The Dissertation Committee for Michael Wood Certifies that this is the approved version of the following Dissertation:

Development of Ligands Targeting the Sigma-2 Receptor and the Molecular Identification of the Sigma-2 Receptor as TMEM97, the Total Synthesis of (±)-Alstoscholarisine E, and Progress Toward the Total Synthesis of Pierisketolide A.

Committee:

Stephen F. Martin, Supervisor

Michael J. Krische

Eric V. Anslyn

Walter Fast

Development of Ligands Targeting the Sigma-2 Receptor and the Molecular Identification of the Sigma-2 Receptor as TMEM97, the Total Synthesis of (±)-Alstoscholarisine E, and Progress Toward the Total Synthesis of Pierisketolide A

by

Michael Dean Wood

Dissertation

Presented to the Faculty of the Graduate School of

The University of Texas at Austin

in Partial Fulfillment

of the Requirements

for the Degree of

Doctor of Philosophy

The University of Texas at Austin

August 2020

Dedication

To my fiancé, for all of your love and support.

Acknowledgements

There are many who I must thank, but first and foremost I would like to thank Professor Stephen F. Martin for bringing me into the group and supporting me throughout this journey. You have provided critical guidance and taught me to be a better scientist, with oversight that kept me on track, but also with the freedom to explore and learn from my mistakes. I feel fortunate to have had the opportunity to work on several meaningful projects under your tutelage, and none of our success would have been possible without your persistence and insight. You were always available to provide help when needed, and you went above and beyond to ensure that I was successful. For that, I will always be grateful. I could not have asked for more from a research advisor, and I am thankful for your support over the years.

None of my success in graduate school would have been possible without the efforts of many current and former members of the Martin group. Much of my research builds on years of prior work from our group that laid the foundation for these endeavors. In addition, Dr. Dan Klosowski's early work on the total synthesis of Alstoscholarisine E was essential, and I am thankful that I was able to contribute to that effort. I have learned a great deal from each of the group members that I have had the privilege to work with. This includes Zach White, Dr. Rachel Wypych, and Dr. Tim Hodges who were members of lab three that contributed significantly to my development during my early years in the group. I'm also thankful to Chris Farley for his enthusiasm in our discussions about chemistry and his willingness to provide critical feedback. But most importantly, I am thankful to each of the former group members that I have worked with, as well as Zhipeng Wang, Grant Walby, and Luiza Cruz, for their friendship over the years, the fun

nights at The Crown, and the all of the little moments that made graduate school more enjoyable.

The love and support from my mother and father were essential in getting me to this point. I specifically want to thank my father for teaching me to work hard and never give up, because often, those things that are most meaningful are only attained through persistent effort. I also want to thank my brother Jesse for providing an example that changed my perspective. You demonstrated what was possible with your own accomplishments, and it altered the trajectory of my life. I might not have made it to this point without your encouragement to pursue undergraduate research, as well as graduate school, and I am grateful for your guidance.

My close friend AJ has been constant source of support and encouragement during this process. Your friendship has been a bright spot during my time in graduate school, and joking with you every day has helped keep me from getting lost in my work. You've never failed to keep pushing me forward when things have been tough. Thank you for being a great friend.

Most importantly, I want to thank my fiancé Cassie. In 2014, I asked you to move to Texas while I pursued graduate school, and you were crazy enough to say yes. Much has changed in the time since, but your love and support has not waivered. My long work hours and high levels of stress could not have been easy for you, not to mention the Texas heat. Despite this, you were by my side through it all, and you even said yes when I asked you to marry me. You encouraged me to work hard, but you also never let me forget that some things matter more than my work. I'm so thankful that you were always there to bring a smile to my face when I came home, even during the tough times, and I could not have asked for more. There have been many challenges on this journey, but we made it through them together. I cannot wait to start the next chapter with you.

Abstract

Development of Ligands Targeting the Sigma-2 Receptor and the Molecular Identification of the Sigma-2 Receptor as TMEM97, the Total Synthesis of (±)-Alstoscholarisine E, and Progress Toward the Total Synthesis of (–)-Pierisketolide A.

Michael Wood, Ph.D.

The University of Texas at Austin, 202

Supervisor: Professor Stephen F. Martin

Our laboratory has shown that ligands constructed using an appropriately substituted norbenzomorphan-derived scaffold exhibit high affinity and selectivity for the sigma-2 receptor (σ2R) and that several of these analogs display promising activity in models of neurodegenerative and neurological conditions. Herein, we report the development of a novel set of ligands that target the σ2R using a scaffold simplification strategy for modification of the norbenzomorphan motif to a tetralin scaffold. Systematic evaluation of structure-activity relationships (SAR) was conducted in four regions of the scaffold and across a range of substitution patterns. This effort resulted in the identification of critical pharmacophore elements and the development of several potent and selective σ2R ligands. One of these, JVW-1601, displayed promising anti-inflammatory properties in the 5XFAD mouse model of Alzheimer's disease. In addition, unique structural features of the simplified scaffold and critical insight from the SAR

investigation were leveraged to enable the molecular identification and cloning of the long sought-after σ2R.

The total synthesis of (±)-alstoscholarisine E, a pentacyclic indole alkaloid, was completed in a longest linear sequence of seven steps from commercially available reagents and 15.2% overall yield, the shortest and most high-yielding synthesis reported to date. The approach features a unique variant of the vinylogous Mannich reaction and tandem intramolecular hetero Diels–Alder reaction to quickly access the core. Diastereoselective reduction of the cyclic vinyl ether moiety was accomplished via a stereoselective acyloxyacetal formation/reduction. A mild procedure to form the bridging aminal ring was discovered that occurs via iridium–catalyzed hydrosilylation of the lactam and spontaneous cyclization of the intermediate hemi-aminal with the indole nitrogen atom, thereby completing the total synthesis of (±)-alstoscholarisine E.

Pierisketolide A is a rearranged *ent*-kaurene diterpene that possesses a bicyclo[3.2.1]octane ring with a fused 5,7-membered ring and a spirotetronate moiety. Enantioselective access to the bridged core structure was achieved using a unique Pauson-Khand reaction with a highly substituted cyclopentane that was prepared from (–)-linalool in five steps. Efforts to optimize this preliminary discovery are ongoing, and further elaboration of the tricyclic core is anticipated to complete the total synthesis of pierisketolide A.

Table of Contents

List of Tables

List of Figures

List of Schemes

THE DESIGN AND SYNTHESIS OF LIGANDS TARGETING THE SIGMA-2 RECEPTOR

Chapter 1: Sigma Receptors

1.1 JOURNEY FROM TOTAL SYNTHESIS TO SIGMA RECEPTORS

1.1.1 Introduction

Research in the Martin laboratories has long been focused on utilizing the structural complexity found in natural products and their mimics as a platform for broader discovery and innovation.[1] These efforts have led to the development of interesting strategies and chemical transformations with broad utility for the construction of small molecules with promising biological activity. Recent work in the Martin group constructing small molecules that target the sigma receptors (σR) exemplifies this approach and highlights important discoveries that arise from challenging targets in both chemistry and biology.

The path that led the Martin group to investigating σRs commenced with early work on the total synthesis of heteroyohimbine natural products. Challenges encountered during the course of that work established a key reaction sequence for the expedient formation of an oxahydroisoquinolne ring system.[2] Ultimately, this gave rise to a more general strategy for accessing diverse heterocyclic scaffolds that were subsequently elaborated to create libraries of small molecules.[3] These molecular libraries were subjected to a variety of assays in order to probe for potential biological activity and a variety of hits were identified. However, a subset of compounds constructed with a norbenzomorphan scaffold displayed affinity for σRs, an interesting target that piqued our interest.[4]

Decades of study has indicated that σRs, which are comprised of the pharmacologically related sigma-1 (σ1R) and sigma-2 receptor (σ2R) subtypes, are potential therapeutic targets for a broad range of diseases including cancer and neurological disorders.[5] Yet despite extensive efforts, much remains unknown about this relatively enigmatic receptor class. The σ1R was successfully cloned in 1996, allowing a more thorough investigation, and a crystal structure was finally obtained in 2016.[6] In contrast, when we initiated our work the σ2R had not yet been cloned, thereby blocking access to modern tools for investigation. A wide variety of structurally diverse ligands bind the σ1R and σ2R, with substantial overlap in their binding profiles, which has resulted in additional challenges that are compounded by the absence of structural information about the protein.[7] However, the potentially untapped medicinal value of the σ2R suggested that the challenges posed by this elusive target might be an opportunity for much needed discovery.

Accordingly, the Martin group forged ahead with an investigation of the norbenzomorphan scaffold, as well as other scaffolds derived from it, for targeting the σ2R.[4,8] These efforts revealed important structural features of the scaffold that can be used to affect σ1R and σ2R affinity.[9] At the time, the σ1R had been implicated in neurological disorders, but the σ2R had largely been pursued as a target for the treatment and diagnosis of cancer and little was known about its role in central nervous system (CNS) disorders.[7,10] Discoveries in the Martin group demonstrated that modulating the σ2R can have beneficial outcomes in models of several CNS disorders including Alzheimer's disease (AD), neuropathic pain, and traumatic brain injury (TBI), as well as alleviating symptoms of alcohol withdrawal.[11-14] However, the expanding therapeutic potential of the σ2R highlights the need for an increased understanding of its biological

role, which would be aided through the development of additional tool compounds and by access to the cloned receptor.

1.1.2 Total Synthesis Leads to MCAP

Research in the Martin group has long been focused on accessing a variety of natural product and natural product-like molecules.[1] A central tactic in this endeavor has been to develop chemical transformations that efficiently access structural subunits that are common to these compounds. Among these, the hydroisoquinoline and oxahydroisoquinoline ring systems were identified as a shared structural feature of many indole alkaloids in the yohimbine family of natural products (Figure 1.1).[15] A synthetic approach that provides efficient access to these *cis*-fused heterocycles would therefore be broadly applicable for the construction of a variety of natural products.

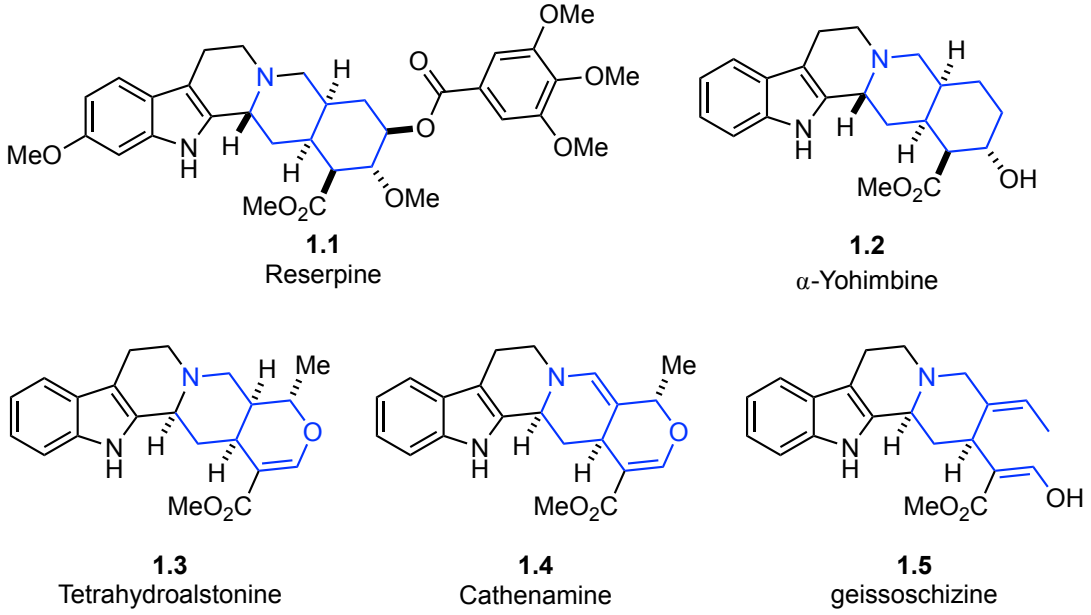

Figure 1.1. Yohimbine natural products.

Accordingly, the Martin group devised a strategy to access this structural motif using an intramolecular Diels–Alder (IMDA) or hetero Diels–Alder reaction (HDA) with

a strategically placed amide moiety that linked the diene and dienophile (Scheme 1.1). Initial investigations proved the utility of this IMDA approach for accessing the hydroisoquinoline subunit and the transformation was extended as a key step in the total syntheses of reserpine (**1.1**) and yohimbine (**1.2**).[16,17] In the event, propargyl alcohol **1.6** was converted to the benzyl amine **1.7** and subsequently acylated to afford triene **1.9**. Consistent with preliminary studies, thermolysis of **1.9** induced cyclization to provide diene **1.10** in 93% yield.[18,19] Refunctionalization of cycloadduct **1.10** via regioselective epoxidation and nucleophilic ring–opening afforded acyloxy analog **1.11**, which was elaborated over 10 steps to yield the advanced indole intermediate **1.12**. Oxidative cyclization with $Hg(OAc)_2$ provided reserpine **1.1** in 35% yield after zinc mediated reduction of the crude reaction mixture.[16,17] Acyloxy analog **1.11** was also elaborated to access yohimbine (**1.2**) through a similar reaction sequence.[17,20]

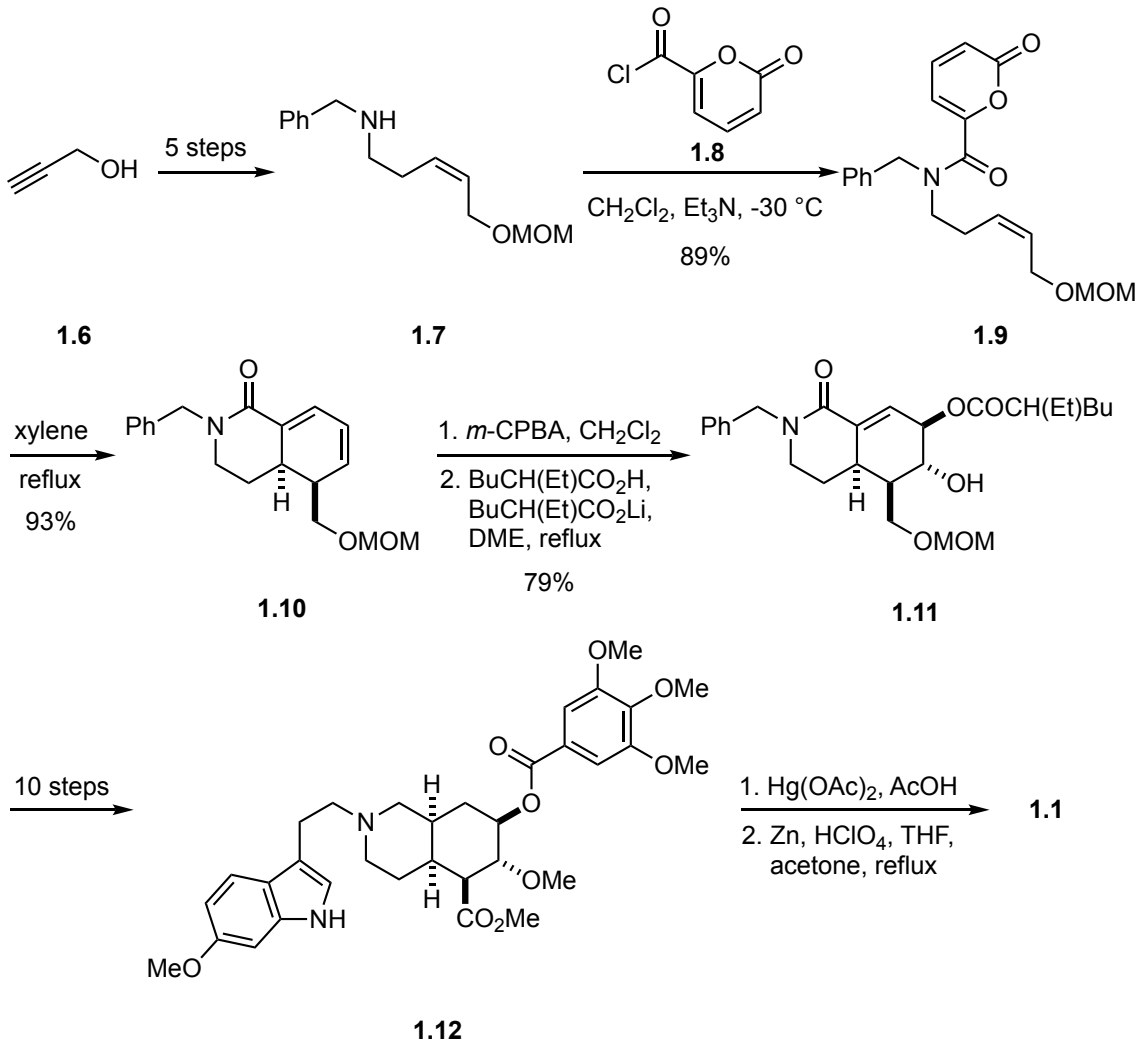

Scheme 1.1. Total synthesis of yohimbine natural products.[17]

These successful total syntheses demonstrated the value of this IMDA approach for accessing yohimbine natural products, while related investigations suggested that the HDA reaction was equally effective for accessing the oxahydroisoquinoline subunit in tetrahydroalstonine (**1.3**), a heteroyohimbine natural product.[20] However, deficiencies in the final oxidative iminium cyclization to form the C ring, as well as other lengthy manipulations, highlighted the need for a more efficient strategy. This led to a second-generation approach that sought to forge the C ring of **1.13** at an early stage of the

synthesis and subsequent refunctionalization would set the stage for a similar HDA reaction to construct the pentacyclic ring system of **1.3** (Figure 1.2).[2]

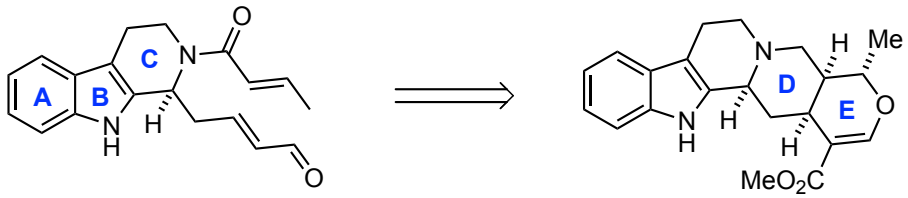

1.13 **1.3**

Figure 1.2. Second generation approach to construct heteroyohimbine natural products.

Expedient access to the HDA precursor **1.12** was critical to assess the feasibility of this modified approach and the known 3,4-dihydro-β-carboline (**1.14**), which is accessible in two steps from tryptamine, was identified as a promising entry point to this system. An interesting one-pot procedure was developed for functionalization of the carboline imine through treatment with an acyl chloride to form an activated *N*-acyliminium with subsequent nucleophilic addition.[15] In the event, treating **1.15** with crotonyl chloride (**1.16**) in the presence of the trimethylsilyloxydiene **1.17** promoted the vinylogous Mannich reaction to afford *N*-acylated triene **1.13** (Scheme 1.2).[21] Refluxing **1.13** in mesitylene induced the HDA reaction to provide the cycloadducts **1.18** in 80% yield. Cycloadduct **1.18** was subsequently elaborated in a few additional steps to complete the total syntheses of (±)-tetrahydroalsonine (**1.3**), (±)-cathenamine (**1.4**), and (±)-geissoschizine (**1.5**).[2,15]

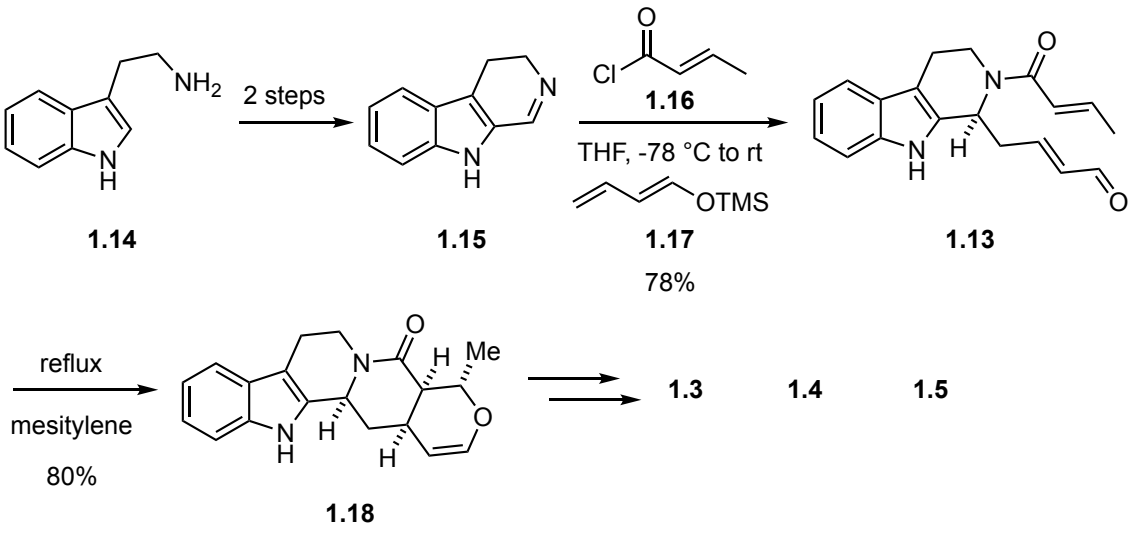

Scheme 1.2. Development of a one-pot vinylogous Mannich reaction.

It is notable that the developed sequence provided access to the pentacyclic core of the heteroyohimbine alkaloids in only four steps from commercially available reagents. Indeed, the initial challenge of constructing the oxahydroisoquinoline subunit provided an opportunity to develop a concise approach to the HDA precursor reaction via in interesting vinylogous Mannich reaction. This endeavor highlighted the utility of combining a vinylogous Mannich reaction in tandem with a HDA reaction to construct challenging alkaloid natural products.[21-26] However more generally, this demonstrated that nucleophilic addition to an activated N-acyliminium in tandem with a cycloaddition reaction might be a powerful tool for the assemblage of a variety of structurally complex heterocycles.[1]

1.1.3 MCAP

Early work in the Martin group to access heteroyohimbine natural products is representative of a target-oriented approach, in which the genesis of the synthetic strategy was born out of the need to access a specific molecule of interest via retrosynthetic

analysis.[27] Target oriented synthesis (TOS) is designed to start from readily available starting materials and access a finite area of chemical space. An alternative strategy is to efficiently access a maximum amount of unique chemical space from simple materials, an approach that Schreiber defined as diversity oriented synthesis (DOS) in 2000.[28] This has been a useful strategy for drug discovery projects, in which large libraries of diverse and complex molecular skeletons are generated and screened for activity against a panel of biological targets.[29] Because there is not a specific target, the screen can identify both a biological target of interest and a small molecule scaffold that modulates it from diverse chemical space, thereby avoiding some structural bias that might be present in a TOS approach.[30]

The strategy for the preparation of DOS chemical libraries often relies on diversity generating processes to transform a collection of relatively similar substrates into a collection of more diverse products.[29] The libraries should be accessible through efficient synthetic sequences, ideally less than five steps without protecting group manipulations. Thus, the sequential use of complexity generating reactions, in which the product of one reaction is used directly in the next complexity building step, is particularly valuable.

Multi-component coupling reactions (MCRs) have emerged as a powerful approach to generate molecular complexity by creating multiple bonds in a single step from less complex inputs.[31] Combining sequential transformations into a single-pot process is useful for increasing synthetic efficiency, as well as operational simplicity. An MCR that displays broad functional group tolerance can facilitate the introduction of orthogonal handles for a variety of transformations.[32-35] This provides an opportunity for a multitude of tandem complexity generating reactions, including annulations and

refunctionalizations that are well suited for accessing numerous scaffolds in a DOS application, an approach that is commonly referred to as build/couple/pair.[36]

Shortly after it's conception, the Mannich-like reaction sequence that was developed during our efforts toward alkaloid synthesis was envisaged to provide more general access to heterocyclic scaffolds. The modular nature of the three-component reaction sequence is distinct from MCRs because introduction of the reactants must be synchronized to obtain the desired reactivity, rather than occurring with simultaneous addition.[37,38] However, the efficiency of the process derives from the one-pot nature of the operation, as opposed to the timepoint of reagent addition. Therefore, by providing a similar ability to incorporate orthogonal functional handles for subsequent diversification, it was expected to be useful from a DOS perspective.

An opportunity to more fully explore this utility later presented itself when the Martin group became involved in the National Institutes of Health (NIH) Molecular Libraries Initiative (MLI). The goal of the program was to facilitate downstream drug development using high-throughput screening (HTS) of chemically diverse, molecular libraries to identify small molecule modulators of thousands of biological targets.[39,40] This effort to expand HTS to the public sector, which was designed to accelerate target validation and identification of chemical probes, required production of chemical libraries that accessed unique areas of chemical space. Thus, the Martin group sought to generalize the tandem vinylogous Mannich and hetero Diels-Alder reaction sequence to provide access to structurally diverse heterocyclic scaffolds for this purpose.

The sequence previously developed to access complex alkaloid natural products can be broadly characterized as the addition of a carbon nucleophile to an iminium ion that is generated in situ from an imine and an acylating agent. A related sequence was designed for application in DOS, in which the condensation of an amine **1.19** and an

aldehyde **1.20** afford an intermediate imine that is converted to an activated *N*-acyl iminium ion in situ via treatment with acylating agent **1.21**. Subsequent addition of a nucleophile ("Nu") **1.22** provides the functionalized amide adduct **1.23** (Scheme 1.3) in a single reaction vessel.[41,42] This one-pot, four-component coupling reaction, identified as the multicomponent assembly process (MCAP), generates considerable complexity from an assortment of simple and readily available reagents. The modular nature of the reaction facilitates the incorporation of orthogonal functional handles that can be used in sequenced annulation reactions, creating additional skeletal complexity in the resulting polycyclic heterocycles **1.24**. Further functional group (FG) interconversions and diversification provide a library of unique scaffolds that are differentiated into various analogs **1.25**. Through the judicious choice of input components, the MCAP sequence provides rapid access to diverse scaffolds that access unique regions of chemical space.

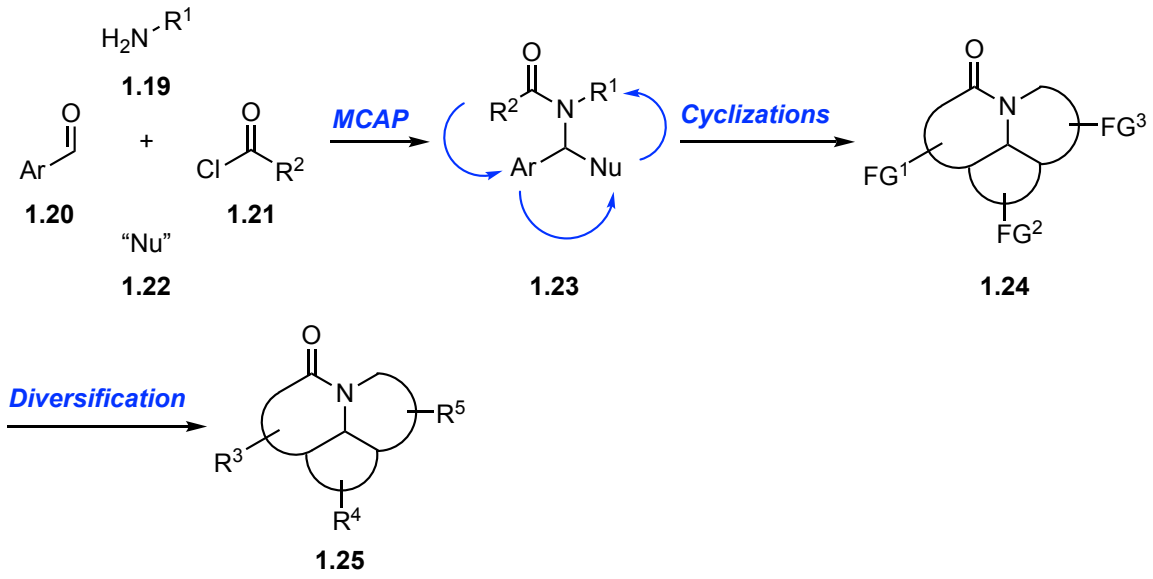

Scheme 1.3. Development of the MCAP for the assemblage of polycyclic heterocycles.

The efficiency of the one-pot MCAP sequence was leveraged to access over 900 compounds comprised of a variety of heterocyclic scaffolds that broadly probed a range of chemical space.[1] The structural diversity achieved with this approach is represented by the benzazepines (**1.26-1.27**), benzodiazepine (**1.28**), polycyclic indoles (**1.29-1.30**), isoindolinone (**1.31**), tetrahydroisoquinolines (**1.32-1.33**), quinazolone (**1.34**), 2-arylpiperidines (**1.35-1.36**), tetrahydrobenzonaphtheridine (**1.37**), benzoxazocine (**1.38**), and the norbenzomorphan (**1.39**) scaffolds that were accessed with this strategy (Figure 1.3).[3,43-50] The prepared compounds were screened at various NIH facilities to evaluate for potential biological activity as part the MLI program and indeed many of the compounds provided hits at various biological targets. Because the norbenzomorphan framework **1.39** is structurally related to the benzomorphan subunit of morphine and has shown promise as a molecular framework for designing acetylcholinesterase (AChE) inhibitors, it was particularly interesting as a platform for HTS.[51-53]

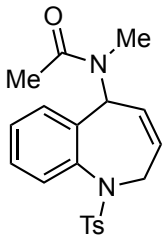

1.26

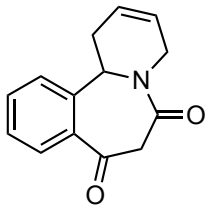

1.27

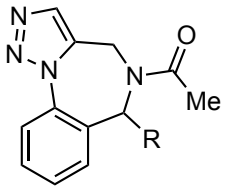

1.28

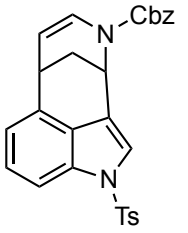

1.29

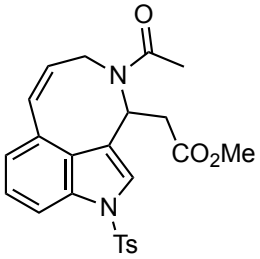

1.30

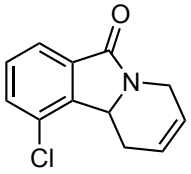

1.31

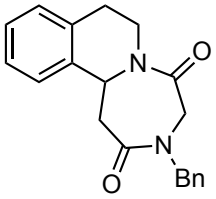

1.32

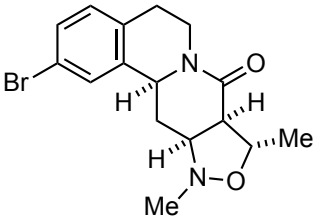

1.33

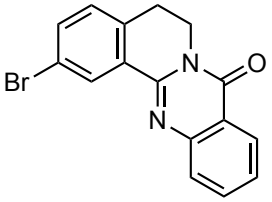

1.34

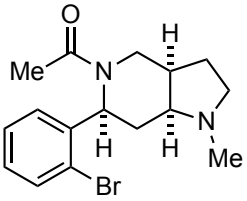

1.35

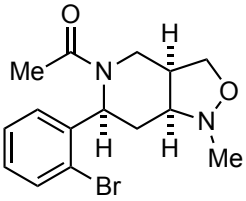

1.36

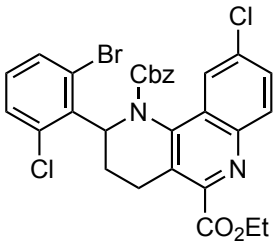

1.37

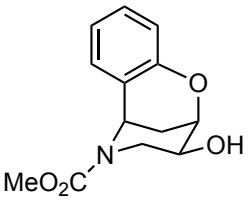

1.38

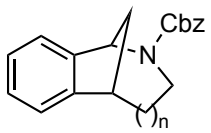

1.39

Figure 1.3. Representative scaffolds constructed with the MCAP.

The Martin group prepared a library of nornbenzomorphan analogs using the MCAP procedure from commercially available 2-bromo-5-chlorobenzaldehyde (**1.40**) and 2-bromo-4-chlorobenzaldehyde (**1.41**) (Scheme 1.4).[50] Condensation with allyl amine (**1.42**) provided intermediate imines **1.43** and **1.44** that were subsequently activated with benzyl chloroformate, followed by addition to of allyl zinc bromide to provide dienes **1.45** and **1.46** in 89-91% yield. Ring closing metathesis (RCM) proceeded smoothly to deliver 2-arylpiperidines **1.47** and **1.48**, and a subsequent Heck cyclization furnished the bridged enecarbamates **1.49** and **1.50** in 92-94% yield. Reduction of the olefin was achieved by treatment with Et_3SiH in the presence of trifluoroacetic acid to deliver the 7-chloro-norbenzomorphan **1.51** and 8-chloro-norbenzomorphan **1.52** scaffolds. Refunctionalization of the heterocyclic nitrogen atom and cross coupling reactions with the aryl chloride readily converted the norbenzomorphan core to a collection of diversely functionalized analogs **1.53**.

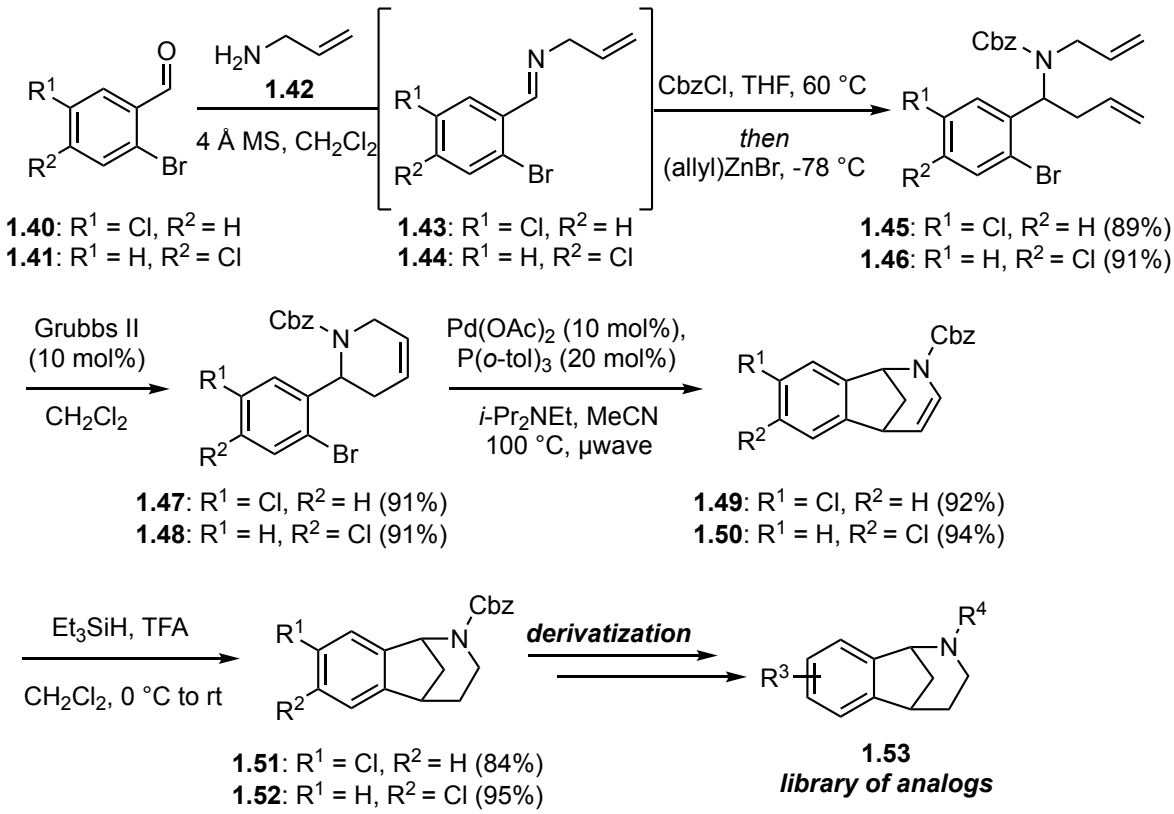

Scheme 1.4. Synthesis of norbenzomorphan analogs using the MCAP.

The initial series of analogs was screened for activity in a range of phenotypic and target-based assays at the NIH Molecular Library Probe Production Center Network (MLPCN), the National Institute of Mental Health's (NIMH) Psychoactive Drug Screening Program (PDSP), and Eli Lilly's Open Innovation Drug Discovery (OIDD) Program.[50] Notable activity was observed for several of the analogs across a spectrum of biological targets, but low nanomolar affinity for the σ1R and σ2R was observed among a subset of derivatives (Figure 1.4).[54] Some early hits with distinct substitution patterns, including compounds **1.54-1.55**, displayed little preference for either σR subtype. Alternatively, morpholine substituted norbenzomorphan **1.56** displayed modest selectivity for the σ1R, whereas phenethylamine substituted norbenzomorphan **1.57**

displayed low levels of selectivity for the σ2R. It was not immediately clear how the substitution pattern was imparting the observed selectivity, but the results suggested that altering the functionality might enable modulation of σR subtype selectivity. Additional investigation revealed the σR to be an intriguing biological target for a range of therapeutic implications, but the absence of definitive characterization data for the receptors made them enigmatic targets.[5] With the DOS initiative having identified an interesting biological target, as well as an easily diversifiable molecular scaffold that modulates it, some additional investigation was warranted.

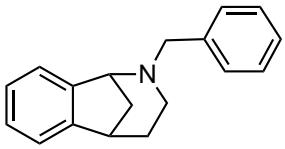

1.54
σ1R K_i (nM): 139
σ2R K_i (nM): 100

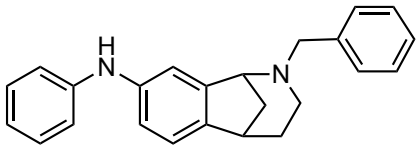

1.55
σ1R K_i (nM): 98
σ2R K_i (nM): 78

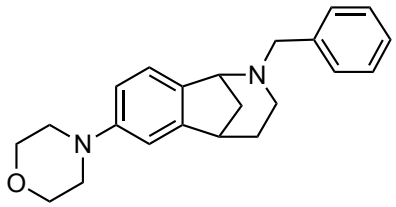

1.56
σ1R K_i (nM): 17
σ2R K_i (nM): 562

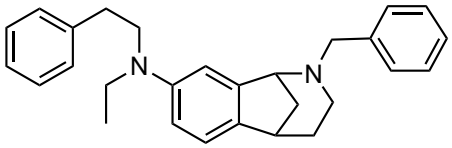

1.57
σ1R K_i (nM): 594
σ2R K_i (nM): 147

Figure 1.4. Representative examples of preliminary norbenzomorphan analogs with affinity for the σRs.[54]

1.2 THE HISTORY OF SIGMA RECEPTORS

1.2.1 The Early Discovery of Sigma Receptors and Their Misclassification

The receptors that have now been classified as σRs were originally discovered in 1976 in the seminal work of Martin *et al.* that identified several opioid receptor subtypes through pharmacological evaluation of morphine and a series of structurally related analogs (Figure 1.5).[55] The classical approach relied on observation of distinguishable behavioral responses to drug administration in dogs, and the receptor category was named according the first letter in the name of the corresponding compound it bound. The administration of morphine (**1.58**) diminished nociceptive responses with general apathy toward external stimuli, but notably the dogs did not sleep. This response was attributed to activity at mu (μ) opioid receptors and was accompanied by a depression in body temperature and pulse rate. In contrast, dosing with ketocyclazocine (**1.59**) produced a notable sedative effect, without altering body temperature or pulse rate, and was attributed to activity at the kappa (κ) opioid receptors. Administration of the benzomorphan SKF-10,047 (**1.60**) produced a dose dependent increase in pulse rate, but did not alter body temperature. However, a pronounced change in behavior was observed as mania and symptoms of delirium ensued, which was associated with activity at sigma (σ) opioid receptors. The unique physiological response to each chemically related compound was blocked by naloxone, an established opioid antagonist, supporting the hypothesis that the behavioral responses resulted from agonism of related opioid receptors.

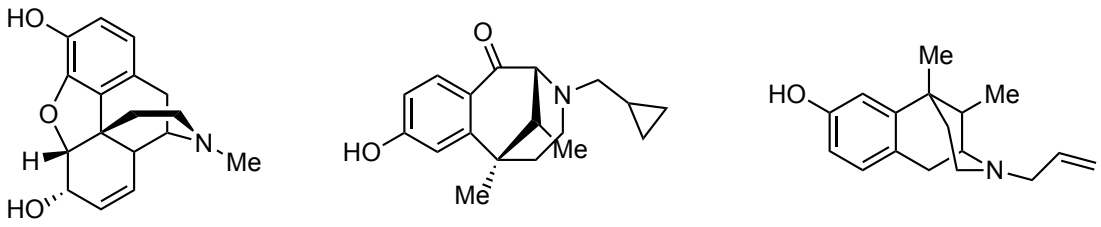

1.58
(-)-morphine

1.59
(-)-ketocyclazocine

1.60
(±)-SKF-10,047

Figure 1.5. Compounds used to distinguish opioid receptor classes

Following Martin's initial discovery of σRs, there were continued pharmacological investigations to probe the nature of the SKF-10,047 binding site, and these suggested that it was a receptor class distinct from the opioid receptors.[56,57] Previous studies indicated that the levorotatory isomers of opioids had higher affinity for μ-opioid receptors than the corresponding dextrorotatory isomer and that the opioid *l*-etorphine had non-specific high affinity for opioid receptors.[58-60] However in 1982, Su *et al.* reported that the racemic, tritiated version of the prototypic σR ligand [^{3}H]-(±)-SKF-10,047 had affinity for a site in the guinea-pig (GP) brain that was not accessible by *l*-etorphine.[56] They also found that the dextrorotatory isomer of benzomorphans (**1.61**-**1.63**) had much greater affinity for the *l*-etorphine inaccessible site, in contrast to the levorotatory isomers which interacted preferentially with opioid receptors (Figure 1.6). In 1983, Tam provided similar evidence that dextrorotatory benzomorphans had affinity for a site inaccessible by the opioid antagonist naloxone in the rat brain.[57] Collectively, evidence provided by Su and Tam indicated that the σR was distinct from opioid receptors.

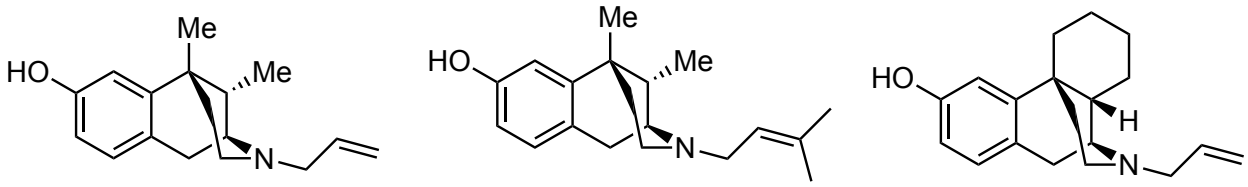

1.61
(+)-SKF-10,047
σR IC_{50} (nM) = 294 ± 45

1.62
(+)-pentazocine
σR IC_{50} (nM) = 41 ± 16

1.63
(+)-dextrallorphan
σR IC_{50} (nM) = 67 ± 13

Figure 1.6. Dextrorotatory benzomorphans with affinity for *l*-etorphine inaccessible site in GP brain using [^{3}H]-SKF-10,047 in the presence of *l*-etorphine to mask opioid sites.

While evidence was emerging to suggest that the σR was a unique receptor class, concurrent pharmacological characterization of the phenylcyclidine (PCP) receptor led to some speculation that σR ligands and PCP act at the same site.[61] Pert and coworkers reported in 1981 that the binding of tritium labeled PCP ([^{3}H]-PCP) in rat brain was not affected by morphine or naloxone, but was displaced by σR binding benzomorphans such as SKF-10,047 (**1.60**), even at low concentrations.[62] The psychotomimetic activity and other behavioral responses that resulted from administration of SKF-10,047 was similar to that observed with PCP, supporting the hypothesis that they acted at the same site.[63-66] However, Su and Tam both demonstrated that σR ligands did not have similar potency at the PCP site and Tam reported differences in regional distribution of the two receptors, suggesting that they were not synonymous.[56,57] The PCP receptor was later revealed to be located within the N-methyl-D-aspartate (NMDA) receptor, and additional investigations with high affinity and noncompetitive radiolabeled NMDA receptor ligands found that these sites were separate from those labeled by the σR ligand [^{3}H]-(±)-SKF-10,047.[67-69] Eventually, a committee at the 1987 "International Seminar on Phencyclidine and Sigma-like Compounds as Molecular Probes in Biology" unanimously approved a proposal for

classifying the PCP and σR as distinct sites based on ligand affinity and selectivity patterns.[70]

The reports by Su and Tam helped establish that the σR was indeed a unique class of receptors with affinity for structurally diverse opiates (**1.61**-**1.63**) and non-opioid (**1.64**-**1.69**) drugs, inspiring additional investigations to characterize pharmacological features of the novel receptor (Figure 1.7).[56,57] This aided the identification of additional drugs that interacted with the σR, some of which were radiolabeled for competition binding analysis and autoradiographic studies including haloperidol (**1.64**), which had the highest σR affinity among these early ligands.[57] Unfortunately, many of these had a lack of specificity for σR which stymied early characterization efforts, but in 1984 Snyder reported that (+)-3-(3-hydroxyphenyl)-N-propylpiperidine (3-PPP) (**1.68**) had high affinity for the σR with greater selectivity.[71] However, (+)-3-PPP was also a presynaptic dopamine autoreceptor agonist, and a truly selective σR ligand was still needed. The crucial advance came in 1986 when Weber *et al.* reported that the achiral, symmetric guanidine derivative 1,3-di-*o*-tolylguanidine (DTG) (**1.69**) displayed high affinity for the σR and that it was selective over the opioid receptors, dopamine D_2 receptors, and the PCP binding site.[72] This specificity was similar to that of (+)-3-PPP (**1.68**), but the structural simplicity of the achiral ligand made it more attractive as a prototypic σR selective ligand, suggesting that the radiolabeled analog [^{3}H]-DTG (**1.70**) would prove beneficial in additional investigations.

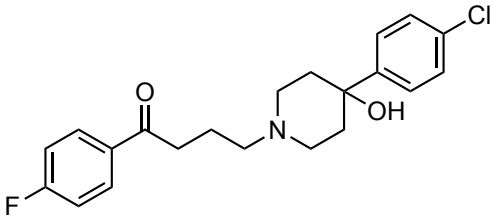

1.64
Haloperidol
σR IC_{50} (nM) = 5 ± 0.3

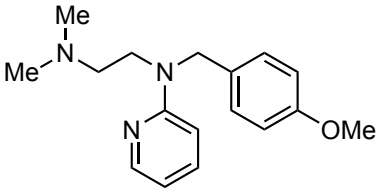

1.65
Pyrilamine
σR IC_{50} (nM) = 142 ± 38[a]

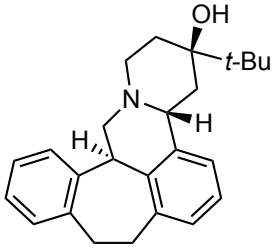

1.66
(-)-Butaclamol
σR IC_{50} (nM) = 530 ± 49

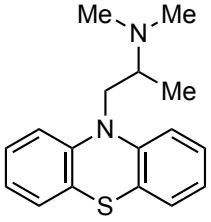

1.67
Promethazine
σR IC_{50} (nM) = 190 ± 27[a]

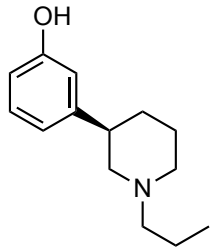

1.68
(+)-3-PPP
σR IC_{50} (nM) = 76 ± 4

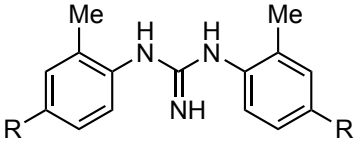

1.69 DTG: R = H
1.70 [^{3}H]-DTG: R = ^{3}H
σR IC_{50} (nM) = 28 ± 1

Figure 1.7. Non-opioids with affinity for σR. Determined using GP brain against [^{3}H]-DTG unless noted otherwise. [a] Determined using [^{3}H]-EKC in the presence of naloxone in rat spinal cord membrane.

1.2.2 Two Sigma Receptor Subtypes

The σR binding site originally identified in Martin's seminal work had become an intriguing target because of its pharmacological profile along with the poor

characterization and misidentification that plagued early studies, but the arrival of selective σR ligands enabled more thorough biochemical characterization. At the time, the σR was pharmacologically distinguished from other receptors according to the binding profile against a range of established ligands.[70] High affinity for (+)-benzomorphans, such as pentazocine (**1.62**) and dextrallorphan (**1.63**) was a defining feature of the σR.[56,57] Additionally, the σR binding site was insensitive to naloxone and *l*-etorphine opioids and had much lower affinity for (-)-benzomorphans, which interacted preferentially with opioid receptors. Another critical defining feature of the σR was notably high affinity for the non-benzomorphan ligands haloperidol (**1.64**), as well as (+)-3-PPP (**1.68**), and DTG (**1.69**), which were more σR selective ligands.[57,71,72] After a decade of research that had been plagued by misidentification, this unique binding pattern comprised the core features of σRs, but evidence soon emerged that pointed to the existence of two distinct σR subtypes.

Irradiation of opioid receptors with ultra-violet (UV) light was a known method for altering the protein structure and attenuating ligand affinity, leading Bowen *et al.* to pursue a similar strategy for evaluating the σR.[73] In 1989 Bowen disclosed the results from that effort, finding that irradiation of membranes from the rat brain with 254 nM light for five minutes decreased affinity for the non-benzomorphan ligands [^{3}H]-DTG and [^{3}H]-(+)-3-PPP by approximately 50%.[74] In contrast, irradiation with 254 nM light significantly enhanced affinity for the benzomorphan ligand [^{3}H]-(+)-SKF-10,047 by about 190% after 10 minutes of irradiation. Additionally, exposure to UV light reduced the ability of the non-benzomorphan ligands to inhibit benzomorphan binding, whereas benzomorphan inhibition of benzomorphan binding was unaffected. The differing photosensitivity to binding suggested that different proteins with distinct responses to irradiation were binding the structurally unique compounds and that that interaction was

not occurring at a common binding site. Moreover, [^{3}H]-DTG and [^{3}H]-(+)-3-PPP each labeled approximately four-times the number of sites that were labeled by [^{3}H]-(+)-SKF-10,047. Collectively these data supported the existence of a multiple binding site model with structurally distinct σR ligands. Bowen concluded with a noteworthy comment that the photosensitivity in rat membrane discussed in the report was different from what they independently observed using GP brain, a much more common tissue source for σR analysis, leading him to suggest that there may be a species-specific difference in the relative ratio of σR subtypes.[74]

Bowen and Hellewell expanded on those findings in 1990 with a follow up report that compared the σR binding profile in tissues obtained from GP brain and pheochromocytoma (PC12) cells, a tumor cell line derived from the rat adrenal gland.[75] Both tissues displayed similar levels of high affinity for the prototypic σR selective ligand [^{3}H]-DTG, as well as haloperidol, a defining feature of the σR. Both tissues also displayed high affinity for [^{3}H]-(+)-PPP, another selective σR ligand, but in PC12 cells it was approximately one-third of that obtained using GP brain (*i.e.* K_D = 86.3 ± 22 and 27.4 ± 2, respectively). The number of sites labeled by [^{3}H]-DTG in GP brain was also roughly three-times greater than the number of sites labeled by [^{3}H]-(+)-PPP. In addition to differing affinities for established σR selective ligands, the two tissues displayed opposite stereochemical preferences for benzomorphans. The GP brain is a common tissue source for σR studies, and it displayed the typical preference for (+)-benzomorphans, yet little to no affinity for those compounds was observed in PC12 cells that instead had a modest preference for the (-)-isomer with generally low affinity overall. The report also utilized an azide-modified DTG analog for photolabeling studies and determined that a 25 KDa protein was labeled in GP brain, but it was not observed in

PC12 cells. Instead, and 18 and 21 KDa protein was labeled and, in each case, the photolabeling was blocked by haloperidol.

Collectively, the findings of Bowen and Hellewell in 1989 and 1990 provided critical evidence to suggest there were two molecular forms of the σR, which could be differentiated by their binding profile and molecular weight.[74,75] Additional evidence emerged supporting this assertion, prompting leading researchers in the field to propose in 1992 that the sigma bind site be delineated into two subtypes, the σ1R and σ2R.[76] The σ1R subtype exhibits the pharmacological profile that was classically associated with σRs in early work by Su and Tam, including high affinity for DTG and haloperidol, as well as (+)-pentazocine and other (+)-benzomorphans. The σ2R was defined by similar affinity for DTG and haloperidol, but with low affinity for (+)-benzomorphans. The functional role of the σ1R and σ2R was still largely unknown, but these critical studies provided important pharmacological characterization data that established the existence of two distinct receptor subtypes and they also identified σR selective ligands that were employed in decades of future research.

1.3 The Sigma-1 Receptor

1.3.1 Early Characterization of the Sigma-1 Receptor

Early investigations of σRs relied on pharmacological characterization and were confounded by a promiscuous binding profile among structurally diverse opioid and non-opioid drugs that lacked specificity for the receptor. The result was more than a decade of confusion over the identity of the receptor, and the pharmacological effects associated with binding remained ambiguous. This dilemma was transformed with the emergence of ligands selective for the σR, but soon confounded again with the realization that there were in fact two σR subtypes, and many of the early σR selective ligands, such as DTG

and (+)-3-PPP, had high affinity for both. However, (+)-pentazocine was identified as a high affinity and specific σ1R ligand that was selective over σ2R, providing a useful tool for additional characterization efforts that was not yet available for the σ2R.[75] In fact, [^{3}H]-(+)-pentazocine remains the radioligand of choice for determining σ1R affinity, whereas σ2R affinity is still commonly determined with [^{3}H]-DTG in the presence of (+)-pentazocine to block binding at the σ1R.[77]

Delineation of σR subtypes using selective radioligands for binding analysis was a significant milestone that was followed by efforts to obtain structural information regarding the molecular composition and function of the receptors. The σ1R was the first to be successfully cloned in 1996 by purifying the receptor from GP liver homogenate with eight chromatographic steps while tracking the [^{3}H]-(+)-pentazocine binding activity of the eluent.[78] The human σ1R was subsequently cloned from a human placental choriocarcinoma cDNA library and found to share 93% amino acid sequence similarity to the GP σ1R.[79] Shortly thereafter, the receptor was also cloned from rat and murine tissues.[80,81]

1.3.2 Localization and Function Role of the Sigma-1 Receptor

Determination of the σ1R primary sequence fueled numerous predictions about the topology and function of the protein. The 25.3 KDa protein was comprised of 223 amino acids with over 90% homology across species.[78-81] The molecular weight and binding profile of the cloned protein were consistent with those reported by Bowen and Hellewell for the σ1R.[74,75] Interestingly, the sequence has no significant similarity to any known mammalian protein, but does share some similarity with the yeast C8-C7 sterol isomerase, ERG 2P.[78] However, the cloned mammalian receptor does not possess any

sterol isomerase activity, and the lack of similarity to other known mammalian proteins has made it difficult to ascertain the functional role of the σ1R.[82]

Determination of the σ1R amino acid sequence enabled some predictions about the topology of the membrane protein, but several conflicting models emerged.[83] Hanner and coworkers applied hydrophobicity analysis to predict a single transmembrane portion near the N-terminus, whereas Kekuda and Seth both predicted the single transmembrane portion was located in the middle of the protein.[78,79,81] A later model predicted that a hydrophobic region near the N-terminus, and also in the middle of the protein, both spanned the membrane to form an extracellular loop that contains approximately 50 amino acids with the N- and C-terminus located intracellularly.[84,85] This two-pass transmembrane model gained more acceptance and would form the foundation of additional modeling studies that attempted to ascertain a structural basis for ligand binding.[86,87] However, 20 years after the σ1R was successfully cloned, a crystal structure was finally obtained that suggested the original single transmembrane hypothesis was accurate (*infra vide*).[6]

Access to the cloned gene also enabled expression studies, immunohistochemical, and immunoprecipitation techniques, in addition to radioligand analysis, that indicated wide distribution throughout the CNS and peripheral tissues.[86,88-90] At the subcellular level, σ1R is thought to be primarily located at the endoplasmic reticulum (ER) and specifically localized at the mitochondrial associated membrane (MAM).[91] The MAM are specialized microdomains of the ER that form junctions with the mitochondria and regulate diverse cellular functions that are important for cell survival, including Ca^{2+} transfer and protein folding.[92] At the MAM in its dormant state, the σ1R is part of a complex with binding immunoglobulin protein (BiP), a chaperone protein that is known to form mass assemblies with other ER chaperones that respond to stress.[91] In response to

either a depletion of cellular Ca^{2+} levels or ligand activation, the σ1R dissociates from BiP, a critical step that allows it to exert its modulatory function with a chaperone at a myriad of other cellular proteins.[93]

In this model, the σ1R is proposed to function as a ligand-operated receptor chaperone at the MAM, but can also translocate to other regions within the cell to interact with other proteins.[94] At the MAM, it serves to stabilize the conformation of the inositol triphosphate receptor (IP_3R) and couple it to ankyrin B to control Ca^{2+} signaling between the mitochondria and the ER, which is related to ER stress and cellular survival.[91] It also helps control transmission of ER stress to the nucleus by interacting with the inositol requiring enzyme 1 (IRE1), an ER stress response protein that results in enhanced production of antistress and antioxidant proteins.[95] The σ1R can also translocate to the plasma membrane, where it interacts with ion channels and G-protein coupled receptors (GPCRs).[94,96] Additionally, the σ1R can also translocate to the nuclear membrane to help regulate gene expression.[94,97]

These models notwithstanding, the precise physiological role of the σ1R remains somewhat ambiguous given that an endogenous ligand has not yet been identified. Some steroid hormones have significant affinity for the σ1R, most notably progesterone (**1.71**) (K_i = 55 ± 15 nM against [^{3}H]-(+)-pentazocine for recombinant human σ1R in Jurkat cells), which has been proposed as an endogenous ligand (Figure 1.8).[98] However, a wide range of K_i values (30-300 nM) for progesterone in various tissues have been reported since it was originally proposed and the physiological relevance of the interaction remains unclear.[5,10,83,99,100] The natural hallucinogen N,N-dimethyltryptamine (DMT) (**1.72**) has been proposed as an endogenous ligand, but its relatively low affinity for the σ1R (K_i = 14.75 μM) has also led to skepticism about the physiological importance of this interaction.[5,101-103] The long chain sphingoid base D-erythro-sphingosine (**1.73**) (K_i =

140 ± 20 nM) has also been proposed as a potential endogenous ligand, but the identity or existence of a specific endogenous ligand remains uncertain.[104,105]

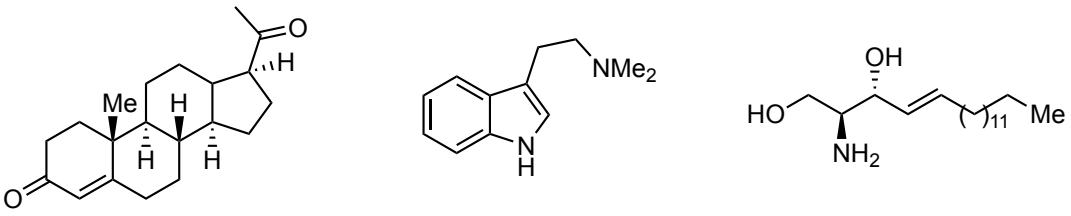

1.71
Progesterone
σ1R K_i (nM) = 30–300

1.72
DMT
σ1R K_i (μM) = 14.75

1.73
D-*erythro*-sphingosine
σ1R K_i (nM) = 140 ± 20

Figure 1.8. Proposed endogenous ligands for σ1R.

The status of the σ1R as an orphan receptor without a relationship to other known proteins has complicated the determination of ligand functional activity. Instead, phenotypic response to ligands have generally been used to assign their functional activity as either agonist or antagonist. Initially, exacerbation of cocaine-induced convulsions in the rat was ascribed to agonist activity, whereas antagonists inhibited the convulsions, but had no affect when administered on their own.[106,107] Later agonist activity was assigned to those compounds that recapitulated the genetic overexpression phenotype.[82] Within the cell, administration of (+)-pentazocine produces agonist activity that results in dissociation of σ1R from BiP.[91] In contrast, haloperidol did not affect the σ1R-BiP complex and blocked the dissociation caused by agonists, consequently it was ascribed antagonist activity. This antagonist functionality is assigned to those ligands that recapitulate the genetic knockdown phenotype.[82] However, the molecular mechanism by which ligand binding produces these effects are not known.

1.3.3 Sigma-1 Receptor as a Therapeutic Target

Initial interest in σR as a therapeutic target undoubtedly resulted from the original presumption that it was an opioid receptor along with its association with psychotomimetic properties, but this grew as an increasing number of structurally diverse, pharmacologically active compounds were found to have σR activity. In the time since, the σ1R has been implicated in a vast number of disorders that creates a complex picture of the receptor's therapeutic potential. Much of the attention has focused on the role σ1R in various neurological disorders,[82,93,108] including Alzheimer's disease (AD),[109] Parkinson's disease (PD),[110,111], Huntington's disease (HD),[112] amyotrophic lateral sclerosis (ALS),[113,114] traumatic brain injury (TBI),[115] and ischemic stroke.[116,117] The σ1R has also emerged as an intriguing, non-opioid target for the treatment of pain,[118,119] as well as addiction.[10] In fact, σ1R ligands are currently in phase II clinical trials for the treatment of neuropathic pain[120] and ischemic stroke,[121] as well as phase II clinical trials for PD[122] and phase IIb/III trials for AD.[123,124] The putative role of σ1R in processes critical to cell survival, such as protein folding and intracellular ion regulation and signal transduction suggests that malfunction or mutation of the protein might have a significant impact even if the exact mechanisms remain unclear.[91,94]

Perhaps unsurprisingly, the receptors role in cell survival has also attracted attention to the σ1R as a potential therapeutic target for the treatment of cancer.[125] Both σ1R and σ2R are overexpressed in a variety of proliferating normal cells and cancerous cells, but significantly higher levels of σ2R expression are observed that has generated more attention in this area (*infra vide*).[126] However, the role of the σ1R in cell survival and proliferation makes it an intriguing target as well. Accordingly, early studies demonstrated that putative σ1R antagonists are correlated with a decrease in cancer cell growth.[127,128] Evidence does not suggest that σ1R is itself an oncogene, but genetic

knockdown of the receptor inhibits cell growth and proliferation in breasts cancer cell lines with little effect on non-cancerous breast cells.[129] This effect was recapitulated to a similar extent in the presence of σ1R antagonists, indicating that small molecule inhibition can diminish proliferation of cancerous tissues. The upregulation of σ1R has also been utilized for visualization with radiolabeled ligands, which could be promising for diagnostic imaging of tumors.[130,131] The σ1R is an attractive target for cancer treatment and imaging, but the molecular mechanisms of the receptor in tumor biology and its antiproliferative effects remain unclear, requiring additional investigation for continued advancement toward the clinic.[125,126]

The broad diversity of diseases and cellular processes impacted by the σ1R highlights the importance of the receptor for maintenance of proper cellular function and viability. Numerous genetic mutations in σ1R have been correlated to a predisposition for disease that is generally linked to the loss of motor neuron function associated with ALS, distal hereditary motor neuropathy, and Silver syndrome.[5] More work is needed to understand the molecular mechanisms at play in these diseases and the mechanism of action associated with its pharmacology. However, these findings emphasize the importance of continued investigation of the receptor as a therapeutic target. Indeed many approved pharmaceuticals including fluvoxamine (Luvox), sertraline (Zoloft), buproprion (Wellbutrin), donepezil (Aricept), and opipramol (Opipram) have σ1R affinity.[10,132] The fact that several approved drugs interact with the σ1R and that ligands targeting the σ1R have continued into phase II and III clinical trials holds promise that the receptor might be safely targeted in humans.

1.3.4 Sigma-1 Receptor Pharmacophore

The potential of the σ1R as a therapeutic target for a range of diseases with unmet medical needs has continued to inspire efforts to construct small molecules that are selective for the receptor. A number of pharmacologically active drugs with σ1R affinity were identified early, but the receptors affinity for a range of structurally diverse ligands posed a challenge for pharmacological characterization. This promiscuity hindered efforts to identify small molecules that were selective for the σ1R, as well as to elucidate the pharmacophore elements that contribute to structure–activity relationships (SAR) that might aid the ligand design process.[133] With the delineation of σR subtypes, it was realized that much of the early binding data was confounded by unclear subtype specificity.[133] Nonetheless, a fertile starting ground for investigation was provided by established ligand classes with affinity for σ1R such as benzomorphan **1.62**, N,N'-disubstituted guanidine **1.69**, and phenyl piperidines **1.64** and **1.68** (Figure 1.9). [56,57,75] A unified pharmacophore model that could bridge the structural dissimilarity among established ligands, connecting common molecular features for optimal σ1R affinity, was highly sought and led to several systematic SAR studies.[133-137]

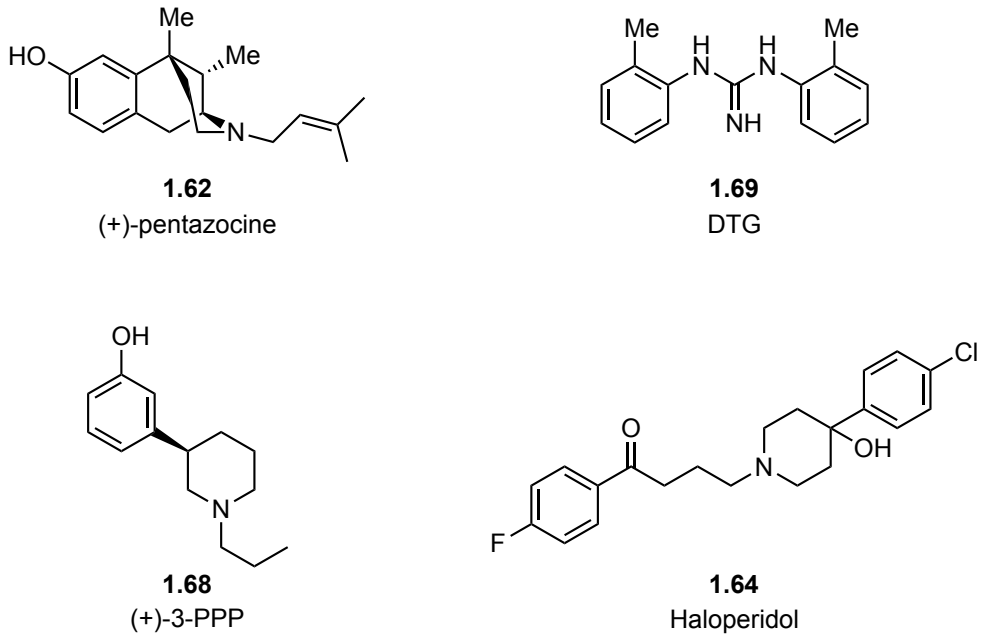

1.62
(+)-pentazocine

1.69
DTG

1.68
(+)-3-PPP

1.64
Haloperidol

Figure 1.9. Ligand classes that have σ1R affinity.

1.3.4.1 Sigma-1 Pharmacophore: Gilligan Model

An extensive SAR study of substituted piperidine analogs that were structurally related to haloperidol led Gilligan and coworkers to report in 1992 a σ1R pharmacophore based on the lead compound (**1.74**) (Figure 1.10.A).[138] Analog **1.74** was characterized with [^{3}H]-SKF-10,047, which is selective for σ1R over σ2R, and found to have high σR affinity (K_i = 6 nM) with selectivity over dopamine D_2 (IC_{50} > 1,000 nM) and PCP receptors (K_i = > 10,000 nM). The four distinct pharmacophore elements (**A**-**D**) of **1.74** were identified as region **A** containing a distal aromatic group that was connected by a linker group (region **B**) to a centrally located piperidine ring (region **C**). The piperidine ring provided a basic nitrogen atom, which is a salient feature of virtually all σR ligands and region **D** was the substituent on the piperidine nitrogen atom.

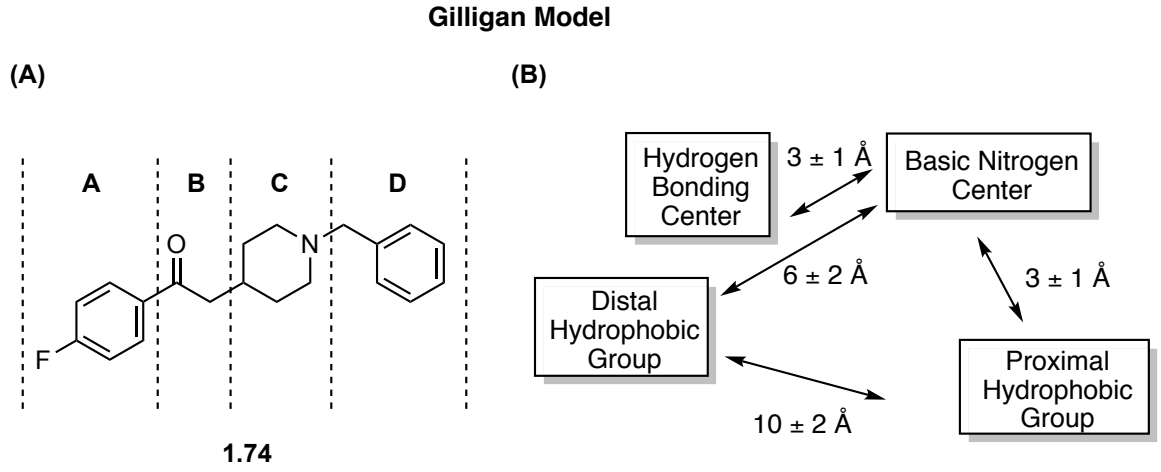

Figure 1.10. Pharmacophore proposed for σ1R by Gilligan based on substituted piperidine analogs.

A series of analogs based on **1.74** were prepared with systematic structural variations in each of the regions **A-D** as part of an SAR study to establish a pharmacophore model for this ligand class.[138] Computational analysis of a subset of these analogs with geometry optimization and energy minimization led Gilligan and coworkers to propose a more detailed four-component model with optimal distances between the critical pharmacophore elements (Figure 1.10.B).[138] The model presented the basic nitrogen atom as the central component, flanked by two hydrophobic groups that extended from the center at different distances. Aliphatic and aromatic groups were accommodated at the proximal hydrophobic site, which was optimally positioned 3 Å from the nitrogen atom. However, it was noted that both the chemical nature and distance of this substituent from the basic amine were critical for obtaining σ1R selectivity over D_2 dopamine and 5-HT_2 serotonin receptors. Heteroaromatic, aromatic and aliphatic carbocycles were well-tolerated at the distal hydrophobic site, optimally positioned 6 Å from the nitrogen center, although aromatic groups were favored for oral potency. The highest potency was generally obtained when the linker between the nitrogen center and

the distal hydrophobic site contained a hydrogen bonding center (*i.e.* carbonyl or ether moiety). While providing interesting insight into the pharmacophoric features, the author acknowledged that the model was limited by the structural similarity of the flexible piperidine analogs, and therefore likely does not define a minimal pharmacophore. The model also made no attempt to account for σR subtype selectivity.

1.3.4.2 Sigma-1 Pharmacophore: Glennon and Ablordeppey Model

In an effort to establish the minimal pharmacophore elements of the (+)-benzomorphan scaffold, Glennon and coworkers sought to simplify the nucleus to the phenethylamine substructure **1.75** (Figure 1.11).[139] The (+)-benzomorphan opiates are archetypal σR ligands, but many only displayed modest potency or suffered from off-target activity, which Glennon hoped to overcome through derivatization of the active pharmacophore subunit. Accordingly, a library of phenethylamine analogs **1.75** were prepared that highlight several important findings from this SAR investigation. Most notably, a continual increase in affinity was observed as the alkyl linker between the nitrogen atom and the phenyl group at R^2 was extended (n = 2-5). It was also noted that stereochemistry had a relatively minimal impact on the binding profile, although there was a modest preference for the *S*-(+)-stereoisomer. This study led to the identification of lead phenylethylamine analog **1.76**, which exemplified the critical pharmacophore elements and in contrast to many benzomorphans, the phenethylamine nucleus provided selectivity over PCP sites. In addition, σR affinity was maintained if the nitrogen atom was a secondary or tertiary amine. Collectively, these findings suggested that the phenethylamine subunit might represent the active pharmacophore of the benzomorphan, but it should be pointed out that overall σR affinity was determined without distinguishing between σR subtypes.

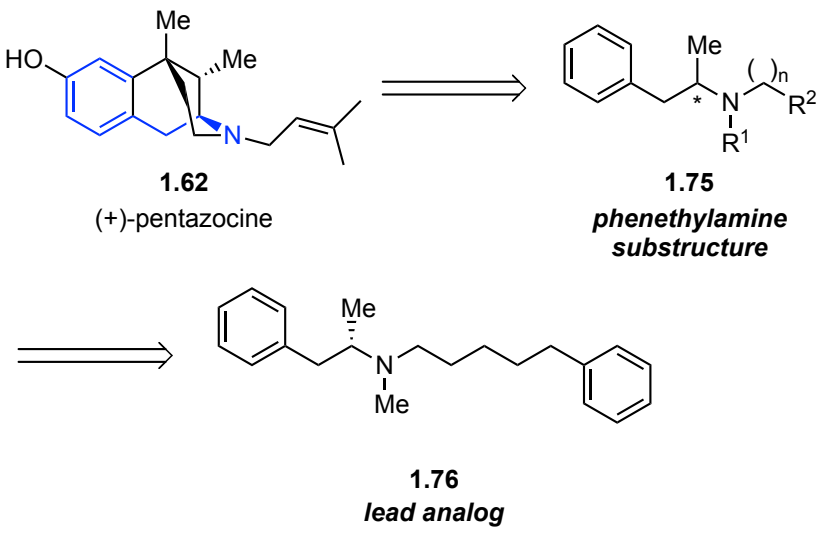

Figure 1.11. Glennon's benzomorphan scaffold minimization approach.

Glennon and Ablordeppey later expanded on the previous study to generate a more thorough pharmacophore model for the σ1R that was generally consistent with their earlier observations, along with a few key points of clarification (Figure 1.12).[140,141] The primary hydrophobic site was found to be critically important for σ1R affinity and was generally occupied by an aryl group, although the group was not required to be aromatic and other aliphatic carbocycles could be accommodated. However, the absence of a hydrophobic group at this position considerably diminished σ1R affinity. The optimal alkyl "y-chain" length between the central nitrogen atom and the primary hydrophobic groups was proposed to be 8.3 Å, but some variability could be accomodated. In contrast, the alkyl "x-chain" allowed more variability in length without deleterious effects and the phenyl group that occupied the secondary hydrophobic site was not significant for σ1R affinity. Replacing the phenyl moiety with a methyl or naphthyl group did not have a considerable impact, provided that the x-chain extended to the secondary hydrophobic site. There was minimal bulk tolerance at the basic nitrogen, accommodating a secondary

and tertiary amine, but with variable effects. The methyl substituent alpha to the amine did not to contribute to σ1R affinity and was removed without impact. As in Gilligan's model, no attempt was made to identify features that led to σR subtype selectivity.

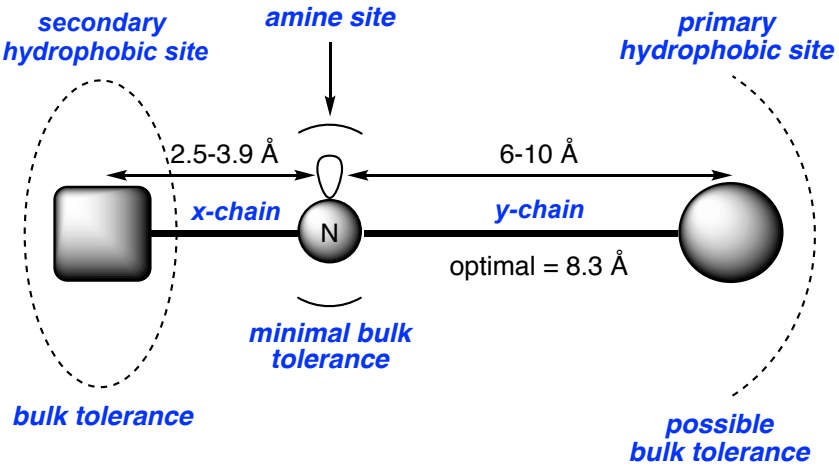

Figure 1.12. Glennon/Ablordeppey pharmacophore model.

The pharmacophore model proposed by Gilligan was followed by Glennon and Ablordeppey's proposal, and the two are quite similar. However, the Glennon and Ablordeppey model does not require the hydrogen bonding group that was suggested in Gilligan's model, but it does allow for hydrophobic bulk at the secondary site. It should be noted that the σ1R is quite promiscuous with affinity for structurally diverse compounds that are not encompassed within this model, but many with high affinity fit well.[141] Both models are defined using conformationally flexible ligands that cannot account for the three-dimensional relationship of the various binding pockets and neither provides a mechanism for obtaining selectivity over the σ2R. At the time there were few ligands with selectivity for the σ2R over the σ1R to enable this distinction, but the similarity in their binding profiles highlights the need for a pharmacophore model that can distinguish between σR subtypes.[141]

1.3.4.3 Sigma-1 Pharmacophore: Laurini Model

The absence of a σ1R crystal structure continued to prohibit structure–based-design strategies, but technological advances enabled more detailed computational predictions of pharmacophore models.[133] Zampieri *et al*. utilized a computational approach in an effort to generate a predictive 3-D pharmacophore model by applying computational software to assess the features of 31 structural variants of the benzooxazolone ligand **1.77** that had a wide range of σ1R affinities (Figure 1.13).[142] The highest ranked quantitative SAR (QSAR) model correlated the predicted and empirically determined binding affinity values (K_i) within four-fold error for most analogs in the training set (24 of 31 < 4-fold error).

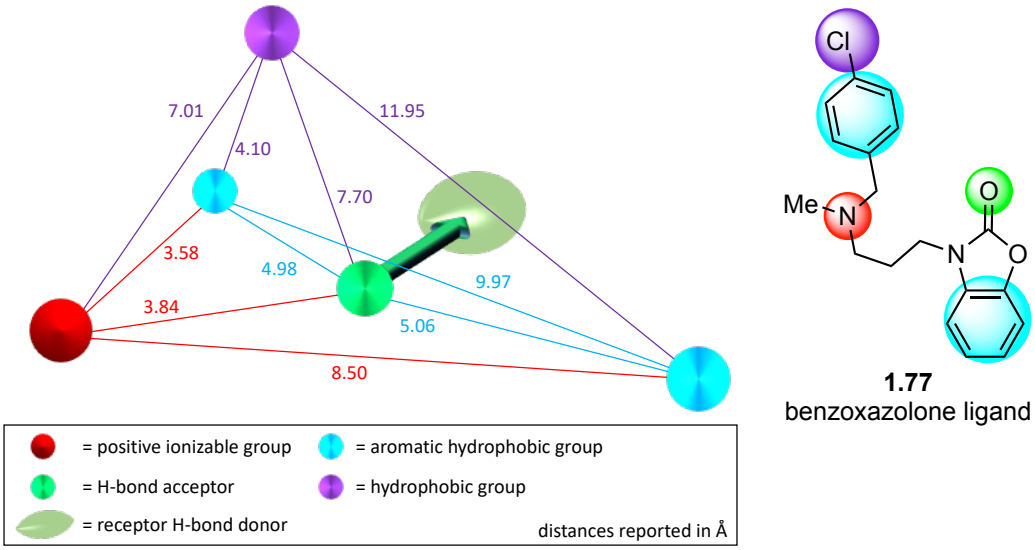

Figure 1.13. Zampieri pharmacophore model using benoxazolone ligands. Adapted with permission.[143] Copyright (2009) American Chemical Society.

The derived pharmacophore aligned well with the Glennon/Ablordeppey and Gilligan models with some variation that might be attributable to the specific structural features of the training set. For instance, the Zampieri model divided the primary

hydrophobic site from the earlier models into an aromatic and an aliphatic hydrophobic site at similar distances (8.5 and 7 Å, respectively) from the positive ionizable group represented by the central basic amine.[142] An additional hydrophobic site was posited to exist 3.6 Å from the positive ionizable group that corresponded well with the secondary hydrophobic site from earlier models. Similar to the Gilligan model, the Zampieri model also accommodates a hydrogen bond acceptor group, which was present in the training set. The model was validated by comparing predicted and experimentally determined binding affinities for six newly developed piperidine analogs that are structurally similar to haloperidol (error 1.1- 4.4-fold), along with three known haloperidol analogs that have high σ1R affinity (error 2.6-9.5 fold).[142] This 3-D model expands on the spatial relationship of key pharmacophore elements and provides some additional basis for structure-based ligand design in the absence of a crystal structure, but the predictive power is unclear given the error observed for ligands outside of the training set. Like earlier models, this 3-D model focuses only on features for optimal σ1R binding without distinguishing between σR subtypes.

1.3.4.4 The Sigma-1 Receptor: A 3-D Homology Model

In 2011, Laurini and colleagues published the first 3-D model of the σ1R that was generated and optimized using homology modeling techniques.[87] The overall 3-D structure was constructed using four different proteins with ≥30% sequence similarity to the σ1R and their crystal structures formed templates that were linked together to build the transmembrane potions of the protein, along with optimization processes that created missing loops. The modeling relied on previous structural predictions, including two membrane spanning portions, an assumption that was shown to be incorrect in the recently obtained crystal structure.[6] The homology model was then further refined by

leveraging data from the Zampieri 3-D pharmacophore model, along with information gleaned about the binding pocket from previous ligand docking studies and mutagenesis experiments.[142] The early site-directed mutagenesis experiments were critical for establishing that Asp126 and Glu172 were essential for ligand binding, likely through interaction with the basic amine moiety of the ligand, and therefore comprised the putative binding site within the recpeptor.[144]

The model was validated by docking a series of ligands with binding affinities that spanned 4-orders of magnitude and comparing the predicted and empirically determined σ1R affinities.[87] The structurally diverse series included benzoxazocine and aryl piperidine analogs, as well as the traditional ligands (+)-pentazocine and haloperidol. Impressively, the ligand affinities were predicted in the correct order, and the calculated values were quite similar to the experimental values (R^2 = 0.93). The 3-D homology model was then used for in silico characterization of a benzoxazocine ligand, and the protein-ligand interactions were identified as: (1) Asp126 formed a critical salt bridge with the basic amine site; (2) favorable van der Waals and electrostatic interactions between Glu172 and the benzoxazocine heterocycle, and between Arg119 and the *p*-Cl-phenyl moiety; (3) hydrogen bonding between the benzoxazolone carbonyl moiety and the -NH donor of the THR151 and Val152; (4) stabilizing π-π interactions between the benzylamine aromatic ring and Trp121 as well as between the benzoxazolone phenyl ring and Tyr173; and (5) generally favorable hydrophobic interactions with Ile128, Thr151, and Val152 (Figure 1.14). It is perhaps unsurprising that these interactions were observed during docking given that several were predicted in the Zampieri pharmacophore model that was used to optimize the protein structure in the homology model.

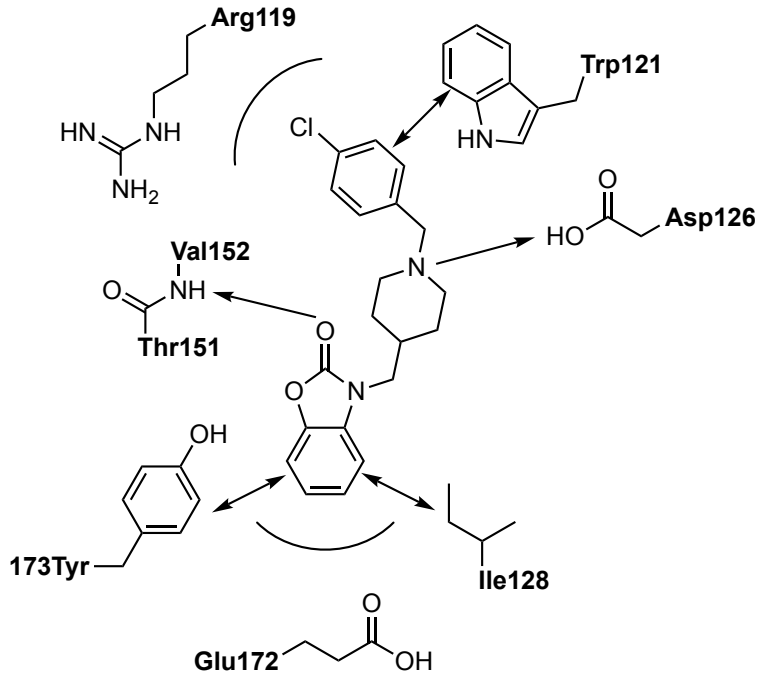

Figure 1.14. 2-D depiction of the predicted protein-ligand interactions in homology model. Adapted with permission.[145] Copyright (2011) American Chemical Society.

Having characterized the relevant protein interactions in the binding pocket, three new ligands were constructed with structural features designed to interact with the protein and provide a range of high, medium, and low affinity analogs.[87] Indeed, the calculated affinities closely aligned with experimental values, which suggested that the 3-D model might resemble the natural topology of the protein and might be a useful predictive tool for structure-based ligand design. Numerous subsequent studies by Laurini and others utilized this homology model in the design of structurally diverse σ1R ligands with good agreement between the in silico and empirical binding affinities.[146-151] Another study recapitulated in silico the effects of site directed mutagenesis among a variety of DNA-mutant proteins variants, confirming that the protein-ligand interactions outlined in the homology model were in fact important for binding (+)-pentazocine.[152] In 2015, Ortega-

Roldan made additional progress toward structural characterization of σ1R with a solution NMR study that revealed the secondary structure of the protein independently of the homology model.[153] The NMR study predicted a cytosolic domain that consisted of three α-helices, one of which was relatively mobile (residues 81-85), as well as a second transmembrane helix (residues 91-107). The experimentally determined structure correlated well with the 3-D homology model, further supporting the validity of the predicted structure.[133]

1.3.4.5 Summary of Sigma-1 Receptor Pharmacophore Models

Since the σ1R was first cloned in 1992, considerable progress has been made toward determining the overall structure of the protein and generating a predicative pharmacophore model for structure-based ligand design. In the absence of a crystal structure for the protein, there has been surprising consistency between early pharmacophore models that relied on extensive SAR studies and more recent computational efforts to generate 3-D structural information. However, definitive structural information remained unavailable, and much was unclear about the molecular mechanisms and the structural basis for agonist and antagonist activity.[154] Access to the cloned σ1R protein enabled major leaps in our understanding of the receptor topology and pharmacophore model, but the σ2R had not yet been cloned, blocking access to similar biochemical tools for characterization. Thus, the predictive models did not provide rationale for designing ligands that were selective for σ1R over σ2R, a formidable challenge given the overlap and their binding profiles.

1.3.5 Sigma-1 Receptor: X-ray Crystal Structure

In 2016, 20 years after the σ1R was first cloned, Kruse *et al*. reported the first crystal structure of the protein.[6] Purification and crystallization of the integral membrane protein had long eluded researchers, but recent advances in the area of membrane protein structural biology have enabled the use of lipid-based crystallization methods, along with mild detergents and improved X-ray diffraction methods with microcrystals.[155] Kruse and coworkers leveraged these modern advances in a GPCR-inspired approach that utilized a mild maltoside detergent to extract the protein from S*f*9 insect cells expressing high levels of a σ1R construct.[6,155] Subsequent purification with antibody affinity chromatography provided pure and minimally altered protein that was crystallized using the lipidic cubic phase technique.

The crystal structure revealed a triangular trimeric assembly in which each promoter contains a single transmembrane domain (α-1, residues 6-31) at the outer corners (Figure 1.15.A).[6] Interestingly, the single-pass transmembrane structure is consistent with early predictions, but is contrary to the more widely accepted two-pass transmembrane models.[78,85,133] The cytosolic portion of the structure is comprised of a β-barrel (residues 81-176) bordered by α-helices (α-2 to α-5) (Figure 1.15.B).[6] The α-helices that cover the β-barrel opening (α-4 and α-5, residues 177-223) adjacent to the membrane contain hydrophobic amino acids facing the membrane. Although the protein contains only one transmembrane portion, this face of the trimer is likely embedded in the membrane.[155] The ligand-binding site is located in the center of the β-barrel portion of the protein, which is structurally similar to the active sites of oligomeric bacterial enzymes in the cupin family.[6] The wider opening of the β-barrel is proximal to the membrane and gated by α-helices (α-4 and α-5) and the more narrow polar opening of

the β-barrel is blocked by Gln135. In fact, the binding pocket is entirely blocked from solvent and the pathway for ligand entry is unclear.[6]

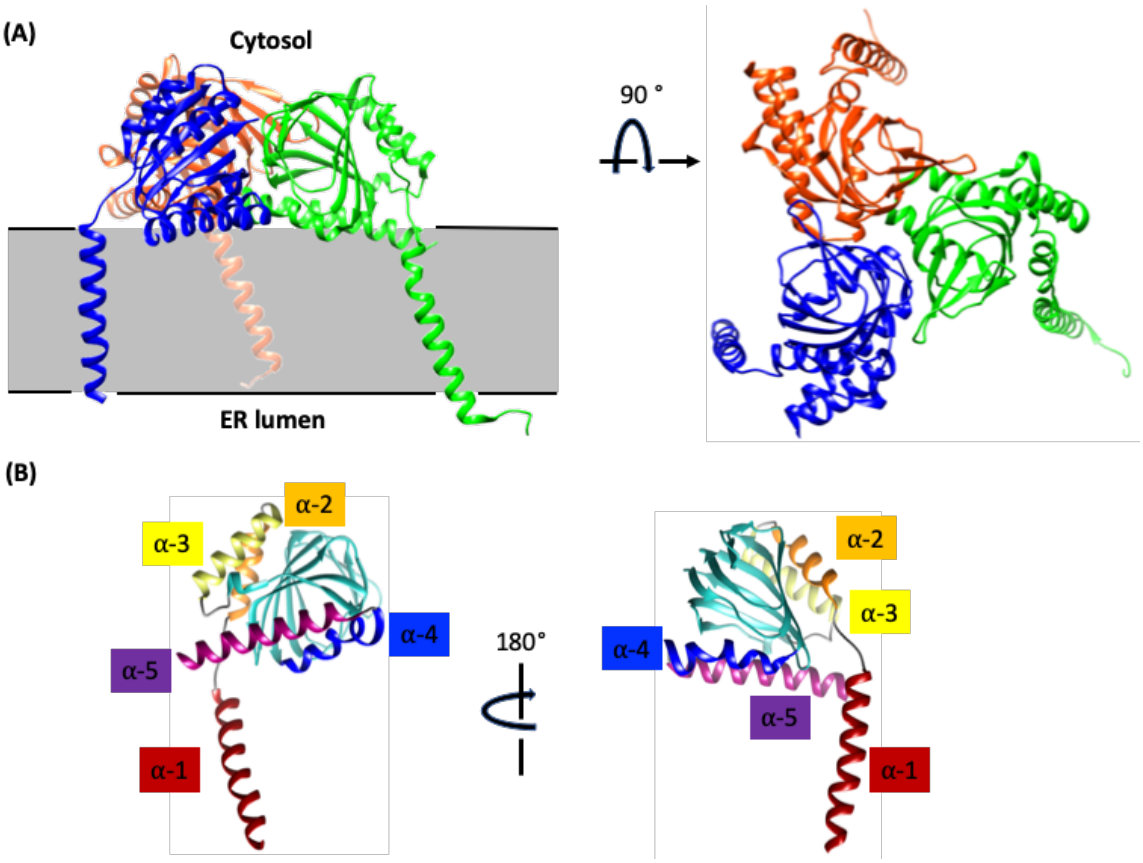

Figure 1.15. (A)X-ray crystal structure of σ1R trimeric complex. Membrane shown in grey. (B) Structure of single σ1R protomer. Adapted by permission from Springer Nature Customer Service Centre GmbH: Springer Nature Nature Structural & Molecular Biology] Schmidt, H.R., Betz, R.M., Dror, R.O. et al. Structural basis for σ1receptor ligand recognition. Nat. Struct. Mol. Biol. 25, 981–987 (2018). Copyright (2018).

The σ1R crystal structure was originally obtained in complex with two structurally distinct ligands, PD144418 (**1.78**) (Figure 1.16.A) and 4-IBP (not shown) and later reported in complex with the classical σ1R ligands pentazocine (**1.62**) and haloperidol (**1.64**) (Figure 1.16.B).[6,154] An interesting attribute of the σ1R is its ability to

bind a wide range of structurally diverse ligands that fit into the general pharmacophore model described by Glennon and Ablordeppey, most critically a basic amine site. The crystal structure revealed that the amine forms a salt bridge with Glu172, a highly conserved acidic residue that prior mutation studies confirmed was necessary for binding.[144] Another acid residue, Asp126 is also important for binding and forms a 2.7 Å hydrogen bond that helps position Glu172.[6,154] Aside from these polar amino acids, the binding pocket consists of primarily aromatic and hydrophobic residues including Val84, Trp,89, Met93, Leu95, Phe107, Ile124, Trp164, and Leu 182. In addition, Tyr103 interacts with ligands via aromatic stacking, but also forms a critical hydrogen bond with Glu172 to help orient the acidic residue. Replacing this important residue, which was previously thought to be part of the second transmembrane domain, with a Y103F mutant resulted in a significant reduction in binding affinity, confirming its critical role in binding.[156]

(A)

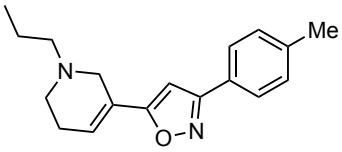

1.78
PD144418

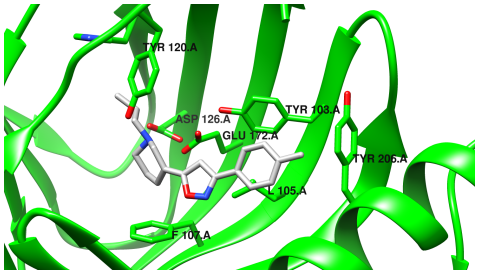

(B)

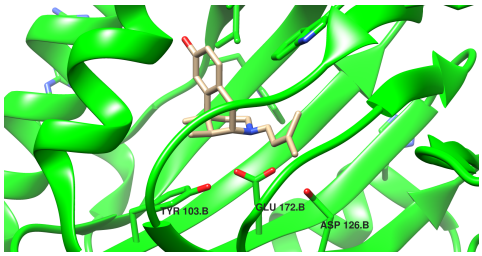

(C)

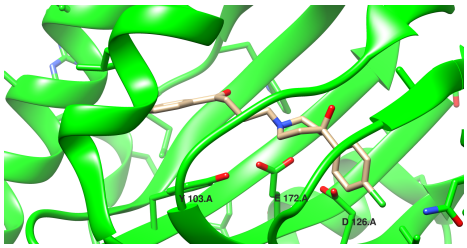

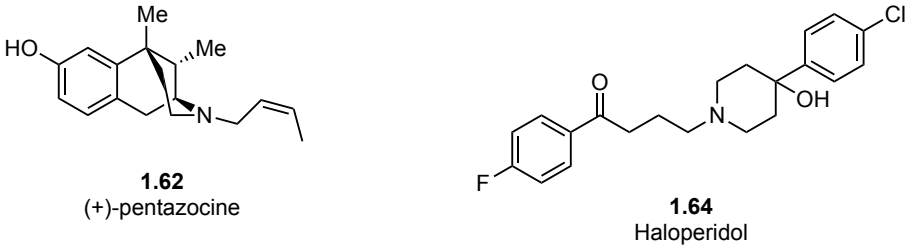

Figure 1.16. (A) X-ray crystal structure of σ1R with PD144418. (B) X-ray crystal structure of σ1R with (+)-pentazocine. (C) X-ray crystal structure of σ1R with haloperidol. Adapted by permission from Springer Nature Customer Service Centre GmbH: [Springer Nature][Nature Structural & Molecular Biology] Schmidt, H.R., Betz, R.M., Dror, R.O. et al. Structural basis for σ1receptor ligand recognition. Nat. Struct. Mol. Biol. 25, 981–987 (2018). [Copyright] 2018.

The initial crystal structures obtained with nonclassical σ1R ligands provided for the first-time definitive structural information about the receptor that was critical for continued advancement. In 2018, Kruse expanded on this work with a more detailed examination of the molecular basis for ligand binding and activity using the classical σ1R agonist (+)-pentazocine (**1.62**) and antagonist haloperidol (**1.64**) (Figure 1.16.B).[154] The study found that agonists have a binding pose that is unique from antagonists, which tend to favor a more linear orientation that positions the primary hydrophobic group toward the space between the α-4 and α-5 helices. In contrast, agonists tended to project the primary hydrophobic group toward the α-4 helix, forcing the helix to shift 1.1-1.8 Å from the α-5 helix. The shift did not disrupt the protomer interface of the trimeric structure. Importantly, Kruse pointed out that crystallization favors low-energy states and therefore may not be representative of a fully activated state. In a higher-energy state, a larger shift could potentially disrupt oligomerization, which is consistent with prior

reports of σ1R agonists biasing toward lower molecular weight oligomers.[157,158] Conversely, antagonist are associated with higher molecular weight oligomers, suggesting that the oligomerization state might be important for to the molecular basis of σ1R function.[159]

A detailed view of ligand recognition has emerged that unites early pharmacophore models with molecular interactions that will enable true structure-based design efforts in the future. The discrepancy between relevant protein-ligand interaction observed in the 3-D homology model and the crystal structure of bound ligands highlights the limitations of these predictive models. The considerable structural diversity of σ1R ligands is attributed to the largely hydrophobic, flexible binding pocket that was observed in the crystal structure.[6] However, a rationale for applying this information to structure-based design strategies that provide selectivity over the σ2R remain unclear. The availability of definitive structural information for the σ1R provides a foundation for continued advancement that will likely transform our understanding of the receptor's molecular mechanisms and function, expanding its potential as a therapeutic target.

1.4 THE SIGMA-2 RECEPTOR

1.4.1 Sigma-2 Receptor: An Enigmatic Target

The σRs have been the subject of considerable research for more that 40 years, during which time the σ1R has benefited from significant characterization advancements that have furthered our understanding of the receptor and paved the way for additional discoveries. In contrast, the σ2R had evaded characterization efforts, until the research outlined through the course of this work resulted in the successful cloning of the receptor (*vide infra*).[160] Accordingly, the σ2R has only recently entered the modern era of biological investigation and has instead relied on classical pharmacological approaches

since its initial discovery. These investigations had continued to endure many of the same challenges that afflicted early σ1R research efforts including misidentification of the receptor, absence of an endogenous ligand, and a promiscuous binding profile with a poorly defined pharmacophore.

The σ2R was pharmacologically distinguished from the σ1R in 1990 following consecutive reports from Bowen and coworkers outlining several characteristics that were unique from the σ1R.[74,75] As previously discussed, the σ2R was defined by its high affinity for the classical σR ligands DTG and haloperidol and its low affinity for (+)-benzomorphans, whereas the σ1R displayed high affinity for each of these ligands. Bowen *et al.* also found the σ2R to be approximately 21.5 kDa, smaller than the σ1R which was approximately 25 kDa. Critically, this work identified the benzomorphan (+)-pentazocine (**1.62**) as a σ1R selective ligand, but at the time there were no selective σ2R ligands available. In fact, many ligands that were developed were either selective for σ1R or had high affinity for both the σ1R and σ2R.[161,162] Consequently, tool compounds for continued pharmacological characterization of σ1R were more readily available. Additionally, previous characterization efforts often relied on benzomorphans based on the seminal findings of Su and Tam and were likely more indicative of σ1R activity.[56,57] These attributes, along with the successful cloning of the σ1R and the more recently published crystal structure have led to a better understanding of the σ1R in comparison to the σ2R, which has been much more enigmatic.[5]

Characterization of the σ2R has relied almost entirely on pharmacological approaches in the absence of a cloned gene and with no structural information available. This has blocked access to modern biological techniques for elucidation of central features of the receptor. Protein knock-down and over-expression studies have not been available to assess the functional role of the receptor and ascribe the pharmacological

effects of various ligands.[5] Lacking knowledge of the structure of the 2σR has also prevented the development of highly specific antibodies for unambiguous characterization with immunohistochemical and immunoprecipitation techniques. Researchers have instead relied on less selective binding assays that commonly use the non-σR specific ligand [^{3}H]-DTG in the presence of (+)-pentazocine to mask σ1R binding sites.[77,83] Information gleaned about the anatomical distribution and subcellular localization has often had to utilize radioligand assays or other photoaffinity labeling approaches with molecules designed to selectively target the receptor.[83] Because structural information for the σ2R has not been available and it has not been possible to use structure-based design strategies for increasing σR subtype selectivity. Moreover, the considerable overlap in σ2R and σ1R ligand binding profiles, has presented a formidable challenge for the development of σ2R selective compounds.[161]

Despite the challenges associated with σ2R research the receptor has continued to attract attention due to its potential as a therapeutic target for a range of disorders. This has largely focused on treatment and diagnostic imaging of cancer due to high levels of σ2R expression in cancer cells.[77] More recently, important findings from the Martin group[11-14,163] and other contemporaneous reports,[164-168] have indicated that the σ2R might be a target for the treatment of some neurological disorders. Interestingly, the σ2R and σ1R were also recently highlighted as a potential targets for treatment of the novel coronavirus SARS-CoV-2, which has resulted in the current COVID-19 global pandemic people leading to significant loss of life, and catastrophic social and economic upheaval.[169] Although the exact role of the σ2R in these disease remains unclear, the receptor appears to have a critical role in cell viability that highlights the need for continued investigation.

1.4.2 Sigma-2 Receptor: Characterization

1.4.2.1 Sigma-2 Receptor: Localization and Physiological Role

Autoradiographic and photoaffinity labeling studies indicate that the σ2R has wide anatomical distribution in both the CNS and peripheral organs. Labeling studies in brain tissue using [^{3}H]-DTG in the presence of (+)-pentazocine have shown wide distribution of the σ2R with higher densities observed in areas associated with posture control and movement such as the motor cortex, cerebellum, oculomotor nuclei, central gray matter, and the substantia nigra pars reticulata.[170] The σ2R is also found outside of the central nervous system with high densities in liver and kidney tissues,[171] as well as tumors and proliferating tissues.[83,172] At the subcellular level, fluorescent ligands with selectivity for the σ2R over σ1R were found to colocalize with fluorescent markers of the mitochondria, lysosomes, ER, and plasma membrane suggesting distribution among several cellular organelles.[173] The σ2R has also been proposed to localize specifically within lipid raft microdomains of the membrane, which require harsh detergents for protein extraction and likely contributes to challenges associated with isolation of functional σ2R protein.[174]

The precise role of the σ2R in biological systems and its molecular mechanisms remain unclear. Without an endogenous ligand or gene-knockout models, the effects of receptor agonism and antagonism can only be hypothesized based on interactions with synthetic compounds. Unfortunately, a standardized system has not been used, and a variety of physiological effects have been associated with activation of σ2R (*i.e.* agonist activity).[175] This seemingly makes the use of ligand descriptors such as agonist and antagonist somewhat arbitrary, but reliance on pharmacological characterization has prevented use of a less ambiguous approach. Early studies classified ligands as either

agonists or antagonists based on behavioral responses. For instance, Matsumoto and coworkers reported that the pan-σR selective ligand BD-1047 (**1.79**) was able to attenuate dystonia in the rat that was induced by DTG and haloperidol, but had no effect on its own (Figure 1.17).[176] The authors ascribed this to antagonism at both σ1R and σ2R, although the lack of σR subtype specificity is confounding and makes this result unclear.

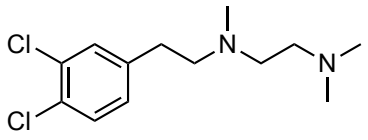

1.79
BD-1047
σ1R IC_{50} (nM) = 0.93 ± 0.14
σ2R IC_{50} (nM) = 47 ±0.60

Figure 1.17. Pan-σR selective ligand BD-1047 that was classified as an antagonist.

1.4.2.2 Sigma-2 Receptor: Expression in Proliferating Cells

The σ2R has remained an enigmatic target since it was first delineated from the σ1R with relatively little known about its precise physiological role and its potential as a therapeutic target. However, the majority of investigations have focused on the involvement of the σ2R in cancer, inspired by early reports that it is overexpressed in cancer cell lines with respect to the corresponding non-malignant cell line. Indeed, high expression levels of the σ2R in PC12 pheochromocytoma and C6 glioma rodent derived cancer call lines, were critical for establishing the existence of the σ2R.[75] Vilner *et al.* followed with a broader examination and found high expression of both σR subtypes in a wide variety of human and murine cancer cell lines, but the σ2R was typically expressed

at much higher level.[172] This suggested that the σ2R might play in an integral role in cellular function and might also be useful for diagnostic imagining purposes.

To expand on this potential, Wheeler *et al*. investigated the relationship between σ2R expression and the proliferative status of cancerous cells.[177] The ability to accurately ascertain the proliferative status of a tumor is useful for determining an effective treatment regimen in the clinic, but technical challenges associated with biopsy and assay methods present some difficulties.[178,179] Therefore, a noninvasive assay to directly visualize whole tumor proliferation status with positron emission tomography (PET) methods would be valuable.[77] Wheeler *et al*. examined mouse mammary adenocarcinoma cell in their active proliferating state (P-cells) and found that σ2R expression was approximately ten-fold higher than in their corresponding quiescent state (Q cells), which was also greater than in nonmalignant cells.[177] A follow up study indicated that the P:Q ratio in solid tumors was significantly elevated and in good agreement with the P:Q ratio observed in tissue culture.[180] These results suggested that the overexpression of σ2R in cancerous tissue might be effective not just for distinguishing tumors from proximal healthy tissue, but also for assessing the proliferative status.

Validation of the σ2R as a biomarker for the proliferative status of solid tumors led to a concerted effort to generate σ2R selective radioligands that could be used for PET imaging. Relatively few selective σ2R ligands were known, but while developing dopamine D_3 ligands Mach *et al.* inadvertently discovered that benzamide analog YUN252 (**1.80**) had high affinity and selectivity for the σ2R (Figure 1.18).[181] This inspired the development of several structural analogs with ^{11}C- and ^{18}F-radiotracers incorporated for PET imaging, including [^{11}C]-RHM-1 (**1.81**) and [^{18}F]-ISO-1 (**1.82**).[7,182,183] MicroPET studies and tumor uptake imaging with the ^{11}C analog **1.81** provided promising initial results, although the short half-life (^{11}C $t_{1/2}$ = 20.4 min) was

not favorable for PET imaging in the clinic, but the ^{18}F analog **1.82** has a half-life that is more favorable [^{18}F] ($t_{1/2}$ = 109.8 min).[183] Subsequent analysis of [^{18}F]-ISO-1 (**1.82**) indicated high tumor uptake with good tumor/normal tissue ratios and rapid clearance from the blood in the mouse. These promising results were followed with successful in human studies using [^{18}F]-ISO-1 (**1.82**) for PET imaging of proliferative status of solid tumors and is currently undergoing clinical trials.[184,185]

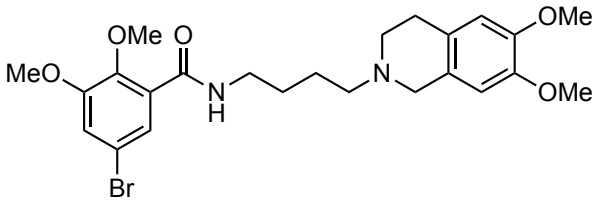

1.80
YUN252

σ1R K_i (nM) = 12,900
σ2R K_i (nM) = 8.2

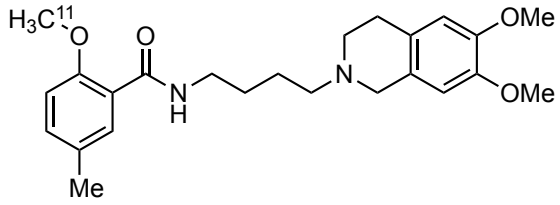

1.81
[^{11}C]-RHM-1

σ1R K_i (nM) = 3,078
σ2R K_i (nM) = 10.3

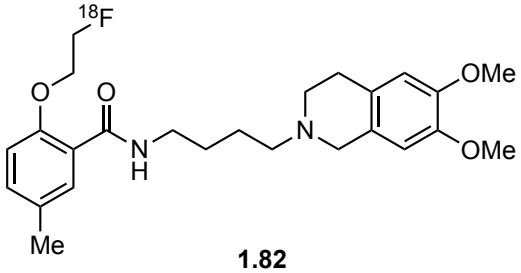

1.82
[^{18}F]ISO-1

σ1R K_i (nM) = 330
σ2R K_i (nM) = 7

Figure 1.18. σ2R ligands developed for PET imaging.

1.4.2.3 Putative Sigma-2 Activation and Cytotoxicity in Cancerous Cells

The σ2R has notably high expression levels in cancerous tissue that attracted attention for the development of tumor diagnostic imaging agents, but the increased

expression level was also indicative of a role in cell viability. Putative activation of the σ2R has been associated with modulation of intracellular calcium levels, which is important for signaling and regulation of cellular processes.[186] Treatment with the σ2R selective ligand CB-64D (**1.83**) was reported to induce a brief, but rapid release of Ca^{2+} from stores within the endoplasmic reticulum (ER) in human SK-N-SH neuroblastoma cells that returned to baseline levels within five minutes (Figure 1.19).[187] Subsequent removal of the ligand produced no further changes in Ca^{2+} levels with no observed morphological changes associated with cytotoxicity. However, continued exposure for an additional 20 minutes led to an additional rise in Ca^{2+} levels that was sustained for up to 60 minutes. This Ca^{2+} release was insensitive to thapsigargin, and was therfore proposed to be derived from the mitochondria rather than the ER. The sustained Ca^{2+} increase also led to morphological signs of apoptotic cell death, which were not observed during the initial transient release. This increase in cytosolic Ca^{2+} levels was not observed in the presence of σ1R selective ligands and was attributed to activation of σ2R, an effect that was blocked by the putative pan-selective σR antagonist BD-1047 (**1.79**).

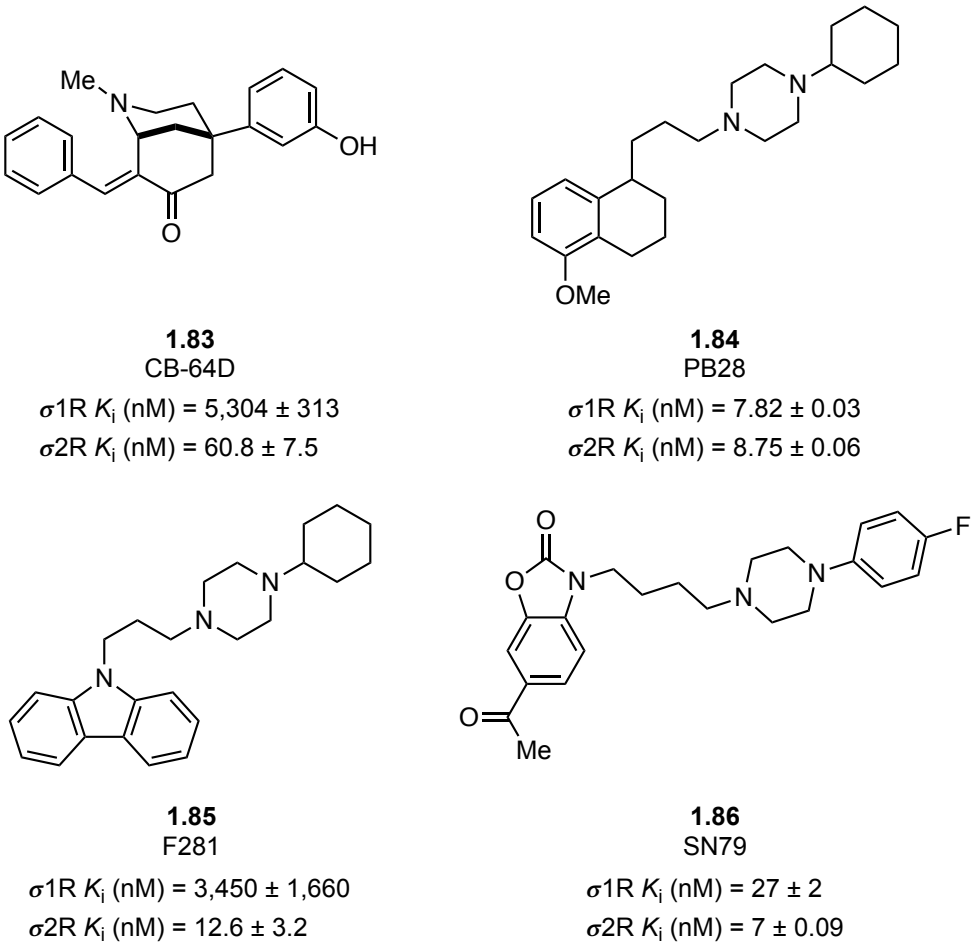

1.83
CB-64D
σ1R K_i (nM) = 5,304 ± 313
σ2R K_i (nM) = 60.8 ± 7.5

1.84
PB28
σ1R K_i (nM) = 7.82 ± 0.03
σ2R K_i (nM) = 8.75 ± 0.06

1.85
F281
σ1R K_i (nM) = 3,450 ± 1,660
σ2R K_i (nM) = 12.6 ± 3.2

1.86
SN79
σ1R K_i (nM) = 27 ± 2
σ2R K_i (nM) = 7 ± 0.09

Figure 1.19. σ2R selective ligands investigated for modulation of intracellular Ca^{2+} levels.

Intracellular calcium provides an important signaling mechanism for proliferation and cell viability,[186] but its link to σ2R activation and cytotoxicity is not entirely clear.[188] For instance, the high affinity σ2R ligand PB28 (**1.84**) was found to inhibit Ca^{2+} release in SK-N-SH neuroblastoma cells, but also has potent cytotoxicity in the same cell line (Figure 1.19).[128,189] However treatment of SK-N-SH cells with F281 (**1.85**), a structural analog of PB28, resulted in immediate and non-transient increase in intracellular Ca^{2+} concentration derived from the ER, as well as thapsigargin insensitive sites (Figure 1.19).[190,191] The F281 analog also proved to be more cytotoxic than PB28, but it should

be pointed out that PB28 also has high affinity for the σ1R making interpretation of these results somewhat difficult.[128] Another σ2R ligand, SN79 (**1.86**) has been proposed to have antagonist activity because it attenuates cocaine-induced convulsions and locomotor activity in behavioral models (Figure 1.19).[192] However, treating SK-N-SH cells with SN79 produces a small Ca^{2+} signal even though no appreciable cytotoxicity is observed.[193] These reports indicate a role for σ2R in Ca^{2+} homeostasis, but the underlying mechanisms remain uncertain.

Inhibition of proliferation and σ2R mediated cytotoxicity has been observed in a variety of malignant cell lines and has been the most common phenotypic response associated with activation of σ2R, but the underlying cellular mechanism requires further clarification .[175,194-196] An early report by Bowen and coworkers revealed that treatment of numerous cancer cell lines of neuronal and non-neuronal origin with a variety of σR ligands had cytotoxic effects.[194] Additional investigations found that treating MCF-7 breast cancer cells with the putative σ2R agonist CB-64D (**1.83**) resulted in dose dependent cytotoxicity. The mechanism of cell death was attributed to caspase-independent apoptosis, as evidenced by DNA fragmentation and Annexin V binding, and cytotoxicity was independent of mutations in the tumor suppressor gene *p53*.[196] Mach *et al*. developed several high affinity σ2R selective ligands that also possessed micromolar level cytotoxicity in EMT-6 mouse breast cancer cells and MDA-MB-435 human melanoma cells (Figure 1.20).[7,188] However, the mechanism of cell death was at least in part caspase-3 dependent becasue the caspase inhibitor Z-VAD-FMK partially inhibits DNA fragmentation and cytotoxicity. Autophagosome markers were also observed with each of the bicyclononane ligands, WC-26 (**1.87**), SV119 (**1.88**), and tropane analog RHM-138 (**1.89**) suggesting autophagy might play a role in cell death.

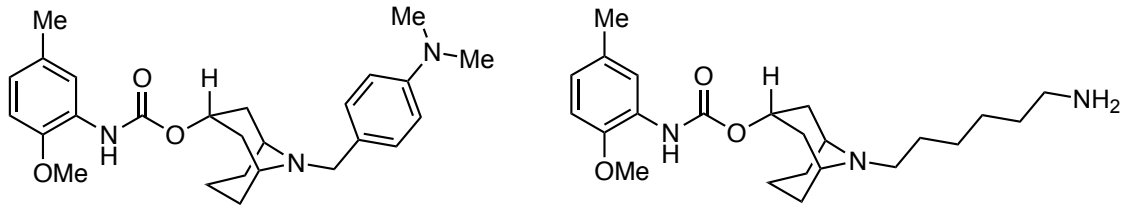

1.87
WC-26
σ1R K_i (nM) = 1,436
σ2R K_i (nM) = 2.6

1.88
SV119
σ1R K_i (nM) = 1,417
σ2R K_i (nM) = 5.2

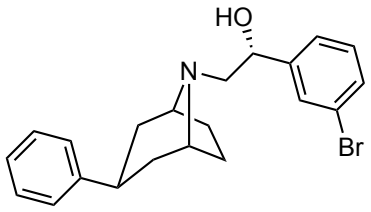

1.89
RHM-138
σ1R K_i (nM) = 544
σ2R K_i (nM) = 12.3

Figure 1.20. Selective σ2R ligands that have cytotoxic effects of malignant cell lines.

Siramesine (**1.90**) is a ligand with subnanomolar affinity for the σ2R that was originally developed for the treatment of anxiety and depression (Figure 1.21).[197] Although it ultimately lacked efficacy in clinical trials, it was well-tolerated in humans, and the reports of σ2R mediated cytotoxicity in cancer cell lines suggested that it might be promising as a cancer therapeutic. This led Ostenfeld *et al*. to investigate tumor cell death in a variety of cancer cell lines, including MCF-7 human breast cancer and ME-180 human cervix carcinoma, upon treatment with siramesine (< 10 μM).[198] Similar to some earlier reports, caspase-independent apoptotic cell death was observed, and cytotoxicity was independent of the tumor suppressor *p53* protein; however, siramesine was significantly more potent than previously reported σ2R ligands. A significant increase in cellular reactive oxygen species (ROS) was observed prior to cell death, which was

inhibited by the antioxidant α-tocopherol, suggesting that oxidative stress may be involved. Additional studies indicated an accumulation of siramesine in lysosomes that induced a rapid rise in pH and destabilization, resulting in lysosomal leakage and dysfunction that triggered caspase-independent cell death.[199] In contrast, a report by Turk *et al.* found that treating HaCaT cells with an increased concentration of siramesine (> 20 μM) resulted in rapid cell death that was not the result of lysosomal leakage.[200] Instead, generation of ROS caused destabilization of the mitochondria by loss of mitochondrial membrane potential and release of cytochrome *c* that triggered caspase-3 mediated cell death.

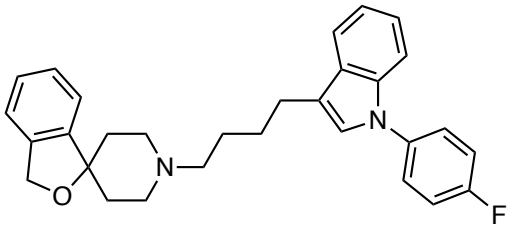

1.90
Siramesine

σ1R K_i (nM) = 17.0
σ2R K_i (nM) = 0.12

Figure 1.21. The σ2R selective ligand siramesine that is associated with cytotoxic effects in malignant cell lines.

Although the mechanisms remain unclear, σ2R ligand induced cytotoxicity is prevalent in cancer cell lines, providing a convenient phenotypic metric for comparison. This led Mach *et al.* to proposed a system for classifying functional activity of σ2R ligands based on cell viability in comparison to siramesine (**1.90**) as a standard ligand (Figure 1.22).[201] Mach *et al*. refers to siramesine as a well-accepted σ2R agonist, which appears to originate from its high σ2R affinity and high cytotoxic potency in cancer cell

lines, a feature that has commonly been associated with σ2R activation.[198,201] However, it is worth reiterating that the functional role of σ2R in cell viability is not clear, and a variety of mechanism could be associated with cell death that might confound results, which is supported by recent findings from Mach's group.[202] This notwithstanding, Mach *et al.* proposed that σ2R ligands (50 μM for 24 h) that possess cytotoxicity (EC_{50} in EMT-6 or MDA-MB-435 cells) greater than 90% relative to siramesine (EC_{50} = 15.9 ± 2.7 μM), are classified as full agonists. Ligands that possess cytotoxicity that is less than 10% relative to siramesine, are classified as antagonists, and ligands that falls in the intermediate range are classified as partial agonists. Using this approach Mach assigned the azabicyclononane SV119 (**1.88**) and tropane RHM-138 (**1.89**) analogs as full agonists, azabicyclononane analogs WC-26 (**1.87**) and YUN245 (**1.91**) as partial agonists, and the azabicyclononane SV95 (**1.92**) and the flexible benzamide RHM-1 (**1.93**) as antagonists (Figure 1.22). It is interesting that derivatives of the azabicyclononane scaffold elicit such a wide range of cytotoxicities, but recent findings suggest that this effect may not be mediated by the σ2R.[202]

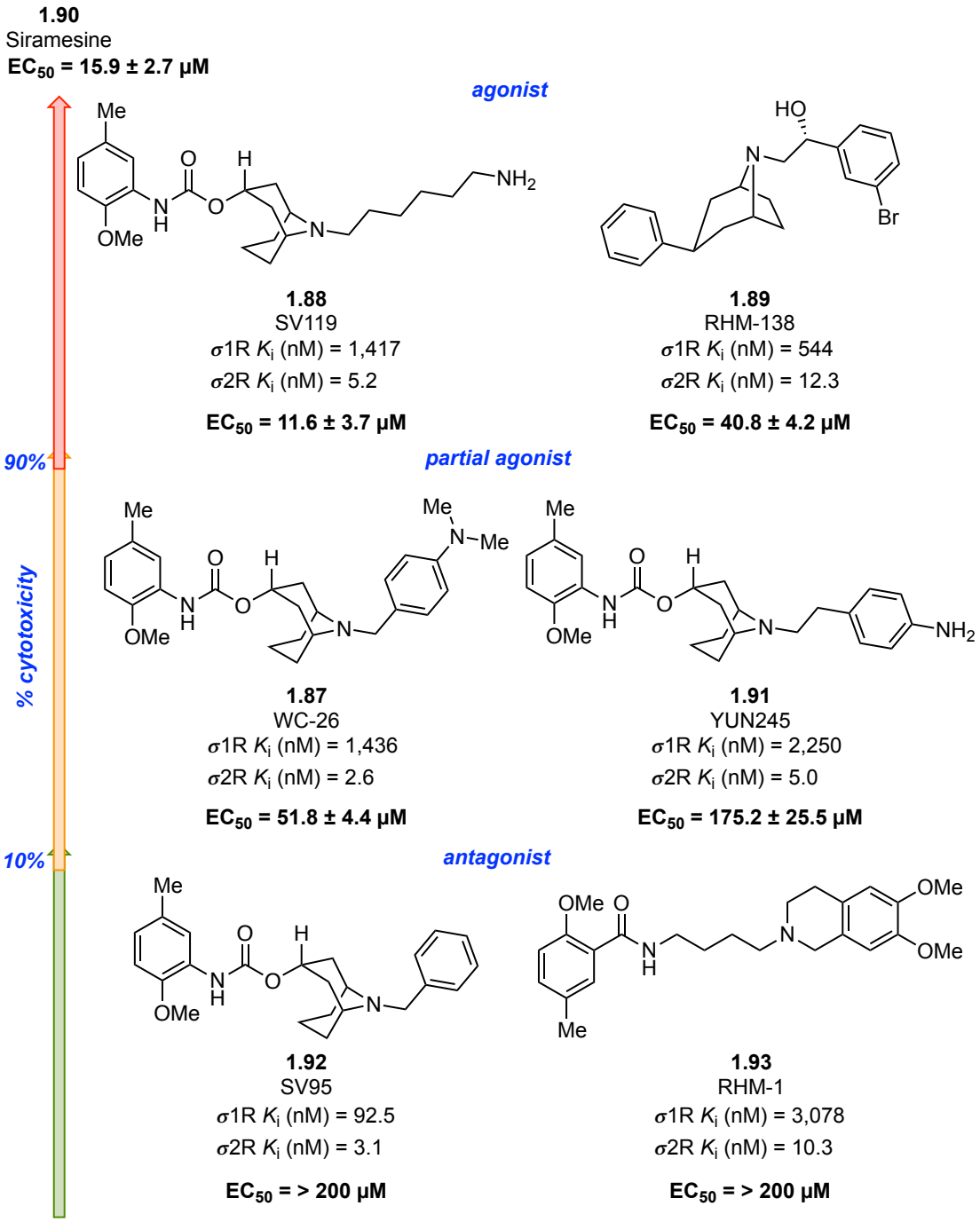

Figure 1.22. Functional activity assignment for σ2R ligands based on cytotoxicity in EMT-6 cells.

The cumulative results from these studies produce a complex picture of the functional role of σ2R in cell viability and the molecular mechanisms for its cytotoxic effects. Modulation of the σ2R appears to have an effect in Ca^{2+} homeostasis, which is known to play a critical role in cellular signaling that affects cell viability. However, some studies suggest that it is difficult to directly correlate σ2R mediated cell death with an increase in intracellular Ca^{2+} levels.[175] In addition, the σ2R mediated cytotoxicity in cancer cell lines appears to occur through multiple pathways that can be both caspase-dependent and independent and that the mechanism might depend on ligand concentration and cancer type.[7] Determination of the functional role of σ2R in these processes requires more investigation that would be aided by access to the σ2R gene, but the receptor seems to be firmly linked to cancer biology and cell viability. The importance of obtaining a better understanding of the therapeutic potential of σ2R is highlighted by the fact that the potent σ2R ligand siramesine was safe for humans in clinical trials and many studies have found σ2R mediated toxicity toward tumor cells to have little effect on nonmalignant tissues.[203]

1.4.2.4 Sigma-2 Receptor: Putative Antagonism and Neurobiological Disorders

Pharmacological manipulation of the σ2R has long been the only mechanism for assessing functional activity of ligands, but selective antagonists of σ2R are surprisingly sparse in the literature. This has been attributed to a dearth of selective σ2R ligands and a lack of unambiguous characterization of the role of this receptor.[204] Behavioral studies have provided one criterion for assigning functional activity, with attenuation of DTG or psychostimulant induced dystonic head movement in the rat being ascribed to σ2R antagonists.[176,205] This strategy was used to assign the high affinity σ2R ligands SM21 (**1.94**),[177] benzamide **1.95,**[206] BD-1047 (**1.79**), and SN79 (**1.86**) as antagonists (Figure

1.23).[192] However, among the limited number of putative σ2R antagonists, many suffer from either modest σ2R affinity or a lack of specificity.[207] The limited availability of unambiguous σ2R antagonists has resulted in relatively few studies of their biological effects, but some evidence is emerging that antagonist action at the σ2R might be beneficial in the treatment of addiction and some neurological disorders.[208]

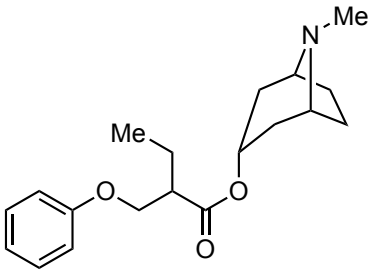

1.94
SM21

σ1R K_i (nM) = 1,050
σ2R K_i (nM) = 145

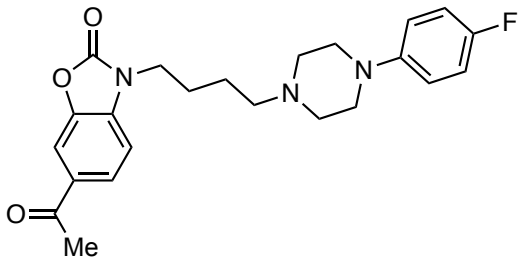

1.86
SN79

σ1R K_i (nM) = 27 ± 2
σ2R K_i (nM) = 7 ± 0.09

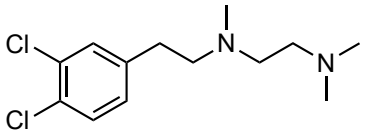

1.79
BD-1047

σ1R IC_{50} (nM) = 0.93 ± 0.14
σ2R IC_{50} (nM) = 47 ±0.60

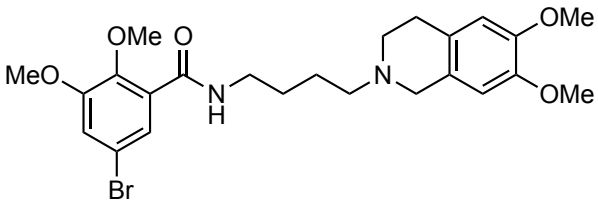

1.95

σ1R K_i (nM) = 12,900
σ2R K_i (nM) = 8.2

Figure 1.23. Putative σ2R antagonists based on behavioral models.

Recently, Izzo *et al.* discovered that some modulators of the σ2R are competitive antagonists for β-amyloid (Aβ) 1–42 oligomers at neuronal synapses.[164] This study determined that Aβ oligomers exhibit saturable binding to neuronal synapses at a single site that results in aberrant membrane trafficking and synapse loss, giving rise to

inhibition of learning and memory.[164,165] Because the involvement of Aβ in synaptotoxicity is of interest for the treatment of AD, Izzo *et al.* screened a propriety library of small molecules for their ability to displace Aβ and identified lead compounds CT0109 (**1.96**) and CT01202 (**1.97**) for their potent inhibition of Aβ binding, which were subsequently determined to be potent and selective for the σ2R (Figure 1.24).[164] The σ2R ligands and their structural analogs CT01344 (**1.98**) and CT01812 (**1.99**) effectively blocked the downstream deficits associated with Aβ binding and also restored behavioral deficits in the transgenic hAPP$^{Lond/Swed}$ mouse model of AD. One of the identified compounds, CT1812 (**1.99**), was advanced and is currently undergoing phase II clinical trials for the treatment of AD.[209] These findings highlight the promise of the σ2R as a new therapeutic target for the treatment of AD and also corroborated independent results in the Martin group that pointed to similar neuroprotective attributes of ligands that modulate the σ2R (*vide infa*).

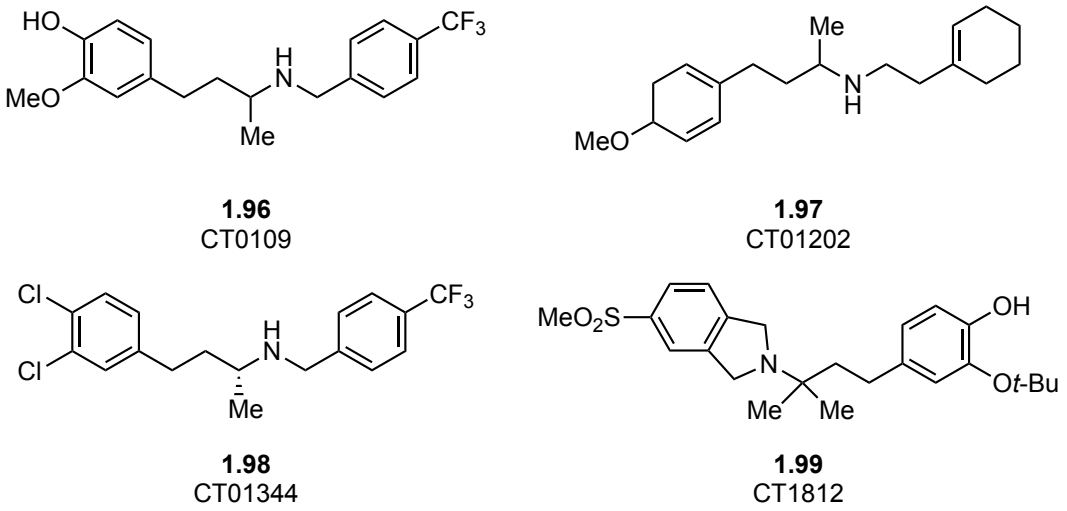

1.96
CT0109

1.97
CT01202

1.98
CT01344

1.99
CT1812

Figure 1.24. σ2R analogs that are competitive antagonists for Aβ neural binding site

Another ligand that modulates the σ2R and is thought to act as an antagonist is roluperidone (**1.100**), which was developed by Minerva for the treatment of schizophrenia (Figure 1.25).[167,210] Rodent models with roluperidone (**1.100**) have demonstrated that it is efficacious against the negative symptoms of schizophrenia, and although it is essentially equipotent for both the σ2R and the serotonin 5–HT_{2A}, its activity at the σ2R is thought to modulate relevant dopamine and glutamatergic pathways.[167] The mechanistic role of roluperidone is not entirely clear, but it is proposed to act through synergistic antagonism of 5–HT_{2A} and the σ2R.[210] Roluperidone is currently undergoing phase III clinical trials for the treatment of schizophrenia, suggesting that high affinity modulators of the σ2R are safe in humans for the treatment on CNS disorders.[211]

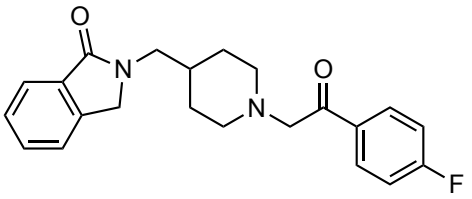

1.100
Roluperidone (MIN-101)

σ2R K_i = 8.19 nmol/L
5–HT_{2A} K_i = 7.53 nmol/L

Figure 1.25. Ligand that modulates σ2R undergoing clinical trials for the treatment of schizophrenia.

1.4.3 Attempts to Identify the Sigma-2 Receptor Protein

It is somewhat surprising that despite decades of research and an increasing number of reports highlighting its medical relevance, the identity of σ2R has evaded researchers. The many publications that point to the receptor as a valuable therapeutic

target are based almost entirely on pharmacological manipulation, which has often been limited by the use of less selective ligands.[212] The enigmatic receptor had not yet entered the modern biological era and our understanding of the σ2R remains underdeveloped in comparison to many other receptors, including the σ1R.[5] Despite the considerable importance of identifying the protein sequence and its coding gene, the literature reveals only two attempts prior to our successful effort disclosed herein.

1.4.3.1 Sigma-2 Receptor: Identity Proposed as a Histone Binding Protein

Protein identification is commonly achieved with chemical proteomic approaches using small molecules functionalized in a way that allows downstream analysis of the protein binding partner. Affinity chromatography methods are a classical technique for purifying the target protein from other components of the biological matrix.[213] This strategy often relies on a small molecule with high affinity for the target that is immobilized on a solid support using a molecular linker. The linker must allow the small molecule to interact with the target without interference from the solid support and without deleterious effects on affinity for the target, and extensive SAR knowledge about the small molecule probe is often required.[213] A variety of linker types and lengths have been used with longer and more rigid linkers providing some benefit, but increasing the hydrophobic surface can increase levels of non-specific interactions that might pose a challenge for downstream identification.[214-216] After immobilization of the molecular probe, it is incubated with a cell lysate to capture the target and the undesired matrix is rinsed away. The target is then released from the immobilized probe, often with a competitive ligand, where it can then be processed with sodium dodecyl sulfate polyacrylamide gel electrophoresis (SDS-PAGE) to isolate specific protein bands for sequence identification using mass-spectrometry (MS).[213]

In 2006, Colabufo *et al*. utilized an affinity chromatography approach in an attempt to purify the σ2R from human SK-N-SH neuroblastoma, which had been shown to have high levels of σ2R expression.[217] A small molecule probe was inspired by the high affinity pan-σR ligand PB28 (**1.84**) that lacked chemical functionality to directly install a linker for immobilization (Figure 1.26). Accordingly, a nitrogen atom was installed on the tetralin moiety to provide **1.101**, which was subsequently coupled with an activated ester on a stationary phase. It was posited that substitution at this position of the tetralin moiety would not affect σ2R affinity based on previous SAR studies. However, that work did not evaluate amide substituents on the tetralin aromatic ring, nor did it incorporate any substituents at the site that was modified in this work.[218] The modified scaffold was also not subjected to independent competition binding analysis to confirm affinity and selectivity.

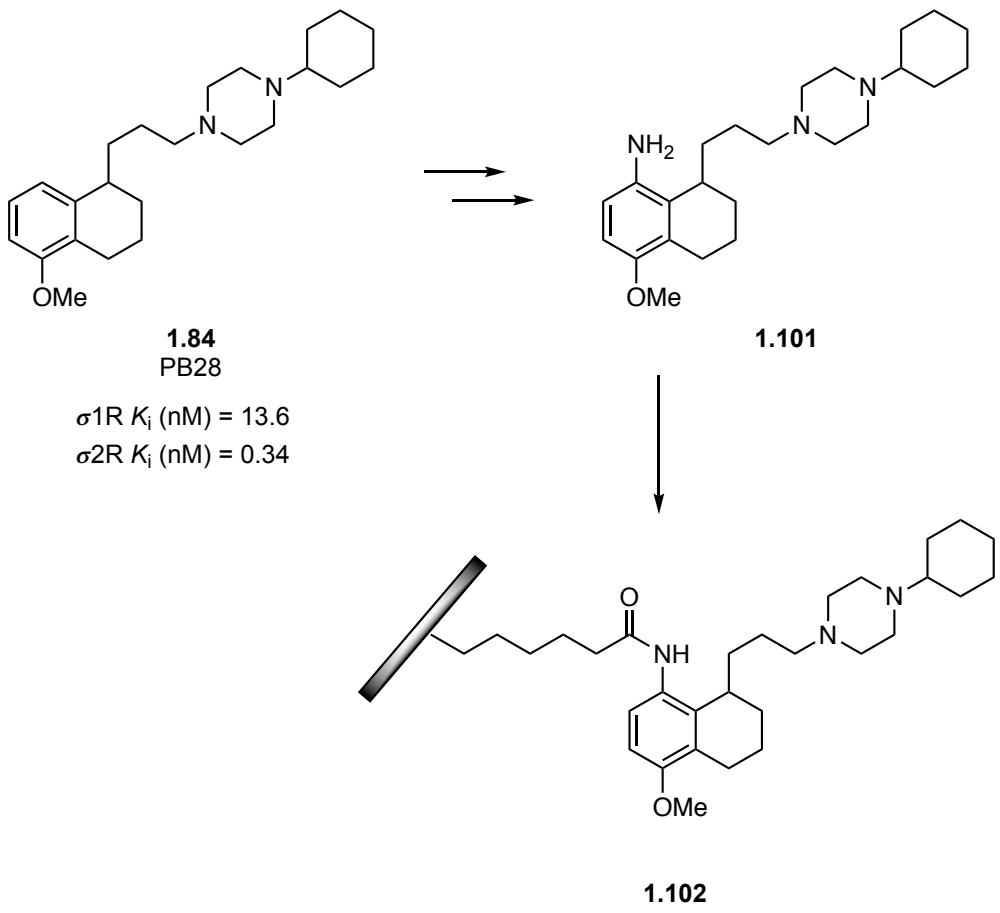

Figure 1.26. Structural modification of PB28 and for affinity purification.

SK-N-SH cells were lysed, and a protein membrane preparation was eluted through an affinity column containing **1.101** while monitoring (SDS-PAGE), to isolate H3.3A (kDa = 15.3), H2B (kDa = 13.8), H2A.5 (kDa = 14.1), and H2.1 (kDa = 21.2) histone proteins.[217] Saturation binding analysis of the eluted cell fractions with [^{3}H]-DTG was consistent with values obtained for the crude material leading to the hypothesis that σ2R is a histone protein. The authors conceded that the σ2R ligand may also have affinity for the histone proteins and that they may not be synonymous, which was corroborated using [^{3}H]-PB28 and reconstituted human histone protein to reveal nanomolar affinity.[219] Later studies indicated that [^{3}H]-PB28 accumulated primarily in

the nucleus, which was not supported by data using selective σ2R fluorescent ligands that showed no significant accumulation in nuclei.[220] Ultimately, the hypothesis had not been widely accepted, with some noting that the study lacked rigorous validation and that histone proteins lacked characteristic σ2R features.[77] It is plausible that the modified molecular probe had diminished affinity for the σ2R, combined with a lack of specificity that contributed to unsuccessful purification. Alternatively, the immobilized ligand might not have the ability to interact with the σ2R binding site which could have prevented efficient protein capture.

1.4.3.2 Sigma-2 Receptor: A Potential Association with the PGRMC1

The molecular identity of the σ2R continued to evade researchers, leading the Mach group to purse an alternative approach for identifying the protein that was reported in 2011.[221] This strategy sought to utilize the molecular probe WC-21 (**1.103**) that was based on RHM-1 (**1.93**), a selective σ2R ligand previously developed by the group. Ligand **1.93** was contained an azide moiety for covalently linking the probe to the protein and a fluorescein isothiocyanate group (FITC) for fluorescent visualization (Figure 1.27). The new molecular probe WC-21 (**1.103**) was characterized using the atypical radioligand [^{125}I]-RHM-4 (**1.104**) that was also developed by the group and determined to have high σ2R affinity and specificity. Having confirmed that WC-21 (**1.103**) displayed affinity for the target, it was incubated with rat liver membrane homogenate and irradiated to crosslink the probe and protein complex. Subsequent western blot analysis with anti-FITC antibodies revealed a ~24 kDa protein band that was labeled with the FITC-probe. Proteomic analysis of the band with MS identified the 22kDa putative progesterone-binding protein and the 25 kDa protein 25-Dx, both sharing the genetic name, progesterone receptor membrane component 1 (*PGRMC1*). Notably, WC-21

labeling of the protein band was inhibited by classical σ2R ligands DTG and haloperidol, as well as [^{125}I]-RHM-4 (**1.104**), which supported the conclusion that the protein band contained the σ2R.

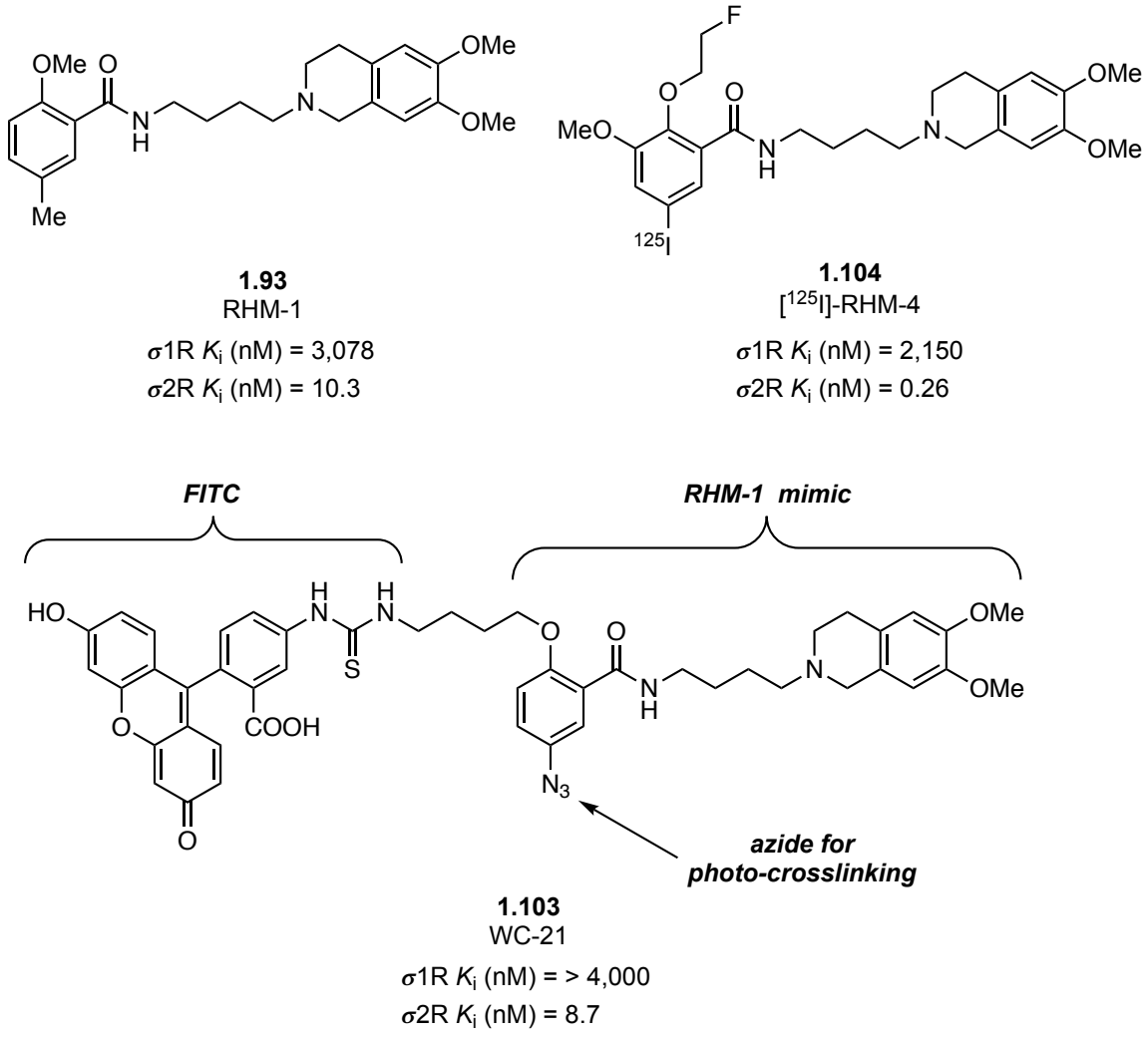

1.93
RHM-1
σ1R K_i (nM) = 3,078
σ2R K_i (nM) = 10.3

1.104
[^{125}I]-RHM-4
σ1R K_i (nM) = 2,150
σ2R K_i (nM) = 0.26

1.103
WC-21
σ1R K_i (nM) = > 4,000
σ2R K_i (nM) = 8.7

Figure 1.27. Molecular probe for photo-crosslinking with the σ2R protein.

PGRMC1 is a known protein that has been sequenced and cloned from several species including humans, enabling Mach to perform additional studies that assessed similarities between the σ2R and PGRMC1.[221] Competitive binding analysis using [^{125}I]-RHM-4 (**1.104**) revealed that the radioligand was readily displaced by the known

PGRMC1 ligand AG-205, as well as the σ2R ligands DTG (**1.70**), siramesine (**1.90**), SV119 (**1.88**), and WC-26 (**1.87**) in HeLa cell membrane homogenate. Additionally, the siRNA knockdown of PGRMC1 reduced [^{125}I]-RHM-4 binding, whereas overexpression using PGRMC1 cDNA increased radioligand binding (~60%) in HeLa cells. PGRMC1 and σ2R were also found to be colocalized within the cell using confocal microscopy with a PGRMC1 antibody and a σ2R fluorescent probe. Taken together, these data led Mach to conclude that the putative σ2R binding site resides within a PGMRC1 protein complex.

1.4.3.3 The PGRMC1

The literature provides a number of insights into PGRMC1 that offer some support for Mach's proposal. The sequenced and cloned protein has an approximate mass of ~25-28 kDa, notably heavier than the reported 21.5 kDa mass reported for σ2R.[171,222] However, the PGRMC1 amino acid sequence is 21.54 kDa for an unmodified isoform without the *N*-terminal methionine, which is consistent with the σ2R.[161] PGRMC1 has similar anatomical distribution with high levels of expression in the liver and kidney, but is also found among other peripheral tissues, as well as distribution in the brain and CNS.[223] Within the cell, PGRMC1 is found to localize in ER, microsomal, and mitochondrial fractions, which is consistent with σ2R subcellular localization studies.[77] Importantly, PGRMC1 is overexpressed in a variety of cancer types where it has been associated with cell viability, a well-established σ2R feature.[224]

PGRMC1 is a member of the membrane associated progesterone receptor (MAPR) subfamily of proteins that contain cytochrome b_5 ($Cytb_5$) domain, which is associated with heme-binding.[225] PGRMC1 is a multifunctional protein that has been implicated in a variety of cellular processes, and its X-ray crystal structure was recently

disclosed showing that the protein forms a stable dimeric species upon binding with heme, which is critical to its function.[226,227] PGRMC-1 has been associated with cholesterol biosynthesis through activation of specific cytochrome P-450 (cyP450) enzymes involved in sterol synthesis.[228] The σ2R has been proposed to be a cyP450 protein as a result of high σ2R affinity among some cyP450 inhibitors and substrates leading Mach to suggest a PGRMC1–cyP450 protein complex might constitute the σ2R binding site.[77,229,230]

Much like the σ2R, the exact functional role of PGRMC1 has been difficult to elucidate, although as its name implies it has been associated with binding of progesterone. However, while it does seem to be involved in progesterone responses, there is little evidence for direct progesterone binding to purified recombinant PGRMC1 protein.[231-233] Nonetheless, progesterone has been proposed as an endogenous ligand for PGRMC1, suggesting that *in vivo* binding might occur with post-translationally modified PGRMC1 as many high molecular weight isoforms have been identified.[224] Partially purified PGRMC1 has been found to have high affinity for progesterone (apparent K_d = 11-35 nM), although the discrepancy with purified recombinant protein in confounding.[222,234] The affinity of progesterone for σ1R and σ2R in rat liver membrane is modest, 239 and 441 nM respectively, notably lower than partially purified PGRMC1 even though the implications of this result are not entirely clear.[235] However, the pan-σR ligand haloperidol was competitive with the [^{3}H]-progesterone binding site in porcine liver membrane (K_i = 20 nM), whereas the σ1R selective ligand (+)-pentazocine had much lower affinity for the same site (K_i = 1.13 μM).[236]

Collectively these data provide some evidence that does not rule out the possibility of the σ2R binding site being located in or associated with PGRCM1. The similar anatomical distribution, subcellular localization, and demonstrated role in cancer

biology provide the clearest support for the hypothesis. Indeed, the significant levels of overexpression of PGRMC1 in a variety of cancer types where it was shown to promote proliferation in tumors was consistent with a common feature of the σ2R. It is perplexing that knockdown of PGRMC1 was associated with decreased proliferation, whereas activation of σ2R has been correlated with the same effect.[226,237] However, since the exact molecular mechanisms of σ2R activation remain unclear and have instead been assigned somewhat arbitrarily, this discrepancy is not completely surprising. Taken together with Mach's fluorescent labeling and proteomic studies, there was compelling evidence to suggest a relationship between the σ2R and PGRMC1, and the hypothesis gained some acceptance, although unequivocal evidence from cloning of the σ2R remained to be acquired.

1.4.3.4 The Sigma-2 Receptor is not Synonymous with PGRMC1

The link between the σ2R and PGRMC1 was viewed as a substantial leap forward in σ2R research that brought molecular identification and cloning closer to being realized. Indeed, the commonality in certain biological features was compelling, and an increasing number of reports ostensibly identified the two proteins as synonymous (e.g. σ2R/PGRMC1).[165,238-240] However, important questions regarding the aforementioned discrepancies between the two proteins remained unanswered leading to some controversy about the true identity of σ2R.[126] Most notably, the PGRMC1 was a 25 kDa protein that was distinctively heavier than the 21.5 kDa mass originally reported for the σ2R. Evidence suggested that splice variants and post-translational modification of PGRMC1 existed with a mass that was consistent the σ2R and therefore the identification could not be precluded based on that criteria, but it did prompt concern among some.[224] In addition, the σ2R was defined by its high affinity for DTG and haloperidol, but at the

time the affinity of these ligands for PGRMC1 was conspicuously absent from the literature.[241]

In an effort to provide some clarity on this issue, Abate *et al*. independently examined the σ2R binding characteristics of MCF7 breast cancer cells with genetic knockdown and overexpression of PGRMC1.[242] Interestingly, scatchard binding analysis using the prototypic σ2R ligand [^{3}H]-DTG revealed no significant change in saturation levels between the MCF7 control cells and the MCF7 cells with altered PGRMC1 expression levels. This suggested that the σ2R binding site might be distinct from the PGRMC1 protein. In addition, the antiproliferative effects of six σ2R ligands with known cytotoxic effects were evaluated in MCF7 cells overexpressing PGRMC1 and little change was observed in proliferation, as compared to control cells.[242] The MCF7 cells with PGRMC1 knockdown displayed increased sensitivity to the antiproliferative effects, but this was attributed to the prosurvival characteristics of PGRMC1 that were diminished due to lower expression levels. In the presence of a known PGRMC1 inhibitor, a synergistic effect was observed that led to increased cytotoxicity in MCF7 control cells that also pointed to separate pathways for inducing cell death. Collectively, these results led Abate *et al.* to suggest that the σ2R and PGRMC1 are unique proteins and that the photoaffinity label used in Mach's study likely had affinity for both proteins.

The report from Abate's group was followed by corroborating results from Ruoho *et al.* using the motor neuron-like NSC34 cell line with altered PGRMC1 expression.[241] In this study, complete knockout of PGRMC1 in NSC34 cells was enabled using CRISPR/Cas9 technology to remove any ambiguity that might derive from the low expression levels obtained with the knockdown approaches used by Mach and Abate.[221,242] Similar to Abate, Ruoho *et al.* found that NSC34 cells lacking PGRMC1 provided no reduction in σ2R density according to scatchard analysis with [^{3}H]-DTG as

compared to control cells.[241] The photoaffinity probe [^{125}I]-IAF (**1.105**) is σ1R selective with micromolar affinity for the σ2R, but after incubation with PGRMC1 knockout cells two DTG-sensitive protein bands were visualized at approximately 26 and 18 kDa, corresponding to σ1R and σ2R respectively (Figure 1.28).[243] This suggested that the defining features of σ2R, namely a 18-21.5 kDa protein with high affinity for DTG, were still present in cells devoid of PGRMC1, thus the two proteins must be derived from distinct genes as opposed to resulting from a splice variant or modified protein complex. The affinities of DTG and haloperidol for PGRMC1 in rat liver membrane were also assayed using [^{3}H]-progesterone and determined to be lower (> 3 orders of magnitude) than for the σ2R in the same tissue, although as previously discussed the PGRMC1 does not appear to directly bind progesterone so the meaning of this result is not entirely clear.[241] However, these collective results support the conclusion that PGRMC1 and σ2R are not synonymous and are instead genetically distinct.

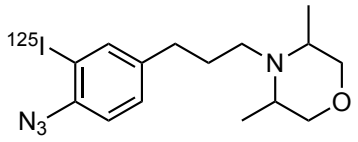

1.105
[^{125}I]IAF
σ1R K_i (nM) = 194 ± 27.5 nM
σ2R K_i (nM) = 2,780 ±1,060 nM

Figure 1.28. Molecular probe for photo-crosslinking with the σ1R and σ2R.

The report from Mach *et al.* that the σ2R binding site was located within the PGRMC1 protein complex initially seemed to provide long sought-after clarity about the molecular identity of the elusive receptor. However, independent reports from other groups suggested that the two proteins are not synonymous based on expression studies

using cell lines different from those originally described by Mach. The reason for the discrepancy between research groups is not clear, but it is possible that the photoaffinity probe used by Mach *et al.* either had off-target affinity for PGRMC1 or that the PGRMC1 is in close proximity to the σ2R and was irreversibly labeled while the probe interacted with the σ2R binding site.[161] It is important to point out that this does not necessarily invalidate Mach's original hypothesis that the binding site was part of a PGRMC1 protein complex and that σ2R could be a partner protein in. However, it does seem increasingly likely based on genetic manipulation studies that the two proteins are not synonymous and that the σ2R is not a modified form of PGRMC1. If it is a partner protein in a larger complex, then it remains unclear if PGRMC1 is essential for σ2R function.[13,224] This produces a rather complex picture about the relevant association of the σ2R and PGRMC1 that requires additional investigation, but it does suggest that the true molecular identity of σ2R had yet to be determined.

1.4.4 Sigma-2 Receptor Pharmacophore and Selective Ligands.

It is somewhat surprising that in spite of decades of research and an increasing number of reports highlighting the medical relevance of the σ2R that its true identity continued to evade researchers. The absence of a crystal structure prevents the use of typical structure-based design strategies, similar to the challenges faced in σ1R ligand design prior to 2016.[6] However, unlike the σ1R, 3-D homology models and mutagenesis studies are also not available to provide structural insights because the σ2R protein has not been identified and the sequence is unknown. Unfortunately, there is considerable overlap in the σ1R and σ2R ligand binding profile, and neither the σ1R crystal structure nor the previously discussed σ1R pharmacophore models addressed strategies for obtaining subtype selectivity.[133,141]

Lack of a 3-D model for the σ2R binding site has resulted in a longstanding challenge for designing ligands that have both high affinity for the σ2R and high selectivity over σ1R.[77,162,203] In fact, the first high affinity ligands with reasonable selectivity for the σ2R over the σ1R were not reported until 1995 and some of these were only identified by happenstance during the course of investigations targeting other receptors.[161,244] Since then, many high affinity σ2R ligands have been developed that exhibit varying degrees of selectivity over the σ1R and that have been derived from extensive SAR studies within a given ligand class.[77,162,203,220] An online searchable database was compiled in 2017 containing known σ2R ligands with selectivity over σ1R (*i.e.* K_i σ1R/K_i σ2R > 1).[245] At the time of this writing, this database contained 592 σ2R ligands meeting this criteria, but less than half of these had greater than 10-fold selectivity over σ1R, and only 90 had greater than 100-fold selectivity. This limited number of compounds with high levels of selectivity highlights the persistent and ongoing challenge of ligand design. In addition, the σ2R binds a large variety of structurally diverse ligands and the lack of crystal structure has made it difficult to identify common pharmacophore features.[162] There have been several attempts to identify σ2R pharmacophore models, but these have generally be restricted to structurally similar molecules from within specific ligand classes and do not provide broadly predictive information.[142,246,247] In addition, these models often used ligands that lacked sufficient subtype selectivity so their discussion will be limited. However, a brief survey of several ligand classes that are selective for the σ2R over the σ1R and the associated SAR investigations of these ligands will provide some insight into structural features that have provided enhanced potency and selectivity.

1.4.4.1 Sigma-2 Receptor Ligands: The Benzomorphan-7-one Scaffold

The benzomorphan-7-one scaffold **1.107** reported by Bowen *et al.* in 1995 was among the first σ2R selective ligand classes disclosed, and it was discovered inadvertently.[248] Initial efforts were focused on modulating the μ-opioid affinity of 3-hydroxyphenylmorphan **1.106**, a potent opioid analgesic, through the introduction of an *E*-benzylidene group on the parent scaffold to give analogs of **1.107** (Scheme 1.5). Notably, this structural change produced a modest decrease in opioid affinity in the modified scaffold that was accompanied by an increase in affinity for the σ1R and σ2R.

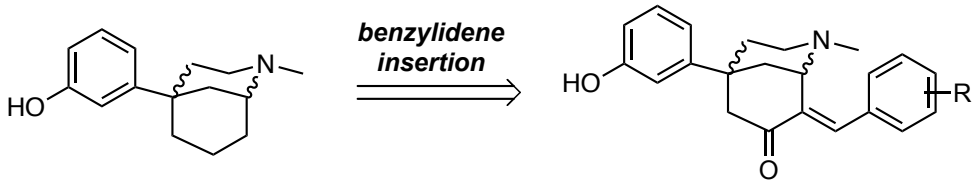

(±)-1.106 **(±)-1.107**

Scheme 1.5. Introduction of an *E*-benzylidnene group in the 3-hydroxyphenyl-morphan scaffold

Recognizing that benzomorphan-7-one (±)-**1.107** represented a unique scaffold for targeting the σRs, a more detailed investigation of the SAR was conducted.[244,249] Initial examination of the benzomorphan-7-one stereoisomers CB-64D (**1.83**) and CB-64L (**1.110**) revealed that levorotatory isomer **1.110** had significantly higher affinity for the σ1R than the corresponding dextrorotatory isomer **1.83**.[249] In fact, the (+)-benzomorphan-7-one displayed high affinity for the σ2R and remarkable selectivity over the σ1R, an enantiomeric preference that is opposite the preference that is typically observed with (+)-benzomorphans. The same trend was observed upon introduction of the dichlorinated benzylidenes moiety in CB-182 (**1.112**) and CB-184 (**1.111**). Indeed, the chlorine substituents further decreased σ1R affinity in the (+)-benzomorphan-7-one

analog CB-184 (**1.111**) and led to 554-fold subtype selectivity favoring the σ2R.[249] The effect of a single chlorine atom on the benzylidene aromatic ring was found to be a bit more pronounced at R^2 (**1.114**) than R^1 (**1.113**), but incorporating both had a notable synergistic effect in CB-184 (**1.111**).[244] Introduction of a single iodine atom at R^2 (**1.115**) was not as effective as the chlorine substituent for reduction of σ1R affinity. However, introduction of a polar methoxy substituent at R^2 (**1.116**) was favorable and led to 157-fold selectivity for σ2R over σ1R.[244] It is notable that each of the (+)-benzomorphan-7-one analogs maintained high affinity for the σ2R, and σ1R affinity was modulated by altering the substitution pattern. The (+)-benzomorphan-7-one analog CB-184 (**1.111**) was the most σ2R subtype selective ligand known at the time, although the μ-opioid affinity was still high detracting from its utility as a truly σ2R selective ligand.[248] Nonetheless, CB-64D (**1.83**) and CB-184 (**1.111**) provided an advancement in selective ligand design and were used for many additional studies probing the cytotoxicity of σ2R ligands in a range of cancer cell lines.[187,196]

Table 1.1. Binding affinity of benzomorphan-7-one analogs.

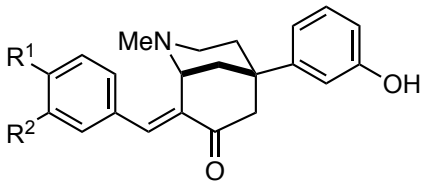

(+)-1.108

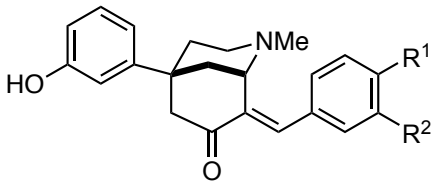

(–)-1.109

				K_i (nM)		K_i ratio
Compd. (name)	(+)/(–)	R^1	R^2	σ1R	σ2R	(σ1R/σ2R)
1.83 (CB-64D)	(+)	H	H	3,063 ± 78	16.5 ± 2.7	185
1.110 (CB-64L)	(–)	H	H	10.5 ± 1.6	154 ± 3	0.07
1.111 (CB-184)	(+)	Cl	Cl	7,436 ± 308	13.4 ± 2	554
1.112 (CB-182)	(–)	Cl	Cl	27.3 ± 2.8	35.5 ± 8.8	0.77
1.113	(+)	Cl	H	759.3 ± 59.8	6.4 ± 0.4	119
1.114	(+)	H	Cl	3,100 ± 350	22.4 ± 2.1	138
1.115	(+)	H	I	1,620 ± 170	24.0 ± 1.5	68
1.116	(+)	H	OMe	6,000 ± 750	38.2 ± 3.5	157

1.4.4.2 Sigma-2 Receptor Ligands: The Tropane Scaffold

The first tropane identified with high affinity for the σ2R and selectivity over the σ1R was BIMU-1 (**1.117**), discovered while probing the tropane based structure as a ligand for the serotonin receptors (5-HT_3 and 5-HT_4) (Figure 1.29).[250] The 200-fold σ2R subtype selectivity possessed by BIMU-1(**1.117**) was an interesting discovery, and it represented a useful tool compound, although it maintained high affinity for the serotonin receptors. The tropane-based compound SM-21 (**1.94**) and many structural analogs that

were first prepared by Gualtieri *et al.* in 1994 were found to have potent antinociceptive activity that was attributed to their activity as a cholinergic modulator.[251,252] However, the σR affinity of SM-21 (**1.94**) was evaluated after it was discovered that the structurally similar tropane BIMU-1 (**1.117**) had high σ2R affinity. In fact, Mach reported that SM-21 (**1.94**) has higher affinity for σ2R than the muscarinic receptor it was designed to target and suggested that it might serve as a lead compound for developing additional σ2R selective ligands.[253]

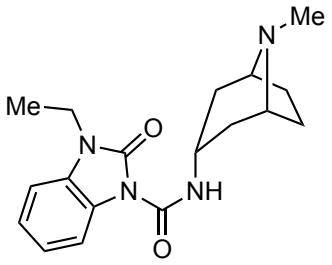

1.117
BIMU-1

σ1R K_i (nM) = 6,300
σ2R K_i (nM) = 32
K_i ratio (σ1R/σ2R) = 197

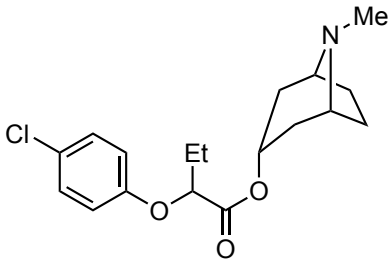

1.94
SM-21

σ1R K_i (nM) = > 1,000
σ2R K_i (nM) = 67.5 ± 8
K_i ratio (σ1R/σ2R) = 185

Figure 1.29. Tropane-based analogs with selectivity for σ2R over σ1R.

Inspired by the discovery that SM-21 displayed selectivity for the σ2R, the tropane derivatives originally prepared by Gualtieri *et al.* in 1994 as potential analgesics or nootropics were also determined to have σR affinity.[254] Three regions were identified among 48 tropane derivatives for construction of a computationally derived pharmacophore model: (1) hydrophobic region–1, (2) hydrophobic region–2, and (3) the positive ionizable nitrogen area that was labeled as hydrogen bond (HB) donor region (Figure 1.30.A).[246] Interestingly, many of the derivatives displayed only modest affinity for σ2R and low levels of selectivity over σ1R (i.e. 1-5 fold) a fact that signifiacntly

restricts the utility of the model. Nevertheless, the results can be briefly summarized as follows: (1) There was little difference when hydrophobic region–1 contained a phenoxy or phenthio group (R^2 = ArO–, ArS–, but an aniline group (R^2 = ArNH–, ArNMe–) decreased σ2R affinity; (2) converting the ester moiety (Y = O) to and ether linkage (Y = H) increased affinity for both σ1R and σ2R, thereby eliminating σ2R selectivity; and (3) a methyl substituent was preferred in hydrophobic region–2 (Z = Me) and switching to a benzyl group increased σ1R, again eroding selectivity.[254] A pharmacophore model was proposed from these results using grid-independent descriptor (GRIND) computational methods that proposed optimal distances between the three pharmacophore elements (Figure 1.30.B).[246] Overall, the model is similar to the σ1R pharmacophore model proposed by Gilligan, but with modified distances to favor the σ2R. However, the modest affinity and low σ2R selectivity displayed by the tropane derivatives makes it difficult to extrapolate the reported distances to a more general model that can be used in the design of additional σ2R selective ligands.

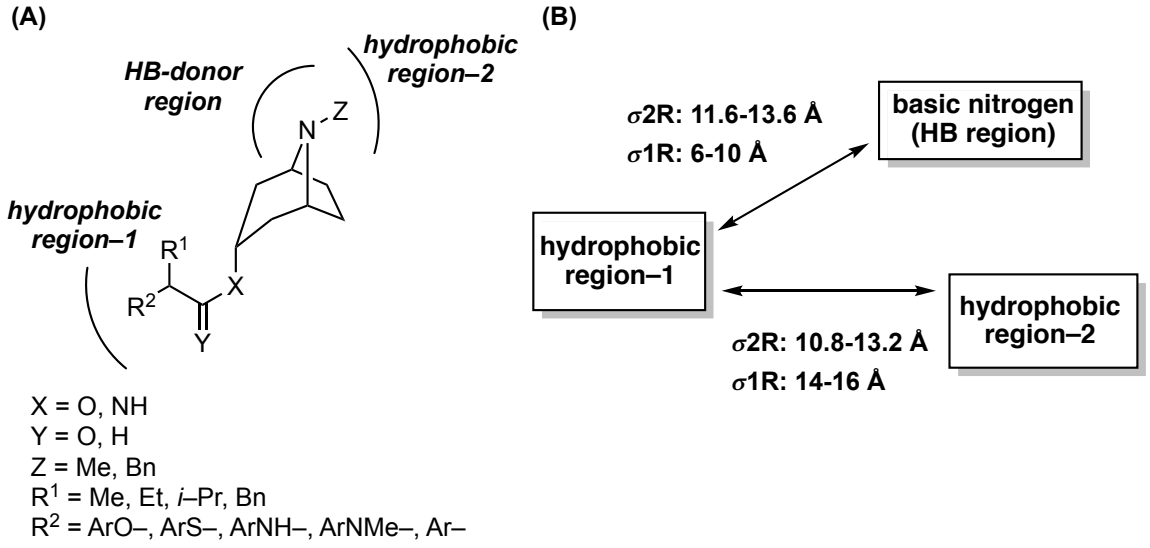

Figure 1.30. (A) Pharmacophore elements of tropane derivatives. (B) σ2R pharmacophore model for tropane derivatives proposed by Cratteri.[246]

1.4.4.3 Sigma-2 Receptor Ligands: The Granatane Scaffold

The tropane derivative BIMU-1 (**1.117**) was serendipitously discovered as a high affinity σ2R ligand with selectivity over σ1R, but it suffered significant off-target interactions leading Mach *et al.* to investigate structural modifications as part of an extensive SAR investigation (Figure 1.31).[255] The *N*-methyl moiety of BIMU-1 was thought to be the source of high 5-HT_3 and 5-HT_4 affinity because that functionality was observed in several antagonists targeting those receptors, hence replacing the methyl group with a benzyl moiety was investigated to suppress off-target interactions. The benzimidazole moiety was replaced with a phenyl carbamate moiety to more easily evaluate a range of substituted aromatic groups in this region. The tropane core was also targeted for modification with a structurally similar granatane unit envisioned as an alternative. These structural changes were embodied in the *N*-benzyl tropane **1.118** and *N*-benzyl granatane **1.119** scaffolds that were designed to interrogate these key SAR features.

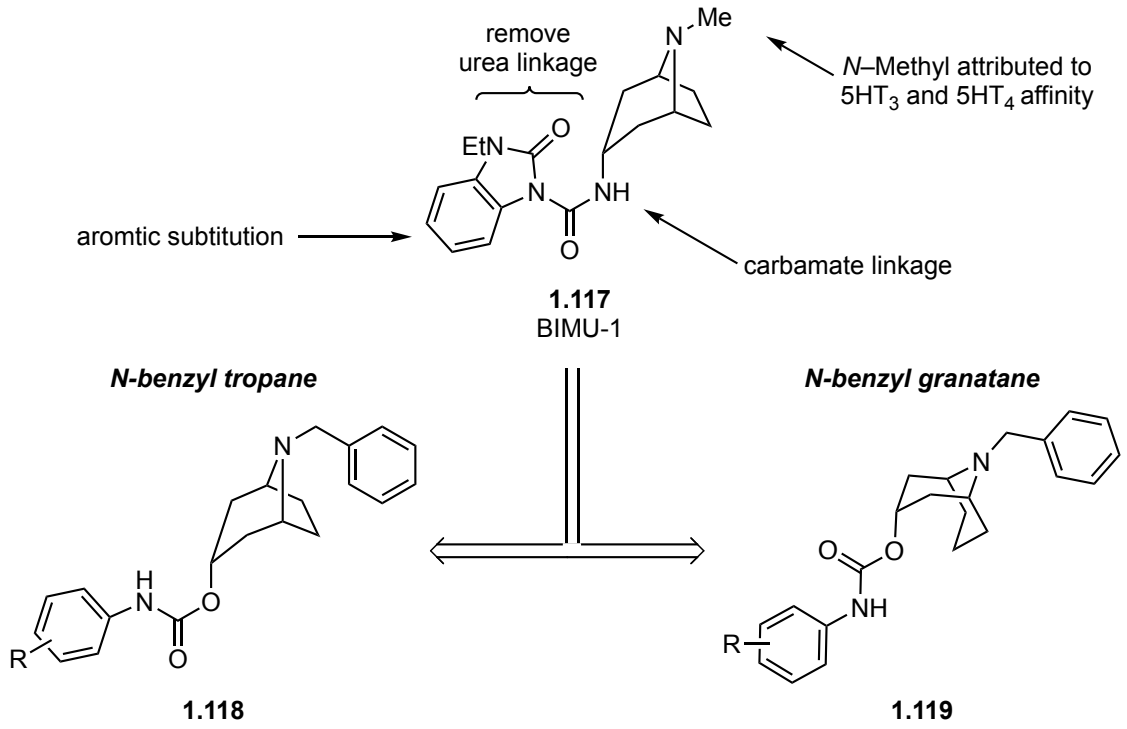

Figure 1.31. Structural modification of BIMU-1 leads to *N*-benzyl tropane and granatane scaffolds.

Importantly, Mach discovered that exchange of the *N*-methyl substituent with an *N*-benzyl group significantly diminished affinity for 5-HT_3 and 5-HT_4 in most of the analogs, while high σ2R affinity was maintained (Table 1.2).[255] Additionally, the incorporation of aromatic substituents on the phenyl carbamate had a pronounced impact on σ1R affinity. For example, the 2,5-dimethylcarbamate moiety on the tropane **1.120** and granatane **1.121** scaffolds had high affinity for both the σ1R and σ2R with a slight preference for the σ1R. In contrast, the methoxy substituent in tropane **1.122** and granatane **1.123** decreased affinity for the σ1R, an effect that was more pronounced for granatane **1.123** leading to 30-fold selectivity for the σ2R. The most σ2R selective tropane was the 2-methoxy-5-nitro analog **1.124**, which had 7-fold selectivity over σ1R.

Interestingly, the analogous granatane **1.125** displayed decreased σ2R affinity and only 2-fold selectivity. However, a number of the *N*-benzyl granatane analogs displayed modest levels of selectivity for the σ2R over the σ1R, suggesting that it was the preferred scaffold arrangement.

Table 1.2. Binding affinity of *N*-benzyl tropane and granatane analogs.

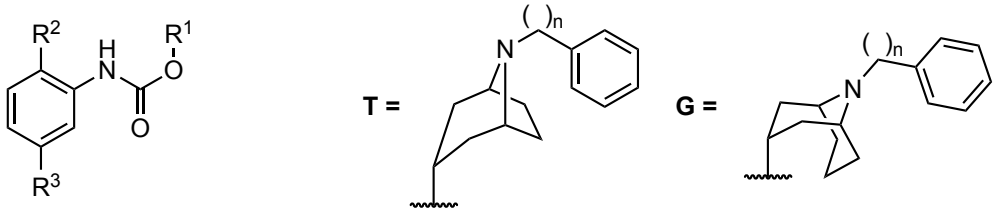

					K_i (nM)		K_i ratio
Compd.	R^1	R^2	R^3	n	σ1R	σ2R	(σ1R/σ2R)
1.120	T	Me	Me	1	9.2 ± 1.2	14.6 ± 0.4	0.6
1.121	G	Me	Me	1	6.0 ± 1.5	7.6 ± 0.2	0.8
1.122	T	OMe	Me	1	14.4 ± 0.1	3.2 ± 0.4	4.5
1.123	G	OMe	Me	1	92.5 ± 11	3.1 ± 0.8	30
1.124	T	OMe	NO_2	1	37.9 ± 3.3	5.4 ± 1.1	7
1.125	G	OMe	NO_2	1	67.8 ± 2.1	16.7 ± 0.4	2
1.126	G	OMe	OMe	1	329.1 ± 26.1	26.8 ± 7.9	12
1.127	G	OMe	Me	2	59.9 ± 4.6	1.2 ± 0.1	50
1.128	G	OMe	Me	3	73.0 ± 1.6	2.0 ± 0.1	37
1.129	G	OMe	Me	4	65.5 ± 4.3	2.9 ± 0.2	23
1.130	G	OMe	Me	5	17.3 ± 1.2	1.8 ± 0.2	10
1.131	G	OMe	Me	6	214 ± 24	7.6 ± 0.4	28

This finding generated additional interest in the granatane scaffold and a variety of additional analogs were evaluated.[203] These efforts identified granatane **1.127** in which the aromatic group was optimally positioned with a two-carbon spacer (n = 2) between the granatane nitrogen atom providing 50-fold selectivity over the σ1R (Table 1.2).[256] Interestingly, spacers up to 6-carbons in length (n = 1-6) provided high σ2R affinity and modest selectivity over the σ1R. A second basic amine at the terminus of the tethered group significantly decreased affinity for the σ1R, providing 510-fold selectivity with aniline analog **1.91** and 273-fold selectivity with the primary amine analog **1.88** (Figure 1.32).[256,257] The range of spacer lengths and hydrophobic bulk that was tolerated at the tethered aromatic group inspired considerable investigation and led to the installation of fluorescent tags in this region for visualizing the σ2R in tumors, as well as a tethered biotin unit.[257] It is interesting that there are no reports attempting to pulldown the σ2R with the biotinylated compound. Nonetheless, the granatane scaffold has been the subject of extensive SAR investigations, providing highly selective σ2R ligands that were useful as tool compounds for investigating the receptor.

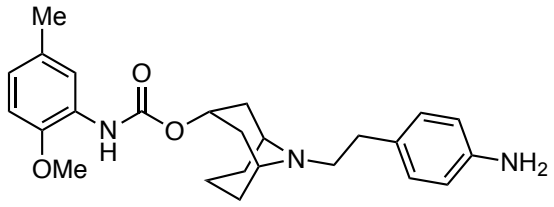

1.91
yun245

σ1R K_i (nM) = 2,250 ± 73
σ2R K_i (nM) = 5.0 ± 0.2
K_i ratio (σ1R/σ2R) = 510

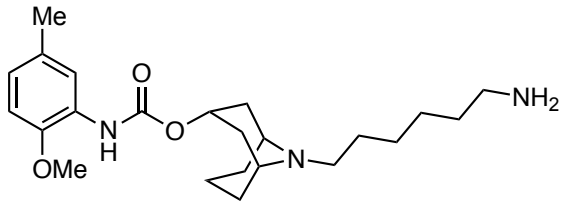

1.88
SV119

σ1R K_i (nM) = 1,418 ± 439
σ2R K_i (nM) = 5.19 ± 0.8
K_i ratio (σ1R/σ2R) = 273

Figure 1.32. Granatane analogs with a second basic amine.

1.4.4.4 Sigma-2 Receptor Ligands: Siramesine Analogs

Perregaard *et al.* reported a series of aryl piperazine analogs (**1.132**) in 1995 that were originally developed as low efficacy serotonin 5-HT_{1a} agonists, but were also potent σR ligands.[197] Interested in exploring this feature, an SAR strategy was devised to evaluate functionality that might enhance affinity and selectivity for the σ2R over the σ1R (Figure 1.33). Initially a series of aryl substituents at R^1 were targeted for investigation, as well exchange of the aniline nitrogen with a carbon atom in **1.133**. In addition, substitution of the nitrogen atom of the tethered indole moiety would also be probed.

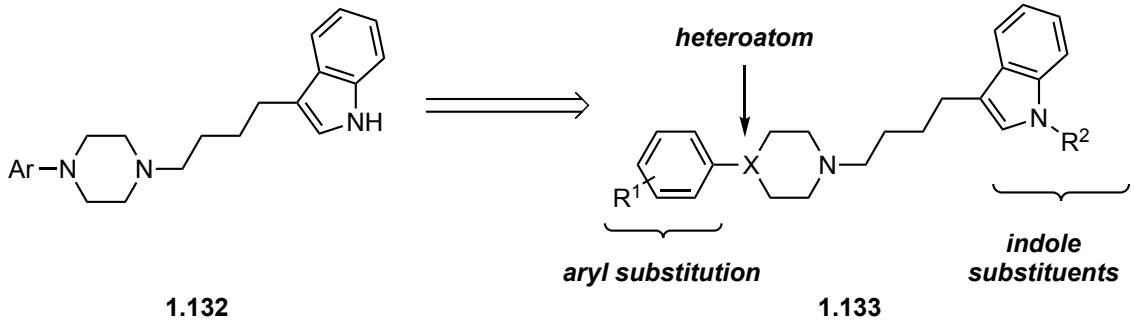

Figure 1.33. Modification of aryl piperazines analogs to enhance σ2R affinity.

The initial iteration of SAR revealed that each of these structural units could be modified to enhance the overall binding profile (Table 1.3).[197] For instance, the aryl substituent at R^1 impacted overall affinity for the σRs and switching from a 2-methoxy in **1.134** to a 4-fluoro substituent in **1.135** increased affinity for both σR receptors with low selectivity for the σ2R (4.3-fold). Replacement of the aniline nitrogen atom with a carbon atom (**1.136**) further increased affinity for the σ1R, slightly favoring it over the σ2R, which suffered a slight decrease in affinity. However, replacing the 4-fluoro substituent at R^1 with a hydrogen atom (**1.137**) increased σ2R affinity to subnanomolar levels, although

with only a slight preference over the σ1R (3.1 fold). Unfortunately, each of the unsubstituted indole analogs (**1.134-1.137**) had considerable off-target affinity for the serotonin N 5-HT_{1a} and 5-HT_{2a}, dopamine D_2, and the α_1 adrenergic receptors. However, introduction of the 4-fluorophenyl substituent at the indole nitrogen (**1.138-1.139**) greatly reduced these off-target interactions and also decreased σ1R affinity, affording up to 100-fold selectivity for the σ2R.

Table 1.3. Binding affinity of indole analogs

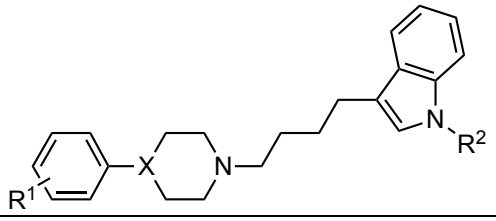

				K_i (nM)		K_i ratio
Compd.	X	R^1	R^2	σ1R	σ2R	(σ1R/σ2R)
1.134	N	2-OMe	H	14	21	0.67
1.135	N	4-F	H	5.6	1.3	4.3
1.136	CH	4-F	H	1.4	4.0	0.35
1.137	CH	H	H	1.5	0.48	3.1
1.138	CH	4-F	4-F-phenyl	16	0.27	59
1.139	CH	H	4-F-phenyl	44	0.44	100

Inspired by reports of other σR ligands with a spirocyclic piperidine moiety, Perregaard *et. al.* next constrained the aryl group in **1.140** as a phthalane–piperidine spirocycle (**1.141**) (Figure 1.34).[197] The length of the carbon chain that tethered the indole moiety was also evaluated to determine the optimal length for enhancing σ2R selectivity.

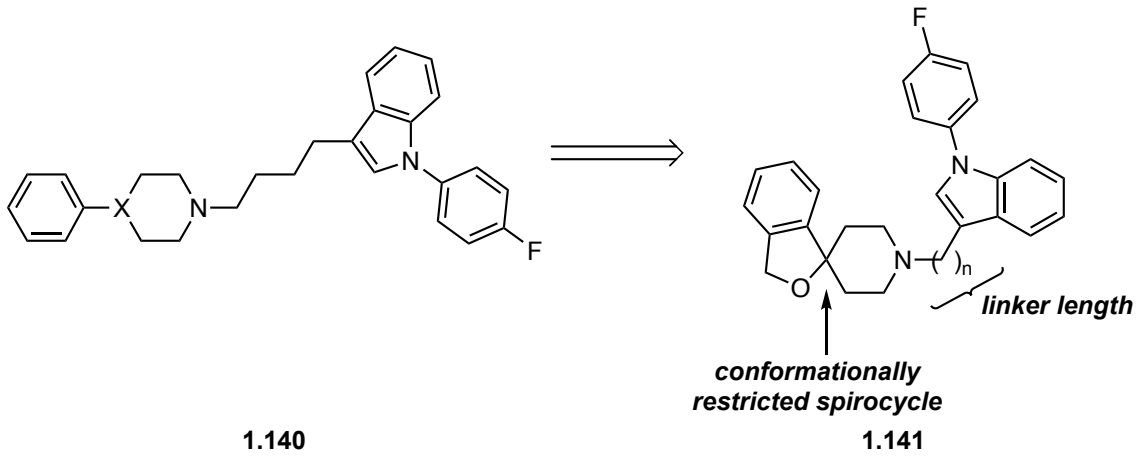

Figure 1.34. Introduction of the spirocyclic piperidine moiety.

Indeed, Perregaard *et al.* discovered that the spirocycle **1.90** had increased σ2R affinity to 0.12 nM, along with a modest increase in σ1R affinity that resulted in a 140-fold preference for the σ2R (Table 1.4). Attempts to decrease the length of the carbon-linker (n = 1–4) connected to the indole moiety decreased affinity for the σ2R and increased σ1R affinity, thereby eroding selectivity (**1.142-1.144**). Analog **1.90**, which came to be known as siramesine, benefits from remarkably high affinity for the σ2R and has potent cytotoxic activity in cancer cell lines, leading to its prominent use as a reference compound for investigations of the receptor.[201,220]

Table 1.4. Binding affinity of spirocyclic piperidine analogs.

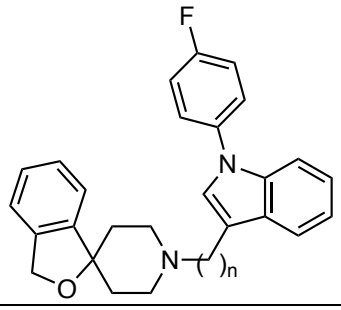

		K_i (nM)		K_i ratio
Cmpd.	n	σ1R	σ2R	(σ1R/σ2R)
1.90	4	17	0.12	140
1.142	3	10	2.8	3.6
1.143	2	15	3.0	5
1.144	1	3.0	4.7	0.64

1.4.4.5 Sigma-2 Receptor Ligands: Benzamide Analogs

In 2004, the efforts of Mach and coworkers to design ligands targeting dopamine D_3 receptors selectively over the D_2 receptors and the σRs resulted in the fortuitous discovery of some of the most σ2R selective ligands reported to date.[77] Previous work from the group identified pyrrole analog **1.145** with modest selectivity for D_3 over D_2 and low off-target affinity for the σRs (Figure 1.35.A).[258] The naphthamide analog **1.146** had improved selectivity for D_3 over D_2, but showed high affinity for the σ1R and σ2R (Figure 1.35.B).[259] Accordingly, Mach sought to construct a series of hybrid ligands **1.147** to improve D_3 over D_2 selectivity and reduce σR affinity by combining the amide linker of **1.146** with various structural arrangements of the 2,3-dimethoxyphenyl (Group

i) and tetrahydroisoquinoline (Group ii) elements from **1.145** with the 2-methoxynaphthyl (Group iii) moiety from **1.146** (Figure 1.35.C).[181]

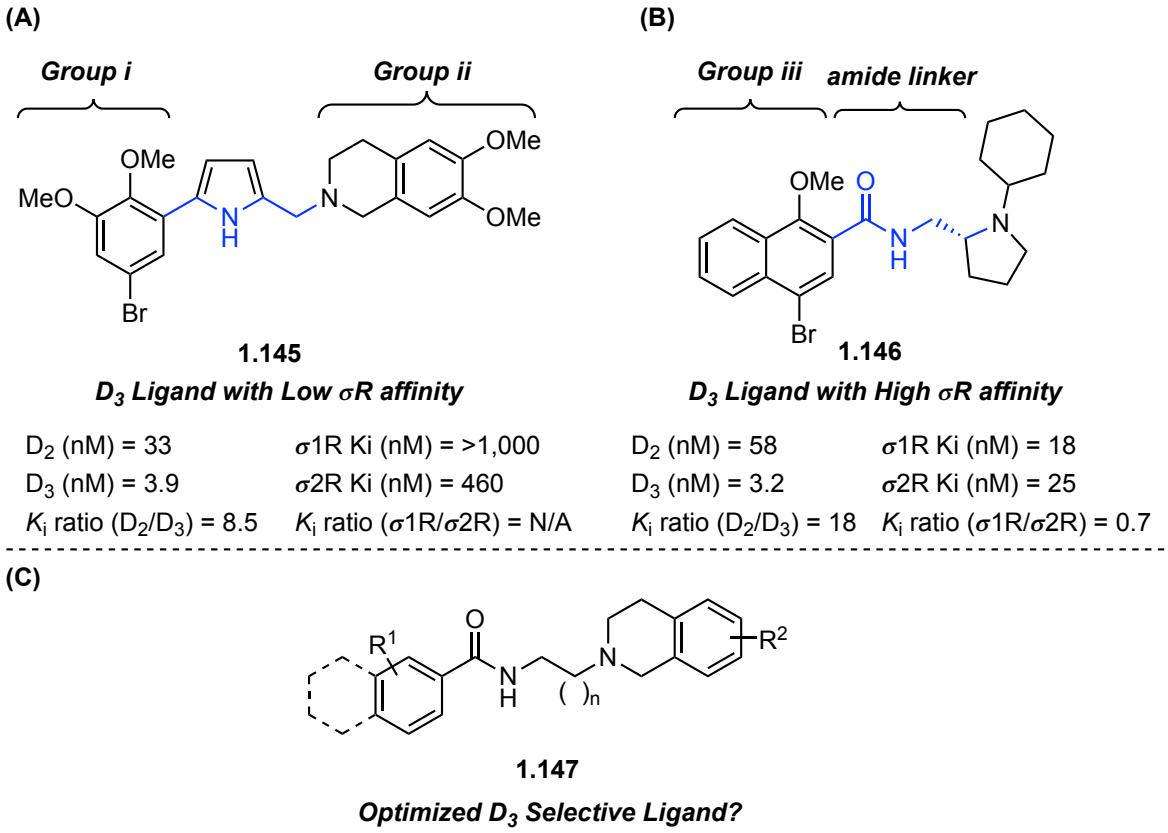

Figure 1.35. A) Pyrrole analog with modest D_3 selectivity and low σR affinity. B) Pyrrole analog with improved D_3 selectivity and high σR affinity. C) Design of benzamide analog for optimized D_3 selectivity.

The study revealed that the benzamide analogs **1.148** typically displayed high affinity for the σ2R, and affinity for the σ1R and dopamine receptors could be modulated by altering the substitution pattern (Table 1.5).[181] For instance, the 2-methoxynaphthylamide (R^1 = A) and the unsubstituted tetrahydroisoquinoline (R^2 = H) separated by a two-carbon spacer (**1.149**) displayed high affinity for both σRs, but introduction of the 6,7-methoxy substituents (**1.150**) attenuated σ1R affinity and provided

modest selectivity (9-fold) and both **1.149** and **1.150** maintained significant affinity for the dopamine receptors. The same pattern in σ2R selectivity was observed when the naphthyl group was replaced with a 2-methoxyphenylamide group (R^1 = B) (**1.151**-**1.152**), but 442-fold selectivity over the σ1R was achieved. In addition, both **1.151** and **1.152** benefited from diminished dopamine D_3 receptor activity. Transitioning to the 2,3-dimethoxyphenylamide (R^1 = C) (**1.153**) increased affinity for σ1R and the D_3 receptor. However, when the spacer group was increased to four-carbon atoms as in **1.80** there was a considerable decrease in σ1R affinity that produced a remarkable 1,573-fold selectivity for the σ2R subtype and further diminished dopamine receptor affinity. Finally, installation of the 2-methoxy-4-methyl-phenylamide (R^1 = D) as in **1.154**, increased affinity for the σ1R and the D_3 receptor, eroding selectivity, but decreasing the length of the spacer group to 2-carbons in **1.155** attenuated this effect and provided 783-fold selectivity for the σ2R over the σ1R and with very low potency at the D_3 receptor.

Table 1.5. Binding affinity of benzamide analogs

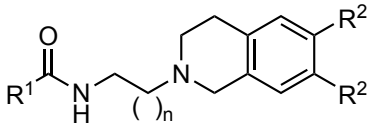

1.148

A = 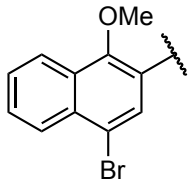

B = 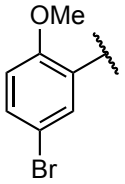

C = 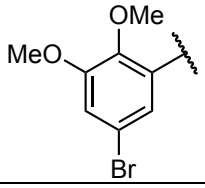

D = 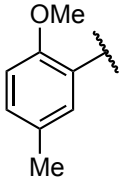

				K_i (nM)			K_i ratio
Cmpd.	R^1	R^2	n	σ1R	σ2R	D_3	(σ1R/σ2R)
1.149	A	H	1	15.1 ± 1.7	47.7 ± 2.5	81.6	0.32
1.150	A	OMe	1	189.1 ± 2.6	21.2 ± 0.1	126.5	9.0
1.151	B	H	1	21.8 ± 5.6	89.4 ± 13.9	310.7	0.24
1.152	B	OMe	1	5,484 ± 266	12.4 ± 1.8	488	442
1.153	C	OMe	1	2,932 ± 28	16.4 ± 2.0	21.4	179
1.80	C	OMe	3	12,900 ± 28	8.2 ± 1.4	627	1,573
1.154	D	OMe	3	3,078 ± 87	10.3 ± 1.5	313	299
1.155	D	OMe	1	10,412 ± 462	13.3 ± 0.1	3,760	783

The remarkable levels of σ2R selectivity achieved with the benzamide scaffold led to the construction of a variety of analogs that were used extensively in biological investigations of the receptor.[77] Some follow up SAR investigations revealed the importance of the conformationally constrained amine of the tetrahydroisoquinoline. For example, the ring-opened analog **1.156** displayed substantially reduced affinity for the σ2R. as compared to **1.80** (Figure 1.36.A).[260] The importance of the 6,7-dimethoxy

substituents of the tetrahydroisoquinoline moiety was also revealed through replacement with a constrained ethylenedioxy ring (**1.157**) that resulted in a dramatic increase in σ1R affinity (Figure 1.36.B).[260] Further investigations of the 2,3-dimethoxyphenyl amide substitution pattern identified the 2-methoxy substituent to play an important role that was hypothesized to result from a hydrogen bonding interaction with the amide N-H that forced a coplanar orientation of the aromatic ring (Figure 1.36.C).[261] This inspired the constrained cyclic amide **1.159** with a conformational constraint that forces a coplanar orientation and delivered good levels of σ2R selectivity.

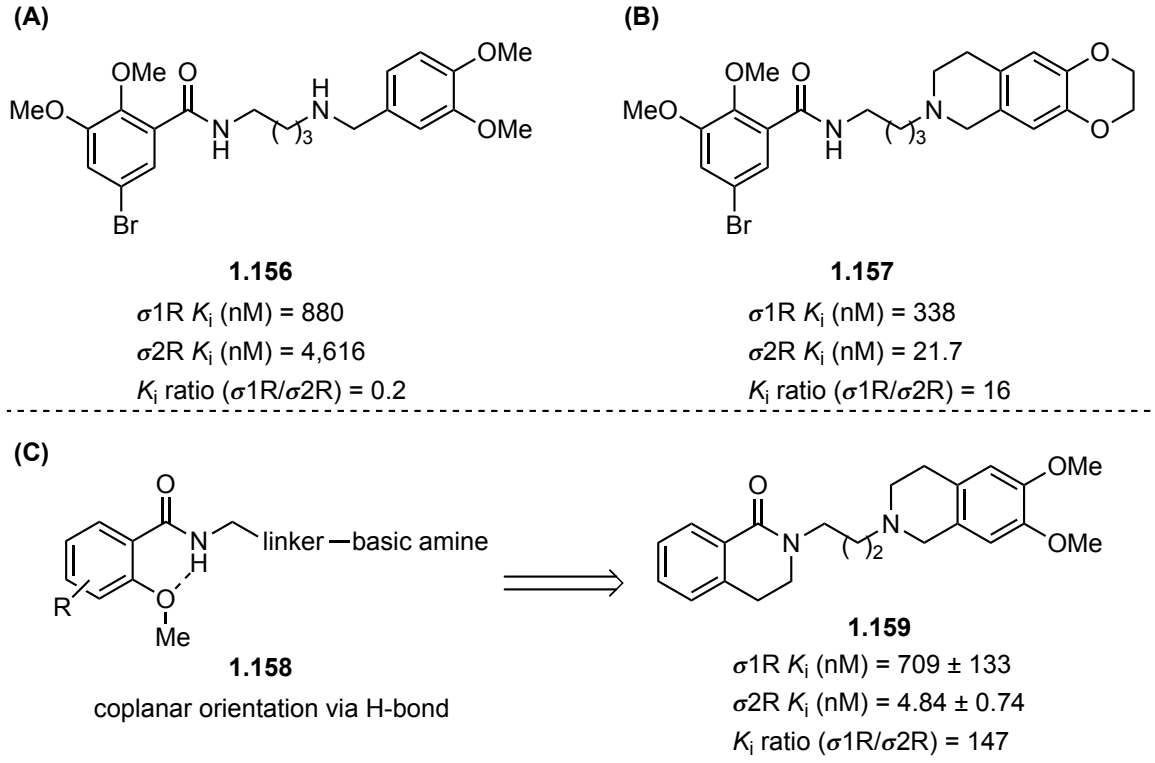

1.156
σ1R K_i (nM) = 880
σ2R K_i (nM) = 4,616
K_i ratio (σ1R/σ2R) = 0.2

1.157
σ1R K_i (nM) = 338
σ2R K_i (nM) = 21.7
K_i ratio (σ1R/σ2R) = 16

1.158

1.159
σ1R K_i (nM) = 709 ± 133
σ2R K_i (nM) = 4.84 ± 0.74
K_i ratio (σ1R/σ2R) = 147

Figure 1.36. A) Benzamide analog with ring-opened tetrahydroisoquinoline. B) Benzamide analog with ethylenedioxy ring. C) Proposed hydrogen bond with *ortho*-methoxy group that promotes coplanar orientation.

1.4.4.6 Sigma-2 Receptor Ligands: Cyclohexylpiperazine Analogs

Analogs constructed with a cyclohexylpiperazine motif have also been well-studied due to their high affinity for both the σ1R and σ2R, but most members of this family do not achieve meaningful levels of subtype selecitvity.[220] This is exemplified by the prototypic member of this ligand class PB-28 (**1.84**), which achieves subnanomolar affinities for the σ1R and σ2R and has potent antiproliferative activity (Figure 1.37).[262] The cyclohexylpiperazine moiety is important for maintaining σ2R affinity, but unlike siramesine, replacing it with a piperidine ring (**1.160**) has a deleterious effect on σ2R affinity and high σ1R affinity is maintained.[262] The particularly high affinity of PB-28 (**1.84**) for the σ2R has attracted attention for additional SAR studies, but attempts to prepare structural analogs of PB-28 with enhanced selectivity for the σ2R have been generally unsuccessful.[261,262] A notable exception is F281 (**1.85**) wherein the 5-methoxytetraline group of **1.84** is replaced with a carbozole moiety that diminishes affinity for both σRs, but because this effect is less pronounced at σ2R there is 274-fold selectivity for the σ2R. Despite the modest reduction in σ2R affinity, F281 has more potent antiproliferative activity in SK-N-SH cells than **1.84**.[190,262] In addition, exchange of the 5-methoxytetraline group in **1.84** with the 2(3H)-benzothiazolone moiety to give **1.161** led to higher affinity for the σ2R and a modest decrease for σ1R, affording 11-fold selectivity. Although unremarkable for σ2R selectivity the cyclohexylpiperazine motif does afford high potency and, in some cases, the tethered aromatic group can be altered to attenuate σ1R affinity.

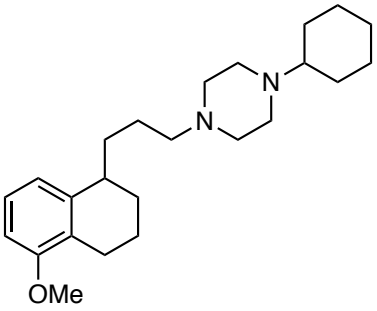

1.84
PB28

σ1R K_i (nM) = 0.38 ± 0.10
σ2R K_i (nM) = 0.68 ± 0.20
K_i ratio (σ1R/σ2R) = 0.56

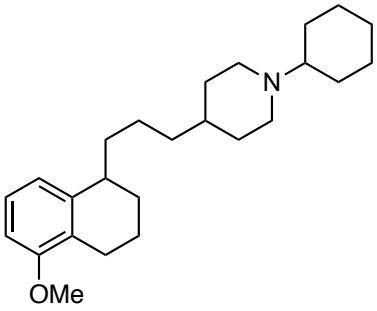

1.160

σ1R K_i (nM) = 1.1 ± 0.71
σ2R K_i (nM) = 26.6 ± 9.6
K_i ratio (σ1R/σ2R) = 0.04

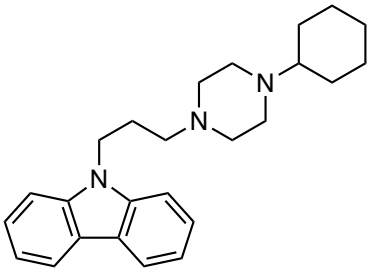

1.85
F281

σ1R K_i (nM) = 3,450 ± 1,660
σ2R K_i (nM) = 12.6 ± 3.2
K_i ratio (σ1R/σ2R) = 274

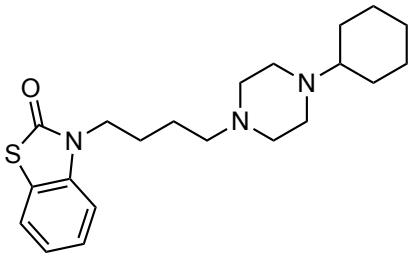

1.161

σ1R K_i (nM) = 4.17 ± 0.62
σ2R K_i (nM) = 0.39 ± 0.06
K_i ratio (σ1R/σ2R) = 11

Figure 1.37. Cyclohexylpiperazine analogs.

1.4.4.7 Sigma-2 Receptor Ligands: Summary

There are relatively few ligand classes that achieve high levels of selectivity for the σ2R over the σ1R and frequently such selective compounds were discovered by happenstance during extensive SAR investigations. A unifying pharmacophore model that is predictive for ligand design has not yet emerged. However, comparing the ligands discussed above reveals several principles that might guide future design strategies (Figure 1.38). The ligands are generally comprised of a cyclic tertiary amine site that a

has a hydrophobic substituent. This basic group is frequently either a piperidine or a piperazine ring that might be bridged by another carbocycle. The basic amine is typically flanked by two hydrophobic/aromatic groups, one that that is relatively close in proximity and another that is more distant. This model is quite similar to pharmacophore models proposed for the σ1R, and the structural diversity accommodated by both receptors increases the complexity of designing σ2R-selective ligands. Indeed, many ligands with high affinity for σ2R also have high affinity for the σ1R and obtaining selectivity relies on relatively subtle structural changes that disfavor interaction with the σ1R.

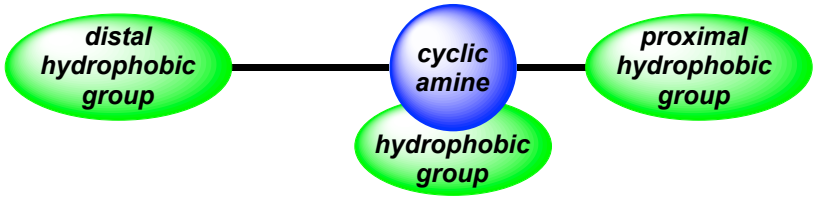

Figure 1.38. Hypothetical 2-D representation of a σ2R pharmacophore.

High affinity for the σ2R can be obtained with either a flexible or rigid linker that connects the distal hydrophobic/aromatic group to the amino group and shifting its position can have a dramatic effect on σ1R affinity. The optimal distance is not entirely clear and seems to exist within a variable range as demonstrated by the benzamide ligand class. A significant decrease in σ1R affinity was observed as the linker for 2,3-dimethoxybenzamide **1.153** was extended from two to four carbon atoms in **1.80**. In contrast, the structurally similar 2-methoxybenazmide **1.155** displayed an equally substantial decrease in σ1R affinity when the linker was shortened from four to two carbon atoms in **1.154**. During the SAR investigations of potential σ2R ligands, adjustments to the position of the distal hydrophobic/aromatic group might be critical for

obtaining selectivity, even if the preferred position is not necessarily obvious or predictable.

The position of the proximal hydrophobic group is also important for obtaining high σ2R affinity and selectivity over the σ1R, although it is again difficult to predict the optimal distance. Conformational restriction of this hydrophobic group seems to be somewhat more important and many ligands that display selectivity over the σ1R impart conformational rigidity with a carbocycle. This can be seen in the tetrahydroisoquinoline moiety of benzamide analogsthe spirocyclic ring fusion of siramesine (**1.90**), and the benzylidene moiety of (+)-benzomorphan-7-one analogs. However, the existence of multiple binding modes has been proposed and might present a challenge for discerning between the hydrophobic sites based on their relative position.[247] During the design of σ2R ligands, subtle perturbations in positioning of the proximal hydrophobic group and employing conformational restrictions can significantly impact subtype selectivity.

Variations in the substituents on these aromatic groups also significantly impacts σ1R affinity. For instance, incorporation of the 6,7-dimethoxy substituents on the tetrahydroisoquinoline of benzamide analogs produced a significant reduction in σ1R affinity as compared to the corresponding unsubstituted analog. Likewise, introduction of two chlorine atoms on the benzylidene moiety of the (+)-benzomorphan-7-one analogs had a synergistic effect that afforded a considerable decrease in σ1R affinity. Probing aryl substitution patterns is an important consideration during an SAR investigation of ligands targeting the σ2R.

These trends are unfortunately somewhat speculative and vague because they are based on general observations among the few selective σ2R ligands available. Structural information about the σ2R remains elusive, access to the cloned gene would facilitate mutation studies and homology models based upon the predicted structure of σ2R would

provide additional insights. However, the lack of σ2R selective ligands and an understanding of how they modulate biological pathway justifies additional efforts to design potent and selective σ2R binding ligands with favorable drug–like properties.

1.5 THE NORBENZOMORPHAN: A NEW CLASS OF SIGMA LIGANDS

1.5.1 Identification of Lead Compound Classes

As previously discussed, the Martin group developed a rapid process for construction of the halogenated norbenzomorphan scaffold **1.162**, and preliminary investigations revealed that some analogs had affinity for the σRs with selectivity favoring either σ2R or σ1R being observed in some instances. Intrigued by the medicinal relevance of the σ2R and the relative ambiguity of the protein, along with historical challenges of developing selective ligands, the possibility of developing a new molecular scaffold that selectivity targets the σ2R warranted additional investigations. Accordingly, the Martin group expanded the SAR study to probe diverse substitution patterns that might provide enhanced affinity and selectivity for the σ2R. The easily diversifiable core allowed for the incorporation of varied functionality via cross-coupling reactions with the aryl halide and nitrogen refunctionalization reactions, similar to the approach previously discussed (Scheme 1.6).

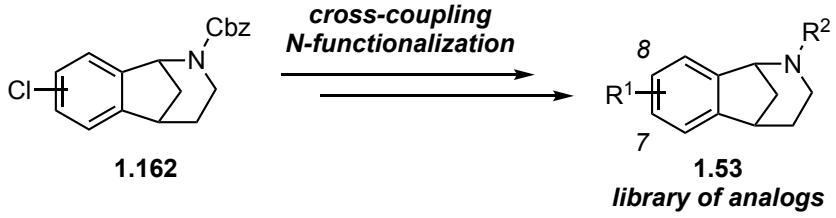

Scheme 1.6. General strategy for diversification of the norbenzomorphan core.

Among the ligands screened as part of the preliminary investigation, a subset emerged with discernable substitution patterns that provided favorable results, particularly with the piperazine substituted norbenzomorphans (**1.163**-**1.165**) (Figure 1.39). Installation of *N*-methylpiperazine at C-8 in **1.163** provided high affinity for the σ2R (<100 nM) with modest selectivity over the σ1R. The requisite basic nitrogen atom is located on the piperazine rather than the nitrogen atom of the norbenzomorphan core, which is instead acylated. Notably, the benzyl carbamate of **1.163** that was originally installed as a nitrogen protecting group provides similar levels of σ2R potency as the 3-chlorobenzamide derivative **1.164**, but with lower σ1R affinity that affords 9.3-fold selectivity. This might be attributed to minor changes in the positioning of the distal aromatic group in relation to the basic amine, similar to observations among known σ2R selective ligands. In addition, when the core nitrogen atom was functionalized as a benzyl carbamate, installation of the *N*-methylpiperazine at C-7 in **1.165** resulted in a significant increase in affinity for the σ1R, that is accompanied by a modest decrease in σ2R affinity. This reversed the σR selectivity preference to favor the σ1R, an interesting feature that might also result from the subtle changes in the position of the distal aromatic group with respect to the substituted basic nitrogen atom.

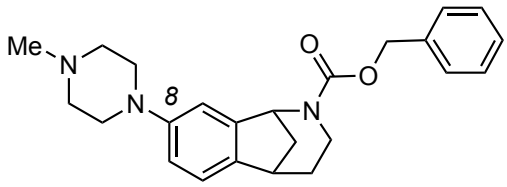

1.163

σ1R K_i (nM) = 841

σ2R K_i (nM) = 90

K_i ratio (σ1R/σ2R) = 9.3

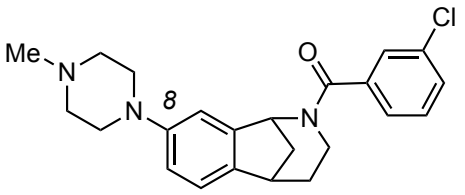

1.164

σ1R K_i (nM) = 203

σ2R K_i (nM) = 96

K_i ratio (σ1R/σ2R) = 2.1

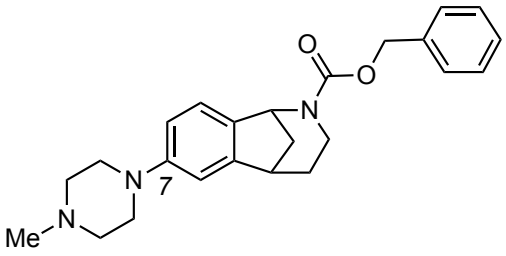

1.165

σ1R K_i (nM) = 63

σ2R K_i (nM) = 269

K_i ratio (σ1R/σ2R) = 0.23

Figure 1.39. Piperazine substituted norbenzomorphans with σR subtype selectivity.

Another series of norbenzomorphan analogs emerged, in which the core nitrogen atom served as the requisite basic amine (**1.166-1.170**) (Figure 1.40). In a subset of these derivatives the nitrogen atom was substituted with a benzyl group and variation of the substituent on the core arene ring had a significant effect on σR affinity. The unsubstituted arene **1.166** was nearly equipotent at σ1R and σ2R, but installation of a morpholine substituent at C–7 (**1.167**) increased affinity for the σ1R and decreased affinity for the σ2R. In contrast, incorporating the morpholine substituent at C–8 in dicholobenzyl analog **1.168** provided a considerable reduction in σ1R affinity in relation to unsubstituted analog **1.166** and afforded 32-fold selectivity for the σ2R. A similar result was obtained when an aryl group was installed at C–7 in **1.169** leading to a

preference for the σ1R, whereas introduction of an aromatic group at C–8 in the *N*–methyl analog **1.170** increased affinity for the σ2R and provided some selectivity.

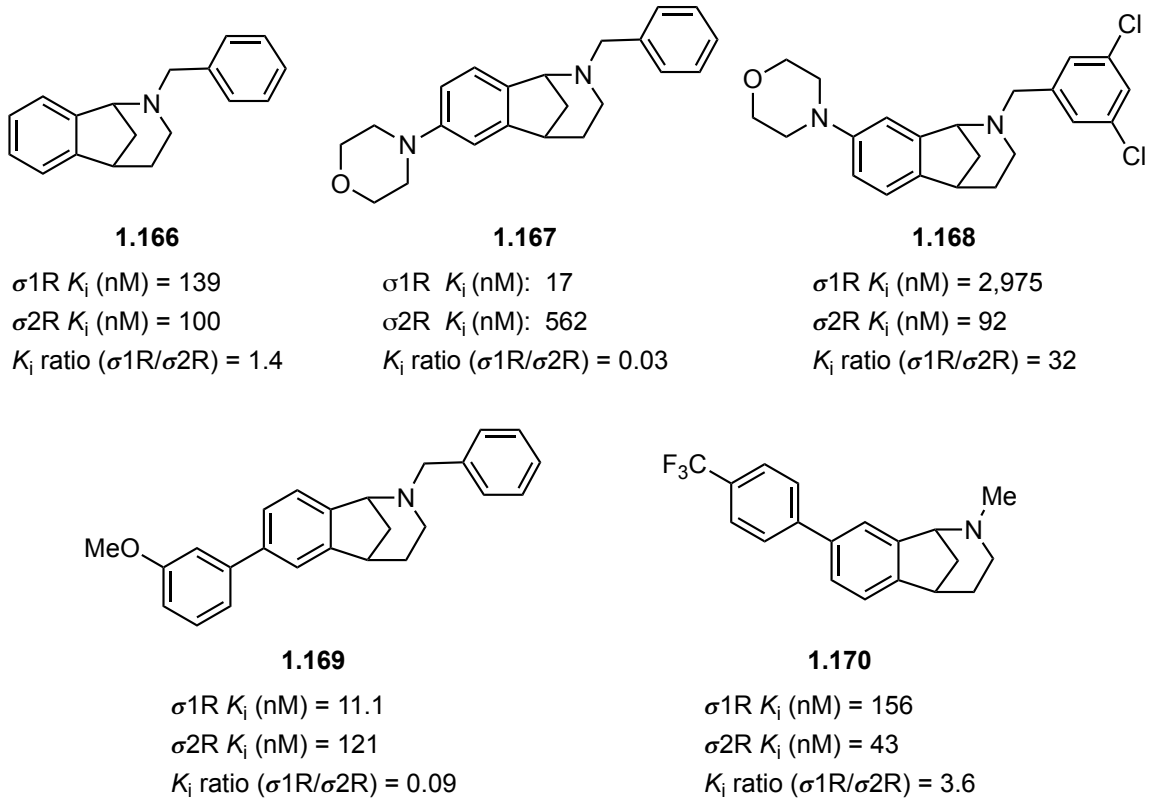

1.166

σ1R K_i (nM) = 139
σ2R K_i (nM) = 100
K_i ratio (σ1R/σ2R) = 1.4

1.167

σ1R K_i (nM): 17
σ2R K_i (nM): 562
K_i ratio (σ1R/σ2R) = 0.03

1.168

σ1R K_i (nM) = 2,975
σ2R K_i (nM) = 92
K_i ratio (σ1R/σ2R) = 32

1.169

σ1R K_i (nM) = 11.1
σ2R K_i (nM) = 121
K_i ratio (σ1R/σ2R) = 0.09

1.170

σ1R K_i (nM) = 156
σ2R K_i (nM) = 43
K_i ratio (σ1R/σ2R) = 3.6

Figure 1.40. Norbenzomorphans analogs with a basic amine in the core.

This preliminary SAR study highlighted several key structural features in lead compounds that inspired additional investigations. Critically, the scaffold existed in two distinct categories in which the requisite basic nitrogen atom was incorporated either as an substituent on the benzene ring of the norbenzomorphan scaffold or by the norbenzomorphan nitrogen atom. In both cases, substitution at the C–8 position favored the σ2R, whereas substitution at C–7 favored the σ1R. Substitution of the norbenzomorphan benzene ring with a piperazine group provided favorable σ2R affinity

particularly when the core nitrogen was functionalized as a benzyl carbamate, as exemplified by lead compound **1.163**. Alternatively, substitution on the arene ring with a morpholine or aryl group also provided high σ2R affinity and modest selectivity as demonstrated by compounds **1.168** and **1.170**.

The Martin group was particularly interested in pursuing the σ2R because little was known about its role in neuroscience and it therefore presented fertile ground for discovery. The optimal structural arrangement for favoring the σ2R was not clear, but preliminary investigations revealed that subtle changes in substitution patterns and spatial orientation of these groups could have a dramatic effect on subtype selectivity. Accordingly, a multifaceted SAR study was devised for continued investigation of the norbenzomorphan substitution pattern to favor the σ2R. In addition, a concurrent scaffold simplification initiative to assess the importance of some norbenzomorphan structural features and to provide alternative lead scaffolds that might have more favorable properties was also conducted.

1.5.2 SAR of the Piperazine Substituted Norbenzomorphan Scaffold

The piperazine substituted norbenzomorphan scaffold presented several opportunities for this SAR effort (Figure 1.41). The basic nitrogen is a critical pharmacophore element of ligands that bind σRs, thus it stands to reason that modifications to the nitrogen substituent might have considerable impact on σR selectivity. Interestingly, relatively little information is available from the literature about systematic alteration of *N*-substituents in σ2R selective ligands because it has typically been part of a constrained ring system and substituted with an alkyl spacer group that connects to the distal hydrophobic/aromatic group.[203] The cyclohexylpiperazine analogs provide the closest comparison (Figure 1.37), but those analogs displayed little σ2R

selectivity. Early results suggested that the position of the piperazine substituent on the arene core is important with placement at C–8 favoring the σ2R.

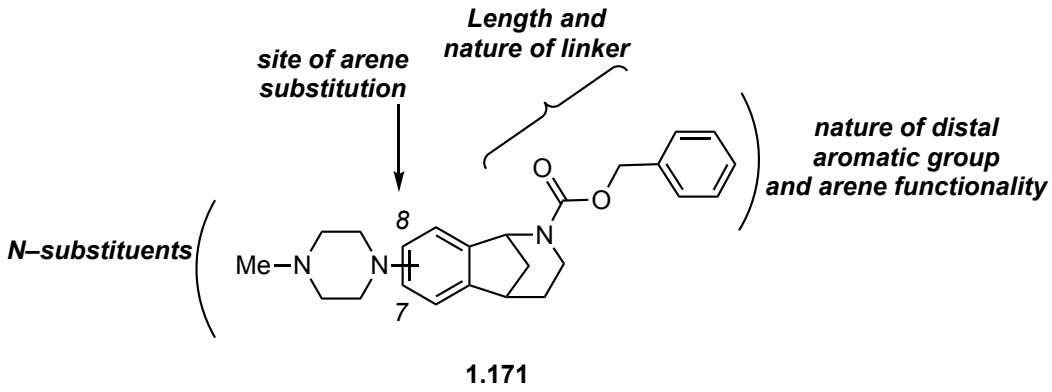

Figure 1.41. Strategy for SAR investigation of piperazine substituted norbenzomorphan scaffold

The nitrogen atom of the norbenzomorphan core is functionalized with a carbamate linker attached to aromatic group that presented several areas for an SAR investigation (Figure 1.41). Many σ2R selective ligands have a hydrogen bond acceptor (HBA) group such as the benzyl carbamate of 1.17, but assessing its contribution to the binding profile would require additional investigation. The distal hydrophobic/aromatic group is known to have a significant effect on the binding profile suggesting that both the position and nature of that group should be examined. Likewise, substituents on the distal aromatic group have been previously observed to impart selectivity and were therefore targeted for further SAR analysis. A large number of compounds were prepared, but this discussion will summarize general trends from the SAR investigation as represented by a subset of those analogs.

1.5.2.1 Investigation of the Linker and Distal Aromatic Group

The SAR investigation commenced with evaluation of the distal aromatic group and the linker that connects it to the scaffold. The *N*–methylpiperazine from lead compound **1.163** was maintained for comparison (Figure 1.39). The C–8 halogenated norbenzomorphan **1.51** was prepared according to the previously discussed MCAP procedure and then diversified to a variety of analogs for analysis. Subsequent Buchwald-Hartwig cross-coupling of **1.51** using $Pd(OAc)_2$ and JohnPhos with an excess of piperazine (**1.172**) afforded the substituted norbenzomorphan **1.173** in 72% yield,[50] followed by reductive amination with paraformaldehyde to provide the *N*–methylated analog **1.163** (Scheme 1.7).[4] Reductive removal of the Cbz-protecting group in **1.163** produced impurities that were difficult to separate.[263] Alternatively stirring a solution of **1.163** in CH_2Cl_2 with TMSI followed by acidic workup provided the deprotected product **1.174** in 88% yield. The core nitrogen atom was subjected to a variety of *N*-functionalization reactions including acylation with acyl chlorides, chloroformates, and isocyanates or sulfonylation to afford final analogs.[4,9,263]

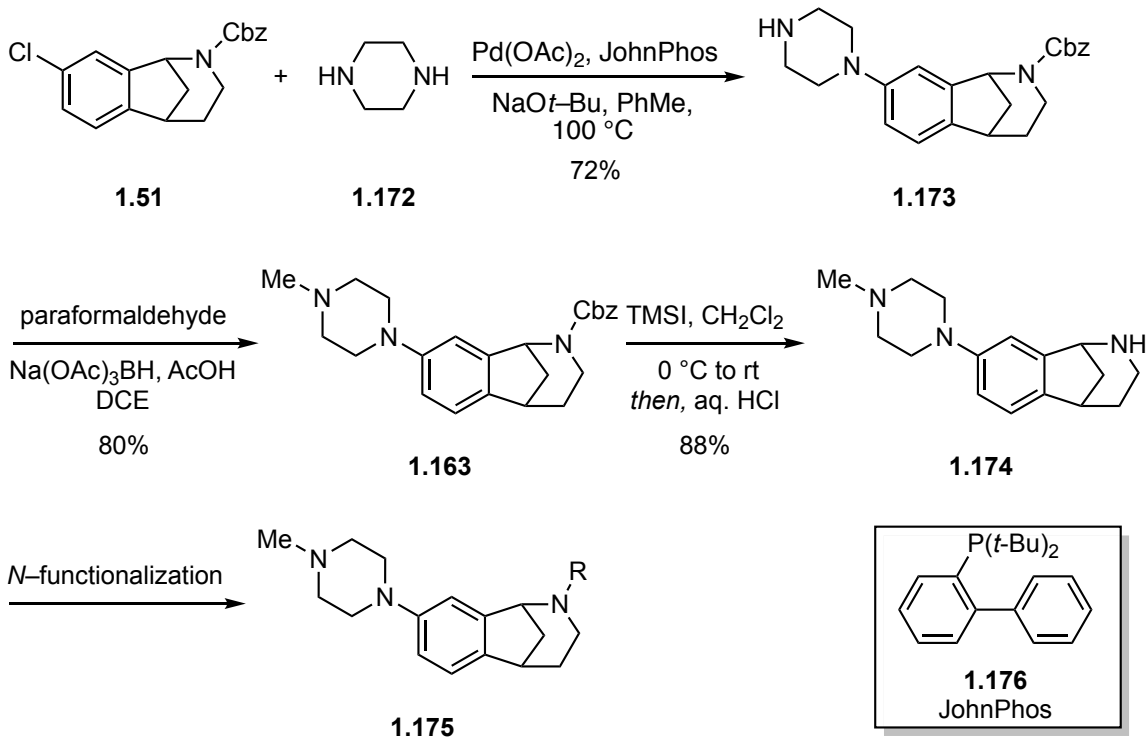

Scheme 1.7. General strategy for diversification of the norbenzomorphan core nitrogen.

The SAR investigation of the distal aromatic group of the and the linker connecting it to the norbenzomorphan scaffold indicated the significance of this group for maintaining high affinity and selectivity for the σ2R (Table 1.6).[263] The carbamate functionality of the linker in **1.163** was first examined by replacing the benzylic oxygen atom with a nitrogen atom and a carbon in **1.176** and amide **1.177**, respectively. Both suffered similar decreases in σ2R affinity in comparison to carbamate **1.163**, but amide **1.177** also displayed increased affinity for the σ1R. Decreasing the length of the linker in the amide group also had a negative effect on σ2R selectivity. Compared with the two-carbon spacer in amide **1.177**, the single methylene linker **1.178** provided reduced affinity for the σ2R and increased affinity for σ1R, whereas potency was diminished for both σRs with benzamide **1.179**. Similarly, phenyl carbamate **1.180** displayed reduced

affinity for both σRs, as compared to benzyl carbamate **1.163** with an additional methylene spacer. Replacement of the benzyl carbamate moiety with an alloc group (**1.183**) also diminished σR affinity indicating the importance of the aromatic group, as opposed to an alternative unsaturated alkyl group. Likewise, removal of the benzyl carbamate functionality eliminated detectable σR binding in acetamide analog **1.184** and unsubstituted amine analog **1.174**.

Table 1.6. Binding affinity of *N*-methylpiperazine-norbenzomorphan analogs.

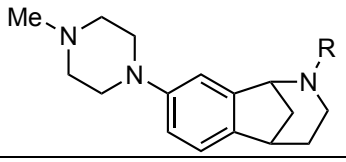

		K_i (nM)		K_i ratio
Cmpd.	R	σ1R	σ2R	(σ1R/σ2R)
1.163	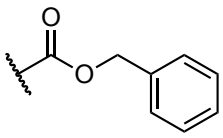	841	89.7	9.4
1.176	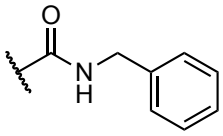	935	360	2.6
1.177	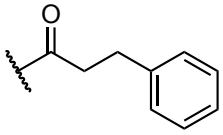	294	357	0.82
1.178	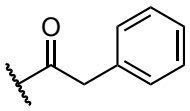	431	930	0.46

Table 1.6. Binding affinity of *N*-methylpiperazine-norbenzomorphan analogs.

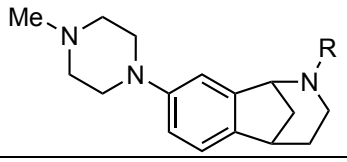

		K_i (nM)		K_i ratio
Cmpd.	R	σ1R	σ2R	(σ1R/σ2R)
1.179	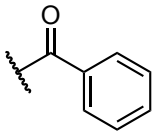	1,875	1,642	1.1
1.180	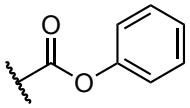	>10,000	445	> 22
1.181	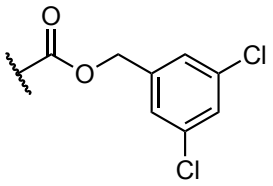	428	31	14
1.182	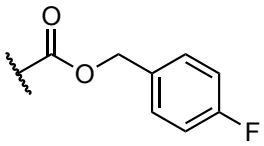	264	37	7.1
1.183	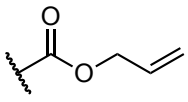	2,105	442	4.8
1.184		>10,000	>10,000	N/A

Table 1.6. Binding affinity of *N*-methylpiperazine-norbenzomorphan analogs.

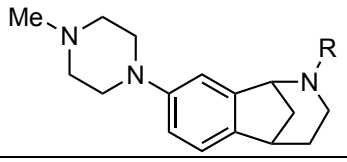

		K_i (nM)		K_i ratio
Cmpd.	R	σ1R	σ2R	(σ1R/σ2R)
1.174		>10,000	>10,000	N/A
1.185	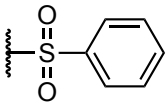	>10,000	764	>13
1.186	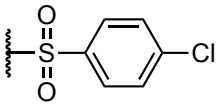	476	309	1.5
1.187	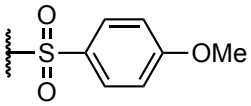	664	301	2.2
1.188	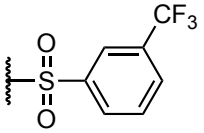	73	41	1.8

Table 1.6. Binding affinity of *N*-methylpiperazine-norbenzomorphan analogs.

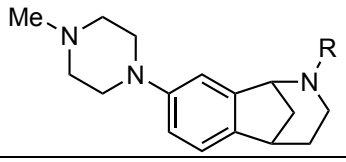

		K_i (nM)		K_i ratio
Cmpd.	R	σ1R	σ2R	(σ1R/σ2R)
1.189	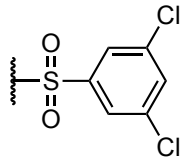	442	27	16

K_i values determined from non-linear regression of radioligand competition binding isotherms by PDSP. Unless indicated otherwise, σ1R was sourced from guinea pig brain and σ2R was sourced from rat PC12 cells.

The positional requirements of the distal aromatic group could also be satisfied if the core nitrogen atom was functionalized as an aryl sulfonamide, although a sensitivity to aryl substituents was evident within this series (Table 1.6). Namely, σ2R binding of the unsubstituted aryl sulfonamide **1.185** was much less favorable than the benzyl carbamate **1.163**. However, the corresponding substituted analogs **1.186** and **1.187** were more potent for both σRs than **1.185**, with little subtype selectivity. Interestingly, the 3,5-dichloro analog **1.189** increased affinity for the σ2R and provided 16-fold selectivity. The trifluoromethyl–substituted analog **1.188** exhibited σ2R affinity that was similar to **1.189**, but also increased affinity for the σ1R leading to little selectivity. The same trend was observed for the benzyl carbamate series in which the 3,5-dichlorobenzyl analog **1.181** had a notable increase in σ2R affinity relative to **1.163** with a less pronounced change at σ1R that afforded 14-fold selectivity. Likewise, the fluorobenzyl carbamate analog **1.182** displayed increased affinity for both σRs with only 7.1-fold subtype selectivity. The

optimal aromatic substitution pattern requires more investigation, but consistent with other selective σ2R ligands, dichlorination at this site appears to be favorable.

Collectively, these data indicate that the distal aromatic group is a key pharmacophore element of the piperazine substituted norbenzomorphan scaffold. Relatively minor changes in its position that result from alterations in the length and composition of the linker can lead to large shifts in σ1R and σ2R affinity, although the exact orientation of the aryl group that is preferred is not clear. Additonally, aryl substituents on the distal aromatic group can also lead to increased affinity for the σ1R and σ2R that can either enhance or diminish σ2R selectivity. Among the *N*-acylated analogs, functionalization of the core nitrogen atom as a benzyl carbamate seems to provide the favorable σ2R affinity and selectivity.

1.5.2.2 Investigation of Piperazine Substituents

Having identified that the benzyl carbamate functionality on the norbenzomorphan core nitrogen atom delivered generally favorable σ2R selectivity, attention turned toward the piperazine nitrogen-substituent. The unsubstituted piperazine **1.173**, previously prepared by cross-coupling with the halogenated norbenzomorphan core, was subjected to a variety of *N*–functionalization reactions including reaction with alkyl halides, reductive alkylation, and conjugate addition to various Michael acceptors to access a series of analogs to assess the effects of different aliphatic substituents at the piperazine nitrogen atom.[4,9,263]

A trend emerged in which an increase in size of the aliphatic substituent led to higher affinity for the σ1R and σ2R (Table 1.7).[4,9,263] For example, as the length of the linear alkyl group was increased from methyl (**1.163**) to propyl (**1.191**), the affinity increased for both σRs, but the increase was more pronounced for σ2R, achieving 5.1 nM

affinity and 45-fold selectivity over the σ1R for the propyl piperazine analog **1.191**. The same trend was observed for analogs with branched alkyl groups (**1.192-1.193**). Similarly, cyclic alkyl groups (**1.194-1.196**) displayed high affinity for the σRs that favored σ2R selectivity, but larger carbocycles also increased affinity for the σ1R, thereby eroding selectivity. Thus, the cyclobutyl **1.194** and cyclopentyl **1.195** analogs were 42 and 36–fold selective for σ2R, respectively, whereas the cyclohexyl analog **1.196** was only 2.4–fold selective. Aliphatic substituents from three to five–carbon atoms typically provide greater than 10 nM affinity for the σ2R and 30-fold selectivity.

Table 1.7. Binding affinity of saturated piperazine substituents

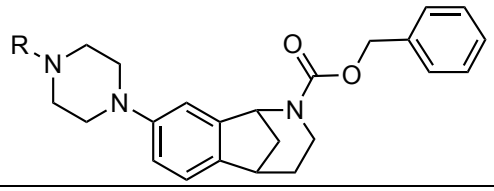

		K_i (nM)		K_i ratio
Cmpd.	R	σ1R	σ2R	(σ1R/σ2R)
1.163		841	89.7	9.4
1.190	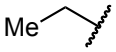	600	32.5	18
1.191	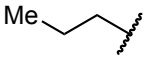	230	5.1	45
1.192	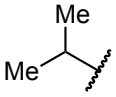	473	14.5	33
1.193	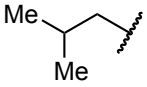	111	1.8	62
1.194	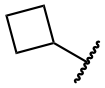	208	5.0	42
1.195	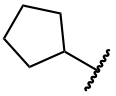	130	3.6	36
1.196	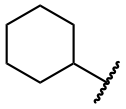	29.8	12.5	2.4

K_i values determined from non-linear regression of radioligand competition binding isotherms by PDSP. Unless indicated otherwise, σ1R was sourced from guinea pig brain and σ2R was sourced from rat PC12 cells.

A similar series was prepared to assess the effects of unsaturated *N*-alkyl substituents (Table 1.8).[4,9,263] The introduction of unsaturation in **1.197** decreased affinity for σ1R and σ2R as observed with analog **1.191**. The isobutylene analog **1.198**

provided results that were similar to the propyl piperazine analog **1.191**, although somewhat less potent and selective. Introduction of a benzyl group (**1.200**) was also less favorable, leading to an increase in σ1R affinity and eroding selectivity to 1.5–fold, which again suggests that large hydrophobic groups in this region favor the σ1R.

Table 1.8. Binding affinity of unsaturated piperazine substituents

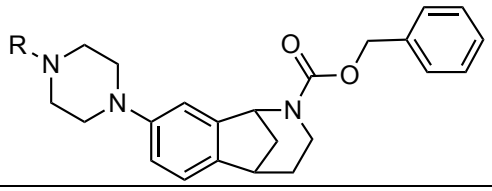

		K_i (nM)		K_i ratio
Cmpd.	R	σ1R	σ2R	(σ1R/σ2R)
1.191	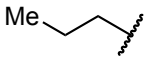	230	5.1	45
1.197	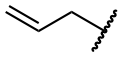	931	76.4	12
1.198	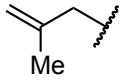	413	17.5	24
1.199	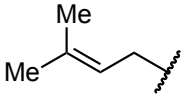	62	23	2.7
1.200	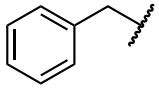	119	80.8	1.5

K_i values determined from non-linear regression of radioligand competition binding isotherms by PDSP. Unless indicated otherwise, σ1R was sourced from guinea pig brain and σ2R was sourced from rat PC12 cells.

A series of analogs that incorporated polar functional groups on the aliphatic substituent was also evaluated (Table 1.9).[4,9,263] Interestingly, many of these analogs displayed dramatically lower affinity for the σ1R. For instance, both the ethyl alcohol **1.201** and propyl alcohol **1.202** analogs exhibited decreased affinity for the σ1R relative

to the corresponding aliphatic analogs **1.190** and **1.163**, respectively, but affinities for the σ2R were relatively in comparison, thereby increasing selectivity. A similar effect was noted for the substituents with a carbonyl moiety, such as ethyl ester analog **1.203**, which achieved micromolar affinity for the σ1R and 280-fold σ2R selectivity, albeit with a modest decrease in σ2R affinity. Similar results were obtained with amide **1.204** and nitrile **1.205**, although with some reduction in σ2R affinity. Introduction of cyclic alkyl substituents containing a heteroatom, such as tetrahydropyran **1.206** and *N*-methylpiperidine **1.207**, led to a more modest reduction in σ1R affinity, but these analogs still provided a relative increase in selectivity as compared to the corresponding aliphatic substituents.

Table 1.9. Binding affinity of polar piperazine substituents

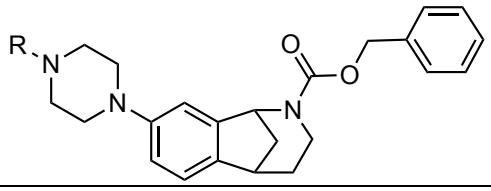

		K_i (nM)		K_i ratio
Cmpd.	R	σ1R	σ2R	(σ1R/σ2R)
1.191	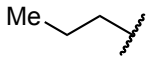	230	5.1	45
1.201	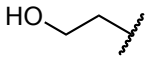	1,1216	39	31
1.202	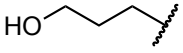	524	5	105
1.203	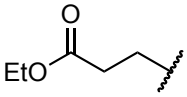	6,660	23.8	280
1.204	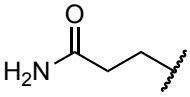	3,919	45	87
1.205	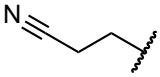	5,890	414	14
1.206	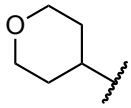	121	3.5	35
1.207	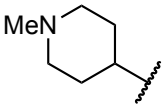	150	26	5.8

K_i values determined from non-linear regression of radioligand competition binding isotherms by PDSP. Unless indicated otherwise, σ1R was sourced from guinea pig brain and σ2R was sourced from rat PC12 cells.

Investigation of substituents at the piperazine nitrogen atom revealed several interesting trends for modulating σR selectivity. Generally high affinity for the σ2R is observed for a variety of groups at this position, and there is more variability in affinity for the σ1R. There are limits with respect to the size of the hydrophobic group, and as the size increases the σ2R selectivity is eroded by increasing σ1R affinity. The optimal σ2R selectivity seems to be obtained with saturated aliphatic substituents that contain three-to five–carbon atoms. Incorporating polar functional groups on the nitrogen substituent produces a pronounced reduction in binding at the σ1R and represents a significant mechanism for modulating σ2R selectivity. The effect was particularly favorable with alcohol or ester functional groups positioned two to three carbon-atoms from the amine. The specific negative interaction with the σ1R binding site that produces this effect is not clear, but the close proximity of the polar functional group to the essential basic amine site of the ligand suggests that it might be disrupting this key ligand-protein interaction is some way. For instance, the electron withdrawing nature of this group likely results in decreased basicity of the nitrogen atom that might weaken the formation of the critical salt-bridge that was previously observed in the crystal structure of the σ1R.[6,154,264] While the exact mechanism requires additional investigation, the fact that the reduction in potency in more pronounced for the σ1R than the σ2R is a meaningful finding and it might allow for additional optimization in the future.

1.5.2.3 Site of Piperazine Installation on the Norbenzomorphan Core

As previously discussed, installation of the piperazine ring at the C–8 position of the norbenzomorphan core seemed to provide enhanced selectivity for the σ2R over the σ1R. However, after a more thorough investigation of the SAR revealed optimal piperazine substituents, this hypothesis was again tested with several sets of C–7 and C–8

substituted analogs (Table 1.10).[9] Interestingly, installing the N-substituted piperazine at the C–7 position resulted in a a modest decrease in σ2R affinity that was accompanied by a significant increase in σ1R affinity. The result was a reversal in the subtype preference that switched from favoring the σ2R at the C–8 position to favoring the σ1R at the C–7 position for each analog tested (**1.208**-**1.211**). This was even true for C–7 ethyl ester analog **1.211** that displays a slight preference for the σ1R, but the corresponding C–8 analog **1.203** displayed 280-fold selectivity for the σ2R.

Table 1.10. Binding affinity of unsaturated piperazine substituents

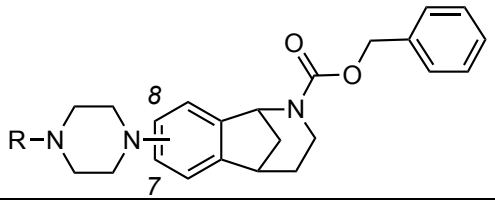

			K_i (nM)		K_i ratio
Cmpd.	R	C–7/C–8	σ1R	σ2R	(σ1R/σ2R)
1.208	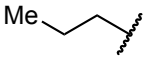	C–7	8.7	29.3	0.30
1.163		C–8	230	5.1	45
1.209	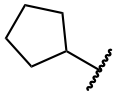	C–7	4.6	11.1	0.41
1.195		C–8	130	3.6	36
1.210	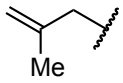	C–7	18.5	46.7	0.40
1.198		C–8	413	17.5	24
1.211	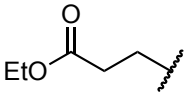	C–7	108	111	0.97
1.203		C–8	6,660	23.8	280

K_i values determined from non-linear regression of radioligand competition binding isotherms by PDSP. Unless indicated otherwise, σ1R was sourced from guinea pig brain and σ2R was sourced from rat PC12 cells.

The discovery that the orientation of a substituent on the norbenzomorphan scaffold leads to changes in σR subtype selectivity is highly notable. It was somewhat surprising that merely changing the position of the substituent could have such a dramatic effect. Although limited in predictive power, the pharmacophore models that have been proposed for both the σ1R and σ2R have suggested optimal positions for the proximal

and distal hydrophobic sites in relation to the basic amine site. In this case, shifting the basic amine site to the C–7 position of the norbenzomorphan scaffold alters its relative position in relation to the distal hydrophobic site in a way that is more favorable for the σ1R. Indeed, a related trend was observed within the benzamide ligand class, in which changing the length of the spacer group between the benzamide moiety and the tetrahydroisoquinoline by two methylene groups produced a remarkable decrease in σ1R affinity, while σ2R was relatively unaffected (Table 1.5). This likely represents a similar alteration in the position of the distal hydrophobic group relative to the basic amine site. It is interesting that the σ2R seems to be less sensitive to this change, suggesting that this is a structural feature that can be used to bias against σ1R interaction. If this speculation is correct, then the rigidity of the norbenzomorphan scaffold might provide a useful mechanism to control the position of these groups and might be optimized in future studies.

1.5.2.4 Enantiomeric Preference of The Piperazine-Substituted Norbenzomorphan

The σ2R was defined based on the preference of (+)-benzomorphans to bind the σ1R, but not the σ2R. It is therefore not surprising that some ligand classes have displayed enhanced σ2R selectivity for a particular enantiomer. As previously discussed, the (-)–benzomorphan-7-one CB-182 (**1.112**) possessed high affinity for both σR subtypes, but the (+)-enantiomer CB-184 (**1.111**) had greatly reduced σ1R affinity and achieved 554-fold selectivity for the σ2R. It therefore stands to reason that the norbenzomorphan scaffold might also display an enantiomeric preference. Accordingly, the enantiomers of the *N*-propylpiperazine analog **1.191** were separated via chiral HPLC and evaluated individually.[263] Both enantiomers (**1.212-1.213**) possessed nearly identical affinity for the σ1R, which was relatively unchanged from the racemic mixture (σ1R K_i

= 230 nM) (Figure 1.42). However, **1.212** showed a modest decrease in affinity for the σ2R as compared to the racemic mixture (σ2R K_i = 5.1 nM), the affinity of **1.213** for the σ2R was nearly identical to the racemic mixture. It is interesting that a more pronounced difference was not observed. However, this might be because the source of chirality is not in close proximity to the basic amine site of the piperazine-substituted norbenzomorphan as it is in the benzomorphan-7-one ligands.

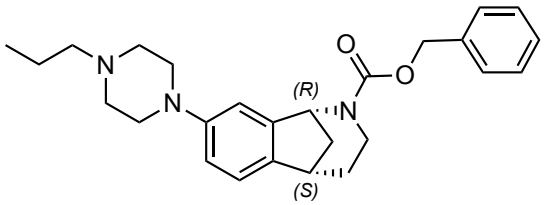

1.212

σ1R K_i (nM) = 250
σ2R K_i (nM) = 20
K_i ratio (σ1R/σ2R) = 13

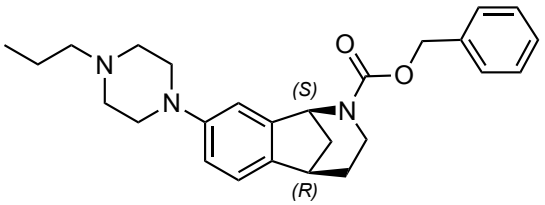

1.213

σ1R K_i (nM) = 251
σ2R K_i (nM) = 2.7
K_i ratio (σ1R/σ2R) = 93

Figure 1.42. Binding affinity of enantiomerically pure *N*-propylpiperazine analogs.

1.5.2.5 Other Structural Features of the Piperazine-Substituted Norbenzomorphan

Having investigated a wide variety of substitution patterns on the piperazine-substituted norbenzomorphan, a few analogs were prepared to interrogate structural features of the scaffold. As previously discussed, many high affinity σ2R ligands contain a basic nitrogen atom within a constrained ring system, commonly a piperidine nitrogen atom. The contribution of the less basic, aniline nitrogen of the piperazine substituted norbenzomorphan was not clear as it may not be involved in interactions with acidic residues of the protein. Accordingly, the aniline nitrogen atom in **1.191** was removed in piperidine analog **1.214**, which maintained high affinity for the σ2R (Figure 1.43). However, a modest increase in σ1R affinity that eroded selectivity was also observed.

This finding suggests that the aniline nitrogen of the piperazine ring is beneficial for enhancing σ2R selectivity and thus was maintained in ongoing SAR studies.

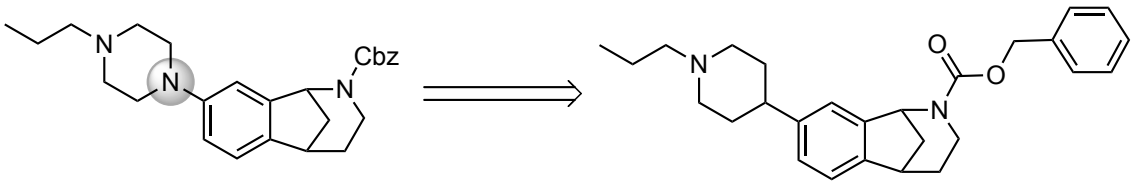

1.191
σ1R K_i (nM) = 230
σ2R K_i (nM) = 5.1
K_i ratio (σ1R/σ2R) = 45

1.214
σ1R K_i (nM) = 132
σ2R K_i (nM) = 9.7
K_i ratio (σ1R/σ2R) = 14

Figure 1.43. A propylpiperidine analog of the norbenzomorphan scaffold.

The norbenzomorphan scaffold possessing a bridged 7-membered ring system was the primary subject of SAR investigations. As part of ongoing efforts in the Martin group to assess the effect of different structural modifications of the norbenzomorphan scaffold, compounds having the expanded methanobenzazocine ring in **1.215** were also evaluated (Figure 1.44). The ring expanded analog maintained high σ2R affinity, but an increase in σ1R affinity was also observed that eroded selectivity.

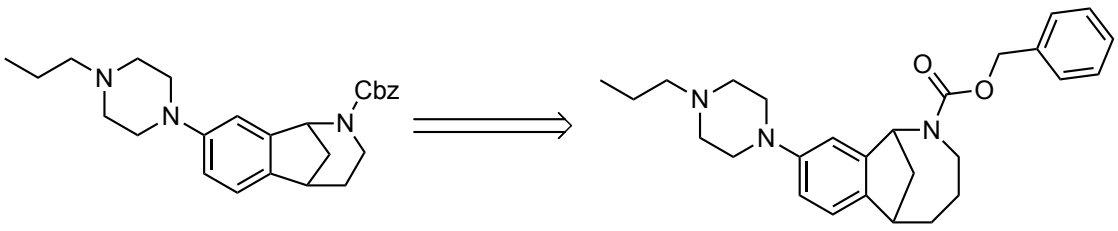

1.191
σ1R K_i (nM) = 230
σ2R K_i (nM) = 5.1
K_i ratio (σ1R/σ2R) = 45

1.215
σ1R K_i (nM) = 70
σ2R K_i (nM) = 8.3
K_i ratio (σ1R/σ2R) = 8.4

Figure 1.44. Binding affinity of a ring expanded methanobenzazocine analog.

1.5.3 The Aryl-Substituted Norbenzomorphan Scaffold

An alternative substitution pattern of the norbenzomorphan core is one in which the nitrogen atom of the norbenzomorphan ring provides the requisite basic amine site and was also evaluated during early investigations of the scaffold. Thus, a brief overview of SAR features of this scaffold is also warranted. As previously discussed, substitution of the norbenzomorphan core with an aryl substituent at C–8 provided high affinity σ2R ligands. Specifically, the 4-trifluoromethylphenyl substituent led to high σ2R affinity and selectivity and inspired examination of an expanded series in which the *N*-alkyl group was varied (Table 1.11).

Table 1.11. Binding affinity of biaryl analogs.

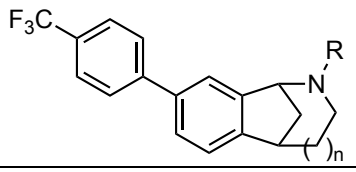

			K_i (nM)		K_i ratio
Cmpd. (name)	R	n	σ1R	σ2R	(σ1R/σ2R)
1.170		1	156	43	3.6
1.216	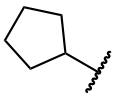	1	609[a]	82[b]	7.4
1.217 (DKR-1051)	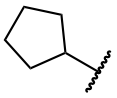	2	556	61	9.1
1.218	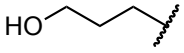	1	154 [a]	19 [b]	8.1
1.219 (UKH-1114)	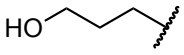	2	1,279	46	28
1.220	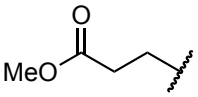	2	3,049	59	52
1.221		2	27 [a]	21 [b]	1.3

K_i values determined from non-linear regression of radioligand competition binding isotherms by PDSP. Unless indicated otherwise, σ1R was sourced from guinea pig brain and σ2R was sourced from rat PC12 cells. [a] determined using HEK293 cells expressing recombinant human σ1R. [b] determined using HEK293 cells expressing recombinant human σ2R/TMEM97.

The *N*-methyl analog **1.170** displayed modest affinity for the σ2R, but low selectivity over the σ1R. An *N*–cyclopentyl group in **1.216** reduced affinity for both σRs, but the effect was the effect more pronounced for the σ1R leading to 7.4-fold selectivity

favoring the σ2R.[4] A similar trend was observed for the corresponding ring-expanded methanobenzazocine DKR-1051 (**1.217**) as compared to **1.170**.[11] Introduction of a propyl alcohol substituent on norbenzomorphan **1.218** increased affinity for both σRs, but retained 8.1-fold selectivity favoring the σ2R. The corresponding methanobenzazocine UKH-1114 (**1.219**) showed a considerable reduction in σ1R affinity that afforded 28-fold selectivity for the σ2R.[11] The reason for the difference between the two ring sizes is not clear, but the methanobenzocine provides higher levels of selectivity. The ring expanded analog with an ester substituent (**1.220**) also displayed decreased σ1R affinity with 52-fold selectivity for the σ2R. The importance of an *N*-alkyl substituent at this position was confirmed with the unsubstituted analog **1.221** which achieves high potency for both σRs, but is not subtype selective.

It is interesting that similar SAR trends are observed for norbenzomorphan and methanobenzazocine analogs that possesses the basic amine moiety within the heterocyclic scaffold or as a substituent on the arene core. In both cases, hydrophobic substituents at the basic nitrogen are increase σR affinity and incorporation of a polar functional group on those substituents diminshes σ1R affinity. Likewise, each displays optimal σ2R selectivity when the piperazine or aryl group is installed at the C–8 position of the scaffold. Although the methanobenzazocine JVW-1034 (**1.222**) also achieves high affinity for the σ2R with modest selectivity over σ1R, when a chlorine is installed at the C–8 position (Figure 1.45).[13]

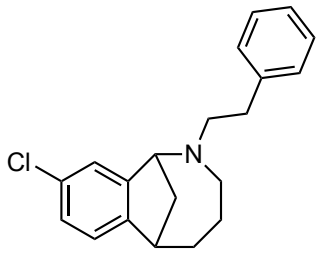

1.222
JVW-1034
σ1R K_i (nM) = 248
σ2R K_i (nM) = 23
K_i ratio (σ1R/σ2R) = 11

Figure 1.45. Binding affinity of the chloro-substituted methanobenzazocine analog.

1.5.4 Norbenzomorphan Ligands in Neuropsychiatric Disorders

1.5.4.1 The Sigma-2 Receptor as a Therapeutic Target for Neurological Disorders

It is unsurprising that the σ2R has attracted considerable attention with respect to a role in cancer given its significant overexpression in malignant cells, but its demonstrated role in cell survival and wide expression in the CNS suggests that it might also be an intriguing target for neurological disorders.[170] It is therefore somewhat perplexing that this area of research has received significantly less attention, particularly since the pharmacologically similar σ1R has been implicated in a variety of CNS disorders. Indeed the σ2R was defined by its ability to bind some neuroleptic drugs and psychotomimetic compounds.[75,76] However more recently, evidence has emerged that the σ2R might be a target for a range of difficult-to-treat neurological disorders, and the Martin group has been at the forefront of this area of research with pioneering studies that utilize the norbenzomorphan scaffold.[208]

1.5.4.2 Norbenzomorphan Ligands and APP Induced Neurodegeneration

Because the σ1R is associated with a range of CNS disorders, but little was known about the role of the σ2R in neurological disorders, and the recent discovery that norbenzomorphan analogs were capable of selectively modulating the σ2R, the Martin group was inspired to investigate the effects of these compounds in models of neurodegeneration. A *Caenorhabditis elegans (C. elegans)* model that mimics age-related neurodegeneration associated with AD was recently developed by the Pierce-Shimomura group at the University of Texas at Austin, providing a promising assay for assessing ligands that bind the σ2R as potential neuroprotective agents.[12] In humans, the amyloid precursor protein (APP) is produced in large quantities in neurons and processed to produce β-amyloid protein (Aβ), but genetic mutation of the human APP gene gives rise to Aβ accumulation that is correlated with AD progression.[265] *C. elegans* have orthologs for approximately two-thirds of all human genes and work by the Pierce-Shimomura group revealed that inserting a single copy of the human amyloid precursor protein (SC_APP) 695 gene into the worm genome results in age-dependent degeneration of cholinergic neurons, similar to AD progression in humans.[12,266] These neurons can be labeled with green fluorescent protein for visualization of progressive neurodegeneration.

The gene that codes for the σ2R was not known and thus, an ortholog had not been identified in *C. elegans,* but the worm possesses the PGRMC1 ortholog vem–1.[267] The increase in neurodegeneration associated with SC_APP in the worm model was reduced to control levels upon genetic knockout of vem-1, suggesting that PGRMC1 might be involved in the SC_APP associated degenerative pathway.[12] As previously discussed, evidence indicated that the PGRCM1 and σ2R are not synonymous and the true genetic identity of the σ2R was unknown, but work by Mach *et al*. suggested the two proteins might be associated to some extent.[221] As a result, the worm model could

provide some insights on the ability of σ2R ligands to recapitulate the diminished neurodegenerative effects of vem-1 knock out.

The Martin group pursued a collaboration with the Pierce-Shimomura group to assess the effects of σ2R selective norbenzomorphans in the SC_APP worm model. Gratifyingly, treating the SC_APP worm with SAS-0132 (**1.163**) and JVW-1009 (**1.55**) reduced neurodegeneration as compared to the control SC_APP worm that was administered vehicle only (Figure 1.46).[12] Conversely, DKR-1051 (**1.217**) and DKR-1005 (**1.168**) led to enhanced neurodegeneration relative to the control SC_APP worm. Genetic knockdown of vem-1 with RNA*i,* both in the presence and absence of SAS-0132 (**1.163**) and JVW-1009 (**1.55**), provided similar levels of diminished neurodegeneration, thus supporting a hypothesis that the σ2R binding ligands acted through the vem-1 pathway.[12] Moreover, SAS-0132 (**1.163**) improved cognitive performance, and rescued AD–related behavioral deficits in the Thy-1 $hAPP^{Lond/Swe+}$ transgenic mouse model of AD. Interestingly, it also provided enhanced cognitive performance in healthy wild-type mice.[12] Collectively these result suggest that ligands that modulate the σ2R can alleviate Aβ–induced neurodegeneration and improve cognitive deficits associated with animal models of AD.

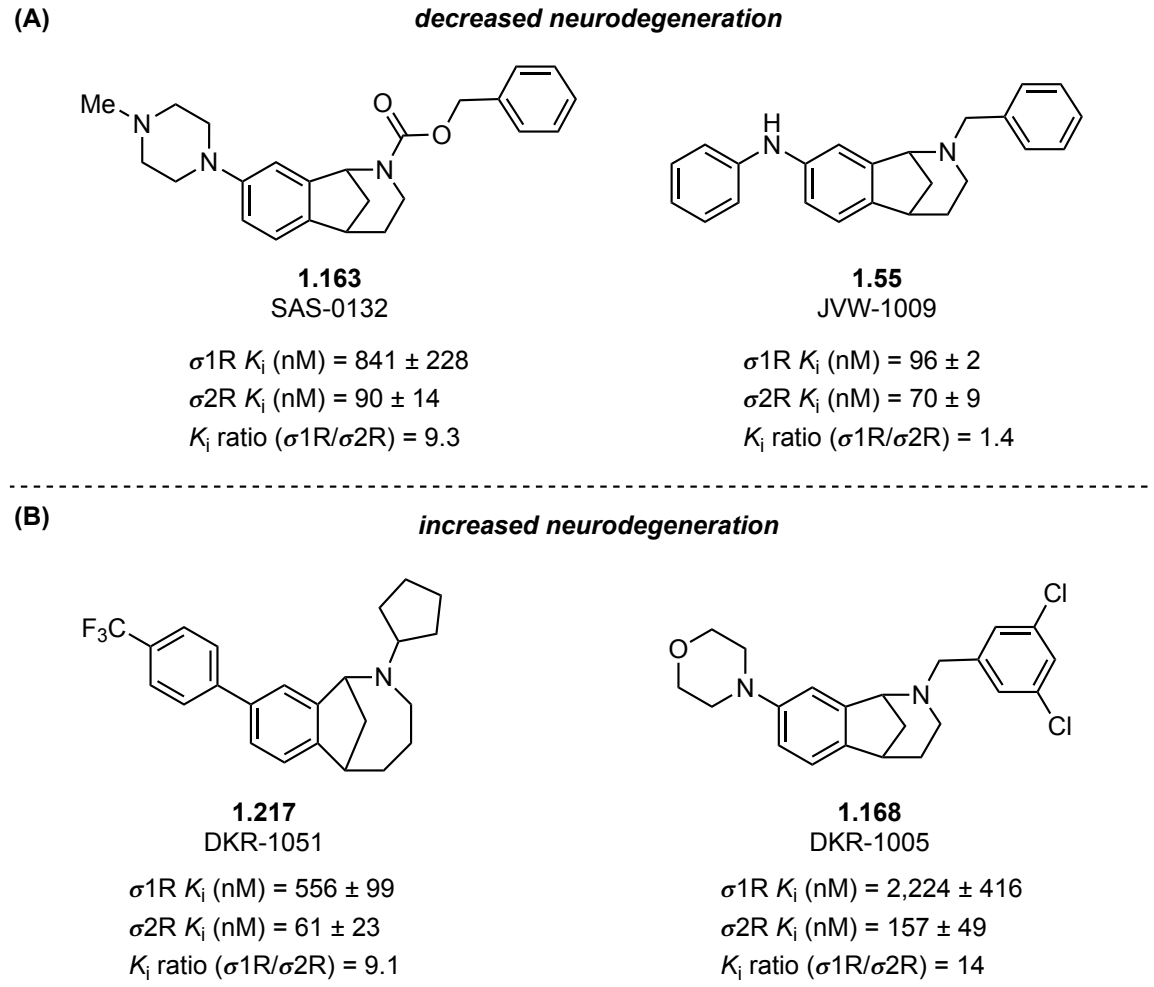

Figure 1.46. A) Norbenzomorphan analogs that decreased neurodegeneration in SC_APP *C. elegans* model. B) Norbenzomorphan analogs that increased neurodegeneration in SC_APP *C. elegans* model.

At the time of this initial discovery there were no other reports that linked modulation of σ2R with attenuation of Aβ–related neurodegeneration, although Izzo *et al.* soon reported that putative σ2R antagonists could block Aβ oligomer–induced synaptotoxicity.[164,165] The exact mechanism of σ2R–associated neuroprotection remains to be clarified, but the report from Izzo *et al.* corroborates these early findings from the Martin group and suggests that more investigation is warranted. The promising results of the SAS-0132 (**1.163**) in this early study, along with pharmacokinetic properties that

supported good bioavailability and brain/plasma ratio, led the Martin group to pursue the piperazine-substituted norbenzomorphan scaffold in a number of continuing studies.[12]

1.5.4.3 Norbenzomorphan Analogs and Neuropathic Pain

Neuropathic pain is a troubling medical condition that is associated with pain caused by damage or disease of the somatosensory system, which is responsible for the perception of pain, pressure, temperature, vibration, and touch.[268] The pain arises from altered transmission of sensory signals into the CNS and is mechanistically distinct from pain attributed to inflammation making treatment more challenging. Common first-line treatment options include gabapentinoids and various antidepressants, but low efficacy is associated with these therapeutic options that are effective in less than 50% of patients with chronic neuropathic pain.[269] As previously discussed, antinociceptive properties are associated with the σ1R, and ligands that modulate this receptor are currently in phase II clinical trials for the treatment of neuropathic pain, but the σ2R had not been investigated for this purpose .[118,270] However, the σ2R is expressed in the mouse and human dorsal root ganglion, which contain the cell bodies of sensory neurons, as well as the spinal cord, suggesting that the σ2R might be a therapeutic target for this condition.[11]

The Martin group in collaboration with the Price group at The University of Texas at Dallas selected several norbenzomorphan and methanobenzazocine analogs for evaluation in the mouse spared nerve injury (SNI) model, which generates persistent and robust neuropathic pain via lesions on the sciatic nerve while leaving the sural nerve intact (Figure 1.47).[271] This nerve injury results in increased responsiveness to mechanical sensitivity that was assayed after intrathecal injection (10 μg dose) of the test compounds.[11] Significant antimechanical hypersensitivity was observed 24 h after injection of DKR-1005 (**1.168**) and DKR-1051 (**1.217**), peaking at 48 h. In addition,

further enhanced antimechanical hypersensitivity was observed for the more potent and σ2R selective analog UKH-1114 (**1.219**) at the same time points. The effects of UKH-1114 (**1.219**) could be blocked by SAS-0132 (**1.163**), which displayed neuroprotective activity that was opposite to that observed with DKR-1005 (**1.168**) and DKR-1051 (**1.217**) in the SC_APP *C. elegans* model of neurodegeneration. This suggests that the two compounds might act through differing functional activity pathways at the σ2R.

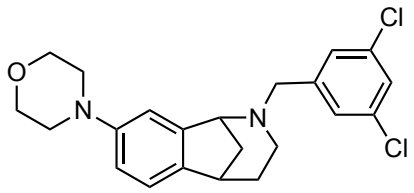

1.168
DKR-1005

σ1R K_i (nM) = 2,224 ± 416
σ2R K_i (nM) = 157 ± 49
K_i ratio (σ1R/σ2R) = 14

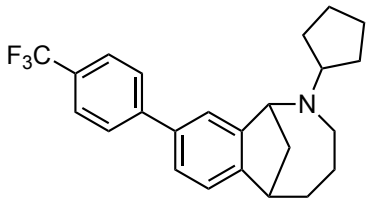

1.217
DKR-1051

σ1R K_i (nM) = 556 ± 99
σ2R K_i (nM) = 61 ± 23
K_i ratio (σ1R/σ2R) = 9.1

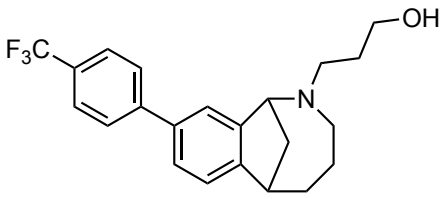

1.219
UKH-1114

σ1R K_i (nM) = 1,279 ± 548
σ2R K_i (nM) = 46 ± 1
K_i ratio (σ1R/σ2R) = 28

Figure 1.47. Norbenzomorphan and methanobenzazocine analogs with antinociceptive effects.

Encouraged by these behavioral results, UKH-1114 (**1.219**) was advanced as the lead compound for additional analysis with systemic dosing (10 mg/kg) and compared to

gabapentin, a standard treatment for neuropathic pain.[11] Treating mice after SNI with gabapentin (100 mg/kg), fully alleviated mechanical hypersensitivity between 1 and 3 h after administration. Interestingly, UKH-1114 (**1.219**) also ameliorated hypersensitivity with an equivalent level of efficacy, but with longer duration that peaked between 24 and 48 h, which may point to a unique mechanism of action. UKH-1114 (**1.219**) displays 28-fold selectivity for the σ2R over the σ1R and negligible affinity for a panel of 55 other targets, strongly implicating the σ2R in the observed antinociceptive activity.[11] This is the first study identifying the σ2R as a potential therapeutic target for the treatment of neuropathic pain and might offer a mechanism of action that is unique from current treatment options. More investigation is needed to fully understand the role of σ2R in pain and its cellular mechanisms, but this work expands upon the medical value of the receptors and highlights the need for additional investigation of the σ2R in CNS disorders.

1.5.4.4 Norbenzomorphan Analogs and Traumatic Brain Injury

Traumatic brain injury (TBI) is associated with a primary injury to the brain that then gives rise to secondary, non-mechanical mechanisms of injury that can result in progressive neuronal death, leading to cognitive decline and numerous psychological problems.[272] Unfortunately, the condition is widespread, with 1.7 million cases reported annually in the United States, but there are currently no FDA–approved treatments that prevent TBI–induced neurodegeneration.[273,274] Accumulating evidence indicates that norbenzomorphan-derived modulators of the σ2R are neuroprotective and this finding prompted the Martin group to investigate σ2R ligands in models of TBI.

The piperazine-substituted norbenzomorphan DKR-1677 (**1.191**) is structurally related to SAS-0132 (**1.163**), which had promising neuroprotective attributes in animal

models of AD, but DKR-1677 is more potent at the σ2R and has enhanced selectivity for the σ1R (Figure 1.48).[14] The increased σ2R selectivity of this structural congener along with its ability to achieve effective brain exposure suggested that it was a good candidate for analysis in animal models of TBI. Because TBI can occur through numerous pathways and give rise to a variety of secondary injury mechanisms, both a blast and cortical controlled impact (CCI) models were assessed.[14]

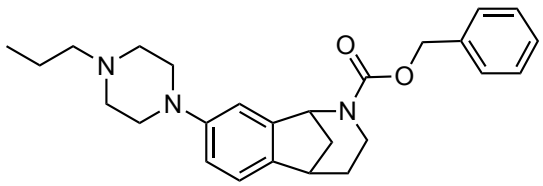

1.191
DKR-1677

σ1R K_i (nM) = 5.1
σ2R K_i (nM) = 230
K_i ratio (σ1R/σ2R) = 45

$t_{1/2}$ (IP, 3 mg/kg) = 1.2 h
T_{max} (IP) = 5 min
brain conc. (IP, 4 h) = 32 nM
brain/plasma ration (4 h) = 3.5
P-gp ration = 0.6

Figure 1.48. Norbenzomorphan analog DKR-1677 and its pharmacological characteristics

The blast injury model applies a pressure wave to the head of a mouse that leads to impaired performance in behavioral models that assess hippocampal-dependent learning and memory functions, as well as widespread axonal degeneration.[275] Treatment with DKR-1677 (**1.191**) 30 min after the blast injury and continuing daily for seven days revealed dose dependent (1, 3, 10 mg/kg/day) preservation of memory in the Morris water maze model of memory and learning.[14] The improved memory functions were correlated with diminished axonal degeneration for the 10 mg/kg dose regimen as compared to the control group, which displayed significant axonal degeneration after the blast injury.

The CCI model applies a direct impact to the exposed cortex with an accelerated metal rod to mimic a concussive injury that causes localized cell death.[276] The resulting loss of neurons and oligodendrocytes was partially mitigated by treatment with DKR-1677 (**1.191**) 1 h after the injury and continuing daily for 7 days (3 mg/kg/day).[14] Collectively, these data point to the neuroprotective properties associated with modulation of the σ2R by DKR-1677 (**1.191**) and for the first time indicate that the receptor might present a therapeutic opportunity for the treatment of TBI. Although the mechanism for protection remains to be clarified, it provides further support for the role of the σ2R in CNS disorders.

1.5.4.5 Norbenzomorphan Analogs and Alcohol Withdrawal

Alcohol use disorder is a common problem, but FDA approved drugs that treat alcohol addiction suffer from low success rates that often result in relapse.[277,278] During the course of chronic alcohol use the neurocircuitry associated with positive reinforcement is altered and might be associated with the symptoms of withdrawal.[279] The duration of abstinence can be affected by a patient's ability to tolerate the symptoms, which can range in severity.[280] This suggests that treatments targeting withdrawal symptoms might be a useful approach for treating alcohol use disorder. Ligands that modulate the σ2R have previously been associated with an ability to attenuate the behavioral responses and toxic effects of cocaine in rodent models and ligands that target the σ1R have shown promise for the treatment addiction.[10,192,281,282] Therefore, we queried whether σ2R ligands might also be effective for modifying alcohol-related behaviors.

The effects of alcohol withdrawal have been modeled in *C. elegans* behavioral studies to assess performance upon removal of alcohol following chronic exposure.[283,284]

The model evaluates *C. elegans* in a food-race assay, in which the target area contains an attractant and a paralytic for immobilization upon reaching the target. Following preconditioning of *C. elegans* with ethanol and subsequent cessation, a withdrawal period ensues in which impaired navigation in the food-race is observed.[283] Performance can be recovered if sufficient time is allowed in the withdrawal period, prior to the race, and also with low-dose administration of alcohol, suggesting that the compromised performance is the result of withdrawal symptoms.[283] The number of *C. elegans* that navigate to the endpoint during the course of the race enable a comparison of withdrawal effects under various conditions. Although the system does not fully mimic the complexity of alcohol abuse in humans, it does provide a convenient platform for screening compounds that target withdrawal symptoms, and *C. elegans* have previously been used to identify genes that affect alcohol-related behaviors.[285]

In collaboration with the Pierce group at the University of Texas at Austin, we selected a small series of methanobenazocine derived analogs with high σ2R affinity and selectivity over the σ1R in order to assess their ability to modulate alcohol related behaviors (Figure 1.49).[13] As previously discussed, analogs substituted with a 4-trifluoromethylphenyl group on the benzene ring, such as UKH-1114 (**1.219**) and DKR-1051 (**1.217**), reduced mechanical hypersensitivity in models of neuropathic pain.[11] Therefore these analogs, along with several similarly substituted derivates (not shown) were included in the screen. Several structurally related methanobenzazocine analogs with a chlorine substituent on the benzene ring (**1.222**–**1.224**) were discovered to have high σ2R affinity with modest selectivity over the σ1R and were also included in the study in order to identify novel compounds with promising activity.

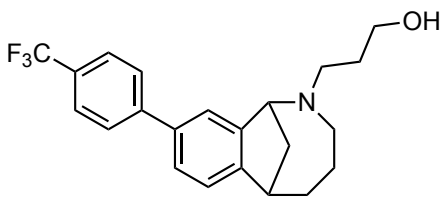

1.219
UKH-1114

σ1R K_i (nM) = 1,279
σ2R K_i (nM) = 46
K_i ratio (σ1R/σ2R) = 28

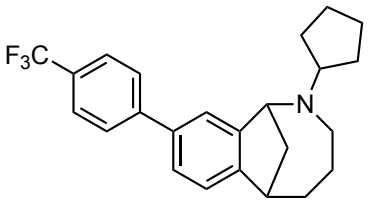

1.217
DKR-1051

σ1R K_i (nM) = 556
σ2R K_i (nM) = 61
K_i ratio (σ1R/σ2R) = 9.1

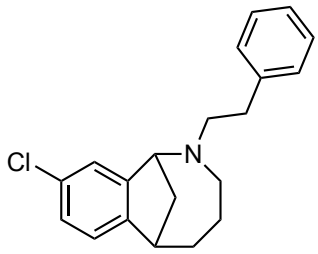

1.222
JVW-1034

σ1R K_i (nM) = 248
σ2R K_i (nM) = 23
K_i ratio (σ1R/σ2R) = 11

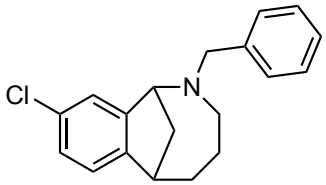

1.223

σ1R K_i (nM) = 205
σ2R K_i (nM) = 39
K_i ratio (σ1R/σ2R) = 5.3

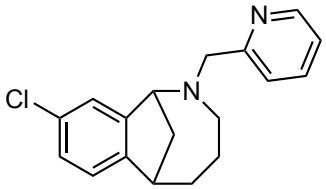

1.224

σ1R K_i (nM) = 826
σ2R K_i (nM) = 122
K_i ratio (σ1R/σ2R) = 6.8

Figure 1.49. Methanobenzazocine analogs evaluated in C. elegans model of alcohol abuse.

The Peirce group conducted the assay by removing ethanol conditioned *C. elegans* from alcohol exposure onto plates seeded with the test ligands (100-200 μM) for one hour, during which time the internal alcohol level returned to baseline levels.[13] After the one-hour withdrawal period, *C. elegans* were evaluated in the food-race. Similar to the reported protocol, significant impairment was observed in the nematodes treated with vehicle alone (DMSO) and the fraction on target was greatly reduced as compared to nematodes naive to ethanol.[13,283] Administration of UKH-114 (**1.219**) and DKR-1051 (**1.217**) did not produce a notable effect, nor did other similarly substituted biaryl

analogs. In contrast, the chlorine substituted analogs **1.222** and **1.223** did reduce behavioral deficits in the assay, and notably JVW-1034 (**1.222**) improved performance to levels observed with the naive nematode.[13] Administration of these compounds to *C. elegans* that were not exposed to ethanol had no effect on their behavior, suggesting that these σ2R ligands may reduce alcohol withdraw symptoms.

Having identified novel analogs that modulate alcohol-related behaviors, the effect was compared to the well-characterized σR ligands siramesine and opipramol. Administration of siramesine, which possesses high σ2R affinity (0.12 nM) and selectivity over the σ1R (142-fold), also recovered behavioral deficits in *C. elegans* preconditioned to ethanol. However, the behavior of ethanol-naïve nematodes was also altered, with some performance enhancement observed in the food-race. This provides additional support using a structurally distinct ligand that the σ2R may be involved in alleviating symptoms of alcohol withdrawal. Opipramol has low nanomolar affinity for the σ1R (0.2 nM) and is selective over the σ2R (280-fold) and did not provide any notable effect in the assay, indicating the σ1R may not be responsible for the activity.

The results from the *C. elegans* food-race assay were corroborated in higher order animals using a rodent model of alcohol dependence.[286] The voluntary ethanol consumption of the ethanol-dependent rats during the withdrawal period was significantly attenuated by administration of JVW-1034 (**1.222**). These findings provide evidence for the first time, that modulation of σ2R with small molecules effects behaviors associated with alcohol withdrawal. This expands the therapeutic potential of the σ2R and suggests that small molecules targeting the receptor might be useful for treating alcohol-abuse disorder.

1.6 SCAFFOLD MODIFICATION OF THE NORBENZOMORPHAN

1.6.1 Scaffold Simplification

These studies show that the norbenzomorphan scaffold is a promising molecular template for the construction of ligands that selectively target the σ2R and have promising activity in animal models of neurological disorder. Motivated by the underexplored therapeutic potential of the receptor and the longstanding challenges associated with the protein, SAR investigations of various substitution patterns were performed. However, despite the obvious merits of norbenzomorphan–derived σ2R modulators, it was not clear if this scaffold presented the optimal orientation of substituents or pharmacological properties for continued advancement. Accordingly, an investigation was initiated to modify the scaffold using a structural simplification approach. The hit-to-lead development process can frequently result in an increased number of rings and atoms that increase molecular complexity, as well as the molecular weight and lipophilicity, as a result of efforts to enhance potency.[287] The structural simplification process attempts to remove nonessential groups as part of lead optimization and generally focuses on reducing the number of rings.[288] This approach can provide alternative lead compounds that have shed unnecessary complexity and might exhibit pharmacokinetic (PK) properties that are more favorable than the parent scaffold. Indeed, it is often strategically important to identify multiple diverse structures with suitable potency, selectivity, and PK profiles to increase the likelihood of successful lead optimization and advancement during development.[289]

Analysis of the norbenzomorphan structure revealed the bridged ring system as an obvious source of structural complexity, but it was unknown if the feature was necessary for the pharmacological profile. Accordingly, a simplified scaffold was envisioned that

would arise from excision of bridging methylene in **1.53** to afford the tetrahydro-2-benzazepine ring system in **1.225** (Figure 1.50).[8] Further evaluation of **1.225** would involve contraction of the heterocyclic ring to assess various ring sizes in **1.226** (n = 1-3). Of course, the bridged ring system imparts conformational rigidity to the norbenzomorphan that will be absent in the modified scaffold.

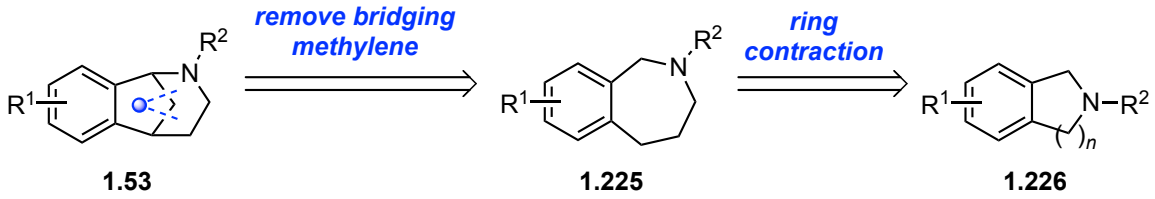

Figure 1.50. Scaffold simplification via excision of the bridging carbon atom.

The halogenated regioisomers of **1.226** (R = Br, n = 1-2) are known and accessible with slight modification of literature procedures, whereas hydrobenzazepine **1.225** (R = Cl) was prepared in a five-step procedure from the commercially available dihalogenated aldehydes **1.227-1.228** (Scheme 1.8).[8] In the event, Suzuki cross-coupling of **1.227-1.228** with potassium vinyltrifluoroborate provided the styrenes **1.229-1.230** that were subjected to reductive amination with allylamine followed by installation of the benzyl carbamate to afford dienes **1.231-1.232**. Ring closing metathesis of **1.231-1.232** with Grubbs 2nd generation catalyst (Grubbs II) and subsequent hydrogenation of the resultant olefin with Adam's catalyst delivered the halogenated hydrobenzazepines **1.233-1.234**.

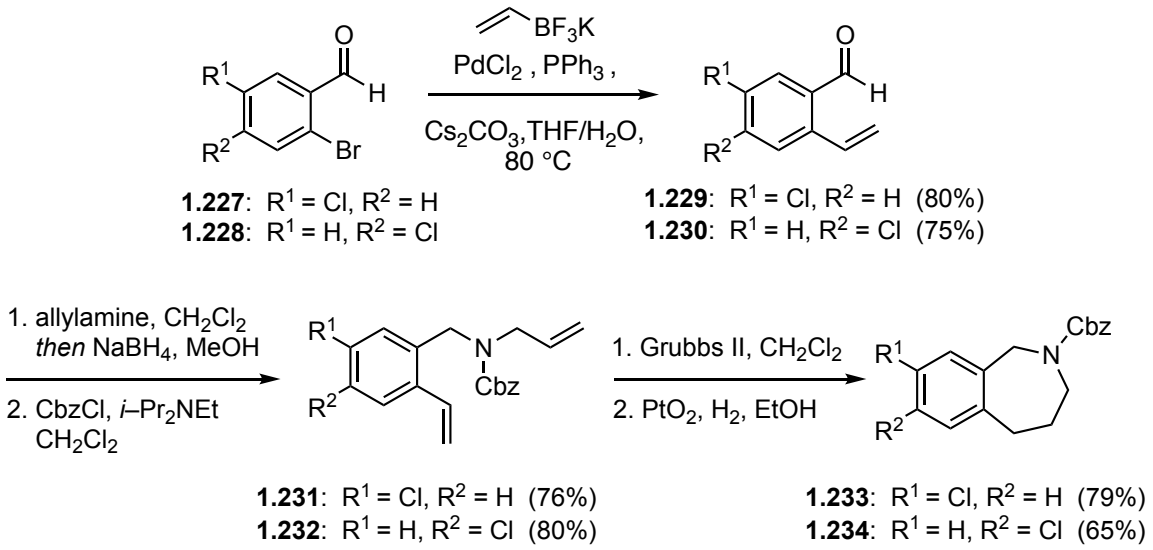

Scheme 1.8. Synthesis of the halogenated hydrobenzazepine scaffold.

These halogenated scaffolds **1.233**-**1.234** were easily diversified in a manner similar to the norbenzomorphan, as previously discussed. A series of substituted piperazine analogs that corresponded to σ2R selective norbenzomorphans were prepared, revealing that excision of the bridging methylene had a pronounced effect on the binding profile (Table 1.12).[8] In addition, the size of the heterocyclic ring system (n = 1-3), as well as the nature of the alkyl substituents on the piperazine affected affinity and selectivity. For instance, the propyl piperazine substituent provided high σ2R affinity and 45-fold selectivity with norbenzomorphan **1.91**. However, the same substituent on the simplified scaffolds (**1.235**-**1.237**) provided less than 2-fold σ2R selectivity resulting from increased σ1R affinity and diminished σ2R affinity. Increasing the ring size in **1.235**-**1.237** (n = 1-3) increased the σ2R affinity, and the lowest σ1R affinity was obtained with the tetrahydroisoquinoline scaffold **1.236** (n = 2). A similar trend was observed with an unsaturated alkyl substituent on the piperazine (**1.238**-**1.240**), and in this instance tetrahydroisoquinoline **1.239** achieved 10-fold selectivity for the σ2R. The

greatest σ2R affinity (K_i = 2.7 nM) was obtained for tetrahydroisoquinoline scaffold **1.242** with a cyclopentyl substituent at the piperazine nitrogen atom, a notable increase that provided 19-fold selectivity over the σ1R. Previously, introduction of an alkyl substituent bearing an ester moiety delivered a considerable decrease in σ1R affinity with norbenzomorphan **1.203**, but little effect was observed at the σ2R. Interestingly, this effect was not as pronounced for the simplified scaffold (**1.244**-**1.246**) and was accompanied by decreased σ2R affinity, giving rise to < 5-fold selectivity over the σ1R.

Table 1.12. Binding affinities of the piperazine substituted-simplified scaffold.

A = 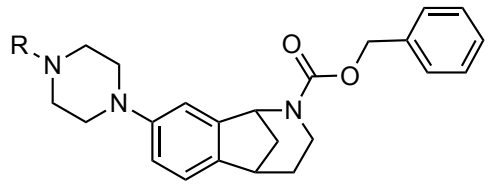

B = 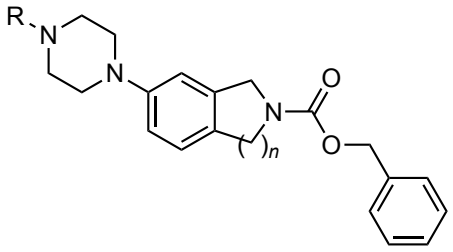

				K_i(nM)		K_i ratio
cmpd.	n	scaffold	R	σ1R	σ2R	(σ1R/σ2R)
1.191	N/A	A		230	5.1	45
1.235	1	B	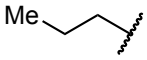	19	77	0.25
1.236	2	B		85	50	1.7
1.237	3	B		15	14	1.1
1.210	N/A	A		413	17.5	24
1.238	1	B	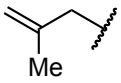	92	153	0.6
1.239	2	B		245	25	10
1.240	3	B		48	19	3
1.209	N/A	A		130	3.6	36
1.241	1	B	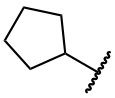	44	8.2	5
1.242	2	B		52	2.7	19
1.243	3	B		49	13	4
1.203	N/A	A		6,660	23.8	280
1.244	1	B	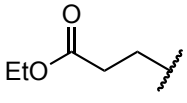	352	134	3
1.245	2	B		407	198	2
1.246	3	B		368	83	4

Relatively minor changes in the position of the distal aromatic group with respect to the more basic nitrogen atom of the piperazine ring were previously demonstrated to have a significant impact on σ1R affinity. Indeed, the norbenzomorphan scaffold displayed much lower affinity for the σ1R when the piperazine was installed at C–8, as opposed to C–7.[9] The isoindoline scaffold **1.226** (n = 1) has a symmetry element that prevents examination of a similar regioisomeric preference. However, the orientation of the piperazine on **1.247** and **1.249** provides a slight preference for the σ2R, whereas **1.248** has a modest preference for the σ1R (Figure 1.51).[8] The bridging methylene group of the norbenzomorphan scaffold seems to plays a role in obtaining selectivity for the σ2R. Excision of this group in hydrobenzazepine scaffold **1.249** likely altered the orientation of the core nitrogen atom and the distal aromatic group that is attached at this site in a manner that favors σ1R binding. In order to examine alternative linkers to the distal aromatic group, the benzyl carbamate of **1.249** was exchanged with an aryl sulfonamide in **1.250**, which provided increased affinity for both σRs, but with little change in selectivity (Figure 1.51.B).

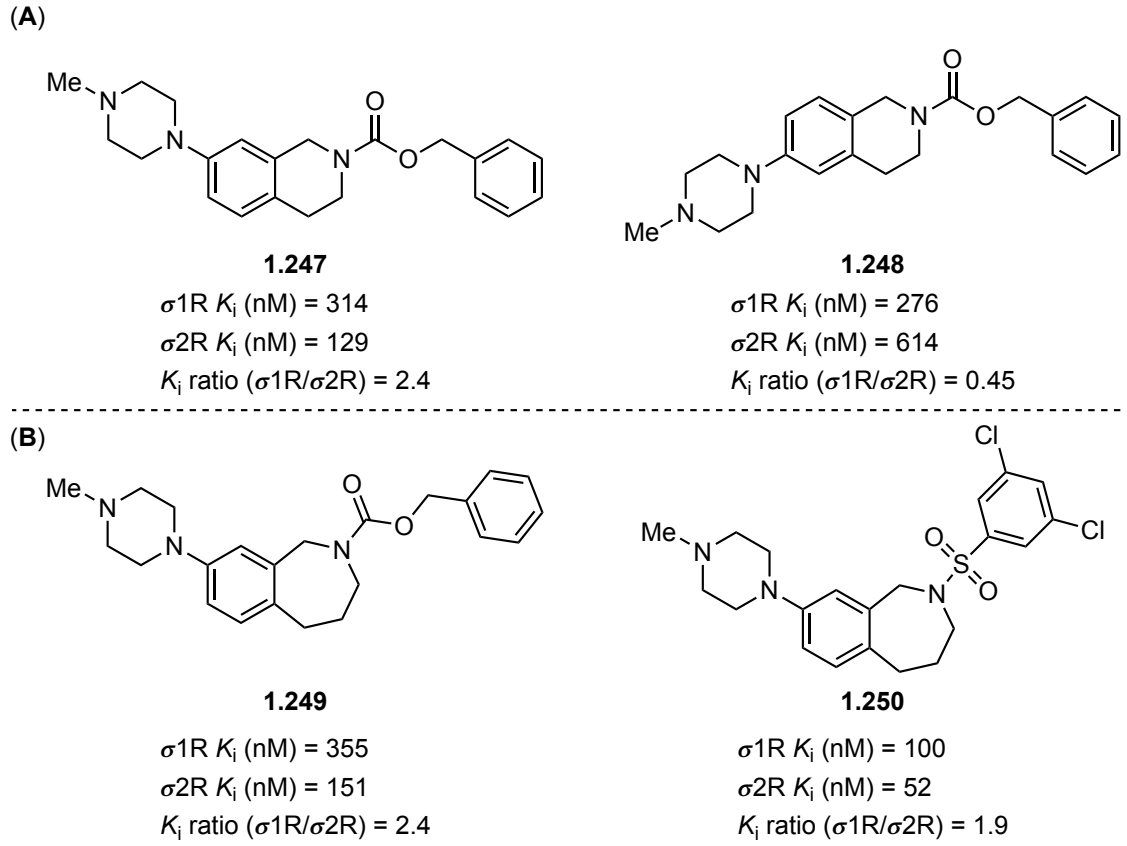

Figure 1.51. A) Regioisomers of piperazine substituted tetrahydroisoquinoline. B) Variations in the aryl substituent on the hydrobenzazepine nitrogen atom.

The norbenzomorphan scaffold demonstrated an ability to obtain σ1R selectivity, when substituted at the C–7 and this proved to be effective strategy for accessing σ1R selective ligands using the simplified scaffold (Table 1.13).[8,9] The morpholine substituted scaffolds (**1.251**-**1.253**) achieved low nanomolar affinity for the σ1R, and isoindoline **1.251** achieved 28-fold selectivity over the σ2R. Likewise, the aryl substituted scaffold displayed high affinity for the σ1R, with isoindoline **1.254** obtaining 4.1 nM for the σ1R and 16-fold selectivity over the σ2R. In both cases, the modified scaffold is more potent at the σ1R than the corresponding norbenzomorphan suggesting

that removal of the bridging methylene is an effective simplification strategy for developing σ1R selective ligands.

Table 1.13. Binding affinity of simplified scaffold with σ1R selectivity.

A = 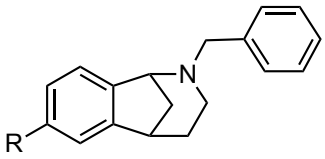

B = 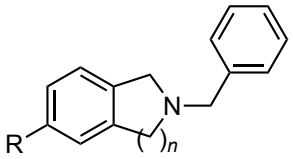

				K_i (nM)		K_i ratio
cmpd.	n	scaffold	R	σ1R	σ2R	(σ2R/σ1R)
1.56	N/A	A		16.5	562.3	34
1.251	1	B	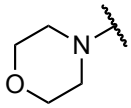	5.9	166	28
1.252	2	B		1.7	33	19
1.253	3	B		6.1	81	13
1.169	N/A	A		11.1	121	11
1.254	1	B	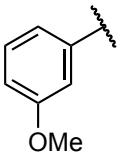	4.1	65	16
1.255	2	B		4.9	57	12
1.256	3	B		21	440	21

K_i values determined from non-linear regression of radioligand competition binding isotherms by PDSP.

Collectively, these results provide additional evidence that the relative position of the basic nitrogen and the distal aromatic group are important pharmacophore elements for obtaining σ2R selectivity. Moreover, the bridging methylene group appears to be an important structural feature for preferential σ2R binding and this simplification strategy suggests that excision of this group had a deleterious effect in the bicyclic heterocycles. Modest σ2R selectivity was achieved in some in some instances with the bicyclic scaffold, but the norbenzomorphan achieves greater levels of σ2R selectivity with similar

substitution patterns, suggesting that it provides a more favorable orientation of key pharmacophore elements.

1.7 CONCLUSION

The σ1R and σ2R are intriguing receptors that have been implicated in a broad range of diseases, and ligands that modulate the σRs are currently undergoing clinical trials. This expanding medicinal relevance highlights the need for a thorough understanding of the cellular mechanism of action involving these receptors, but the σ2R has been an enigmatic target that has relied on pharmacological characterization and remains poorly defined. Identification of the σ2R protein and access to the cloned gene will provide access to modern tools for investigation that should enable much needed advancement. This underscores the need for molecular tools with high specificity for the σ2R, but ligands that are selective over the σ1R have been elusive in the absence of structure-based-design strategies.

The Martin group has developed a new σR ligand class using an efficient an easily diversifiable synthetic strategy that enabled an extensive SAR investigation and identified substitution patterns that modulate σ1R and σ2R affinity. Some of these norbenzomorphan derived analogs show promising activity in models of several neurological disorders that were previously unknown, suggesting that continued development is warranted. Structural features of the norbenzomorphan nucleus that contribute to the binding profile were interrogated using a scaffold simplification strategy as part of ongoing hit-to-lead development aimed at optimizing pharmacological activity and discovering alternative lead scaffolds with unique PK profiles. This effort revealed that the bridged ring system of the norbenzomorphan might play an important role as a conformational constraint to provide selectivity over the σ1R. However, it also suggests

that selectivity can be obtained using other scaffolds if the proper orientation of critical substituents can be obtained. Thus, continued investigation of molecular variants of the norbenzomorphan scaffold might provide useful tool compounds that elucidate key features of the SAR and potentially provide alternative lead compounds with improved pharmacological and PK properties

Chapter 2: Structural Modification of the Norbenzomorphan Scaffold for Targeting the σ2R and the Molecular Identification of the σ2R as TMEM97[1]

2.1 Scaffold Simplification: An Alternative Approach

2.1.1 Introduction

In the time since their initial discovery, the σRs have generated considerable interest that revealed the enigmatic nature of the protein, but also their promising therapeutic potential.[5] Following their early mischaracterization as an opioid receptor subtype, the σRs were delineated into the σ1R and σ2R receptor subtypes that were unique from opioid receptors.[55,75] Molecular identification and cloning of the σ1R followed shortly thereafter, enabling significant advancements, and more recently the structure of the protein was finally revealed via X-ray crystallography.[6,78] Increased access to these characterization data improved our understanding of the cellular role of the σ1R and have implicated it in the regulation of cellular processes important for cell viability.[10] Genetic mutations of the σ1R have been linked to disorders associated with neuronal decline,[5] and it has been implicated in a variety of conditions that range from cancer to neuropsychiatric disorders. Ligands that modulate the σ1R are currently in clinical trials for the treatment of neuropathic pain, AD, and stroke.[10,108,119-124]

In contrast, the σ2R has proved to be a much more elusive target and the protein was only recently identified and cloned through the course of the work presented herein.[160] As a result, pharmacological characterization has been the primary mechanism

[1] Sections of this chapter are based on previously published work from Michael D. Wood that Prof. Stephen F. Martin served as an advisor for. See Alon, A.; Schmidt, H. R.; Wood, M.D.; Sahn, J. J.; Martin S. F.; Kruse, A. C. Identification of the Gene that Codes for the σ2 Receptor. *Proc. Natl. Acad. Sci. U.S.A.* **2017**, *114*, 7160-7165. Contributions from Michael D. Wood include the development and synthesis of the ligand used for affinity purification of the σ2 receptor.

for investigation of the σ2R, and although numerous studies posit promising therapeutic potential of the receptor, the molecular mechanism remained unclear.[7] These challenges notwithstanding, the σ2R had attracted considerable attention for treatment and diagnostic imaging of cancer.[77,161,203] More recently, important findings from the Martin group[11-14,163] and others have indicated that the σ2R might be a target for the treatment of some neurological and addiction disorders, and ligands that modulate the receptor are currently undergoing clinical trials for the treatment of AD and schizophrenia.[164-168,211]

The Martin group recently discovered that derivatives of the norbenzomorphan scaffold can have high affinity for the σ2R. Importantly, a SAR investigation revealed that affinity for the σ1R can be effectively modulated through several unique variations in substitution pattern (Figure 2.1).[263] Among the key findings, the position of the piperazine moiety on the core arene and alterations to the position of the distal aromatic group had a pronounced impact on affinity, particularly with respect to the σ1R.[9,263] Several of the compounds developed during the course of these investigations displayed promising neuroprotective activity in animal models of some CNS disorders that inspired continued investigation as part of hit-to-lead development.[11-14,163] However, the SAR studies focused on identifying substitution patterns on norbenzomorphans that enhanced potency and selectivity for the σ2R, but the importance of specific structural features of the norbenzomorphan nucleus itself required additional clarification.

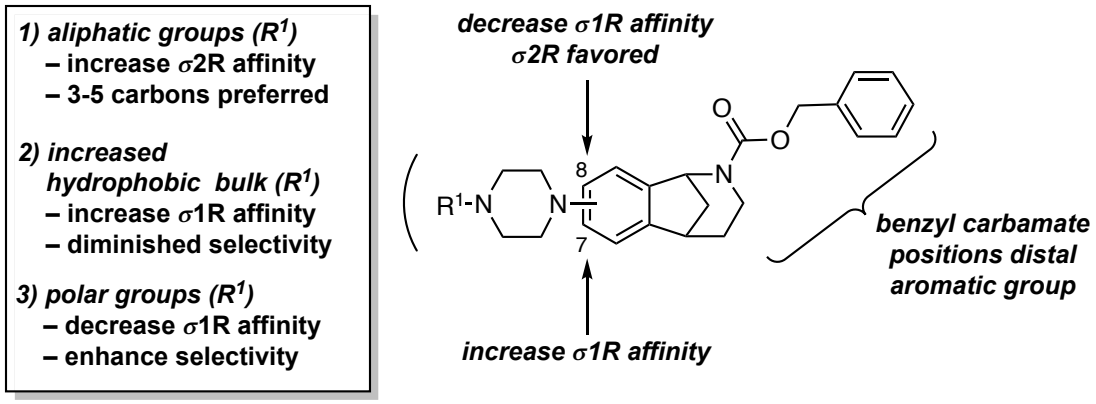

Figure 2.1. Summary of SAR for piperazine-substituted norbenzomorphan.

Scaffold simplification , which is a common strategy during hit-to-lead development, aims to achieve a similar orientation of key pharmacophore elements with an alternative scaffold arrangement that is less structurally complex.[288] This tactic can potentially provide alternative lead scaffolds that possess unique physiochemical or PK properties that might be beneficial, and it also allows the importance of various structural characteristics of the scaffold to be assessed. During the course of ongoing studies that probed the effects of various substitution patterns on the norbenzomorphan scaffold, there were also concurrent efforts to assess structural modifications via a scaffold simplification approach. As discussed in the preceding chapter, the bridged ring system was identified as a potential source of unnecessary structural complexity. Thus, one scaffold simplification approach involved excision of the bridging methylene, but interestingly, this generally enhanced affinity for the σ1R and eroded selectivity for the σ2R (Figure 2.2).[8] These results suggested that the bridged ring system might play an important role, possibly through conformationally constraining the scaffold in an orientation that was less favorable for interaction with the σ1R. However, if this speculation is correct, then it might be possible to obtain selectivity over the σ1R with an

alternative scaffold, provided that critical pharmacophore elements are constrained in a favorable position.

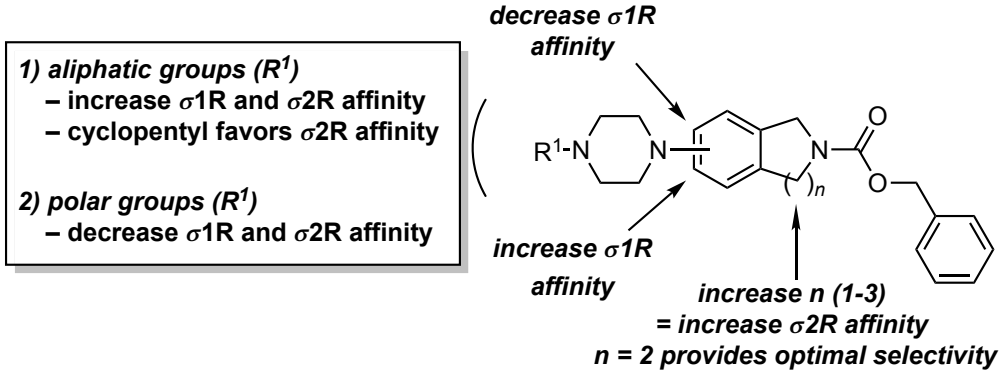

Modified scaffold possess increased σ1R affinity and diminished σ2R selectivity relative to similarly substituted norbenzomorphan congeners

Figure 2.2. Summary of SAR for piperazine-substituted scaffolds with the bridging methylene removed.

2.1.2 Development of an Aminotetralin Scaffold

During the course of these investigations, an alternative strategy for scaffold simplification of the bridged ring system was devised. In this unique approach, scission of the seven-membered ring in **1.53** and ring-expansion of the bridging five-membered ring gives rise to the aminotetralin scaffold **2.1** (Figure 2.3.A). Importantly, this tactic transitioned the benzylic nitrogen atom to an exocyclic position that is less conformationally restricted. As evidenced by preliminary studies of the norbenzomorphan, seemingly minor alterations in substitution at this position can have a considerable impact on σ2R selectivity, indicating that it is an important pharmacophore element. This suggests that the proposed structural modification in the simplified scaffold might provide a unique binding profile by perturbing the orientation of important groups.

In addition, aminotetralin **2.1** presents a new site of substitution at the exocyclic nitrogen atom (R^3), thereby allowing access to unexplored chemical space that might be leveraged to enhance the binding profile or other physiochemical properties.

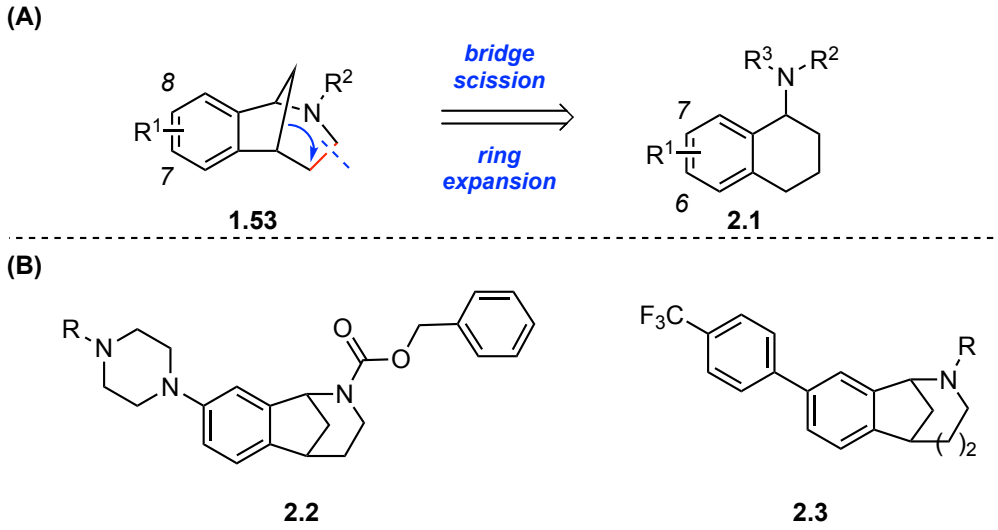

Figure 2.3. **A**) Strategy for scaffold simplification via a tetralin based scaffold. **B**) Structural configurations of the norbenzomorphan that will be mimicked on the tetralin scaffold.

In order to assess the effects of these structural changes, an initial evaluation was devised to incorporate substitution patterns that were favored the σ2R on the norbenzomorphan scaffold. At the time, initial SAR results with the norbenzomorphan scaffold pointed toward unique structural configurations that provided reasonable levels of σ2R selectivity in addition to promising activity in models of neurodegeneration (Figure 2.3.B). One such construction was the piperazine-substituted norbenzomorphan **2.2**, in which the core nitrogen atom was functionalized as a benzyl carbamate, and the requisite basic amine moiety was incorporated as a substituent on the aromatic ring. An alternative arrangement presented the core nitrogen atom as the basic amine site and the aromatic ring was substituted with a 4-trifluoromethylphenyl group in **2.3**. Each of these

could be mimicked on aminotetralin scaffold **2.1** for direct comparison to their norbenzomorphan derived congeners in order to assess the impact of these structural changes on the binding profile. Because the position of the substituent on the aromatic ring of the norbenzomorphan nucleus **1.53** significantly impacted affinity for the σ1R and σ2R, we foresaw an investigation of substituents at C–6 and C–7 of the tetralin scaffold **2.1**. However, an initial emphasis was placed on installation of the substituent at the C–7 position because it corresponded to the norbenzomorphan C–8 position that was more favorable for σ2R selectivity (Figure 2.3.A). A methyl group was envisioned at the newly accessible site of substitution on the nitrogen atom (R^3) in **2.2** to resemble the substitution present in the parent scaffold, while also avoiding added hydrophobic bulk and unnecessary complexity.

A synthetic strategy that provides efficient access to the core tetralin moiety and is readily diversifiable was required for a systematic investigation. The initial approach was inspired by the MCAP that was used to construct the norbenzomorphan scaffold because of the synthetic versatility that it provided.[3,4,9,43,48,50] The halogenated aldehydes **1.227** and **1.228** are commercially available and represented convenient starting materials for an MCAP approach (Scheme 2.1). Suzuki cross-coupling of **1.227** and **1.228** with potassium vinyltrifluoroborate (**2.4**) was catalyzed by palladium acetate (5 mol%) and triphenylphosphine according to slight modification of a literature procedure and occurred selectively at the arylbromide to afford styrene intermediates **1.229** and **1.230** in 72% and 79% yield, respectively.[290-292] Subsequent addition of an ethanolic solution of methylamine to a mixture containing the aldehyde intermediate **1.229** or **1.230** and $MgSO_4$ in CH_2Cl_2 delivered **2.5** and **2.6** in 99% yield, and these compounds were used directly without purification.

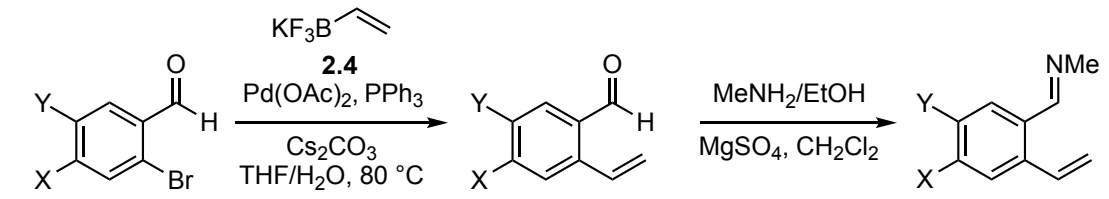

1.227: X = H, Y = Cl
1.228: X = Cl, Y = H

1.229: X = H, Y = Cl (72%)
1.230: X = Cl, Y = H (79%)

2.5: X = H, Y = Cl (99%)
2.6: X = Cl, Y = H (99%)

Scheme 2.1. Synthesis of the halogenated imine as MCAP precursor.

With imines **2.5** and **2.6** in hand, the stage was set for installation of the homoallylic benzyl carbamate using the one-pot MCAP according to established protocol.[3,50] In the event, stirring a solution of imine **2.6** and benzyl chloroformate (CbzCl) in THF at 60 °C for three hours followed by addition of allyl zinc bromide at -78 °C delivered in intractable mixture (Equation 2.1).

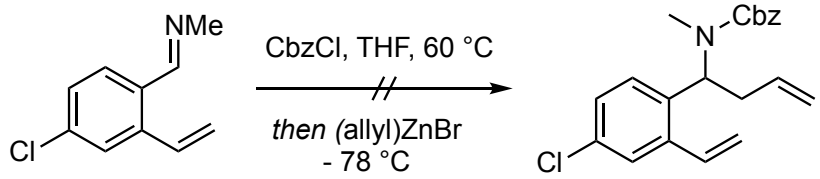

2.6 **2.7** **(2.1)**

Suspecting that formation of an activated *N*-acyliminium ion in the presence of the styrene moiety might be problematic, the one-pot reaction was divided into a related two-step sequence. Thus, allyl zinc bromide was added directly to imine intermediates **2.5** and **2.6** to afford the homoallylic amines **2.8** and **2.9** in 80% and 88%, respectively (Scheme 2.2). The amines **2.8** and **2.9** were subsequently acylated with benzyl chloroformate to deliver **2.10** and **2.11** in 99% and 92% yield, respectively. RCM proceeded smoothly by treating dienes **2.10** and **2.11** with Grubbs II catalyst to afford dihydronaphthalenes **2.12** and **2.13** in 88% and 89% yield, respectively. Reduction of the

resulting olefin was accomplished via catalytic hydrogenation using Adam's catalyst to afford the halogenated aminotetralin scaffolds **2.14** and **2.15**.

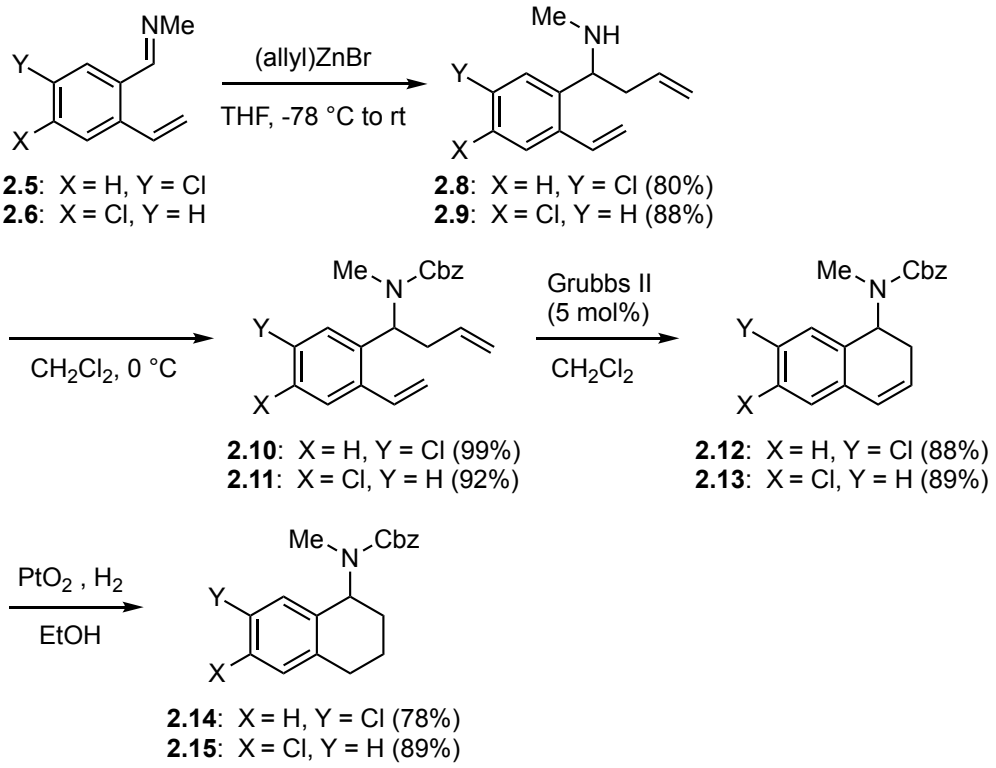

Scheme 2.2. Synthesis of the halogenated aminotetralin scaffolds.

2.1.3 Preliminary Validation of the Aminotetralin Scaffold

With halogenated scaffold **2.14** in hand, attention was shifted toward the preparation of a small series of analogs for direct comparison to corresponding norbenzomorphan derivatives. The aryl chloride moiety provided a convenient handle for cross-coupling using Buchwald-Hartwig amination reactions that were established for derivatization of the norbenzomorphan core **1.53**.[4,9] Thus, heating a toluene solution of **2.14** and excess piperazine (**1.172**) at 100 °C in the presence of palladium acetate (5 mol%) and JohnPhos delivered amine **2.16** in 56% yield (Scheme 2.3). Subsequent

reductive alkylation of **2.16** with paraformaldehyde provided *N*-methylpiperazine analog **2.17** in 52% yield.

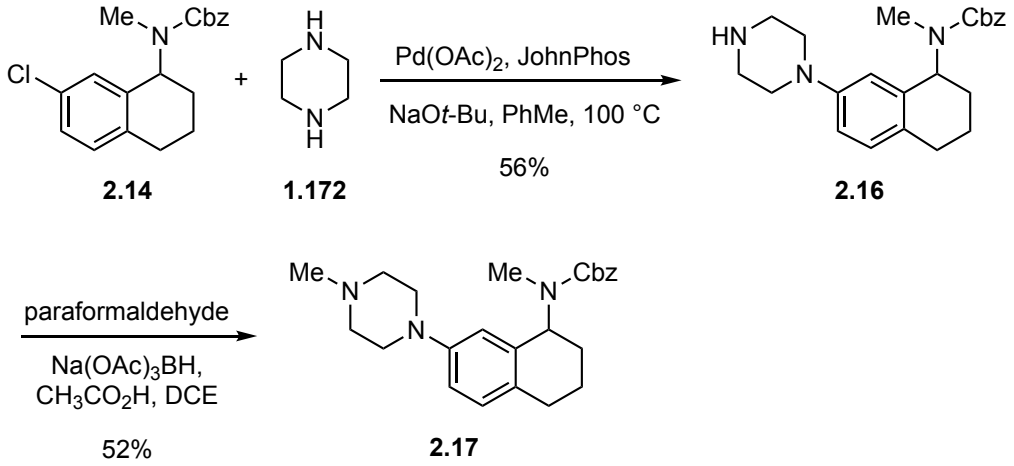

Scheme 2.3. Synthesis of *N*-methylpiperazine analog.

The binding profile was determined by the National Institutes of Health (NIH) Psychoactive Drug Screening Program (PDSP) at UNC-Chapel Hill via competition binding analysis.[54] The σ1R binding affinity was determined for a range of test ligand concentrations (0.1 nM – 10 μM) using [^{3}H]-(+)-pentazocine with tissue typically sourced from guinea pig unless indicated otherwise. A modified protocol was recently established using membrane preparations from HEK293T cells transfected with human σ1R to obtain high levels of protein expression. The σ2R binding affinity was determined with the same range of ligand concentrations using [^{3}H]-DTG in the presence of (+)-pentazocine to block σ1R binding sites with membrane preparations from rat PC12 cells. Following the molecular identification and cloning of the σ2R discussed in this work, a modified protocol using membrane preparations from HEK293T cells transfected with human σ2R was established. The IC_{50} was calculated from dose-response curves obtained for each test ligand and from that, the K_i was determined according to the

Cheng-Prusoff equation and is reported as the common measure of binding affinity.[293] All K_i values for tetralin derived analogs were determined from a single experiment using non-linear regression.

Gratifyingly, binding analysis revealed that the piperazine-substituted aminotetralin **2.17** displayed 10-fold selectivity for the σ2R over the σ1R, which is similar to the corresponding norbenzomorphan **1.163** (Figure 2.4). Although the affinities of aminotetralin **2.17** for the σ1R and σ2R were somewhat diminished, this preliminary result suggested that the modified scaffold might be a viable alternative to the more structurally complex norbenzomorphan. However, a more thorough SAR investigation of the simplified scaffold was needed for determination of preferred substitution patterns.

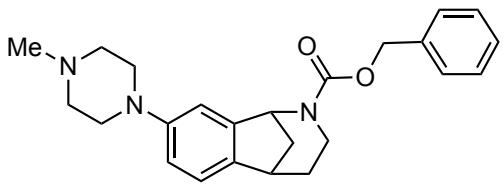

1.163

σ1R K_i (nM) = 841
σ2R K_i (nM) = 90
K_i ratio (σ1R/σ2R) = 9.3

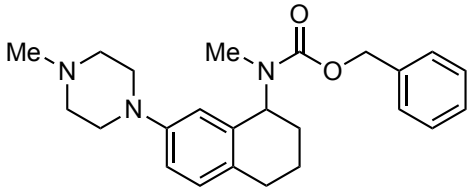

2.17

σ1R K_i (nM) = 2,944
σ2R K_i (nM) = 284
K_i ratio (σ1R/σ2R) = 10

Figure 2.4. Comparison of the piperazine-substituted aminotetralin scaffold and the similarly substituted norbenzomorphan.

To further evaluate alternative scaffold substitutions, an analog of the 4-trifluoromethylphenyl substituted methanobenzazocine **1.219** was also prepared (Scheme 2.4). Suzuki cross-coupling of halogenated aminotetralin **2.14** with arylboronic acid **2.18** in the presence of Pd(t-Bu_3P)$_2$ delivered the biaryl substrate **2.19** in 78% yield.[11] Reductive removal of the Cbz-group in **2.19** provided the secondary amine **2.20** in 91% yield and reaction of **2.20** with ethyl acrylate (**2.21**) at 40 °C afforded the alkylated

analog **2.22** in 75% yield. Reduction of the ester moiety of **2.22** with lithium borohydride gave the 4-trifluoromethylphenyl analog **2.23** in 50% yield.

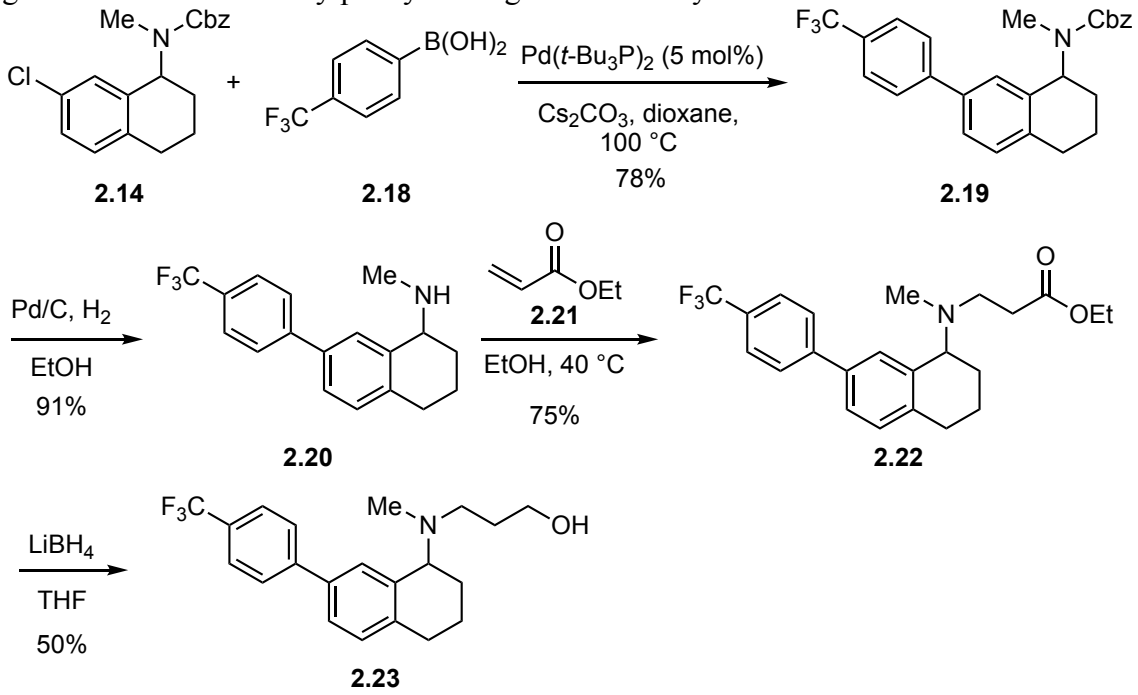

Scheme 2.4. Synthesis of the 4-trifluoromethylphenyl-substituted aminotetralin analog.

Comparison of the σR binding profile of the aminotetralin **2.23** with the corresponding methanobenzazocine **1.219** revealed close similarities (Figure 2.5). Namely, the affinity of **2.23** for the σ2R of 50 nM was similar to the related methanobenzazocine congener **1.219**. Likewise, affinity for the σ1R of the aminotetralin **2.23** was 1,268 nM, leading to a 25-fold preference for the σ2R, which is comparable to the methanobenzazocine analog **1.219**.

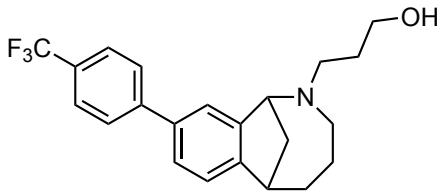

1.219
UKH-1114
σ1R K_i (nM) = 1,279
σ2R K_i (nM) = 46
K_i ratio (σ1R/σ2R) = 28

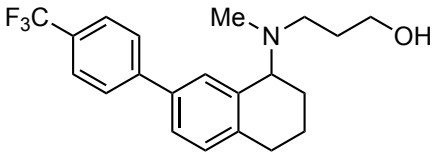

2.23

σ1R K_i (nM) = 1,268
σ2R K_i (nM) = 50
K_i ratio (σ1R/σ2R) = 25

Figure 2.5. Comparison of the 4-trifluoromethylphenyl-substituted tetralin scaffold and the corresponding methanobenzazocine.

Preliminary analysis of analogs having the aminotetralin scaffold revealed binding profiles that were commensurate with similarly substituted norbenzomorphans. Importantly, this observation suggested that this simplified ring system maintains a similar orientation of critical pharmacophore elements. However, more data were needed to assess the merits of this modified scaffold.

2.2 Expanded SAR of the Piperazine-Substituted Aminotetralin Scaffold

Norbenzomorphans, in particular those bearing a piperazine group, that modulate the σ2R yielded encouraging results in some models of neurodegeneration.[12,14] A preliminary study showed that the piperazine-substituted aminotetralin scaffold **2.17** possessed a binding profile that was similar to the corresponding norbenzomorphan derivatives, suggesting that the modified scaffold might also possess similar activity in neurodegenerative models. As a result, we embarked on an expanded SAR investigation to elucidate trends in the binding profile and hopefully to identify useful tool compounds for ongoing assessment of the therapeutic potential of the σ2R in neurophysiological disorders.

Interrogation of the aminotetralin SAR was conducted concurrently with the norbenzomorphan **1.53** and hydrobenzazepine **1.226** derived scaffolds, and trends in substitution pattern that favor the σ2R were just beginning to emerge. However, the piperazine moiety was identified as a preferred ligand subtype. The presence of a basic amine is a mandatory requirement for high affinity σR ligands, and the σ1R crystal structure demonstrated a critical interaction between a basic site on the molecule and acidic residues within the σ1R binding pocket.[6] The existence of related interactions in the binding pocket of the σ2R were not known because the protein had not been identified, but the ubiquitous nature of this functional group among ligands that bind the σ2R suggests that salt bridges might also play an important role for σ2R ligand binding.[220]

Based on these considerations, it seemed reasonable that variations in substituents at the piperazine nitrogen atom of aminotetralin **2.24** may modulate affinity for the σ1R and σ2R, which was the subject of SAR region **A** (Figure 2.6). At the time, the importance of the distal aromatic group in SAR region **D** was not entirely clear, although the benzyl carbamate did appear to be favorable on the norbenzomorphan. Thus, the intial SAR investigation would retain the benzyl *N*-methylcarbamate functionality in region **D** present in **2.17**. Likewise, the position of the piperazine was fixed at the C–7 position in region **B**.

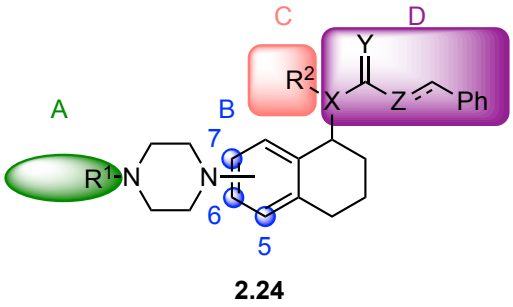

2.24

Figure 2.6. SAR regions targeted on the aminotetralin scaffold.

2.2.1 The C–7 Piperazine-Substituted Aminotetralin Scaffold

2.2.1.1 Synthesis of C-7 Piperazine Analogs

The first-generation synthesis of the aminotetralin scaffold (Scheme 2.2) provided both C–6 and C–7 halogenated scaffolds that were easily diversifiable, but six steps were needed to access the key intermediate **2.14**. Given our interest in more thoroughly exploring piperazine substituents at the C–7 position, a more expedient approach to that regioisomer was developed. Tetralone **2.25** possesses the bicyclic ring system present in the aminotetralin scaffold, but incorporation of a halogen substituent on the aromatic ring was first needed. Direct bromination of tetralone **2.25** was accomplished according to a literature protocol via addition of bromine to a mixture of **2.25** and excess $AlCl_3$ that had been heated at 70 °C for 1 hour to deliver a separable mixture of **2.26** and **2.27** in 76% combined yield (ca. 1:1) (Equation 2.2).[294] The C–7 regioisomer **2.26** is commercially available, although somewhat costly; notably this protocol also provides efficient access to C–5 regioisomer **2.27**, which can be used to probe previously unexplored chemical space.

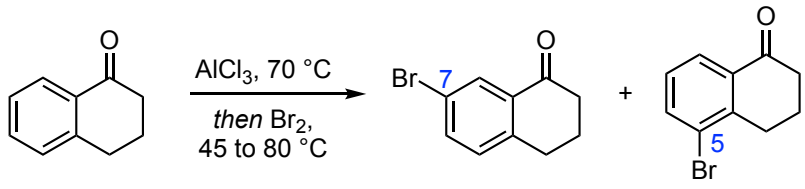

2.25 **2.26**: 36% **2.27**: 40% **(2.2)**

With 7-bromotetralone (**2.26**) in hand, the next step required introduction of the benzyl carbamate moiety. Initial attempts to install the amine via reductive amination of tetralone **2.26** with $MeNH_3Cl$ in the presence of sodium cyanoborohydride resulted in poor conversion, and amine **2.28** was isolated in only 38% yield (Equation 2.3). However, efficient conversion to the amine **2.28** was realized by stirring a solution of **2.26**, $MeNH_3Cl$, triethylamine, and $Ti(O\textit{i}\text{-}Pr)_4$ in ethanol for 22 hours followed by addition of $NaBH_4$ to afford amine **2.28** in 79% yield (Equation 2.4).[295] Subsequent treatment of **2.28** with benzyl chloroformate at 0 °C delivered the halogenated scaffold **2.29** in 98% yield and two steps from commercially available **2.26**.

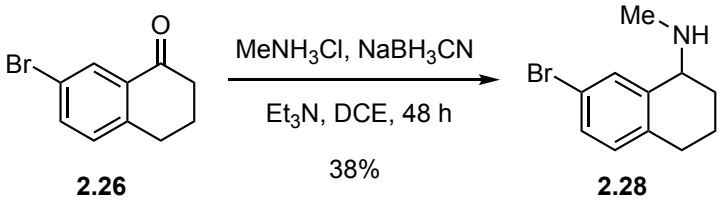

2.26 **2.28** **(2.3)**

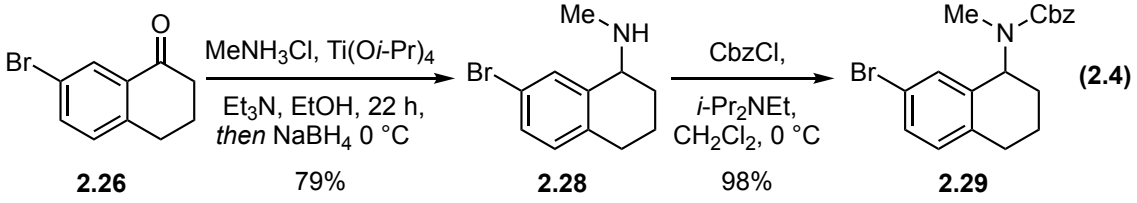

2.26 **2.28** **2.29** **(2.4)**

With an efficient route to 7-bromotetralin scaffold **2.29** in hand, a piperazine moiety was installed via Buchwald-Hartwig cross-coupling using $Pd(OAc)_2$ and

JohnPhos (**1.176**) at 100 °C, following a protocol reported for the norbenzomorphan scaffold (Scheme 2.5).[4,9] However, **2.16** was obtained in only 37% yield. Concurrent investigations with similar substrates revealed that low and variable yields were often obtained using these conditions and loss of the Cbz-group was frequently observed upon analysis of the crude reaction mixtures. Investigation of more mild conditions using Pd_2dba_3 and RuPhos (**2.30**), a phosphine ligand with improved reactivity, in the presence of excess piperazine (**1.172**) in THF at 70 °C afforded **2.16** in 91% yield.[296,297]

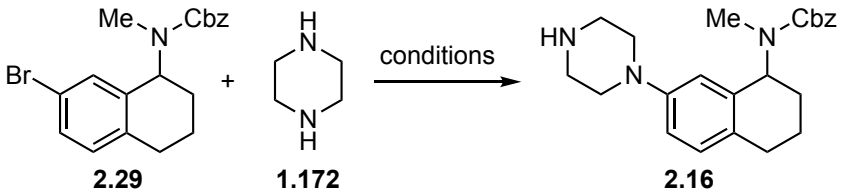

2.29 **1.172** **2.16**

conditions

$Pd(OAc)_2$, JohnPhos, NaO*t*-Bu, PhMe, 100 °C (37%)
Pd_2dba_3, RuPhos, THF, 70 °C (91%)

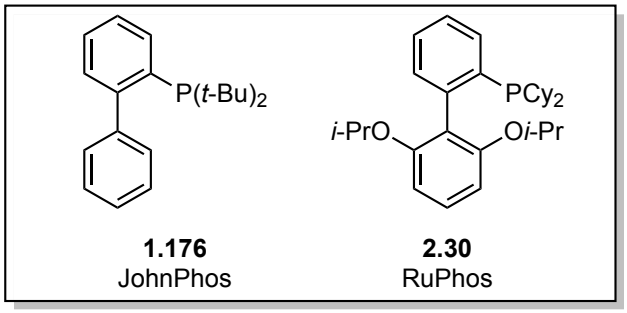

1.176 JohnPhos **2.30** RuPhos

Scheme 2.5. Buchwald-Hartwig amination conditions.

The secondary amine intermediate **2.16** was easily diversified using a variety of *N*–alkylation reactions to access a range of substituted analogs. For instance, reductive alkylation of **2.16** with an aldehyde or ketone delivered analogs **2.31**-**2.35** in high yields (Equation 2.5). Alternatively, reaction of **2.16** with alkyl halides delivered analogs **2.36**-**2.41** in modest to good yields (Equation 2.6). Ester analogs **2.42**-**2.43** were accessed via

conjugate addition of **2.16** with an appropriate acrylate (Equation 2.7). Finally, the ether analog **2.44** was obtained directly from Buchwald-Hartwig amination of the halogenated aminotetralin **2.14** with the commercially available piperazine **2.45** (Equation 2.8). These analogs were submitted to the PDSP for binding analysis according to the protocols previously discussed.

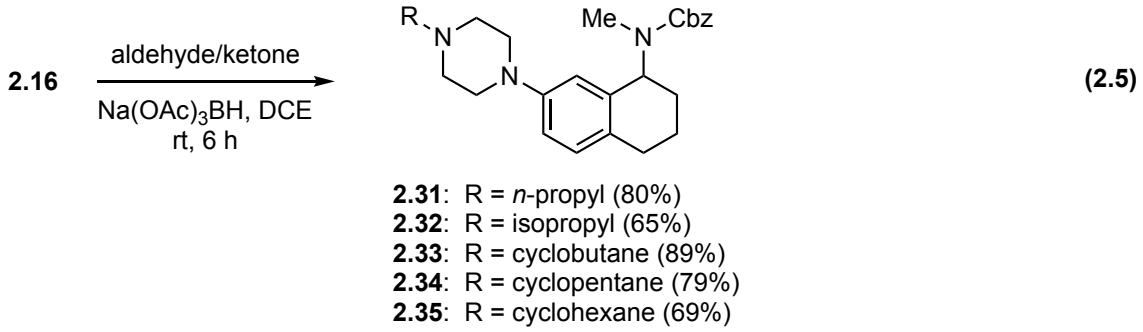

(2.5)

2.31: R = *n*-propyl (80%)
2.32: R = isopropyl (65%)
2.33: R = cyclobutane (89%)
2.34: R = cyclopentane (79%)
2.35: R = cyclohexane (69%)

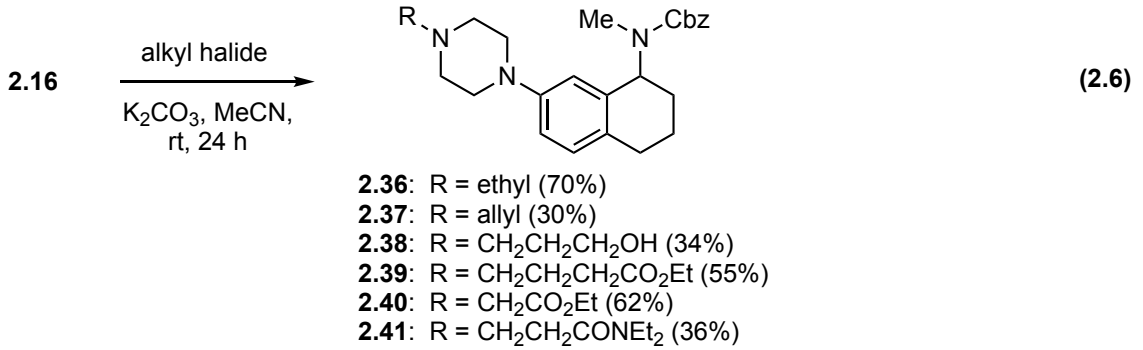

(2.6)

2.36: R = ethyl (70%)
2.37: R = allyl (30%)
2.38: R = $CH_2CH_2CH_2OH$ (34%)
2.39: R = $CH_2CH_2CH_2CO_2Et$ (55%)
2.40: R = CH_2CO_2Et (62%)
2.41: R = $CH_2CH_2CONEt_2$ (36%)

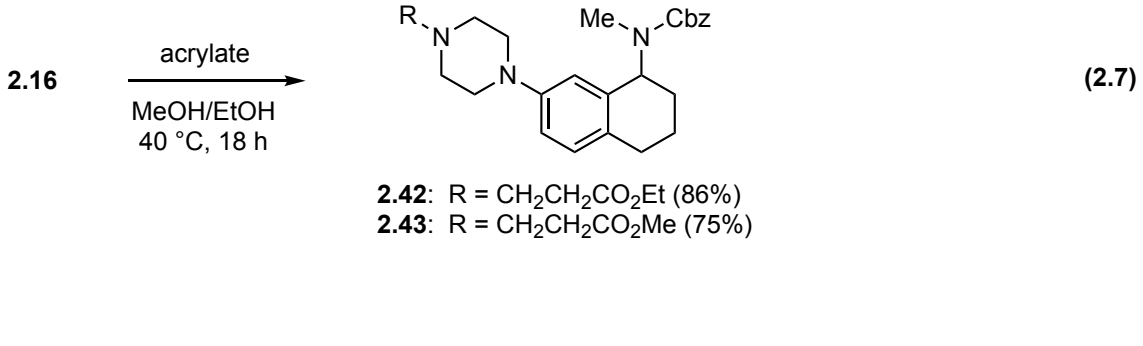

(2.7)

2.42: R = $CH_2CH_2CO_2Et$ (86%)
2.43: R = $CH_2CH_2CO_2Me$ (75%)

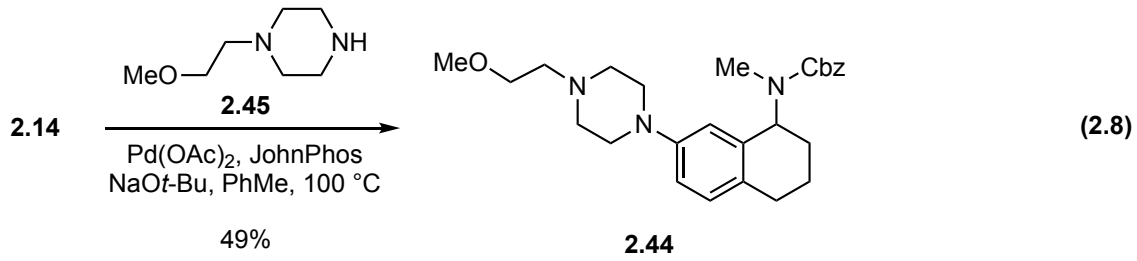

(2.8)

2.2.1.2 Effect of Varying Hydrophobic Piperazine Substituents

The first series of analogs were designed to assess the effect of hydrophobic substituents of increasing size at the piperazine nitrogen atom on binding affinity for the σ1R and σ2R (Table 2.1). The *N*-methylpiperazine analog **2.17** had modest affinity and selectivity for the σ2R. Interestingly, the unsubstituted piperazine analog **2.16** showed increased affinity for both the σ1R and σ2R relative to **2.17**, but the selectivity for the two compounds was similar. However, increasing the length of a linear alkyl group from one to three carbon atoms (**2.17**, **2.36**, **2.31**) increased affinity for both σRs. The observed increase generally favored the σ2R as illustrated by the *n*-propyl analog **2.31**, which has 5.5 nM affinity for the σ2R and 36-fold selectivity over the σ1R. Branching in the aliphatic substituent had comparatively little effect as reflected in the isopropyl analog **2.32**, but introduction of unsaturation with the allyl group in **2.37** resulted in a nearly 20-fold decrease in σ2R affinity.

Table 2.1. Binding affinity of aminotetralins with aliphatic piperazine substituents.

AT = 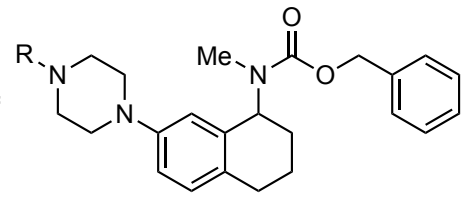

NB = 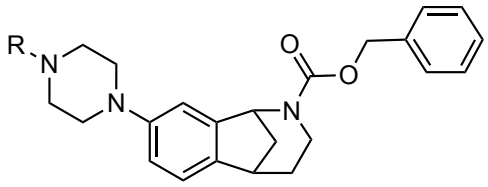

			K_i (nM)		K_i ratio
Cmpd.	R	Scaffold	σ1R	σ2R	(σ1R/σ2R)
2.16		AT	280[a]	32[b]	8.8
1.173		NB	1,624	25	65
2.17		AT	2,944	284	10
1.163		NB	841	90	9.3
2.36	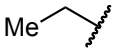	AT	887	35	25
1.190		NB	600	32.5	18
2.31	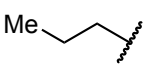	AT	200	5.5	36
1.191		NB	230	5.1	45
2.32	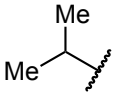	AT	223	8.3	27
1.192		NB	473	14.5	33
2.37	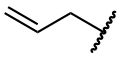	AT	820	105[b]	7.8
1.197		NB	931	76.4	12

K_i values for aminotetralin analogs (single point) determined from non-linear regression of radioligand competition binding isotherms by PDSP. Unless indicated otherwise, σ1R was sourced from guinea pig brain and σ2R was sourced from rat PC12 cells. [a] Determined using HEK293T transfected with human σ1R. [b] Determined using HEK293T cells transfected with human σ2R/TMEM97.

The ligands in this aminotetralin (AT) series were also compared to similarly substituted norbenzomorphan (NB) analogs (Table 2.1). Fortunately, the binding affinity

for each pair was remarkably consistent across the entire range of alkyl groups that were tested. These results provided compelling evidence that the simplified aminotetralins are viable replacements for norbenzomorphans. The unsubstituted piperazine analog **2.16** is the lone exception with σ2R affinity similar to norbenzomorphan **1.173**, but considerably higher σ1R affinity. However, it is notable that σ1R affinity for **2.16** was determined using HEK293T cells transfected with human σ1R, as opposed to the classical assay using GP tissue that was utilized with other ligands. This difference makes a direct comparison more challenging.

Having established that linear aliphatic substituents of increasing size were associated with increased affinity, attention shifted toward *N*-cycloalkyl analogs (Table 2.2). As the ring size is increased from four to six-carbons (**2.33**-**2.35**) affinity for both σRs increases. Among the cyclic hydrocarbon substituents, the cyclopentyl group in **2.34** provides the greatest affinity for the σ2R (2.1 nM) and selectivity (41-fold) for the σ2R over the σ1R. Expanding the ring size to a cyclohexyl group in **2.35** produces a notable increase in σ1R affinity with no change in σ2R affinity, resulting in a more modest 7.6-fold preference for the σ2R. Hydrophobic bulk appears to be well tolerated near the basic nitrogen atom by both the σ1R and σ2R, and σR affinity is enhanced as the group size increases. Similar to linear aliphatic groups, there is a high level of consistency between analogs derived from the simplified aminotetralin scaffold and similarly substituted norbenzomorphan analogs, further validating the simplified scaffold.

Table 2.2. Binding affinity of aminotetralins with carbocyclic piperazine substituents.

AT = 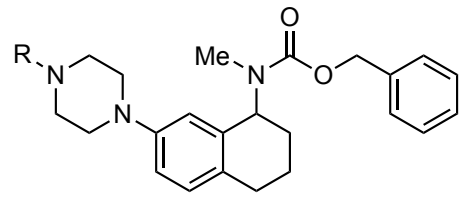

NB = 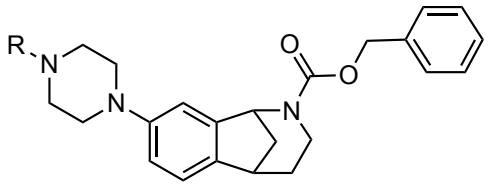

			K_i (nM)		K_i ratio
Cmpd.	R	Scaffold	σ1R	σ2R	(σ1R/σ2R)
2.33	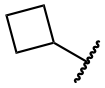	AT	266	12	22
1.194		NB	208	5.0	42
2.34	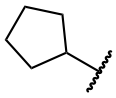	AT	86	2.1	41
1.195		NB	130	3.6	36
2.35	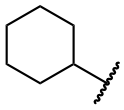	AT	16	2.1	7.6
1.196		NB	29.8	12.5	2.4

K_i values for aminotetralin analogs (single point) determined from non-linear regression of radioligand competition binding isotherms by PDSP. Unless indicated otherwise, σ1R was sourced from guinea pig brain and σ2R was sourced from rat PC12 cells.

2.2.1.3 Polar Functional Groups on the Piperazine Substituent

Having assessed a range of aliphatic groups on the piperazine nitrogen atom, attention turned toward incorporating polar functionality on these substituents. Large hydrophobic groups in close proximity to the basic nitrogen atom appear to be readily accommodated by the σ1R and σ2R. However, the data indicate that high σ2R affinity can be obtained with or without large hydrophobic groups, whereas such groups are imperative for high σ1R affinity. This observation suggested that introducing polar functionality at this site might disrupt the preference for hydrophobic interactions in this

region by the σ1R, but perhaps with less impact on σ2R binding, thereby enhancing σ2R selectivity.

To examine this hypothesis, a series of analogs with several polar functional groups at various locations on the *N*–alkyl substituent were evaluated (Table 2.3). In comparison to propyl piperazine analog **2.31**, each compound had diminished affinity for the σ1R, but the impact on σ2R potency was generally more subtle. For instance, the incorporation of an ethyl ester in **2.42** resulted in an 8-fold decrease in σ1R affinity, but potency for the σ2R was virtually unchanged, affording a remarkable 366-fold preference for the σ2R. Extending the length of the carbon chain between the basic amine and the carbonyl moiety from two to three-carbons in **2.39** provided a modest decrease in σ2R affinity that resulted in a more modest 68-fold preference for σ2R. In contrast, decreasing the length of the aliphatic chain from two to one-carbon atoms in **2.40** significantly reduced affinity for both σRs. It is notable that a structurally related amine with an α-ester moiety similar to **2.40** has significantly reduced basicity as compared to a β-ester moiety similar to **2.42** (ΔpK_a ca. -1.5).[264] Thus, the diminished σR affinity of **2.40** might be attributed to a decrease in basicity that mitigates formation of a strong salt-bridge interaction in the receptor binding site. Decreasing the length of the alkoxy-carbon chain in methyl ester analog **2.43** provided similarly diminished σ1R, although with a more pronounced decrease in σ2R affinity. A similarly positioned carbonyl moiety in diethylamide analog **2.41** reduced σ1R affinity to micromolar levels, but low nanomolar affinity was retained for the σ2R, resulting in a 292-fold preference over the σ1R. The propyl alcohol analog **2.38** displayed a modest reduction in σ1R affinity (ca. 2-fold), accompanied by decreased σ2R affinity (ca. 4-fold) and a similar effect was observed in methyl ether analog **2.44** with a more prominent reduction in potency at both the σ1R and σ2R. As observed with hydrophobic groups, the binding profile of the aminotetralin and

norbenzomorphan analogs are generally similar, although with somewhat more variability that might be attributed to an increased sensitivity toward minor changes in the position of polar functionality.[298]

Table 2.3. Binding affinity of aminotetralins with polar substituents at the piperazine.

AT = 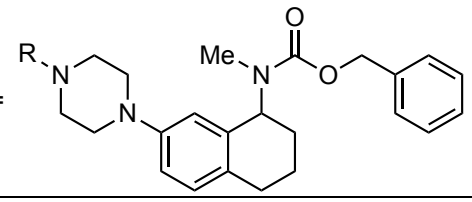

NB = 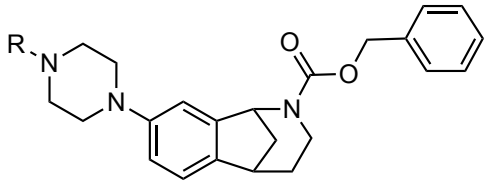

			K_i (nM)		K_i ratio
Cmpd.	R	Scaffold	σ1R	σ2R	(σ1R/σ2R)
2.31	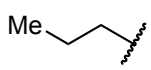	AT	200	5.5	36
1.191		NB	230	5.1	45
2.38	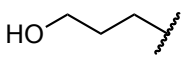	AT	474	21	23
1.202		NB	524	5	105
2.44	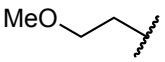	AT	1,054	128	8
2.46		NB	583	26	22
2.40	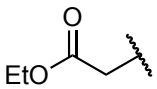	AT	>10,000	894	>11
–		NB	*N/A*	*N/A*	*N/A*
2.42	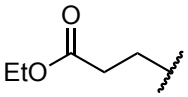	AT	1,649	4.5	366
1.203		NB	6,660	23.8	280
2.39	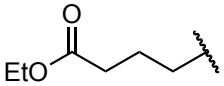	AT	1,369	20[b]	68
–		NB	*N/A*	*N/A*	*N/A*
2.43	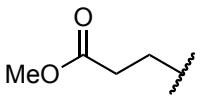	AT	2,864	43	67
2.47		NB	2,275	11	207

Table 2.3. Binding affinity of aminotetralins with polar substituents at the piperazine.

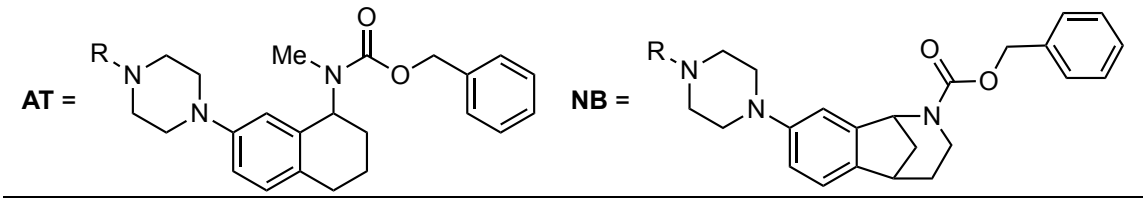

			K_i (nM)		K_i ratio
Cmpd.	R	Scaffold	σ1R	σ2R	(σ1R/σ2R)
2.41	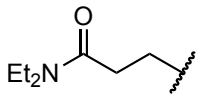	AT	2,101	7.2	292
2.48		NB	963[a]	7.7[b]	125

K_i values for aminotetralin analogs (single point) determined from non-linear regression of radioligand competition binding isotherms by PDSP. Unless indicated otherwise, σ1R was sourced from guinea pig brain and σ2R was sourced from rat PC12 cells. [a]Determined using HEK293T transfected with human σ1R. [b]Determined using HEK293T cells transfected with human σ2R/TMEM97.

Among the analogs tested, those with an alkyl substituent installed at the piperazine nitrogen atom possessing a carbonyl moiety that is separated from the amine by a two-carbon chain achieved approximately 300-fold selectivity for the σ2R over the σ1R. This represents an important discovery for modulating σ2R selectivity that is not clearly demonstrated among structurally unrelated σ2R ligands. It is important to note that a carbonyl group at this position has minimal impact on σ2R affinity, while significantly disfavoring interaction with the σ1R. As previously discussed, many of the more σ2R selective ligands incorporate some HBA group or other polar functionality, but a relationship with respect to its proximity to the basic amine site has not been clearly estabilished.[162,203,220] This provides support for the hypothesis that the σ1R requires a large hydrophobic group near the basic nitrogen and that polar functionality in this region

can disrupt binding. These results represent a valuable observation that could potentially be further optimized to enhance selectivity for the σ2R.

2.2.1.4 Nitrogen Containing Heterocycles in SAR Region A

During lead optimization, lipophilic bulk is often accumulated on molecules and such changes can frequently give rise to enhanced potency. However, increased lipophilicity can also result in physiochemical properties that are not ideal, contributing to downstream attrition of drug candidates.[299] It is therefore important to more broadly consider molecular attributes that are favorable not just for potency, but also for adsorption, distribution, metabolism, excretion, and toxicity (ADMET). The lipophilicity of a compound is often related in terms of its computed *n*-octanol and water partition coefficient (cLog*P*) with higher values corresponding to increased lipophilicity. This parameter is a particularly important component in many factors associated with drug properties.[298,300] Indeed, cLog*P* values greater than five were associated with a decreased likelihood of oral bioavailability by Lipinksi.[301] Later, nearly 30,000 compounds were profiled by GlaxoSmithKline (GSK) finding that on average those with cLog*P* values less than four and molecular weights below 400 exhibited more favorable ADMET profiles.[302]

The propensity of basic compounds to inhibit the human ether-a-go-go related gene (hERG) potassium ion channels, a particularly promiscuous protein that is associated with life-threatening heart arrhythmias, is magnified with increased lipophilicity.[303] In fact, among the basic molecules reviewed by GSK, those with cLog*P* values greater than four had, on average, a higher likelihood of hERG inhibition along with lower solubility and lower bioavailability, as compared to compounds with cLog*P* values less than four.[302] The balance of these molecular features is certainly more

nuanced than these general parameters, but they provide guidelines that can be applied during development.[298]

The discovery that polar functional groups in region **A** significantly attenuate affinity for the σ1R with little disruption in σ2R affinity was an intriguing finding and provides a useful strategy for augmenting selectivity. This was particularly effective with either an ester or amide moiety positioned two to three-carbons from the basic amine group. The investigation of aliphatic substituents in this region revealed that considerable hydrophobic bulk was also well-tolerated by the σ2R. However, the series of analogs that probed polar functional groups was limited to flexible, linear substituents. These observations raised the possibility that more bulky heterocycles possessing similar functionality in this region, but with potentially unique physiochemical properties, might also provide a similar effect. Thus, the incorporation of polar heterocycles in region **A** could potentially decrease lipophilicity and enhance σ2R.

The previous investigation of substituents in this region revealed that an amide moiety provided low nanomolar affinity for the σ2R and 292-fold selectivity over the σ1R in analog **2.41**, suggesting that structural variants might also be promising. A lactam was envisioned as a heterocyclic replacement that would provide similar functionality in region **A** as part of a conformationally constrained ring system. Accordingly, heating a solution of piperazine analog **2.16** and the known lactam 1-(chloroethyl)-2-pyrolidinone (**2.49**) at 65 °C for 72 h provided **2.50**, albeit in only 25% yield along with significant unreacted starting material (Equation 2.9).[304] However, a sufficient quantity of material was obtained for an initial evaluation before additional optimization was pursued.

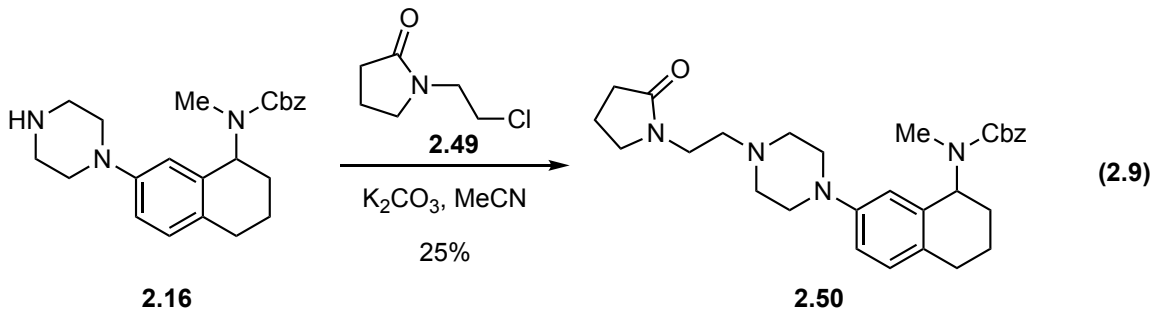

2.16 **2.50** **(2.9)**

Alternatively, a common strategy during development of drug candidates is the replacement of a functional group with a bioisosteric equivalent that elicits a similar biological effect, but is structurally unique. This strategy is often employed to exchange metabolically labile groups with more robust groups or as a means of modulating physiochemical and ADMET properties.[305] Ester and amide groups are frequently targeted for bioisostere replacement, and many functional groups have been established for this purpose, particularly azole heterocycles.[305] Exchanging the carbonyl moiety in ester **2.42** and amide **2.41** with a known heterocyclic bioisostere might provide similarly potent and selective σ2R ligands, but with decreased cLog*P* values and more favorable ADMET properties.

To test this hypothesis, a small series of analogs was desinged to probe the effects of heterocyclic isosteres in this region. The 1,2,4-oxadiazole ring system is a well-established bioisostere for amide and ester functional groups that can be accessed via a nitrile intermediate.[305,306] Accordingly, a solution of piperazine analog **2.16** in methanol at 0 °C was treated with acrylonitrile (**2.51**) to deliver the 1,4-addition product **2.52** in 70% yield (Scheme 2.6). Nucleophilic addition of hydroxylamine to nitrile **2.52** delivered amide-oxime **2.53** in 45% yield. Notably, significant formation of piperazine **2.16** was observed in the crude reaction mixture, presumably resulting from retro-Michael addition under the reaction conditions. 1,2,4-Oxadiazoles are commonly constructed by acylating

amide-oximes with either an acid chloride or anhydride followed by base promoted condensation to form the heterocycle.[307] However, refluxing **2.53** with acetic anhydride in pyridine delivered in intractable mixture containing only a trace amount of oxazole **2.54**.[308] An alternative two-step sequence was conducted according to a reported protocol by first acylating amide-oxime **2.53** with acetyl chloride then treating the crude reaction mixture with tetrabutylammonium fluoride (TBAF) to promote cyclization afforded trace quantities of oxazole **2.54** as part of a complex mixture that was could not be purified.[309]

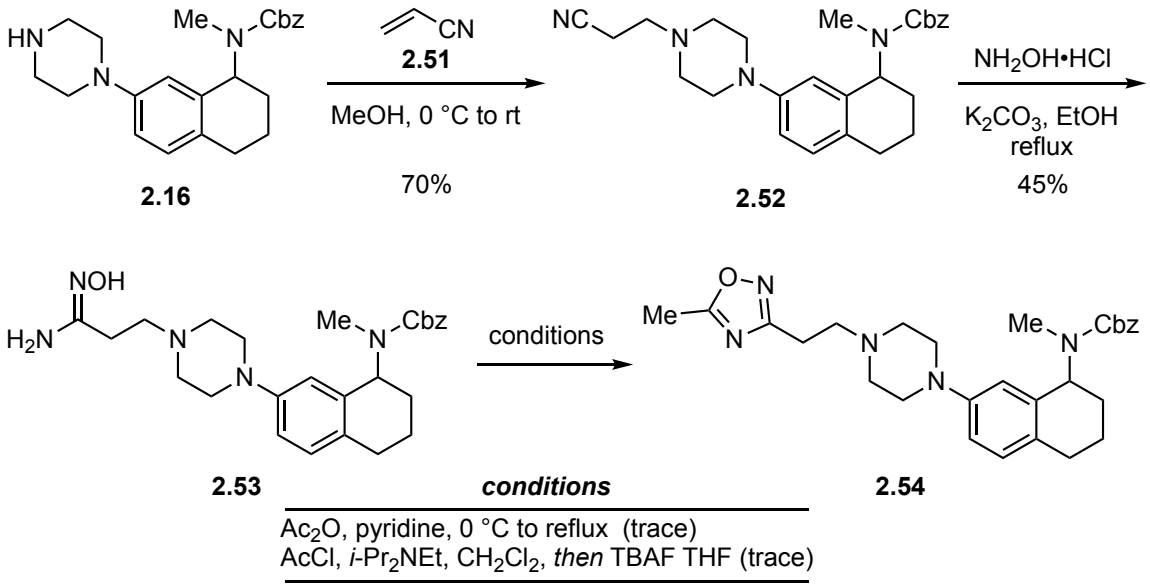

Scheme 2.6. Synthesis 1,2,4-oxadiazole analog.

The assemblage of 1,2,4-oxadiazole **2.54** through a nitrile precursor proved somewhat challenging and suffered from low yields during formation of the amide-oxime intermediate. As a result, an alternative approach was devised utilizing ester analog **2.42** as a potential divergent intermediate for accessing structurally distinct oxazoles. In the event, ester **2.42** was heated under reflux with amide-oxime **2.55** to deliver 1,2,4-oxadiazole **2.56** in 71% yield (Scheme 2.7.A).[310,311] Alternatively, nucleophilic addition

of hydrazine to ester **2.42** provided the hydrazide intermediate **2.57** accompanied by formation of the retro-Michael addition product **2.16** that could not be separated (Scheme 2.7.B).[312] Thus, the crude reaction mixture was subjected to microwave irradiation with excess trimethyl orthorformate to afford 1,3,4-oxadiazole analog **2.58** in 63% yield over two-steps.

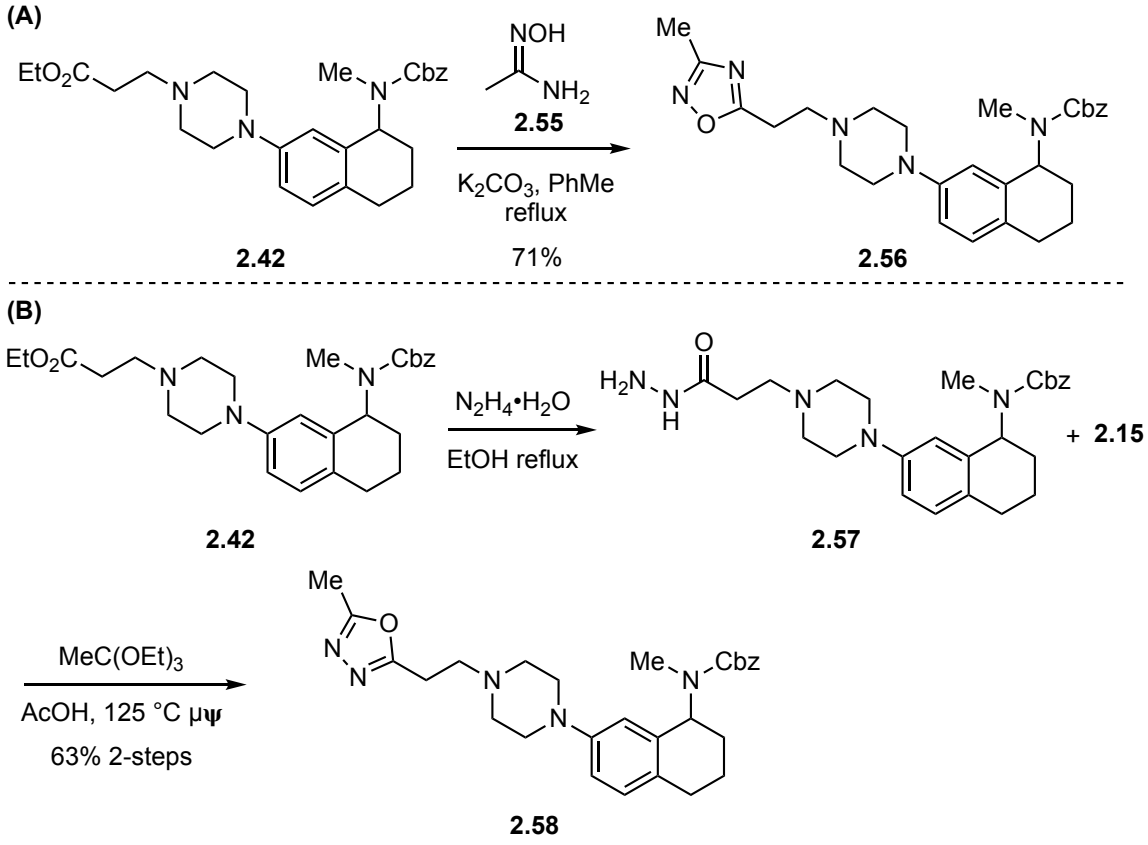

Scheme 2.7. A) Synthesis 1,2,4-oxadiazole analog. B) Synthesis of 1,3,4-oxadiazole analog.

Analogs **2.50**, **2.56**, and **2.58** were submitted to the PDSP but are still awaiting complete binding analysis (Table 2.4). Interestingly, lactam **2.50** suffered from a complete loss of activity at the σ2R, but was accompanied by a greater than 11-fold

increase in σ1R potency. This is a profound shift that highlights a potential unforeseen sensitivity to polar groups in this region. Binding analysis of oxazoles **2.56** and **2.58** has been delayed due to COVID-19, but a preliminary single point assay (10 μM test-ligand) yielded encouraging results. Oxazole analog **2.56** displayed high levels of σ2R inhibition (94%) and lower inhibition at the σ1R (88%), a notable decrease at such a high test-ligand concentration. Oxazole analog **2.58** exhibited much lower inhibition of σ1R (64%), and retained high levels of σ2R inhibition (96%). These preliminary results are encouraging, but determination of inhibition constants will be necessary before the results can be interpreted. Nonetheless, it is interesting that lactam **2.50** suffered complete loss of σ2R inhibition in a single point assay (10 μM), whereas oxazoles **2.56** and **2.58** displayed significant inhibition suggesting that heterocyclic ester and amide isosteres in this region may be promising. In addition, comparison of cLog*P* values for these compounds reveals that analogs **2.56** and **2.58** with oxazole substituents attained cLog*P* values below four, a notable reduction as compared to amide analog **2.41**. While these are merely predicted values, it suggests that physiochemical properties might be effectively modulated with polar heterocycles in this region.

Table 2.4. Binding affinity of aminotetralins with polar heterocycles in region **A**.

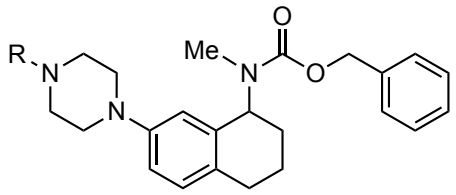

2.23

			K_i (nM)		K_i ratio
Cmpd.	R	cLog*P*[c]	σ1R	σ2R	(σ1R/σ2R)
2.41	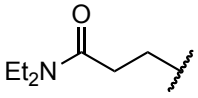	5.7	2,101	7.2	292
2.50	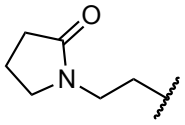	4.4	188	>10,000[b]	< 0.019
2.56	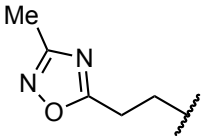	3.4	pending	pending	pending
2.58	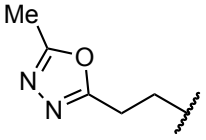	3.3	pending	pending	pending

K_i values for aminotetralin analogs (single point) determined from non-linear regression of radioligand competition binding isotherms by PDSP. Unless indicated otherwise, σ1R was sourced from guinea pig brain and σ2R was sourced from rat PC12 cells. [a]Determined using HEK293T transfected with human σ1R. [b]Determined using HEK293T cells transfected with human σ2R/TMEM97. [c] cLogP values calculated using BioByte with ChemDraw Professional 16.0.

2.2.1.5 Summary of Piperazine Substituents in SAR Region A

Collectively, the investigation of SAR region **A** helped elucidate several important findings on the aminotetralin scaffold (Figure 2.7). A broad range of substitution patterns demonstrated that hydrophobic substituents in region **A** are

sufficient, but not necessary to obtain high affinity for the σ2R and that a secondary nitrogen atom can provide modest selectivity over the σ1R. However, enhanced σ2R potency is obtained with aliphatic groups that are either linear or cyclic and that optimally contain three to five-carbon atoms. Within this size range, potency for the σ2R increases as the size increases, providing reasonable selectivity over the σ1R that is diminished as the size is further increased. The discovery that substituents with polar HBA or HBD groups disfavor interaction with the σ1R is significant. Critically, a carbonyl moiety positioned two to three-carbons from the basic amine was established as an effective tactic for disfavoring the σ1R with little impact on σ2R potency. Thus, varying the substitution pattern on the piperazine nitrogen atom in region **A** delivered analogs with low nanomolar affinity for the σ2R that are capable of obtaining up to 366-fold selectivity over the σ1R.

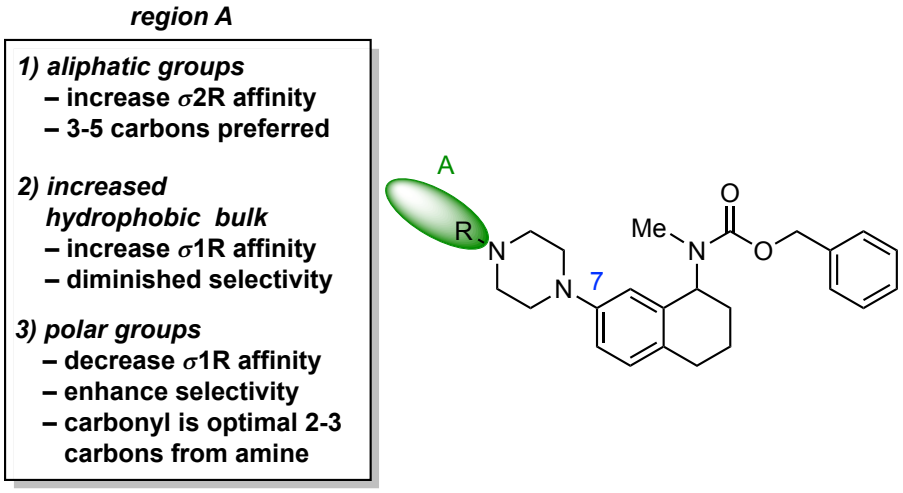

Figure 2.7. Summary of SAR observation in region **A**.

Most importantly, this SAR investigation validated the aminotetralin scaffold as a useful simplified variant of the norbenzomorphan nucleus. The binding profiles of

ligands constructed around this template are quite similar to the norbenzomorphan with a broad range of linear and cyclic hydrophobic groups in region **A**, as well as substituents with polar functionality. This suggests that the modified scaffold provides similar orientations of critical pharmacophore elements among ligands with diverse substitution patterns in this region. Critically, this strategy has resulted in a new scaffold that might possess altered physicochemical or ADMET properties that could be useful during ongoing hit-to-lead development.

2.2.2 Position of the Piperazine on the Aminotetralin Core

A range of hydrophobic and polar substituents were installed in region **A** that elucidated several important trends, but was restricted to the C–7 piperazine-substituted scaffold, which corresponds to C–8 substituted norbenzomorphans. However, it was not clear if the simplified scaffold would offer a σR binding profile that was similar to the norbenzomorphan when the substituents were repositioned on the core benzene ring, thus we explored the SAR in region **B** (Figure 2.8).

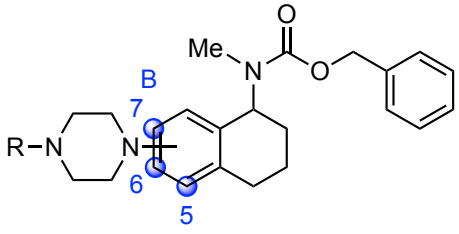

2.59

Figure 2.8. Investigation of the position of piperazine ring in region **B**.

We first prepared the C–6 halogenated aminotetralin scaffold **2.15** using an MCAP inspired approach as previously discussed. The chlorine provided a convenient functional handle for probing the effect of positioning the piperazine at this site. Additionally, the C–5 brominated tetralone **2.27** was accessed according to the

aforementioned bromination protocol to provide access to the 5-substituted analogs. Based on the SAR derived from region **A**, compounds corresponding to *N*-propylpiperazine analog **2.31** and ester analog **2.42** were targeted for comparison.

The synthesis of C–5 and C–6 analogs was similar to that employed for related C–7 analogs. Namely, Buchwald-Hartwig amination of the halogenated scaffolds **2.15** and **2.27** with excess piperazine (**1.172**) was catalyzed by palladium acetate and JohnPhos to afford the piperazine-substituted products **2.60** and **2.61** in 57% and 35% yield, respectively (Equation 2.10). Reductive alkylation of **2.60** and **2.61** with propionaldehyde (**2.62**) delivered the C–5 *N*-propylpiperazine analog **2.63** and the corresponding C–6 analog **2.64** in 71% and 68% yield, respectively (Equation 2.11). Alternatively, treating **2.60** and **2.61** with ethyl acrylate (**2.21**) in ethanol at 40 °C provided the C–5 substituted ester analog **2.65** and the corresponding C–6 analog **2.66** in 84% and 59% yield respectively (Equation 2.12).

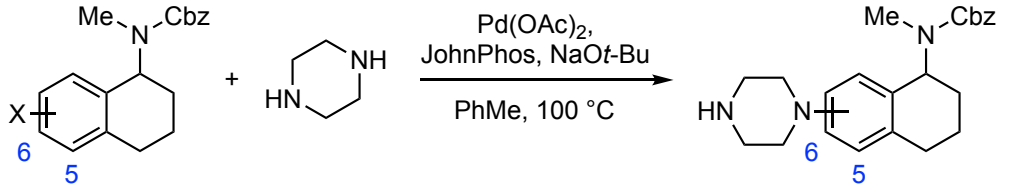

2.27: C–5 = Br
2.15: C–6 = Cl

1.172

2.60: C–5 piperazine (57%)
2.61: C–6 piperazine (35%)

(2.10)

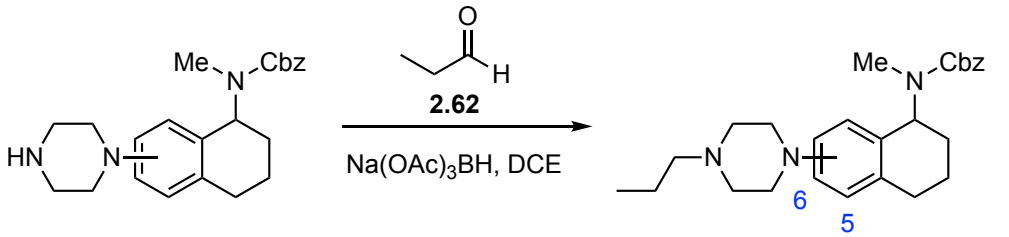

2.60: C–5 piperazine
2.61: C–6 piperazine

2.63: C–5 piperazine (71%)
2.64: C–6 piperazine (68%)

(2.11)

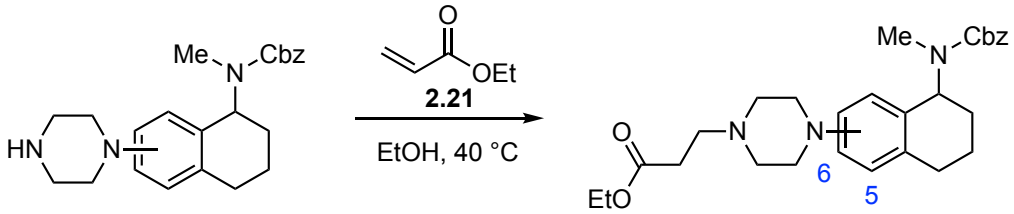

2.60: C–5 piperazine
2.61: C–6 piperazine

2.65: C–5 piperazine (84%)
2.66: C–6 piperazine (59%)

(2.12)

Compounds **2.63**-**2.66** were submitted to the PDSP to determine their σR binding profile and comparison of these binding affinities with those of the corresponding C–7 analog confirmed that substitution at C–7 imparts the greatest σ2R potency with the lowest levels of σ1R affinity (Table 2.5). For example, the C–7 *N*-propylpiperazine in **2.31** exhibited 200 nM affinity for the σ1R, but the C–6 substituted analog **2.64** was 5-fold more potent, whereas the C–5 derivative **2.63** had 17-fold higher affinity for σ1R. In contrast, less-pronounced reductions in σ2R affinity were observed for the C–6 and C–5 congeners **2.64** and **2.63**. Thus, repositioning the piperazine ring from C–7 in **2.31** to the C–5 position in **2.63** switches the σR that is favored from σ2R preferring in **2.31** (36-fold) to σ1R in **2.63** (2.2-fold). As discussed in the preceding chapter, the norbenzomorphan **1.163** that possessed an *N*-propylpiperazine at C–8 favored the σ2R (45-fold), but the same substituent at C–7 in 1.208 switched the σR preference to favor the σ1R (3.4-fold) (Table 1.10). A similar trend is observed in σ1R potency for ester analogs **2.65**-**2.66**, but the carbonyl group appears to still attenuate interaction at σ1R, again highlighting the effect of this functional group. A more pronounced decrease in σ2R affinity is also observed with ester analogs **2.65**-**2.66**, and the lowest σ2R potency is observed in the C–6 analog **2.66**.

Table 2.5. Binding affinity of aminotetralins with varied substitution on the core arene.

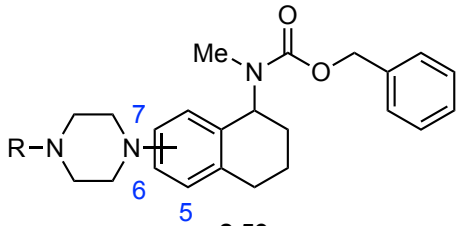

2.59

			K_i (nM)		K_i ratio
Cmpd.	R	position	σ1R	σ2R	(σ1R/σ2R)
2.31	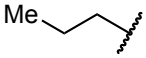	C–7	200	5.5	36
2.64		C–6	40	13	3.1
2.63		C–5	12	26	0.46
2.42	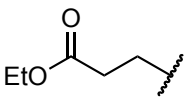	C–7	1,649	4.5	366
2.66		C–6	647	91	7.1
2.65		C–5	303	34	8.9

K_i values for aminotetralin analogs (single point) determined from non-linear regression of radioligand competition binding isotherms by PDSP. Unless indicated otherwise, σ1R was sourced from guinea pig brain and σ2R was sourced from rat PC12 cells.

The probe of SAR region **B** demonstrated that the optimal position for the piperazine substituent on the aminotetralin scaffold for σ2R binding is C–7. Importantly, this trend was confirmed using two dissimilar groups on the piperazine nitrogen atom, suggesting that the effect was not limited to hydrophobic groups. As previously discussed, a related trend was observed with the norbenzomorphan scaffold. Therefore, collectively these data highlight a useful strategy for disfavoring interaction with the σ1R by tuning the position of key pharmacophore elements around the rigid tetralin and norbenzomorphan scaffolds.

2.2.3 Summary of the Scaffold Simplification Strategy: SAR Regions A and B

The SAR investigation of regions **A** and **B** revealed several important characteristics (Figure 2.9). Examination of the cumulative data set reveals that many of the aminotetralin derived ligands displayed high affinity for the σ2R, with greater than 100 nM affinity being observed for the majority of analogs constructed using a range of substitution patterns in both regions **A** and **B**. This illustrates the promiscuous nature of the σ2R and its ability to accommodate considerable structural diversity. However, the σ1R appears to be more sensitive to variations in substitution pattern on the aminotetralin scaffold. Seemingly minor alterations in functional groups or substituent position lead to large shifts in σ1R potency that can range from nanomolar to micromolar levels.

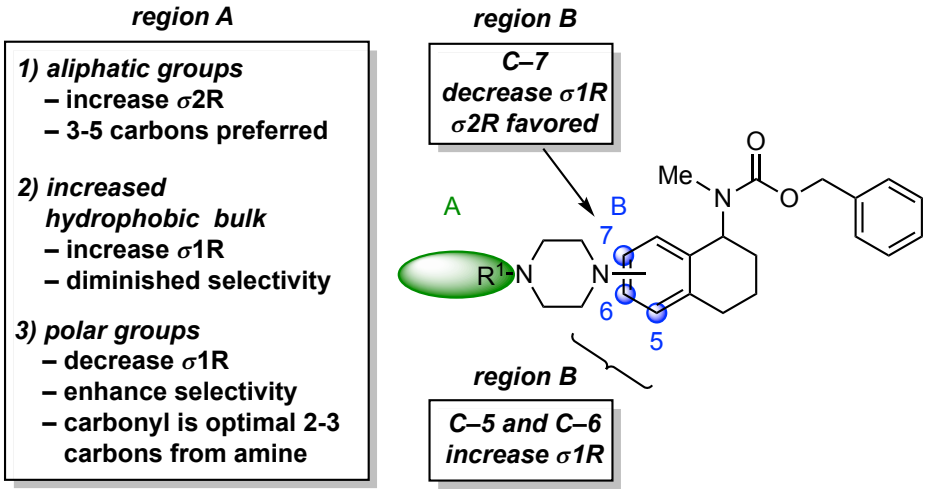

Figure 2.9. Summary of SAR trends in regions **A** and **B**.

Examination of the SAR in region **A** revealed that most hydrophobic substituents provided greater the 35 nM affinity for the σ2R with increasing size leading to enhanced potency for both σ1R and σ2R that results in low nanomolar affinity for both receptors. Therefore, an optimum size range between three and five-carbon atoms avoids significant

increases in σ1R affinity, but high σ2R potency is retained. Installation of alkyl substituents with a carbonyl moiety that is separated from the basic amine by two-carbon atoms decreased affinity for the σ1R to micromolar levels, with relatively little change in σ2R affinity as compared to related hydrophobic substituents. This provides a useful strategy for disfavoring interaction with the σ1R and enhancing σ2R selectivity. In addition, evaluation of the SAR in region **B** demonstrates that installation of the piperazine at C–7 disfavors binding at the σ1R and provides the highest levels of σ2R selectivity. This trend is consistent with observations for the norbenzomorphan and establishes an effective strategy for modulating σR subtype selectivity through the positioning of key pharmacophore elements around the rigid scaffold.

As discussed in the preceding chapter, the pharmacophore models available for the σ1R and σ2R lack predictive power for selective ligand design, but the relative positions of the basic amine and the distal aromatic group have been highlighted as important pharmacophore elements.[138,140,246] In the aminotetralin, the distal aromatic group is represented by the benzyl group of the carbamate moiety (Figure 2.10). It stands to reason that installation of the piperazine moiety at C–7 constrains the basic amine in an orientation relative to the benzylcarbamate that disfavors the σ1R, but remains favorable for the σ2R. If this hypothesis is correct, then it suggests that structural changes that alter the relative orientation of these pharmacophore elements can significantly impact affinity for the σ1R and either enhance or erode σ2R selectivity.

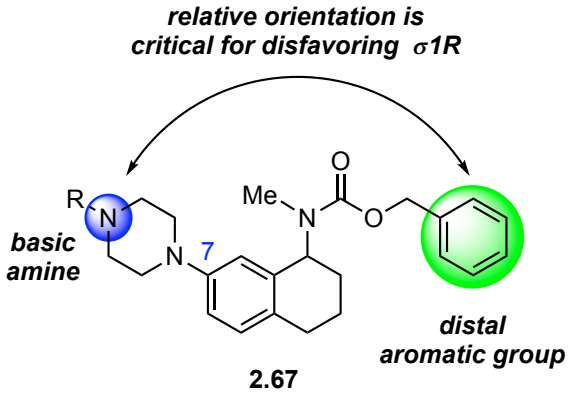

Figure 2.10. The relative orientation of the basic amine and distal aromatic group is a critical pharmacophore feature.

The aminotetralin scaffold was born of a multifaceted scaffold simplification strategy that was aimed at probing the σ2R pharmacophore, while potentially developing alternative leads having improved ADMET and PK profiles. The initial goal of this effort was a comparison of the binding profiles of aminotetralins with that of similarly substituted norbenzomorphan analogs. A high degree of similarity was observed between the norbenzomorphan and the aminotetralin scaffolds in nearly every ligand pair over a range of substitution patterns and structural configurations. These results signify that the orientation of critical pharmacophore elements on the aminotetralin scaffold and the norbenzomorphan is similar. The significance of the position of the distal aromatic group with respect to the basic amine likely indicates that the aminotetralin achieves a similar orientation of these group without the need for a bridged ring system. This highlights the utility of this scaffold simplification strategy for removal of unnecessary structural complexity and validates the aminotetralin as a viable alternative scaffold.

The scaffold simplification strategy that led to the aminotetralin scaffold **2.67** was conducted concurrently with an alternative strategy that delivered the hydrobenzazapine derived scaffolds **2.68** (n = 0-2) (Figure 2.11). Both approaches evaluated removal of the

bridged ring system in norbenzomorphan **2.69**, but the heterocycles **2.68** (n = 0-2) retained a nitrogen atom in the ring and these analogs were generally less selective and less potent for both σRs. Collectively, these results indicate that the relative orientation of the piperazine and the distal aromatic group is more favorable in norbenzomorphan **2.69** and aminotetralin **2.67** scaffolds than in bicyclic heterocycles **2.68**. It also suggests that the aminotetralin and norbenzomorphan might provide similar orientations of these groups which is not as readily achieved with the bicycle **2.68**.

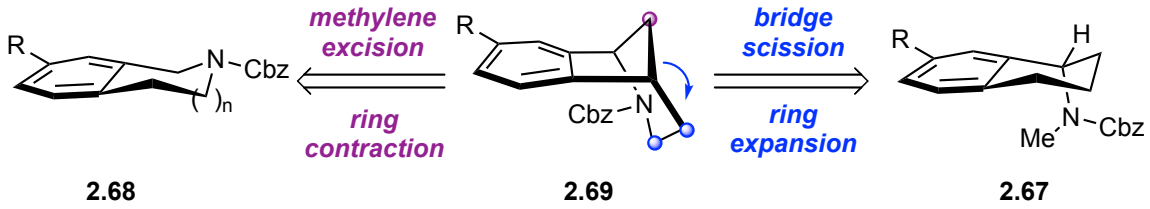

Figure 2.11. Comparison of the scaffold simplification strategies.

Following the elucidation of critical pharmacophore features of the norbenzomorphan and its structurally simplified variants, a picture emerges that might explain the differences observed in the two simplification strategies (Figure 2.10). The bridged ring system of the norbenzomorphan **2.69** projects the core nitrogen atom out the plane of the aromatic ring. Excision of the bridging methylene removes that conformational constraint, providing a more flexible system in which the nitrogen atom preferentially adopts an orientation more in plane with the aromatic ring. The resultant alteration in the position of the benzyl carbamate moiety likely disrupts the relative orientation of the basic amine and distal aromatic group that is critical for disfavoring the σ1R and favoring the σ2R. In contrast, the position of the norbenzomorphan nitrogen atom is more reliably mimicked by the aminotetralin scaffold **2.67** in which the nitrogen

atom is directed out of the plane of the aromatic ring to minimize steric interactions with hydrogen atom of the aromatic ring.[313,314]

2.2.4 Evaluation of the Core Nitrogen Atom

2.2.4.1 Substituents on the Carbamate Nitrogen Atom

The structural modifications to the norbenzomorphan that delivered the aminotetralin scaffold significantly altered the nature of the core nitrogen atom from a heterocyclic motif to and exocyclic amine. This modification generated a newly accessible site of substitution in **2.70** (R^2) that had not yet been explored (Figure 2.12). Accordingly, a brief evaluation of substituents at this position was necessary to determine the optimal substitution pattern of this nitrogen atom. Indeed, investigation of polar and hydrophobic substituents in SAR region A identified trends in nitrogen substituents that delivered considerable enhancements in σ2R selectivity. Therefore, region **C** was devised to assess a series of hydrophobic and polar substituents installed at the core nitrogen atom (R^2), while structural features that favored the σ2R in regions **A** and **B** were retained.

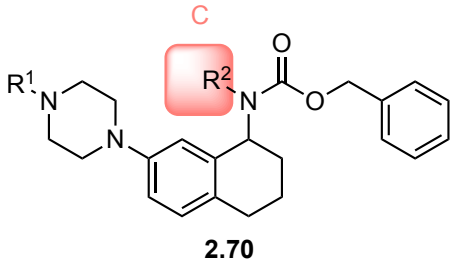

2.70

Figure 2.12. SAR region **C**.

Analogs with hydrophobic groups in region **C** were first prepared via reductive amination of tetralone **2.26** with a primary amine in the presence on sodium cyanoborohydride (Scheme 2.8). As noted in earlier investigations, this reaction

proceeded slowly with significant amounts of starting material being present. The amine intermediate was separated from the crude reaction mixture via acid extraction and the crude residue was treated directly with benzyl chloroformate to delivery halogenated aminotetralin scaffolds **2.71** and **2.72** in 51% and 44% yield over two steps, respectively. Subsequent Buchwald-Hartwig amination with excess piperazine (**1.172**) catalyzed by palladium acetate and JohnPhos delivered the piperazine-substituted scaffolds **2.73** and **2.74** in 73% and 70% yield, respectively.

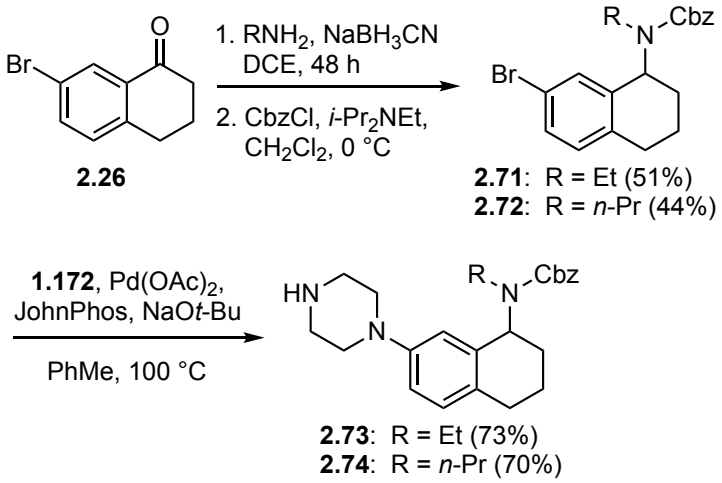

Scheme 2.8. Synthesis of piperazine substituted aminotetralin scaffold with aliphatic group at the benzyl carbamate nitrogen atom.

Similarly, a solution of tetralone **2.26** and ammonium acetate in methanol was heated at 60 °C in the presence of sodium cyanoborohydride to give an intermediate amine that was separated from the crude reaction mixture via acid extraction and the crude residue was treated directly with benzyl chloroformate to deliver the halogenated aminotetralin **2.75** in 63% yield over two steps (Scheme 2.9). Buchwald-Hartwig amination with excess piperazine (**1.172**) using the same conditions delivered the

piperazine-substituted scaffold **2.76**, albeit in 43% yield with loss of Cbz-group observed as a considerable side-product in the crude reaction mixture.

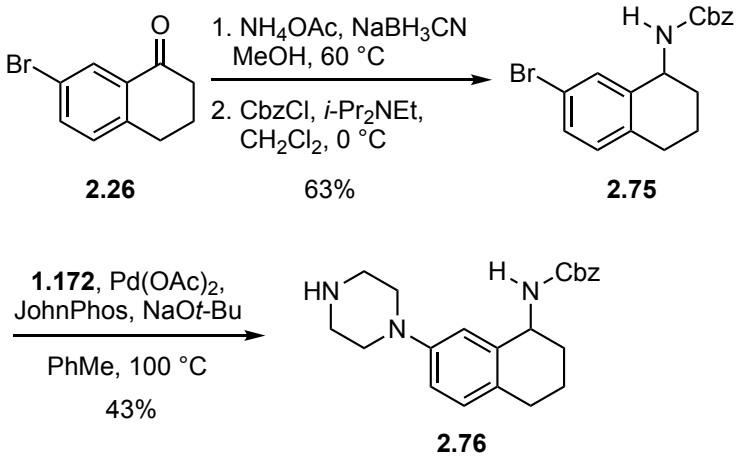

Scheme 2.9. Synthesis of piperazine substituted aminotetralin scaffold.

The synthesis of final analogs was completed through alkylation of the piperazine nitrogen atom with an *n*-propyl group or ethyl ester group to enable comparison to the parent compounds **2.31** and **2.42**. Thus, reductive amination of **2.73**-**2.74** and **2.76** with propionaldehyde (**2.62**) afforded **2.77**-**2.79** in good yield (Equation 2.13). Alternatively, reaction of **2.73**-**2.74** and **2.76** with ethyl acrylate (**2.21**) at 40 °C delivered **2.80**-**2.82** in high yield (Equation 2.14).

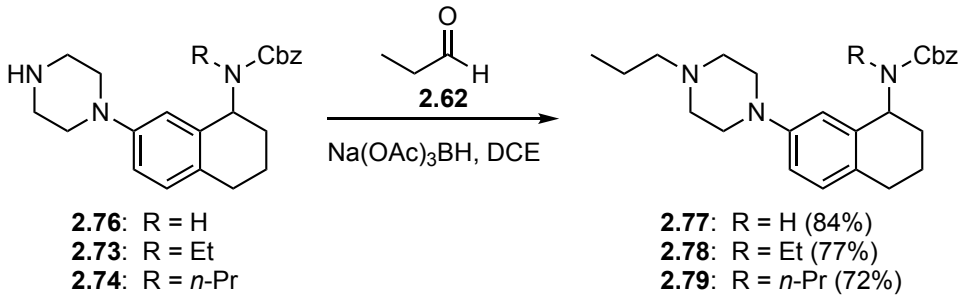

2.76: R = H
2.73: R = Et
2.74: R = *n*-Pr

2.77: R = H (84%)
2.78: R = Et (77%)
2.79: R = *n*-Pr (72%)

(2.13)

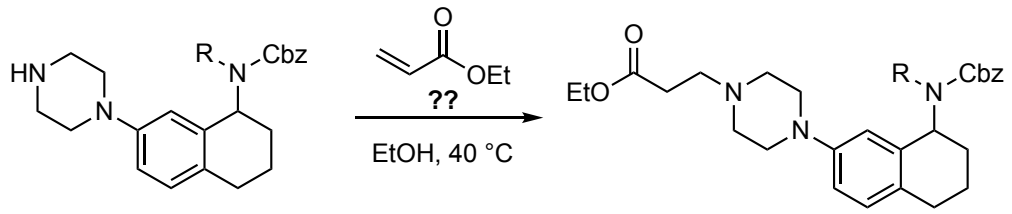

(2.14)

2.76: R = H
2.73: R = Et
2.74: R = *n*-Pr

2.80: R = H (80%)
2.81: R = Et (92%)
2.82: R = *n*-Pr (86%)

Compounds **2.77**-**2.79** and **2.80**-**2.82** were submitted to the PDSP for determination of σR binding affinity according to the protocol previously discussed. Increasing the size of the hydrophobic substituent at the carbamate nitrogen atom (R^2) had relatively little impact on the binding profiles for *N*-propylpiperazine analogs **2.78**-**2.79**, with less the 2-fold change observed in both σ1R and σ2R affinity as compared to benzyl *N*-methylcarbamate analog **2.31** (Table 2.6). A similar trend was observed for the corresponding ester analogs **2.81**-**2.82**, although with a more notable decrease in σ2R affinity was observed with increased size of the *N*–alkyl group (ca. 4-fold). The lowest σ1R affinity was observed with an ethyl group installed at the carbamate nitrogen atom (R^2) in **2.78** and **2.81**, but the reduction was modest as compared to the corresponding methyl substituent. In both cases, the secondary carbamate was not well tolerated with **2.77** and **2.80** suffering from diminished σ2R affinity as compared to the corresponding benzyl *N*-methylcarbamate analogs **2.31** and **2.42**, perhaps pointing toward a modest conformational preference for the tertiary carbamate.

Table 2.6. Binding affinity of benzyl *N*-substituted carbamates.

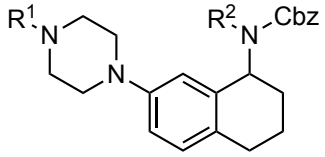

2.70

			K_i (nM)		K_i ratio
Cmpd.	R^1	R^2	σ1R	σ2R	(σ1R/σ2R)
2.77		H	174	56	3.1
2.31		Me	200	5.5	36
2.78	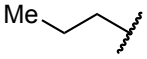	Et	321	4.6	70
2.79		*n*-Pr	199	9.4	21
2.80		H	2,256	80	28
2.42		Me	1,649	4.5	366
2.81	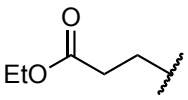	Et	3,315	20	166
2.82		*n*-Pr	2,364	19	124

K_i values for aminotetralin analogs (single point) determined from non-linear regression of radioligand competition binding isotherms by PDSP. Unless indicated otherwise, σ1R was sourced from guinea pig brain and σ2R was sourced from rat PC12 cells.

Because varying the size of the hydrophobic groups at the carbamate nitrogen atom had little effect attention shifted toward incorporating polar functional groups in region **C**. However, we recognized that a more divergent approach was needed to enable an efficient investigation of substituents on the core nitrogen atom. Installation of a substituted piperazine moiety prior to incorporation of the amino moiety was envisioned to provide more rapid access to greater structural diversity. Accordingly, 7-bromotetralone (**2.26**) was subjected directly to Buchwald-Hartwig amination with piperazine (**1.172**) to afford the cross-coupled product **2.83** in 88% yield (Scheme 2.10).

Because 7-bromotetralone (**2.26**) possesses an enolizable ketone, the reaction conditions were modified using cesium carbonate in *tert*-butanol rather than sodium *tert*-butoxide, which can be problematic in the presence of acidic protons.[296] Earlier studies revealed that the tetralone ketone moiety was reticent to undergo reductive amination at room temperature, suggesting that reductive alkylation of the piperazine nitrogen atom should occur preferentially. In the event, treating piperazine substituted tetralone **2.83** with excess propionaldehyde (5 eq.) in the presence of sodium triacetoxyborohydride delivered alkylated product **2.84**, but in only 33% yield. Interestingly, considerable formation of a mixture of a side products that were consistent with an aldol side-reaction to provide **2.85** as a mixture of diastereomers. Reducing the equivalents of propionaldehyde (1.1 eq.) provided modest improvement, affording **2.84** in 55% yield. Ultimately, slow addition of a solution of propionaldehyde (**2.62**) in dichloroethane to a stirred solution of tetralone **2.83** and sodium triacetoxyborohydride delivered **2.84** in 77% yield on a multigram scale. With efficient access to this key intermediate, tetralone **2.84** was subjected to reductive amination with an appropriate amine in the presence of Ti(O*i*-Pr)$_4$, followed by addition of sodium borohydride to afford aminoteralins **2.86**-**2.88** in good yields.

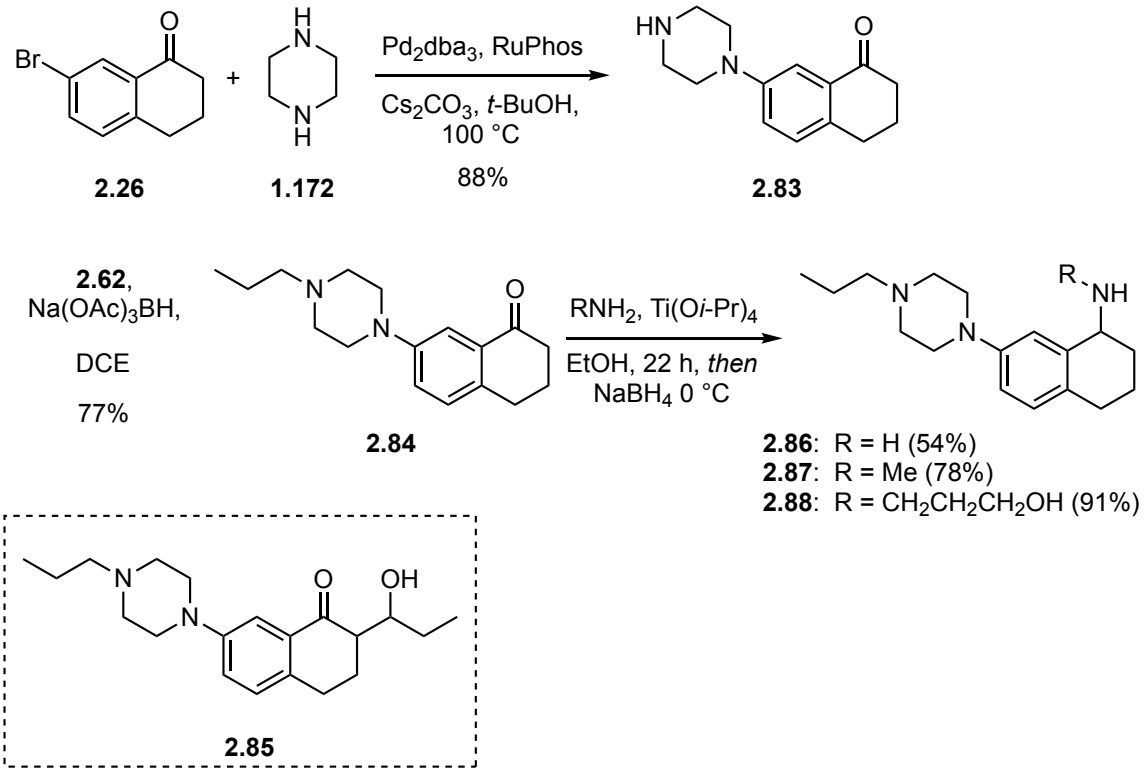

Scheme 2.10. Synthesis of a piperazine-substituted tetralone divergent intermediate.

The primary amine **2.86** was then diversified to probe the effects of ester, ether, and alcohol functional groups in region **C**. Conjugate addition of **2.86** with ethyl acrylate (**2.21**) followed by treatment with benzyl chloroformate delivered ester **2.89**, albeit in only 21% yield over two steps (Equation 2.15). Alternatively, treating **2.86** with 3-oxetanone (**2.90**) in the presence of Ti(O*i*-Pr)$_4$ followed by addition of sodium borohydride and subsequent treatment with benzyl chloroformate afforded **2.91** (Equation 2.16). Notably, reductive amination of tetralone **2.86** with **2.20** in the presence of sodium triacetoxyborohydride failed to deliver the desired product. Lastly, **2.88** was treated with benzyl chloroformate predicting that the amine might react preferentially react over the alcohol moiety, but perhaps unsurprisingly a mixture of products was obtained and **2.92** was isolated in only 19% yield (Equation 2.17). Each of these reactions was low yielding,

but importantly considerable structural diversity was accessed through the common divergent intermediate **2.86** to provide analogs for preliminary analysis. Because our primary interest was determining the effect of polar functional groups in this region on σR affinity, additional optimization was delayed pending binding analysis.

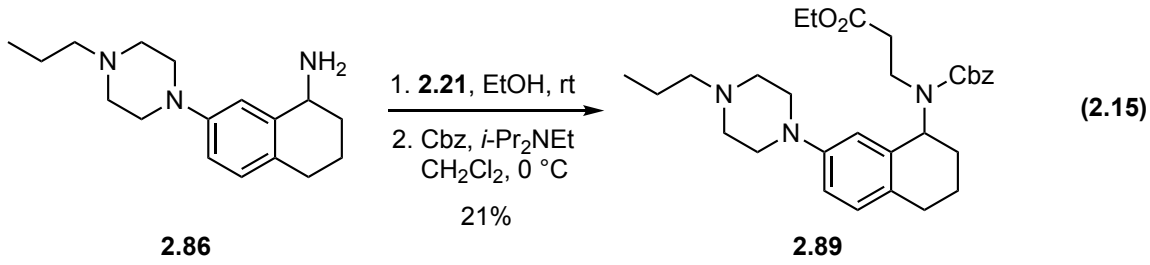

2.86 **2.89** **(2.15)**

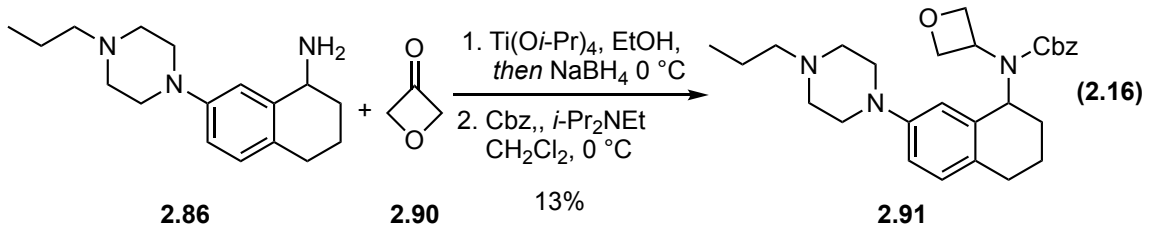

2.86 **2.90** **2.91** **(2.16)**

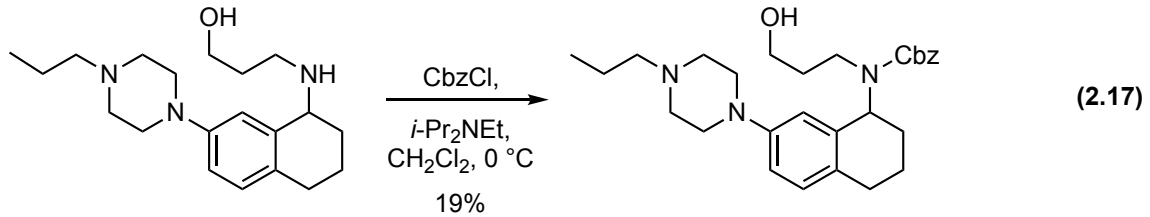

2.88 **2.92** **(2.17)**

Binding analysis of the prepared analogs was conducted by the PDSP revealing that polar groups in SAR region **C** were generally less favorable (Table 2.7). For example, the impact on σ1R was relatively minimal for ester analog **2.89** and alcohol analog **2.92** as compared to the methyl group in **2.31**, but each suffered from diminished σ2R affinity that eroded selectivity. Alcohol analog **2.92** displayed the most pronounced

reduction in σ2R affinity (ca. 24-fold) as compared to benzyl *N*-methylcarbamate **2.31**, whereas ester analog **2.89** suffered a more modest decrease (ca 6-fold). The cyclic ether analog **2.91** also suffered from diminished σ2R affinity (ca. 10-fold) that was accompanied by a modest increase in σ1R affinity. Collectively, these data suggest that polar functional groups in region **C** have a deleterious effect on σ2R affinity and selectivity.

Table 2.7. Binding affinity of analogs with polar groups in region **C**.

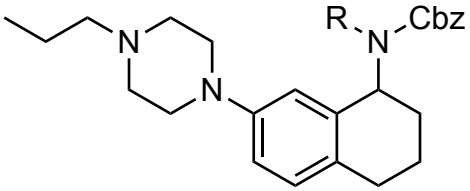

		K_i (nM)		K_i ratio
Cmpd.	R	σ1R	σ2R	(σ1R/σ2R)
2.31		200	5.5	36
2.89	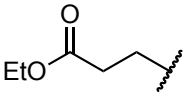	187	35[b]	5.3
2.92	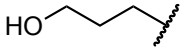	254	135[b]	1.0
2.91	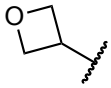	105[a]	57[b]	1.8

K_i values for aminotetralin analogs (single point) determined from non-linear regression of radioligand competition binding isotherms by PDSP. Unless indicated otherwise, σ1R was sourced from guinea pig brain and σ2R was sourced from rat PC12 cells. [a]Determined using HEK293T transfected with human σ1R. [b]Determined using HEK293T cells transfected with human σ2R/TMEM97.

2.2.4.2 Evaluation of the Benzyl Carbamate Functionality

Previous SAR investigations of the aminotetralin retained the benzyl carbamate functionality, thus we now sought to probe the effects of changing this group. Variations

in this region of the norbenzomorphan had been limited, but studies had shown that the benzyl carbamate group could be replaced with an aryl sulfonyl group, but not amide groups, without a loss of potency. Additionally, substituents on the aromatic ring of this groups provided enhanced potency. Hence, a number of analogs were designed in which substitution in region **D** was varied (Figure 2.13).

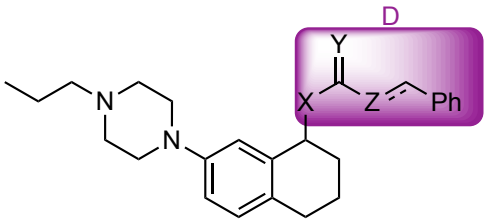

Figure 2.13. SAR region **D**.

The propyl piperazine **2.87** was efficiently accessed in three steps as previous described (Scheme 2.10) and this served as the key intermediate for preparing a range of *N*–substituted derivatives. In the event, stirring a solution of **2.87** in dichloromethane with an appropriate acyl chloride delivered a series of *N*–acylated analogs **2.93**-**2.94** (Equation 2.18).

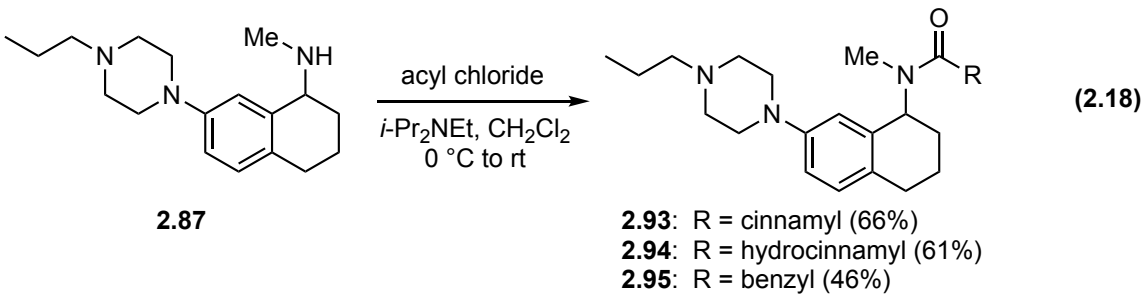

(2.18)

Analogs **2.93**-**2.95** were assayed by the PDSP revealing that different acyl groups were well-tolerated (Table 2.8). Exchanging the benzyl carbamate in **2.31** with a

cinnamamide moiety in analog **2.93** resulted in relatively minimal change in σ1R and σ2R affinities. Interestingly, the affinity of the related hydrocinnamamide analog **2.94** for the σ1R decreased by 4.9-fold as compared to benzyl carbamate **2.31**, leading to increased σ2R selectivity (57-fold). This notable increase in selectivity for the more conformationally restricted cinnamamide analog **2.93** highlights the importance of the orientation of the distal aromatic group. Reducing the length of the spacer by one-carbon atom in amide analog **2.95**, which had similar σ1R potency as the benzyl carbamate analog **2.31**, reduced σ2R affinity (9.6-fold). These results suggest that at least a three-atom linker between the nitrogen atom and the aromatic ring is needed for significant σ2R potency.

Table 2.8. Binding affinity of aminotetralins with varied *N*-acyl groups.

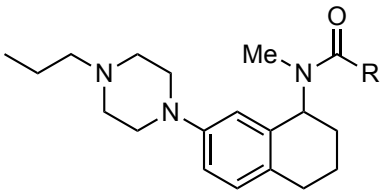

??

		K_i (nM)		K_i ratio
Cmpd.	R^1	σ1R	σ2R	(σ1R/σ2R)
2.31	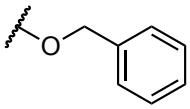	200	5.5	36
2.93	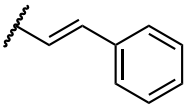	196[a]	9.6[b]	20
2.94	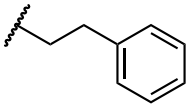	973	17[b]	57
2.95	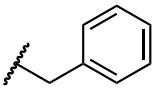	188[a]	53[b]	3.5

K_i values for aminotetralin analogs (single point) determined from non-linear regression of radioligand competition binding isotherms by PDSP. Unless indicated otherwise, σ1R was sourced from guinea pig brain and σ2R was sourced from rat PC12 cells. [a]Determined using HEK293T transfected with human σ1R. [b]Determined using HEK293T cells transfected with human σ2R/TMEM97.

We then worked to assess the importance of the nitrogen atom itself to determine if it was essential, or if it was merely an atom in the linker that might be replaced with another atom, such as an oxygen atom. To probe this question, tetralone **2.84** was treated with $NaBH_4$ to afford benzylic alcohol intermediate **2.96** for diversification (Scheme 2.11). Reaction of **2.96** with sodium hydride followed by alkylation with several alkyl bromides (**2.97**-**2.98**) delivered analogs **2.99** and **2.100** for analysis. In addition, catalytic hydrogenation of the cinnamyl ether analog **2.100** afforded the corresponding

hydrocinnamyl ether **2.101** (Equation 2.19). Alternatively, treatment of alcohol **2.96** with hydrocinnamoyl chloride (**2.102**) delivered ester analog **2.103** (Equation 2.20).

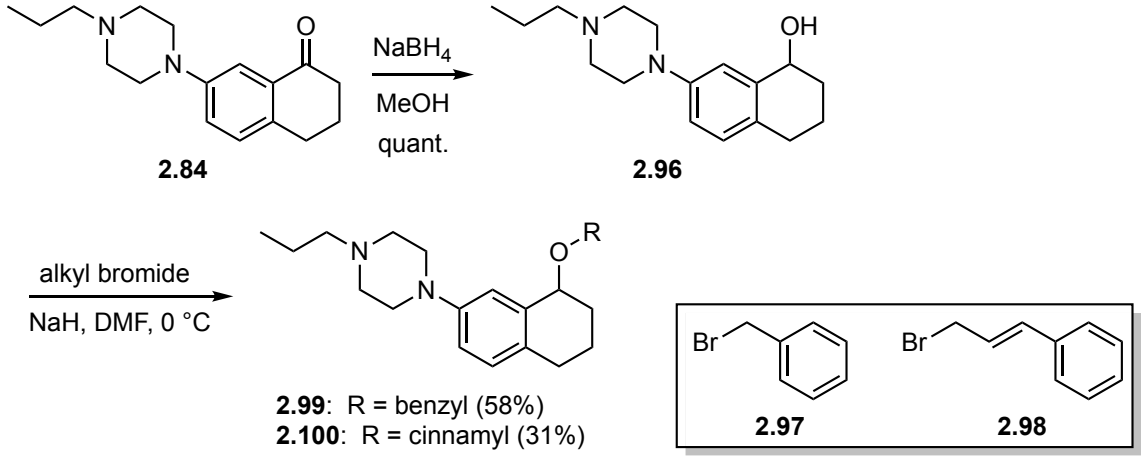

Scheme 2.11. Synthesis of ether substituted tetralin analogs.

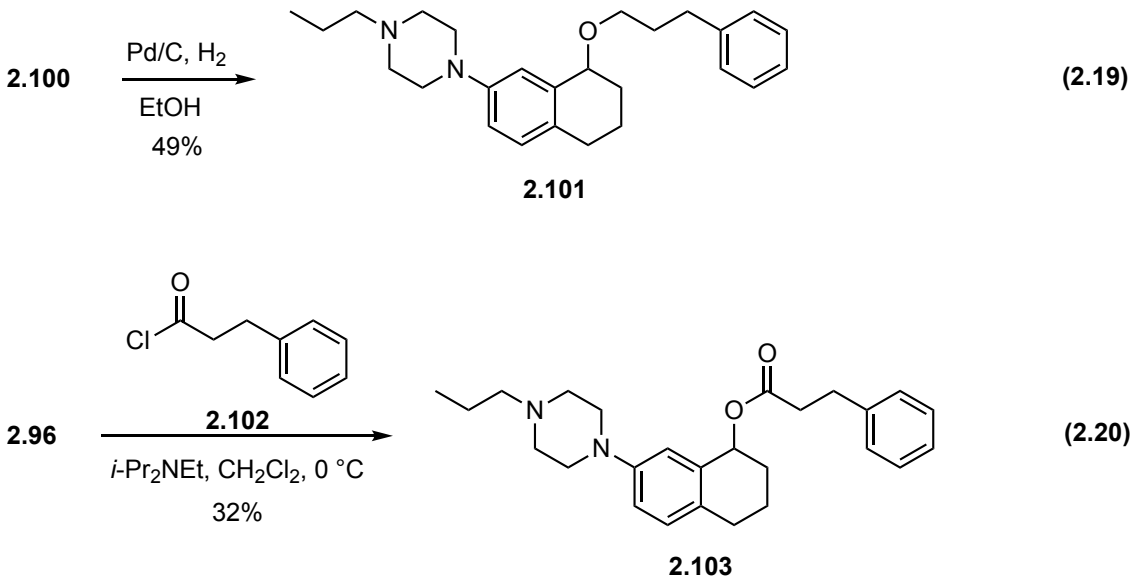

Interestingly, each of the oxygen analogs **2.99-2.101 and 2.103** displayed a considerable increase in σ1R affinity relative to the parent benzyl carbamate analog **2.31** and a modest reduction in σ2R affinity (Table 2.9). For example, hydrocinnamic ether and ester analogs **2.101** and **2.103**, were approximately equipotent for both σRs. However, introduction of an olefin in the side chain of **2.100** diminished σ1R affinity and restored modest levels of σ2R selectivity (9-fold). This is a particularly interesting result because it suggests for the first time that the nitrogen atom is not necessary for σ2R selectivity and again points to a dependence on the precise positioning of the distal aromatic group as a critical pharmacophore element. Similar to the nitrogen derived compounds, shortening the length of the carbon chain in benzyl ether analog **2.99** was unfavorable and decreased σ2R affinity.

Table 2.9. Binding affinity of oxygenated tetralin analogs.

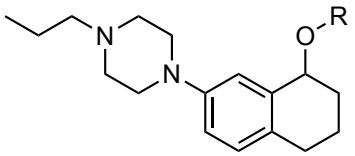

??

		K_i (nM)		K_i ratio
Cmpd.	R^1	σ1R	σ2R	(σ1R/σ2R)
2.103	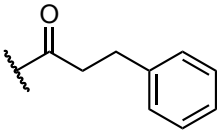	33	25	1.3
2.101	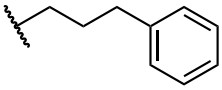	21	17[b]	1.2
2.100	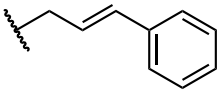	140	15[b]	9
2.99	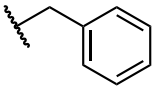	104	50	2.1

K_i values for aminotetralin analogs (single point) determined from non-linear regression of radioligand competition binding isotherms by PDSP. Unless indicated otherwise, σ1R was sourced from guinea pig brain and σ2R was sourced from rat PC12 cells. [a]Determined using HEK293T transfected with human σ1R. [b]Determined using HEK293T cells transfected with human σ2R/TMEM97.

Intrigued by the discovery that the nitrogen atom is not be a required structural feature, two additional analogs were prepared (Scheme 2.12). Treating a solution of tetralone **2.84** and potassium hydroxide in ethanol with benzaldehyde (**2.104**) resulted in aldol condensation to deliver benzylidene analog **2.105** in 59% yield as a mixture of *E*/*Z* isomers (ca. 8:1). Interestingly, analysis of this mixture revealed that σ1R and σ2R affinities were remarkably similar to the cinnamyl ether analog **2.100** with a modest preference for the σ2R (8-fold). Catalytic hydrogenation of the olefin in **2.105** delivered

2-benzyl tetralone **2.106**, albeit in only 28% yield due to competitive reduction of the benzylic ketone moiety that was observed in analysis of the crude reaction mixture. Binding studies of **2.106** showed a notable increase in σ1R potency relative to **2.105** resulting in a slight preference for the σ1R over the σ2R. These results again suggested that the specific positioning of the distal aromatic group, which can be controlled with a conformational constraint, is required to disfavor binding at the σ1R.

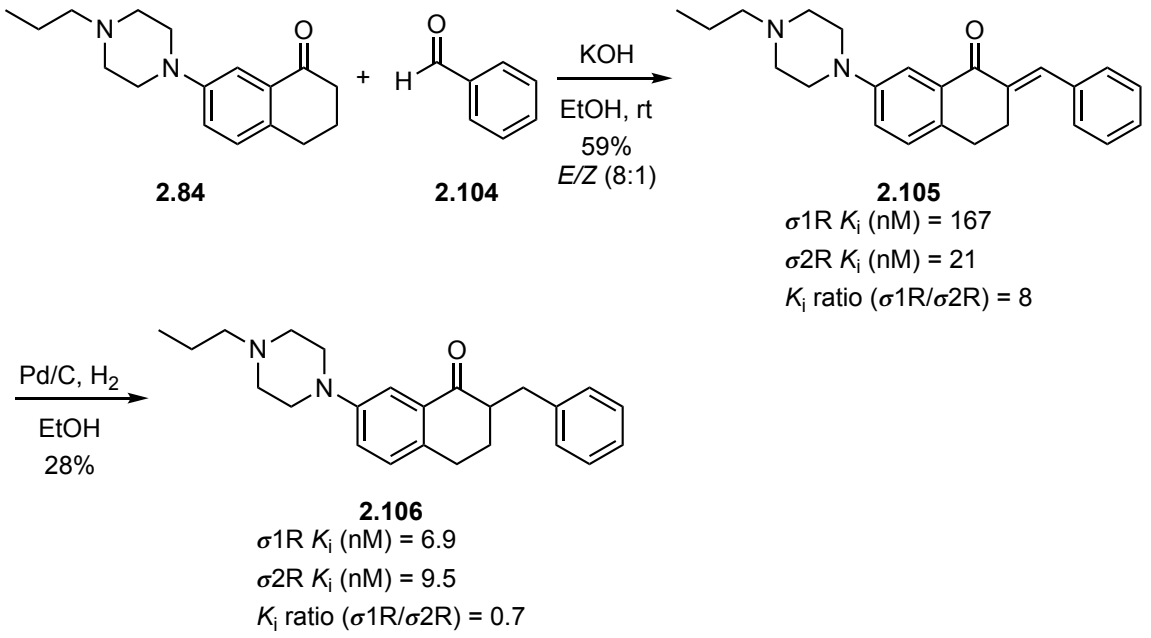

Scheme 2.12. Synthesis of benzylidene derived analogs.

As discussed in the proceeding chapter, substituents on the distal aromatic ring of σ2R ligands, including the norbenzomorphan scaffold, have been observed to significantly alter potency and selectivity.[203,220] Accordingly, we sought to evaluate the effect of placing halogen atoms and more polar methoxy groups on the aromatic ring of this group on the aminotetralin scaffold. In order to access a range of substituents on the piperazine nitrogen atom, the piperazine in **2.83** was first Boc-protected to afford

carbamate **2.107** in 75% yield (Scheme 2.13). Subsequent condensation of **2.107** with $MeNH_3Cl$ in the presence of $Ti(O\textit{i}\text{-}Pr)_4$ followed by addition of sodium borohydride afforded amintotetralin **2.108**. A solution of 4-fluorobenzyl alcohol (**2.109**) in a mixture of toluene and THF (1:1) was treated with phosgene at 0 °C to generate a chloroformate that was allowed to react with aminotetralin **2.108** to deliver the 4-fluorobenzylcarbamate intermediate **2.110** in 73% yield. Removal of the Boc-protecting group with trifluoroacetic acid provided the unsubstituted piperazine analog **2.111**. Reductive alkylation of **2.111** with propionaldehyde (**2.62**) provided *N*-propylpiperazine analog **2.112** (Equation 2.21), and alkylation with the known alkyl bromide **2.113** provided diethylamide analog **2.114** in 94% yield (Equation 2.22).[315]

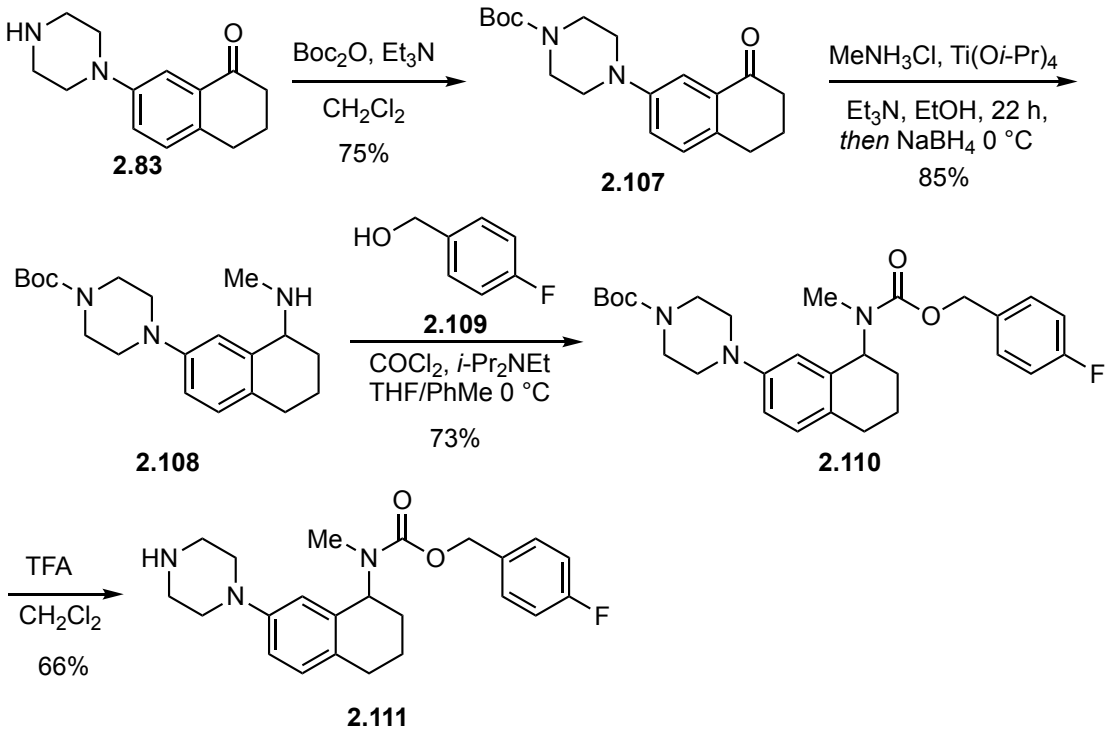

Scheme 2.13. Synthesis of an aminotetralin scaffold with a 4-fluorobenzyl carbamate.

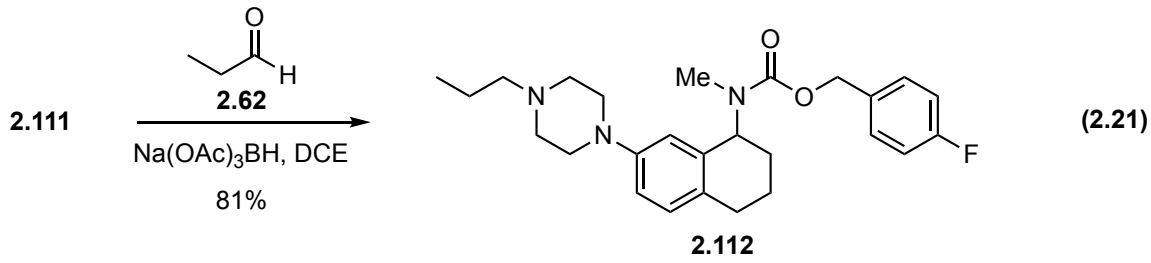

(2.21)

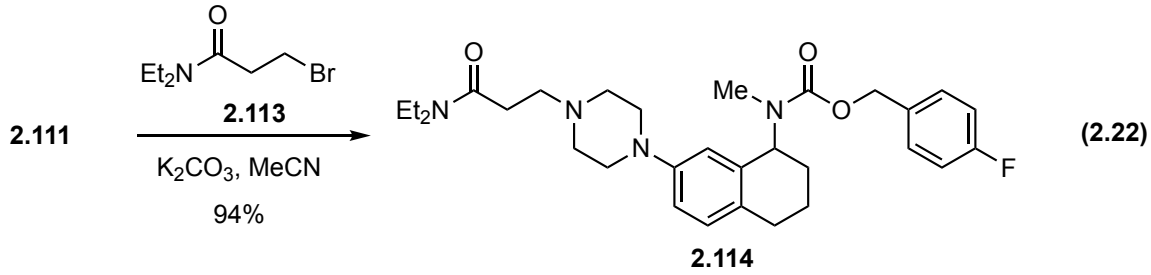

(2.22)

Binding analysis of the 4-fluorobenzyl analogs **2.111**-**2.112** and **2.114** revealed that they had σ2R affinities similar to their benzyl carbamate analogs (Table 2.10). Interestingly, the affinities of analogs **2.112** and **2.114**, which possess an alkyl substituent at the piperazine nitrogen atom, for the σ1R increased, thereby eroding selectivity. In contrast, the σ1R affinity of unsubstituted piperazine analog **2.111** was relatively unchanged. These results suggest that incorporation of a fluorine substituent at the 4-position of the benzyl group generally has a deleterious effect on σ2R selectivity with the aminotetralin scaffold, whereas the same group in norbenzomorphan **1.182** provided an increase in σ2R affinity.

Table 2.10. Binding affinity of 4-fluorobenzyl N-substituted carbamates.

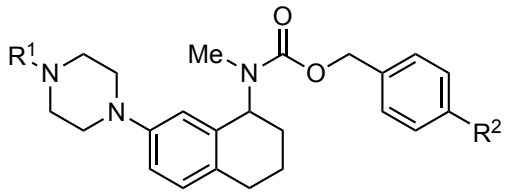

2.115

			K_i (nM)		K_i ratio
Cmpd.	R^1	R^2	σ1R	σ2R	(σ1R/σ2R)
2.16		H	280[a]	32[b]	8.8
2.111		F	237[a]	35[b]	6.8
2.31	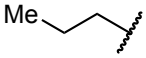	H	200	5.5	36
2.112		F	52[a]	4.4[b]	12
2.41	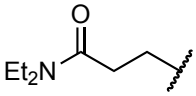	H	2,101	7.2	292
2.114		F	355[a]	3.1[b]	115

K_i values for aminotetralin analogs (single point) determined from non-linear regression of radioligand competition binding isotherms by PDSP. Unless indicated otherwise, σ1R was sourced from guinea pig brain and σ2R was sourced from rat PC12 cells. [a]Determined using HEK293T transfected with human σ1R. [b]Determined using HEK293T cells transfected with human σ2R/TMEM97.

A series of aminotetralin analogs was also designed to probe the effects of more polar methoxy substituents on the aromatic ring. Because the cinnamamide analog **2.93** displayed nearly identical binding affinity for the σ1R and σ2R as the benzyl carbamate analog **2.31**, we decided to study the effect of methoxy-substituted cinnamamides. (Table 2.7). Thus, the aminotetralin **2.87** was coupled with the appropriate cinnamic acid using EDCI to deliver the 2-methoxy, 3-methoxy, and 4-methoxy analogs **2.116**-**2.118** in good yields (Equation 2.23). A similar tactic was used to exchange the phenyl group with a furan moiety in **2.120** that might also provide interesting results with an alternative

aromatic group that is more polar in nature (Equation 2.24). Binding analysis of these analogs has been delayed due to COVID-19, but is anticipated to provide insight into the tolerance of polar functional groups in this region of the molecule.

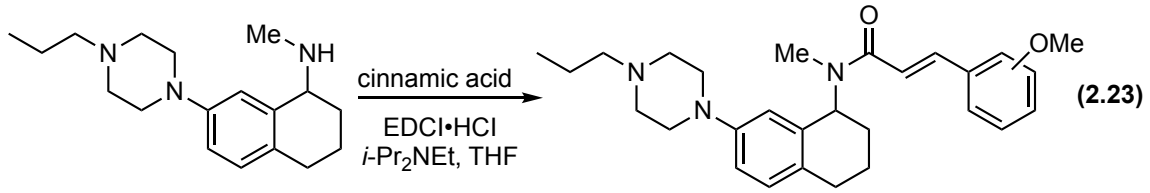

2.87

2.116: 2–OMe (70%)
2.117: 3–OMe (75%)
2.118: 4–OMe (69%)

(2.23)

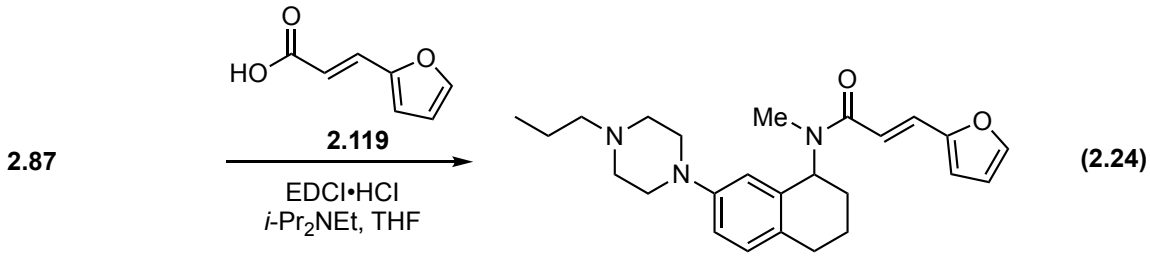

2.120

(2.24)

2.2.5 Investigation of the Aminotetralin Enantiomers

It is well established that some some ligands in their optically pure form preferentially bind either the σ1R or σ2R. As outlined in the preceding chapter, the σRs were originally defined based on their preference for (+)-benzomoprhans, a feature that was later attributed specifically to the σ1R.[56,57] The σ2R was later defined in part, by its low affinity for the (+)-benzomoprhans.[75] A related trend was observed with the benzomorphan-7-one σ2R ligand classes, in which (+)-CB-184 (**1.111**) displayed greater than 500-fold selectivity for the σ2R over the σ1R, whereas as the enantiomer displayed a modest preference for the σ1R (Table 1.1).[249] However, little difference was observed between the enantiomers of the *N*-propylpiperazine-substituted norbenzomorphans **1.212**-

1.213 and the corresponding racemate **1.191**, although **1.212** did show a modest reduction in σ2R affinity (3.9-fold) (Figure 1.42). However, it remained to be determined if the enantiomers of the aminotetralin scaffold exhibited preferential binding for the σ2R that might enhance selectivity.

A common tactic for resolving enantiomers is through formation of diastereomeric salts from a racemic mixture by selective crystallization of a particular diastereomeric form.[316] The proximity of the basic amine moiety to the chiral center of *N*-methyl aminotetralin **2.28** suggested that it was an ideal intermediate for optical resolution using this strategy. Fortunately, Welch and Williams of Pfizer disclosed the resolution of (*R*)-**2.122** during their preparation of sertraline in greater than 99% enantiomeric excess (*ee*) by crystallization of the *N*-acetyl-L-phenylalanine salt.[317] In accordance with the reported protocol, a solution of *N*-acetyl-L-phenylalanine and **2.28** was stirred in hot ethanol and allowed to cool whereupon crystallization occurred (Scheme 2.14). The collected solids were recrystallized again from ethanol to deliver *S*-enriched salt (> 97:3 *dr*) along with the mother liquors containing *R*-enriched salt. The *R*-enriched residue obtained from the mother liquors was converted to the free base and subjected to the same procedure using *N*-acetyl-D-phenylalanine to afford the *R*-enriched salt (> 97:3 *dr*). Treatment of the salts thus obtained with aqueous sodium hydroxide afforded aminotetralins (*S*)-**2.121** and (*R*)-**2.122** in 32% and 25% overall yield, respectively (based on a theoretical yield comprised of both enantiomers).

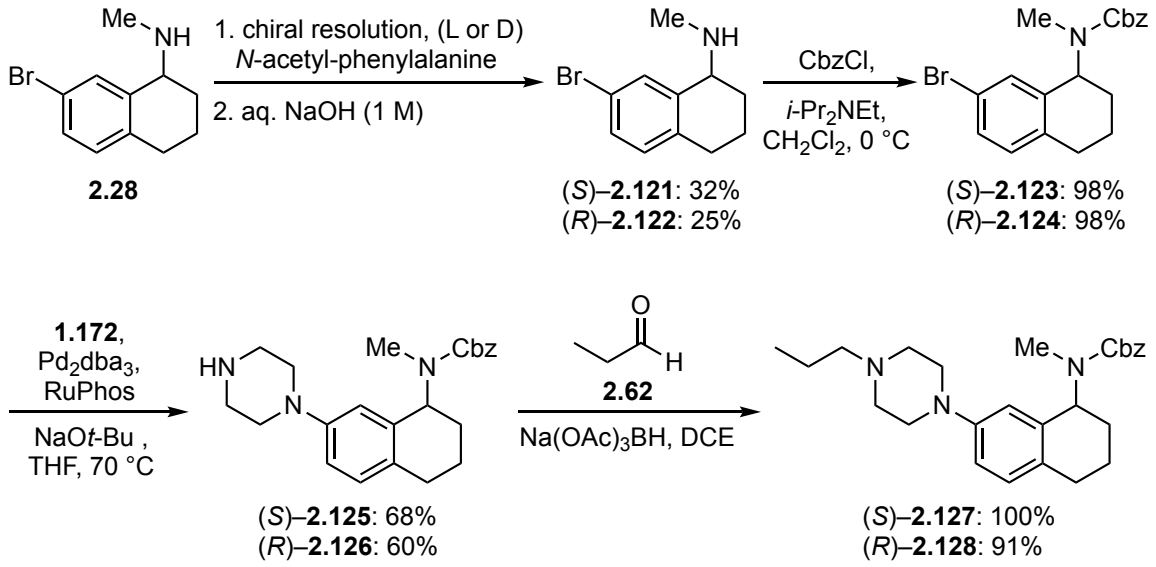

Scheme 2.14. Synthesis enantioenriched analogs through chiral resolution of **2.28**.

The enantiomers (*S*)-**2.121** and (*R*)-**2.122** were subsequently converted to *N*-propylpiperazine analogs for comparison to the racemic mixture (Scheme 2.14). Similar to the previously discussed protocol, (*S*)-**2.121** and (*R*)-**2.122** were treated with benzyl chloroformate to deliver (*S*)-**2123** and (*R*)-**2.124** in 98% yield. Subsequent Buchwald-Hartwig amination of (*S*)-**1.123** and (*R*)-**2.124** with piperazine (**1.172**) catalyzed by $Pd_2(dba)_3$ and RuPhos afforded intermediates (*S*)-**2.125** and (*R*)-**2.126** in 68% and 60% yield, respectively. Reductive alkylation of (*S*)-**2.125** and (*R*)-**2.126** with propionaldehyde (**2.62**) provided (*S*)-**2.127** and (*R*)-**2.128** in greater than 99% *ee*.

The enantioenriched analogs were submitted to the PDSP for binding analysis, that indicated that the two enantiomers had different binding profiles (Table 2.11). The effect toward the σ1R was the most pronounced, with a 5.3-fold increase in σ1R affinity in (*R*)-**2.128**, as compared to (*S*)-**2.127**. Interestingly, (*S*)-**2.127** possessed similar σ1R affinity as the racemate. The σ2R potency of (*R*)-**2.128** and (*S*)-**2.127** was relatively unchanged, leading to enhanced σ2R selectivity in (*S*)-**2.127** (35-fold), which is similar

to the racemate. However, it is worth noting that different protocols were used for the σ1R binding assay of the racemate and the enantiomers that makes a direct comparison more challenging. Somewhat surprisingly, the difference in σ1R affinity for the aminotetralin enantiomers is distinct from the similarly substituted norbenzomorphan enantiomers, which had nearly identical affinity for the σ1R.

Table 2.11. Binding affinity of enantioenriched analogs.

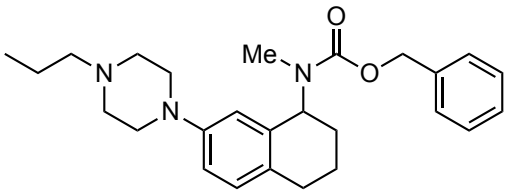

	K_i (nM)		K_i ratio
Cmpd.	σ1R	σ2R	(σ1R/σ2R)
(±)-**2.31**	200	5.5	36
(*R*)-**2.128**	37[a]	8.4[b]	4.4
(*S*)-**2.127**	195[a]	5.5[b]	35

K_i values for aminotetralin analogs (single point) determined from non-linear regression of radioligand competition binding isotherms by PDSP. Unless indicated otherwise, σ1R was sourced from guinea pig brain and σ2R was sourced from rat PC12 cells. [a]Determined using HEK293T transfected with human σ1R. [b]Determined using HEK293T cells transfected with human σ2R/TMEM97.

2.2.6 Summary of the Aminotetralin SAR Investigation

A scaffold simplification strategy applied to the norbenzomorphan framework gave rise to the aminotetralin scaffold (Figure 2.14). SAR investigations in region **A** and **B** suggest that compounds that have the aminotetralin scaffold had similar binding profiles to the corresponding norbenzomorphan. The aminotetralin scaffold displayed

high affinity and selectivity for the σ2R over the σ1R when a piperazine ring was installed at the C–7 position in region **B**. The highest levels of σ2R selectivity, up to 366-fold, were obtained with aliphatic substituents possessing a carbonyl moiety installed on the piperazine nitrogen atom in region **A**. Hydrophobic groups in this region that were between three and five- carbon atoms provide optimum σ2R selectivity if a carbonyl group is not present. The relative orientation of the substituted piperazine moiety and the distal aromatic group appear to be critical for achieving selectivity for the σ2R over the σ1R. Indeed, Further investigation of the aminotetralin scaffold in region **D** revealed that the position of the aromatic group appears to be a significant component for disfavoring binding to the σ1R. A linker of at least three atoms connecting the distal aromatic group is important for retaining high σ2R affinity, and selectivity over the σ1R is achieved with carbamate, amide, and ether heteroatom configurations in the chain. However, the hydrocinnamamide group provided the highest levels of σ2R selectivity among similarly substituted analogs. The newly accessible site of substitution on the nitrogen atom in SAR region **C** provided no benefit, with minimal change observed from hydrophobic groups of increasing size and polar groups leading to enhanced σ1R affinity. However, this feature was leveraged in our efforts to identify the σ2R.

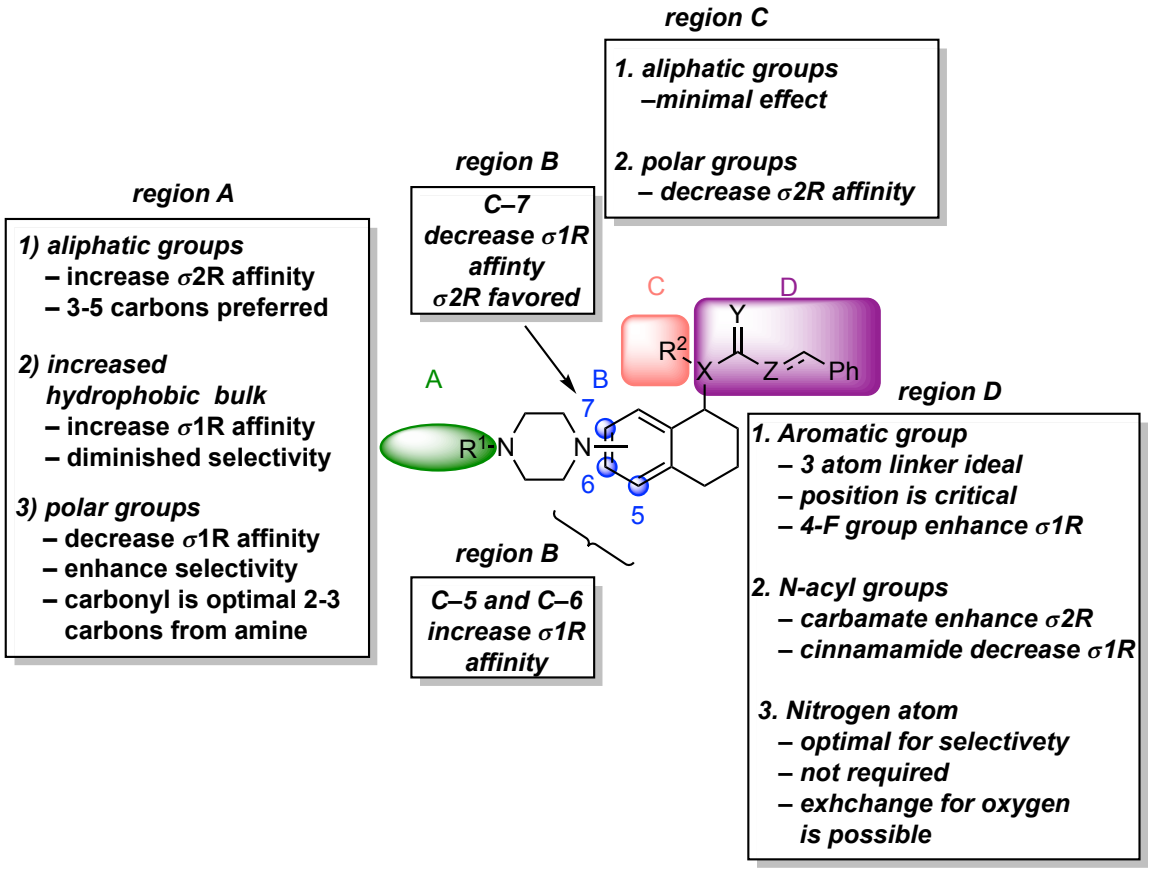

Figure 2.14. Summary of the aminotetralin SAR.

2.3 Sigma-2 Modulation in the 5XFAD Transgenic Mouse Model

2.3.1 Introduction

Alzheimer's Disease (AD) is an age-related neurodegenerative disorder that is clinically characterized by progressive loss of cognitive function and deficits in learning and memory that are associated with dementia.[318] Typical pathological characteristics of the disease include extracellular buildup of Aβ plaques and formation of intracellular neurofibrillary tangles, along with chronic neuroinflammation that collectively contribute to synaptic loss and ultimately neuronal death.[319-321] Current FDA approved drugs for the treatment of AD include the acetylcholinesterase inhibitors rivastigmine, galantamine,

and donepezil, as well as the NMDA receptor antagonists memantine, but these only provide temporary symptomatic relief.[318] There are currently no disease altering treatment options that are capable of slowing or halting the progressive neuronal death associated with AD, which currently impacts more than five million people in the United States and is expected to increase in prevalence as the population ages.[318] This dire situation highlights the need for continued development of novel therapeutic strategies for the treatment of AD.

The σ2R has recently emerged as a potential target for the treatment of several neuropsychiatric disorders, and neuroprotective properties in some disease models suggest that modulating this receptor might provide a unique approach for treating AD. As discussed in the preceding chapter, the Martin group discovered that SAS-0132 (**1.163**) was neuroprotective in a *C. elegans* model of age related neurodegeneration.[12] Administration of SAS-0132 also improved cognitive performance, rescuing AD-related behavioral deficits in a Thy-1 $hAPP^{Lond/Swe+}$ transgenic mouse model of AD.[12] Notably, reduced levels of the proinflammatory cytokine IL1β, which is associated with the neuroinflammatory response and AD progression, were observed in the transgenic mice relative to control levels following the dosing regimen.[322,323] In addition, the structurally related analog DKR-1677 (**1.191**), which possesses enhanced σ2R potency and selectivity over the σ1R, provided decreased axon degeneration and improved behavioral deficits in mouse models of TBI (Figure 2.15)..[14] A structurally unique ligand class that modulates the σ2R was observed to displace Aβ oligomers from the neuronal synapse leading to reduced synaptotoxicity an improved memory in mouse models of AD.[164,165] This led to the development of Elayta (CT1812), which is currently undergoing phase II clinical trials for the treatment of AD.[166,209]

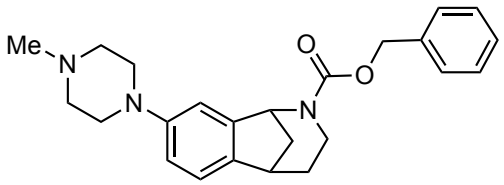

1.163
SAS-0132
σ1R K_i (nM) = 841 ± 228
σ2R K_i (nM) = 90 ± 14
K_i ratio (σ1R/σ2R) = 9.3

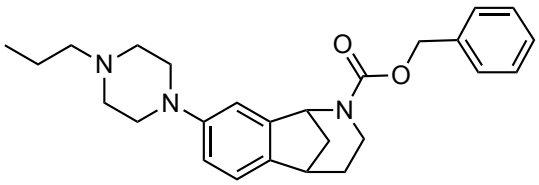

1.191
DKR-1677
σ1R K_i (nM) = 230
σ2R K_i (nM) = 5.1
K_i ratio (σ1R/σ2R) = 45

Figure 2.15. Norbenzomorphan analogs with neuroprotective properties.

Because of the promising activity of SAS-0132 and DKR-1677 in models of neurodegeneration, we queried whether the corresponding aminotetralin JVW-1601 (**2.31**) might also possess similar neuroprotective activity (Figure 2.16). Accordingly, we evaluated DKR-1677 and JVW-1601 in the FXFAD transgenic mouse model.

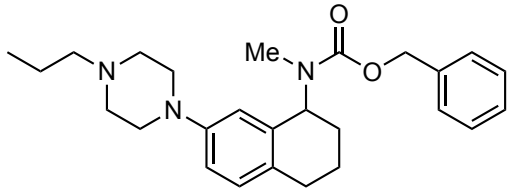

2.31
JVW-1601
σ1R K_i (nM) = 200
σ2R K_i (nM) = 5.5
K_i ratio (σ1R/σ2R) = 36

Figure 2.16. Aminotetralin analog selected for evaluation in 5XFAD model.

Transgenic 5XFAD mice are derived from overexpression of mutated versions of three human amyloid precursor protein (APP) genes and two human presenilin-1 (PSEN1) genes associated with early onset familial AD.[324] This gives rise to increased production of Aβ that accumulates and forms plaques, a pathological hallmark of AD.

Although there is much about the underlying mechanism and its role in the disease that remain unclear, the amyloid cascade hypothesis suggests that an accumulation of Aβ oligomers that results from in imbalance in Aβ production and clearance is correlated with AD onset.[319,325,326] The predominant forms of Aβ consist of 40 ($A\beta_{40}$) and 42 ($A\beta_{42}$) amino acid residues; they are soluble in their monomeric form, but readily aggregate into a variety of assemblies that can lead to soluble oligomers or insoluble plaques that are associated with AD.[327] However, soluble oligomers possess more potent neurotoxicity.[328] The rapid accumulation of Aβ in the 5XFAD mouse model provides a useful assay for evaluating the ability of small molecules to alleviate the negative effects associated with this pathological feature of AD.[324] Because compounds that modulate the σ2R have demonstrated an ability to mitigate Aβ oligomer synaptotoxicity, the 5XFAD mouse model was selected in collaboration with the Shamloo group at Stanford University to assess the neuroprotective attributes of JVW-1601 and DKR-1677.

2.3.2 Bioavailability and Specificity

Prior to evaluation in the 5XFAD transgenic mouse study, JVW-1601 and DKR-1677 were assessed for metabolic stability and bioavailability (Quintara Discovery, Inc. Hayward, CA) (Figure 2.17). Both displayed low metabolic stability ($t_{1/2} < 5$ min) upon incubation with liver microsome, indicating similar metabolic liabilities for both scaffolds that would eventually limit their potential for oral administration. The P-glycoprotein (P-gp) is an efflux transporter that is widely expressed in major organs, but specifically in the capillaries of the blood brain barrier (BBB) where it can restrict brain penetration of potential CNS drugs.[329] Madin Darby canine kidney (MDCK) cells with the *MDR1* gene (ABCB1) that encodes for P-glycoprotein (P-gp) provide a useful assay to assess permeability and P-gp efflux liability.[330] Analysis of known CNS drugs suggests

that a P-gp efflux ratio greater than 2.5 is considered a P-gp liability, but JVW-1601 and DKR-1677 display efflux ratios of 1.0 and 0.6 respectively, suggesting that good brain penetration is anticipated.[330] The PK properties of JVW-1601 and DKR-1677 were also assessed *in vivo* and found to be bioavailable and to readily cross the BBB in mice. The brain concentrations four hours after a single intraperitoneal (IP) dose of JVW-1601 (10 mg/kg) and DKR-1677 (3 mg/kg) were 95 nM and 32 nM, respectively. In the same experiment, the brain to plasma ratio was 2.8 for JVW-1601 and 3.5 for DKR-1677.

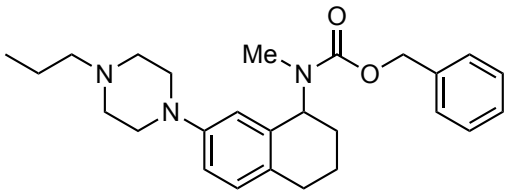

2.31
JVW-1601

σ1R K_i (nM) = 200
σ2R K_i (nM) = 5.5
K_i ratio (σ1R/σ2R) = 36

$t_{1/2}$ (IP, 10 mg/kg) = 1.2 h
T_{max} (IP) = 5 min
brain conc. (IP, 4 h) = 95 nM
brain/plasma ratio (4 h) = 2.8
P-gp ratio = 1.0

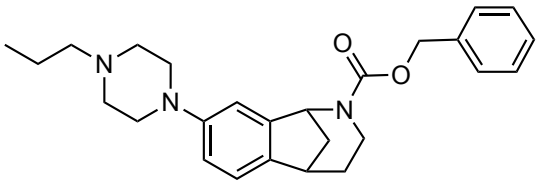

1.191
DKR-1677

σ1R K_i (nM) = 230
σ2R K_i (nM) = 5.1
K_i ratio (σ1R/σ2R) = 45

$t_{1/2}$ (IP, 3 mg/kg) = 1.2 h
T_{max} (IP) = 5 min
brain conc. (IP, 4 h) = 32 nM
brain/plasma ratio (4 h) = 3.5
P-gp ratio = 0.6

Figure 2.17. Bioavailability of analogs.

Because obtaining selectivity for the σ2R over the σ1R has been historically challenging, the initial SAR investigation of the aminotetralin scaffold placed emphasis on that particular parameter. However, JVW-1601 was also screened against a panel of more than 50 proteins relevant to the CNS by the PDSP and greater than 100-fold selectivity was obtained against targets other than the σ2R (Supplements Table S.1). The few exceptions observed are the σ1R (36-fold), several of the serotonin receptors (25–66-

fold), and the histamine-1 receptor (4-fold). This is similar to DKR-1677, which had greater than 100-fold selectivity for many of the same targets with the exception of the σ1R (45-fold), alpha-2A adrenergic receptor (69-fold), and histamine-1 receptor (20-fold). This suggest that JVW-1601 and DKR-1677 share similar binding profile with respect to σRs and also other CNS proteins.

2.3.3 Administration in the 5XFAD Model

In collaboration with the Shamloo laboratory at Stanford University, age-matched wildtype (N = 6–7) and 5XFAD transgenic (N = 6–7) mice were assigned to vehicle and drug groups and administered JVW-1601 or DKR-1677 (10 mg/kg) daily via IP for 60 days beginning at approximately four weeks of age. The animals were weighed daily and no adverse effects were observed on body weight for the duration of the dosing regimen (Figure 2.18). At the completion of the 60-day dosing schedule, the animals were sacrificed and the blood and major organs were harvested. No significant alterations in the mass of these organs (brains, heart, lungs, livers, spleens, kidneys, testes, intestines) was observed. Additionally, analysis of the blood for 22 chemical biomarkers revealed no notable discrepancies between the vehicle and drug groups. Collectively, this suggests that chronic dosing with JVW-1601 or DKR-1677 presents no obvious toxic effect.

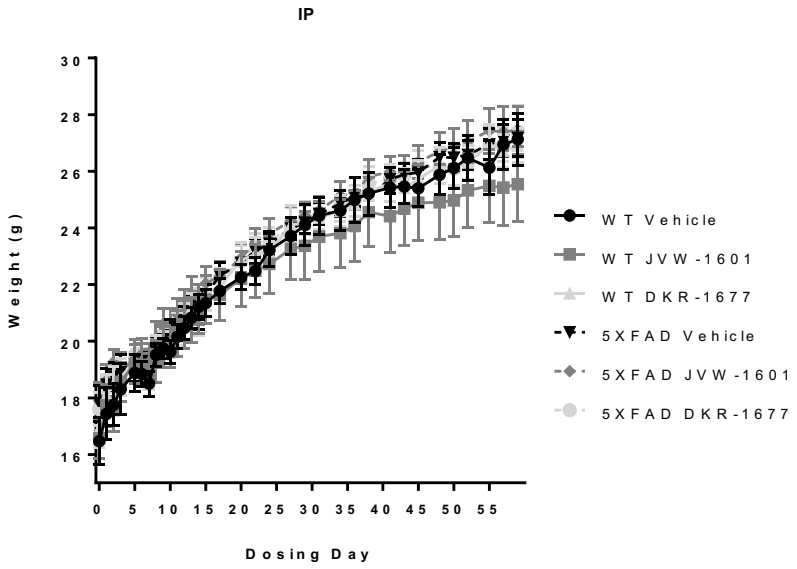

Figure 2.18. Body weight of wildtype and 5XFAD transgenic mice in vehicle and drugs groups measured daily.

AD is characterized by Aβ and tau pathologies, along with neuroinflammation and neurodegeneration. The 5XFAD transgenic mouse model rapidly accumulates Aβ and gives rise to plaque formation and neurodegeneration associated with disease progression.[319] Therefore, the effect of JVW-1601 or DKR-1677 on Aβ burden in cortical tissues of the 5XFAD group was assessed. Soluble $A\beta_{40}$ and $A\beta_{42}$ was extracted with tris-buffered saline (TBS) and quantified using an enzyme-linked immunosorbent assay (ELISA) kit revealing that administration of JVW-1601 and DKR-1677 led to decreased levels of soluble $A\beta_{40}$ and $A\beta_{42}$, as compared to the vehicle-treated group (Figure 2.19). In both cases, the reduction was much more pronounced for the norbenzomorphan compound DKR-1677 than the aminotetralin JVW-1601. A similar trend was observed for insoluble $A\beta_{40}$ and $A\beta_{42}$ with reduced solubility that was extracted from the same homogenized tissue with guanidine HCl (GdHCl) buffer and quantified. Minor reduction

in insoluble $A\beta_{40}$ and $A\beta_{42}$ levels was observed with administration of JVW-1601 as compared to the vehicle-treated group, whereas DKR-1677 provided a more pronounced reduction. These preliminary result point toward diminished Aβ burden following chronic dosing with DKR-1677 and its simplified variant JVW-1601, although additional testing is needed to confirm statistical significance.

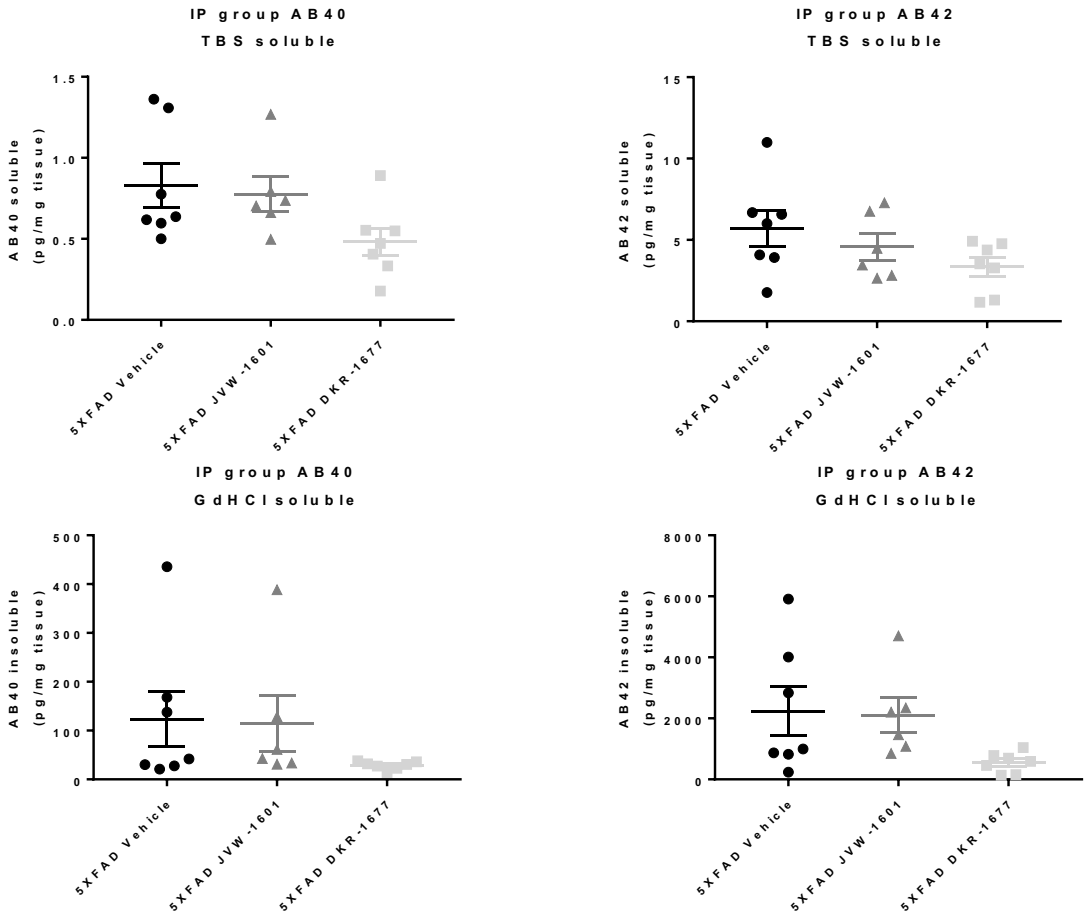

Figure 2.19. Levels of soluble $A\beta_{40}$ and $A\beta_{42}$ determined by TBS extraction of cortical tissues. Levels of insoluble $A\beta_{40}$ and $A\beta_{42}$ determined by extraction of the same tissues with GdHCl.

The role of neuroinflammation in AD is not well-defined, but it is considered a symptom of neurodegeneration that might result from Aβ and tau pathologies, as well as a cause of additional neuron damage that can contribute to progression of the disease.[321] Immune responses in recognition of damage gives rise to the activation of microglial cells that secrete a variety of inflammatory components including the pro-inflammatory cytokines interleukin-1β (IL-1β) and tumor necrosis factor-α (TNF-α). Enhanced expression of pro-inflammatory cytokines has been observed in AD patients, and there is evidence that mRNA expression of these neuroinflammatory markers is elevated in the 5XFAD transgenic model and is accompanied by increased neurodegeneration.[331,332] Moreover, compounds that are neuroprotective and restore behavioral deficits in models of AD, including the norbenzomorphan SAS-0132, have provided decreased mRNA expression of neuroinflammatory cytokines.[12,332]

The mRNA expression level of several inflammatory markers in the cortex were assessed by quantitative real-time polymerase chain reaction (qRT-PCR). Consistent with previous results, some elevated expression of the pro-inflammatory cytokines TNF-α and IL-1β were observed in 5XFAD transgenic mice as compared to wildtype (Figure 2.20).[332] Wildtype mice treated with JVW-1601 and DKR-1677 possessed similar expression levels of TNF-α as compared to the control group, whereas IL-1β expression was suppressed in the same wildtype groups. The elevated gene expression of TNF-α and IL-1β that was observed in 5XFAD transgenic mice was suppressed in groups that were subjected to chronic dosing of JVW-1601 and DKR-1677. In both instances the reduction was more pronounced with the norbenzomorphan DKR-1677 than with aminotetralin JVW-1601. These preliminary results show there is a reduction of neuroinflammatory markers resulting from administration of JVW-1601 and DKR-1677 that is consistent with an anti-inflammatory effect.[12,332]

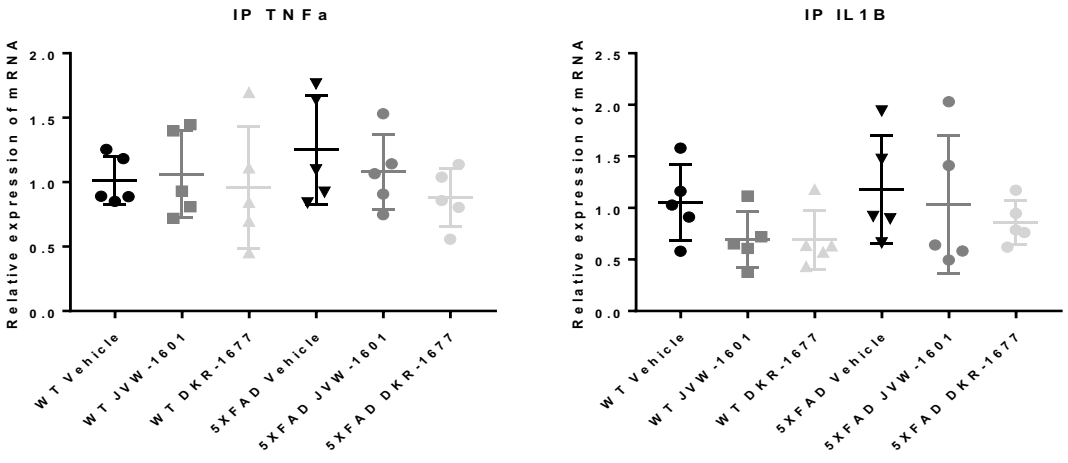

Figure 2.20. Relative mRNA expression of pro-inflammatory cytokines.

Increased levels of inflammatory cytokines such as TNF-α and IL-1β activate astrocytes as part of the neuroinflammatory response, resulting in gliosis that is characterized by an upregulation of glial fibrillary acidic protein (GFAP).[333] An increase in gliosis and corresponding GFAP is observed in neurodegenerative disorders, including Alzheimer's disease, although the contribution of gliosis is complex and requires further clarifiaction.[334] Gliosis levels were measured by immunohistochemical staining of GFAP that indicated increased gliosis in the striatal and hippocampal region of the vehicle-treated 5XFAD transgenic group, as compared to the vehicle-treated wildtype group (Figure 2.21). Chronic dosing with JVW-1601 and DKR-1677 in 5XFAD transgenic mice diminished gliosis as compared to the vehicle-treated 5XFAD group, although the observed reduction in staining appears to be more pronounced for DKR-1677.

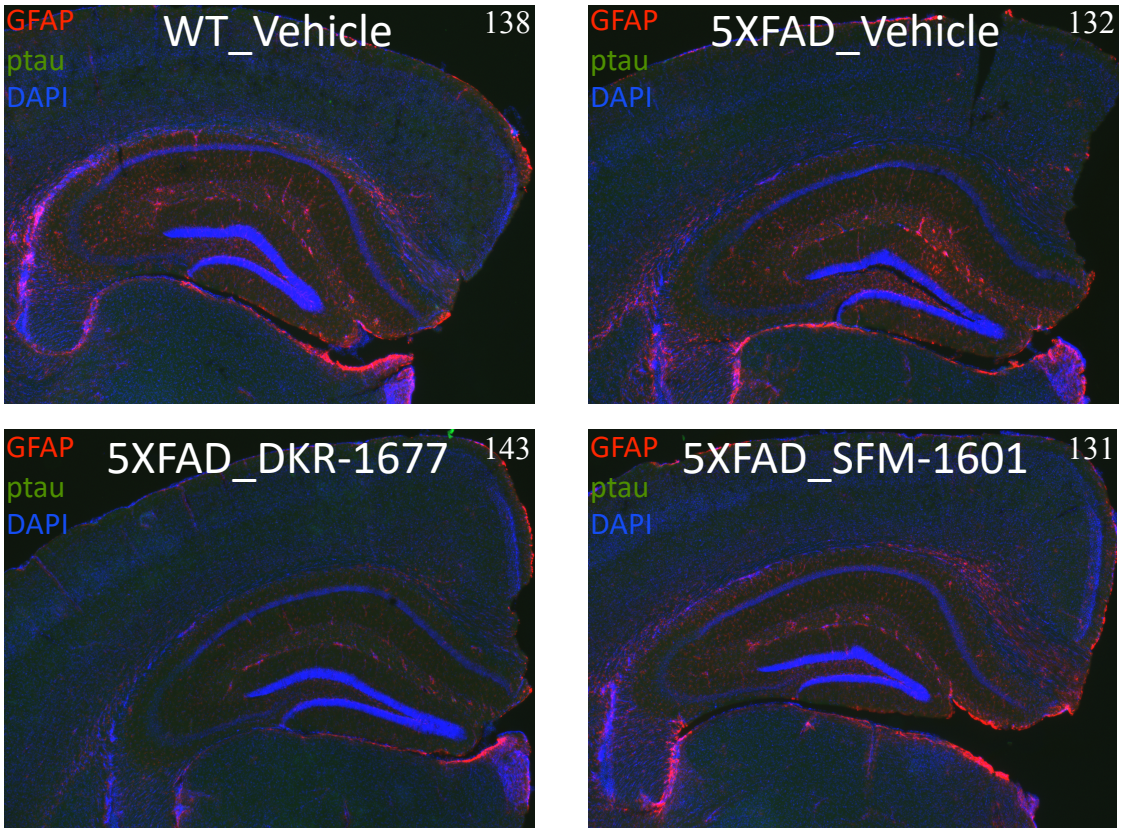

Figure 2.21. Hippocampal regions of the brain stained with GFAP (red). Cell nuclei stained with 4',6-diamino-2-phenylindole (blue).

2.3.4 Summary

These studies were conducted to determine if the norbenzomorphan analog DKR-1677 and its simplified variant JVW-1601 mitigated the negative effects associated with Aβ pathology in 5XFAD transgenic mice and to compare the properties these scaffolds. Analysis of the PK profile and bioavailability in vitro and in vivo revealed that JVW-1601 and DKR-1677 were similarly susceptible to rapid metabolism by liver microsome. In addition, they possessed similar half-life times (IP), and both displayed a favorable ability to cross the BBB, achieving good brain exposure with low predicted risk of P-gp

liability. The off-target profile against a range of CNS related proteins was also generally similar.

Chronic dosing with JVW-1601 and DKR-1677 indicated that they were well tolerated, and no signs of toxicity or variation of chemical biomarkers was observed. At the completion of the 60-day dosing regimen, both JVW-1601 and DKR-1677 displayed anti-inflammatory properties in 5XFAD transgenic mice as observed through a reduction in pro-inflammatory cytokines and diminished gliosis. In addition, some reduction of soluble and insoluble Aβ was observed suggesting that each of these compounds decreased Aβ burden in this model. In each instance, the effect was more pronounced with DKR-1677 than JVW-1601, which may indicate that the norbenzomorphan scaffold is more advantageous in this system. Collectively, the anti-inflammatory properties exhibited by these compounds suggest that they may help mitigate the negative effects of Aβ pathology, but further experiments are needed to confirm statistical significance and to probe their ability to rescue cognition in behavioral models.

2.4 Molecular Identification of the Sigma-2 Receptor as TMEM97

2.4.1 Introduction

The σ2R has been an enigmatic target since it was initially distinguished from the σ1R in 1990, but it has continued to attract considerable interest due to its implication in a range of disorders.[75] During this time, the σ2R had evaded all attempts to identify its molecular structure and its coding gene.[212] As a result, pharmacological characterization methods have been the primary mechanism for investigating the σ2R, which has greatly limited our understanding of its biological role.[5] As previously discussed, the σ2R has recently emerged as a potential target for the treatment of several neurodegenerative disorders including AD, neuropathic pain, and TBI.[11-14] Moreover, ligands that modulate

the σ2R are currently undergoing clinical trials for the treatment of AD, schizophrenia, and for the diagnostic imaging of cancer.[166,184,185,209,211] The increasing medicinal potential of the σ2R highlights the critical need to understand the cellular mechanisms and biological role of this protein.

Given the decades of research focused on the σ2R, it is rather surprising that the molecular identity of the protein has proven to be so evasive. Recently, Mach *et al.* reported that the σ2R binding site resides within a PGRMC1 protein complex.[221] However, follow up studies revealed that modulation of PGRMC1 expression levels did not affect [^{3}H]-DTG binding, indicating that the proteins were not synonymous and that the true identity remained unknown.[224,241,242] Because the need for identification of the protein was critical for continued advancement, efforts in the Martin group shifted toward molecular identification of the σ2R in a collaboration with the Kruse group at Harvard University.

2.4.2 Aminotetralin Analogs for Affinity Purification of the Sigma-2 Receptor

Our plan to identify the σ2R was a classical affinity purification approach that required immobilization of a high affinity ligand on a solid support to enable separation of the target protein from the biological matrix. This is similar to other approaches undertaken that attempted to purify the σ2R.[217,221] However, because the small molecule is a central component in the purification strategy, we hypothesized that different structural arrangements available on high affinity σ2R ligands developed in our laboratories might prove useful. As discussed in preceding chapter, the linker for immobilization must be installed on the small molecule in manner that allows the ligand to interact with the binding pocket of the receptor without interference from the solid support and without a deleterious impact on potency.[213] This task requires thorough

knowledge of the small molecule's SAR and an ability to install a range of linkers at several unique positions on the scaffold.[213]

Our SAR investigation of a range of aminotetralin analogs provided this relevant insight and the readily diversifiable scaffold could easily be modified for installation of linkers at several locations. Analysis of the SAR for the four regions investigated (**A**-**D**), revealed that regions **A** and **C** tolerated hydrophobic groups of increasing size with only modest changes in σ2R affinity (Figure 2.22.A). This observation suggested that linkers installed at these sites might not disrupt ligand affinity, and the nitrogen present in each region provided a function handle for linker attachment. Linker groups that possessed an aldehyde or primary amine at one terminus could readily be installed on the scaffold in a manner similar to other diversification strategies that were previously developed, whereas a Boc-protected amine at the other linker terminus could easily be deprotected to enable immobilization on a solid surface that possessed activated ester sites (Figure 2.22.B).

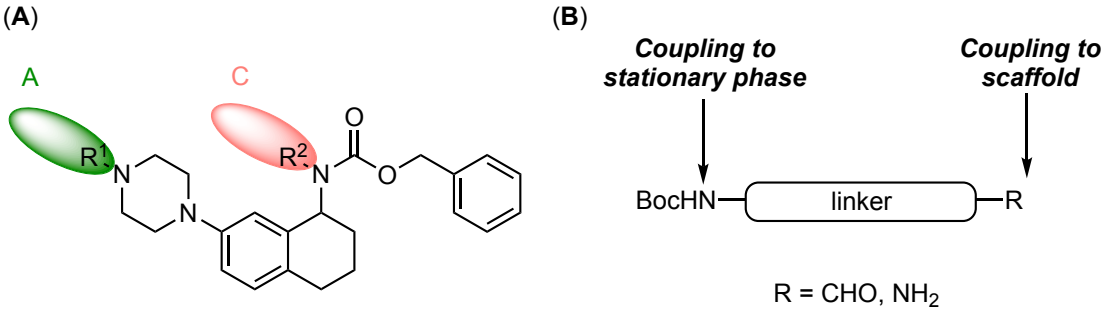

Figure 2.22. (A) Regions targeted for linker installation. (B) Strategy for incorporating a range of linkers at scaffold nitrogen atoms.

Because the length and nature of the linker that would enable the small molecule to effectively interact with the σ2R binding site after immobilization was not known, we sought to install a short (six-carbon atoms) and long (11-carbon atoms) linker at each site. The 6-carbon linker with an aldehyde moiety was constructed according to a slightly

modified literature procedure wherein amino acid **2.129** was treated with Boc-anhydride to afford the *N*-Boc amino acid **2.130** (Scheme 2.15). The crude reaction mixture was treated with lithium aluminum hydride to afford the primary alcohol **2.131** that was subjected to Swern oxidation without purification to deliver the known aldehyde **2.132** in 67% yield over three steps.[335,336]

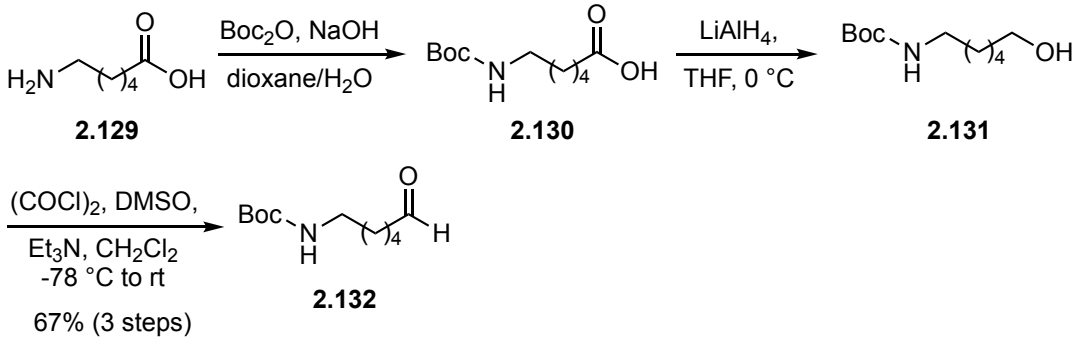

2.129 **2.130** **2.131** **2.132**

Scheme 2.15. Synthesis of the six-carbon linker bearing an aldehyde functional group.

A slightly modified procedure was used to construct the 11-carbon linker bearing an aldehyde functional group (Scheme 2.16). In the even, amino acid **2.133** was treated with Boc-anhydride to afford *N*-Boc amino acid **2.134**. The crude reaction mixture was reduced according to a reported protocol by treating **2.134** with isobutyl chloroformate (**2.135**) to generate the mixed anhydride *in situ* followed by addition of sodium borohydride and subsequent dropwise addition of methanol to afford alcohol **2.136**.[337] The operational simplicity and mildness of this reduction strategy was preferred to lithium aluminum hydride reduction. The crude reaction mixture thus obtained was subjected to Swern oxidation to deliver the known aldehyde **2.137** in 71% yield over three steps.[338]

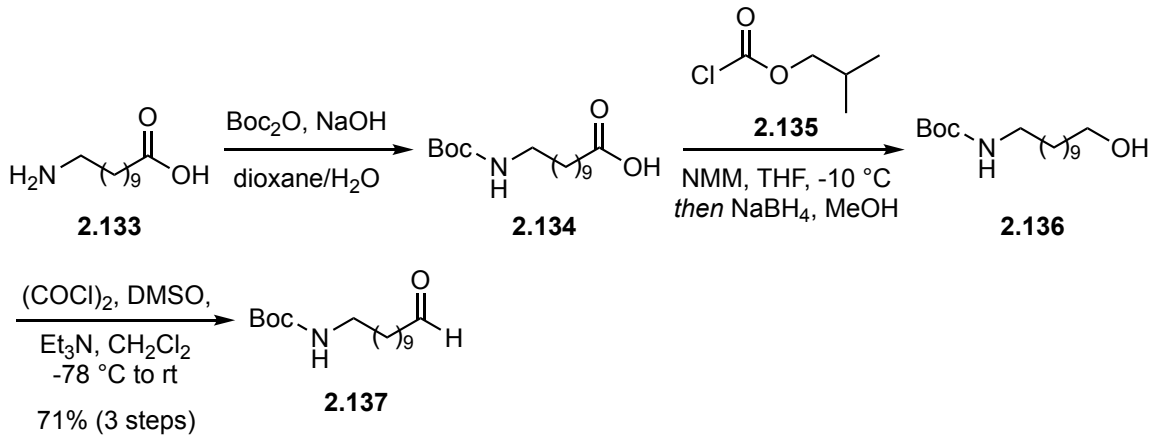

Scheme 2.16. Synthesis of the six-carbon linker bearing an aldehyde functional group.

The aldehyde functionality on the aliphatic chains of **2.132** and **2.139** proved to be an effective handle for attachment to **2.16** via reductive amination, as a variety of groups were previously appended in this manner. Stirring a solution of **2.16** in dichloroethane with **2.132** or **2.137** in the presence of sodium triacetoxyborohydride delivered alkylated analogs **2.138** and **2.139** (Equation 2.25).

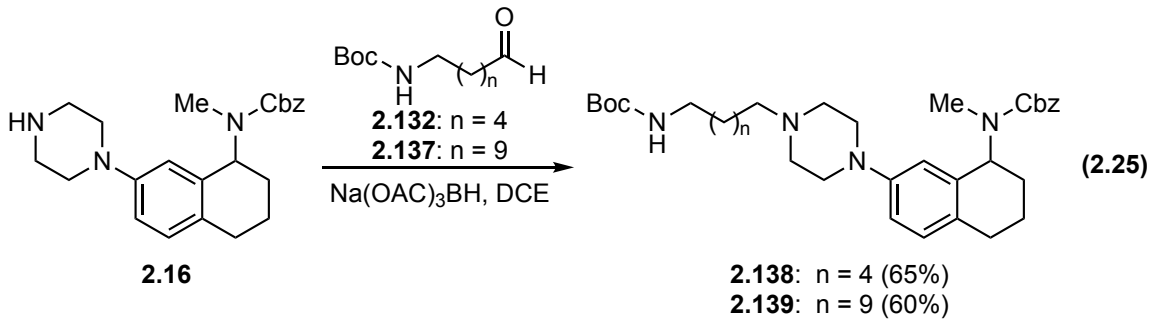

A related tactic was employed to attach these linking groups at the carbamate nitrogen atom. Accordingly, reductive amination of 7-bromotetralone (**2.26**) with ammonium acetate delivered aminotetralin **2.140** (Scheme 2.17). Condensation of **2.140** with aldehyde **2.132** provided an intermediate imine that was reduced *in situ* with sodium

borohydride, and the resultant amine was treated with benzyl chloroformate to deliver **2.141** with a six-carbon spacer between the carbamate nitrogen and the Boc-protected amine, in 67% yield over two steps. Buchwald-Hartwig amination of **2.141** with excess piperazine (**1.172**) using the same conditions as previously discussed delivered **2.142**, and subsequent reductive alkylation with propionaldehyde (**2.62**) delivered **2.143**.

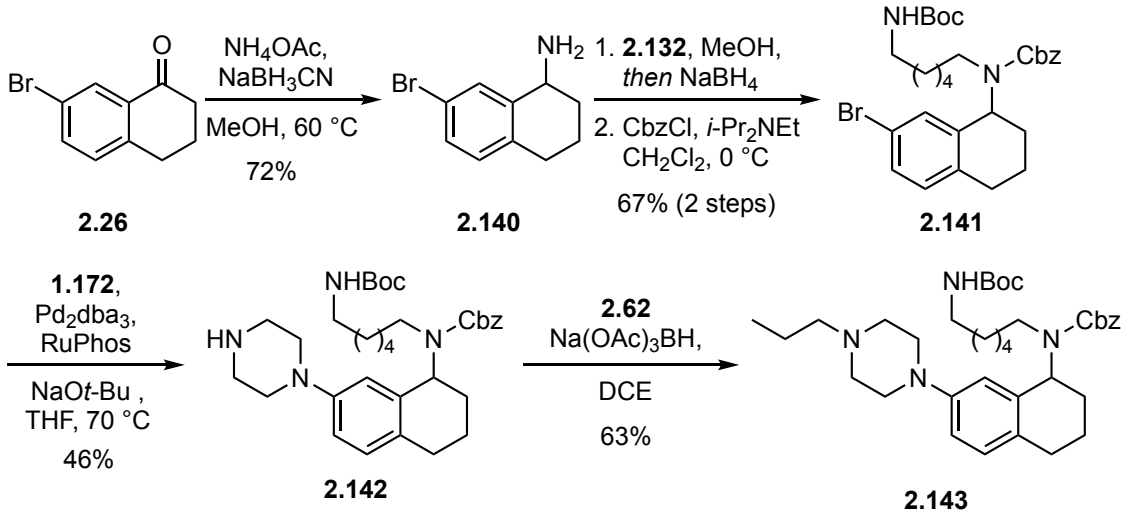

Scheme 2.17. Synthesis of aminotetralin analog with a six-carbon linker at the carbamate.

This strategy enabled late-stage diversification of the substituent at the piperazine nitrogen atom if needed, but the high σ2R affinity of the related *N*-propylpiperazine analog **2.31** suggested that a propyl group at that position should be sufficient. However, this synthesis of **2.143** required introduction of the aliphatic linker at an early stage of the synthetic sequence, a significant drawback for evaluating a range of linkers. Because the nature and the length of the linker that would prove most effective for application to affinity chromatography was not known, a more divergent strategy was devised in order to increase efficiency of analog preparation. An aliphatic linker with a primary amine moiety was anticipated to allow reductive amination directly with the tetralone

intermediate **2.84**. Therefore 11-aminoundecanoic acid (**2.133**) was Boc-protected, and the acid was subsequently reduced via activation as a mixed anhydride to deliver the known alcohol intermediate **2.136** in 92% yield over two steps (Scheme 2.18).[339] A solution of **2.136** in toluene was treated with methansulfonyl chloride followed by addition of sodium azide to afford intermediate **2.144**, and the crude reaction mixture was subjected to catalytic hydrogenation to provide the known mono-Boc-protected diaminoalkane **2.145** in 50% yield over two steps.[340]

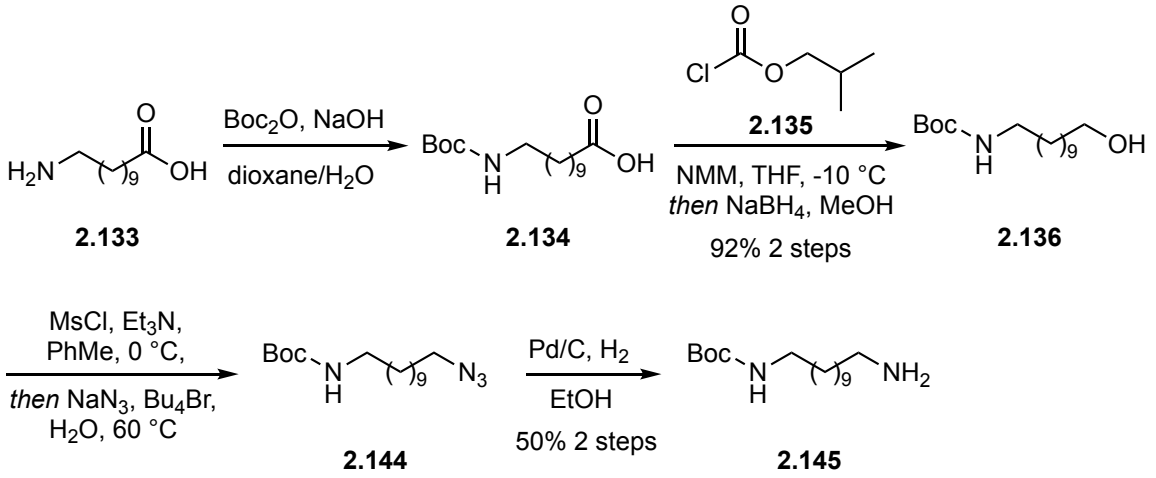

Scheme 2.18. Synthesis of mono-Boc-protected diaminoalkane **2.145**.

After some experimentation, we discovered that heating a solution of **2.84** and **2.145** in ethanol in the presence of excess Ti(O*i*-Pr)$_4$ provided full conversion to the imine intermediate that was reduced in situ by addition of sodium borohydride to deliver the secondary amine **2.146** in 87% yield (Scheme 2.19). Notably, this transformation required the use of excess Ti(O*i*-Pr)$_4$ (10 eq.) for efficient conversion to the imine intermediate. The use of three equivalents of Ti(O*i*-Pr)$_4$ resulted in only partial conversion (ca. 1:1) after 15 h and heating provided little benefit. Treating **2.146** with benzyl chloroformate delivered final analog **2.147** in 80% yield.

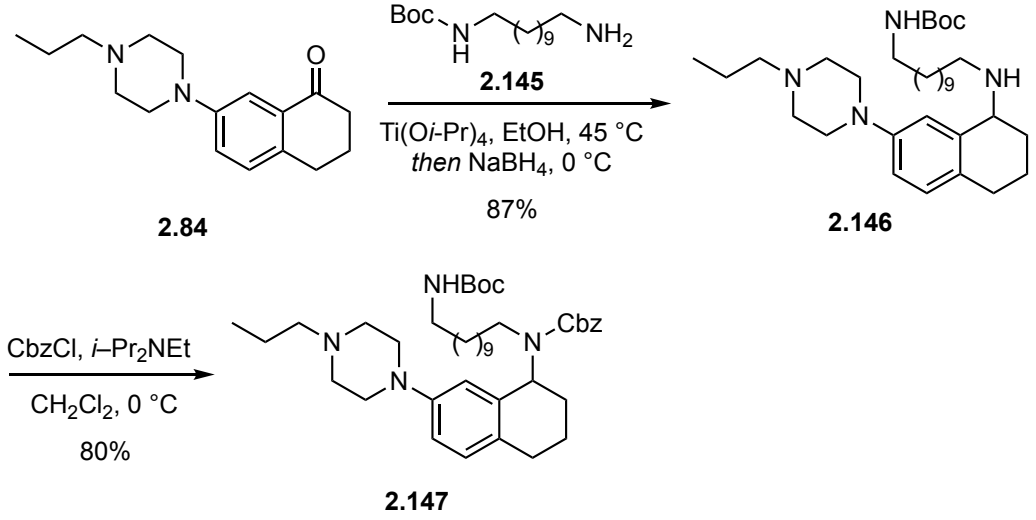

Scheme 2.19. Synthesis of pull-down analog **2.147**.

The putative pull-down ligands **2.138**-**2.139**, **2.143**, and **2.147** were then assessed for their ability to bind the σ2R. Single point binding analysis with the test ligands (1μM) was conducted by the Kruse group at Harvard University using PC-12 cell membrane preparations and [^{3}H]-DTG (30 nM) in the presence of SKF-10,047 (2 μM) to mask the σ1R binding site (Figure 2.23.A). The single point assay included the related norbenzomorphan analog **2.148** possessing a six-carbon aliphatic group at the piperazine nitrogen atom, as well as haloperidol (σ2R K_i = 48.7 nM) and the aminotetralin **2.42** (σ2R K_i = 4.5 nM) as standards for comparison.[75] Several of the ligands performed well in the assay with competitive [^{3}H]-DTG binding that were similar to or less than haloperidol. However, **2.147** possessing an 11-carbon linker at the carbamate nitrogen atom, displayed notably lower levels of competitive [^{3}H]-DTG binding that suggested higher affinity for the σ2R. Thus, **2.147** was progressed as a lead compound, along with the norbenzomorphan analog **2.148**, which provided an alternative scaffold with a unique immobilization site for comparison. Competition binding analysis confirmed that **2.147**

possessed 0.4 nM affinity for the σ2R and that norbenzomorphan **2.148** displayed 3.1 nM σ2R affinity, indicating that introduction of the aliphatic chain at these positions did not have a deleterious effect on potency (Figure 2.23.B).

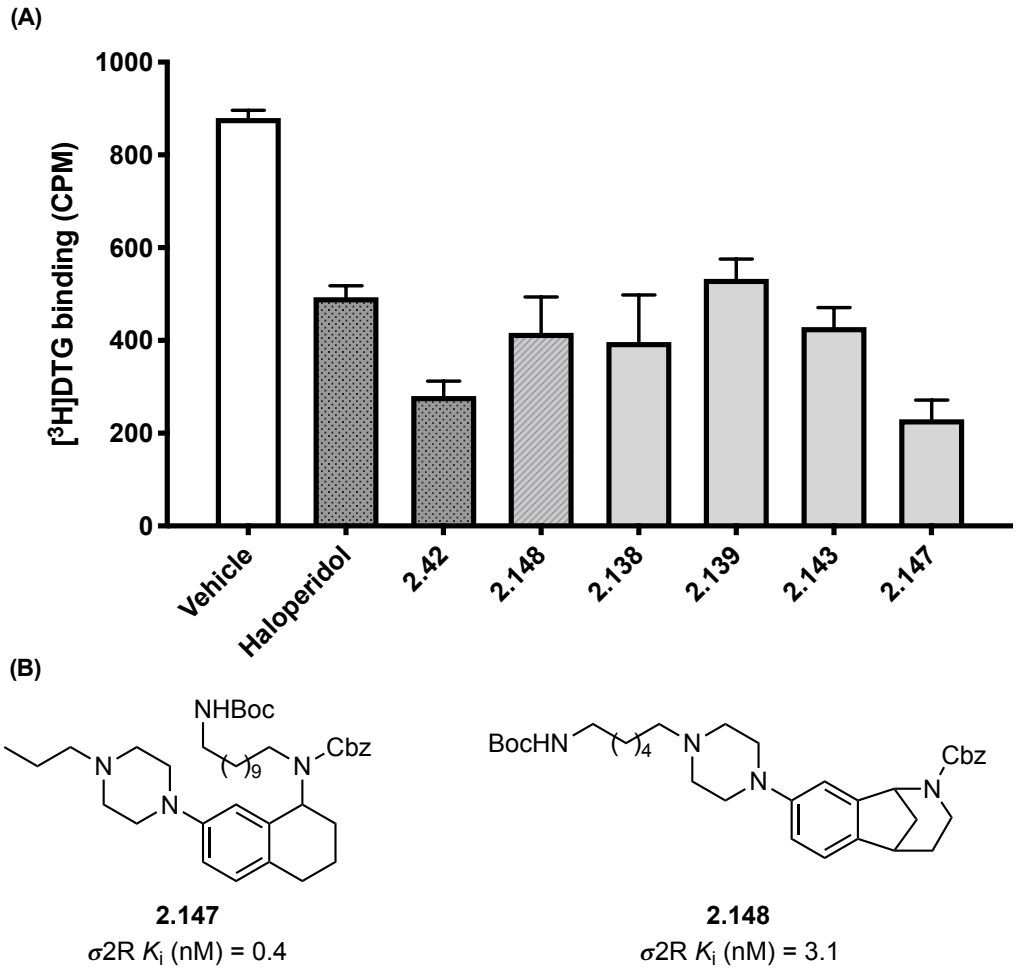

Figure 2.23. (A) Single point binding analysis of test ligand at 1 μM with PC12 cells using [^{3}H]-DTG (30 nM) in the presence of SKF-10,047 (2 μM) (B) K_i values (single experiment) for lead analogs.

The lead analogs **2.147** and **2.148** were next assessed for their ability to capture the σ2R from calf liver membrane homogenate by the Kruse group. Accordingly,

removal of the Boc-protecting group was accomplished by treating **2.147** with a solution of HCl in dioxane to deliver JVW-1625 (**2.149**) with the requisite primary amine for immobilization. Competition binding analysis confirmed that JVW-1625 possessed 16.6 nM affinity for the σ2R (Equation 2.26). An affinity resin was prepared by coupling JVW-1625 (**2.149**) to affi-gel 10 resin at a range of coupling densities (50-2,000 μM) for use in preparing affinity columns (Figure 2.24).[160] Calf liver membrane extract was flowed onto the column, and σ2R capture was assessed by determination of [^{3}H]-DTG binding in the column flow through. Critically, the affinity resin prepared with JVW-1625 (**2.149**) demonstrated efficient depletion of radioligand binding at all coupling densities examined, and no [^{3}H]-DTG binding was observed at a 2,000 μM coupling density.[160] A similar analysis with an affinity resin prepared using the norbenzomorphan analog **2.148** revealed that protein capture was much less effective. It is not clear if the reduction in protein capture derives from the decreased length of the linker used for immobilization or due to the alternative immobilization site on the scaffold itself.

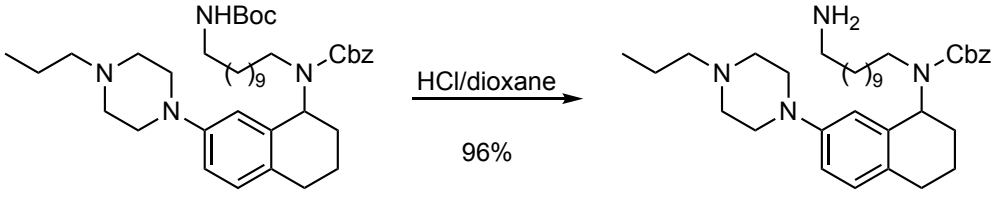

2.147

2.149
JVW-1625
σ2R K_i (nM) = 16.6

(2.26)

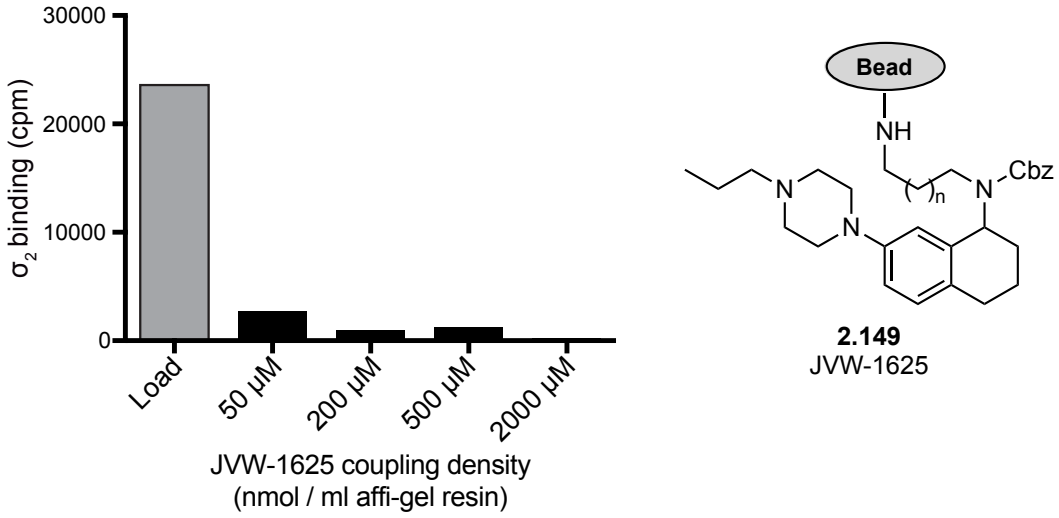

Figure 2.24. Affinity column prepared with JVW-1625 coupled to affi-gel 10 resin at the specified coupling density. Binding assay performed on column flowthrough of calf liver membrane extract with [^{3}H]-DTG (25 nM). Copyright (2017) National Academy of Sciences / modified from original to show only binding depletion assay (A) and JVW-1625 coupled to bead.[160]

Longer linkers can often provide superior results by projecting the small molecule further away from the stationary phase, but additional hydrophobicity in the linker can create challenges with solubility and non-specific binding.[214,216] During the course of the binding depletion assay, some clumping was observed in the resin that was attributed to the hydrophobicity of JVW-1625, and this clumping posed a potential problem for scale up during isolation studies. An effort was made to prepare a similar analog that possessed a PEG-linker that might provide improved solubility. Therefore, the known diamino-PEG-chain **2.150** was installed on tetralone **2.84** via reductive amination according to the previously discussed protocol to afford **2.151** in 69% yield (Scheme 2.20).[341] Subsequent treatment with benzyl chloroformate delivered **2.152**. Unfortunately, binding analysis of

2.152 by the PDSP revealed diminished σ2R affinity, which is consistent with prior observations in SAR region **C**, suggesting that **2.152** might not be a suitable candidate.

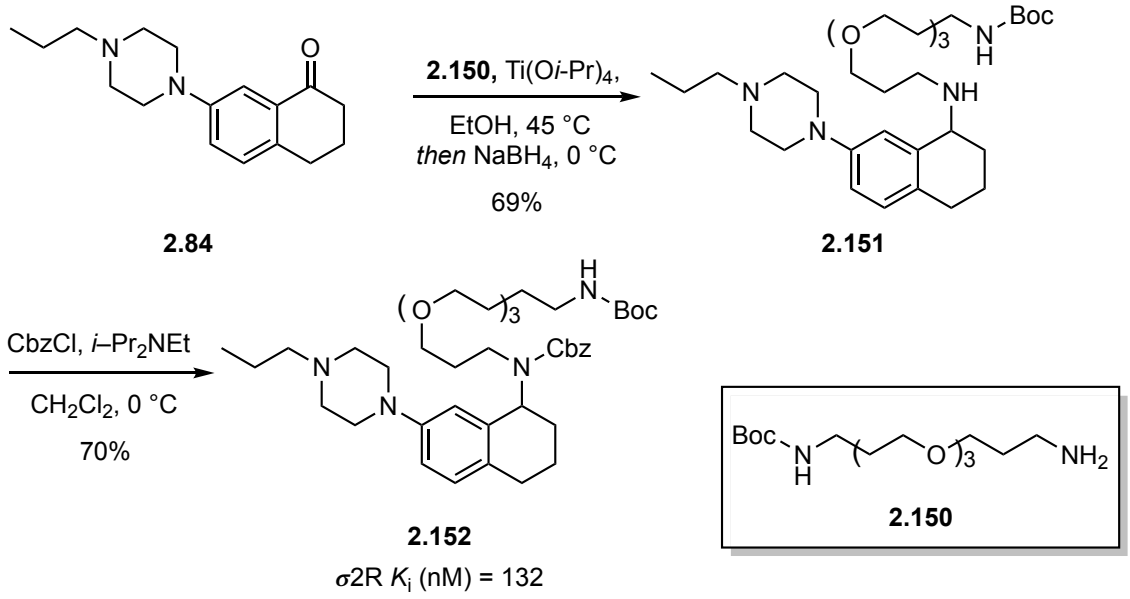

Scheme 2.20. Synthesis of an amainoteralin analog with a PEG-linker at the carbamate.

Fortunately, efficient protein capture was observed using an affinity resin prepared with JVW-1625 even at low coupling densities. Thus, scaled up affinity purification was conducted by the Kruse lab using the JVW-1625 affinity resin (2 mL) at 100 μM coupling density.[160] Solubilized σ2R from calf liver homogenate was flowed through the column in order to wash away undesired components of the biological matrix, followed by eluent containing DTG (100 μM) to release the desired protein. The obtained protein was processed with SDS-PAGE, and the portion of the gel that was consistent with a mass range of 15-25 kDa was analyzed via LCMS/MS at Harvard's Faculty of Arts and Sciences Mass Spectrometry and Proteomics Resource Laboratory and also at the Harvard Medical School Taplin Mass Spectrometry Facility.

Known protein candidates were selected from the identified proteins for follow up analysis because their molecular weight was consistent with the range predicted for the σ2R, in addition to PGRMC1 due to its association with the σ2R. Each was overexpressed in HEK293 cells and assayed for [^{3}H]-DTG binding, but only the transmembrane protein 97 (TMEM97) displayed significant activity (Figure 2.25).[160] Notably, mRNA expression of Tmem97 was reduced by approximately 60% in PC-12 cells using siRNA knockdown, which produced a similar reduction in σ2R expression as determined with [^{3}H]-DTG saturation binding studies. This discovery supported the hypothesis that the σ2R might be TMEM97, but more rigorous conformation was required.

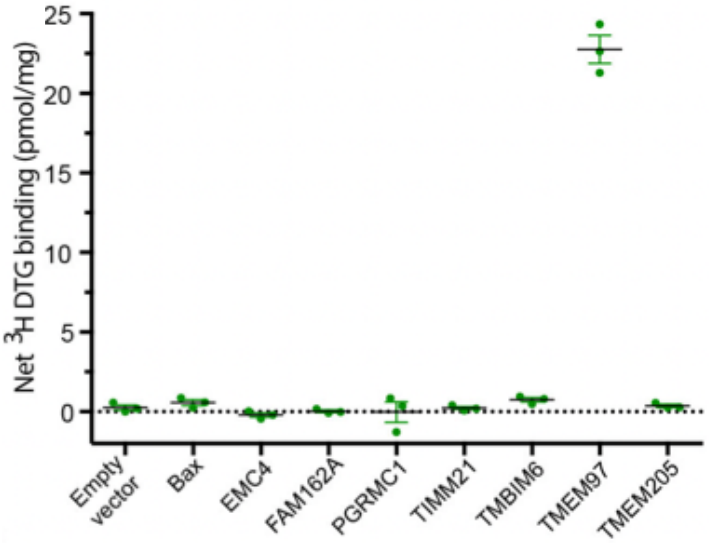

Figure 2.25. Single point binding assay performed in triplicate on membrane preparations of expi293 cells expressing hits identified via LCMS/MS with [^{3}H]-DTG (10-30 nM). Shown as means ± SEM. Copyright (2017) National Academy of Sciences / modified from original to show only binding assay results.[160]

Additional validation studies were conducted by the Kruse lab to confirm the potential identification of the σ2R as TMEM97 based on the well characterized σ2R binding profile.[160] The *Sf9* insect cells line does not possess a TMEM97 ortholog and does no display affinity for [^{3}H]-DTG.[342] However, upon overexpression of human TMEM97, these cells exhibited saturable [^{3}H]-DTG binding with 11.3 nM affinity, which is within the range of reported values (17.9-37.6 nM).[75,172,242] Having discovered that the expression of TMEM97 in *Sf9* cells imparted an ability to bind [^{3}H]-DTG, a central pharmacological characteristic that defined the σ2R and was otherwise absent, a range of well-characterized σ2R ligands were assessed in the same cell line (Table 2.12).[75] Notably, the inhibition constant of each liagnd was consistent with the values reported in the literature. For example, high σ2R affinity was observed for DTG, haloperidol, and PB-28, as well as the norbenzomorphan analog SAS-1121. However, low or nondetectable affinity was displayed by the (+)-benzomorphans (+)-SKF-10,047 and (+)-pentazocine, another defining characteristic of the σ2R. In addition, the σ2R possessed similar affinities for Elacridar and Ro 48-8071, which were recently reported as TMEM97 ligands.[343]

Table 2.12. Binding affinities of known ligands at recombinant TMEM97 and native σ2R expressed in cell membranes.

		K_i (nM)	
entry	ligand	TMEM97 in sf9 cells	σ2R
1	DTG	19.6 ± 3.0	21.2[a]
2	haloperidol	54.1 ± 6.7	48.7[a]
3	PB-28	2.0 ± 0.3	1.8[b]
4	(+)-pentazocine	2,467 ± 436	1,402 – 3,890[b]
5	(+)-SKF 10,047	>10,000	no inhibition[a]
6	SAS-1121	25.2 ± 3.8	23.8[c]
7	Elacridar	6.5 ± 1.1	4.7 ± 0.7
8	Ro 48-8071	971 ± 228	817 ± 226

The inhibition constants were determined by the Kruse group with sf9 cells expressing recombinant TMEM97 and MCF-7 cell membranes expressing native σ2R using [^{3}H]-DTG in the presence of (+)-SKF-10,047 (1.8 μM). [a] *Values reported by Hellewell and Bowen.*[75] [b] *Values reported by Colabufo et al.*[128] [c] *Values reported by Sahn et al.*[9] *Copyright (2017) National Academy of Sciences / modified from original to reformat table.*[160]

2.4.3 The Sigma-2 Receptor is Synonymous with TMEM97

The σ2R was pharmacologically distinguished from the σ1R in 1990 based on a unique ligand binding profile that was distinct from the σ1R.[75] The defining features of the σ2R were high affinity for the classical σR liagnds DTG and haloperidol, as well as low affinity for (+)-benzomorphans. Following affinity purification of calf liver membrane extract using the high affinity σ2R ligand JVW-1625 that was developed through an extensive SAR investigation of the aminotetralin scaffold, TMEM97 was identified as a candidate protein a search for the molecular identity of the σ2R. Subsequent expression studies confirmed that TMEM97 expression is necessary and

sufficient for [^{3}H]-DTG binding. Moreover, the ligand binding profile that pharmacologically defined the σ2R was recapitulated in cells expressing recombinant TMEM97. Collectively, this led us to conclude that the σ2R and TMEM97 are synonymous and will henceforth be referred to as TMEM97/σ2R.[160] This identification resolves a mystery that had evaded researchers for decades and should enable more thorough characterization of the biological functions and cellular mechanisms of TMEM97/σ2R.

Successful identification of the elusive of TMEM97/σ2R protein was enabled by the discovery and development of the aminotetralin scaffold as a new σ2R ligand class. The unique structural features of the aminotetralin scaffold provided the pivotal attachment point for immobilization of the ligand that facilitated efficient protein capture. This highlights the utility of this scaffold simplification strategy for the development of alternative lead scaffolds as tool compounds that aid the study of challenging biological targets.

2.5 TMEM97/σ2R Overview and New Discoveries

2.5.1 TMEM97/σ2R Structure and Function

As the name suggests, TMEM97 is an integral membrane protein and it was originally identified in 1993 as a gene with altered expression in meningiomas that was referred to as meningioma-associated protein (MAC30).[344] The membrane protein, is comprised of 176 amino acids and high expression levels were observed in a several cancers prior to its identification as TMEM97/σ2R, although little is known about its molecular function.[345,346] However, increased expression of TMEM97/σ2R in tumors was correlated with poor prognosis in cancer patients and inhibition of cancer cell migration and proliferation in vitro was observed upon downregulation of TMEM97/σ2R.[347-350]

TMEM97/σ2R has also been proposed as a sterol response element binding protein (SREBP) target gene located at the ER and lysosomes that is involved in regulation of cellular cholesterol levels.[351] In addition, TMEM97/σ2R interacts with NPC1, which is required for shuttling cholesterol out of lysosomes and its dysfunction results in an accumulation of lysosomal lipids that is associated with Niemann-Pick disease type C (NP-C).[352] Reduction of TMEM97 levels was observed to increase levels of NPC1 and also increase cholesterol and lipid transport from lysosomes, suggesting that TMEM97/σ2R might be a target for the treatment of NP-C disease, a fatal neurodegenerative disorder that is associated with cognitive decline.[352] The σRs were previously implicated in cholesterol metabolism and the TMEM97/σ2R identification provides conformation of this important cellular role.[353,354]

As part of our effort to identify and clone TMEM97/σ2R, computational and mutagenic analysis were conducted to predict the structure of the protein (Figure 2.26.A).[160] A four-pass transmembrane topology is predicted with an ER retention sequence at the C-terminus, which is located in the cytosolic domain. With respect to interactions occurring within the binding pocket, a ubiquitous structural feature of ligands with high affinity for TMEM97/σ2R is the presence of a basic amine site, which indicates that a pivotal salt-bridge interaction might be present that is similar to those observed in the σ1R crystal strucutre.[6,155] To further probe the structural basis for TMEM97/σ2R ligand recognition, each Glu and Asp residue was subjected to site directed mutagenesis and its ability to bind [^{3}H]-DTG was assessed.[160] Mutation of both D29N and D56N abolished binding and ab initio structural prediction indicated that both acid residues were located in close proximity (Figure 2.26.B).[355] This supports the hypothesis that a hydrogen bond complex, similar to the one observed in the σ1R, might

be involved in ligand binding, but this remains be determined definitively by an X-ray structure of a TMEM97/σ2R ligand complex.

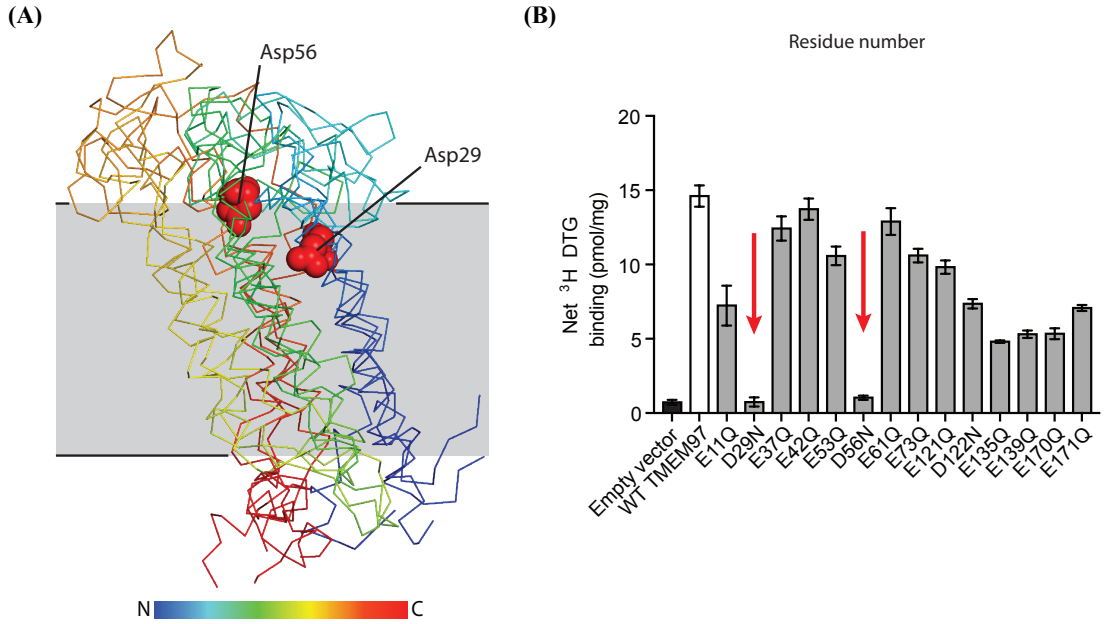

Figure 2.26. (A) Overlay of top four ranked molecular models generated from evolutionary coupling analysis. Asp29 and Asp56 are represented as red spheres. (B) Single point [^{3}H]-DTG (10-30 nM) binding assay of membrane preparations from Expi293 cells expressing TMEM97 with point mutation at specified residue number. Copyright (2017) National Academy of Sciences / modified from original to show only molecular models (A) and mutation study (B).[160]

Following our report on the molecular identification and cloning of TMEM97/σ2R, several studies that have been aided by access to Crisper-Cas9 gene editing technology have been disclosed in which TMEM97/σ2R expression is modulated in order to examine its cellular role. For example, an interaction between TMEM97/σ2R and low-density lipoprotein (LDL) was recently demonstrated.[356] In this study, TMEM97/σ2R knockout reduced LDL internalization by the LDL-receptor, which was

suggested to derive from a ternary protein complex involving PGRMC1, TMEM97/σ2R, and the LDL receptor.[356] Another study utilized TMEM97/σ2R ligands that were previously associated with cytotoxic activity and discovered that knockout of TMEM97/σ2R did not change the ligand concentration required to achieve 50% cell death.[202] This finding was particularly interesting because it suggested that the cytotoxic effects that had long been associated with TMEM97/σ2R agonism in cancer cells might not be mediated by TMEM97/σ2R.[188,201]

In collaboration with the Pierce group at the University of Texas at Austin, we recently utilized the molecular identification and cloning of TMEM97/σ2R to expand on our earlier findings that ligands that modulate the receptor mitigate negative effects of alcohol withdrawal in *C. elegans.*[13] In order to assess the effect of genetic manipulation, Y38H6C.16 was identified as a potential TMEM97/σ2R ortholog in *C. elegans* that shared 30% sequence similarity to TMEM97/σ2R and possessed a similar predicted secondary structure along with partial conservation of the aspartate residues that were identified as critical for ligand binding.[13,160] The putative TMEM97/σ2R ortholog was required for activity of JVW-1034 in the *C. elegans* model with no recovery of performance being observed in the *Y38H6C.16* null strain.[13] Critically, the activity of these compounds was rescued upon reintroduction of endogenous *Y38H6C.16* or the human TMEM97/σ2R gene. This supports the role of TMEM97/σ2R in modulation of alcohol withdrawal symptoms and points to a conserved TMEM97/σ2R signaling pathway that could be useful for additional studies. This is also the first report that utilizes genetic modulation of TMEM97/σ2R in a behavioral study to assess its function. Interestingly, the PGRMC1 ortholog, VEM-1, was also required for activity of JVW-1034, providing additional support for its hypothesized involvement in the TMEM97/σ2R signaling mechanism.[356,357]

2.6 SUMMARY

The enigmatic nature of TMEM97/σ2R has posed a considerable challenge to researchers for decades and has stymied critical advancement for elucidation of its function and therapeutic potential. Even basic strategies for the design of selective TMEM97/σ2R ligands has been surprisingly elusive. Through the course of the work described herein, a new molecular scaffold was developed that possesses high affinity and selectivity for TMEM97/σ2R relative to the σ1R. This aminotetralin scaffold was derived from the norbenzomorphan scaffold via a simplification strategy to remove structural complexity and provide an alternative scaffold for hit-to-lead development. This tactic proved successful, given that the simplified scaffold exhibits a binding profile and biological properties that are generally quite similar to corresponding norbenzomorphan analogs.

Despite the numerous studies that highlight the therapeutic potential of TMEM97/σ2R, including ongoing clinical trials for the treatment of several CNS disorders, the role of the receptor in these diseases has been unclear due to a reliance on pharmacological characterization. However, as a direct result of the work described herein, the research landscape has now changed dramatically. The SAR studies conducted with the aminotetralin scaffold identified structural features unique to this scaffold that were leveraged to enable the molecular identification and cloning of the long sought-after TMEM97/σ2R. This discovery will now enable access to a suite of modern biological tools that should increase our understanding of the role of TMEM97/σ2R in a range of neurodegenerative disorders. In the time since this discovery, genetic manipulation of TMEM97/σ2R expression has already linked the receptor to a potential role in LDL and cholesterol transport that was previously unknown and enabled unambiguous characterization of ligands that were previously thought to

mediate cytotoxic effects in cancer cells, an effect that now seems less likely.[202,356] Moreover, it permitted the first study that utilized genetic manipulation in a behavior model to confirm that TMEM97/σ2R plays a role in modulating the effects of alcohol withdrawal.[13] The identification of TMEM97/σ2R also facilitates work to obtain a crystal structure of the TMEM97/σ2R protein, which is the focus of continuing efforts in the Martin and Kruse groups that should enable structure-based ligand design strategies in the future. Application of the aminotetralin scaffold for the molecular identification and cloning of TMEM97/σ2R was not envisioned at the outset of this work, but it is perhaps the most significant component of this research that has resolved a longstanding mystery in the field and paved the way for critical advancements in the future.

THE STEREOSELECTIVE TOTAL SYNTHESIS OF ALSTOSCHOLARISINE E

Chapter 3: Isolation and Previous Syntheses

3.1 ISOLATION AND BIOLOGICAL ACTIVITY

Progressive neuronal decline is a feature associated with a range of CNS disorders, including Alzheimer's disease, Parkinson's disease, and amyotrophic lateral sclerosis.[358] There are currently no disease altering treatment options for these disorders that attenuate the neuronal deficits associated with disease progression. However, stem-cell based therapies have emerged as a potentially useful strategy for the development of novel therapeutic remedies and several are undergoing phase I and II clinical trials for the treatment of Alzheimer's disease.[359] Because small molecules have been shown to influence neural stem cell proliferation, natural products that possess this ability have garnered increasing attention as privileged molecular scaffolds for further exploration of treatment options.[360,361]

Alstoscholarisines A-E (**3.1**-**3.5**) are unique monoterpenoid indole alkaloids, isolated from the leaves of *Alstonia scholaris* in the Yunnan Province of China by Luo *et al.* in 2014, that were reported to promote neuronal stem cell (NSC) proliferation (Figure 3.1).[362] Each of these alkaloids **3.1**-**3.5** (10 μg/mL) were found to enhance adult NSC proliferation relative to control cells treated with DMSO.[362] Alstoscholarisines A (**3.1**) and E (**3.5**), respectively were among the most potent and **3.1** provided a dose dependent response (0.1 – 20 μg/mL). Furthermore, alstoscholarisine A (**3.1**) promoted NSC sphere formation and neuronal fate commitment. Because these natural products appear to modulate NSC proliferation and neurogenic fate they are intriguing candidates for additional analysis in neurodegenerative models.

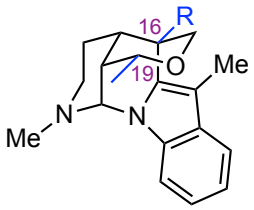

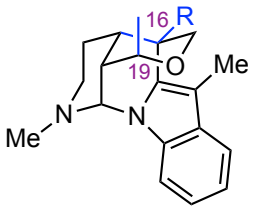

3.1 (–)-alstoscholarisine A R = H
3.2 (–)-alstoscholarisine B R = CO_2Me

3.3 (–)-alstoscholarisine C R = CO_2Me
3.4 (–)-alstoscholarisine D R = CO_2H
3.5 (–)-alstoscholarisine E R = H

Figure 3.1. The structures of (–)-Alstoscholarisines A-E.

The alstoscholarisine alkaloids **3.1-3.5** are comprised of a similar pentacyclic structure that contains a *cis*–fused oxahydroisoquinolone ring system bearing five contiguous stereocenters. Notably, the indole nitrogen forms a cyclic aminal with the piperidine ring of the *cis*-oxahydroisoquinolone, bridging the tetrahydropyran ring and forming a highly caged structure. The core scaffolds of **3.1-3.5** differ in their orientation of the methyl group at the C–19 center and the substituent at the C-19 bridgehead carbon. An equatorial methyl group is exhibited by **3.1** and **3.2**, whereas **3.3-3.5** possess an axial methyl group at this position. Additionally **3.2-3.4** contain a carboxylic acid or ester group at the C–16 bridgehead center, whereas **3.1** and **3.5** possess a tertiary bridgehead (R = H).

The structural complexity of these natural products and their intriguing biological activity quickly captured the interest of the synthetic community. The first synthesis of racemic alstoscholarisine A was reported by Bihelovic and Ferjancic in 2016,[363] followed shortly thereafter by an enantioselective approach disclosed the same year by Yang.[364] Weinreb achieved a synthesis of (±)-alstoscholarisines B and C in 2017 via a divergent approach that was also utilized to access (±)-alstoscholarisines A, D, and E in 2018.[365,366] More recently, the synthesis of (–)-alstoscholarisines A and E was also disclosed by Liao.[367]

3.2 PREVIOUS SYNTHESES OF THE ALSTOSCHOLARISINE ALKALOIDS

3.2.1 Bihelovic and Ferjancic Synthesis of (±)-Alstoscholarisine A

The first successful synthesis of (±)-alstoscholarisine A was achieved by Bihelovic and Ferjancic in 2016 using a domino-enamine cyclization as a key step to assemble the core.[363] The synthesis commenced with preparation of the starting material **3.9** according to a reported protocol via oxidative radical alkylation of 3-methylindole (**3.6**) with the xanthate ester **3.7** to deliver the known 2,3-disubstituted indole **3.8** in 63% yield (Scheme 3.1).[368] Subsequent treatment of **3.8** with Boc-anhydride afforded indole ester **3.9** in 60% yield. Treating a solution of **3.9** in THF with lithium diisopropylamide (LDA) generated the corresponding ester enolate followed by addition of the known *N*-protected aldehyde **3.10** to generate the aldol product **3.11**.[369] Subsequent dehydration of the crude reaction mixture with sodium hydride resulted in migration of the *N*-Boc protecting group to the oxygen atom generating a carbonate that was spontaneously eliminated to afford **3.12** as a single isomer in 75% yield. Palladium mediated removal of the allyloxycarbonyl (alloc) protecting group in **3.12** provided secondary amine **3.13** and set the stage for the key domino cyclization.

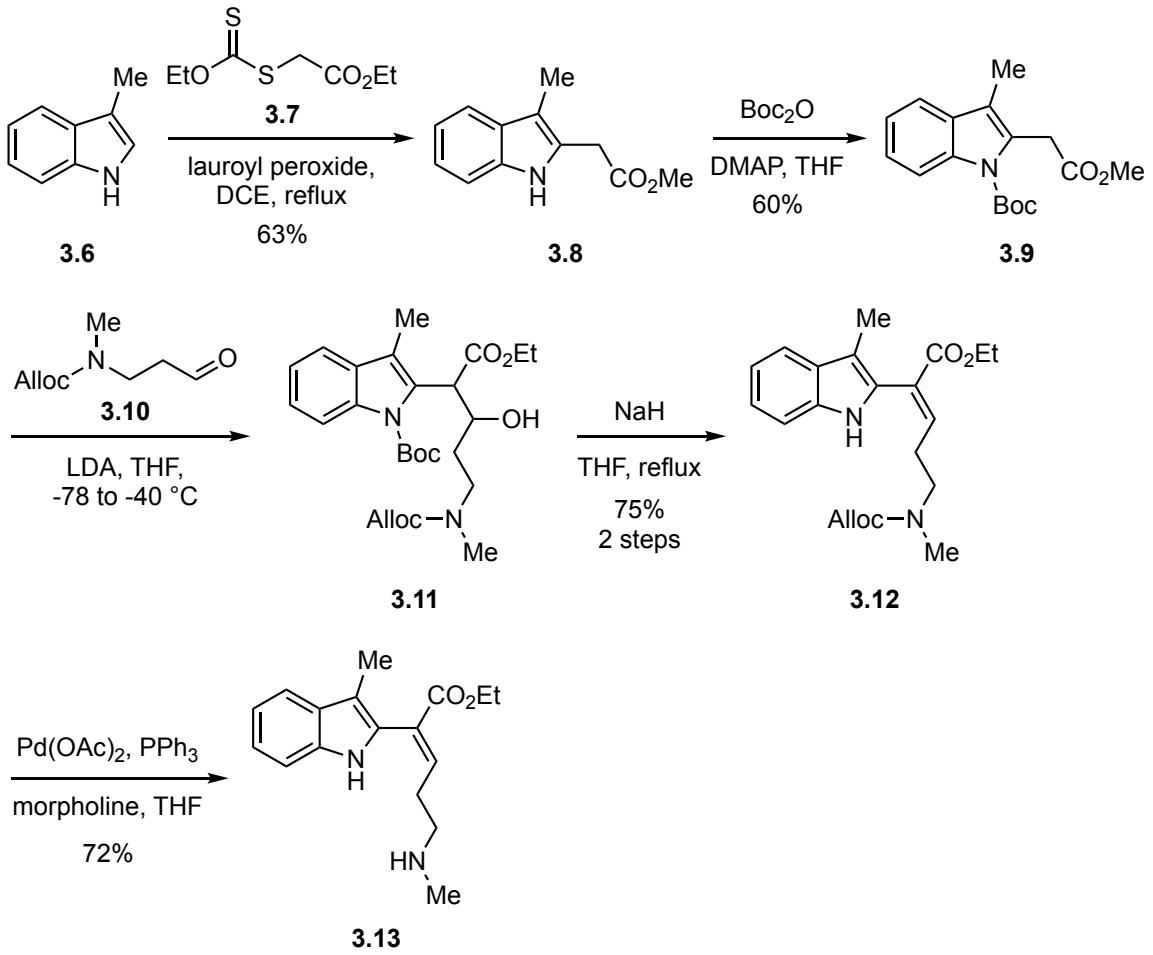

Scheme 3.1. Synthesis of the domino-cascade reaction precursor.

In the event, a solution of amine **3.13** with 4-(phenylselanyl)butanal (**3.14**) in acetonitrile was heated under reflux in the presence of 4 Å molecular sieves (MS) resulting in condensation to generate enamine **3.15** that underwent an intramolecular Michael addition to the α,β-unsaturated ester moiety to generate the cyclic iminium ion in intermediate **3.16** (Scheme 3.2). Subsequent spontaneous cyclization with the indole nitrogen atom formed the aminal ring in the tetracyclic product **3.17** as a mixture of diastereomers (1:1). Heating a solution of ethanol containing the crude reaction mixture

and DBU resulted in thermodynamic equilibration of the ester moiety, and **3.18** was isolated in 71% yield over two steps.

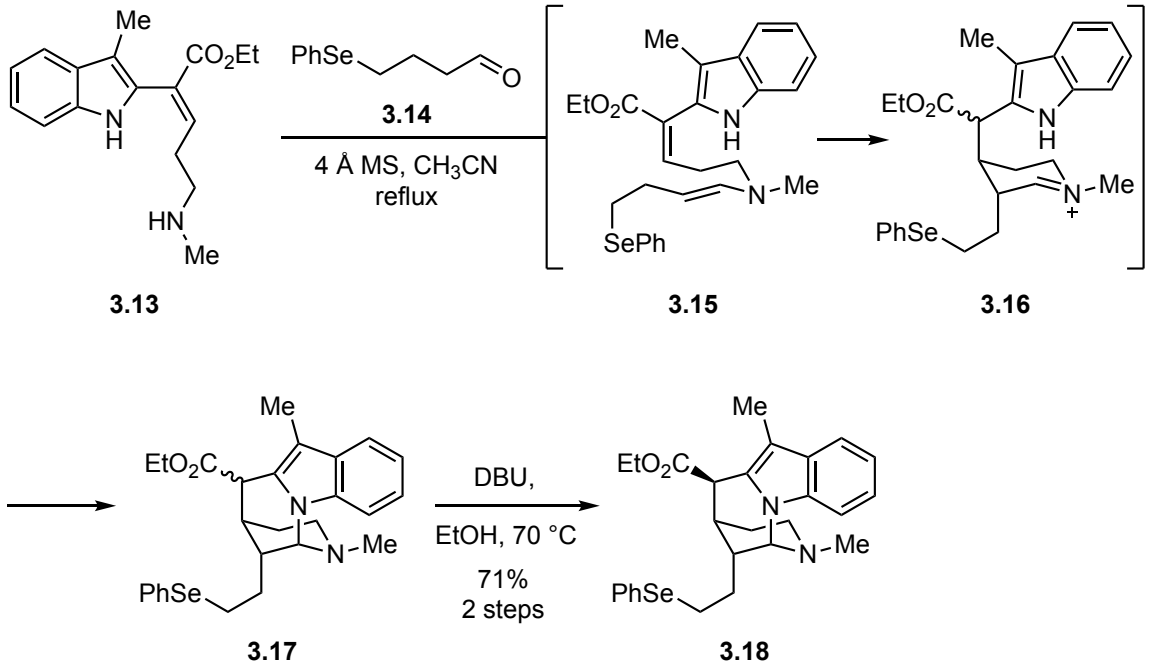

Scheme 3.2. Enamine–Michael cascade reaction sequence.

The axial orientation of the alkylselenide side chain in **3.18** was not predicted at the outset and inversion at this center would ultimately be required. The stereochemical outcome was rationalized to occur through equilibration of enamine **3.19** under the reaction conditions (Scheme 3.3). The equatorial sidechain in **3.20** was posited to be less favorable due to gauche interactions that were alleviated upon equilibration to the axial position in **3.16**, which might be favored because the presence of the nitrogen atom in the ring alleviates the 1,3-diaxial interaction that would otherwise be present.

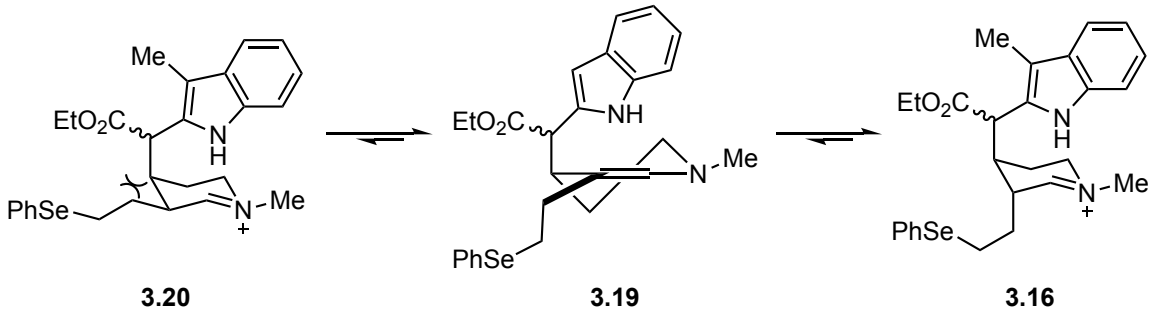

Scheme 3.3. Equilibration of alkylselenide side chain in **3.20** and **3.16**.

Having successfully executed the key domino reaction in the assemblage of tetracyclic core **3.18**, attention turned toward late-stage construction of the tetrahydropyran ring. Oxidation of the selenide moiety of **3.18** was accomplished via treatment with *meta*-chloroperoxybenzoic acid (*m*-CPBA) to generate the selenoxide that was eliminated *in–situ* to afford the terminal alkene in **3.21** in 83% yield (Scheme 3.4). The ester moiety of **3.21** was reduced with diisobutylaluminum hydride (DIBAL-H) to deliver the primary alcohol intermediate **3.22**. Subsequent Upjohn dihydroxylation of the terminal olefin in **3.22** followed by oxidative cleavage with lead tetraacetate generated aldehyde **3.23** that was used directly, without purification. Upon treatment of **3.23** with DBU, epimerization of the aldehyde to the equatorial position occurred, resulting in spontaneous cyclization to deliver hemiacetal intermediate **3.24** that was oxidized *in–situ* with Dess–Martin periodinane (DMP) to afford lactone **3.25** in 34% yield, over three steps. Addition of methyllithium to lactone **3.25** yielded the hemiketal intermediate **3.26** in 66% yield. Lewis acid-catalyzed reduction of the hemiketal in **3.26** using triethylsilane in the presence of trimethylsilyl trifluoromethansulfonate (TMSOTf) resulted in diastereoselective, axial delivery of the hydride from the convex face to complete the synthesis of (±)-alstoscholarisine A (**3.1**).

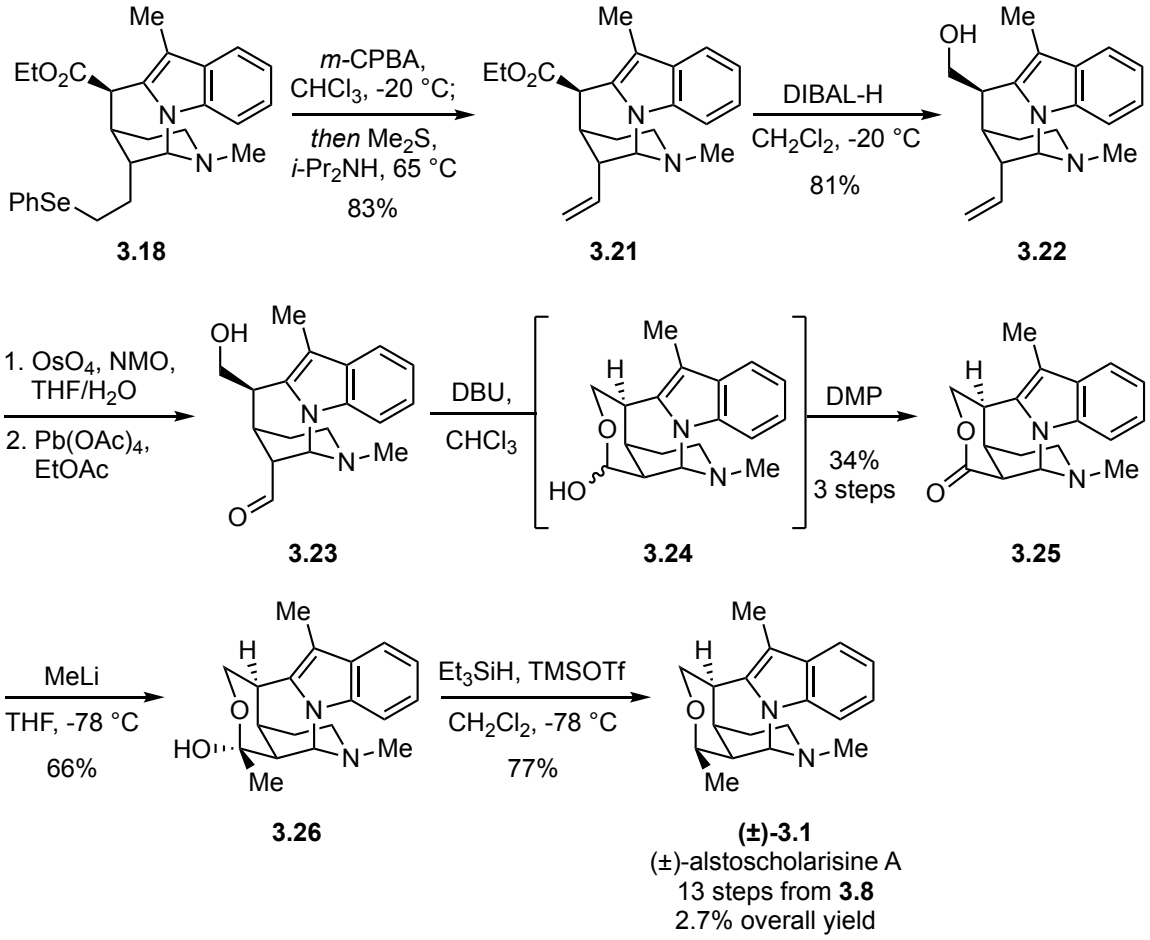

Scheme 3.4. Construction of the tetrahydropyran ring of (±)-alstoscholarisine A

The route to (±)-alstoscholarisine A developed by Bihelovic and Ferjancic was accomplished in 13 steps and 2.7% overall yield from the known 2,3-disubstituted indole **3.9**. The key step involved an enamine–Michael addition and aminal cyclization cascade that assembled a portion of the core structure in six steps, in its longest linear sequence (LLS). Unfortunately, the strategy for late-stage construction of the tetrahydropyran ring was somewhat lengthy and required numerous redox manipulations that detracted from

the overall efficiency of the synthesis. Despite this shortcoming, the synthesis is notable as the first reported synthesis of an alkaloid from this family of natural products.

3.2.2 The Yang Synthesis of (±)-Alstoscholarisine A

The first synthesis of (–)-alstoscholarisine A was reported by Yang *et al.* shortly after the report from Bihelovic and Ferjancic .[364] The synthesis began from known butyrolactone **3.30**, which was prepared in two steps from the commercially available ester **3.27** according to a reported protocol via ozonolysis and subsequent addition of vinylmagnesium chloride to provide the cyclized product **3.30** (Scheme 3.5).[370] Butyrolactone **3.30** was then used in a Lewis acid promoted acylation of 3-methylindole (**3.6**) to form the *N*-acylated product **3.31** in 75% yield. This intermediate set the stage for the key iridium-catalyzed enantioselective Friedel-Crafts cyclization at the 2-position of indole **3.31** using Carreira's chiral ligand **3.32** and scandium triflate to afford the lactam product **3.33** in 75% yield (99% *ee*).[371]

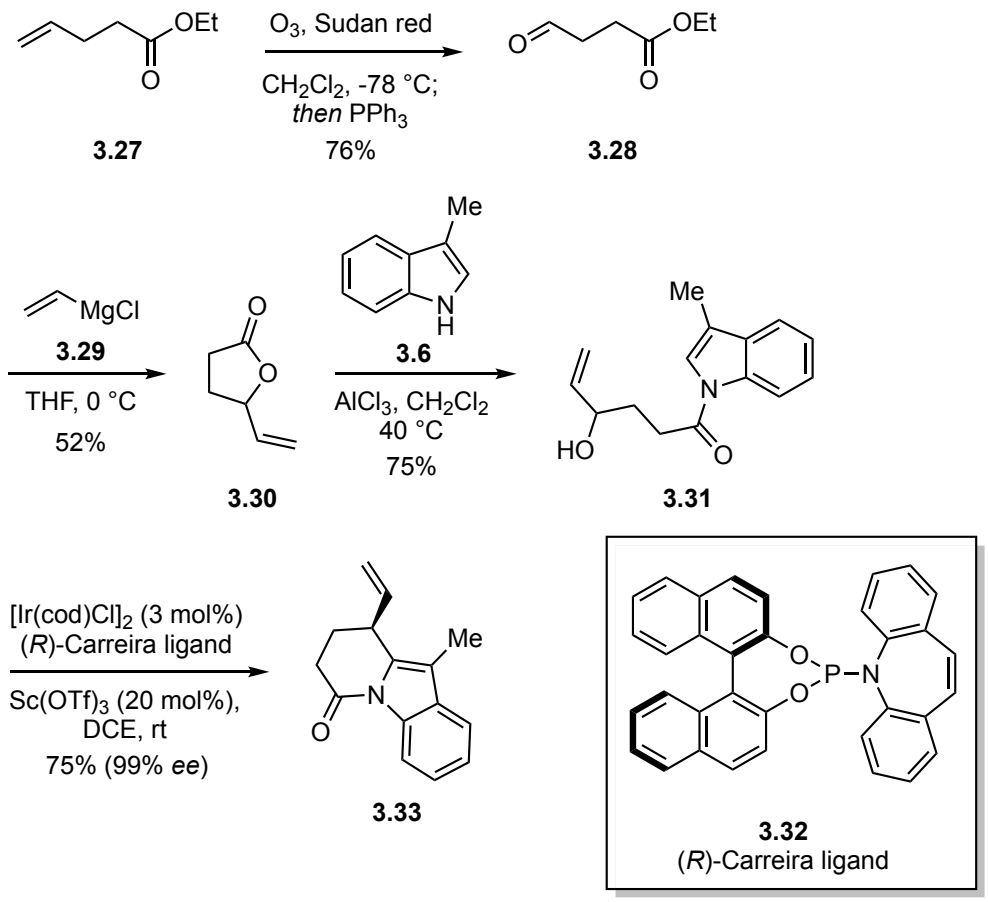

Scheme 3.5. The asymmetric Friedel-Crafts cyclization in Yang's synthesis of (–)-alstoscholarisine A.

With the critical stereocenter established in **3.33**, the terminal olefin was then dihydroxylated with osmium tetroxide to afford diol **3.34** as a mixture (5:1) of diastereomers (Scheme 3.6). The crude mixture thus obtained was converted to the corresponding acetonide with 2,2,-dimethoxypropane (**3.35**) and the major diastereomer **3.36** was separated in 75% yield over two steps. Deprotonation of lactam **3.36** with lithium bis(trimethylsilyl)amide (LiHMDS) followed by addition of phenylselenyl bromide provided the selenide intermediate **3.37** that was then oxidized and eliminated to afford α,β-unsaturated lactam **3.38** in 70% yield over two steps.

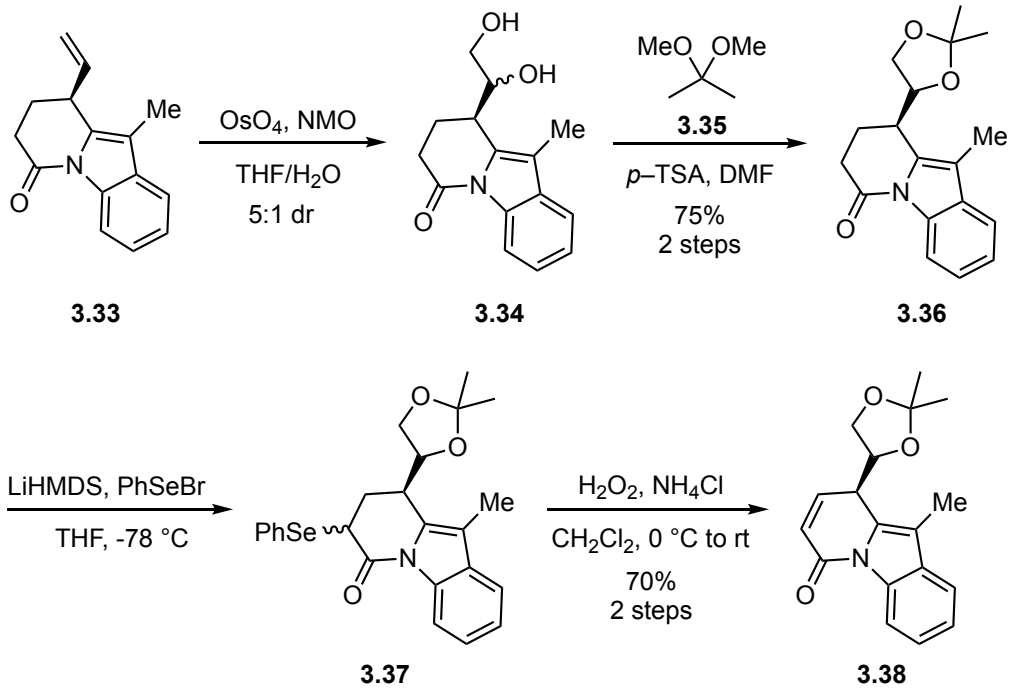

Scheme 3.6. Yang's synthesis of **3.38**.

With **3.38** in hand, the subsequent copper iodide mediated conjugate addition of vinylmagnesium bromide (**3.39**) proceeded smoothly with substrate-controlled stereoselective addition from the most accessible face (Scheme 3.7). The resulting enolate was trapped with acetaldehyde to afford **3.40** as the major diastereomer (8:1) in 75% yield. Stirring a solution of **3.40** in methanol with aqueous HCl revealed the diol intermediate **3.41** that was oxidatively cleaved *in-situ* by addition of sodium periodate ($NaIO_4$) to give aldehyde **3.42** that spontaneously cyclized to deliver lactol **3.43** in 86% yield as an inconsequential mixture (1:1) of diastereomers. Subsequent Lewis acid-promoted ionic reduction of **3.43** with triethylsilane completed construction of the tetrahydropyran ring in **3.44**.

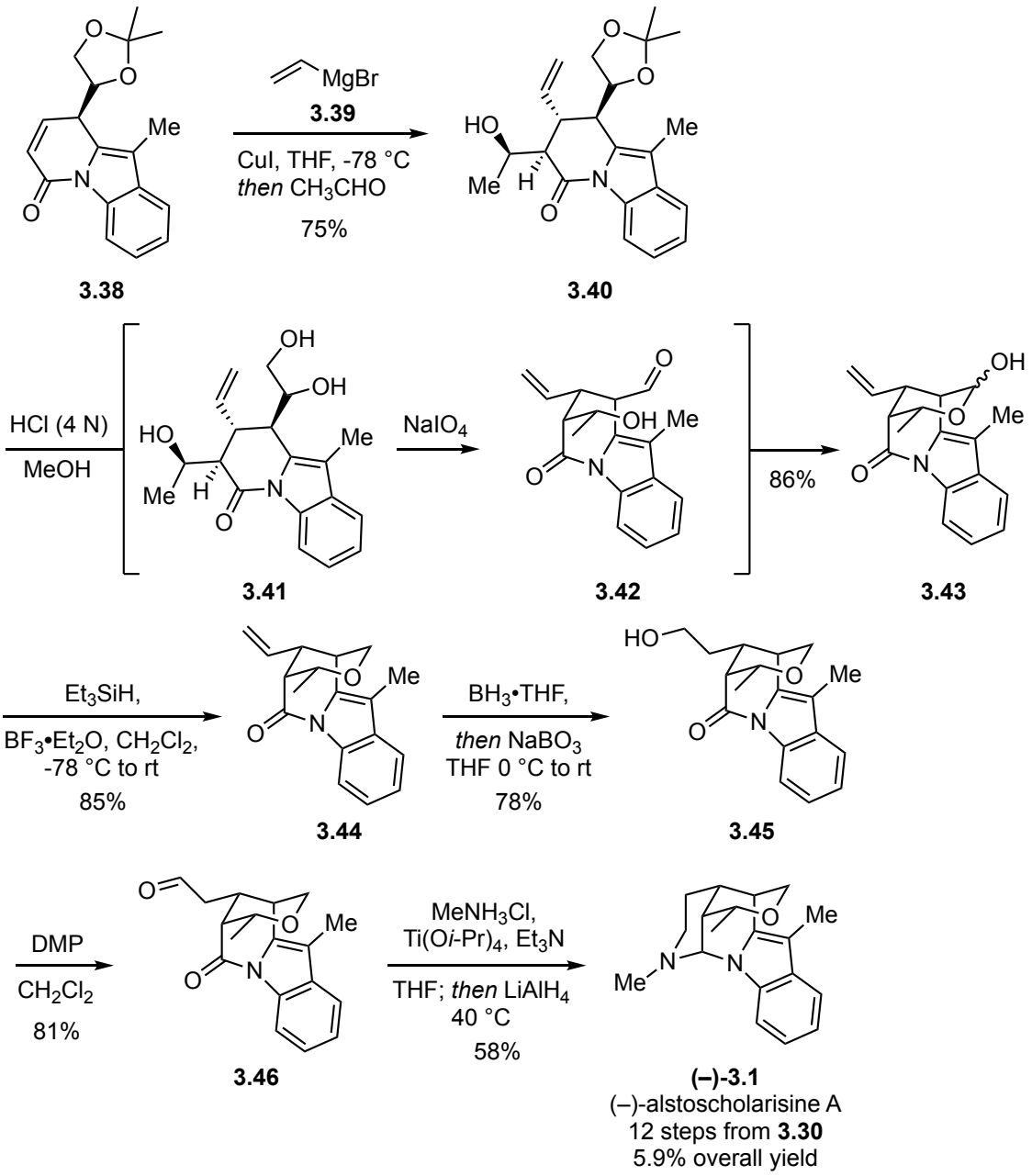

Scheme 3.7. Completion of the total synthesis of (–)-alstoscholarisine A.

Attention next turned toward construction of the cyclic aminal ring. Thus, hydroboration and oxidation of the terminal olefin in **3.44** provided the primary alcohol intermediate **3.45** and subsequent oxidization with Dess–Martin periodinane yielded

aldehyde **3.46** (Scheme 3.7). The aldehyde moiety in **3.46** was converted to an imine via condensation with methylamine, followed by reduction with lithium aluminum hydride that also reduced the indole lactam resulting in aminal formation and completing the synthesis of (–)-alstoscholarisine A.

Yang and coworkers achieved the first synthesis of (–)- alstoscholarisine A in 12 steps (LLS) from known starting material **3.30** and 5.9% overall yield.[364] A critical stereocenter was established early in the synthesis using Carreira's methodology for iridium-catalyzed polyene cyclization to forge the lactam ring in **3.33**. This enabled sufficient substrate control in subsequent transformations. In contrast to other strategies, late-stage construction of the aminal ring was used to complete the enantioselective synthesis.

3.2.3 The Weinreb Synthesis of (±)-Alstoscholarisine B and C

Weinreb later developed a more divergent approach to access several of the alstoscholarisine alkaloids.[365,366] The synthesis commenced with preparation of known *N*-sulfonylvalerolactam **3.48** from commercially available valerolactam **3.47** according to a reported protocol (Scheme 3.8).[372] Deprotonation of **3.48** with excess LiHMDS (2.2 eq.) followed by sequential addition of allyl chloroformate (AllocCl) and phenylselenyl bromide delivered the β-ketoester intermediate **3.49** in 71% yield.[365] Oxidation and elimination of the selenide in **3.49** provided α,β-unsaturated lactam **3.50**, which was not stable to purification and was used directly as a Michael acceptor in the conjugate addition with known 2,3-disubstituted indole **3.8** to afford Michael–adduct **3.51** in 69% yield over two steps, as a complex mixture of diastereomers.

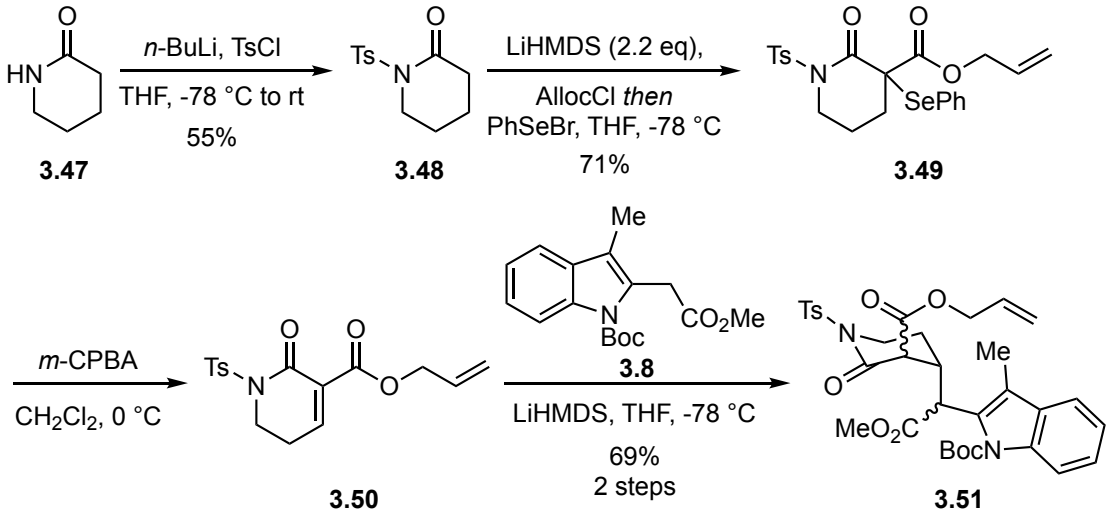

Scheme 3.8. Synthesis of Michael-adduct **3.51**.

The next task involved constructing the appropriately substituted cyclic aminal ring system.[365] A one-pot process involving alkylation of β-ketoester **3.51** with allyl iodide, followed by palladium catalyzed decarboxylation delivered lactam **3.52** in 74% yield as a mixture of C–16 diastereomers (Scheme 3.9). The direct palladium–mediated decarboxylation and allylation of **3.51** proved to be lower yielding than the sequential one-pot sequence. Chemoselective partial reduction of *N*-sulfonyl lactam **3.52** to hemiaminal intermediate **3.53** was accomplished with diisobutylaluminum hydride (DIBAL-H) in 78% yield. Treating **3.53** with trifluoroacetic acid removed of the Boc-protecting group and induced cyclization of the indole nitrogen atom with the hemiaminal moiety to afford the aminal ring system in **3.54**. This served as the key divergent intermediate that possessed four of the five ring systems and would be used to complete the alstoscholarisines via late-stage construction of the tetrahydropyran ring in Weinreb's second generation approach.[365,366]

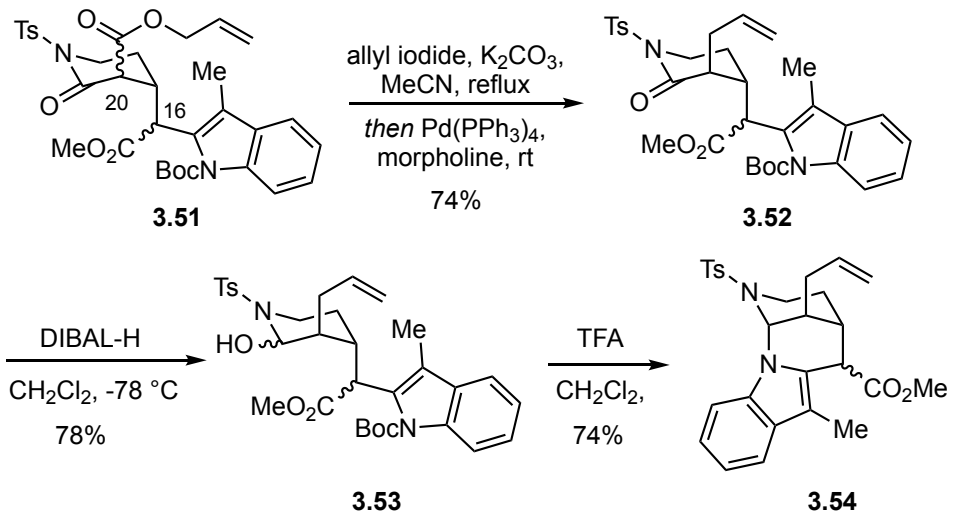

Scheme 3.9. Synthesis of Weinreb's divergent intermediate.

Treatement of **3.54** with potassium bis(trimethylsilyl) amide (KHMDS) followed by addition of formaldehyde from the convex face afforded the aldol adduct **3.55** in 94% yield as a single diastereomer (Scheme 3.10).[365] The primary alcohol of **3.55** was protected as a *tert*-butyldimethylsilyl (TBS) ether in **3.56**. Formation of the tetrahydropyran ring required isomerization of the terminal olefin of **3.56** to a 2-propenyl group. Initial attempts at transition metal catalyzed isomerization were unsuccessful and led to an alternative strategy that transposed the olefin via a thermal ene–reaction with diethyl diazocarboxylate (DEAD) to afford the allylic hydrazide intermediate **3.57** in 77% yield.[366] Subsequent dihydroxylation of the olefin in **3.57** followed by oxidative cleavage revealed the requisite aldehyde moiety of **3.58** in 61% yield over two steps.

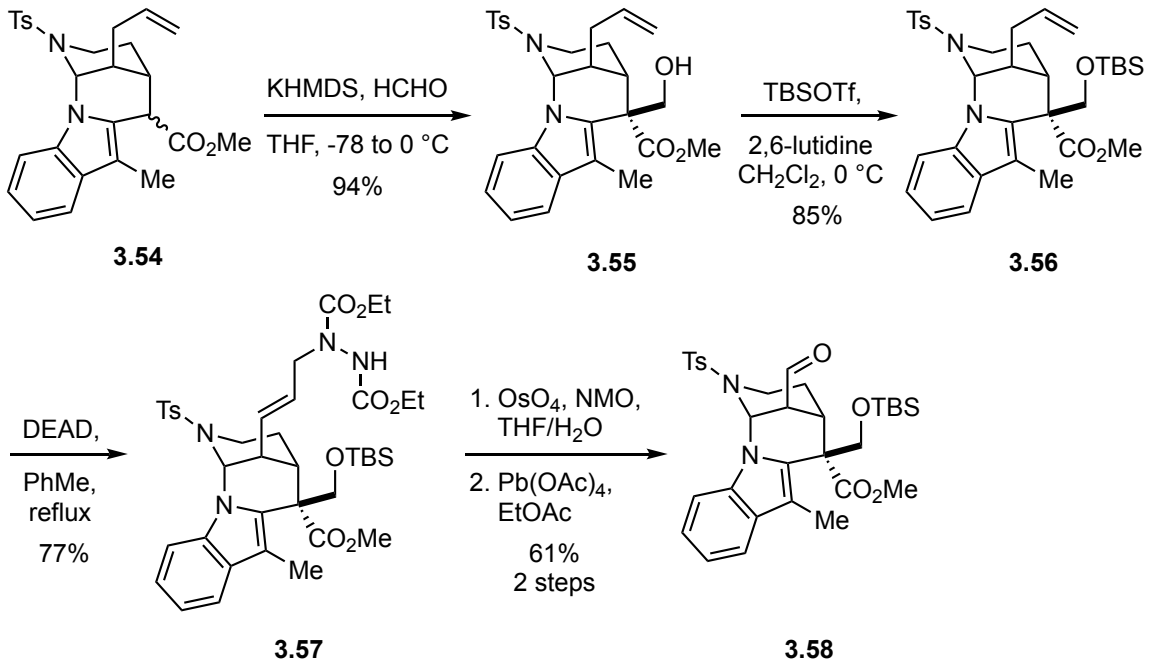

Scheme 3.10. Weinreb's synthesis of **3.58**.

Continuing toward alstoscholarisine C, the TBS-protecting group was next removed from aldehyde **3.58** under acidic conditions to deliver the primary alcohol **3.59** (Scheme 3.11). Similar to the tactic used by Bihelovic and Ferjancic, aldehyde **3.59** was epimerized via treatment with DBU, resulting in spontaneous cyclization to the lactol intermediate that was then acylated *in situ* to afford **3.60** in 77% overall yield from **3.58**. Stirring a solution of **3.60** in dichloromethane in the presence of TMSOTf and trimethylaluminum provided axial delivery of a methyl group to a presumed oxocarbenium intermediate in 75% yield, thereby completing the construction of the tetrahydropyran ring **3.61**. Subsequent removal of the *N*-tosyl protecting group and reductive methylation of the resulting secondary amine completed the synthesis of (±)-alstoscholarisine C (**3.3**).[365]

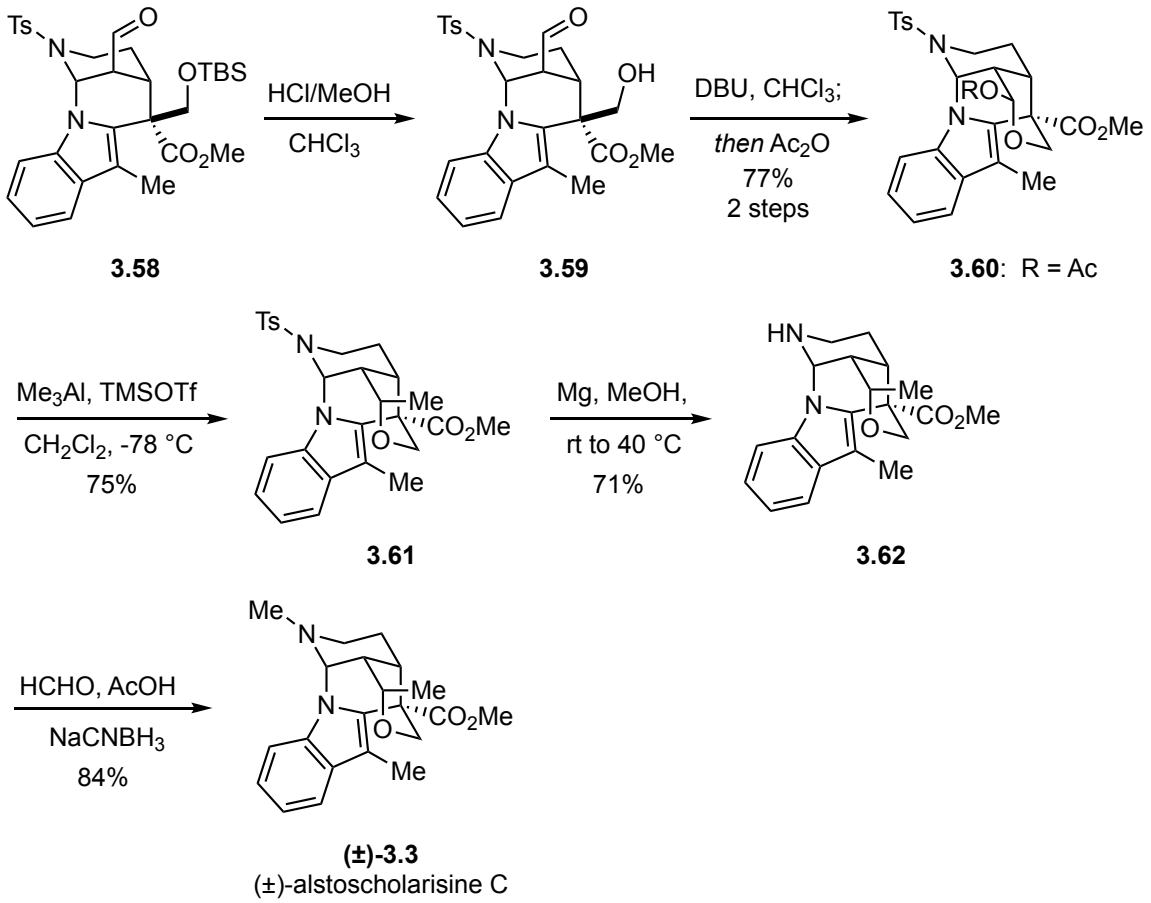

Scheme 3.11. Completion of the total synthesis of (±)-alstoscholarisine C.

A related strategy was used to complete the synthesis of alstoscholarisine B.[365] Removal of the silyl protecting group from **3.58** followed by epimerization of the aldehyde with DBU gave lactol intermediate **3.59**, which was oxidized *in situ* using iodobenzene diacetate and TEMPO to afford lactone **3.63** in 73% yield over two steps (Scheme 3.12) . Addition of methyllithium to lactone **3.63** afforded the hemiketal intermediate **3.64** as a single diastereomer (configuration not determined) in 66% yield. Subsequent ionic reduction of **3.64** with triethylsilane and TMSOTf resulted in axial delivery of the hydride to the oxocarbenium intermediate, thereby establishing the correct stereochemistry of the methyl group on the tetrahydropyran ring in **3.65**. Removal of the

N-tosyl protecting group from **3.65** and reductive methylation of the nitrogen atom completed the synthesis of (±)-alstoscholarisine B.

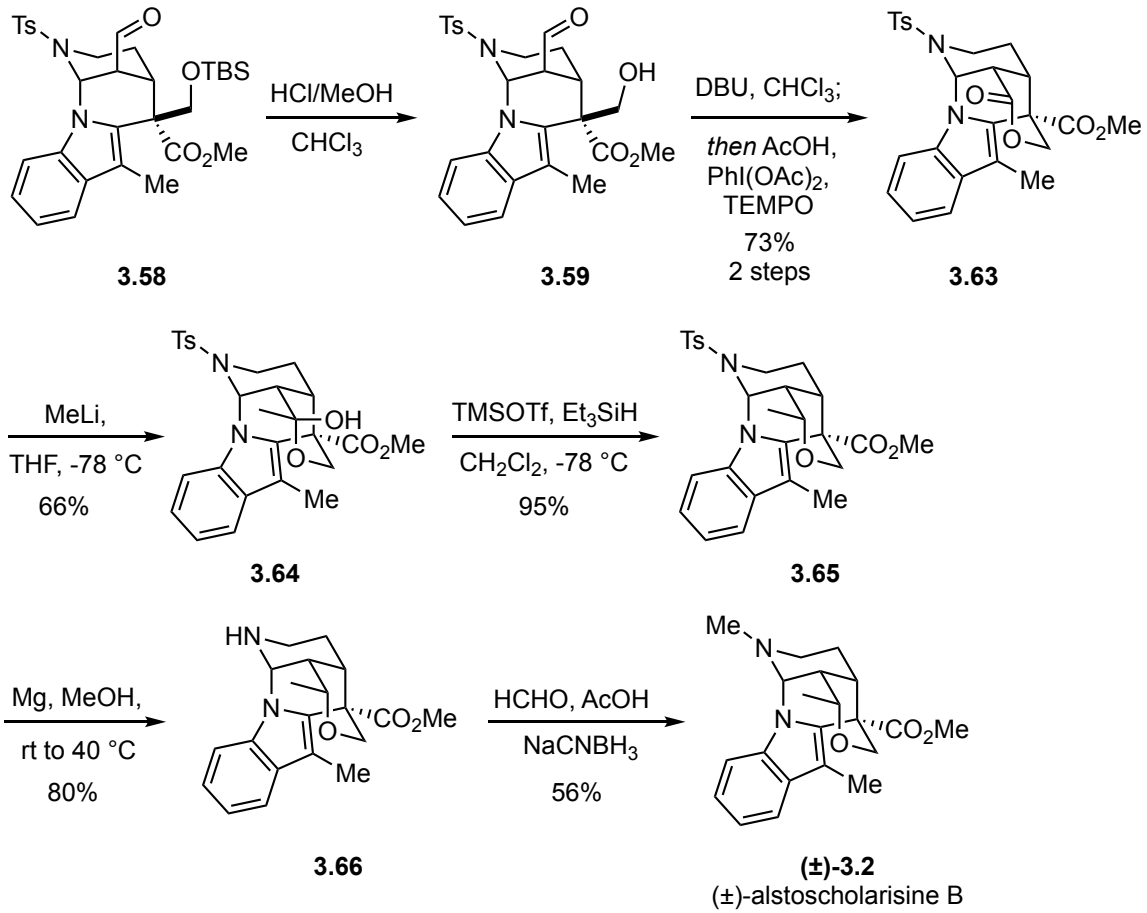

Scheme 3.12. Completion of (±)-alstoscholarisine B.

3.2.4 The Weinreb Synthesis of (±)-Alstoscholarisines A–E

After Weinreb's initial syntheses of (±)-alstoscholarisines B and C in 2017, a follow up report in 2018 disclosed the synthesis of (±)-alstoscholarisines A–E using a slightly improved route.[366] The first generation approach relied on a thermal ene–reaction for isomerization of the terminal olefin in **3.56** (Scheme 3.10). However, upon revisiting

the transition metal catalyzed isomerization, it was discovered that heating a solution of **3.56** and Grubbs II catalyst (10 mol%) in methanol at 60 °C according to a protocol reported by Hanessian *et al.* provided the 2-propenyl intermediate **3.67** in 89% yield as an inconsequential mixture (*ca*. 2.8:1 *E/Z*) of isomers (Scheme 3.13).[373] This alternative tactic improved atom economy and obviated the need to protect the primary alcohol in **3.56**.[366]

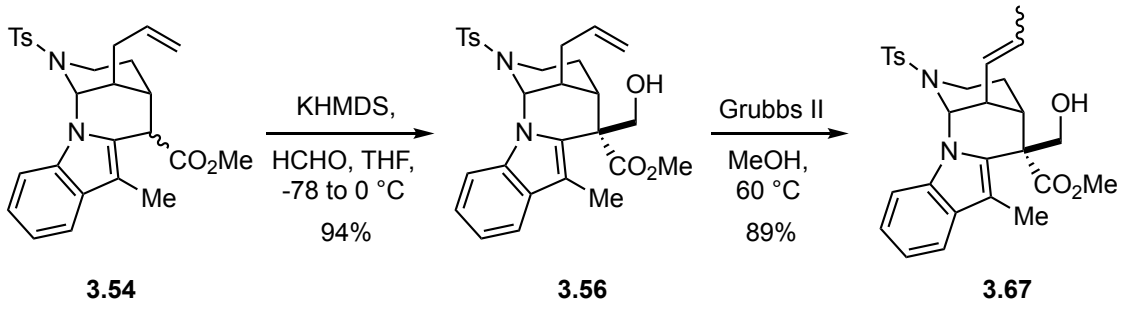

3.54 **3.56** **3.67**

Scheme 3.13. Isomerization of the allyl group using Grubbs II catalyst.

With improved access to a slightly modified divergent intermediate **3.67**, a similar sequence was applied to complete the synthesis of alstoscholarisine alkaloids (Scheme 3.14). A two-step oxidative cleavage of the olefin revealed the aldehyde in **3.59** that was isomerized with DBU and trapped as the acylated lactol intermediate **3.60**, which was prepared in the first-generation approach. Thus, application of the same sequence completed the synthesis of (±)-alstoscholarisine C (**3.3**) in 14 steps from known *N*-sulfonylvalerolactam **3.48** and 5.7% overall yield. Basic hydrolysis of the ester in **3.3** to the carboxylic acid afforded (±)-alstoscholarisine D (**3.4**) in 15 steps from **3.48** and 4.9% overall yield. Alternatively, isomerization of aldehyde intermediate **3.59** with DBU and oxidation of the resulting lactol provided lactone **3.63** that was also accessed in the first-generation synthesis. Accordingly, using the previously developed four-step sequence

completed the synthesis of (±)-alstoscholarisine B (**3.2**) in 15 steps from known *N*-sulfonylvalerolactam **3.48** and 3.6% overall yield.

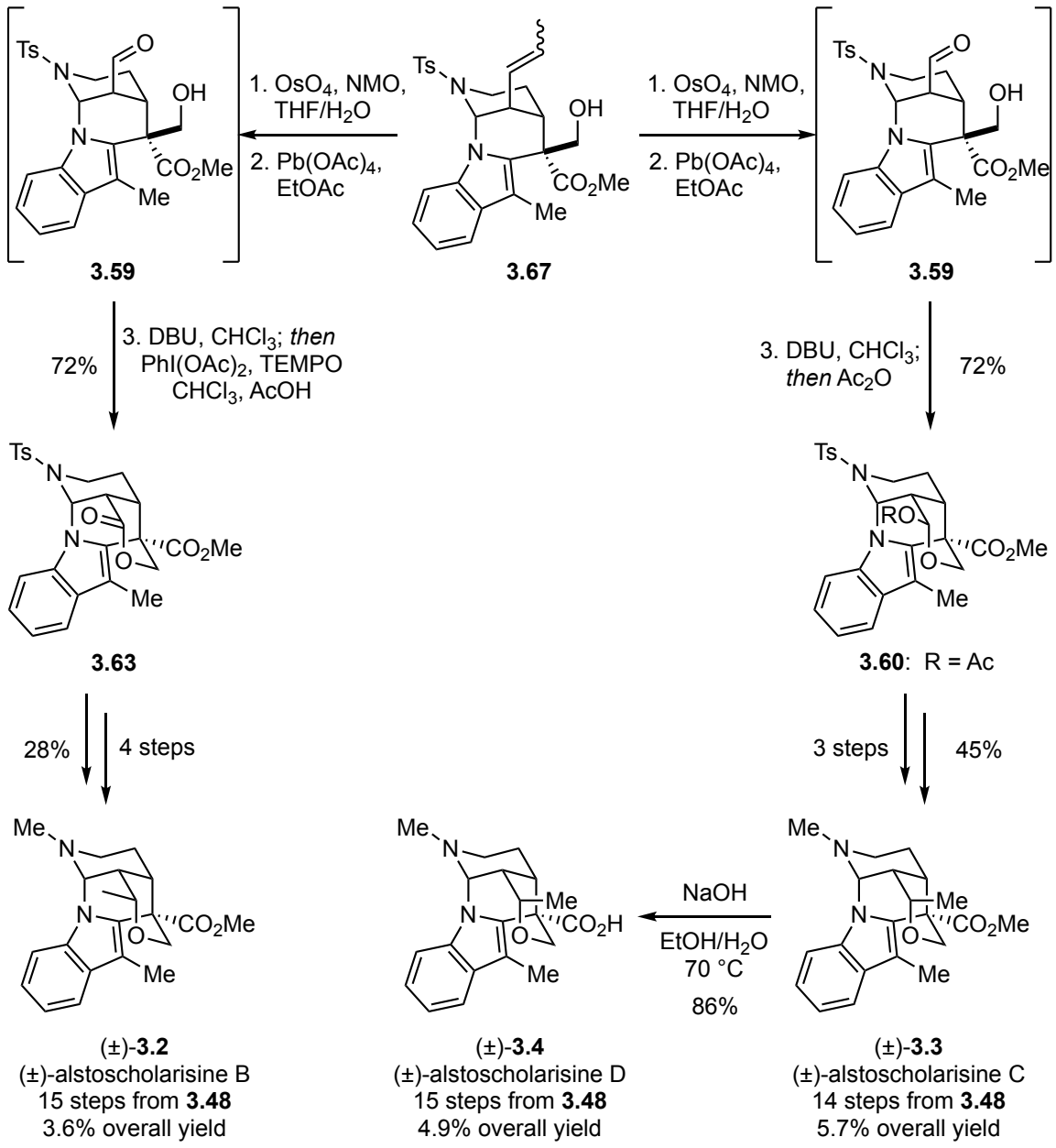

Scheme 3.14. Completion of the total syntheses of alstoscholarisines B–D.

Toward the synthesis of alstoscholarisines A and E, which do not possess the carbonyl moiety at the C–16 bridgehead, the previously constructed aminal intermediate **3.54** which existed as a mixture of diastereomers was epimerized with sodium methoxide to afford **3.68** as a single diastereomer in 95% yield (Scheme 3.15). Isomerization of the allyl group using Grubbs II catalyst proceeded smoothly to afford **3.69** and subsequent reduction of the ester was accomplished via treatment with lithium aluminum hydride to provide primary alcohol **3.70**.

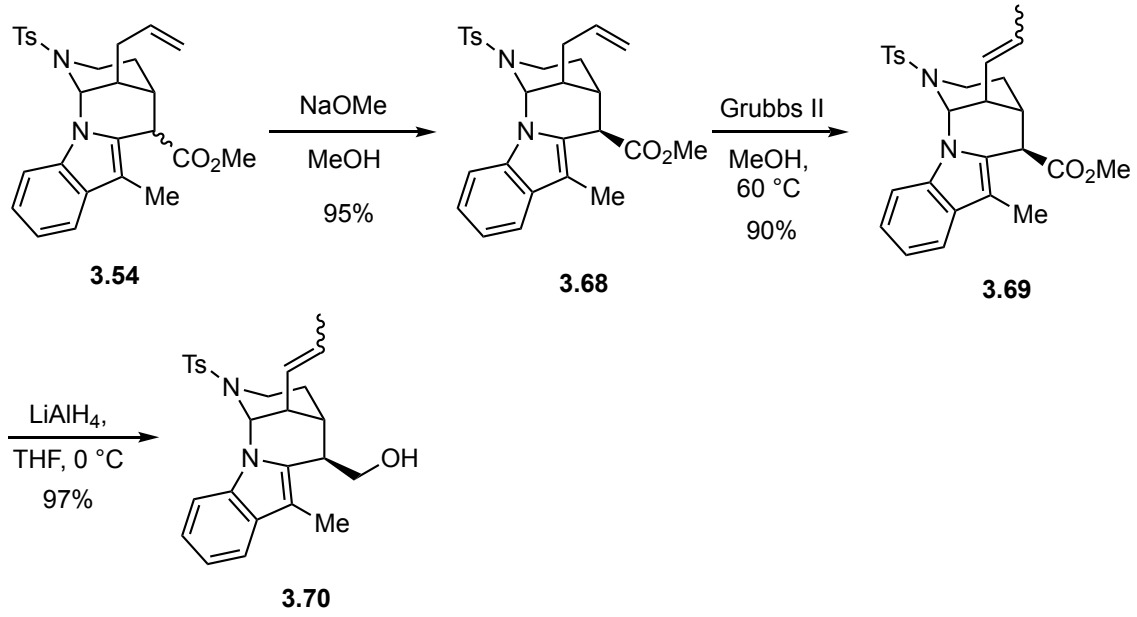

3.54 **3.68** **3.69** **3.70**

Scheme 3.15. Weinreb's synthesis of **3.70** en route to (±)-alstoscholarisines A and E.

Having accessed divergent intermediate **3.70**, the tetrahydropyran ring was constructed in a similar fashion as the previous approach (Scheme 3.16). Namely, oxidative cleavage of the olefin in **3.70** and epimerization of the resultant aldehyde provided a lactol intermediate that was either trapped *in situ* as acylated lactol **3.72** or

oxidized *in situ* to lactone **3.73**. Notably, this sequence was less effective using divergent intermediate **3.70** that lacked a fully substituted C–16 center and proceeded in only 31% and 41% yield over three steps, respectively. The same sequence previously used to complete the syntheses (±)-alstoscholarisines B–D was applied to **3.72** and **3.73** to complete the synthesis of (±)-alstoscholarisine A (**3.1**) in 16 steps from known *N*-sulfonylvalerolactam **3.48** and 1.8% overall yield, as well as the synthesis of (±)-alstoscholarisine E (**3.5**) in 15 steps from **3.48** and 3.1% overall yield.

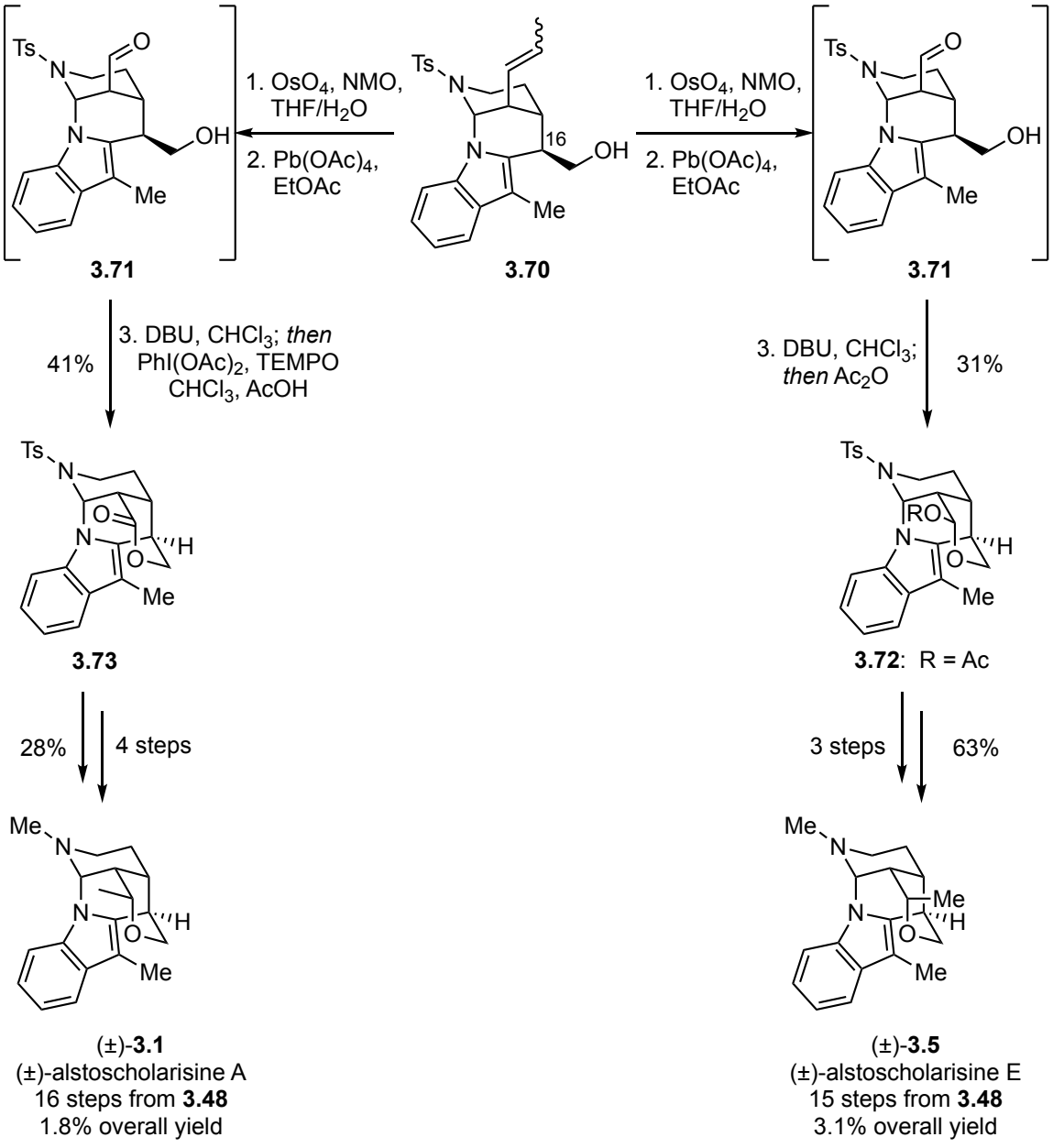

Scheme 3.16. Completion of the syntheses of (±)-alstoscholarisines A and E.

Weinreb and coworkers reported the first synthesis of (±)-alstoscholarisines B-D, as well as the first synthesis of (±)-alstoscholarisines E.[365,366] Their route shares some similarities with the approach developed by Bihelovic and Ferjancic in that the same

indole starting material was used to construct the cyclic aminal ring system early in the synthesis. Additionally, the tactic for late-stage construction of the tetrahydropyran ring was related. While the synthesis did not require the development of new chemistry, it is notable for its divergent nature that enabled the construction of multiple alstoscholarisine alkaloids. This does seem to come at the cost of efficiency, as preparation of (±)-alstoscholarisine A is more lengthy and lower yielding than previously developed routes.

3.2.5 The Liao Synthesis of (–)-Alstoscholarisine A and E

An enantioselective synthesis of (–)-alstoscholarisines A and E was recently reported by Liao and coworkers utilizing the known chiral lactam **3.78**.[367] The staring material was prepared in three steps from commercially available 1-*N*-Boc-2-piperidone (**3.74**) according to a reported protocol via deprotonation of **3.74** with LiHMDS and addition of phenylselenyl chloride to deliver **3.75** (Scheme 3.17).[374] Subsequent oxidation and elimination of the selenide provided α,β-unsaturated lactam **3.76** in 55% yield over two steps. The rhodium catalyzed asymmetric conjugate addition of alkynl(diphenyl)methanol **3.77** to α,β-unsaturated lactam **3.76** was previously reported by Hayahsi to proceed in 86% yield (95% *ee*).[375] Removal of the triisopropylsilyl (TIPS) protecting group with TBAF generated the terminal alkyne substrate **3.79**.[367] Treating **3.79** with dibutylboron triflate (*n*-Bu_2BOTf) and *N*,*N*-diisopropylethylamine followed by acetaldehyde delivered the aldol adduct **3.80** as a mixture of isomers that were not isolated. The crude reaction mixture was subjected to rhodium catalyzed cycloisomerization according to the protocol developed by Trost to afford oxahydroisoquinolones **3.81** in 22% yield and **3.82** as a mixture of diastereomers in 53% yield.[376] The authors indicated that obtaining this mixture was critical to the divergent strategy that was devised to access both (–)-alstoscholarisines A and E.

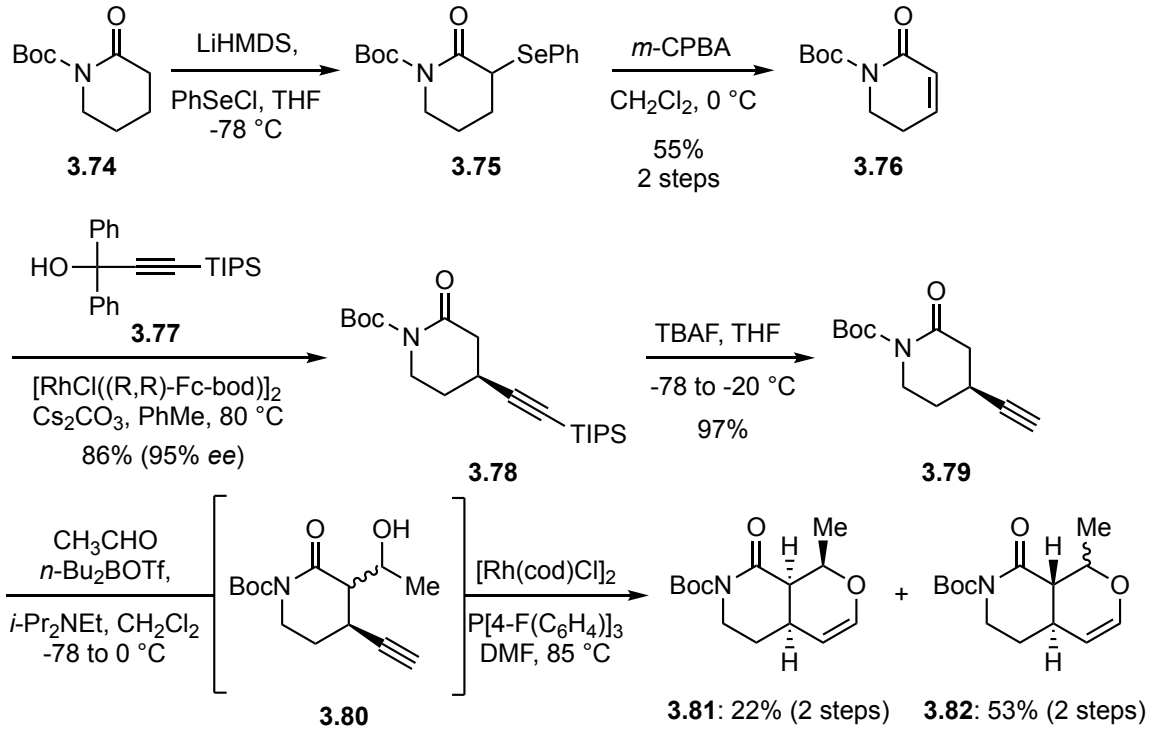

Scheme 3.17. Liao's synthesis of oxahydroisoquinolone ring system.

Continuing toward (–)-alstoscholarisine A, attention turned toward introduction of the indole moiety via a cross-coupling reaction (Scheme 3.18). Thus, oxahydroisoquinolone **3.81** was converted to vinyl iodide **3.83** using *N*-iodosuccinimide (NIS) and catalytic silver nitrate (20 mol%) according to a reported protocol for the conversion of glycals to 2-iodoglycals.[377] A variety of conditions were screened for the Suzuki–Miyaura coupling of vinyl iodide **3.83** with indole boronic acid **3.84**, a challenging substrate that is well-known to easily undergo protodeboronation under the reaction conditions.[378] Ultimately, they found that slight modification of conditions reported by Buchwald and coworkers for the Suzuki-Miyaura coupling of related 2-heterocyclic boronic acids worked well.[379,380] In the event, heating a solution of oxahydroisoquinolone **3.83** and indole boronic acid **3.84** (3 eq.) in a mixture of toluene

and water (5:1) at 60 °C in the presence of the palladium precatalyst Pd SPhos G2 (5 mol%) and K_3PO_4 provided the cross-coupled product **3.85** in 97% yield.[367]

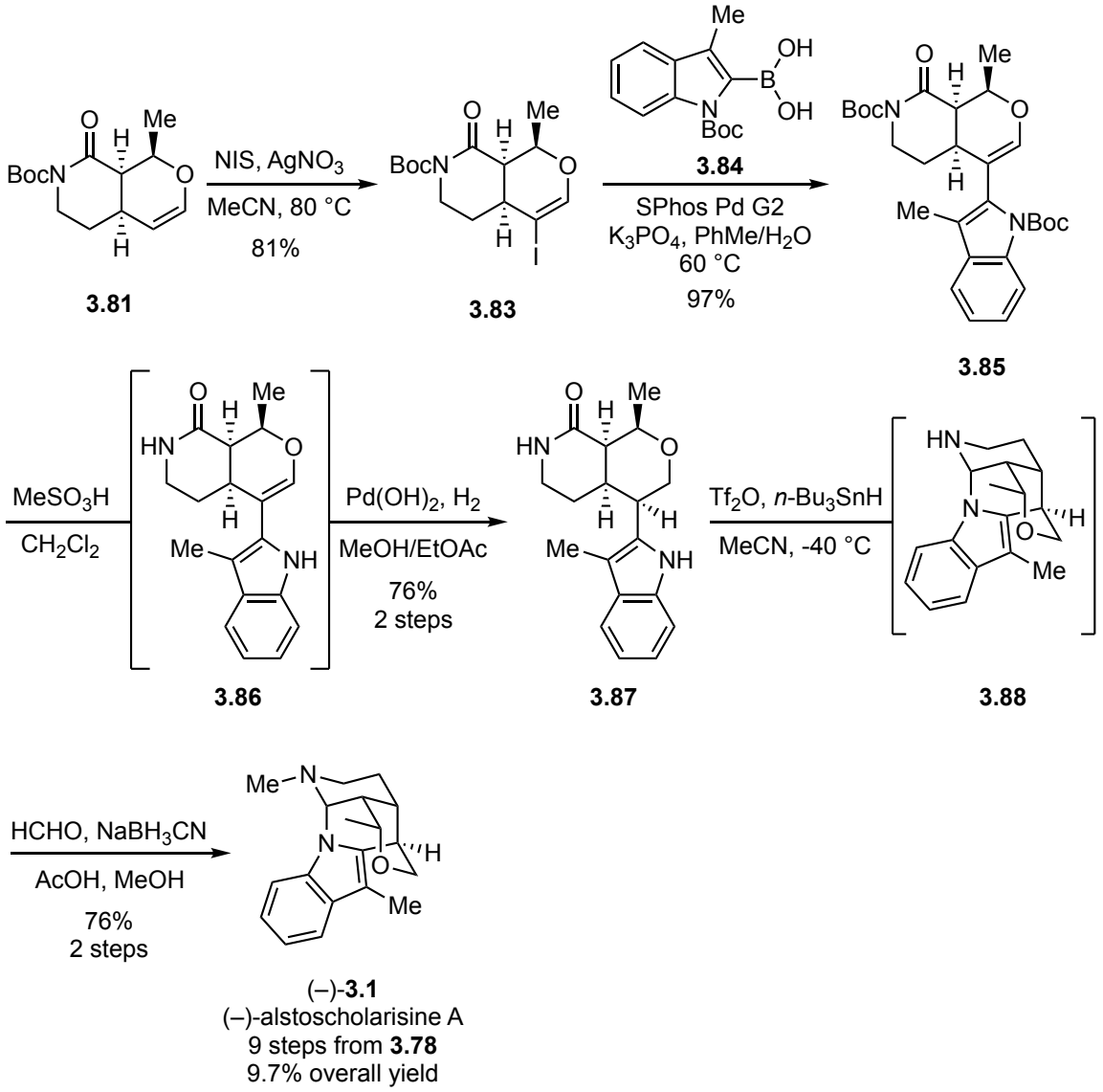

Scheme 3.18. Liao's synthesis of (–)-alstoscholarisine A.

With **3.85** in hand, the next challenge was formation of the bridging aminal ring. Toward this goal, stirring a solution of **3.85** in dichloromethane and methanesulfonic acid

(1:1) resulted in global Boc-deprotection to afford **3.86** (Scheme 3.18). The crude reaction mixture was subjected to hydrogenation using Pearlman's catalyst (100 mol%) to provide the reduced product **3.87** with the correct stereochemistry in 76% yield over two steps. Common conditions for the reduction of lactams to hemiaminal intermediates, including Schwartz reagent and DIBAL-H, were assessed with only small quantities of the cyclized product **3.88** observed. Eventually it was discovered that subjecting **3.87** to conditions developed by Movassaghi, using trifluoromethanesulfonic anhydride (Tf_2O) and tributyltin hydride provided the cyclic aminal **3.88**.[381] The volatiles were removed and the crude product was subjected to reductive alkylation with formaldehyde to afford (–)-alstoscholarisine A in 76% yield over two steps.

Attention next turned toward the synthesis of (–)-alstoscholarisine E from the mixture of oxahydroisoquinolone diastereomers **3.82** previously obtained using the same reaction sequence. Frist, treating the mixture of **3.82** with potassium hydride at -78 °C resulted in epimerization and the desired enantiomer **3.89** was isolated in 61% yield (Scheme 3.19). The same protocol outlined previously was used to convert **3.89** to vinyl iodide **3.90** and subsequent Suzuki–Miyaura coupling with indole boronic acid **3.84** proceeded in 80% yield. Interestingly, the global Boc-deprotection and hydrogenation sequence that was used previously, delivered a mixture of diastereomers **3.39** and **3.94** in 30% and 65% yield, respectively. The authors hypothesized that the axial methyl group in **3.85** provided enhanced selectivity by further blocking the concave face of the molecule, an effect that was absent in **3.84**, resulting in diminished selectivity. The desired diastereomer **3.94** was subjected to Movassaghi's conditions to form the cyclic aminal **3.95** followed by reductive alkylation to afford (–)-alstoscholarisine E in 64% yield over two steps.

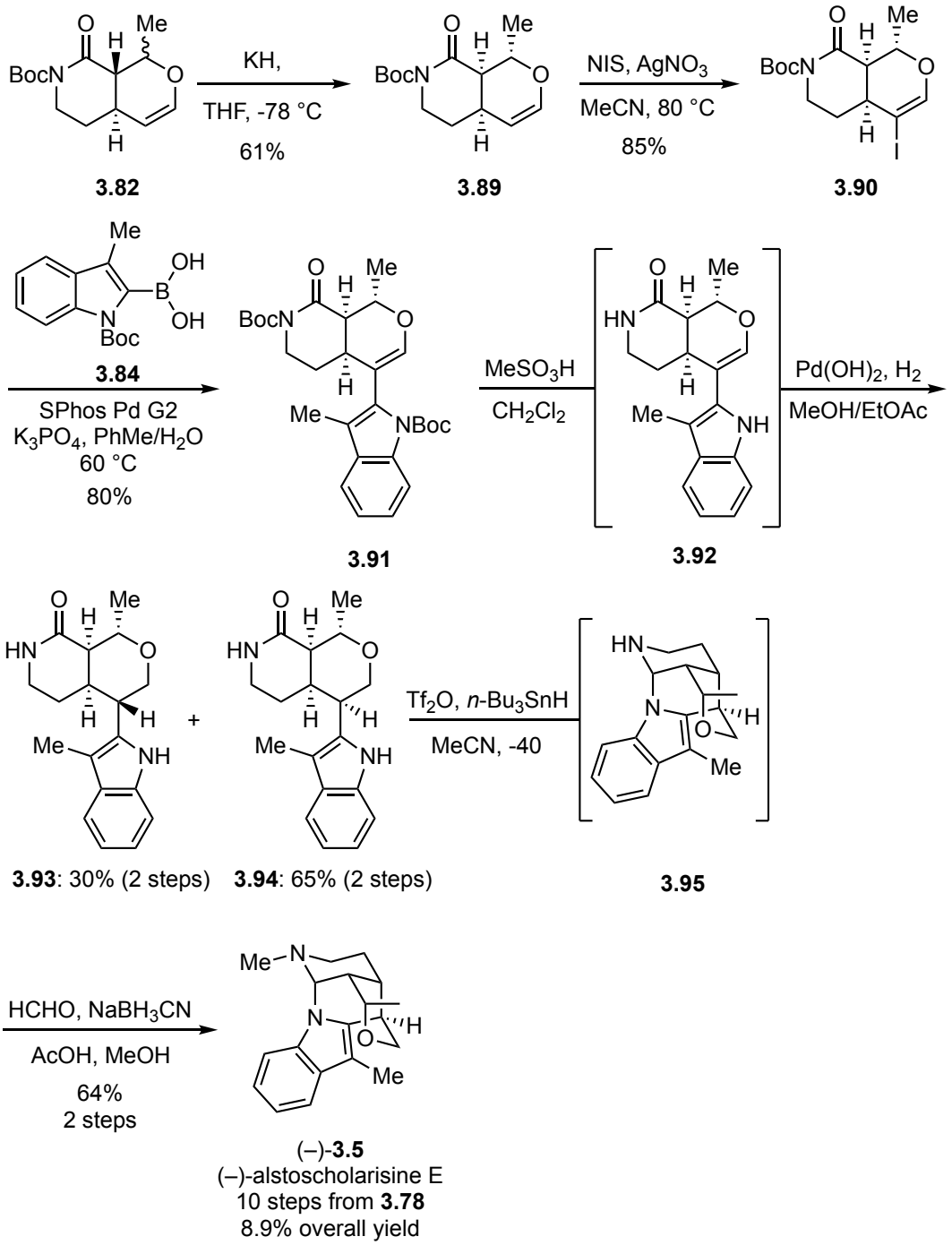

Scheme 3.19. Liao's synthesis of (–)-alstoscholarisine E.

Liao completed the first enantioselective synthesis of (–)-alstoscholarisine E (**3.5**), as well as the synthesis of (–)-alstoscholarisine A (**3.1**).[367] The strategy utilized the known chiral lactam **3.78** that is accessible in three steps from commercially available materials to establish a critical stereocenter in the oxahydroisoquinolone ring system. However, several of the subsequent transformations were plagued by a lack of stereoselectivity. This was most notable in the tandem aldol–cycloisomerization sequence to convert **3.79** to oxahydroisoquinolones **3.81** and **3.89**, which were isolated in 22% and 32% yield respectively, after epimerization to the *cis*-fused ring system. The authors leveraged the lack of selectivity in this sequence to access both (–)-alstoscholarisine A (**3.1**) and (–)-alstoscholarisine E (**3.5**), but it decreases the overall efficiency of the synthesis. In addition, the reduction of **3.92** to **3.94**, in route to (–)-alstoscholarisine E (**3.5**), resulted in a mixture (2.2:1) of diastereomers during the construction of another critical stereocenter. Overall, the synthesis is relatively concise from known materials, but the additional steps required for preparation of the starting chiral lactam **3.78** and the lack of stereoselectivity in the ensuing steps detract from the efficiency of this approach. Despite these shortcomings, the synthesis highlighted late-stage installation of the indole moiety and subsequent aminal cyclization as a convenient tactic for accessing the caged scaffold.

3.3 SUMMARY

The intriguing biological activity and the structural complexity of the alstoscholarisine alkaloids motivated numerous synthetic endeavors in the short time since their isolation was reported in 2014.[362] Bihelovic and Ferjancic first reported the synthesis of (±)-alstoscholarisine A in 2016 using an interesting enamine–Michael addition and aminal cyclization cascade to quickly access a portion of the core

structure.[363] Unfortunately, the late-stage construction of the tetrahydropyran ring was lengthy and detracted from the synthetic efficiency. The enantioselective synthesis of (–)-alstoscholarisine A by Yang followed in close succession using methodology develop by Carreira to establish a critical stereocenter. This alternative approach also required multiple synthetic manipulations to establish the tetrahydropyran ring. Nonetheless the synthesis was accomplished in 12 steps from known staring materials. Weinreb achieved the first synthesis of (±)-alstoscholarisines B and C in 2017 and in 2018 extended this approach to the first synthesis of (±)-alstoscholarisines E and D, as well as other members of this family of natural products. The divergent nature of the synthesis was notable, but the divergent intermediate was accessed early in the synthesis and required numerous transformations to prepare each natural product. In addition, the synthesis of (±)-alstoscholarisines A and E were lower yielding and required 16 and 15 steps to prepare from known starting material in 1.8 and 3.1% overall yield, respectively. The recent synthesis of (–)-alstoscholarisines A and E reported by Liao was more concise, accessing the natural products in 9 and 10 steps from a known chiral starting material, respectively. Unfortunately, the starting material required several steps to prepare and multiple transformations in the sequence lacked stereoselectivity, detracting from the efficiency of this approach.

Chapter 4: The Total Synthesis of (±)-Alstoscholarisine E[2]

4.1 Martin Group Approach to (±)-Alstoscholarisine E

Research in the Martin group has long been focused on the efficient total syntheses of indole alkaloids and we were intrigued by the structural complexity of the alstoscholarisine natural products. We therefore set out to devise a strategy to access alstoscholarisine E (**3.5**), as a representative member of this family of natural products. At the outset of our planning, a successful synthesis of alstoscholarisines A–E had not yet been achieved, although shortly thereafter the racemic and enantioselective synthesis of alstoscholarisine A (**3.1**) was reported.[363,364,382] Only recently was the synthesis of alstoscholarisine E (**3.5**) disclosed.[366,367] Despite these recent successes, the reported syntheses have been somewhat lengthy from commercially available reagents (13-18 steps LLS). We therefore continued forward to develop a concise and high yielding synthesis of alstoscholarisine E.

We envisioned a convergent approach to alstoscholarisine E (**3.5**), in which the advanced intermediate **4.1** would be converted to **3.5** through a selective reduction and cyclization sequence (Scheme 4.1).[383] Stereoselective reduction of the enol ether in **4.1** would be achieved from the convex face. Subsequent selective reduction of the lactam in **4.1** to the cyclic hemiaminal intermediate was expected to result in transannular cyclization with the indole nitrogen atom to form the bridging aminal in **3.5**. The advanced intermediate **4.1** would be accessed by joining an appropriately substituted 3-methylindole **4.2** (Z = ZnCl, $B(OH)_2$, $SnBu_3$) with the halogenated *cis*-

[2] This chapter is based on previously published work from Michael D. Wood that Prof. Stephen F. Martin served as an advisor for. See Wood, M.D.; Klosowski, D. W.; Martin S. F. Stereoselective Total Synthesis of (±)-Alstoscholarisine E. *Org. Lett.* **2020**, *22*, 786-790. Michael D. Wood contributed to complete the full synthetic sequence and optimization therein that delivered alstoscholarisine E.

oxahydroisoquinolone **4.3** (X = Br, I) via a Negishi, Suzuki, or Stille coupling. Facile halogenation of *cis*-oxahydroisoquinolone **4.3** (X = H) was anticipated, which in turn would be accessed via a hetero Diels–Alder (HDA) reaction of **4.4** in accord with prior work from our group that has been showcased as a key step in the synthesis of several natural products.[15,22,384,385] Expedient access to HDA precursor **4.4** was envisioned to occur using a vinylogous Mannich reaction, a reaction discovered and pioneered in the Martin group and used in the assemblage of a range of alkaloid natural products.[21,23-26,386-388] A vinylogous Mannich reaction of trimethylsiloxydiene **1.17** (~9:1 *E/Z*) and an *N*-acyliminium ion that might arise from treating hexahydrotriazine **4.6** with crotonyl chloride (**1.16**). Each of these reagents, **1.16**-**1.17** and **4.5**, are commercially available, making this an ideal entry point to these alkaloids.

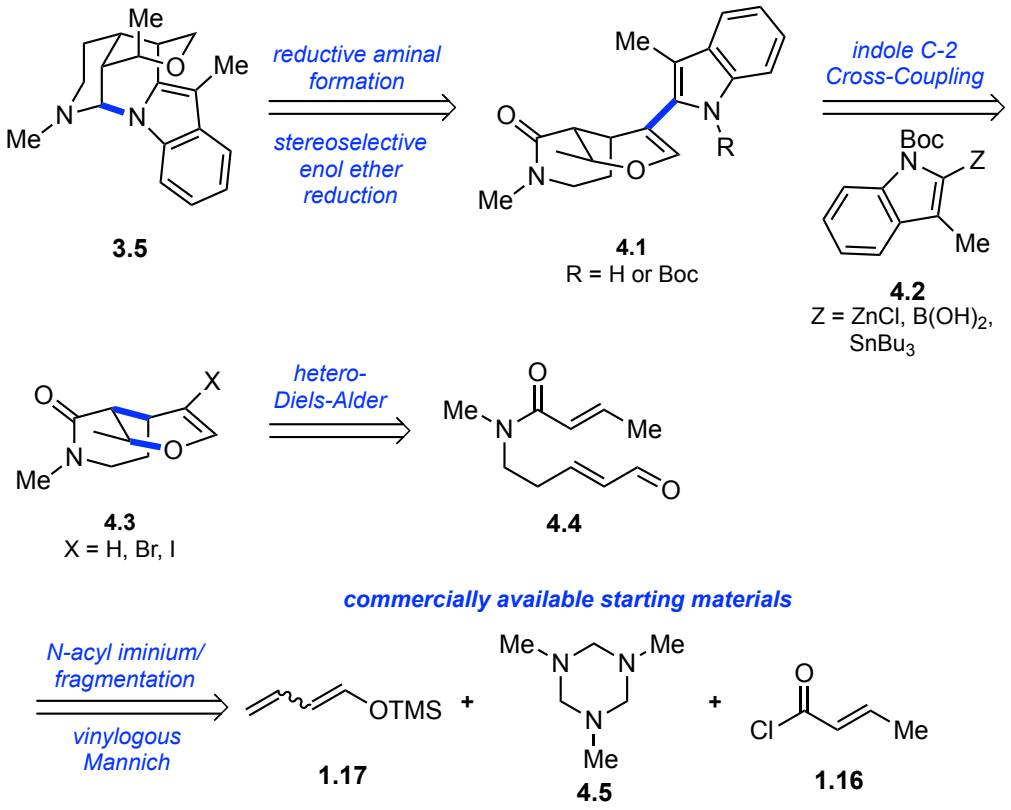

Scheme 4.1. Retrosynthetic analysis of (±)-alstoscholarisine E.

4.2 Construction of the Oxahydroisoquinolone Ring System

As discussed in the first chapter, the Martin group recognized that the hydroisoquinoline and oxahydroisoquinolone ring system is a common structural subunit of many natural products and developed an efficient strategy for their construction using an intramolecular Diels–Alder (IMDA) and hetero Diels-Alder reactions (IMHDA).[2,15-18,20,385,389-394] As part of this endeavor targeting a general entry point to the yohimbine family of natural products, a novel IMHDA reaction between an α,β-unsaturated aldehyde and an α,β-unsaturated amide was developed (Scheme 4.2).[20,389] The synthesis commenced with preparation of the IMHDA precursor **4.13** from protected propargyl alcohol **4.6**. Deprotonation of **4.6** with *n*-butyllithium followed by addition of oxirane

delivered homopropargyl alcohol **4.7** and subsequent partial hydrogenation using Lindlar catalyst provided **4.8**. Successive tosylation of alcohol **4.8** and reaction with benzylamine generated the homoallylic amine **4.10**. Amine **4.10** was subsequently acylated with crotyl anhydride **4.11** to afford benzyl amide **4.12**. After removal of the methoxymethyl (MOM) acetal protecting group from **4.12**, the resulting alcohol was subjected to Swern oxidation to deliver the IMDA precursor **4.13** in eight steps from commercially available reagents. Thermolysis of **4.13** in xylenes at 190 °C delivered the cycloadducts **4.14** and **4.15** (*ca.* 5:1), and the *cis*-oxahydroisoquinolone **4.14** was isolated in 73% yield. A few additional steps were required to transform **4.14** to **4.16**, which completed the formal synthesis of tetrahydroalstonine (**1.3**).[20,389]

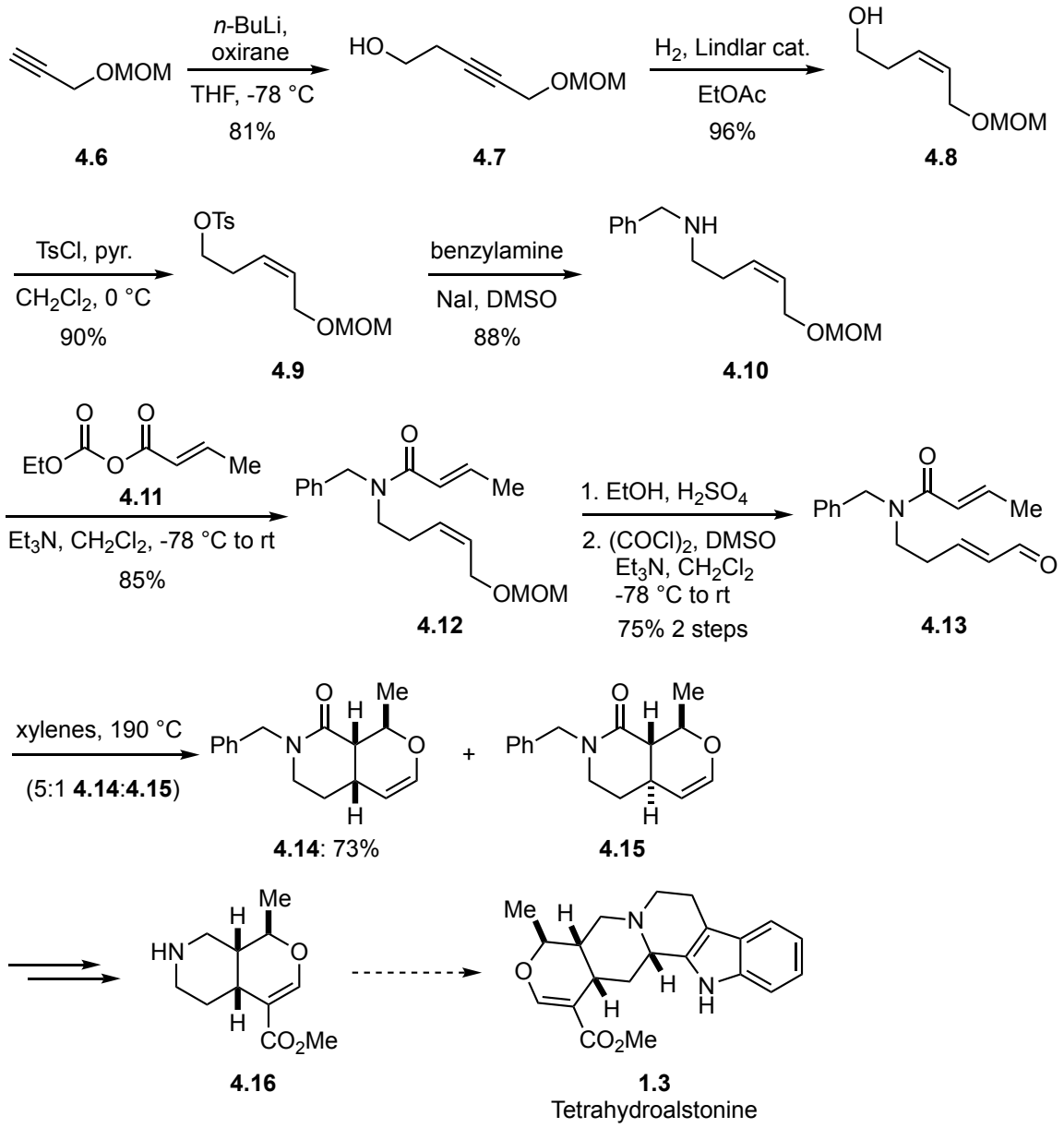

Scheme 4.2. Formal synthesis of tetrahydroalstonine using IMHDA.

The use of an IMHDA reaction with heterotiene **4.13** for the assemblage of an oxahydroisoquinolone ring system was unique at the time because the cycloaddition occurred between an electron deficient α,β-unsaturated aldehyde as the diene partner and an electron deficient dienophile.[20,389] The use of electron rich dienophile components that

are better electronically matched for cycloaddition with α,β-unsaturated aldehydes was more common, particularly for the construction of dihydropyrans.[395] Therefore, this work established an IMDHD as a useful tool for accessing these fused heterocyclic ring systems, particularly within the context of natural product synthesis.[1] The preference for the *cis*-fused ring system attained using heterotrienes related to **4.13** was the subject of computational studies from our group,[15] as well as Tanitillo and Houk.[396] The models generated from these studies were in agreement that the endo, boat-like transition state is favored, giving rise to the *cis*-fused ring system. The favorability of the boat-like transition state has been attributed to the amides ability to maintain planarity in this conformation, whereas the chair-like transition state requires considerable rotation out of planarity to achieve proper orbital overlap for the cycloaddition (Figure 4.1). Thus, the energetic penalty associated with steric interactions in the boat-like transition state is offset by the planar conformation of the amide that is lower in energy. The experimental product ratio was consistent with those predicted by these theoretical studies.

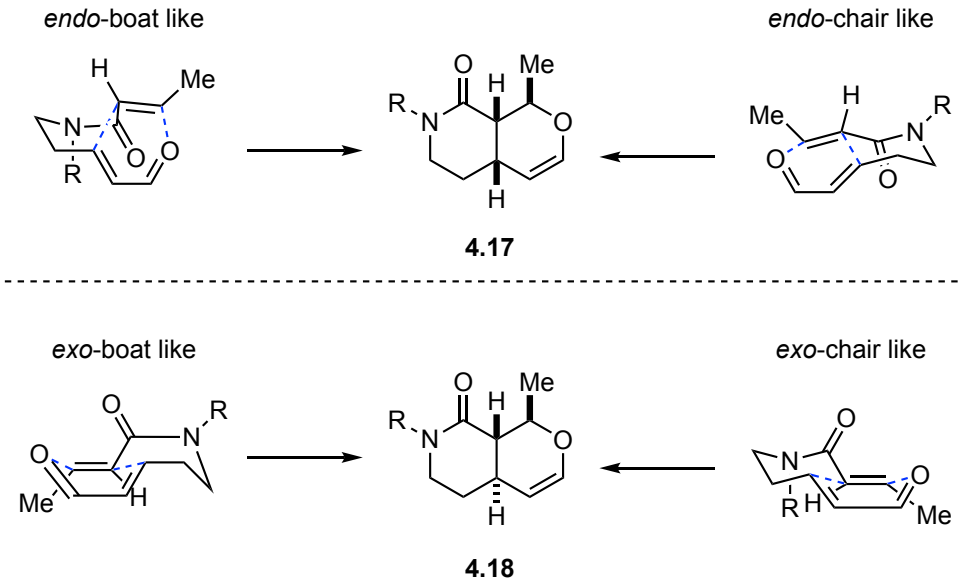

Figure 4.1. Endo and exo-transition states leading to IMDA cycloadducts.

The heterotriene **4.13** that was used in these seminal studies is notably quite similar in structure to **4.4**, which was targeted for construction of the oxahydroisoquinolone ring system of alstoscholarisine E. This provides encouraging precedent that the *cis*-fused cycloadduct would be expected from thermolysis of **4.4**. Unfortunately, the synthesis of the IMHDA precursor **4.13** in earlier work from our group required eight steps to prepare.[20,389] Because we required a more expedient approach for this synthetic endeavor, our attention turned to related work from the Martin group for further inspiration. The Martin group previously recognized the value of the IMHDA reaction for the construction of the oxahydroisoquinolone subunit, but were aware that more efficient access to the heterotriene precursor would expand the utility of this methodology for natural product synthesis. Specifically, in their quest to access the heteroyohimbine alkaloid core **1.18**, the IMHDA precursor **1.13** was envisioned to provide a more direct approach (Figure 4.2).[2,15] However, a clear tactic for the concise construction of **1.13** was not immediately clear and required some innovation.

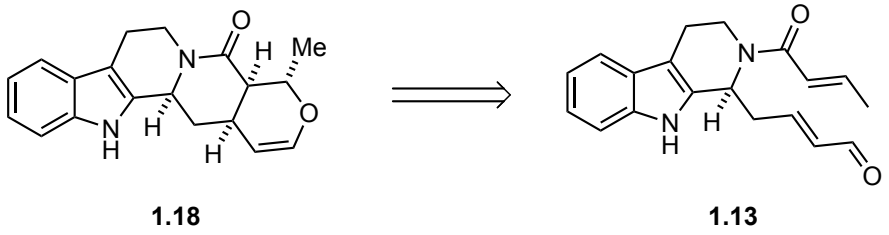

1.18 **1.13**

Figure 4.2. Retrosynthetic analysis of heteroyohimbine core structure accessed from advanced IMHDA precursor **1.13**.

Eventually it was discovered that a vinylogous variant of the venerable Mannich reaction was uniquely suited to access the δ-acrylamide-α,β-unsaturated aldehyde motif present in **1.13**.[2,15] In this newly developed vinylogous Mannich reaction sequence, stirring a solution of 3,4-dihydro-β-carboline (**1.15**), which is accessible in two steps from commercially available tryptamine (**1.13**), in THF with crotonyl chloride (**1.16**) in the presence of 1-(trimethylsiloxy)-1,3-butadiene (**1.17**) provided **1.13** in 78% yield (Scheme 4.3).[15] The reaction is thought to proceed through formation of an *N*-acyl iminium ion that is activated for nucleophilic attack, but notably there was no observation of products that might arise from attack at the α-carbon of **1.17**.[21] Subsequent thermolysis of **1.13** in refluxing mesitylene provided the *cis*-fused cycloadduct **1.18** in 80% yield.[2,15] Critically, the vinylogous Mannich reaction developed through the course of this work provided access to the pentacyclic heteroyohimbine core in just four steps from commercially available materials and only a few additional steps were required to complete the total synthesis of tetrahydroalstonine (**1.3**), cathenamine (**1.4**), and geissoschizine (**1.5**).[2,15]

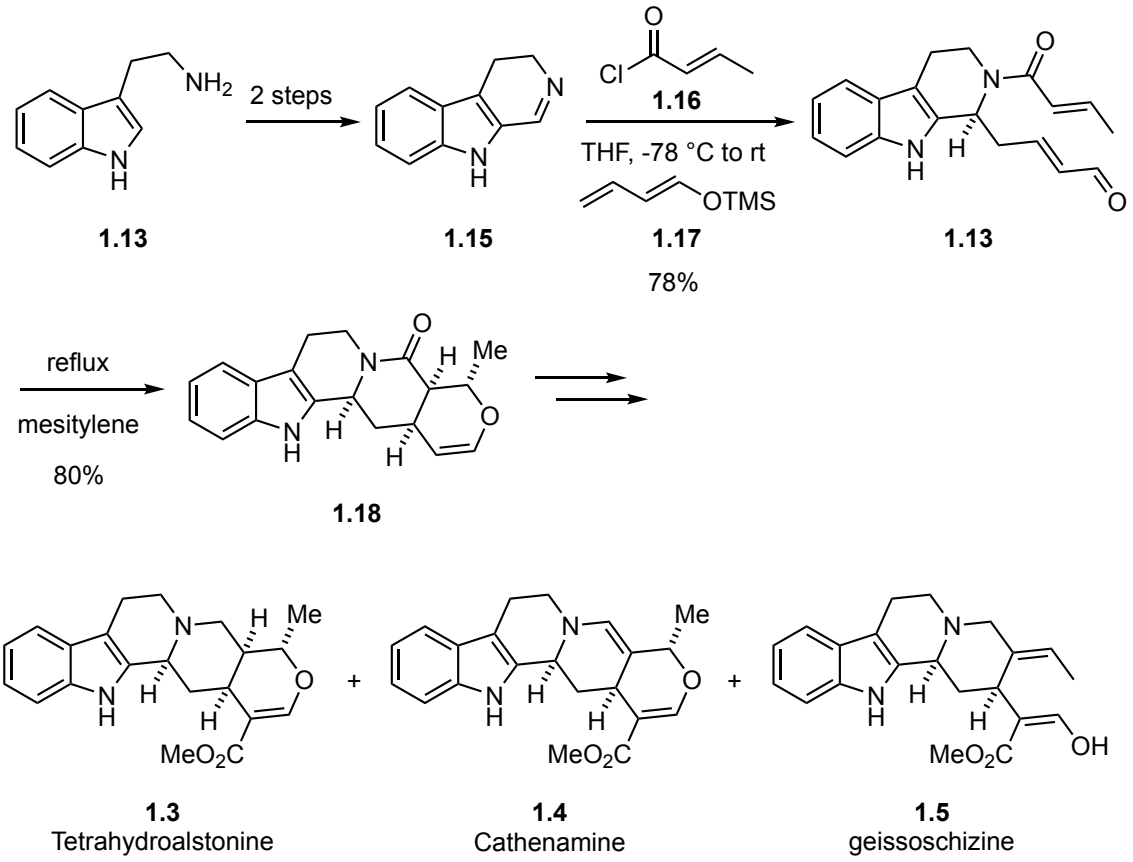

Scheme 4.3. Development of the vinylogous Mannich reaction to access IMHDA precursors.

4.3 The Vinylogous Mannich Reaction For Preparation of the Hetero Diels–Alder Precursor

4.3.1 Hexahydrotriazines as a Formaldehyde Equivalent in the Mannich Reaction

The reaction sequence developed above demonstrated the utility of combining a tandem vinylogous Mannich reaction and IMHDA reaction for the efficient construction of alkaloid natural products and inspired a wide range of additional investigations from our laboratory, including the development of the MCAP.[1,21] We queried whether we might utilize a related strategy to access the IMHDA substrate **4.4** that was targeted for the total synthesis of alstoscholarisine E (**3.5**). Hexahydrotriazines such as **4.19** have been

shown to fragment upon treatment with an acyl chloride **4.20** to generate *N*-substituted-*N*-(chloromethyl)amides **4.22**, that might provide a synthon for N-acyliminium ion **4.21** (Scheme 4.4).[397] Furthermore, intermediate **4.22** has been reacted with a range of nucleophilic partners to afford N-substituted amides.[397-401] This suggests that 1-(trimethylsiloxy)-1,3-butadiene (**1.17**) might be a suitable nucleophile to react with either the N-acyl iminium **4.21** or N-(chloromethyl)amide **4.22** that is generated upon acyl chloride mediated breakdown of hexahydrotriazine **4.19** in order to access the IMHDA precursor **4.4**.

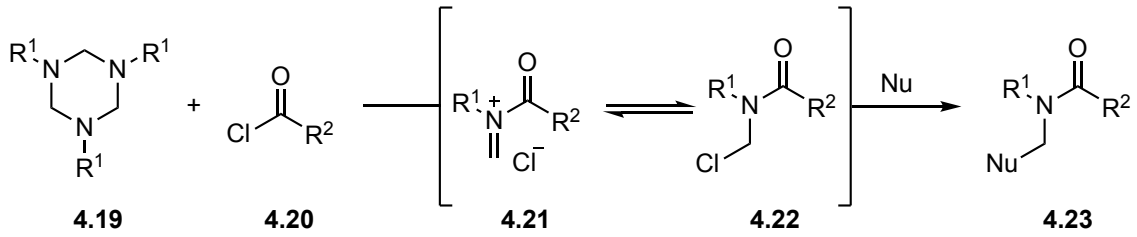

Scheme 4.4. Acyl chloride mediated breakdown of hexahydrotriazines.

We are not aware of any reports applying the *N*-acylation of hexahydrotriazines such as **4.5** in a vinylogous Mannich reaction with π–nucleophiles such as **1.17**. A related Mannich reaction using hexahydrotriazine **4.5** and a series of silyl enol ether analogs was disclosed by Ikeda *et al*. in 1981.[401] In a representative example, a solution of hexahydrotriazine **4.5** in dichloromethane at 0 °C was treated with acetyl chloride (**4.24**) (3 molar eq.), and after stirring at room temperature for one hour, silyl enol ether **4.26** (2.7 molar eq.) and titanium tetrachloride were added at 0 °C to afford the Mannich reaction product **4.27** in 40% yield (Scheme 4.5). Although this example provides a proof of concept for a related approach, the yields were quite low, ranging from 23-55% with less than 50% yield obtained for most substrates. Additionally, there were no examples

using a silyl enol ether vinylogue, which suggested that modifications might be required with our planned substrates.

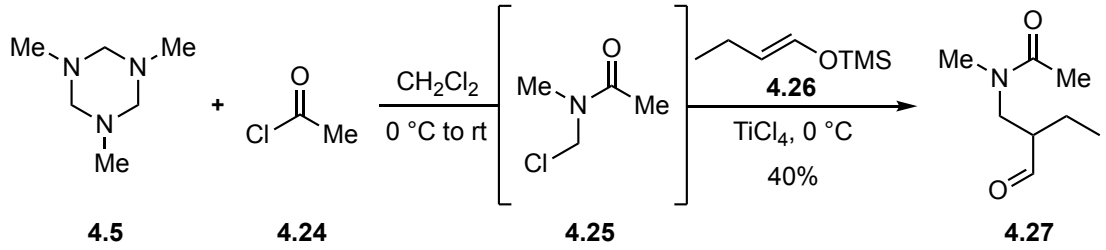

Scheme 4.5. Reported Mannich reaction of hexahydrotriazine **4.5** upon acyl chloride mediated breakdown.

4.3.2 Development of a Hexahydrotriazine Vinylogous Mannich Reaction

Our preliminary investigation was conducted by Dr. Klosowski and began with exploration of vinylogous Mannich conditions that were previously reported by our group.[382] Accordingly, crotonyl chloride (**1.16**) was added dropwise to a solution of hexahydrotriazine **4.5** and 1-(trimethylsiloxy)-1,3-butadiene (**1.17**) in THF at -78 °C (Equation 4.1). Gratifyingly, these conditions did lead to the formation of **4.4**, albeit in low yield (~33%), along with formation of a side product that was difficult to separate.

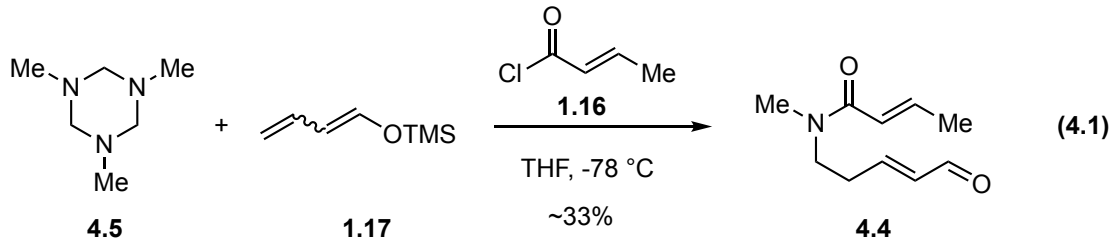

(4.1)

The optimization process began by first assessing the acyl chloride mediated breakdown of hexahydrotriazine **4.5**, which could be evaluated using nuclear magnetic

resonance (NMR) spectroscopy of aliquots taken directly from the reaction mixture. Interestingly, treating a solution of hexahydrotriazine **4.5** in THF at -78 °C did not lead to significant formation of *N*-methyl-*N*-(chloromethyl)amide **4.28**, rather a by-product whose structure is consistent with **4.29** based was observed as the major product based on crude LCMS and NMR analysis (Scheme 4.6). Among related examples of acyl chloride mediated breakdown of hexahydrotriazines, dichloromethane has commonly been used as the solvent and the reaction has been performed at 0 °C, although a report by Siver *et al.* acknowledged the formation of a *bis*-adduct related to **4.29** using these conditions.[397-401] Thus, a range of solvents and temperatures were screened to assess the transformation of **4.5** to **4.28** (Scheme 4.6). Performing the reaction in THF at elevated temperatures (0 °C to reflux) led to intractable mixtures. Switching the solvent to dichloromethane was beneficial and a positive correlation between increased temperatures and the formation of **4.28** was observed, but *bis*-adduct **4.29** remained prevalent. Switching the solvent to toluene resulted in an intractable mixture. However, when crotonyl chloride (**1.16**) was added to a solution of hexahydrotriazine **4.5** in acetonitrile at 0 °C and then heated to 70 °C for two hours, complete conversion to putative *N*-methyl-*N*-(chloromethyl)amide **4.28** was observed based on NMR analysis of an aliquot from the reaction mixture .[382] It should be noted that this result stands in contrast to the report from Siver *et al.*, which indicated that maintaining a low temperature was critical for suppressing formation of the *bis*-adduct.[400] Taken together, these results suggest that solvent and temperature are both important parameters for this transformation

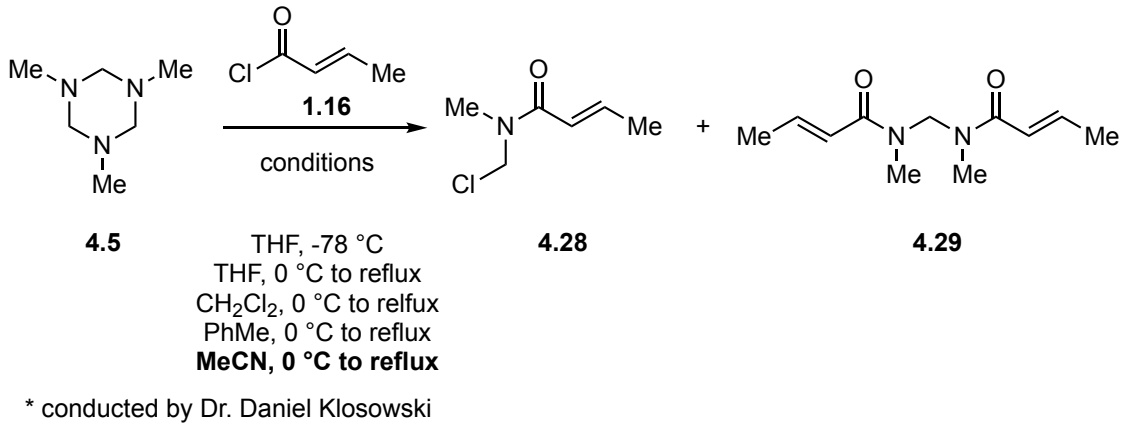

Scheme 4.6. Solvent and temperature screen for acyl chloride mediated breakdown of **4.5**.

Applying these conditions for the quantitative formation of *N*-methyl-*N*-(chloromethyl)amide **4.28** followed by sequential addition of 1-(trimethylsiloxy)-1,3-butadiene (**1.17**) and catalytic (10 mol%) trimethysilyl trifluoromethane sulfonate (TMSOTF) at 0 °C provided the IMHDA precursor **4.4** in 62% yield (Equation 4.2).[382] Interestingly, the regioisomer **4.30** that results from nucleophilic addition at the α-carbon of **1.17** was also isolated in 10% yield. We were encouraged that the alkylated products **4.4** and **4.30** were isolated in a combined 72% yield, enabling continued progress toward alstoscholarisine E. However, sustained efforts were made to further optimize this transformation.

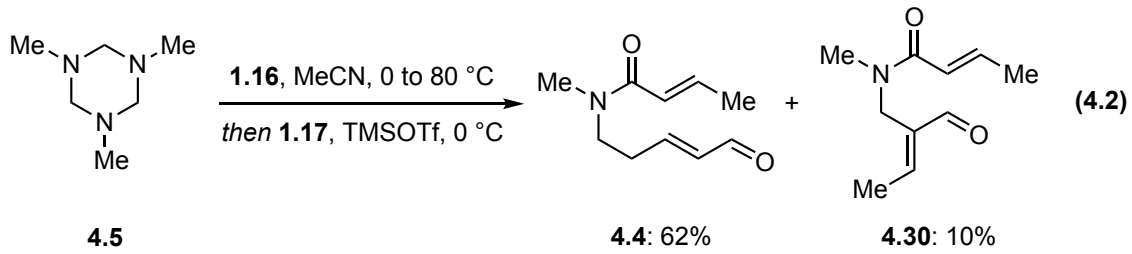

(4.2)

Solvent choice proved to be important for breakdown of hexahydrotriazine **4.5** to putative *N*-methyl-*N*-(chloromethyl)amide **4.28** during preliminary studies and was the subject of a more extensive evaluation in the full reaction sequence (Table 4.1). Exchanging acetonitrile for dichloromethane decreased the yield of **4.4** and **4.30** to 29% and 6%, respectively, which was consistent with the decreased formation of the *N*-methyl-*N*-(chloromethyl)amide **4.28** observed in our earlier studies (entry 1). A similar result was obtained using dichloroethane (entry 2). Switching the solvent to THF provided further diminished yields of **4.4** and **4.30** and none of the desire product was observed when DMF was used as the solvent (entries 4-5). These studies supported the use of acetonitrile as the optimal solvent for this transformation.

Table 4.1. Solvent screen in the vinylogous Mannich reaction.

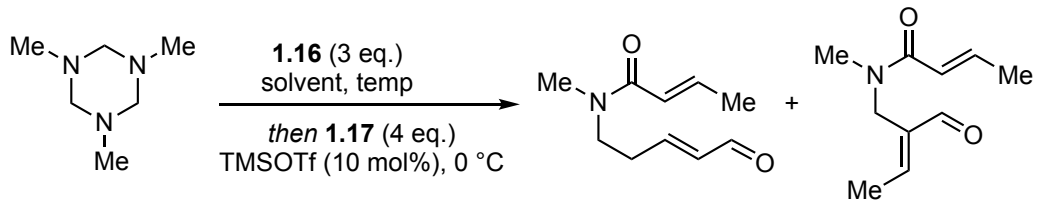

4.5 **4.4** **4.30**

entry	solvent	temp (°C)	% yield **4.4**	% yield **4.30**
1	MeCN	0 to 80	62[a]	10[a]
2	DCM	0 to reflux	29[b]	6[b]
3	DCE	0 to 80	30[b]	13[b]
4	THF	0 to reflux	13[b]	3[b]
5	DMF	0 to 80	0[b]	0[b]

[a] Isolated yield after chromatographic purification. [b] Yield determined by NMR with internal standard.

Results from our preliminary investigation of the vinylogous Mannich reaction with hexahydrotriazine **4.5** provided some indication that the addition of a Lewis acid provided enhanced yields, but it remained to be determined if it was an important component using these optimized reaction conditions (Table 4.2).[382] Indeed, performing the reaction in the absence of a Lewis acid resulted in significantly diminished yields, as compared to the reaction conducted in the presence of TMSOTf (entries 1-2). Exchanging TMSOTf for ethylaluminum dichloride did not result in a significant change (entry 3). However, the use of boron trifluoride diethyl etherate (BF_3•OEt_2) was not as favorable and **4.4** was only obtained in 29% yield (entry 4). These results confirmed that a Lewis acid was an important additive in the reaction, with the best results obtained using TMSOTf.

Table 4.2. Lewis acid screen in the vinylogous Mannich reaction.

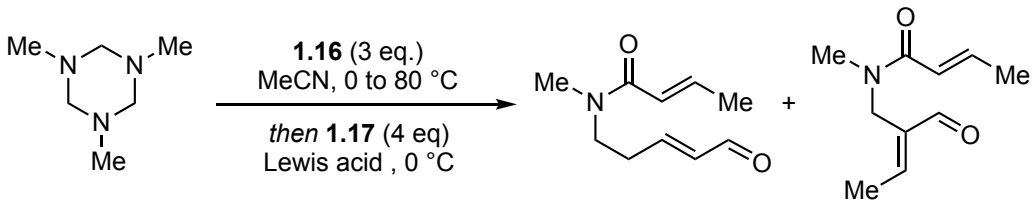

4.5 **4.4** **4.30**

entry	Lewis acid	% yield **4.4**	% yield **4.30**
1	*none*	7[b]	3[b]
2	TMSOTf	62[a]	10[a]
3	$EtAlCl_2$	57[b]	12[b]
4	BF_3•OEt_2	29[b]	5[b]

[a] *Isolated yield after chromatographic purification.* [b] *Yield determined by NMR with internal standard.*

Our initial experiments utilized hexahydrotriazine **4.5** as the limiting reagent assuming acyl chloride mediated breakdown generated three molar equivalents of *N*-methyl-*N*-(chloromethyl)amide **4.28**. Because it was not clear that three equivalents of **4.28** would actually be generated in this process, the reaction was also attempted using 1-(trimethylsiloxy)-1,3-butadiene (**1.17**) as the limiting reagent (Table 4.3). However, reducing the quantity of **1.17** (4 to 2 eq.) had minimal impact on the yield of **4.4** and **4.30** (entries 1-2). Likewise, increasing the amount of **1.17** (6 eq.) did not provide any benefit (entry 3). Based on these results, four equivalents of 1-(trimethylsiloxy)-1,3-butadiene (**1.17**) was used in ongoing investigations.

Table 4.3. Molar equivalents of 1-(trimethylsiloxy)-1,3,butadiene (**1.17**) in the vinylogous Mannich reaction.

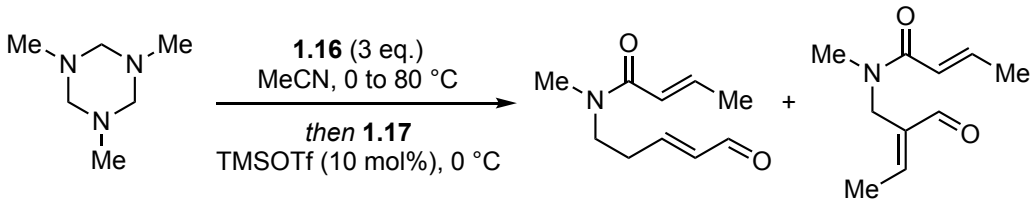

4.5 **4.4** **4.30**

entry	**1.17** (eq.)	% yield **4.4**	% yield **4.30**
1	2	56[b]	11[b]
2	4	62[a]	10[a]
3	6	58[b]	9[b]

[a] *Isolated yield after chromatographic purification.* [b] *Yield determined by NMR with internal standard.*

The optimized reaction sequence furnished the alkylated products **4.4** and **4.30** in 72% combined yield. Formation of the regioisomer **4.30** that resulted from nucleophilic addition at the α-carbon of 1-(trimethylsiloxy)-1,3-butadiene (**1.17**) was somewhat surprising because this had not been observed in previous studies of the vinylogous Mannich reaction from our group.[21] We hypothesized that increasing the size of the silyl group on the diene might suppress nucleophilic addition at the α-carbon and increase the yield of the desired product **4.4**. Therefore the optimized sequence was conducted using the known TBS-analog **4.31** (Equation 4.3).[402] Gratifyingly, **4.4** and **4.30** were obtained in 63% and 6% yield, respectively suggesting that by-product formation could be suppressed with this tactic. However, because 1-(trimethylsiloxy)-1,3-butadiene (**1.17**) was commercially available, we elected to utilize this readily available reagent in the synthesis going forward

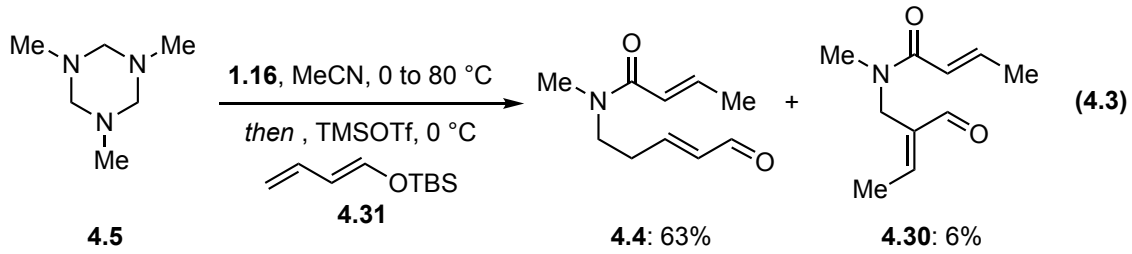

4.4 INTRAMOLECULAR HETERO DIELS–ALDER REACTION

Having developed an optimized one-step procedure to access the IMHDA precursor **4.4** **4.4** in 62% on a gram scale, attention turned toward the IMHDA reaction. Consistent with previous work from our group, heating a solution of **4.4** in degassed mesitylene under reflux afforded a separable mixture (5.4:1) of the *cis*– and *trans*–fused cycloadducts **4.31** and **4.32** in 77% combined yield (Equation 4.4).[15,389]

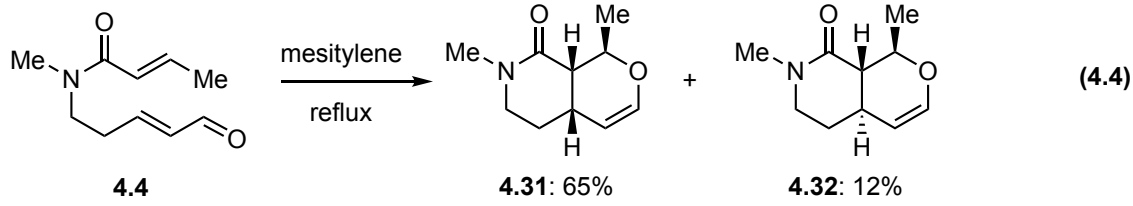

The thermally induced IMHDA reaction provided reliable access to the racemic *cis*–fused core **4.31**, but we queried whether the cyclization might be catalyzed by a chiral Lewis acid to provide **4.31** enantioselectively. As previously discussed, the IMHDA substrate **4.4** is somewhat challenging in that both the diene and dieneophile are electron deficient and contain a carbonyl moiety that might interact with catalyst. Indeed, preliminary attempts to induce Lewis–acid catalyzed cyclizations with substrates similar to **4.4** in our earlier work were unsuccessful.[15] Thus, we were cognizant that realization of this strategy might be challenging particularly since many of the known methods for promoting hetero Diels–alder reactions utilize substrates that are electronically

predisposed to cyclization.[403] These concerns notwithstanding, a brief evaluation of the chiral Lewis acids **4.33**-**4.35**, which are known to promote hetero Diels–Alder reactions, was conducted (Scheme 4.7).[404-406] However, treating **4.4** with each of these catalysts failed to produce detectable quantities of cycloadducts **4.31** and **4.32**, so we were relegated to using racemic **4.31** to complete the synthesis of (±)-alstoscholarisine E.

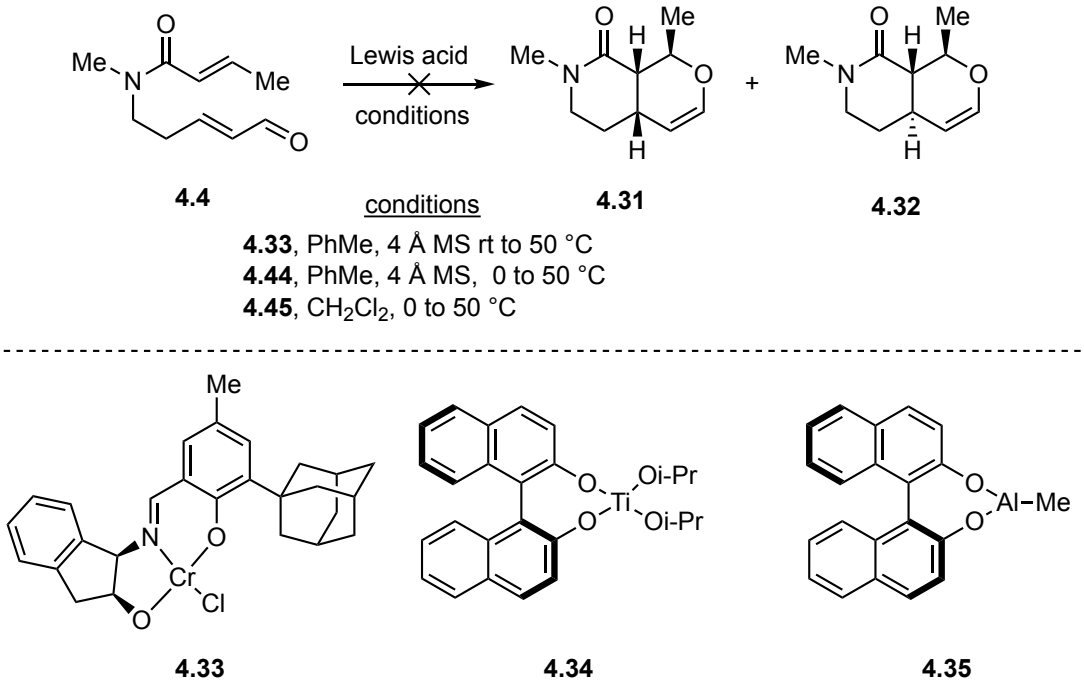

Scheme 4.7. Chiral Lewis acids evaluated in the IMHDA reaction.

4.5 Cross-Coupling of the Oxahydroisoquinolone and Substituted Indole

4.5.1 Halogenation of the Oxahydroisoquinolone

With gram-scale access to the oxahydroisoquinolone core in two steps from commercially available reagents, the next challenge was cross-coupling of the 3-methylindole moiety. This first required installation of a halogen atom at the β-position of the enol ether moiety of **4.31**, which would provide a functional handle in subsequent

cross-coupling reactions. A protocol for the one-step conversion of glycals to 2-iodoglycals was disclosed by Dharuman *et al.* in 2014 using NIS and catalytic silver nitrate (20 mol%) (Scheme 4.8).[377] Earlier work reported that treating a solution of **4.36** with NIS in the absence of other additives results in stereoselective addition to the vinyl ether moiety to afford **4.37** in 95% yield.[407] Alternatively, Dharuman *et al*. discovered that including catalytic silver nitrate (20 mol%) provided 2-iodoglycal **4.38** in 72% yield.

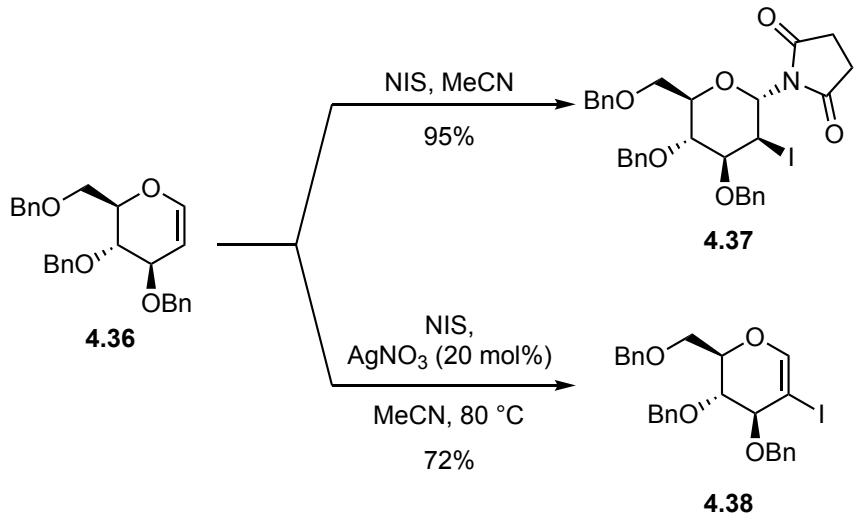

Scheme 4.8. Previously reported reaction of NIS with glycals.[377,407]

The authors proposed a mechanism that involves activation of NIS with silver nitrate via coordination to the carbonyl in **4.40** and subsequent nucleophilic attack by the vinyl ether **4.39** to generate the oxocarbenium intermediate **4.41** (Figure 4.3).[377] The intermediate **4.41** is subsequently captured by the nitrate anion, rather than the silver succinimide **4.42**. Subsequent intramolecular elimination in **4.43** generates vinyl iodide **4.44** and nitric acid (HNO_3), which protonates the silver succinimide intermediate **4.42** and regenerates silver nitrate in the catalytic cycle.

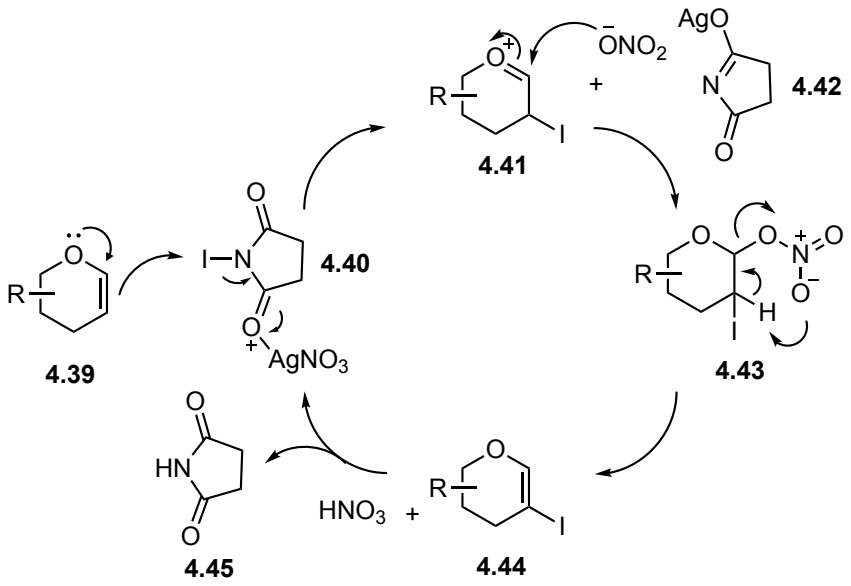

Figure 4.3. Proposed mechanism for conversion of glycals to 2-iodoglycals.[377]

Oxahydroisoquinolone **4.31** was thus treated with NIS and catalytic silver nitrate (20 mol%), according to the protocol reported by Dharuman *et al*., to deliver the vinyl iodide **4.46** in 79% yield (Equation 4.5). In an effort to further improve the yield, the silver nitrate catalyst loading was varied (10-35 mol%). Interestingly, increasing the catalyst loadings (> 20 mol%) resulted in diminished yields of **4.46**, although analysis of the crude reaction mixture by NMR, LCMS, or GCMS analysis did not identify the formation of any significant by-product that could be isolated for further analysis. Indeed, in each instance the crude reaction mixture was surprisingly clean, suggesting that reduced yields might result from diminished recovery. Decreasing the catalyst loading (10 mol%) provided modest improvement and **4.46** was isolated in 83% yield (> 0.5 gram scale).

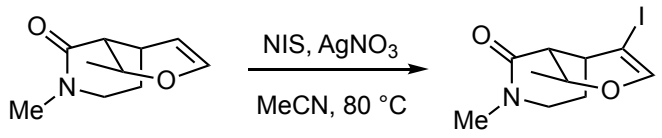

(4.5)

4.31 **4.46**

NIS (mol%)	% yield
35	55
30	67
20	79
10	83

4.5.2 Oxahydroisoquinolone Cross-Coupling with 3-Methylindole

With reliable access to the halogenated oxahydroisoquinolone **4.46**, the stage was set for the cross-coupling of **4.46** with an appropriately substituted 3-methylindole (**4.2**). We first targeted a Negishi coupling in initial work performed by Dr. Daniel Klosowski, because the transformation could be conducted in a single step.[382] After numerous attempts at the Negishi coupling of **4.46** with 3-methylindole **4.47** failed to furnish **4.48**, we pursued an alternative cross-coupling strategy (Equation 4.6).[382]

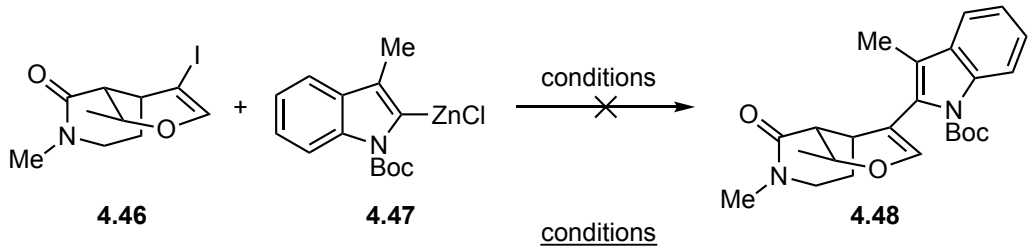

(4.6)

4.46 **4.47** **4.48**

conditions

$Pd(PPh_3)_3$, THF, rt to 125 °C
$Pd(dba)_2$, $P(o\text{-}fur)_3$, THF, tr to 125 °C
$Pd(dba)_2$, RuPhos, THF, 80 °C
$Pd(PPh_3)_3$, DMAc, 80 °C
$Pd(OAc)_2$, RuPhos, DMAc, 80 °C
$Pd(OAc)_2$, DMAc, 80 °C

* performed by Dr. Daniel Klosowski

Our attention next turned to Suzuki–Miyaura coupling of the halogenated oxahydroisoquinolone **4.31** with 3-methylindole boronic acid **4.2** (R = $B(OH)_2$).

Although 2-heterocyclic boronic acids such as **4.2** (R = $B(OH)_2$) are known to be problematic substrates in Suzuki–Miyaura coupling reactions due to competitive protodeboronation under the reaction conditions, innovations in catalyst design by Buchwald have overcome these challenges.[378] One such catalyst is the XPhos Pd G2 precatalyst **4.53**, which was reported to work well for substrates that are prone to protodeboronation based on their ability to undergo rapid reduction to the active phosphine ligated Pd(0) complex using mild conditions, along with their inherent high level of catalytic activity.[379,380,408] It is notable that Buchwald reported a Suzuki–Miyaura coupling of the related indole boronic acid **4.50** and 6-chloro-1-indanone (**4.49**) to afford **4.51** in 88% yield using the XPhos Pd G2 precatalyst with aqueous K_3PO_4 in THF at room temperature (Scheme 4.9).[379]

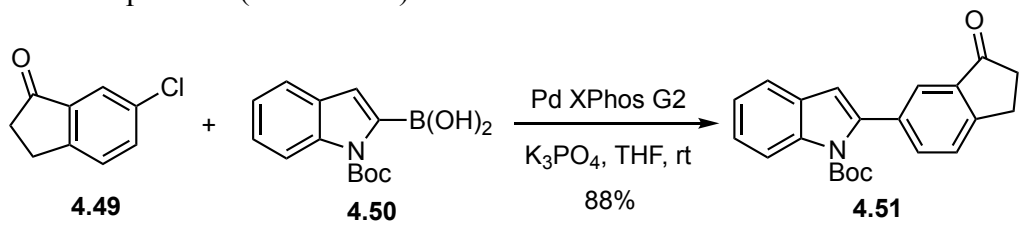

4.49 **4.50** **4.51**

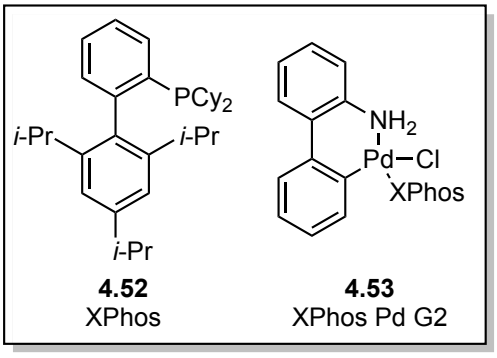

4.52 XPhos **4.53** XPhos Pd G2

Scheme 4.9. Reported Suzuki–Miyaura couple of an indole boronic acid.

We were pursuing this catalyst system for the Suzuki–Miyaura coupling of indole boronic acid **3.84** with oxahydroisoquinolone **4.31**, when Liao contemporaneously

disclosed a related coupling strategy using the SPhos Pd G2 precatalyst in the synthesis of (–)-alstoscholarisine A and E.[367,382] Cognizant of the similarities between the coupling partners, we elected to utilize the coupling conditions reported by Liao. The indole boronic acid **3.84** was prepared through slight modification of a reported protocol by treating a solution of 3-methylindole **4.54** in THF at -78 °C with *tert*-butyllithium, followed by rapid addition of trimethyl borate to the cooled solution and subsequent hydrolysis using aqueous ammonium chloride to afford the indole boronic acid **3.84**.[409,410] Analysis of the crude reaction mixture indicated near quantitative conversion, but because of the reported instability of **3.84**, it was not isolated and was instead used directly in the Suzuki–Miyaura coupling.[409] In the event, heating a solution of indole boronic acid **3.84** (*ca.* 3 eq.) and oxahydroisoquinolone **4.31** at 60 °C in the presence of the SPhos Pd G2 precatalyst (5 mol%) delivered the cross-coupled product, albeit in only 18% yield (Scheme 4.10). Suspecting that the instability of boronic acid **3.84** was the cause of the low yield, the experiment was repeated with an increased quantity of **3.84** (*ca* 4 eq.), which provided some improvement, but further increasing the equivalents of **3.84** (*ca* 5 eq.) did not further enhance the yield. Ultimately, we discovered that increasing the loading of the Pd SPhos G2 precatalyst (10 mol%) and indole **4.54** (4 eq.), relative to the conditions reported by Liao, reliably provided **4.55** in 79% yield on a gram scale.

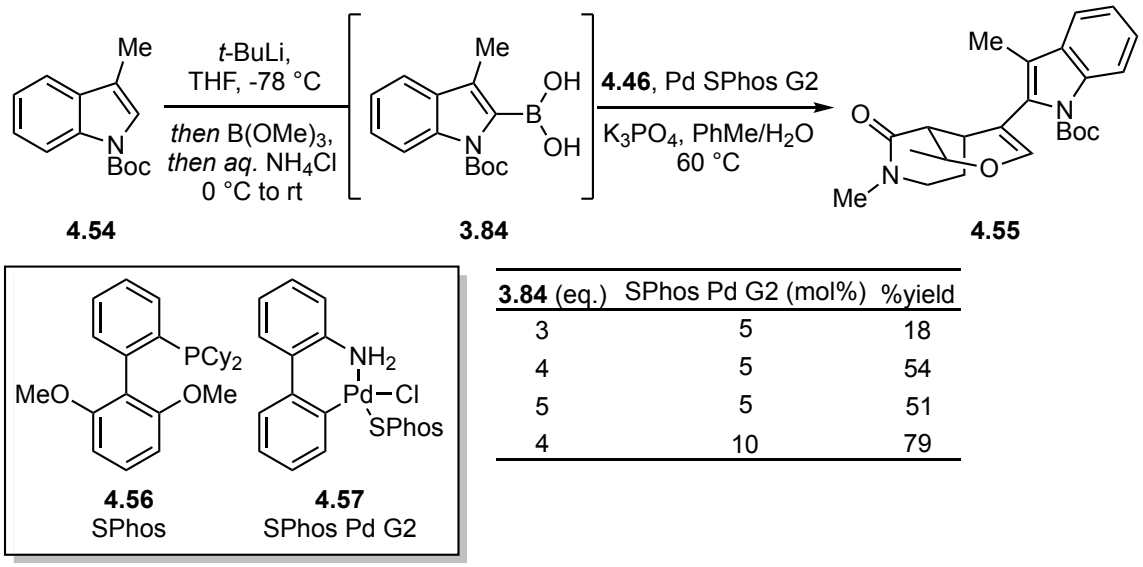

3.84 (eq.)	SPhos Pd G2 (mol%)	%yield
3	5	18
4	5	54
5	5	51
4	10	79

Scheme 4.10. Suzuki–Miyaura coupling of indole boronic acid **3.84** and oxahydroisoquinolone **4.31**.

4.6 COMPLETION OF THE TOTAL SYNTHESIS OF (±)-ALSTOSCHOLARISINE E

4.6.1 Stereoselective Reduction of the Cyclic Vinyl Ether

With **4.55** in hand, we next investigated strategies for the stereoselective reduction of the cyclic vinyl ether moiety. Liao reported a tandem Boc-deprotection and hydrogenation sequence using a related substrate that resulted in a mixture of diastereomers (2.2:1) and notably the Boc-deprotected intermediate was not isolated.[367] Initially, the same sequence was attempted using oxahydroisoquinolone **4.55**, but somewhat surprising, the crude residue obtained following treatment of **4.55** with methanesulfonic acid contained a complex mixture of products (Equation 4.7). The mixture was subjected to hydrogenation using Pearlman's catalyst (100 mol%) according to the reported protocol to furnish a complex mixture. Analysis of the crude residue with LCMS revealed that at least two compounds with a mass corresponding to the reduced

product **4.58** (ca. 3:2) were present, accompanied by a variety of by-products that were not readily identifiable.

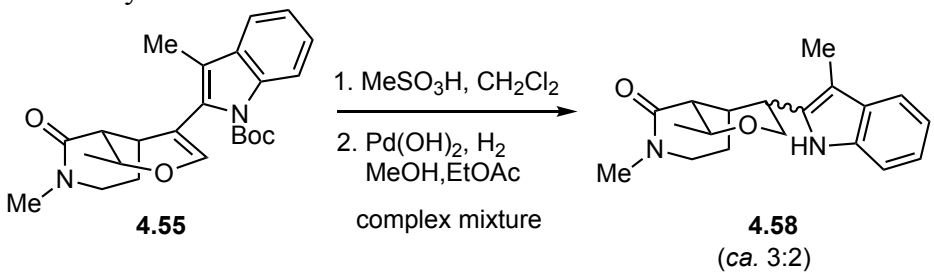

(**4.7**)

Given that an unexpected mixture of products was observed following the treatment of **4.55** with methanesulfonic acid, alternative conditions were attempted for removal of the Boc-protecting group prior to hydrogenation. Thus, trifluoroacetic acid (15 eq.) was added to a solution of oxahydroisoquinolone **4.55** in dichloromethane and stirred at room temperature for 90 minutes (Scheme 4.11). Monitoring the reaction by thin layer chromatography (TLC) suggested smooth conversion of the starting material **4.55**, but again the NMR spectra of the crude reaction revealed a complex mixture of unanticipated by-products. Nonetheless, the crude residue was subjected to hydrogenation with Pearlman's catalys. However, none of the reduced product **4.58** was observed and instead a mixture of products that had a mass consistent with **4.60**, was observed. Cognizant that the addition of methanol to the tetrahydropyran of **4.55** might be expected in the presence of acid, it was somewhat perplexing that the solvent used in the hydrogenation reaction might provide a similar result.

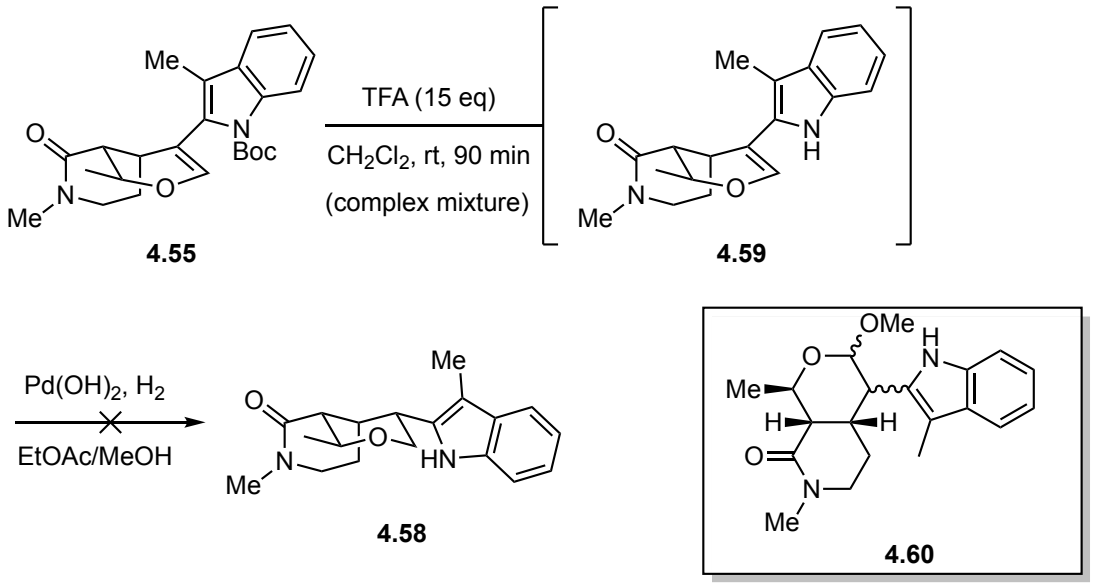

Scheme 4.11. Attempted Boc-deprotection and catalytic hydrogenation sequence.

Intrigued by this finding, we recognized that Lewis acid mediated reduction of the acetal moiety in **4.60** might also be possible and therefore attempted to form the acetal 4.60 directly. Thus, oxahydroisoquinolone **4.55** was treated with methanol under a variety of acidic conditions, that only provided returned starting material (Equation 4.8). Notably, addition of acetyl chloride to a solution of **4.55** in methanol also provided predominantly returned starting material, but was accompanied by a minor by-product (*ca*. 10%). At the time, the identity of the by-product was not clear, but its discovery would ultimately provide critical insight in ongoing investigations.

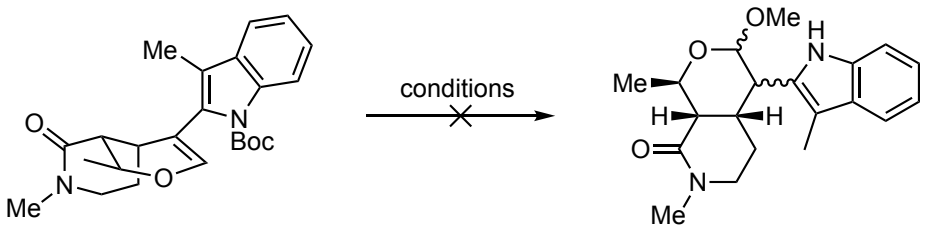

4.55 **4.60** (**4.8**)

conditions	result
p-TsOH (1 eq), MeOH, rt	RSM
TFA (15 eq), MeOH, rt	RSM
PPTS, DCM/MeOH (1:1) 0 °C to reflux	RSM
CH_3COCl, MeOH, rt	RSM/by-product (*ca.* 10%)

Having encountered difficulties during the tandem Boc-deprotection and hydrogenation sequence, we briefly attempted the direct hydrogenation of oxahydroisoquinolone **4.55** (Equation 4.8). Unfortunately, none of the hydrogenation conditions screened led to reduced product **4.58**. Only returned starting material was obtained using palladium on carbon. Use of Pearlman's catalyst and Adam's catalyst appeared to provide a mixture of returned starting material and some reduction of the indole double bond.

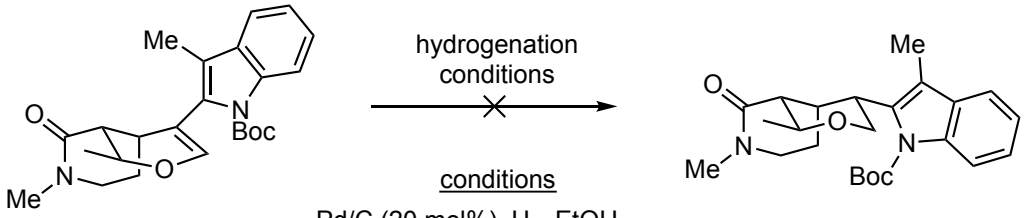

4.55

conditions

Pd/C (20 mol%), H_2, EtOH
$Pd(OH)_2$ (100 mol%), H_2, EtOH
PtO_2, (100 mol%), H_2, EtOH

4.58 (**4.8**)

In light of these challenges, our attention next turned toward ionic reduction as an alternative tactic, aware that chemoselective reduction of the cyclic vinyl ether moiety might be challenging if the Boc-protecting group on the indole nitrogen atom were to be

removed under the reaction conditions.[411] We first attempted conditions that were previously reported for the reduction of a structurally related cyclic vinyl ether that were not anticipated to remove the Boc-protecting group.[412] Accordingly, a solution of oxahydroisoquinolone **4.55** in acetic acid was treated with sodium cyanoborohydride, but only returned starting material was obtained (Equation 4.9).

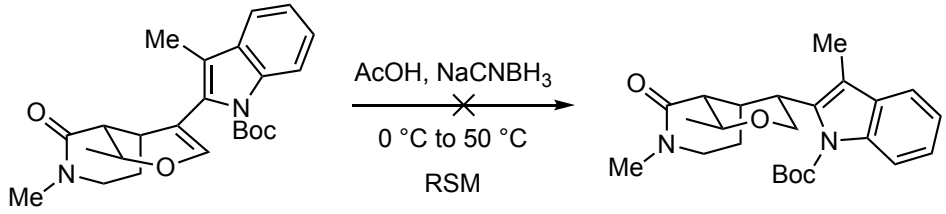

4.55 **4.58** (**4.9**)

We next examined other conditions known to reduce stabilized carbocations.[413] Surprisingly, stirring a solution of oxahydroisoquinolone **4.55** in dichloromethane with triethylsilane and trifluoroacetic acid (5 eq) did not provide the reduced product **4.58** or significant quantities of Boc-deprotected starting material (Scheme 4.12). Instead, the starting material was completely consumed and a mixture of two predominant by-products that were tentatively assigned as the bicyclic acetals **4.61** and **4.62** (*ca*. 1:1) were isolated in 60% combined yield.

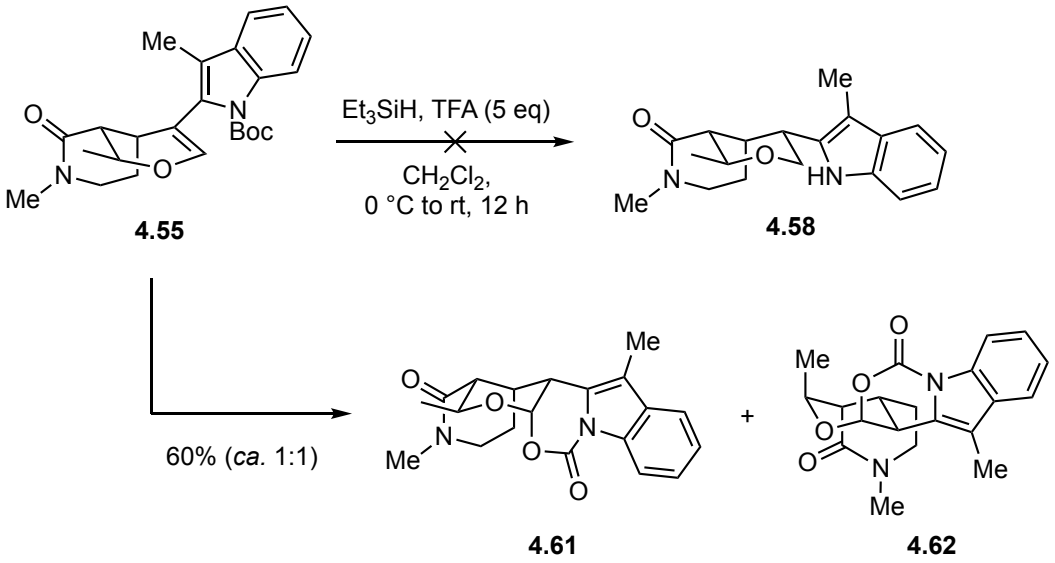

Scheme 4.12. Unanticipated formation of acyloxy acetals.

The exact stereochemistry of the isolated bicyclic acyloxy acetals **4.61** and **4.62** remained to be determined, but it suggested that under acidic conditions, the Boc-carbamate cyclized onto the vinyl ether moiety rather than undergo acid mediated cleavage as expected. The discovery of this unanticipated product enabled a critical review of the challenges that led up to this point. In hindsight, this provided an explanation for the complex mixture of products obtained from the tandem Boc-deprotection and catalytic hydrogenation sequences. Moreover, closer analysis of the mixture obtained from the previous Boc-deprotection reaction using trifluoracetic acid (15 eq, 90 min) indicated that these conditions favored the formation of one diastereomer (*ca.* 1:3) prior to catalytic hydrogenation. Replicating those conditions confirmed this finding with **4.61** and **4.62** (*ca.* 1:3) isolated in 95% combined yield (Scheme 4.13). In contrast, the by-product that was observed (*ca.* 10%) upon stirring oxahydroisoquinolone **4.55** in methanolic HCl appeared to be a single diastereomer. Repeating that reaction with an increased concentration of methanolic HCl provided a complex mixture of

products, but analysis of the crude reaction mixture confirmed that only a single acyloxy acetal diastereomer was present and it was later revealed to be **4.61**.

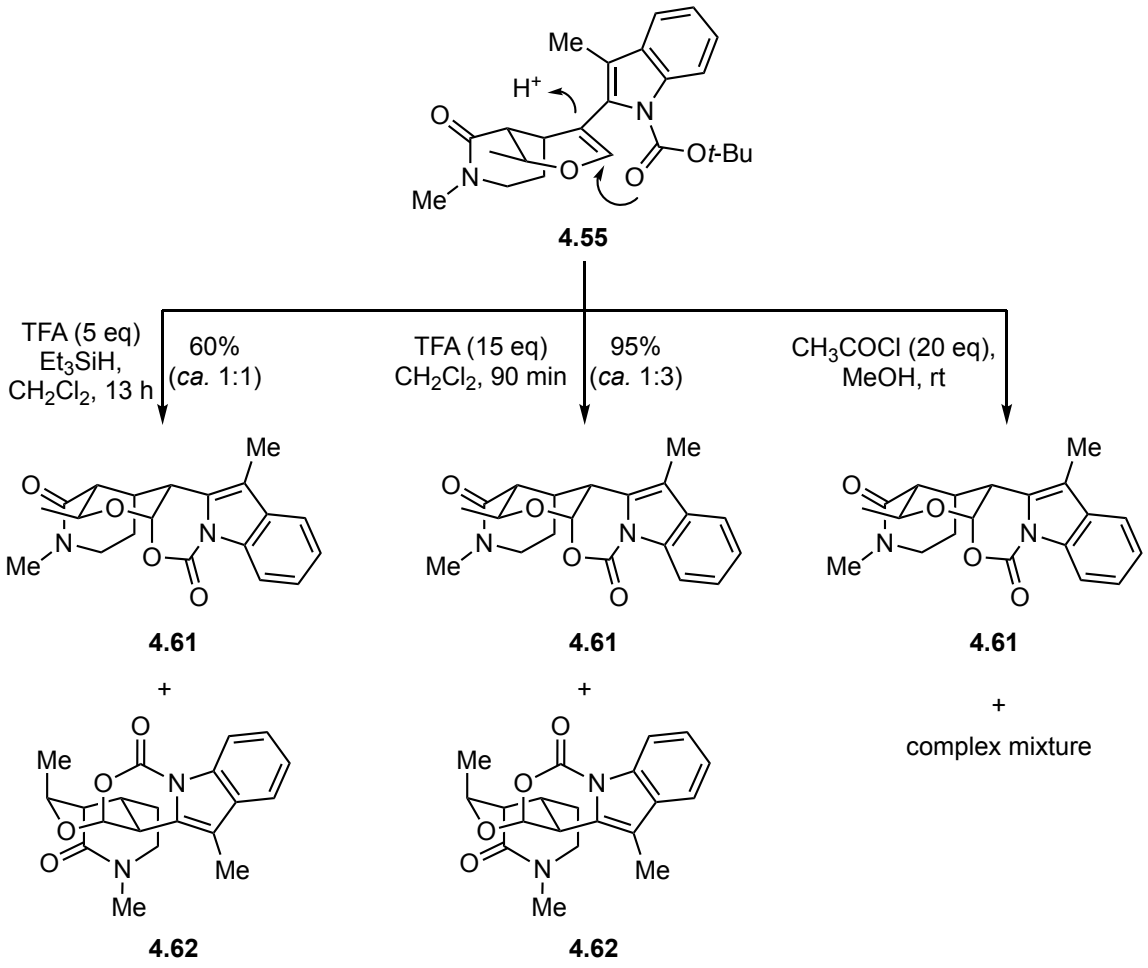

Scheme 4.13. Acid catalyzed formation of acyloxy acetal intermediates.

We recognized that the cyclic carbamate moiety of **4.61** and **4.62** could potentially be reductively cleaved with concomitant decarboxylation to deliver the reduced product **4.58**. Therefore, the fortuitous discovery that the predominant bicyclic acetal diastereomer formed in the cyclization could be modulated through variation of the acidic conditions indicated that this approach might ultimately enable a diastereoselective

reduction sequence. Thus, conditions for the diastereoselective formation of the bicyclic acetal using HCl were further explored (Scheme 4.14). Gratifyingly, we found that stirring a solution of oxahydroisoquinolone **4.55** in dioxane with HCl (2 M) furnished **4.61** as a single diastereomer in 59% yield. Reducing the concentration of HCl (0.4 M) and increasing the reaction time suppressed undesired Boc-deprotection of **4.55**, affording **4.61** in 77% yield and the structure of which was unambiguously confirmed by X-ray crystallography. Notably, **4.61** possesses the same stereochemistry at the indole–oxahydroisoquinolone carbon center as is present in alstoscholarisine E. Stirring oxahydroisoquinolone with trifluoroacetic acid in dioxane provided only unreacted starting material, confirming that that nature of the acid and solvent is important for this transformation.

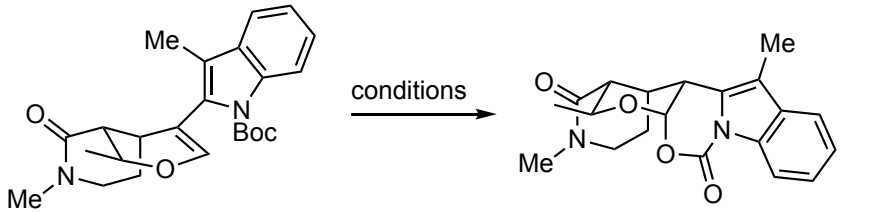

4.55 **4.61**

conditions	% yield
HCl (2 M), dioxane, 3 h	59
HCl (1 M), dioxane, 7 h	71
HCl (0.4 M), dioxane, 30 h	77
TFA/dioxane (1:3), 31 h	RSM

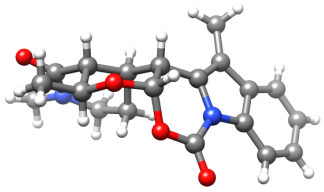

?? (X-ray)

Scheme 4.14. Stereoselective acyloxy acetal formation.

We speculated that **4.61** might be thermodynamically favored over **4.62** and that thermodynamic equilibration under the reaction conditions results in the exclusive formation of **4.61**. To probe this hypothesis, a solution of oxahydroisoquinolone **4.61** in

dichloromethane was stirred with trifluoroacetic acid (5 eq.) for 13 h, at which time the starting material was consumed (Scheme 4.15). Analysis of the crude residue confirmed the formation of mixture of **4.62** and **4.61** (*ca.* 1.2:1). The crude residue thus obtained was subsequently stirred with HCl (0.5 M) in dioxane for 25 h. Examination of the crude product mixture revealed that **4.61** was the major product and that diastereomer **4.62** was no longer observed. This preliminary experiment supports the hypothesis that thermodynamic equilibration favors the formation of **4.61**.

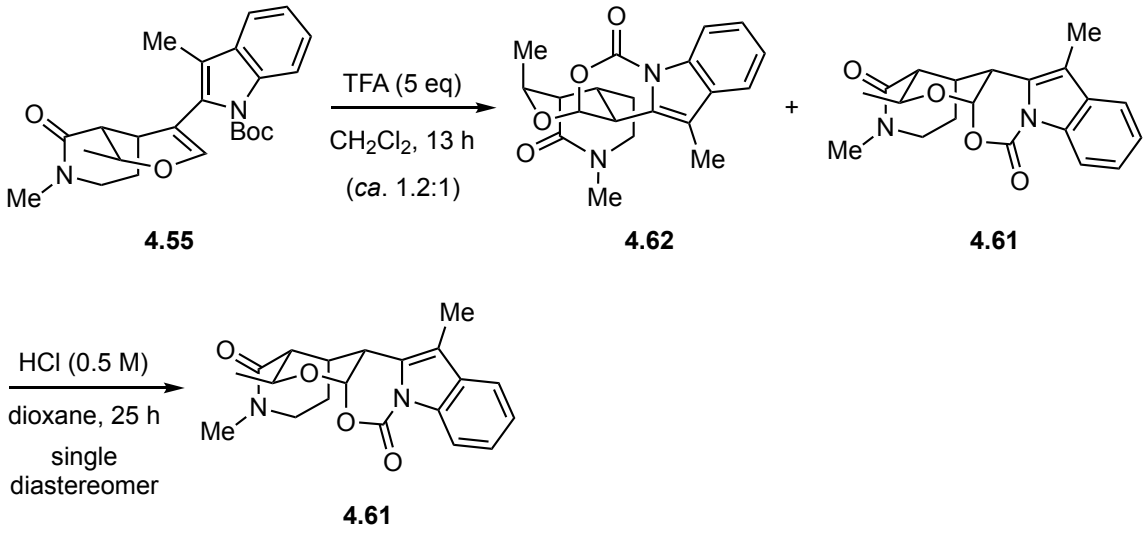

Scheme 4.15. Putative thermodynamic equilibration of acyloxy acetals **4.61** and **4.62**.

Attention next shifted to the reductive opening of bicyclic acetal moiety of **4.61** at the anomeric center, which proved to surprisingly unreactive to a range of conditions. A variety of Lewis acids have been used for the reductive opening of acetals in the presence of triethylsilane, but an example that was analogous to the bicyclic carbamate acetal in **4.61** was not readily identified.[414] However, previous work demonstrated that $TiCl_4$, TMSOTf, and $Sc(OTf)_3$ were effective for the ring opening of structurally related bicyclic lactone acetals at the anomeric carbon.[414-417] Unfortunately, tuse of hese Lewis acids in

the presence of triethylsilane only returned starting material (Equation 4.10). BF_3•OEt_2 also failed to provide any conversion of the starting material. Fortunately, we discovered that treating **4.61** with excess ethylaluminum dichloride (7 eq.) in the presence of triethylsilane led to smooth reductive opening at the anomeric center with subsequent decarboxylation to afford the desired product **4.63** in 97% yield. Attempted reductive opening using less of the Lewis acid (< 5 eq.) provided incomplete conversion of the starting material. The reduction was also found to be slow at lower temperatures, but proceeded rapidly at 0 °C. The diastereoselective reduction of **4.55** developed in this two-step sequence is notable given that catalytic hydrogenation resulted in a mixture of diastereomers.

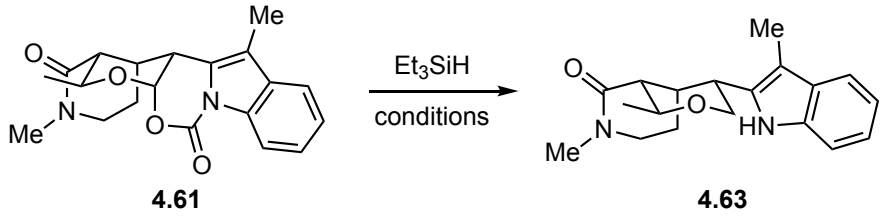

4.61 **4.63** (**4.10**)

conditions	% yield
$TiCl_4$ (20 eq), CH_2Cl_2, -78 to rt	RSM
TMSOTF (5 eq), MeCN, -40 °C to rt	RSM
$Sc(OTf)_3$, (1.5 eq), CH_2Cl_2, 0 °C to rt	RSM
BF_3•OEt_2, (10 eq), CH_2Cl_2, 0 °C	RSM
$EtAlCl_2$ (7 eq), CH_2Cl_2, -40 °C to 0 °C	97%

4.6.2 Formation of the Bridging Aminal Ring

All that remained to complete the synthesis of (±)-alstoscholarisine E (**3.5**) was partial reduction of the lactam moiety of **4.63** to the N,O-hemiaminal followed by cyclization to generate the bridging aminal ring in **3.5**. Such cyclizations are well precedented in the prior art and several methods are known for partial reduction of

amides; however avoiding overreduction to the amine can sometimes be challenging and substrate specific.[364-367,418] At the outset of this work, encouraging precedent for the feasibility of this transformation was found in the total synthesis of (±)-goniomitine (**4.66**) reported by Mizutani *et al*., in which an *N*-benzyl lactam **4.64** was partially reduced with DIBAL-H, resulting in spontaneous cyclization with the indole nitrogen atom to form the aminal ring of **4.65** in 87% yield (Scheme 4.16).[419] Although, the transannular cyclization of oxahydroisoquinolone **4.63** to form the bridging aminal ring in **3.5** was anticipated to be more challenging, this report suggested that using a 2,3-disubstitued indole and tertiary lactam for the intramolecular cyclization was a viable approach.

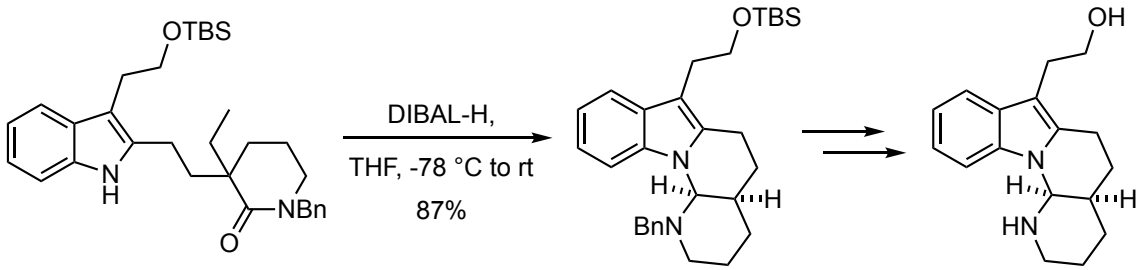

4.64 **4.65** **4.66** (±)-goniomitine

Scheme 4.16. Precedent for formation of a cyclic aminal with and indole nitrogen atom.

We initiated our investigation by screening conditions that were reported for related transformations. Thus, a solution of oxahydroisoquinolone **4.63** in THF was treated with DIBAL-H at -78 °C according to the protocol reported by Mizutani *et al*., but analysis of the crude reaction indicated that over reduction of the lactam to the amine was the major product (Equation 4.11).[419] Switching the solvent to dichloromethane, according to the protocol reported by Weinreb provided similar results.[365,366] The procedure described in Liao's recent synthesis of the alstoscholarisines utilized a similar

substrate that relied on activation of the amide using trifluoromethanesulfonic anhydride in the presence of tributyltinhydride, but using these conditions with oxahydroisoquinolone **4.63** resulted in only trace formation of the desired product **3.5**.[367]

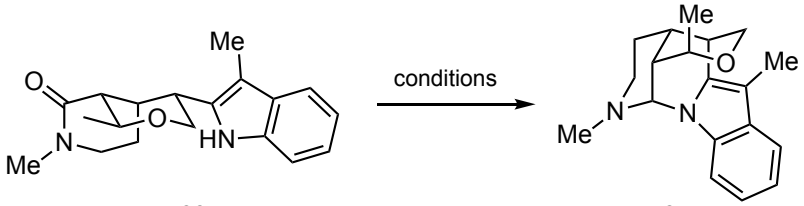

4.63 **3.5** (**4.11**)

conditions	% yield
DIBAL-H, THF, -78	0
DIBAL-H, CH_2Cl_2, -78 °C	trace
Bu_3SnH, Tf_2O, MeCN, -40°C to rt	trace

With methodology from the prior art having failed to deliver quantifiable quantities of the natural product, our focus turned toward other known methods for partial reduction of amides. The hydrozirconation of amides using Schwartz's reagent (Cp_2ZrHCl) is a well-established method for partial reduction of amides under mild conditions, but this too only delivered trace quantities of the cyclized product **3.5** based on LCMS analysis of the crude reaction mixture (Equation 4.12).[420]

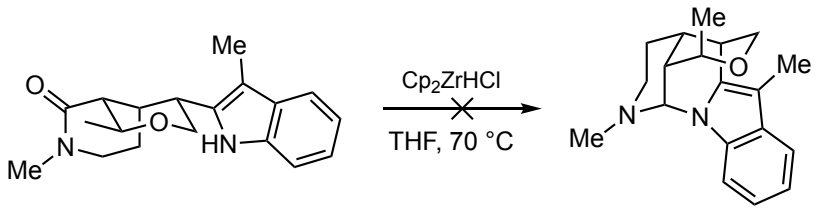

4.63 **3.5** (**4.12**)

Alternatively, hydrosilylation has emerged as a particularly useful strategy for partial reduction of amides.[418,421] An early example using hydrosilanes for reduction of

amides to aldehydes was reported by the Buchwald group in 1996 using titanium(IV) isopropoxide and diphenylsilane (Ph_2SiH_2).[422] The active reducing agent was postulated to be a titanium hydride-like complex that reduced amide **4.67** to hemiaminal **4.68**, which underwent spontaneous elimination to the enamine **4.69** and upon aqueous work-up, the aldehyde **4.70** was obtained in good yields (Equation 4.13). As a result, the reaction was limited to secondary and tertiary amides that possessed an α-hydrogen atom. More recently, a related procedure was reported by Lemaire and coworkers using titanium(IV) isopropoxide and 1,1,3,3-tetramethyldisiloxane (TMDS) as an alternative organosilane reagent.[423] Notably, this protocol was not restricted to enolizable amides and worked well for aromatic and aliphatic tertiary amides.

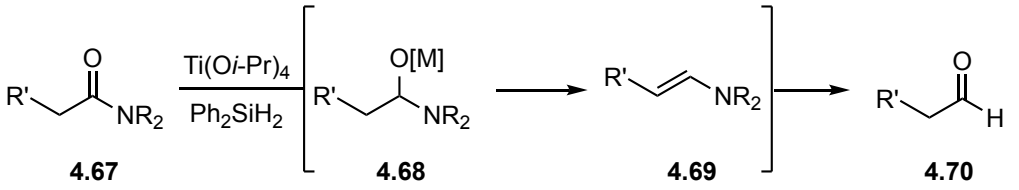

4.67 **4.68** **4.69** **4.70** (**4.13**)

A related iridium–catalyzed process was reported by Nagashima in 2009 for the partial reduction and dehydrogenation of amides to enamines (Figure 4.4.A).[424] The procedure was highly efficient, and using catalytic (0.05 mol%) Vaska's complex ($IrCl(CO)(PPh_3)_2$) with TMDS, a range of aliphatic tertiary amides were converted to the corresponding enamines in high yield. This methodology has been adapted for the reductive functionalization of amides with a variety of carbon nucleophiles by the Dixon group, as well as others.[425-435] For example, Dixon and coworkers discovered that stirring a solution of the tertiary amide **4.74** with Vaska's complex in dichloromethane resulted in full conversion to the partially reduced intermediate **4.75** followed by addition of benzylmagnesium chloride to deliver **4.76** in 86% yield (Figure 4.4.B).[434] In addition, the

Dixon group found that stirring a toluene solution of lactam **4.77** with Vaska's complex for five minutes, followed by addition of trimethylsilyl cyanide afforded the reductive Strecker product **4.78** in 86% yield (Figure 4.4.C).[433] The reactions were shown to work well with aliphatic amides and aromatic amides indicating that nucleophilic capture can outcompete enamine formation. Alternatively, Chida and coworkers reported that partial reduction of lactam **4.79** with Vaska's complex and TMDS delivered the enamine intermediate **4.80** that was then subjected to a vinylogous Mannich reaction with **4.81** in the presence of acid to afford **4.82** in 73% yield (Figure 4.4.D).[427]

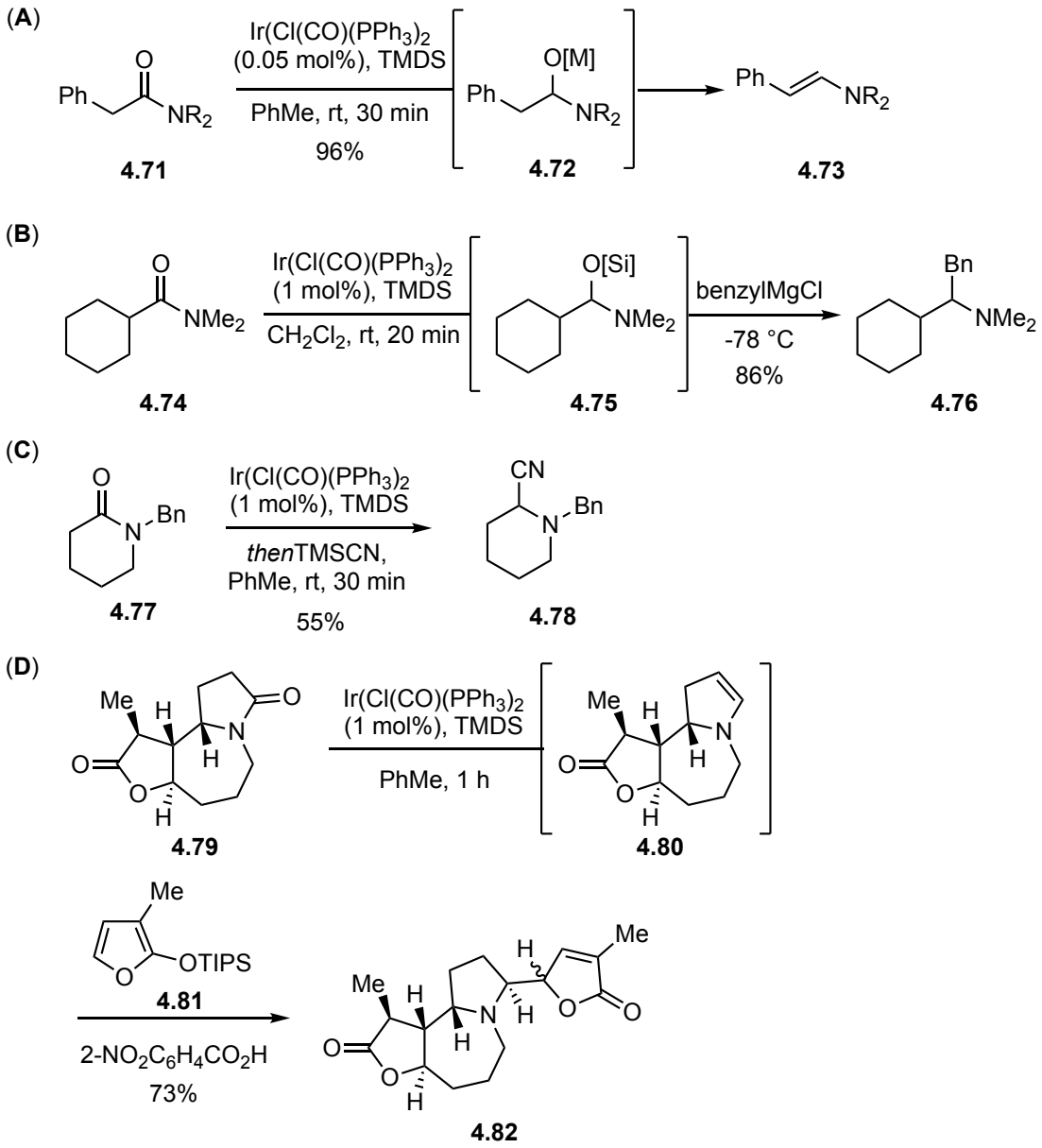

Figure 4.4. Reported examples for the hydrosilylation of amides and their nucleophilic capture.

Encouraged by these promising reports, we focused our attention on the hydrosilylation of oxahydroisoquinolone **4.63** (Scheme 4.17). In the event, treating **4.63** with titanium(IV) isopropoxide and diphenylsilane according to the protocol reported by Buchwald provided a complex mixture containing only trace quantities of the natural

product.[422] A preliminary reaction of **4.63** with titanium(IV) isopropoxide and TMDS according to the procedure reported by Lemaire was observed to provide some product formation, but was slow to react at room temperature.[423] Fortunately, we discovered that heating the reaction to 50 °C led to increased conversion and **3.5** was isolated in 56% yield.

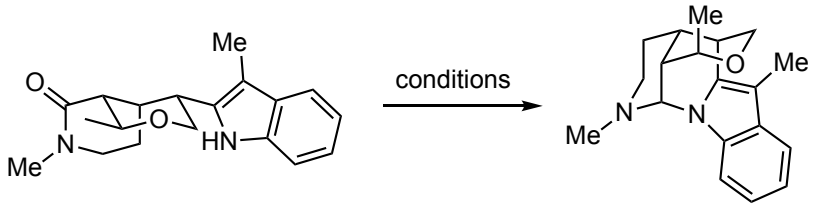

4.63

3.5
(±)-alstoscholarisine E

conditions	% yield
Ph_2SiH_2, Ti(O*i*-Pr)$_4$, THF, 50 °C	trace
TMDS, Ti(O*i*-Pr)$_4$, PhMe, 50 °C	56
TMDS, IrCl(CO)(PPh_3)$_2$, PhMe, rt	56
TMDS, IrCl(CO)(PPh_3)$_2$, CH_2Cl_2, rt	77

Scheme 4.17. Hydrosilylation of oxahydroisoquinolone **4.63** and aminal formation.

Transitioning to catalytic conditions, treating a solution of **4.63** in toluene with catalytic Vaska's complex and TMDS according to the protocol reported by Nagashima, the natural product was isolated in 56% yield.[424] Gratifyingly, merely switching the reaction solvent to dichloromethane delivered (±)-alstoscholarisine E (**3.5**) in 77% yield. The partial reduction of amides using Vaska's complex and TMDS is well-established, but this is the first report we are aware of, in which the intermediate is captured by a nitrogen nucleophile to furnish an aminal. Therefore, this discovery provides a useful extension of existing methodology for the reductive functionalization of amides.

4.7 SUMMARY

In summary, the total synthesis of (±)-alstoscholarisine E was achieved in a mere seven steps (LLS) from commercially available reagents and 15.2% overall yield (Scheme 4.18). The synthesis features a novel variant of the vinylogous Mannich reaction and a tandem IMHDA reaction to rapidly access the *cis*-oxahydroisoquinolone core in just two steps from commercially available reagents. The diastereoselective reduction of the cyclic vinyl ether in **4.55** was accomplished via the fortuitous discovery of a stereoselective acid–catalyzed cyclization and the subsequent Lewis acid–promoted hydride reduction. Mild conditions were developed for aminal formation in an iridium–catalyzed amide reduction and cyclization sequence to complete the synthesis. Notably, the route developed is considerably shorter and more efficient than previously reported syntheses of the alstoscholarisine alkaloids.

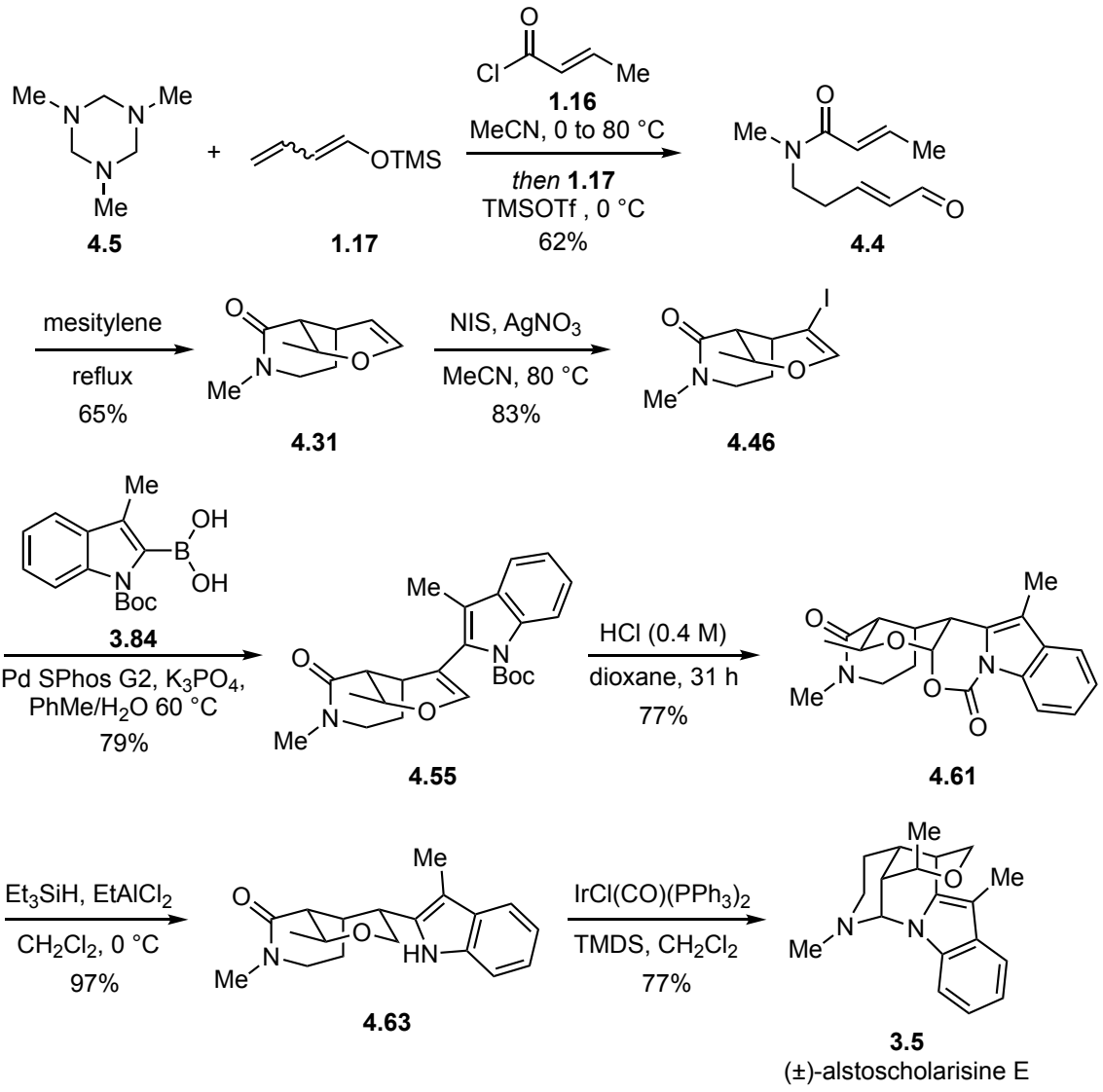

Scheme 4.18. The total synthesis of (+)-alstoscholarisine E.

PROGRESS TOWARD THE ENANTIOSPECIFIC TOTAL SYNTHESIS OF PIERISKETOLIDE A

Chapter 5: Approach to Pierisketolide A

5.1 Isolation and Bioactivity

Pieris Formosa (Wall) D.Don is a shrub belonging to the *Ericaceae* family that is found in south and southwest China, and it has a history of use in traditional Chinese medicine for the treatment of tinea and scabies.[436,437] The genus *Pieris* is smaller than some other members of the family, but is a rich source of diterpenoid natural products.[438] Recently, as part of their effort to discover biologically interesting natural products from traditional Chinese medicines, Niu *et al*. reported the isolation of three pierisketane terpenoids (**5.1–5.3**) from *P. Formosa* that are thought to be derived from *ent*-kaurene (**5.4**) (Figure 5.1).[437] While **5.1–5.3** possess a bicyclo[3.2.1]octane ring that is common among *ent*-kaurenoids, they contain an unusual rearranged A-homo-B-nor-framework.[439] Pierisketones B (**5.2**) and C (**5.3**) are comprised of a tetracyclic skeleton, whereas pierisketolide A (**5.1**) contains a bridged spirotetronate moiety that adds structural complexity. Similar to other natural products isolated from P. *Formosa*, pierisketolide A (**5.1**) exhibits analgesic activity, with a 45% writhe inhibition rate at 10.0 mg/kg an no observable cytotoxicity at 10 μM concentration.[437,440] In contrast, **5.2** and **5.3** did not provide any analgesic effect, suggesting that the unique structural features of pierisketolide A are linked to its bioactivity. Thus, the development of a synthetic strategy to access pierisketolide A might be useful to further evaluate its biological activity, but the synthesis of **5.1** has not yet been achieved.

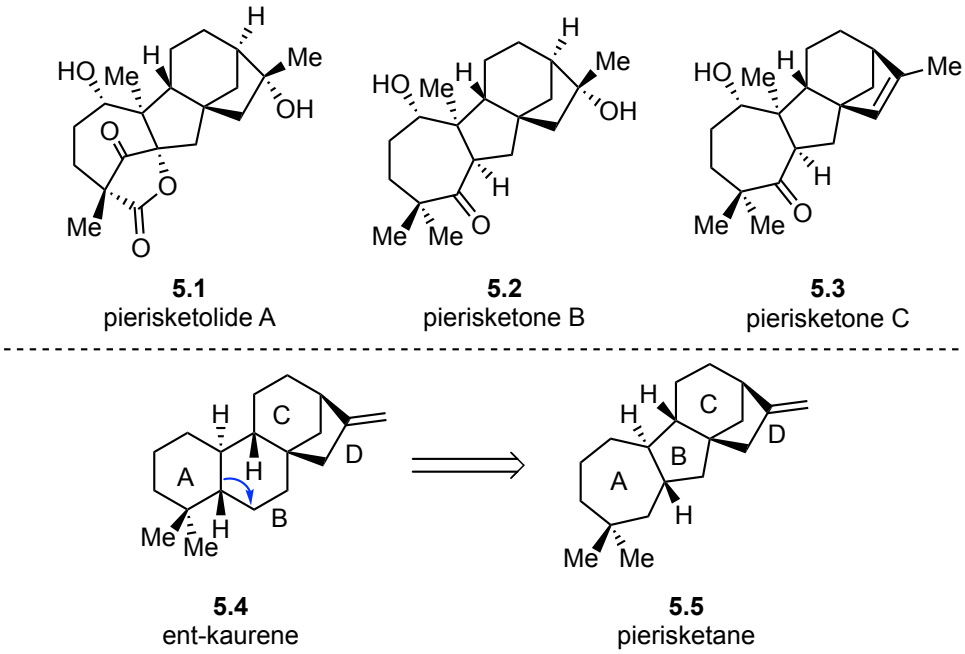

Figure 5.1. The pierisketanes **5.1**-**5.3** derived from *ent*-kaurene.

5.2 SYNTHETIC STRATEGY

Inspired by the structural complexity of pierisketolide A (**5.1**) and its intriguing biological activity, we sought to develop an enantiospecific approach toward **5.1** that would forge the critical bicyclo[3.2.1]octane ring early in the synthesis (Scheme 5.1). Accordingly, we envisioned that the late stage intermediate **5.6** could be transformed into **5.1** via lactonization of a β–ketoester moiety that would arise from the *C*–acylation and methylation of ketone **5.6**. The seven-membered ring of **5.6** could be formed via a SmI_2 mediated pinacol coupling of a tethered carbonyl moiety in ketone **5.7**, which might be installed through a stereoselective Mukaiyama aldol of aldehyde **5.8** with the tricyclic core **5.9** (R = Me or H) following a 1,4-reduction of the enone moiety.[441-444] Key to this approach was expedient access to the tricyclic core **5.9** through a unique Pauson-Khand reaction (PKR) to establish the bridged ring system, for which there is only scant

precedent that related bridged tricycles can be formed using a similar approach.[445-448] Critically, the substituted methylenecyclopentane **5.10**, which possessed the chiral tertiary hydroxyl group, was targeted as the PKR precursor to obviate the need for late–stage redox manipulations. The cyclopentane precursor **5.10** could be readily accessed from methylenation of the known cyclopentenone **5.11** following 1,4-addition addition of alkyne **5.12** (R = Me of TMS).[449]

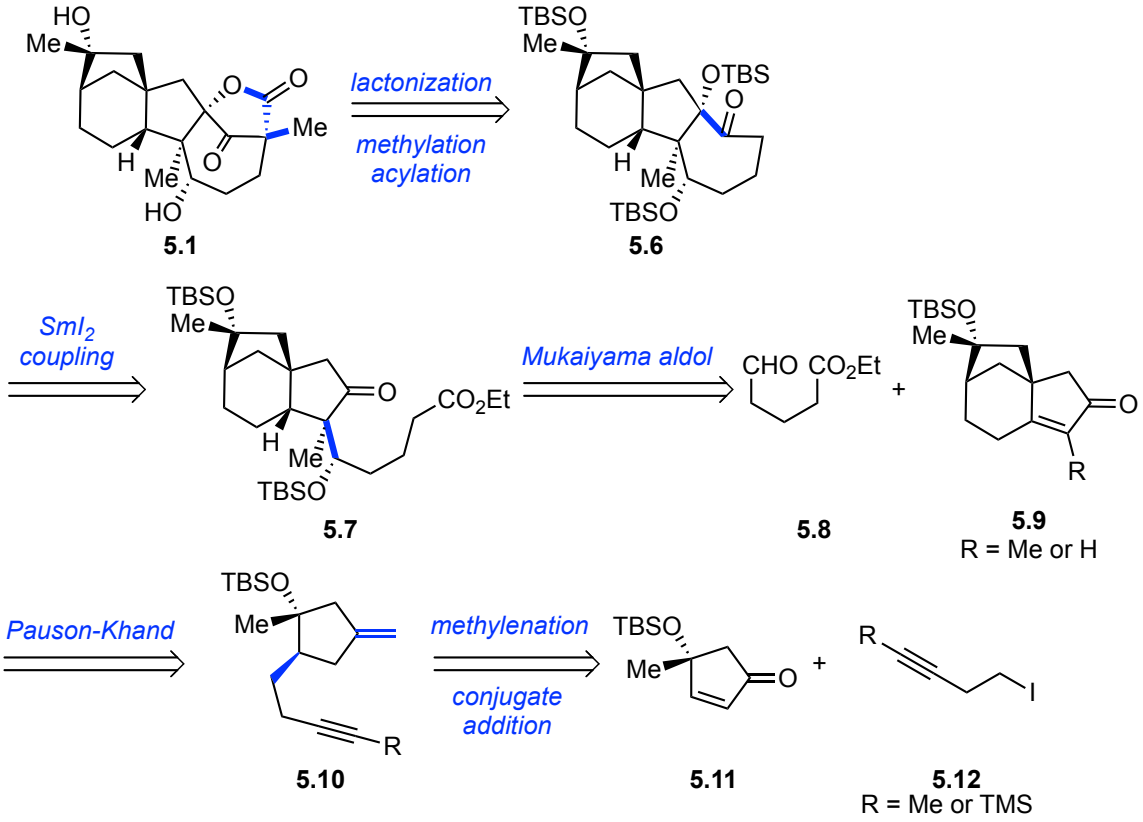

Scheme 5.1. Retrosynthetic analysis of pierisketolide A.

5.2.1 A Model System for the Pauson–Khand Reaction

5.2.1.1 Preparation of the Pauson-Khand Reaction Precursor

Because there was little direct evidence that the bicyclo[3.2.1]octane of **5.9** could be constructed using the devised PKR approach, we initially targeted a simplified model system to assess the feasibility of this transformation. Therefore, our attention first directed toward the known 4-siloxy-2-cyclopentenone **5.15** for preliminary studies. Convenient access to **5.15** was achieved according to a reported protocol for the microwave promoted Piancatelli rearrangement of furfuryl alcohol (**5.13**) (Equation 5.1).[450] The reaction was reported to proceed in up to 80% yield with full conversion of the starting material within four minutes, but in our hands **5.14** was obtained in only 46% yield. The modest yield notwithstanding, the short reaction time enabled rapid access to multi-gram quantities of **5.14** and subsequent protection of the alcohol as a *tert*-butyldimethylsilyl (TBS) ether provided **5.15** in two-steps from commercially available reagents.

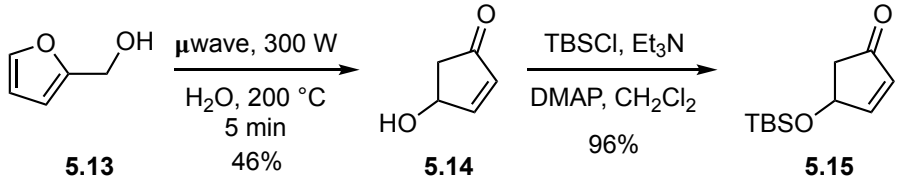

5.13 **5.14** **5.15** **(5.1)**

With **5.15** in hand, the next challenge was identification of conditions for the 1,4-addition of alkyne **5.12** (R = Me or TMS). Related transformations are well precedented using organocopper reagents, particularly in the area of prostaglandin synthesis.[449,451-453] A survey of copper sources reported for the conjugate addition of organocuprates to similar 4-siloxy-2-cyclopentenone substrates was conducted using *n*-butyllithium as a convenient surrogate for **5.12** (Equation 5.2).[449,454-456] In the event, *n*-butyllithium (3 eq.)

was added to a solution of THF containing the copper salt (1.5 eq) at -78 °C and the reaction was warmed to -40 °C, and cyclopentenone **5.15** was added at -78 °C. Both CuI and freshly prepared CuBr•DMS provided only unreacted starting material, whereas CuCN resulted in full consumption of **5.15** and provided the conjugate addition product **5.16** in 46% yield along with a variety of unidentified by-products. It is well established that TMSCl and hexamethylphosphoramide (HMPA) are effective additives for increasing the rate of organocuprate addition to enones to provide the silyl enol ether intermediate.[457,458] Moreover, trapping the intermediate enolate was discovered as an effective strategy to prevent enolate equilibration and the irreversible elimination of the TBS ether group with related 4-silyloxy-2-cyclopentenone substrates.[453,456,459] Fortunately, including these additives with the organocuprate generated from CuI•0.75DMS provided **5.16** in 67% yield after acidic hydrolysis of the silyl enol ether intermediate.

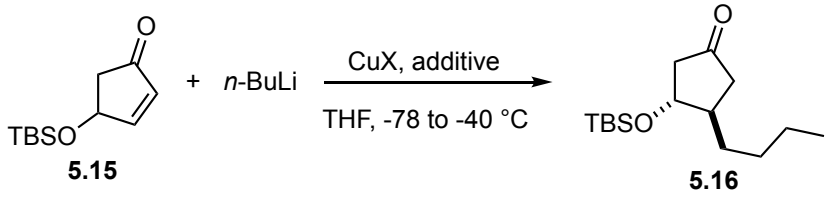

5.15 **5.16** **(5.2)**

CuX	additive	% yield
CuI	–	0
CuBr•DMS	–	0
CuCN	–	46
CuI	TMSCl, HMPA; AcOH	0
CuI•0.75DMS	TMSCl, HMPA; AcOH	67

We next sought to apply these conditions to the 1,4–addition of the organolithium generated from known alkyne **5.17**, which is accessible in one step from the

commercially available alcohol.[460] Accordingly, iodoalkyne **5.17** was converted to organolithium **5.18** via treatment with *tert*-butyllithium, followed by addition of a THF solution containing a soluble copper iodide–dimethylsulfide complex. Subsequent addition of 4-silyloxy-2-cyclopentenone **5.15** and TMSCl afforded the silyl enol ether intermediate **5.19** (Scheme 5.2).[449,461] The crude reaction mixture was hydrolyzed with aqueous acetic acid to provide **5.20** in 62% yield.

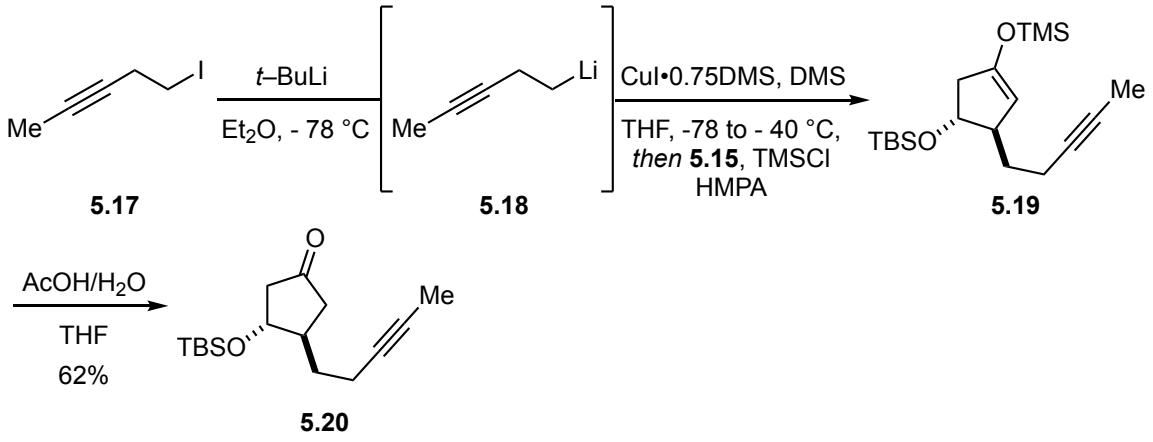

Scheme 5.2. Conjugate addition of iodoalkyne **5.17** with 4-silyloxy-cyclopentenone **5.15**.

Unfortunately, this initial result proved difficult to reproduce and subsequent attempts provided only unreacted starting material. In order to identify the source of this problem, it was necessary to evaluate individual steps of the multi-step reaction. Because the reaction was successful using a commercially available organolithium reagent, we hypothesized that the lithium-halogen exchange of **5.17** might be the culprit. To further examine this transformation, a solution of iodoalkyne **5.17** in diethyl ether was treated with *tert*-butyllithium and after stirring for one hour, the reaction was quenched with freshly distilled benzaldehyde (**5.21**) (Scheme 5.3). Interestingly, none of the addition product **5.22** was observed in the crude reaction mixture, and instead alcohol **5.23**

appeared to be a major by-product. This indicated that dissolved oxygen in the solvent might be consuming the intermediate organolithium. Although the diethyl ether was sparged with N_2 prior to being passed through neutral alumina according to the procedure reported by Grubbs, more rigorous degassing might be required.[462] Thus, the reaction was repeated after deassing the solvent via several freeze-pump-thaw cycles, as well as with diethyl ether distilled from sodium benzophenone ketyl, and the addition product **5.22** was obtained in 69% and 82% yield respectively.

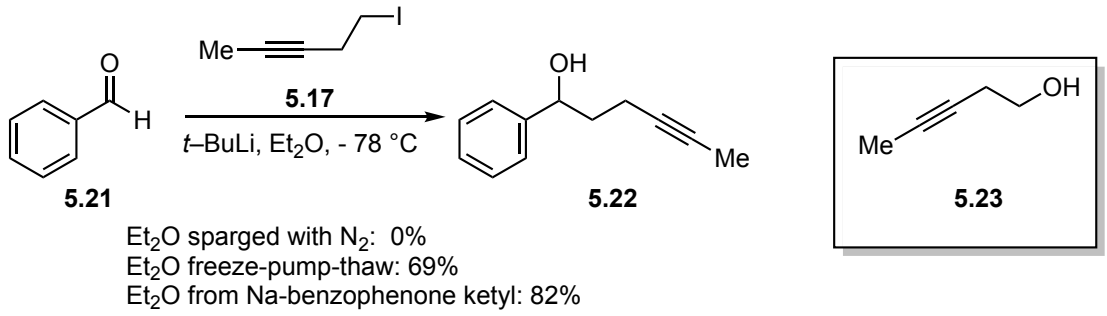

Scheme 5.3. Lithium-halogen exchange using degassed solvent.

After establishing conditions for successful lithium-halogen exchange with **5.17**, the conjugate addition was further optimized to reduce the quantity of alkyne required for the transformation by including 2-thienyllithium as a nontransferable ligand. Thus, a slightly modified protocol was developed using TMS-alkyne **5.23**, which was also targeted for investigation in the PKR (Scheme 5.4). In the event, treating **5.23** with *tert*-butyllithium in degassed diethyl ether induced lithium-halogen exchange, and was transferred to a solution of diethyl ether containing CuI•0.75DMS and 2-thienyllithium. Subsequent addition of cyclopentenone **5.15** and TMSCl afforded silyl enol ether **5.25**, which was hydrolyzed to afford **5.26** in 72% yield.

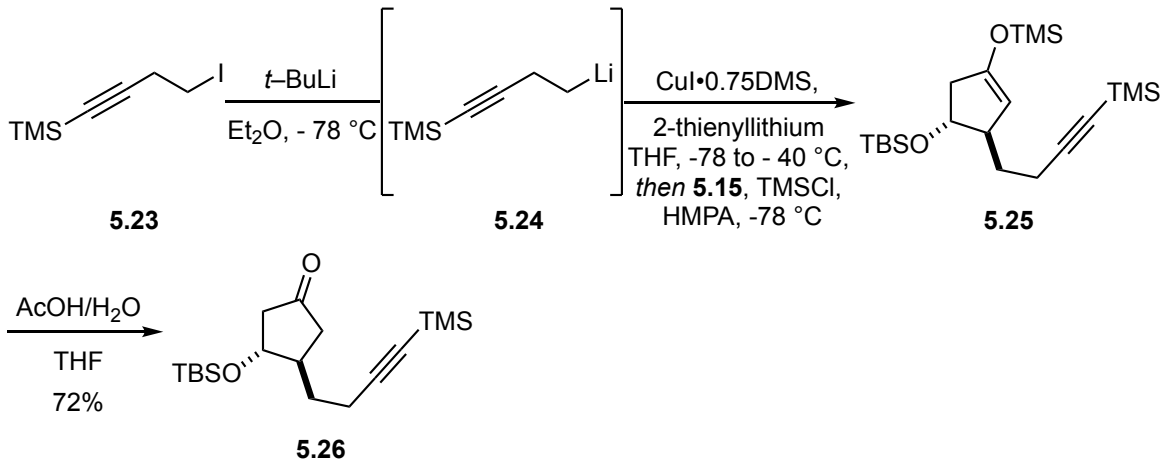

Scheme 5.4. Optimized conditions for the 1,4-addition with cyclopentenone **5.26**.

With substituted cyclopentenones **5.20** and **5.26** in hand, it was necessary to methylenate the carbonyl moiety. Wittig olefination of structurally related β-siloxy– and β-alkoxy–cyclopentanones have been reported to be unsuccessful due to their propensity to undergo β–elimination.[463,464] Accordingly, we examined Petasis reagent for methylenation.[465,466] Thus, treating **5.20** and **5.21** with Petasis reagent afforded the methylenated products **5.27** and **5.28** in 46% and 57% yield, respectively (Scheme 5.5). Although the yields were modest, additional optimization of the reaction was delayed until the feasibility of the PKR could be evaluated. The TMS group in **5.27** was easily removed to deliver the terminal alkyne in **5.29**.

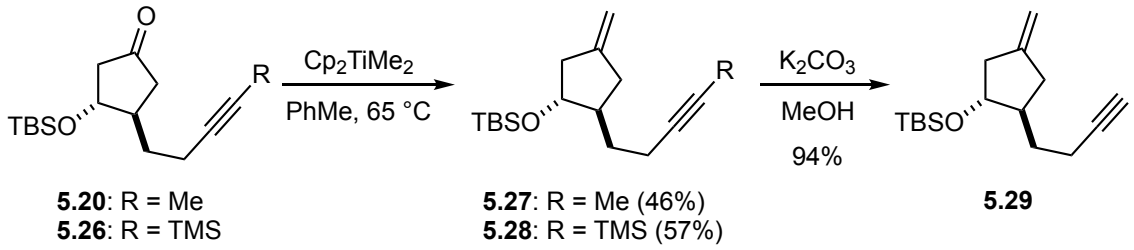

Scheme 5.5. Synthesis of the Pauson–Khand reaction precursor **5.28** and **5.29**.

5.2.1.2 A Preliminary Evaluation of the Pauson-Khand Reaction

The PKR is formally a [2+2+1] cycloaddition of an alkene, an alkyne, and carbon monoxide to form a cyclopentenone product (Scheme 5.6).[467] The putative mechanism, originally proposed by Magnus, involves the initial formation of a stable cobalt-alkyne complex **5.31** upon treatment of an alkyne with dicobalt octacarbonyl.[468,469] A reacting alkene then coordinates with this complex in a ligand substitution step, followed by cobaltacycle formation in **5.34**. Migratory insertion of CO and reductive elimination of the homologated intermediate **5.35** forms the cyclopentenone **5.36**. The traditional conditions typically require high temperatures to promote this transformation, which is thought to be related to decarbonylation in the ligand substitution step.[469,470] However, since its initial discovery a variety of advancements have been made to promote this transformation using more mild conditions, particularly with respect to oxidative and Lewis basic promoters that are thought to increase the rate of the ligand substitution step.[470]

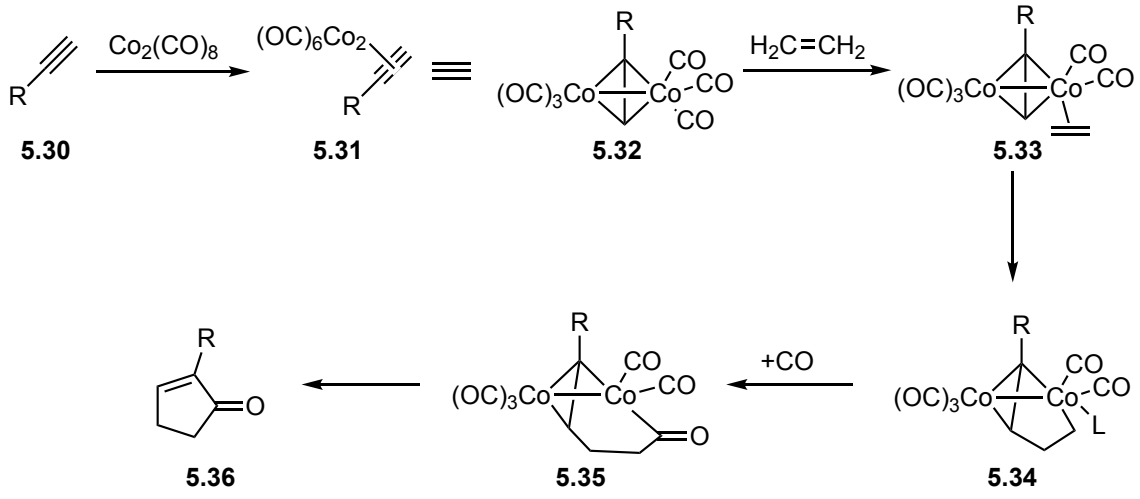

Scheme 5.6. Putative mechanism of the PKR.

The intramolecular variant represents a valuable strategy for accessing fused ring systems possessing considerable molecular complexity from comparatively simple enyne starting materials and has recently been has featured as a key step in the total synthesis of a variety complex natural products.[471-477] Among the numerous reports that use the PKR to assemble fused ring systems, there are few examples in which a bridged ring system is constructed and the carbon bond formation that occurs between the alkene and alkyne establish a newly formed bridgehead center. One example was reported by Pauson and coworkers for construction of the cedrane skeleton **5.38**, toward the formal and total syntheses of several cedrane natural products (Equation 5.3).[445-447] The cycloaddition of the 1,6-enyne proceeded using the oxidative promoters trimethylamine *N*-oxide (TMANO) and 4-methylmorpholine *N*-oxide (NMO), as well as the Lewis basic promoter *n*-butyl methylsulfide to provide **5.38** in high yield under mild reaction conditions. Another example reported by Chirkin *et al.* utilized *Z*-enyne **5.39** in a molybdenum hexacarbonyl–promoted hetero Pauson-Khand reaction to create the bicyclo[3.2.1]octane of **5.40** in 50% yield (Equation 5.4).[448] Each of these examples generate a bridged ring system that is structurally related to the bicyclo[3.2.1]octane of pierisketolide A, although both **5.37** and **5.39** possess structural features that might make cyclization more favorable. Thus, it remained to be determined if a related PKR with enyne **5.27** and **5.29** could be used to construct the tricyclic core of pierisketolide A.

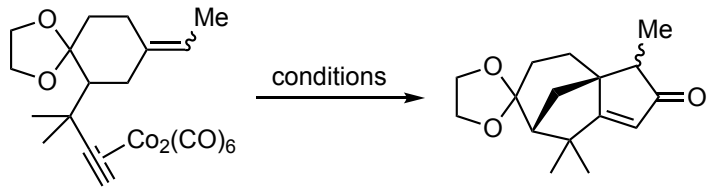

5.37 **5.38**

(5.3)

TMANO•$2H_2O$, acetone, rt; 91%
NMO•H_2O, CH_2Cl_2, rt; 84%
n-BuSMe, DCE, reflux; 95%

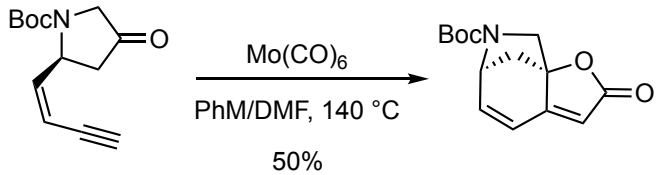

5.39 **5.40**

(5.4)

Inspired by these examples, we focused our attention first on the PKR using the internal alkyne substrate **5.27**. Enyne **5.27** was first treated with dicobalt octacarbonyl to generate the cobalt alkyne complex that was subjected directly to a range of conditions known to promote the PKR (Equation 5.5).[470] Gratifyingly, GCMS analysis of the crude reaction mixtures revealed that trace quantities of the desired adduct **5.41** were formed after refluxing the mixture in toluene. Similarly, trace quantities of **5.41** were also observed when the reaction was conducted in refluxing dichloroethane in the presence of *n*-BuSMe as a Lewis basic promoter.[478] Alternatively, in the presence of cyclohexylamine only alkyne **5.27** was observed, resulting from competitive demetallation.[479] Likewise, the well-established oxidative promoter NMO•H_2O only returned enyne **5.27**. Competitive demetallation of the cobalt-alkyne is a known challenge when using these PKR conditions with less reactive substrates, which indicates that **5.37** might exhibit inherently low reactivity in the PKR. [470,480]

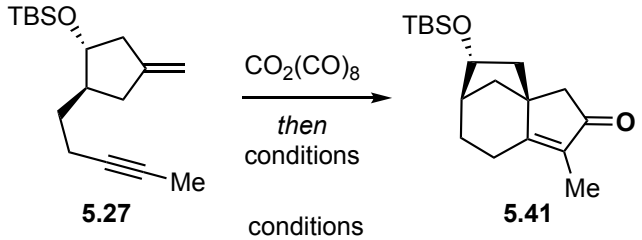

(5.5)

conditions	
PhMe, reflux	trace
n-BuSMe, DCE, reflux,	trace
$cyNH_2$, PhMe, reflux	0%
$NMO•H_2O$, CH_2Cl_2 rt	0%

Nonetheless, we were encouraged by these preliminary findings indicating that the cyclized product was formed in small quantities, and we next evaluated the terminal alkyne substrate **5.29** using similar conditions. We were pleased to discover that stirring a solution of enyne **5.29** and dicobalt octacarbonyl at room temperature for 2 h, followed by heating under reflux for 22 h afforded the PKR adduct in 8% yield, along with some unreacted starting material (Equation 5.6). Given the modest success of the PKR with standard heating conditions, microwave irradiation was pursued as an alternative method for promoting the PKR.[447,481] Enyne **5.29** was treated with dicobalt octacarbonyl and filtered through a short silica plug to afford **5.43** in 91% yield based on mass recovery. Gratifyingly, microwave irradiation of a toluene solution of **5.43** at 130 °C provided increased consumption of the starting material and **5.42** was isolated in 20% yield (Equation 5.7). This suggested that heating under microwave irradiation was superior to standard heating methods. Similar to the reactions conducted with the internal alkyne **5.27**, all attempts to induce the cyclization using known Lewis basic (*n*-BuSMe, tetramethylthiourea, and DMSO) and oxidative promoters ($NMO•H_2O$) did not produce detectable quantities of PKR product **5.42**. These initial results provided some encouragement, but only small quantities of the PKR product were obtained in these

preliminary experiments and it was clear that additional optimization was required. We therefore turned to the desired substrate rather than the model system

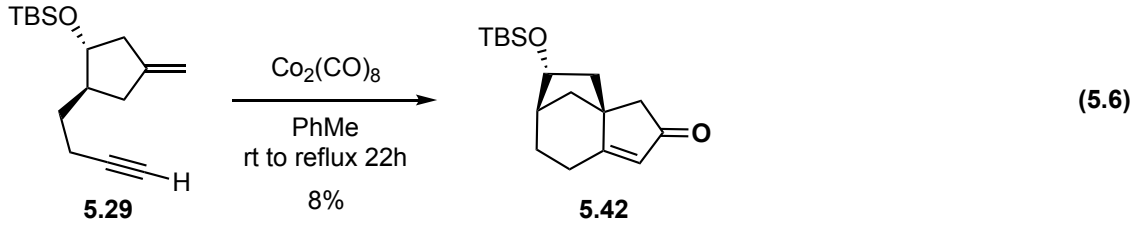

5.29 **5.42** **(5.6)**

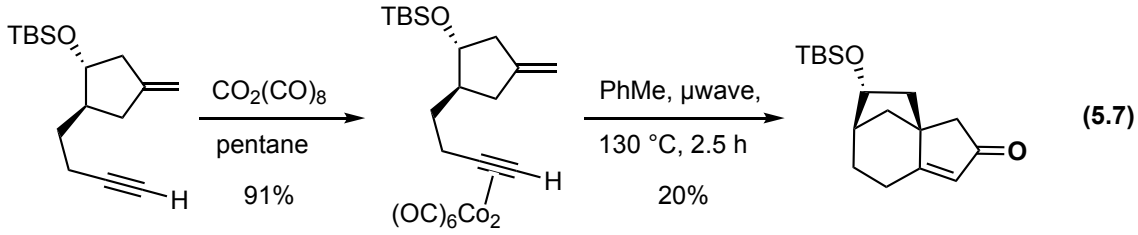

5.29 **5.43** **5.42** **(5.7)**

5.2.2 The Enantiospecific Approach

We thus focused upon accessing the chiral PKR precursor **5.10** using conditions that were developed with the model system. The synthesis commenced with preparation of known cyclopentenone **5.11** from commercially available (–)-linalool (**5.44**) according to the reported protocol.[449] In the event, ring closing metathesis of **5.44** was catalyzed by Hoveyda-Grubbs second generation catalyst (HG II) using solvent-free conditions followed by silylation of the intermediate alcohol with TBSCl gave **5.45** (Equation 5.8). Subsequent ruthenium catalyzed allylic oxidation afforded cyclopentenone **5.11** in 30% yield over two-steps. However, with **5.11** in hand, we pressed ahead toward the PKR precursor.

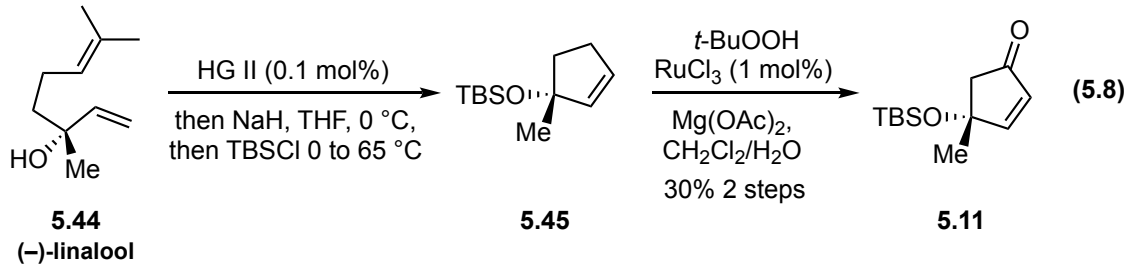

5.44
(–)-linalool

5.45

5.11

(5.8)

Unlike the model system, the carbon center adjacent to the Michael acceptor in **5.11** is fully substituted, and it was unclear if high levels of diastereoselectivity would be achieved in the 1,4–addition.[449] Following lithium-halogen exchange of iodoalkyne **5.23**, the organolithium was added to a solution of diethyl ether containing CuI•0.75DMS and 2-thienyllithium, followed by addition of **5.11** and TMSCl to afford silyl enol ether **5.46** (Scheme 5.7). Acidic hydrolysis of **5.46** delivered **5.47** in 67% yield along with the minor diastereomer in just 3% yield. The stereochemistry was confirmed based analysis of the NOESY spectra for the two diastereomers. Presumably the stereochemical outcome of the reaction is dictated by the steric bulk of the TBS group on the bottom face of the molecule. Subsequent methylenation of **5.47** with Petasis reagent provided enyne **5.48** in 64% yield and removal of the TMS group delivered the PKR precursor **5.49** in 92% yield.

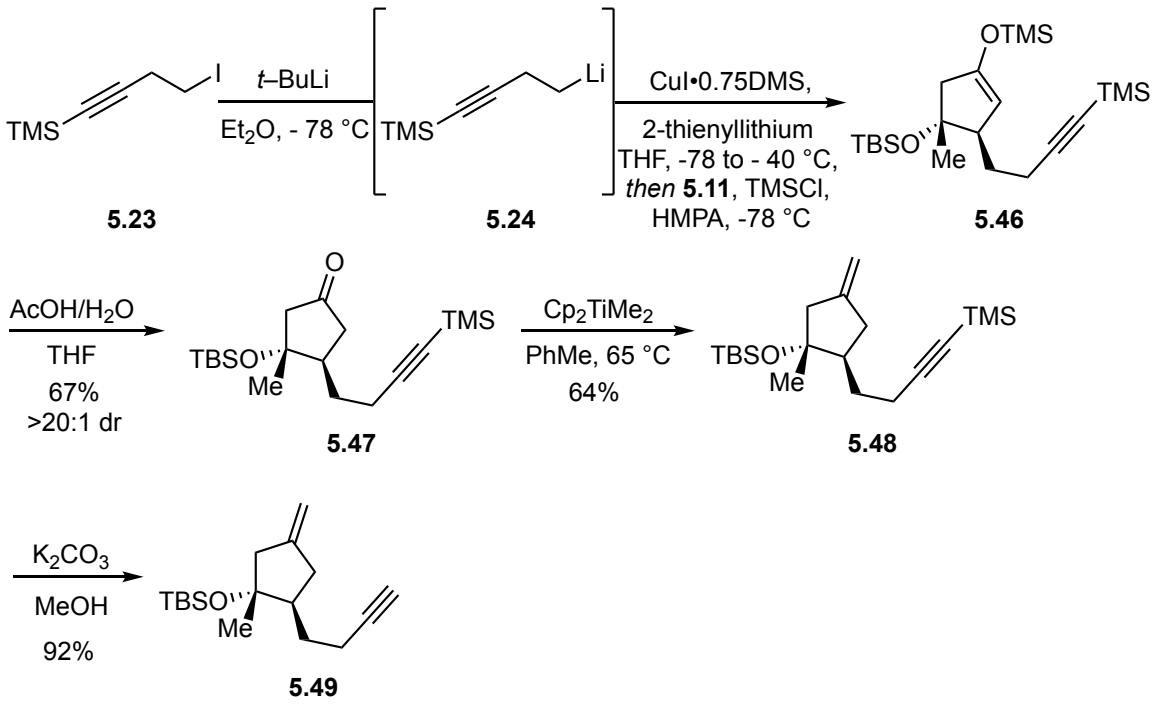

Scheme 5.7. Synthesis of the enantiopure Pauson-Khan precursor.

With reliable access to **5.49** thus established, the PKR was first assessed using conditions that showed promise in preliminary studies with the model substrate. Enyne **5.49** was treated with dicobalt octacarbonyl and after filtration through a silica gel plug, the cobalt alkyne complex **5.50** was dissolved in toluene and subjected to microwave irradiation at 130 °C. Most of the starting material was consumed after heating for four h based on GCMS analysis of the crude reaction mixture and the major peak was consistent with the molecular weight of cyclized product **5.51**, but **5.51** was isolated in only 14% yield (Equation 5.9). Alternatively, after stirring a solution of enyne **5.51** and dicobalt octacarbonyl in mesitylene at room temperature to generate the cobalt–alkyne complex *in situ*, the solution was directly heated to 130 °C for four h (Equation 5.10). Unlike the reaction conducted with microwave irradiation, considerable starting material remained with only trace formation of **5.51** by TLC analysis. The temperature was increased to 150

°C and the reaction was stirred for an additional 15 h, at which point the starting material was no longer observed, yet **5.51** was isolated in only 7% yield. The yields for each of these reactions were consistent with results obtained using the model system and again suggested heating with microwave irradiation was somewhat better than conventional heating.

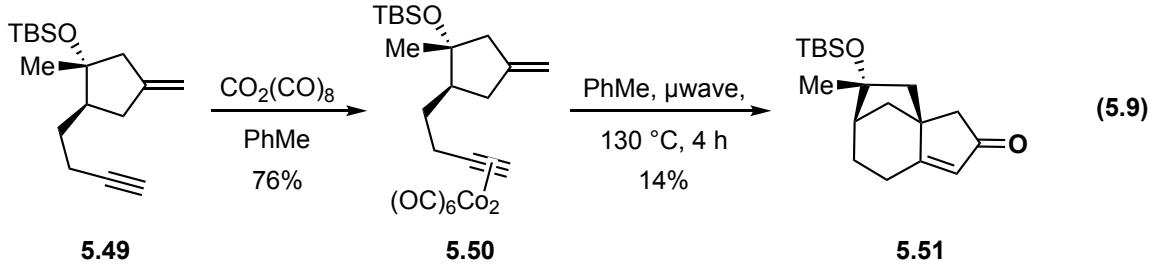

5.49 **5.50** **5.51** **(5.9)**

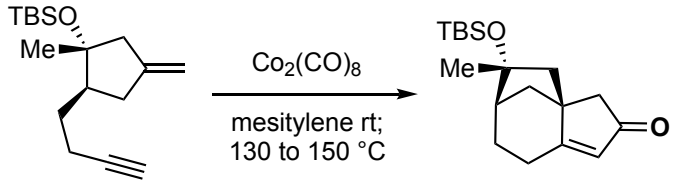

5.49 **5.51** **(5.10)**

In an attempt to further optimize the reaction, a brief survey of alternative conditions was conducted (Equation 5.11). Microwave irradiation was attempted using dichloroethane as a more polar solvent, but this resulted in diminished yields of **5.51** were obtained. Heating enyne **5.49** at 130 °C in the presence of *n*-BuSMe as a Lewis basic promoter provided only trace quantities of **5.51**. Turning to other metal mediators of PKR–like reactions, heating a solution of enyne **5.49** in a mixture of DMF and toluene at 140 °C in the presence of molybdenum hexacarbonyl, according to the protocol reported by Chirkin *et al.* delivered an intractable mixture.[448] Likewise the rhodium–catalyzed PKR using $[RhCl(CO)_2]_2$ (10 mol%) under an atmosphere of carbon monoxide also

produced an intractable mixture.[482] Thus, while initial results provided some encouragement, it is clear that the PKR with this substrate will require a more extensive optimization to identify conditions for the PKR that provide **5.51** in synthetically useful yields.

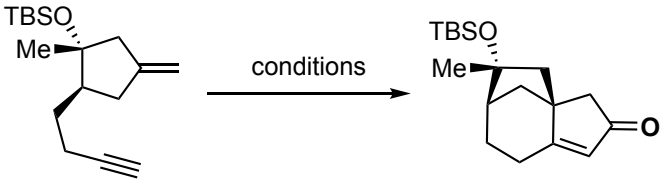

5.49 **5.51** **(5.11)**

conditions	
$Co_2(CO)_8$, DCE, μwave, 130 °C	3%
$Co_2(CO)_8$, mesitylene, *n*-BuSMe ,130 °C	trace
$Mo(CO)_6$, DMF/PhMe, 140 °C	0%
$[RhCl(CO)_2]_2$, CO, PhCl, 130 °C	0%

5.3 SUMMARY

In summary, we have investigated a novel approach to the enantiospecific synthesis of pierisketolide A that begins from readily available chiral starting materials. Conditions were developed for the 1,4-addition of iodoalkyne **5.23** to cyclopentenone **5.11** that achieved high levels of diastereoselectivity (Scheme 5.8). The PKR precursor was accessed in just one to two additional steps, providing a facile entry point for additional optimization studies. In addition, enyne **5.49** was shown to be converted directly to the bicyclo[3.2.1]octane core of pierisketolide A, providing an initial proof–of–concept, but additional optimization of this transformation is still needed. Although our efforts to improve the yields of the PKR have so far been unsuccessful, we remain optimistic that a viable strategy can be developed.

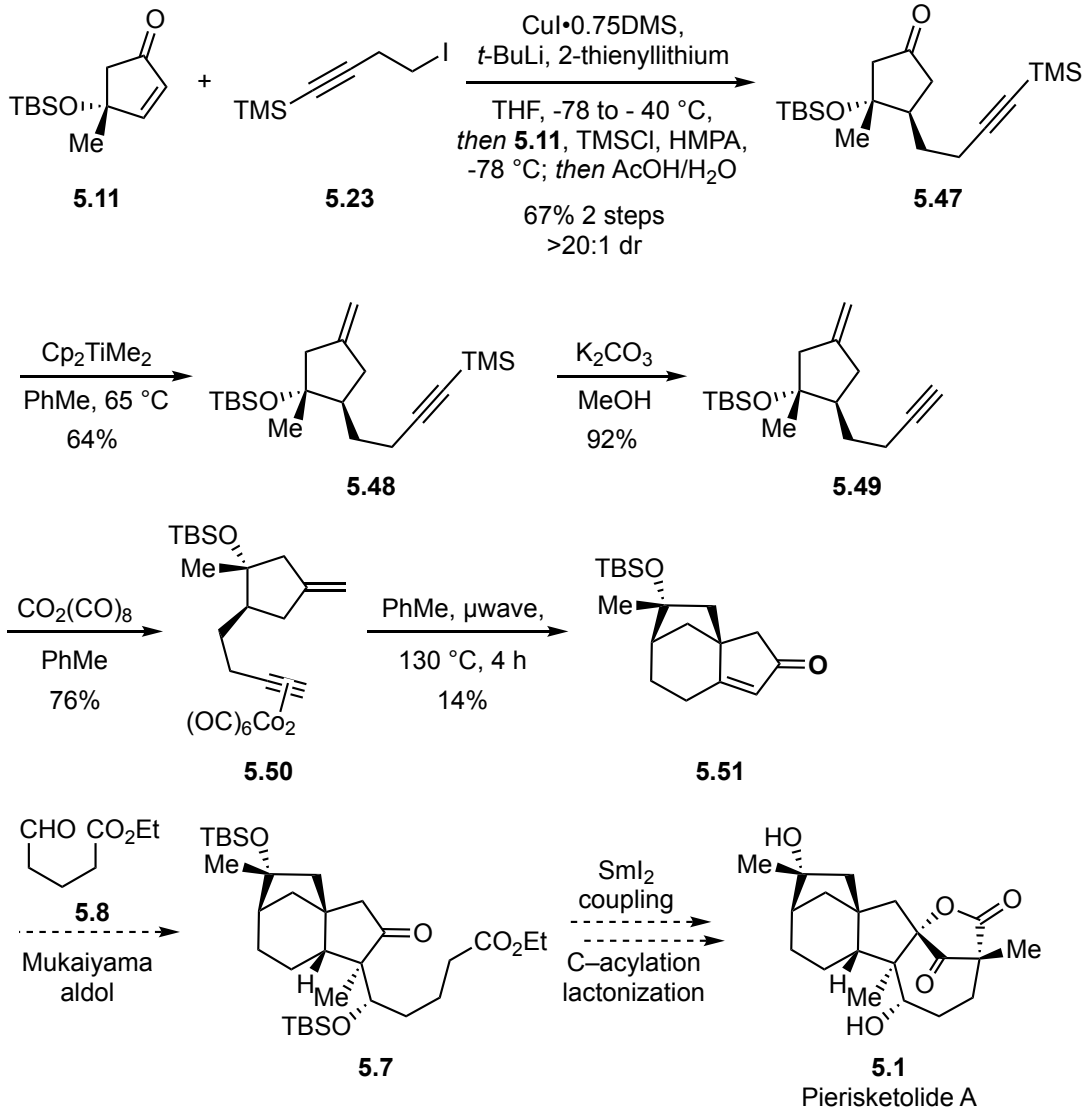

Scheme 5.8. Summary of progress towards the total synthesis of pierisketolide A.

5.4 FUTURE DIRECTIONS

The rapid assembly of the pierisketolide A core using a PKR from enyne **5.49** remains a promising entry point to this natural product and a variety of tactics to improve this transformation remain to be investigated. For instance, we have shown that microwave irradiation is more beneficial than conventional heating conditions, but a

thorough screen of solvents and known promoters is needed to determine optimum conditions. Similarly, an initial evaluation with the oxidative promoter NMO indicated that competitive demetallation was problematic, but recent studies have shown that the addition of ethylene glycol can help stabilize the metal-alkyne complex to allow coordination of the alkene prior to decomposition.[483] There remains an extensive body of literature on the PKR including a range of other metal mediators that might also be evaluated.[484]

Alternatively, a strategy can be envisioned that incorporates a Z-olefin as a conformational constraint similar to the strategy utilized in the hetero–PKR reported by Chirkin *et al.* (Scheme 5.9).[448] It is plausible that the low reactively observed using **5.49** stems from the unfavorable conformation that must be adopted for cyclization to occur. Thus, preorganization of the substrate in the reactive conformation might be a useful tactic to promote cyclization. Although somewhat less direct, this approach might allow rapid construction of the tricyclic core and provides a potential path forward.

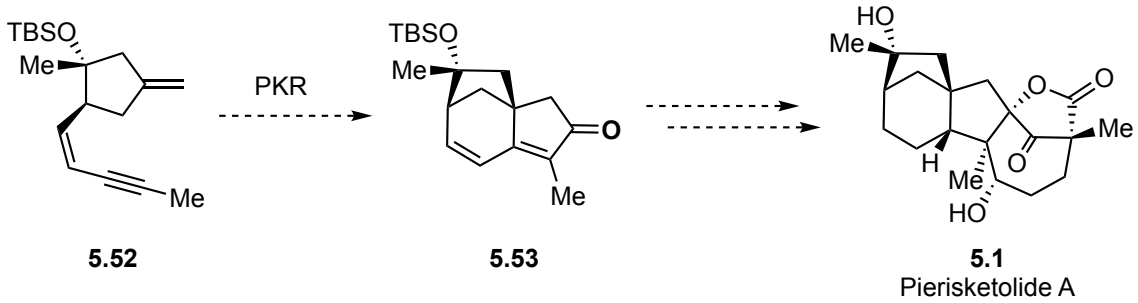

5.52 **5.53** **5.1**
Pierisketolide A

Scheme 5.9. Strategy for incorporating a conformational constraint.

Chapter 6: Supplementary Information

6.1 General Experimental

Solvents were purified unless otherwise noted before use as follows. Tetrahydrofuran (THF) was dried by filtration through two columns of activated, neutral alumina according to the procedure described by Grubbs.[462] Toluene (PhMe) was filtered through one column of activated, neutral alumina and Q5 reactant. Acetonitrile (MeCN) was dried by filtration through two columns of activated molecular sieves. These solvents were determined to have less than 50 ppm H2O by Karl Fischer coulometric moisture analysis. Methylene chloride (CH_2Cl_2), mesitylene, and 1,3,5-trimethylhexahydro-1,3,5-triazine were distilled from CaH_2, and N-Iodosuccinimide (NIS) was recrystallized from dioxane and hexane prior to use. All other reagents and solvents were reagent grade and were used as received unless otherwise noted. Dioxane was determined to have less than 1000 ppm H_2O by Karl Fischer coulometric moisture analysis. For air sensitive reactions, solvents were sparged with nitrogen or argon for at least 15 min. Reactions were performed under a nitrogen or argon atmosphere in round-bottom flasks sealed under rubber septa with magnetic stirring. Volatile solvents were removed under reduced pressure using a Büchi rotary evaporator at a water-bath temperature of 25–30 °C. Water sensitive reactions were performed with flame- or oven-dried glassware, stir-bars, and steel needles. Reaction temperatures are reported as the temperatures of the bath surrounding the vessel. Sensitive reagents and solvents were transferred using plastic syringes and steel needles using standard techniques.

Analytical HPLC separations were performed using a Chiralcel OD (Daicel Chemical Industries, Ltd.) column. Proton nuclear magnetic resonance (1H NMR) and carbon nuclear magnetic resonance (^{13}C NMR) spectra were acquired in $CDCl_3$ unless

otherwise noted. Chemical shifts are reported in parts per million (ppm, δ), downfield from tetramethylsilane (TMS, δ = 0.00 ppm) and are referenced to residual solvent ($CDCl_3$, δ = 7.26 ppm (1H) and 77.16 ppm (^{13}C)). Coupling constants (J) are reported in hertz (Hz), and the resonance multiplicity abbreviations used are: s, singlet; d, doublet; t, triplet; q, quartet; dt, doublet of triplets; dd, doublet of doublets; ddd, doublet of doublet of doublets; dddd, doublet of doublet of doublet of doublets; m, multiplet; comp, overlapping multiplets of magnetically non-equivalent protons. The abbreviations br and app stand for broad and apparent, respectively. Infrared (IR) spectra were obtained with a Thermo Nicolet 380 spectrometer. Melting points were determined using a Thomas-Hoover Uni-melt capillary melting point apparatus. Thin-layer chromatography (TLC) was performed on EMD 60 F254 glass- backed pre-coated silica gel plates and were visualized using one or more of the following methods: UV light (254 nm) and staining with basic potassium permanganate ($KMnO_4$), acidic p-anisaldehyde (PAA), or CAM. Flash chromatography was performed using glass columns and with Silicycle® SiliaFlash F60® (40-63 μm) silica gel eluting with the solvents indicated according to the procedure of Still.[485]

1-(Trimethylsiloxy)-1,3-butadiene (ca 9:1 *E/Z*) is commercially available from Sigma-Aldrich or can be prepared according to literature procedure.[486] N-Boc-3-methylindole was prepared according to literature procedure and the 1H and 13C NMR spectra were consistent with those previously reported.[487]

6.2 EXPERIMENTAL PROCEDURES

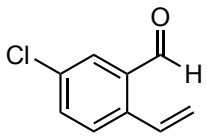

5-Chloro-2-vinylbenzaldehyde (**1.229**) (MDW-4-223). A flask was charged with 2-bromo-5-chlorobenzaldehyde (2.033 g, 9.314 mmol), potassium vinyltrifluoroborate (1.372 g, 10.24 mmol), Cs_2CO_3 (9.103 g, 27.94 mmol), $Pd(OAc)_2$ (104 mg, 0.463 mmol), and PPh_3 (244 mg, 0.930 mmol). The flask was evacuated and backfilled with N_2 three times, whereupon degassed THF (42 mL) and H_2O (5 mL) were added sequentially and the mixture was stirred at room temperature for 2 min. The flask was transferred to an oil bath preheated to 80° C and the reaction was heated under reflux for 6 h. Upon cooling, the reaction was diluted with saturated aqueous $NaHCO_3$ (15 mL) and extracted with Et_2O (3 x 30 mL). The combined organic extracts were washed with brine (1 x 30 mL), dried ($MgSO_4$), and concentrated under reduced pressure. The crude residue was purified via flash chromatography (SiO_2) eluting with hexanes/Et_2O (100:1 to 20:1) to afford 1.222 g (79%) of **1.229** as a pale yellow oil. ^{1}H NMR (400 MHz, $CDCl_3$) δ 10.25 (s, 1H), 7.82 – 7.79 (m, 1H), 7.53 – 7.50 (comp, 2H), 7.44 (dd, *J* = 17.4, 11.0 Hz, 1H), 5.70 (dd, *J* = 17.4, 1.0 Hz, 1H), 5.55 (dd, *J* = 11.0, 1.0 Hz, 1H). ^{13}C NMR (126 MHz, $CDCl_3$) δ 190.9, 139.0, 134.3, 134.0, 133.9, 132.2, 130.4, 129.1, 120.4. HRMS (CI) *m/z* calcd for C_9H_7ClO $(M+H)^+$, 166.0185; found 166.0181.

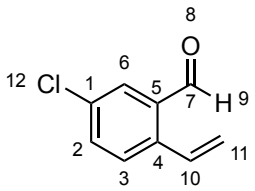

NMR Assignments (**1.229**). ^{1}H NMR (400 MHz, $CDCl_3$) δ 10.25 (s, 1H, 9), 7.82 – 7.79 (m, 1H, 2), 7.53 – 7.50 (comp, 2H, 3, 6), 7.44 (dd, *J* = 17.4, 11.0 Hz, 1H, 10), 5.70 (dd, *J* = 17.4, 1.0 Hz, 1H, 11), 5.55 (dd, *J* = 11.0, 1.0 Hz, 1H, 11). ^{13}C NMR (126 MHz, $CDCl_3$) δ 190.9 (7), 139.0 (4), 134.3 (5), 134.0 (1), 133.9 (6), 132.2 (10), 130.4 (2), 129.1 (3), 120.4 (11).

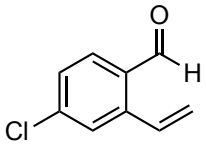

4-Chloro-2-vinylbenzaldehyde (**1.230**) (MDW-4-222). A flask was charged with 2-bromo-4-chlorobenzaldehyde (1.531 g, 6.976 mmol), potassium vinyltrifluoroborate (0.935 g, 6.98 mmol), Cs_2CO_3 (6.821 g, 20.93 mmol), $Pd(OAc)_2$ (78 mg, 0.35 mmol), and PPh_3 (183 mg, 0.698 mmol). The flask was evacuated and backfilled with N_2 three times, whereupon degassed THF (32 mL) and H_2O (4 mL) were added sequentially and the mixture was stirred at room temperature for 2 min. The flask was transferred to an oil bath preheated to 80° C and the reaction was heated under reflux for 6 h. Upon cooling, the reaction was diluted with saturated aqueous $NaHCO_3$ (15 mL) and extracted with Et_2O (3 x 30 mL). The combined organic extracts were washed with brine (1 x 30 mL), dried ($MgSO_4$), and concentrated under reduced pressure. The crude residue was purified via flash chromatography (SiO_2) eluting with hexanes/Et_2O (100:1 to 20:1) to afford 0.834 g (72%) of **1.230** as a colorless solid: mp 37–40 °C. ^{1}H NMR (400 MHz, $CDCl_3$) δ 10.24 (s, 1H), 7.77 (d, *J* = 8.3 Hz, 1H), 7.54 (d, *J* = 2.1 Hz, 1H), 7.48 (dd, *J* = 17.4, 11.0 Hz, 1H), 7.40 (dd, *J* = 8.3, 2.0 Hz, 1H), 5.73 (dd, *J* = 17.4, 0.9 Hz, 1H), 5.57 (dd, *J* = 11.0, 0.9 Hz, 1H). ^{13}C NMR (126 MHz, $CDCl_3$) δ 191.1, 142.2, 140.4, 132.6, 132.3, 131.3, 128.3, 127.6, 120.8. HRMS (CI) *m/z* calcd for C_9H_7ClO $(M+H)^+$, 166.0185; found 166.0178.

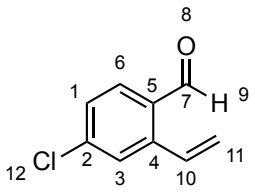

NMR Assignments (**1.230**). ^{1}H NMR (400 MHz, $CDCl_3$) δ 10.24 (s, 1H, 9), 7.77 (d, *J* = 8.3 Hz, 1H, 6), 7.54 (d, *J* = 2.1 Hz, 1H, 3), 7.48 (dd, *J* = 17.4, 11.0 Hz, 1H, 10), 7.40 (dd, *J* = 8.3, 2.0 Hz, 1H, 1), 5.73 (dd, *J* = 17.4, 0.9 Hz, 1H, 11), 5.57 (dd, *J* = 11.0, 0.9 Hz, 1H, 11). ^{13}C NMR (126 MHz, $CDCl_3$) δ 191.1 (7), 142.2 (4), 140.4 (5), 132.6 (6), 132.3 (10), 131.3 (2), 128.3 (1), 127.6 (3), 120.8 (11).

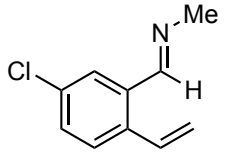

1-(5-Chloro-2-vinylphenyl)-*N*-methylmethanimine (**2.5**) (MDW-4-228). A solution of $MeNH_3$ (33% in EtOH, 0.32 mL) was added to a solution of **1.229** (0.286 g, 1.72 mmol) in CH_2Cl_2 (11 mL) containing $MgSO_4$ (620 mg, 5.51 mmol) and was stirred for 11 h. The reaction was filtered, washing with CH_2Cl_2 (10 mL). The filtrate was concentrated under reduced pressure to afford 0.305 g (99%) of **2.5** as a colorless oil that was used directly without purification. ^{1}H NMR (400 MHz, $CDCl_3$) δ 8.56 (q, *J* = 1.7 Hz, 1H), 7.85 (d, *J* = 2.3 Hz, 1H), 7.40 (d, *J* = 8.4 Hz, 1H), 7.33 (dd, *J* = 8.4, 2.3 Hz, 1H), 7.15 (dd, *J* = 17.4, 11.0 Hz, 1H), 5.62 (dd, *J* = 17.4, 1.1 Hz, 1H), 5.43 (dd, *J* = 11.0, 1.1 Hz, 1H), 3.54 (d, *J* = 1.7 Hz, 3H). ^{13}C NMR (126 MHz, $CDCl_3$) δ 159.5, 136.5, 134.7, 134.1, 133.0, 130.3, 128.3, 127.4, 118.4, 48.8. HRMS (ESI) *m/z* calcd for $C_{10}H_{10}ClN$ $(M+H)^+$, 180.0575; found 180.0575.

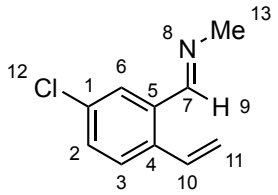

NMR Assignments (**2.5**). ^{1}H NMR (400 MHz, $CDCl_3$) δ 8.56 (q, *J* = 1.7 Hz, 1H, 9), 7.85 (d, *J* = 2.3 Hz, 1H, 6), 7.40 (d, *J* = 8.4 Hz, 1H, 3), 7.33 (dd, *J* = 8.4, 2.3 Hz, 1H, 2), 7.15 (dd, *J* = 17.4, 11.0 Hz, 1H, 10), 5.62 (dd, *J* = 17.4, 1.1 Hz, 1H, 11), 5.43 (dd, *J* = 11.0, 1.1 Hz, 1H, 11), 3.54 (d, *J* = 1.7 Hz, 3H, 13). ^{13}C NMR (126 MHz, $CDCl_3$) δ 159.5 (7), 136.5 (5), 134.7 (4), 134.1 (1), 133.0 (10), 130.3 (2), 128.3 (3), 127.4 (6), 118.4 (11), 48.8 (13).

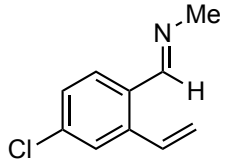

1-(4-Chloro-2-vinylphenyl)-*N*-methylmethanimine (**2.6**) (MDW-4-227). A solution of $MeNH_3$ (33% in EtOH, 0.29 mL) was added to a solution of **1.230** (0.256 g, 1.54 mmol) in CH_2Cl_2 (10 mL) containing $MgSO_4$ (550 mg, 4.57 mmol) and was stirred for 11 h. The reaction was filtered, washing with CH_2Cl_2 (10 mL). The filtrate was concentrated under reduced pressure to afford 0.274 g (99%) of **2.6** as a pale yellow oil that was used directly without purification. ^{1}H NMR (400 MHz, $CDCl_3$) δ 8.57 – 8.53 (m, 1H), 7.78 (d, *J* = 8.4 Hz, 1H), 7.45 (d, *J* = 2.2 Hz, 1H), 7.28 (app dd, *J* = 8.4, 2.1 Hz, 1H), 7.18 (dd, *J* = 17.3, 11.0 Hz, 1H), 5.65 (dd, *J* = 17.3, 1.0 Hz, 1H), 5.46 (dd, *J* = 11.0, 1.1 Hz, 1H), 3.53 (d, *J* = 1.7 Hz, 3H). ^{13}C NMR (126 MHz, $CDCl_3$) δ 159.8, 139.6, 136.4, 133.0, 131.8, 129.2, 128.1, 126.8, 119.0, 48.8. HRMS (ESI) *m/z* calcd for $C_{10}H_{10}ClN$ $(M+H)^+$, 180.0575; found 180.0577.

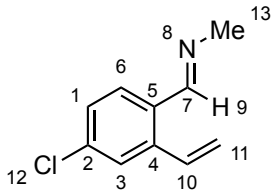

NMR Assignments (**2.6**). ^{1}H NMR (400 MHz, $CDCl_3$) δ 8.57 – 8.53 (m, 1H, 9), 7.78 (d, *J* = 8.4 Hz, 1H, 6), 7.45 (d, *J* = 2.2 Hz, 1H, 3), 7.28 (dd, *J* = 8.4, 2.1 Hz, 1H, 1), 7.18 (app dd, *J* = 17.3, 11.0 Hz, 1H, 10), 5.65 (dd, *J* = 17.3, 1.0 Hz, 1H, 11), 5.46 (dd, *J* = 11.0, 1.1 Hz, 1H, 11), 3.53 (d, *J* = 1.7 Hz, 3H, 13). ^{13}C NMR (126 MHz, $CDCl_3$) δ 159.8 (7), 139.6 (4), 136.4 (2), 133.0 (10), 131.8 (5), 129.2 (6), 128.1 (1), 126.8 (3), 119.0 (11), 48.8 (13).

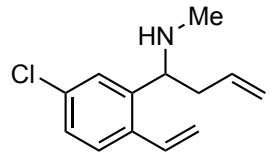

1-(5-Chloro-2-vinylphenyl)-*N*-methylbut-3-en-1-amine (**2.8**) (MDW-4-230). A solution of allylzinc bromide (0.83 M in THF, 5.0 mL, 4.2 mmol) was added dropwise to a solution of crude **2.5** (0.305 g, 1.70 mmol) in THF (8.5 mL) cooled to -78 °C and the reaction was stirred at -78 °C for 6 h. The cooling bath was removed and the reaction was stirred for 30 min at room temperature. The solution was diluted with saturated aqueous NH_4Cl (15 mL) and extracted with Et_2O (3 x 20 mL). The combined organic extracts were washed with brine (1 x 20 mL), dried ($MgSO_4$), and concentrated under reduced pressure. The crude residue was purified via flash chromatography (SiO_2) eluting with hexanes/Et_2O/Et_3N (100:5:1 to 100:10:1) to afford 0.303 g (80% from **1.229**) of **2.8** as a colorless oil. ^{1}H NMR (400 MHz, $CDCl_3$) δ 7.48 (d, *J* = 2.3 Hz, 1H), 7.37 (d, *J* = 8.3 Hz, 1H), 7.18 (ddd, *J* = 8.3, 2.3, 0.6 Hz, 1H), 7.04 (dd, *J* = 17.3, 11.0 Hz, 1H), 5.78 – 5.66 (m, 1H), 5.58 (dd, *J* = 17.3, 1.3 Hz, 1H), 5.32 (dd, *J* = 11.0, 1.3 Hz, 1H), 5.14 – 5.05

(comp, 2H), 3.90 (dd, *J* = 8.3, 4.9 Hz, 1H), 2.44 – 2.35 (m, 1H), 2.31 – 2.21 (comp, 4H), 1.44 (brs, 1H). ^{13}C NMR (126 MHz, $CDCl_3$) δ 142.8, 135.6, 135.1, 134.1, 133.7, 127.9, 127.1, 126.4, 118.1, 116.9, 59.6, 42.0, 34.7. HRMS (ESI) *m/z* calcd for $C_{13}H_{16}ClN$ $(M+H)^+$, 222.1044; found 222.1048.

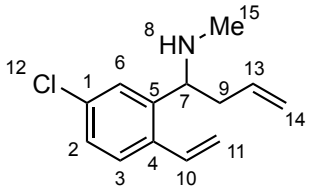

NMR Assignments (**2.8**). ^{1}H NMR (400 MHz, $CDCl_3$) δ 7.48 (d, *J* = 2.3 Hz, 1H, 6), 7.37 (d, *J* = 8.3 Hz, 1H, 3), 7.18 (ddd, *J* = 8.3, 2.3, 0.6 Hz, 1H, 2), 7.04 (dd, *J* = 17.3, 11.0 Hz, 1H, 10), 5.78 – 5.66 (m, 1H, 13), 5.58 (dd, *J* = 17.3, 1.3 Hz, 1H, 11), 5.32 (dd, *J* = 11.0, 1.3 Hz, 1H, 11), 5.14 – 5.05 (comp, 2H, 14), 3.90 (dd, *J* = 8.3, 4.9 Hz, 1H, 7), 2.44 – 2.35 (m, 1H, 9), 2.31 – 2.21 (comp, 4H, 9, 15), 1.44 (brs, 1H, 8).^{13}C NMR (126 MHz, $CDCl_3$) δ 142.8 (1), 135.6 (4), 135.1 (13), 134.1 (5), 133.7 (10), 127.9 (3), 127.1 (2), 126.4 (6), 118.1 (14), 116.9 (11), 59.6 (7), 42.0 (9), 34.7 (15).

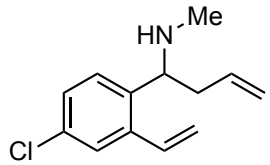

1-(4-Chloro-2-vinylphenyl)-*N*-methylbut-3-en-1-amine (**2.9**) (MDW-4-229). A solution of allylzinc bromide (0.83 M in THF, 4.4 mL, 3.7 mmol) was added dropwise to a solution of crude **2.6** (0.274 g, 1.52 mmol) in THF (7.4 mL) cooled to -78 °C and the reaction was stirred at -78 °C for 6 h. The cooling bath was removed and the reaction was stirred for 30 min at room temperature. The solution was diluted with saturated aqueous NH_4Cl (15 mL) and extracted with Et_2O (3 x 20 mL). The combined organic extracts

were washed with brine (1 x 20 mL), dried ($MgSO_4$), and concentrated under reduced pressure. The crude residue was purified via flash chromatography (SiO_2) eluting with hexanes/Et_2O/Et_3N (100:5:1 to 100:10:1) to afford 0.301 g (88% from **1.230**) of **2.9** as a colorless oil. ^1H NMR (400 MHz, $CDCl_3$) δ 7.43 – 7.39 (comp, 2H), 7.24 (app dd, *J* = 8.3, 2.3 Hz, 1H), 7.06 (dd, *J* = 17.3, 11.0 Hz, 1H), 5.77 – 5.64 (m, 1H), 5.60 (dd, *J* = 17.3, 1.3 Hz, 1H), 5.35 (dd, *J* = 10.9, 1.3 Hz, 1H), 5.13 – 5.04 (comp, 2H), 3.89 (dd, *J* = 8.1, 5.2 Hz, 1H), 2.43 – 2.35 (m, 1H), 2.32 – 2.22 (comp, 4H), 1.46 (brs, 1H). ^{13}C NMR (126 MHz, $CDCl_3$) δ 139.2, 138.9, 135.1, 133.6, 132.6, 128.0, 128.0, 126.4, 118.0, 117.5, 59.4, 42.0, 34.6. HRMS (ESI) *m/z* calcd for $C_{13}H_{16}ClN$ $(M+H)^+$, 222.1044; found 222.1049.

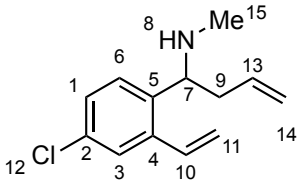

NMR Assignments (**2.9**). ^1H NMR (400 MHz, $CDCl_3$) δ 7.43 – 7.39 (comp, 2H, 3, 6), 7.24 (app dd, *J* = 8.3, 2.3 Hz, 1H, 1), 7.06 (dd, *J* = 17.3, 11.0 Hz, 1H, 10), 5.77 – 5.64 (m, 1H, 13), 5.60 (dd, *J* = 17.3, 1.3 Hz, 1H, 11), 5.35 (dd, *J* = 10.9, 1.3 Hz, 1H, 11), 5.13 – 5.04 (comp, 2H, 14), 3.89 (dd, *J* = 8.1, 5.2 Hz, 1H, 7), 2.43 – 2.35 (m, 1H, 9), 2.32 – 2.22 (comp, 4H, 9, 15), 1.46 (brs, 1H, 8). ^{13}C NMR (126 MHz, $CDCl_3$) δ 139.2 (2), 138.9 (4), 135.1 (13), 133.6 (10), 132.6 (5), 128.0 (3), 128.0 (1), 126.4 (6), 118.0 (14), 117.5 (11), 59.4 (7), 42.0 (9), 34.6 (15).

Representative Procedure A: Reaction of an amine with benzyl chloroformate.

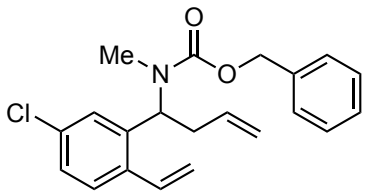

Benzyl (1-(5-chloro-2-vinylphenyl)but-3-en-1-yl)(methyl)carbamate (**2.10**) (MDW-4-236). A solution of **2.8** (0.278 g, 1.25 mmol) and *i*-Pr_2NEt (0.33 g, 0.44 mL 2.5 mmol) in CH_2Cl_2 (6 mL) was cooled to 0 ° C. CbzCl (0.31 g, 0.26 mL, 1.8 mmol) was added dropwise to the cooled solution and the reaction was stirred for 5 h at 0 °C. The cooling bath was removed and the solution was stirred at room temperature for 2 h. The reaction was quenched with 1 N HCl (10 mL) and the aqueous layer was extracted with CH_2Cl_2 (1 x 10 mL). The organic extract was washed with saturated aqueous $NaHCO_3$ (1 x 15 mL) and the aqueous layer was extracted with CH_2Cl_2 (3 x 10 mL). The combined organic extracts were washed with brine (1 x 20 mL), dried (Na_2SO_4), and concentrated under reduced pressure. The crude residue was purified via flash chromatography (SiO_2) eluting with hexanes/EtOAc (20:5) to afford 0.443 g (99%) of **2.10** as a colorless oil. 1H NMR (500 MHz, 130 °C, DMSO-d_6) δ 7.50 (d, J = 8.3 Hz, 1H), 7.40 (d, J = 2.2 Hz, 1H), 7.38 – 7.28 (comp, 6H), 6.94 (dd, J = 17.2, 11.0 Hz, 1H), 5.81 – 5.71 (m, 1H), 5.58 (dd, J = 17.3, 1.4 Hz, 1H), 5.47 (dd, J = 8.8, 6.5 Hz, 1H), 5.22 (dd, J = 11.0, 1.3 Hz, 1H), 5.17 – 5.09 (m, 3H), 5.02 (dd, J = 10.3, 1.7 Hz, 1H), 2.78 – 2.65 (m, 2H), 2.63 (s, 3H). ^{13}C NMR (126 MHz, 130 °C, DMSO-d_6) δ 154.8, 138.1, 136.4, 135.8, 134.0, 132.7, 131.7, 127.5, 127.5, 126.9, 126.9, 126.8, 126.4, 116.4, 116.2, 65.9, 54.0, 33.9, 28.4. HRMS (ESI) *m/z* calcd for $C_{21}H_{22}ClNO_2$ $(M+Na)^+$, 378.1231; found 378.1233.

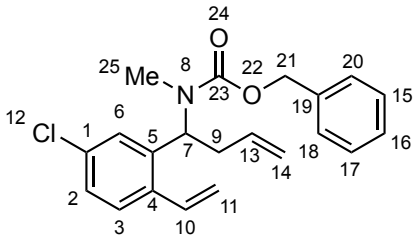

NMR Assignments (**2.10**). ^{1}H NMR (500 MHz, 130 ° C, DMSO-d_6) δ 7.50 (d, J = 8.3 Hz, 1H, 3), 7.40 (d, J = 2.2 Hz, 1H, 6), 7.38 – 7.28 (comp, 6H, 2, 15, 16, 17, 18, 20), 6.94 (dd, J = 17.2, 11.0 Hz, 1H, 10), 5.81 – 5.71 (m, 1H, 13), 5.58 (dd, J = 17.3, 1.4 Hz, 1H, 11), 5.47 (dd, J = 8.8, 6.5 Hz, 1H, 7), 5.22 (dd, J = 11.0, 1.3 Hz, 1H, 11), 5.17 – 5.09 (comp, 3H, 14, 21), 5.02 (dd, J = 10.3, 1.7 Hz, 1H, 21), 2.78 – 2.65 (m, 2H, 9), 2.63 (s, 3H, 25). ^{13}C NMR (126 MHz, 130 ° C, DMSO-d_6) δ 154.8 (23), 138.1 (1), 136.4 (4), 135.8 (5), 134.0 (13), 132.7 (10), 131.7 (19), 127.5 (18, 20), 127.5 (16), 126.9 (3), 126.9 (2), 126.8 (15, 17), 126.4 (6), 116.4 (14), 116.2 (11), 65.9 (21), 54.0 (7), 33.9 (9), 28.4 (25).

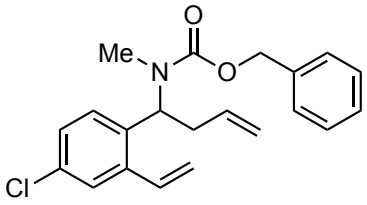

Benzyl (1-(4-chloro-2-vinylphenyl)but-3-en-1-yl)(methyl)carbamate (**2.11**) (MDW-4-235). Prepared from **2.9** (0.276 g, 1.24 mmol) and CbzCl according to representative procedure A. The crude residue was purified via flash chromatography (SiO_2) eluting with hexanes/EtOAc (20:5) to afford 0.409 g (92%) of **2.11** as a colorless oil. ^{1}H NMR (500 MHz, 80 °C, DMSO-d_6) δ 7.52 (d, J = 2.3 Hz, 1H), 7.44 (d, J = 8.4 Hz, 1H), 7.40 – 7.29 (comp, 6H), 6.93 (dd, J = 17.2, 11.0 Hz, 1H), 5.78 – 5.71 (m, 1H), 5.68 (dd, J = 17.2, 1.2 Hz, 1H), 5.48 (dd, J = 9.0, 6.4 Hz, 1H), 5.23 (d, J = 11.0 Hz, 1H), 5.16 – 5.09 (comp, 3H), 5.03 – 4.98 (m, 1H), 2.76 – 2.62 (comp, 2H), 2.55 (s, 3H). ^{13}C

NMR (126 MHz, DMSO-d_6) δ 154.8, 139.1, 136.4, 134.8, 134.1, 132.6, 132.1, 128.5, 127.5, 127.0, 126.8, 126.5, 125.3, 116.9, 116.4, 65.9, 53.8, 34.1, 28.2. HRMS (ESI) *m/z* calcd for $C_{21}H_{22}ClNO_2$ $(M+Na)^+$, 378.1231; found 378.1234.

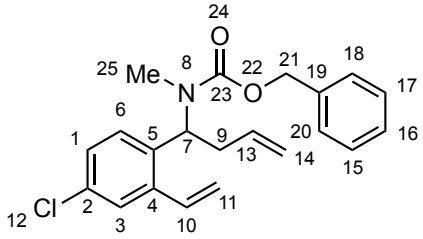

NMR Assignments (**2.11**). ^{1}H NMR (500 MHz, 80 °C, DMSO-d_6) δ 7.52 (d, *J* = 2.3 Hz, 1H, 3), 7.44 (d, *J* = 8.4 Hz, 1H, 6), 7.40 – 7.29 (comp, 6H, 1, 15, 16, 17, 18, 20), 6.93 (dd, *J* = 17.2, 11.0 Hz, 1H, 10), 5.78 – 5.71 (m, 1H, 13), 5.68 (dd, *J* = 17.2, 1.2 Hz, 1H, 11), 5.48 (dd, *J* = 9.0, 6.4 Hz, 1H, 7), 5.23 (d, *J* = 11.0 Hz, 1H, 21), 5.16 – 5.09 (comp, 3H, 14, 21), 5.03 – 4.98 (m, 1H, 11), 2.76 – 2.62 (comp, 2H, 9), 2.55 (s, 3H, 25). ^{13}C NMR (126 MHz, 130 ° C, DMSO-d_6) δ 154.8 (23), 139.1 (2), 136.4 (4), 134.8 (5), 134.1, 132.6, 132.1 (19), 128.5 (3), 127.5 (18, 20), 127.0 (16), 126.8 (15, 17), 126.5 (1), 125.3 (6), 116.9 (14), 116.4 (11), 65.9 (21), 53.8 (7), 34.1 (9), 28.2 (25).

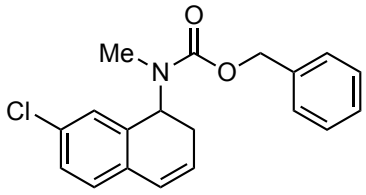

Benzyl (7-chloro-1,2-dihydronaphthalen-1-yl)(methyl)carbamate (**2.12**) (MDW-1-156). Grubbs second generation catalyst (0.163 g, 0.192 mmol) was added to a solution of **2.10** (1.36 g, 3.83 mmol) in CH_2Cl_2 (77 mL) and the reaction was stirred at room temperature for 2 h. DMSO (0.7 mL) was added to the reaction and the solution was stirred for 14 h. The reaction was filtered through a short SiO_2 plug rinsing with

hexanes/EtOAc (85:15) and the filtrate was concentrated under reduced pressure. The crude residue was purified via flash chromatography (SiO_2) eluting with hexanes/EtOAc (92:8) to afford 1.11 g (88%) of **2.12** as a pale yellow oil. ^{1}H NMR (500 MHz, 130 °C, DMSO-d_6) δ 7.39 – 7.35 (comp, 4 H), 7.34 – 7.29 (m, 1 H), 7.26 (ddd, *J* = 8.1, 2.2, 0.8 Hz, 1 H), 7.15 (d, *J* = 8.1 Hz, 1 H), 7.06 – 7.03 (m, 1 H), 6.50 – 6.45 (m, 1 H), 6.12 – 6.07 (m, 1 H), 5.44 (t, *J* = 9.2 Hz, 1 H), 5.18 (s, 2 H), 2.77 (s, 3 H), 2.58 – 2.53 (comp, 2 H). ^{13}C NMR (126 MHz, 130 °C, DMSO-d_6) δ 154.9, 136.4, 134.9, 132.3, 131.3, 127.6, 127.3, 127.0, 126.8, 126.7, 126.7, 125.0, 125.0, 66.0, 51.9, 29.4, 26.5. HRMS (ESI) *m/z* calcd for $C_{19}H_{18}ClNO_2$ $(M+Na)^+$, 350.0918; found 350.0922.

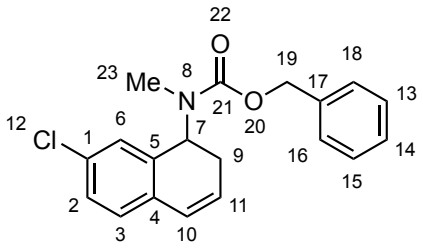

NMR Assignments (**2.12**). ^{1}H NMR (500 MHz, 130 °C, DMSO-d_6) δ 7.39 – 7.35 (comp, 4H, 13, 15, 16, 18), 7.34 – 7.29 (m, 1H, 14), 7.26 (ddd, *J* = 8.1, 2.2, 0.8 Hz, 1H, 2), 7.15 (d, *J* = 8.1 Hz, 1H, 3), 7.06 – 7.03 (m, 1H, 6), 6.50 – 6.45 (m, 1H, 10), 6.12 – 6.07 (m, 1H, 11), 5.44 (t, *J* = 9.2 Hz, 1H, 7), 5.18 (s, 2H, 19), 2.77 (s, 3H, 23), 2.58 – 2.53 (comp, 2H, 9). ^{13}C NMR (126 MHz, 130 °C, DMSO-d_6) δ 154.9 (21), 136.4 (1), 134.9 (4), 132.3 (5), 131.3 (17), 127.6 (16, 18), 127.3 (11), 127.0 (3), 126.8 (10), 126.7 (14), 126.7 (13, 15), 125.0 (2), 125.0 (6), 66.0 (19), 51.9 (7), 29.4 (9), 26.5 (23).

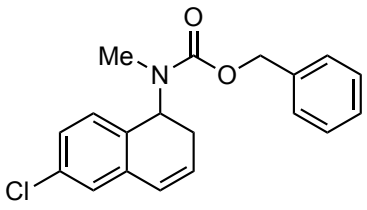

Benzyl (7-chloro-1,2-dihydronaphthalen-1-yl)(methyl)carbamate (2.13) (MDW-1-74). Grubbs second generation catalyst (20 mg, 0.024 mmol) was added to a solution of **2.11** (163 mg, 0.458 mmol) in CH_2Cl_2 (23 mL) and the reaction was stirred at room temperature for 2 h. The reaction was filtered through a short SiO_2 plug rinsing with CH_2Cl_2 and the filtrate was concentrated under reduced pressure. The crude residue was purified via flash chromatography (SiO_2) eluting with hexanes/EtOAc (92:82 to 90:10) to afford 134 mg (89%) of **2.13** as a pale yellow oil. ^{1}H NMR (500 MHz, 80 °C, DMSO-d_6) δ 7.40 – 7.30 (comp, 5H), 7.25 – 7.21 (comp, 2H), 7.06 (d, J = 7.9 Hz, 1H), 6.48 (dt, J = 9.7, 2.0 Hz, 1H), 6.17 – 6.12 (m, 1H), 5.43 (t, J = 9.2 Hz, 1H), 5.15 (s, 2H), 2.73 (s, 3H), 2.57 – 2.52 (comp, 2H). ^{13}C NMR (126 MHz, 80 °C, DMSO-d_6) δ 155.1, 136.6, 135.7, 131.9, 131.5, 128.3, 127.9, 127.3, 127.3, 127.0, 126.7, 125.5, 125.3, 66.2, 51.6, 29.4, 26.9.

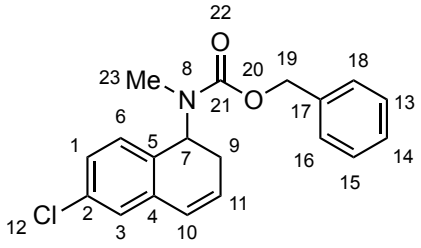

NMR Assignments (**2.13**). ^{1}H NMR (500 MHz, 80 °C, DMSO-d_6) δ 7.40 – 7.30 (comp, 5H, 13, 14, 15, 16, 18), 7.25 – 7.21 (comp, 2H, 1, 3), 7.06 (d, J = 7.9 Hz, 1H, 6), 6.48 (dt, J = 9.7, 2.0 Hz, 1H, 10), 6.17 – 6.12 (m, 1H, 11), 5.43 (t, J = 9.2 Hz, 1H, 7), 5.15 (s, 2H, 19), 2.73 (s, 3H, 23), 2.57 – 2.52 (comp, 2H, 9). ^{13}C NMR (126 MHz, 80 °C, DMSO-d_6) δ 155.1 (21), 136.6 (2), 135.7 (4), 131.9 (5), 131.5 (17), 128.3 (3), 127.9 (16, 18), 127.3 (11), 127.3 (14), 127.0 (13, 15), 126.7 (1), 125.5 (10), 125.3 (6), 66.2 (19), 51.6 (7), 29.4 (9), 26.9 (23).

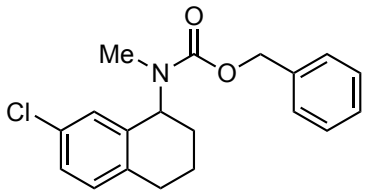

Benzyl (7-chloro-1,2,3,4-tetrahydronaphthalen-1-yl)(methyl)carbamate (**2.14**) (MDW-1-158). A solution of ethanol (9 mL) containing **2.12** (0.300 g, 0.915 mmol) and PtO_2 (10.3 mg, 0.0440 mmol) was sparged with H_2 gas for 5 min and then stirred under an atmosphere of H_2 (1 atm) for 2 h. The reaction was filtered through a pad of Celite and the filter cake was washed with CH_2Cl_2 (20 mL). The filtrate was concentrated under reduced pressure and the crude residue was purified via flash chromatography (SiO_2) eluting with hexanes/EtOAc (4:1) to afford 0.240 g (78%) of **2.14** as a colorless oil. ^{1}H NMR (500 MHz, DMSO-d_6) δ 7.39 – 7.29 (comp, 5H), 7.17 (dd, *J* = 8.2, 2.1 Hz, 1H), 7.13 (d, *J* = 8.2 Hz, 1H), 7.02 – 6.99 (m, 1H), 5.24 (dd, *J* = 9.8, 5.9 Hz, 1H), 5.18 (s, 2H), 2.76 – 2.70 (comp, 2H), 2.68 (s, 3H), 2.03 – 1.91 (comp, 2H), 1.89 – 1.82 (m, 1H), 1.79 – 1.70 (m, 1H). ^{13}C NMR (126 MHz, DMSO) δ 155.4, 137.2, 136.5, 130.1, 130.1, 127.6, 127.0, 126.6, 126.0, 125.3, 103.6, 65.9, 54.3, 29.5, 27.6, 26.2, 20.6. HRMS (ESI) *m/z* calcd for $C_{19}H_{20}ClNO_2$ $(M+Na)^+$, 352.1075; found 352.1079.

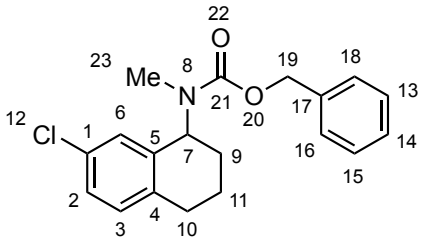

NMR Assignments (**2.14**). ^{1}H NMR (500 MHz, DMSO-d_6) δ 7.39 – 7.29 (comp, 5H, 13, 14, 15, 16, 18), 7.17 (dd, *J* = 8.2, 2.1 Hz, 1H, 2), 7.13 (d, *J* = 8.2 Hz, 1H, 3), 7.02 – 6.99 (m, 1H, 6), 5.24 (dd, *J* = 9.8, 5.9 Hz, 1H, 7), 5.18 (s, 2H, 19), 2.76 – 2.70 (comp, 2H, 10), 2.68 (s, 3H, 23), 2.03 – 1.91 (comp, 2H, 9, 11), 1.89 – 1.82 (m, 1H, 9), 1.79 –

1.70 (m, 1H, 11). ^{13}C NMR (126 MHz, DMSO) δ 155.4 (21), 137.2, 136.5, 130.1, 130.1, 127.6, 127.0, 126.6, 126.0 (14), 125.3 (6), 103.6, 65.9 (19), 54.3 (7), 29.5 (23), 27.6 (10), 26.2 (9), 20.6 (11).

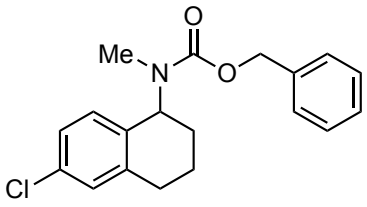

Benzyl (6-chloro-1,2,3,4-tetrahydronaphthalen-1-yl)(methyl)carbamate (**2.15**) (MDW-1-121). A solution of ethanol (20 mL) containing **2.13** (0.639 g, 1.95 mmol) and PtO_2 (22.1 mg, 0.0973 mmol) was sparged with H_2 gas for 5 min and then stirred under an atmosphere of H_2 (1 atm) for 2 h. The reaction was filtered through a pad of Celite and the filter cake was washed with CH_2Cl_2 (20 mL). The filtrate was concentrated under reduced pressure and the crude residue was purified via flash chromatography (SiO_2) eluting with hexanes/EtOAc (4:1) to afford 0.575 g (89%) of **2.15** as a colorless oil. ^{1}H NMR (500 MHz, 130 °C, DMSO-d_6) δ 7.40 – 7.29 (comp, 5H), 7.17 – 7.14 (comp, 2H), 7.04 – 7.00 (m, 1H), 5.26 – 5.21 (m, 1H), 5.17 (s, 2H), 2.81 – 2.68 (comp, 2H), 2.65 (s, 3H), 2.03 – 1.91 (comp, 2H), 1.89 – 1.70 (comp, 2H). ^{13}C NMR (126 MHz, 130 °C, DMSO-d_6) δ 155.4, 139.9, 136.5, 133.8, 130.7, 127.7, 127.7, 127.6, 126.9, 126.6, 125.2, 65.8, 54.0, 29.4, 28.0, 26.4, 20.5. HRMS (ESI) *m/z* calcd for $C_{19}H_{20}ClNO_2$ $(M+Na)^+$, 352.1075; found 352.1082.

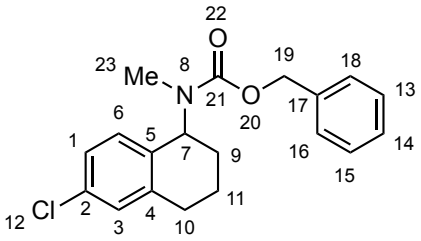

NMR Assignments (**2.15**). 1H NMR (500 MHz, 130 °C, DMSO-d_6) δ 7.40 – 7.29 (comp, 5H, 13, 14, 15, 16, 18), 7.17 – 7.14 (comp, 2H, 1, 3), 7.04 – 7.00 (m, 1H, 6), 5.26 – 5.21 (m, 1H, 7), 5.17 (s, 2H, 19), 2.81 – 2.68 (comp, 2H, 10), 2.65 (s, 3H, 23), 2.03 – 1.91 (comp, 2H, 9, 11), 1.89 – 1.70 (comp, 2H, 9, 11). ^{13}C NMR (126 MHz, 130 °C, DMSO-d_6) δ 155.4 (21), 139.9 (4), 136.5 (17), 133.8 (5), 130.7 (2), 127.7 (3), 127.7 (1), 127.6 (16, 18), 126.9 (14), 126.6 (13, 15), 125.2 (6), 65.8 (19), 54.0 (7), 29.4 (10), 28.0 (9), 26.4 (23), 20.5 (11).

Representative Procedure B: Buchwald-Hartwig amination using $Pd(OAc)_2$ and JohnPhos.

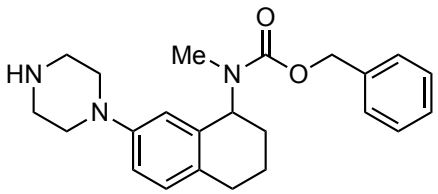

Benzyl methyl(7-(piperazin-1-yl)-1,2,3,4-tetrahydronaphthalen-1-yl)carbamate (**2.16**) (MDW-1-164). A sealable tube was charged with **2.14** (0.679 g, 2.06 mmol), NaO*t*-Bu (0.296 g, 3.09 mmol), and piperazine (0.887 g, 10.3 mmol). The tube was evacuated and backfilled with N_2 three times, whereupon degassed PhMe (4.1 mL) was added and the mixture was stirred for 5 min. A freshly prepared PhMe solution containing $Pd(OAc)_2$ (22 mg, 0.096 mmol) and JohnPhos (29 mg, 0.096 mmol) that had been stirred at room temperature for 30 min was added. The tube was sealed, and the reaction was stirred at 100 °C for 5 h. After cooling to room temperature, the mixture was filtered through Celite and the filter cake was washed with CH_2Cl_2 (20 mL). The filtrate was concentrated and the residue was dissolved in CH_2Cl_2 (20 mL), washed saturated aqueous $NaHCO_3$ (1 x 20 mL), and extracted with 1 N HCl (3 X 20 mL). The combined

acidic extracts were made basic with 6 N NaOH and extracted with CH_2Cl_2 (3 x 50 mL), after which the combined organic extracts were dried (Na_2SO_4) and concentrated. The crude residue was purified via flash chromatography (SiO_2) eluting with CH_2Cl_2/MeOH/Et_3N (100:0:1 to 100:4:1) to afford 0.439 g (56%) of **2.16** as an orange yellow oil. ^{1}H NMR (400 MHz, $CDCl_3$) (rotamers) δ 7.43 – 7.23 (comp, 5H), 6.97 (d, *J* = 8.4 Hz, 1H), 6.77 – 6.71 (m, 1H), 6.60 (dd, *J* = 10.8, 2.1 Hz, 1H), 5.51 – 5.31 (m, 1H), 5.31 – 5.09 (comp, 2H), 3.06 – 2.92 (comp, 8H), 2.73 – 2.59 (comp, 5H), 2.09 – 1.87 (comp, 3H), 1.83 – 1.64 (comp, 2H). ^{13}C NMR (101 MHz, $CDCl_3$) (rotamers) δ 157.1, 156.8, 150.4, 150.4, 137.1, 137.0, 135.7, 135.6, 130.0, 129.8, 129.8, 129.6, 128.5, 127.9, 127.8, 127.7, 115.6, 115.4, 114.5, 114.2, 67.0, 67.0, 55.5, 55.3, 50.7, 50.6, 46.1, 30.2, 29.6, 28.7, 28.6, 28.1, 27.6, 22.2, 22.1. HRMS (ESI) *m/z* calcd for $C_{24}H_{31}N_3O_2$ $(M+H)^+$, 380.233; found 380.2335.

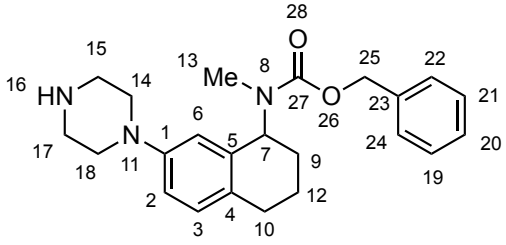

NMR Assignments (**2.16**). ^{1}H NMR (400 MHz, $CDCl_3$) rotamers δ 7.43 – 7.23 (comp, 5H, 19, 20, 21, 22, 24), 6.97 (d, *J* = 8.4 Hz, 1H, 3), 6.77 – 6.71 (m, 1H, 6), 6.60 (dd, *J* = 10.8, 2.1 Hz, 1H, 2), 5.51 – 5.31 (m, 1H, 7), 5.31 – 5.09 (comp, 2H, 25), 3.06 – 2.92 (comp, 8H, 14, 15, 17, 18), 2.73 – 2.59 (comp, 5H, 10, 13), 2.09 – 1.87 (comp, 3H, 9, 12, 16), 1.83 – 1.64 (comp, 2H, 9, 12). ^{13}C NMR (101 MHz, $CDCl_3$) rotamers δ 157.1 (27), 156.8 (27), 150.4 (1), 150.4 (1), 137.1 (5), 137.0 (5), 135.7 (23), 135.6 (23), 130.0 (4), 129.8 (3), 129.8 (3), 129.6 (4), 128.5 (19, 21), 127.9 (22, 24), 127.8 (22, 24), 127.7 (20), 115.6 (6), 115.4 (6), 114.5 (2), 114.2 (2), 67.0 (25), 67.0 (25), 55.5 (7), 55.3 (7),

50.7 (14, 18), 50.6 (14, 18), 46.1 (15, 17), 30.2 (13), 29.6 (13), 28.7 (10), 28.6 (10), 28.1 (9), 27.6 (9), 22.2 (12), 22.1 (12).

Representative Procedure C: Buchwald-Hartwig amination using $Pd_2(dba)_3$ and RuPhosPhos.

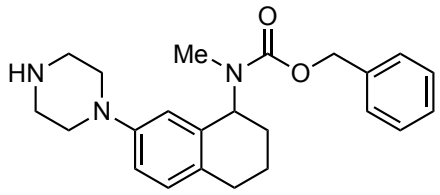

Benzyl methyl(7-(piperazin-1-yl)-1,2,3,4-tetrahydronaphthalen-1-yl)carbamate (**2.16**) (MDW-2-283). A sealable tube was charged with **2.29** (1.494 g, 3.949 mmol), NaO*t*-Bu (0.572 g, 5.95 mmol), and piperazine (1.708 g, 19.83 mmol). The tube was evacuated and backfilled with N_2 three times, whereupon degassed THF (22 mL) was added and the mixture was stirred at 50 °C for 10 min. A freshly prepared THF solution containing $Pd_2(dba)_3$ (73 mg, 0.080 mmol) and RuPhos (74 mg, 0.16 mmol) that had been stirred at 50 °C for 30 min was added. The tube was sealed, and the reaction was stirred at 70 °C for 6 h. After cooling to room temperature, the mixture was filtered through Celite and the filter cake was washed with CH_2Cl_2 (100 mL). The filtrate was concentrated and the residue was dissolved in CH_2Cl_2 (30 mL), washed with 1 N NaOH (3 x 30 mL), and brine (1 x 30 mL). The organic layer was dried (Na_2SO_4) and concentrated. The crude residue was purified via flash chromatography (SiO_2) eluting with CH_2Cl_2/MeOH/Et_3N (97:2:) to afford 1.365 g (91%) of **2.16** as an orange yellow oil. NMR is consistent with **2.16** Prepared using representative procedure A.

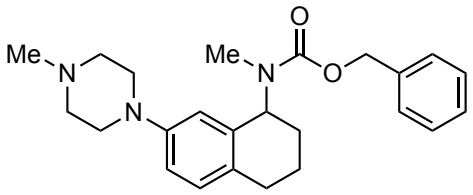

Benzyl methyl(7-(4-methylpiperazin-1-yl)-1,2,3,4-tetrahydronaphthalen-1-yl)carbamate (**2.17**) (MDW-4-233). Paraformaldehyde (64 mg, 2.1 mmol) and CH_3CO_2H (20 μL) were added to a solution of **2.16** (27 mg, 0.071 mmol) in DCE (1.4 mL) and the reaction was stirred for 20 h. Additional paraformaldehyde (64 mg, 2.1 mmol) was added and the reaction was stirred for 3 h until the starting material was consumed by TLC. The reaction was diluted with saturated aqueous $NaHCO_3$ (5 mL) and extracted with CH_2Cl_2 (3 x 10 mL). The combined organic extracts were dried (Na_2SO_4), and concentrated under reduced pressure. The crude residue was purified via flash chromatography (SiO_2) eluting with EtOAc/hexanes/Et_3N (70:29:1) to afford 15 mg (54%) of **2.17** as a colorless oil. ^1H NMR (400 MHz, $CDCl_3$) δ 7.45 – 7.28 (comp, 5H), 6.99 (d, *J* = 8.4 Hz, 1H), 6.76 (dt, *J* = 8.4, 2.9 Hz, 1H), 6.62 (dd, *J* = 9.9, 2.6 Hz, 1H), 5.50 – 5.31 (m, 1H), 5.31 – 5.10 (comp, 2H), 3.22 – 3.05 (comp, 4H), 2.75 – 2.56 (comp, 9H), 2.43 – 2.37 (comp, 2H), 2.07 – 1.91 (comp, 2H), 1.85 – 1.68 (comp, 2H). ^{13}C NMR (101 MHz, $CDCl_3$) δ 157.4, 157.1, 149.8, 149.7, 137.2, 137.1, 136.0, 135.9, 130.5, 130.0, 130.0, 128.6, 128.1, 127.9 127.9, 115.7, 115.4, 114.9,114.6, 67.3, 67.2, 55.7, 55.5, 55.1, 55.0, 49.3, 49.2, 46.0, 30.4, 29.8, 28.9, 28.8, 28.2, 27.7, 22.3, 22.2. HRMS (ESI) *m/z* calcd for $C_{24}H_{31}N_3O_2$ $(M+H)^+$, 394.2489; found 394.2495.

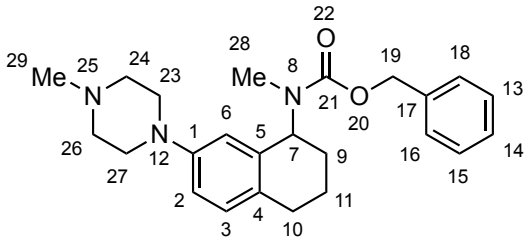

NMR Assignments (**2.17**) ^{1}H NMR (400 MHz, $CDCl_3$) δ 7.45 – 7.28 (comp, 5H, 13, 14, 15, 16, 18), 6.99 (d, *J* = 8.4 Hz, 1H, 3), 6.76 (dt, *J* = 8.4, 2.9 Hz, 1H, 6), 6.62 (dd, *J* = 9.9, 2.6 Hz, 1H, 2), 5.50 – 5.31 (m, 1H, 7), 5.31 – 5.10 (comp, 2H, 19), 3.22 – 3.05 (comp, 4H, 24, 26), 2.75 – 2.56 (comp, 9H, 10, 23, 27, 28), 2.43 – 2.37 (comp, 2H, 29), 2.07 – 1.91 (comp, 2H, 9, 11), 1.85 – 1.68 (comp, 2H, 9, 11). ^{13}C NMR (101 MHz, $CDCl_3$) δ 157.4 and 157.1 (21), 149.8 and 149.7 (1), 137.2 and 137.1 (5), 136.0 and 135.9 (17), 130.5 (4), 130.0 and 130.0 (3), 128.6 (13, 15), 128.1 (14), 127.9, 127.9 (16, 18), 115.7 and 115.4 (6), 114.9 and 114.6 (2), 67.3 and 67.2 (19), 55.7, and 55.5 (7), 55.1 and 55.0 (23, 27), 49.3 and 49.2 (24, 26), 46.0 (29), 30.4 and 29.8 (28), 28.9 and 28.8 (10), 28.2 and 27.7 (9), 22.3 and 22.2 (11).

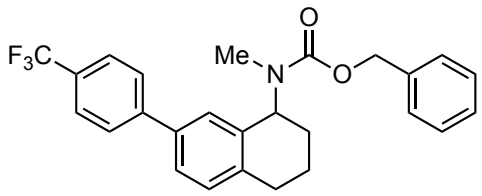

Benzyl methyl(7-(4-(trifluoromethyl)phenyl)-1,2,3,4-tetrahydronaphthalen-1-yl)carbamate (**2.19**) (MDW-2-133). A sealable tube was charged with **2.14** (0.220 g, 0.667 mmol), 4-trifluoromethylphenylboronic acid (0.254 g, 1.34 mmol), cesium carbonate (0.435 g, 1.34 mmol), and Pd(*t*-$Bu_3P)_2$ (0.17 g, 0.033 mmol). The flask was evacuated and backfilled with N_2 three times, whereupon degassed 1,4-dioxane (1.7 mL) was added. The tube was sealed and the reaction was stirred at 100 °C for 6 h. After cooling to room temperature, the reaction was diluted with CH_2Cl_2 (20 mL) and washed with1 N NaOH (1 x 20 mL). The organic layer was separated and the aqueous layer was extracted with CH_2Cl_2 (2 x 20 mL). The combined organic extracts were dried (Na_2SO_4) and concentrated under reduced pressure. The crude residue was purified via flash chromatography (SiO_2) eluting with hexanes/EtOAc (9:1) affording 0.242 g (82%) of

2.19 as a pale yellow oil. 1H NMR (400 MHz, CDCl3)) δ 7.76 – 7.57 (comp, 4 H), 7.52 – 7.31 (comp, 7 H), 7.25 (d, J = 8.0 Hz, 1 H), 5.72 – 5.19 (comp, 3 H), 2.96 – 2.71 (comp, 5 H), 2.22 – 2.03 (comp, 2 H), 1.99 – 1.80 (comp, 2 H). ^{13}C NMR (101 MHz, $CDCl_3$) rotamers δ 157.3, 156.9, 144.6, 144.3, 138.8, 138.5, 137.8, 137.7, 137.0, 137.0, 136.2, 136.1, 130.0, 130.0, 129.4, 129.3, 129.0, 129.0, 128.5, 128.5, 128.0, 127.9, 127.8, 127.8, 127.3, 127.2, 125.8, 125.7, 125.7, 125.7, 125.6, 123.0, 67.3, 55.5, 55.3, 30.3, 29.7, 29.3, 29.3, 28.0, 27.5, 22.1, 21.9. HRMS (ESI) m/z calcd for $C_{26}H_{24}F_3NO_2$ $(M+H)^+$, 440.1832; found 440.1849.

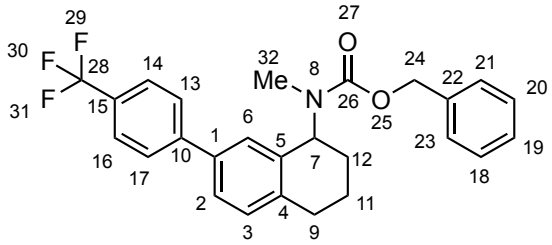

NMR Assignments (**2.19**). ^{1}H NMR (400 MHz, $CDCl_3$) rotamers δ 7.76 – 7.57 (comp, 4H, 13, 14, 16, 17), 7.52 – 7.31 (comp, 7H, 2, 6, 18, 19, 20, 21, 23), 7.25 (d, *J* = 8.0 Hz, 1H, 3), 5.72 – 5.19 (comp, 3H, 7, 24), 2.96 – 2.71 (comp, 5H, 9, 32), 2.22 – 2.03 (comp, 2H, 11, 12), 1.99 – 1.80 (comp, 2H, 11, 12). ^{13}C NMR (101 MHz, $CDCl_3$) rotamers δ 157.3 and 156.9 (26), 144.6 and 144.3 (10), 138.8 and 138.5 (1), 137.8 and 137.7 (5), 137.0 and 137.0 (4), 136.2 and 136.1 (22), 130.0 and 130.0 (3), 129.2 (d, *J* = 32.4, rotamers) (15), 128.5 and 128.5 (18, 20), 128.0 (21, 23), 127.9 (19), 127.8 and 127.8 (6), 127.3 and 127.2 (13, 17), 125.8 (2), 125.7 ($J_{C\text{-}F}$ = comp, rotamers) (14, 16), 123.0 (28), 67.3 (24), 55.5 and 55.3 (7), 30.3 and 29.7 (32), 29.3 and 29.3 (9), 28.0 and 27.5 (12), 22.1 and 21.9 (11).

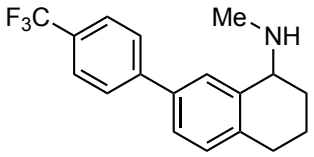

***N*-Methyl-7-(4-(trifluoromethyl)phenyl)-1,2,3,4-tetrahydronaphthalen-1-amine hydrate** (**2.20**) (MDW-1-275). A solution of ethanol (6 mL) containing **2.19** (0.130 g, 0.296 mmol) and 10% Pd/C (47 mg) was sparged with H_2 gas for 5 min and then stirred under an atmosphere of H_2 (1 atm) for 14 h. The reaction was filtered through a pad of Celite and the filter cake was washed with CH_2Cl_2 (20 mL) to provide 0.085 g (94%) of **2.20** as a colorless oil that was of sufficient purity to use without additional purification. ^{1}H NMR (400 MHz, $CDCl_3$) δ 8.04 (s, 1H), 7.97 (d, *J* = 1.9 Hz, 1H), 7.80 (d, *J* = 8.1 Hz, 2H), 7.60 (d, *J* = 8.1 Hz, 2H), 7.43 (dd, *J* = 8.0, 1.8 Hz, 1H), 7.15 (d, *J* = 8.0 Hz, 1H), 4.23 (t, *J* = 5.1 Hz, 1H), 2.93 – 2.64 (m, 2H), 2.48 (s, 3H), 2.20 – 2.03 (m, 3H), 1.84 – 1.68 (m, 1H).

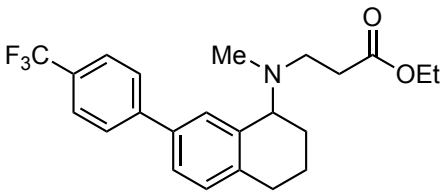

Ethyl 3-(methyl(7-(4-(trifluoromethyl)phenyl)-1,2,3,4-tetrahydronaphthalen-1-yl)amino)propanoate (**2.22**) (MDW-2-34). A solution of crude **2.20** (65 mg, 0.21 mmol) and ethyl acrylate (0.21 g, 0.23 mL, 2.1 mmol) in CH_2Cl_2 (1.1 mL) was stirred at 40 °C for 21 h. The reaction was concentrated and the crude residue was purified via flash chromatography (SiO_2) eluting with hexanes/Et_3N (99:1) affording 64 mg (74%) of **2.22** as a colorless oil. ^{1}H NMR (400 MHz, $CDCl_3$) δ 7.90 (dd, *J* = 2.3, 1.0 Hz, 1H), 7.74 – 7.63 (comp, 4H), 7.36 (dd, *J* = 7.9, 2.2 Hz, 1H), 7.15 (d, *J* = 7.9 Hz, 1H), 4.08 (qd, *J* = 7.2, 1.3 Hz, 2H), 3.97 – 3.89 (m, 1H), 2.86 (td, *J* = 7.1, 3.6 Hz, 2H), 2.83 – 2.74 (comp,

2H), 2.59 – 2.44 (comp, 2H), 2.24 (s, 3H), 2.09 – 1.95 (comp, 2H), 1.76 – 1.65 (comp, 2H), 1.18 (t, J = 7.1 Hz, 3H). ^{13}C NMR (126 MHz, $CDCl_3$) δ 173.0, 145.2, 139.5, 138.6, 137.3, 129.5, 129.0 (d, J = 32.5), 127.4, 127.0, 125.7 (q, J = 3.8, 14, 16), 125.1, 123.5, 62.7, 60.4, 49.7, 37.0, 34.5, 29.8, 22.2, 21.0, 14.4. HRMS (ESI) m/z calcd for $C_{23}H_{26}F_3NO_2$ (M+H)+, 406.1988; found 406.1991.

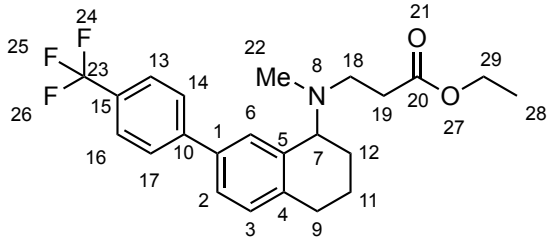

NMR Assignments (**2.22**). ^{1}H NMR (400 MHz, $CDCl_2$) δ 7.90 (dd, J = 2.3, 1.0 Hz, 1H, 6), 7.74 – 7.63 (comp, 4H, 13, 14, 16, 17), 7.36 (dd, J = 7.9, 2.2 Hz, 1H, 2), 7.15 (d, J = 7.9 Hz, 1H, 3), 4.08 (qd, J = 7.2, 1.3 Hz, 2H, 29), 3.97 – 3.89 (m, 1H, 7), 2.86 (td, J = 7.1, 3.6 Hz, 2H, 18), 2.83 – 2.74 (comp, 2H, 9), 2.59 – 2.44 (comp, 2H, 19), 2.24 (s, 3H, 22), 2.09 – 1.95 (comp, 2H, 11, 12), 1.76 – 1.65 (comp, 2H, 11, 12), 1.18 (t, J = 7.1 Hz, 3H, 28). ^{13}C NMR (126 MHz, $CDCl_3$) δ 173.0 (20), 145.2 (10), 139.5 (1), 138.6 (5), 137.3 (4), 129.5 (3), 129.0 (d, J = 32.5) (15), 127.4 (13, 17), 127.0 (6), 125.7 (q, J = 3.8) (14, 16), 125.1 (2), 123.5 (23), 62.7 (7), 60.4 (29), 49.7 (18), 37.0 (22), 34.5 (19), 29.8 (9), 22.2 (12), 21.0 (11), 14.4 (28).

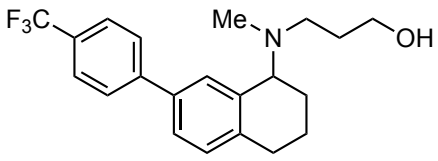

3-(Methyl(7-(4-(trifluoromethyl)phenyl)-1,2,3,4-tetrahydronaphthalen-1-yl)amino)propan-1-ol (**2.23**) (MDW-2-237). $LiBH_4$ (4 mg, 0.2 mmol) was added to a

solution of **2.22** (29 mg, 0.702 mmol) in THF (0.7 mL) cooled to 0 °C. The reaction was stirred at 0 °C for 1 h and the cooling bath was removed. The reaction was stirred for 24 h at room temperature and quenched with saturated aqueous NH_4Cl (1 mL). The aqueous layer was extracted with CH_2Cl_2 (3 x 5 mL), and the combined organic extracts were dried (Na_2SO_2) and concentrated under reduced pressure. The crude residue was purified via flash chromatography (SiO_2) eluting with hexanes/EtOAc/Et_3N (79:20:1) affording 12.8 mg (50%) of **2.23** as a colorless oil. ^{1}H NMR (400 MHz, $CDCl_3$) δ 7.85 – 7.81 (m, 1H), 7.74 (d, *J* = 8.4 Hz, 2H), 7.67 (d, *J* = 8.2 Hz, 3H), 7.41 (dd, *J* = 7.9, 2.0 Hz, 1H), 7.18 (d, *J* = 7.9 Hz, 1H), 4.15 – 4.07 (m, 1H), 3.87 – 3.71 (comp, 2H), 2.82 – 2.74 (comp, 4H), 2.34 (s, 3H), 2.07 – 1.98 (comp, 2H), 1.87 – 1.66 (comp, 5H). ^{13}C NMR (126 MHz, $CDCl_3$) δ 144.6, 139.1, 138.0, 137.6, 129.8, 129.2 (d, *J* = 32.3), 127.2 (13, 17), 127.1 (6), 125.9 (q, *J* = 3.9), 125.4, 124.5 (d, *J* = 271.4), 64.3, 63.1, 53.9, 37.1, 29.9, 28.1, 21.9, 20.7. HRMS (ESI) m/z calcd for $C_{21}H_{24}F_3NO$ (M+H)+, 364.1883; found 364.1888.

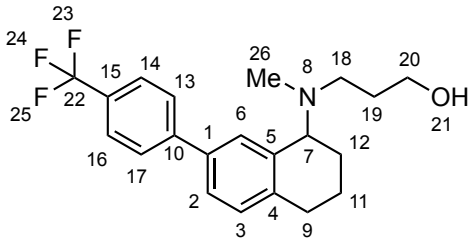

NMR Assignments (**2.23**). ^{1}H NMR (400 MHz, $CDCl_3$) δ 7.85 – 7.81 (m, 1H, 6), 7.74 (d, *J* = 8.4 Hz, 2H, 13, 17), 7.67 (d, *J* = 8.2 Hz, 3H, 14, 16), 7.41 (dd, *J* = 7.9, 2.0 Hz, 1H, 2), 7.18 (d, *J* = 7.9 Hz, 1H, 3), 4.15 – 4.07 (m, 1H, 7), 3.87 – 3.71 (comp, 2H, 20), 2.82 – 2.74 (comp, 4H, 9, 18), 2.34 (s, 3H, 26), 2.07 – 1.98 (comp, 2H, 11, 12), 1.87 – 1.66 (comp, 5H, 11, 12, 19, 21). ^{13}C NMR (126 MHz, $CDCl_3$) δ 144.6 (10), 139.1 (1), 138.0 (5), 137.6 (4), 129.8 (3), 129.2 (d, *J* = 32.3) (15), 127.2 (13, 17), 127.1 (6), 125.9

(q, J = 3.9) (14, 16), 125.4 (2), 124.5 (d, J = 271.4) (22), 64.3 (20), 63.1 (7), 53.9 (18), 37.1 (26), 29.9 (9), 28.1 (19), 21.9 (12), 20.7 (11).

Representative Procedure D: Reduction amination using Ti(O*i*-Pr)$_4$ and an *N*-alkylammonium salt.

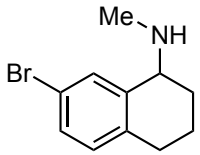

7-Bromo-*N*-methyl-1,2,3,4-tetrahydronaphthalen-1-amine (**2.28**) (MDW-2-260). TiO(*i*-Pr)$_4$ (9.6 g, 10 mL, 34 mmol) and Et_3N (6.8 g, 9.3 mL, 67 mmol) were sequentially added to a solution of 7-bromotetralone (3.00 g, 13.3 mmol) and $MeNH_3Cl$ (4.50 g, 66.6 mmol) in EtOH (27 mL) and the reaction was stirred at room temperature for 17 h. The reaction was cooled to 0 °C and $NaBH_4$ (0.506, 13.4 mmol) was added in a single portion. The reaction was stirred for 30 min and the cooling bath was removed. The solution was stirred for 4 h at room temperature and poured into 2 M aq. NH_4OH (20 mL). Celite was added to the mixture and it was filtered, washing with CH_2Cl_2 (100 mL). The filtrate was concentrated under reduced pressure to remove volatile organics and the mixture obtained was diluted with CH_2Cl_2 (20 mL). The organic layer was separated and the aqueous layer was extracted with CH_2Cl_2 (2 x 10 mL). The combined organic extracts were washed with saturated aqueous NH_4Cl (2 x 30 mL) and extracted with 1 N HCl (3 x 40 mL). The combined acidic extracts were made basic with 6 N NaOH and extracted with CH_2Cl_2 (3 x 50 mL). The combined organic extracts were dried (Na_2SO_4) and concentrated under reduced pressure. The crude residue was purified via flash chromatography (SiO_2) eluting with hexanes/EtOAc/Et_3N (94:5:1 to 79:20:1) affording 2.15 g (67%) of **2.28** as a yellow oil. ^{1}H NMR (400 MHz, $CDCl_3$) δ 7.50 (d, J = 2.2 Hz, 1H), 7.27 – 7.23 (m, 1H), 6.95 (dd, J = 8.2, 1.0 Hz, 1H), 3.62 (t, J = 4.9 Hz, 1H), 2.79 –

2.61 (comp, 2H), 2.49 (s, 3H), 1.98 – 1.82 (comp, 3H), 1.79 – 1.67 (m, 1H), 1.08 (brs, 1H). ^{13}C NMR (126 MHz, $CDCl_3$) δ 141.5, 136.4, 131.7, 130.9, 129.8, 119.3, 57.0, 34.1, 29.0, 27.5, 18.9. HRMS (ESI) m/z calcd for $C_{11}H_{14}BrN$ (M+H)+, 240.0382; found 240.0383.

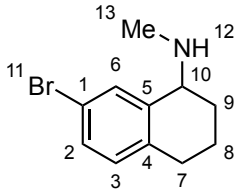

NMR Assignments (**2.28**). ^{1}H NMR (400 MHz, $CDCl_3$) δ 7.50 (d, *J* = 2.2 Hz, 1H, 6), 7.27 – 7.23 (m, 1H, 2), 6.95 (dd, *J* = 8.2, 1.0 Hz, 1H, 3), 3.62 (t, *J* = 4.9 Hz, 1H, 10), 2.79 – 2.61 (comp, 2H, 7), 2.49 (s, 3H, 13), 1.98 – 1.82 (comp, 3H, 8, 9), 1.79 – 1.67 (m, 1H, 8), 1.08 (brs, 1H, 12). ^{13}C NMR (126 MHz, $CDCl_3$) δ 141.5 (5), 136.4 (4), 131.7 (6), 130.9 (3), 129.8 (2), 119.3 (1), 57.0 (10), 34.1 (13), 29.0 (7), 27.5, 18.9 (9).

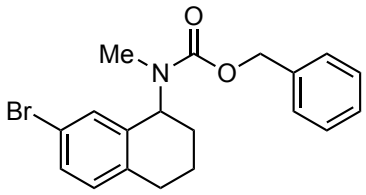

Benzyl (7-bromo-1,2,3,4-tetrahydronaphthalen-1-yl)(methyl)carbamate (**2.29**) (MDW-2-132). Prepared from **2.28** (1.267 g, 5.274mmol) and CbzCl according to representative procedure A. The crude residue was purified via flash chromatography (SiO_2) eluting with hexanes/EtOAc (9:1) to afford 1.954 g (98%) of **2.29** as a white waxy solid. ^{1}H NMR (400 MHz, $CDCl_3$) rotamers δ 7.47 – 7.29 (comp, 5H), 7.28 – 7.23 (comp, 2H), 6.99 – 6.93 (m, 1H), 5.54 – 5.30 (m, 1H), 5.29 – 5.19 (comp, 2H), 2.78 – 2.60 (comp, 5H), 2.09 – 1.94 (comp, 2H), 1.85 – 1.69 (comp, 2H). ^{13}C NMR (101 MHz, $CDCl_3$) rotamers δ 157.0, 156.5, 137.7, 137.6, 137.3, 137.0, 136.8, 136.7, 130.9, 129.9,

129.9, 129.7, 129.6, 128.5, 127.9, 127.7, 119.9, 119.8, 55.1, 54.9, 30.3, 29.5, 28.9, 28.9, 27.5, 27.0, 21.8, 21.7. HRMS (ESI) *m/z* calcd for $C_{18}H_{20}BrNO_2$ $(M+Na)^+$, 396.0570; found 396.0578.

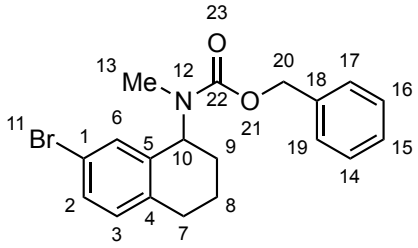

NMR Assignments (**2.29**). ^{1}H NMR (400 MHz, $CDCl_3$) rotamers δ 7.47 – 7.29 (comp, 5H, 14, 15, 16, 17, 19), 7.28 – 7.23 (comp, 2H, 2, 6), 6.99 – 6.93 (m, 1H, 3), 5.54 – 5.30 (m, 1H, 10), 5.29 – 5.19 (comp, 2H, 20), 2.78 – 2.60 (comp, 5H, 7, 13), 2.09 – 1.94 (comp, 2H, 8, 9), 1.85 – 1.69 (comp, 2H, 8, 9). ^{13}C NMR (101 MHz, $CDCl_3$) rotamers δ 157.0 and 156.5 (22), 137.7 and 137.6 (5), 137.3 and 137.0 (18), 136.8 and 136.7 (4), 130.9 (6), 129.9 and 129.9 (1), 129.7 and 129.6 (3), 128.5 (14, 16), 127.9 (15), 127.7 (17, 19), 119.9 and 119.8 (2), 55.1 and 54.9 (10), 30.3 and 29.5 (7), 28.9 and 28.9 (13), 27.5 and 27.0 (9), 21.8 and 21.7 (8).

Representative Procedure E: Reductive amination of the piperazine nitrogen atom with an aldehyde.

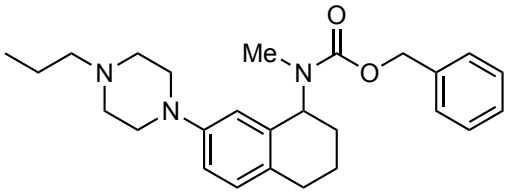

Benzyl methyl(7-(4-propylpiperazin-1-yl)-1,2,3,4-tetrahydronaphthalen-1-yl)carbamate (**2.31**) (MDW-2-286). A solution of **2.16** (0.454 g, 1.20 mmol), $Na(OAc)_3BH$ (0.507 g, 2.39 mmol), and propionaldehyde (81 mg, 0.10 mL, 1.4 mmol) in

DCE (12 mL) were stirred for 1 h at room temperature. The reaction was diluted with saturated aqueous $NaHCO_3$ (5 mL) and extracted with CH_2Cl_2 (3 x 5 mL). The combined organic extracts were washed with brine (1 x 10 mL), dried (Na_2SO_4), and concentrated under reduced pressure. The combined organic extracts were dried (Na_2SO_4) and concentrated under reduced pressure. The crude residue was purified via flash chromatography (SiO_2) eluting with hexanes/EtOAc/Et_3N (84:15:1) affording 0.404 g (80%) of **2.31** as a colorless oil. ^{1}H NMR (500 MHz, $CDCl_3$) rotamers δ 7.46 – 7.28 (comp, 5H), 6.99 (d, J = 8.4 Hz, 1H), 6.82 – 6.74 (m, 1H), 6.62 (dd, J = 12.3, 2.6 Hz, 1H), 5.51 – 5.32 (m, 1H), 5.32 – 5.12 (comp, 2H), 3.16 – 3.03 (comp, 4H), 2.76 – 2.62 (comp, 4H), 2.62 – 2.54 (comp, 4H), 2.39 – 2.32 (comp, 2H), 2.07 – 1.91 (comp, 2H), 1.84 – 1.70 (comp, 2H), 1.61 – 1.50 (comp, 2H), 0.93 (t, J = 7.4 Hz, 3H). ^{13}C NMR (126 MHz, $CDCl_3$) δ 157.3, 157.1, 150.1, 150.1, 137.2, 137.1, 135.9, 135.8, 130.2, 130.0, 129.9, 129.7, 128.6, 128.0, 127.9, 127.9, 115.7, 115.4, 114.7, 114.3, 67.2, 67.2, 60.9, 55.7, 55.5, 53.4, 53.3, 49.7, 49.5, 30.3, 29.8, 28.8, 28.7, 28.2, 27.7, 22.3, 22.2, 20.2, 12.1. HRMS (ESI) *m/z* calcd for $C_{26}H_{35}N_3O_2$ $(M+H)^+$, 422.2802; found 422.2808.

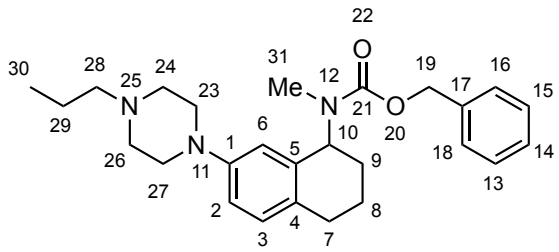

NMR Assignments (**2.31**). ^{1}H NMR (500 MHz, $CDCl_3$) rotamers δ 7.46 – 7.28 (comp, 5H, 13, 14, 15, 16, 18), 6.99 (d, J = 8.4 Hz, 1H, 3), 6.82 – 6.74 (m, 1H, 2), 6.62 (dd, J = 12.3, 2.6 Hz, 1H, 6), 5.51 – 5.32 (m, 1H, 10), 5.32 – 5.12 (comp, 2H, 19), 3.16 – 3.03 (comp, 4H, 23, 27), 2.76 – 2.62 (comp, 4H, 7, 31), 2.62 – 2.54 (comp, 4H, 24, 26), 2.39 – 2.32 (comp, 2H, 28), 2.07 – 1.91 (comp, 2H, 8, 9), 1.84 – 1.70 (comp, 2H, 8, 9),

1.61 – 1.50 (comp, 2H, 29), 0.93 (t, J = 7.4 Hz, 3H, 30). ^{13}C NMR (126 MHz, $CDCl_3$) rotamers δ 157.3 and 157.1 (21), 150.1 and 150.1 (1), 137.2 and 137.1 (5), 135.9 and 135.8 (17), 130.2 and 130.0 (4), 129.9 and 129.7 (3), 128.6 (13, 15), 128.0 (14), 127.9 and 127.9 (16, 18), 115.7 and 115.4 (2), 114.7 and 114.3 (6), 67.2 and 67.2 (19), 60.9 (28), 55.7 and 55.5 (10), 53.4 and 53.3 (24, 26), 49.7 and 49.5 (23, 27), 30.3 and 29.8 (31), 28.8 and 28.7 (7), 28.2 and 27.7 (9), 22.3 and 22.2 (8), 20.2 (29), 12.1 (30).

Representative Procedure F: Reductive amination of the piperazine nitrogen atom with ketone.

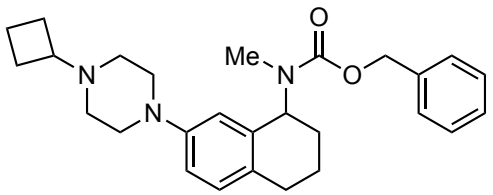

Benzyl (7-(4-cyclobutylpiperazin-1-yl)-1,2,3,4-tetrahydronaphthalen-1-yl)(methyl)carbamate (**2.33**) (MDW-1-162). A solution of **2.16** (25 mg 0.066 mmol), $Na(OAc)_3BH$ (28 mg, 0.13 mmol), cyclobutanone (23 mg, 25 μL, 0.33 mmol), and CH_3CO_2H (8 mg, 8 μL, 0.1 mmol) in DCE (0.7 mL) were stirred for 6 h at room temperature. The reaction was diluted with saturated aqueous $NaHCO_3$ (5 mL) and extracted with CH_2Cl_2 (3 x 5 mL). The combined organic extracts were washed with brine (1 x 10 mL), dried (Na_2SO_4), and concentrated under reduced pressure. The crude residue was purified via flash chromatography (SiO_2) eluting with hexanes/EtOAc/Et_3N (74:25:1) affording 25 mg (89%) of **2.33** as a pale yellow oil. ^{1}H NMR (499 MHz, $CDCl_3$) rotamers δ 7.43 – 7.28 (comp, 5H), 6.98 (d, J = 8.2 Hz, 1H), 6.80 – 6.74 (m, 1H), 6.62 (dd, J = 8.3, 2.2 Hz, 1H), 5.50 – 5.31 (m, 1H), 5.30 – 5.12 (comp, 2H), 3.15 – 3.05 (comp, 4H), 2.84 – 2.61 (comp, 6H), 2.51 – 2.42 (comp, 4H), 2.11 – 1.89 (comp, 6H),

1.80 – 1.68 (comp, 4H). ^{13}C NMR (126 MHz, $CDCl_3$) rotamers δ 157.3, 157.1, 150.1, 137.3, 137.1, 135.9, 135.8, 130.3, 130.0, 129.9, 128.6, 128.0, 127.9, 115.9, 115.5, 114.8, 114.5, 67.3, 67.2, 60.4, 55.7, 55.5, 49.5, 49.5, 49.3, 30.4, 29.8, 29.8, 28.9, 28.8, 28.2, 27.8, 27.1, 22.3, 22.2, 14.5. HRMS (ESI) *m/z* calcd for $C_{27}H_{35}N_3O_2$ $(M+H)^+$, 434.2802; found 438.2819.

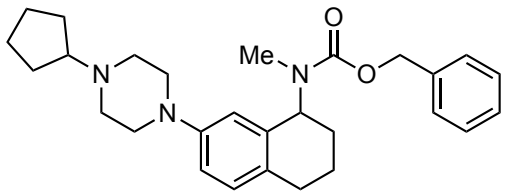

Benzyl (7-(4-cyclopentylpiperazin-1-yl)-1,2,3,4-tetrahydronaphthalen-1-yl)(methyl)carbamate (**2.34**) (MDW-2-235). Prepared from **2.16** (28 mg 0.074 mmol) and cyclopentanone according to representative procedure F. The crude residue was purified via flash chromatography (SiO_2) eluting with hexanes/EtOAc/Et_3N (74:25:1) to afford 26 mg (79%) of **2.34** as a colorless oil. ^{1}H NMR (499 MHz, $CDCl_3$) rotamers δ 7.44 – 7.27 (comp, 5H), 6.99 (d, *J* = 8.3 Hz, 1H), 6.79 – 6.74 (m, 1H), 6.62 (dd, *J* = 7.7, 2.5 Hz, 1H), 5.49 – 5.32 (m, 1H), 5.28 – 5.11 (comp, 2H), 3.16 – 3.05 (comp, 4H), 2.72 – 2.60 (comp, 9H), 2.55 (t, *J* = 8.3 Hz, 1H), 2.05 – 1.88 (comp, 4H), 1.81 – 1.68 (comp, 4H), 1.63 – 1.53 (comp, 2H), 1.52 – 1.41 (comp, 2H). ^{13}C NMR (126 MHz, $CDCl_3$) rotamers δ 157.3, 157.0, 150.0, 137.2, 137.1, 135.9, 135.8, 130.3, 130.0, 129.9, 129.8, 128.6, 128.0, 127.9, 127.9, 115.7, 115.4, 114.7, 114.4, 67.6, 67.2, 67.2, 55.7, 55.5, 52.4, 49.6, 49.4, 30.5, 30.3, 29.8, 28.8, 28.8, 28.2, 27.7, 24.3, 22.3, 22.2. HRMS (ESI) *m/z* calcd for $C_{28}H_{37}N_3O_2$ $(M+H)^+$, 448.2959; found 448.2962.

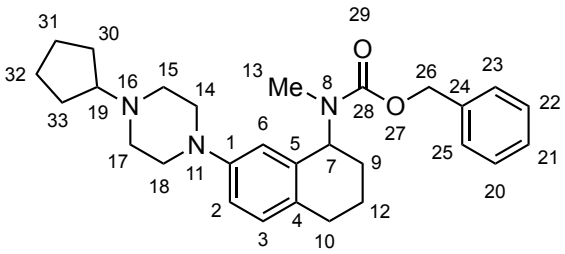

NMR Assignments (**2.34**). ^{1}H NMR (499 MHz, $CDCl_3$) rotamers δ 7.44 – 7.27 (comp, 5H, 20, 21, 22, 23, 25), 6.99 (d, *J* = 8.3 Hz, 1H, 3), 6.79 – 6.74 (m, 1H, 2), 6.62 (dd, *J* = 7.7, 2.5 Hz, 1H, 6), 5.49 – 5.32 (m, 1H, 7), 5.28 – 5.11 (comp, 2H, 26), 3.16 – 3.05 (comp, 4H, 14, 18), 2.72 – 2.60 (comp, 9H, 10, 13, 15, 17), 2.55 (t, *J* = 8.3 Hz, 1H, 19), 2.05 – 1.88 (comp, 4H, 9, 12, 31, 32), 1.81 – 1.68 (comp, 4H, 9, 12, 30, 33), 1.63 – 1.53 (comp, 2H, 30, 33), 1.52 – 1.41 (comp, 2H, 31, 32). ^{13}C NMR (126 MHz, $CDCl_3$) rotamers δ 157.3 (28), 157.0 (28), 150.0 (1), 137.2 (5), 137.1 (5), 135.9 (24), 135.8 (24), 130.3 (4), 130.0 (3), 129.9 (3), 129.8 (4), 128.6 (20, 22), 128.0 (21), 127.9 (23, 25), 127.9 (23, 25), 115.7 (2), 115.4 (2), 114.7 (6), 114.4 (6), 67.6 (19), 67.2 (26), 67.2 (26), 55.7 (7), 55.5 (7), 52.4 (15, 17), 49.6 (14), 49.4 (14, 18), 30.5 (30, 33), 30.3 (13), 29.8 (13), 28.8 (10), 28.8 (10), 28.2 (9), 27.7 (9), 24.3 (31, 32), 22.3 (12), 22.2 (12).

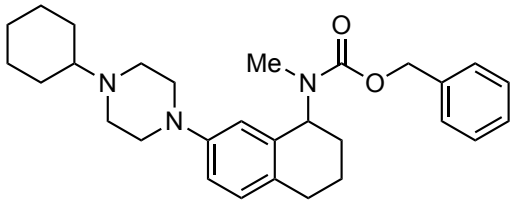

Benzyl (7-(4-cyclohexylpiperazin-1-yl)-1,2,3,4-tetrahydronaphthalen-1-yl)(methyl)carbamate (**2.35**) (MDW-1-205). Prepared from **2.16** (30 mg 0.079 mmol) and cyclohexanone according to representative procedure F. The crude residue was purified via flash chromatography (SiO_2) eluting with hexanes/EtOAc/Et_3N (77:22:1) to afford 25 mg (69%) of **2.35** as a pale yellow oil. ^{1}H NMR (499 MHz, $CDCl_3$) rotamers δ

7.46 – 7.27 (comp, 5H), 6.98 (d, J = 8.4 Hz, 1H), 6.81 – 6.75 (m, 1H), 6.62 (dd, J = 11.3, 2.5 Hz, 1H), 5.50 – 5.32 (m, 1H), 5.31 – 5.10 (comp, 2H), 3.15 – 3.03 (comp, 4H), 2.76 – 2.60 (comp, 9H), 2.34 – 2.25 (m, 1H), 2.07 – 1.89 (comp, 4H), 1.85 – 1.69 (comp, 4H), 1.68 – 1.61 (m, 1H), 1.30 – 1.21 (comp, 4H), 1.18 – 1.09 (m, 1H). ^{13}C NMR (126 MHz, $CDCl_3$) rotamers δ 157.3, 157.1, 150.2, 137.3, 137.1, 135.9, 135.8, 130.2, 129.9, 129.9, 129.6, 128.6, 128.0, 127.9, 115.8, 115.5, 114.7, 114.3, 67.2, 67.2, 63.6, 55.7, 55.5, 50.2, 50.0, 49.1, 49.1, 30.3, 29.8, 29.1, 28.9, 28.8, 28.2, 27.8, 26.4, 26.0, 22.4, 22.2. HRMS (ESI) *m/z* calcd for $C_{29}H_{39}N_3O_2$ $(M+Na)^+$, 484.2934; found 484.2942.

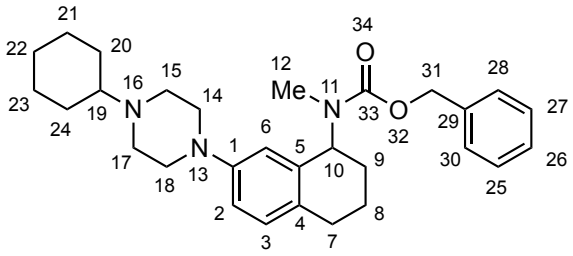

NMR Assignments (**2.35**). ^{1}H NMR (499 MHz, $CDCl_3$) rotamers δ 7.46 – 7.27 (comp, 5H, 25, 26, 27, 28, 30), 6.98 (d, J = 8.4 Hz, 1H, 3), 6.81 – 6.75 (m, 1H, 6), 6.62 (dd, J = 11.3, 2.5 Hz, 1H, 2), 5.50 – 5.32 (m, 1H, 10), 5.31 – 5.10 (comp, 2H, 31), 3.15 – 3.03 (comp, 4H, 14, 18), 2.76 – 2.60 (comp, 9H, 7, 12, 15, 17), 2.34 – 2.25 (m, 1H, 19), 2.07 – 1.89 (comp, 4H, 8, 9, 20, 24), 1.85 – 1.69 (comp, 4H, 8, 9, 21, 23), 1.68 – 1.61 (m, 1H, 22), 1.30 – 1.21 (comp, 4H, 20, 21, 23, 24), 1.18 – 1.09 (m, 1H, 22). ^{13}C NMR (126 MHz, $CDCl_3$) rotamers δ 157.3 (33), 157.1 (33), 150.2 (1), 137.3 (5), 137.1 (5), 135.9 (29), 135.8 (29), 130.2 (4), 129.9 (3), 129.9 (3), 129.6 (4), 128.6 (25, 27), 128.0 (26), 127.9 (28, 30), 115.8 (6), 115.5 (6), 114.7 (2), 114.3 (2), 67.2 (31), 67.2 (31), 63.6 (19), 55.7 (10), 55.5 (10), 50.2 (14, 18), 50.0 (14, 18), 49.1 (15, 17), 49.1 (15, 17), 30.3 (12), 29.8 (12), 29.1 (20, 24), 28.9 (7), 28.8 (7), 28.2 (9), 27.8 (9), 26.4 (22), 26.0 (21, 23), 22.4 (8), 22.2 (8).

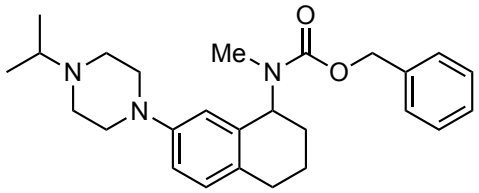

Benzyl (7-(4-isopropylpiperazin-1-yl)-1,2,3,4-tetrahydronaphthalen-1-yl)(methyl)carbamate (**2.32**) (MDW-1-167). Prepared from **2.16** (25 mg 0.066 mmol) and acetone according to representative procedure F. The crude residue was purified via flash chromatography (SiO_2) eluting with hexanes/EtOAc/Et_3N (64:35:1) to afford 18 mg (65%) of **2.32** as a pale yellow oil. ^1H NMR (499 MHz, $CDCl_3$) rotamers δ 7.45 – 7.28 (m, 5H), 6.99 (d, *J* = 8.3 Hz, 1H), 6.80 – 6.75 (m, 1H), 6.63 (dd, *J* = 10.1, 2.2 Hz, 1H), 5.50 – 5.32 (m, 1H), 5.30 – 5.11 (m, 2H), 3.15 – 3.05 (m, 4H), 2.75 – 2.61 (m, 10H), 2.07 – 1.91 (m, 2H), 1.83 – 1.70 (m, 2H), 1.09 (d, *J* = 6.5 Hz, 6H). ^{13}C NMR (126 MHz, $CDCl_3$) rotamers δ 157.3, 157.1, 150.2, 137.3, 137.2, 135.9, 135.8, 130.2, 130.0, 129.9, 129.7, 128.6, 128.0, 127.9, 127.9, 115.8, 115.5, 114.8, 114.4, 67.3, 67.2, 55.7, 55.5, 54.6, 50.1, 49.9, 48.9, 48.9, 30.3, 29.8, 28.9, 28.8, 28.3, 27.8, 22.4, 22.2, 18.8, 18.8. HRMS (ESI) m/z calcd for $C_{26}H_{35}N_3O_2$ $(M+Na)^+$, 444.2641; found 444.2630.

Representative Procedure G: Alkylation of the piperazine nitrogen atom with an alkyl halide.

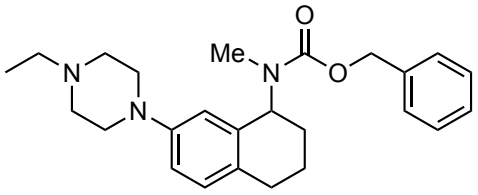

Benzyl (7-(4-ethylpiperazin-1-yl)-1,2,3,4-tetrahydronaphthalen-1-yl)(methyl)carbamate (**2.36**) (MDW-1-161). A solution of **2.16** (30 mg, 0.079 mmol), bromoethane (0.010 g, 7 μL, 0.095 mmol), and K_2CO_3 (22 mg, 0.16 mmol) in MeCN (0.8

mL) was stirred for 24 hours at room temperature. The reaction was diluted with saturated aqueous $NaHCO_3$ (5 mL) and extracted with CH_2Cl_2 (3 x 5 mL). The combined organic extracts were washed with brine (1 x 10 mL), dried (Na_2SO_4), and concentrated under reduced pressure. The crude residue was purified via flash chromatography (SiO_2) eluting with hexanes/EtOAc/Et_3N (69:30:1) affording 23 mg (70%) of **2.36** as a colorless oil. ^1H NMR (499 MHz, $CDCl_3$) rotamers δ 7.45 – 7.28 (comp, 5H), 6.99 (d, J = 8.3 Hz, 1H), 6.81 – 6.75 (m, 1H), 6.63 (dd, J = 11.1, 2.6 Hz, 1H), 5.51 – 5.32 (m, 1H), 5.32 – 5.11 (comp, 2H), 3.18 – 3.06 (comp, 4H), 2.72 – 2.56 (comp, 9H), 2.49 (q, J = 7.2 Hz, 2H), 2.07 – 1.91 (comp, 2H), 1.84 – 1.69 (comp, 2H), 1.14 (t, J = 7.2 Hz, 3H). ^{13}C NMR (126 MHz, $CDCl_3$) rotamers δ 157.3, 157.0, 150.0, 150.0, 137.3, 137.1, 135.9, 135.8, 130.7, 130.2, 130.0, 129.9, 129.7, 128.7, 128.6, 128.1, 128.0, 127.9, 127.9, 127.9, 115.7, 115.4, 114.8, 114.4, 67.2, 67.2, 55.7, 55.5, 52.9, 52.5, 49.6, 49.5, 30.3, 29.8, 29.8, 28.8, 28.8, 28.2, 27.7, 22.3, 22.2, 12.1. HRMS (ESI) *m/z* calcd for $C_{25}H_{33}N_3O_2$ $(M+Na)^+$, 430.2465; found 430.2483

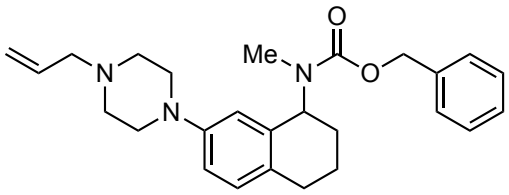

Benzyl (7-(4-allylpiperazin-1-yl)-1,2,3,4-tetrahydronaphthalen-1-yl)(methyl)carbamate (**2.37**) (MDW-2-131). Prepared from **2.16** (55 mg 0.14 mmol) and allyl bromide according to representative procedure G. The crude residue was purified via flash chromatography (SiO_2) eluting with hexanes/Et_2O/Et_3N (39:60:1) to afford 18 mg (30%) of **2.37** as a colorless oil. ^1H NMR (499 MHz, $CDCl_3$) δ 7.45 – 7.27 rotamers (comp, 5H), 6.99 (d, J = 8.3 Hz, 1H), 6.80 – 6.74 (m, 1H), 6.65 – 6.59 (m, 1H), 5.95 – 5.85 (m, 1H), 5.50 – 5.09 (comp, 5H), 3.15 – 3.01 (comp, 6H), 2.74 – 2.52 (comp,

9H), 2.08 – 1.91 (comp, 2H), 1.83 – 1.66 (comp, 2H). ^{13}C NMR (126 MHz, $CDCl_3$) rotamers δ 157.3, 157.0, 150.1, 150.0, 137.3, 137.1, 135.9, 135.8, 135.0, 135.0, 130.2, 130.0, 129.9, 129.7, 128.6, 128.0, 127.9, 127.9, 118.3, 115.7, 115.4, 114.7, 114.4, 67.2, 67.2, 61.9, 61.9, 55.7, 55.5, 53.2, 53.2, 49.7, 49.5, 30.5, 30.3, 29.8, 29.8, 28.8, 28.8, 28.2, 27.8, 22.3, 22.2. HRMS (ESI) *m/z* calcd for $C_{26}H_{33}N_3O_2$ $(M+H)^+$, 420.2646; found 420.2659.

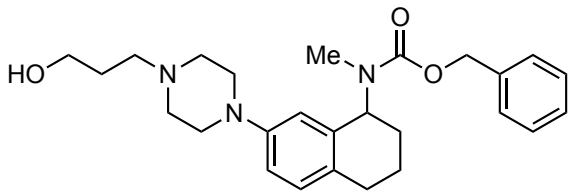

Benzyl (7-(4-(3-hydroxypropyl)piperazin-1-yl)-1,2,3,4-tetrahydronaphthalen-1-yl)(methyl)carbamate (**2.38**) (MDW-1-177). Prepared from **2.16** (100 mg 0.264 mmol) and 3-bromo-1-propanol according to representative procedure G. The crude residue was purified via flash chromatography (SiO_2) eluting with CH_2Cl_2/MeOH/Et_3N (97:2:1) to afford 39 mg (34%) of **2.38** as a colorless oil. ^{1}H NMR (499 MHz, $CDCl_3$) rotamers δ 7.44 – 7.28 (comp, 5H), 6.98 (d, *J* = 8.3 Hz, 1H), 6.78 – 6.71 (m, 1H), 6.59 (dd, *J* = 12.4, 2.6 Hz, 1H), 5.49 – 5.31 (m, 1H), 5.30 – 5.10 (comp, 2H), 3.82 (t, *J* = 5.2 Hz, 2H), 3.13 – 3.01 (comp, 4H), 2.74 – 2.61 (comp, 12H), 2.05 – 1.91 (comp, 2H), 1.82 – 1.68 (comp, 4H). ^{13}C NMR (126 MHz, $CDCl_3$) rotamers δ 157.3, 157.0, 149.8, 149.8, 137.2, 137.1, 135.9, 135.8, 130.4, 130.0, 129.9, 129.9, 128.6, 128.0, 128.0, 127.9, 127.9, 115.8, 115.4, 114.7, 114.5, 67.2, 67.2, 64.7, 58.9, 55.6, 55.4, 53.4, 49.7, 49.6, 30.3, 29.8, 28.8, 28.7, 28.2, 27.7, 27.3, 22.3, 22.1. HRMS (ESI) *m/z* calcd for $C_{26}H_{35}N_3O_3$ $(M+H)^+$, 438.2751; found 438.2759

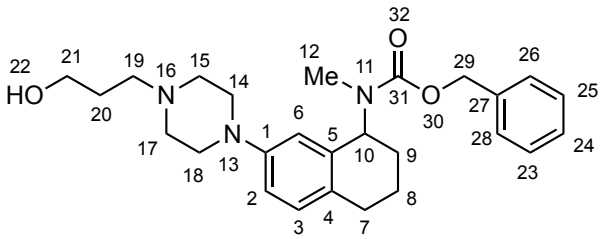

NMR Assignments (**2.38**). ^{1}H NMR (499 MHz, $CDCl_3$) rotamers δ 7.44 – 7.28 (comp, 5H, 23, 24, 25, 26, 28), 6.98 (d, *J* = 8.3 Hz, 1H, 3), 6.78 – 6.71 (m, 1H, 6), 6.59 (dd, *J* = 12.4, 2.6 Hz, 1H, 2), 5.49 – 5.31 (m, 1H, 10), 5.30 – 5.10 (comp, 2H, 29), 3.82 (t, *J* = 5.2 Hz, 2H, 21), 3.13 – 3.01 (comp, 4H, 14, 18), 2.74 – 2.61 (comp, 12H, 7, 12, 15, 17, 19, 22), 2.05 – 1.91 (comp, 2H, 8, 9), 1.82 – 1.68 (comp, 4H, 8, 9, 20). ^{13}C NMR (126 MHz, $CDCl_3$) rotamers δ 157.3 (31), 157.0 (31), 149.8 (1), 149.8 (1), 137.2 (5), 137.1 (5), 135.9 (27), 135.8 (27), 130.4 (4), 130.0 (3), 129.9 (4), 129.9 (3), 128.6 (23, 25), 128.0 (24), 128.0 (24), 127.9 (26, 28), 127.9 (26, 28), 115.8 (2), 115.4 (2), 114.7 (6), 114.5 (6), 67.2 (29), 67.2 (29), 64.7 (21), 58.9 (19), 55.6 (10), 55.4 (10), 53.4 (15, 17), 49.7 (14, 18), 49.6 (14, 18), 30.3 (12), 29.8 (12), 28.8 (7), 28.7 (7), 28.2 (9), 27.7 (9), 27.3 (20), 22.3 (8), 22.1 (8).

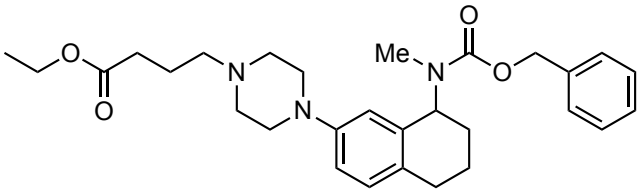

Ethyl 4-(4-(8-(((benzyloxy)carbonyl)(methyl)amino)-5,6,7,8-tetrahydronaphthalen-2-yl)piperazin-1-yl)butanoate (**2.39**) (MDW-2-130). Prepared from **2.16** (55 mg 0.14 mmol) and ethyl 4-bromobutyrate according to representative procedure G. The crude residue was purified via flash chromatography (SiO_2) eluting with hexanes/Et_2O/Et_3N (24:75:1) to afford 39 mg (55%) of **2.39** as a colorless oil. ^{1}H NMR (499 MHz, $CDCl_3$ rotamers δ 7.45 – 7.28 (comp, 5H), 6.99 (d, *J* = 8.3 Hz, 1H),

6.80 – 6.73 (m, 1H), 6.65 – 6.58 (m, 1H), 5.51 – 5.32 (m, 1H), 5.32 – 5.10 (comp, 2H), 4.14 (q, *J* = 7.1 Hz, 2H), 3.13 – 3.02 (comp, 4H), 2.75 – 2.61 (comp, 5H), 2.60 – 2.53 (comp, 4H), 2.42 (t, *J* = 7.3 Hz, 2H), 2.37 (t, *J* = 7.4 Hz, 2H), 2.08 – 1.91 (comp, 2H), 1.90 – 1.67 (comp, 4H), 1.26 (t, *J* = 7.1 Hz, 3H). ^{13}C NMR (126 MHz, $CDCl_3$) δ 173.7, 157.3, 157.0, 150.1, 150.0, 137.2, 137.1, 135.9, 135.8, 130.1, 129.9, 129.9, 129.7, 128.6, 128.0, 127.9, 127.9, 115.7, 115.4, 114.6, 114.3, 67.2, 67.2, 60.4, 57.8, 57.8, 55.7, 55.5, 53.2, 49.7, 49.5, 32.4, 30.4, 30.3, 29.8, 28.8, 28.7, 28.2, 27.7, 22.3, 22.3, 22.2, 14.4. HRMS (ESI) *m/z* calcd for $C_{29}H_{39}N_3O_4$ $(M+H)^+$, 494.3013; found 494.3027.

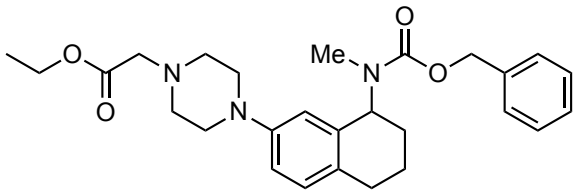

Ethyl 2-(4-(8-(((benzyloxy)carbonyl)(methyl)amino)-5,6,7,8-tetrahydronaphthalen-2-yl)piperazin-1-yl)acetate (**2.40**) (MDW-1-169). Prepared from **2.16** (25 mg 0.066 mmol) and ethyl bromoacetate according to representative procedure G. The crude residue was purified via flash chromatography (SiO_2) eluting with hexanes/EtOAc/Et_3N (69:30:1) to afford 20 mg (62%) of **2.40** as a pale yellow oil. ^{1}H NMR (499 MHz, $CDCl_3$) rotamers δ 7.45 – 7.27 (comp, 5H), 6.99 (d, *J* = 8.4 Hz, 1H), 6.80 – 6.74 (m, 1H), 6.62 (dd, *J* = 12.4, 2.0 Hz, 1H), 5.49 – 5.32 (m, 1H), 5.31 – 5.10 (comp, 2H), 4.25 – 4.17 (comp, 2H), 3.26 (s, 2H), 3.18 – 3.07 (comp, 4H), 2.74 – 2.62 (comp, 9H), 2.06 – 1.92 (comp, 2H), 1.83 – 1.67 (comp, 2H), 1.29 (td, *J* = 7.2, 2.0 Hz, 3H). ^{13}C NMR (126 MHz, $CDCl_3$) δ 170.3, 157.3, 157.1, 150.0, 150.0, 137.2, 137.1, 136.0, 135.9, 130.4, 130.0, 129.9, 129.9, 128.6, 128.1, 127.9, 127.9, 115.8, 115.5, 114.8, 114.5, 67.2, 67.2, 60.8, 59.6, 55.7, 55.5, 53.1, 53.1, 49.6, 49.4, 30.3, 29.8, 29.8, 28.9,

28.8, 28.2, 27.7, 22.3, 22.2, 14.4. HRMS (ESI) *m/z* calcd for $C_{27}H_{35}N_3O_4$ $(M+H)^+$, 466.2700; found 466.2715.

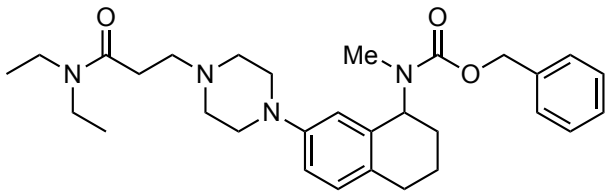

Benzyl (7-(4-(3-(diethylamino)-3-oxopropyl)piperazin-1-yl)-1,2,3,4-tetrahydronaphthalen-1-yl)(methyl)carbamate (**2.41**) (MDW-1-213). Prepared from **2.16** (30 mg 0.079 mmol) and known 3-bromo-N,N-diethylpropanamide, according to representative procedure G.[315] The crude residue was purified via flash chromatography (SiO_2) eluting with EtOAc/*i*-PrOH/Et_3N (98:1:1) to afford 14 mg (36%) of **2.41** as a pale yellow oil. ^1H NMR (499 MHz, $CDCl_3$) rotamers δ 7.45 – 7.28 (comp, 5H), 6.99 (d, *J* = 8.4 Hz, 1H), 6.79 – 6.74 (m, 1H), 6.64 – 6.59 (m, 1H), 5.49 – 5.32 (m, 1H), 5.30 – 5.11 (comp, 2H), 3.42 – 3.30 (comp, 4H), 3.14 – 3.04 (comp, 4H), 2.84 – 2.77 (comp, 2H), 2.74 – 2.61 (comp, 9H), 2.59 – 2.53 (comp, 2H), 2.07 – 1.92 (comp, 2H), 1.80 – 1.71 (comp, 2H), 1.19 (td, *J* = 7.2, 2.0 Hz, 3H), 1.12 (t, *J* = 7.1 Hz, 3H). ^{13}C NMR (126 MHz, $CDCl_3$) rotamers δ 170.6, 157.2, 156.9, 149.9, 149.8, 137.1, 137.0, 135.8, 135.7, 130.2, 129.8, 129.8, 129.7, 128.5, 127.9, 127.7, 127.7, 115.6, 115.4, 114.6, 114.2, 67.1, 67.1, 55.6, 55.3, 54.4, 53.3, 53.3, 49.5, 49.4, 42.0, 40.1, 30.8, 30.2, 29.7, 28.7, 28.6, 28.1, 27.6, 22.2, 22.0, 14.4, 13.1. HRMS (ESI) *m/z* calcd for $C_{30}H_{42}N_4O_3$ $(M+H)^+$, 507.3330; found 507.3346.

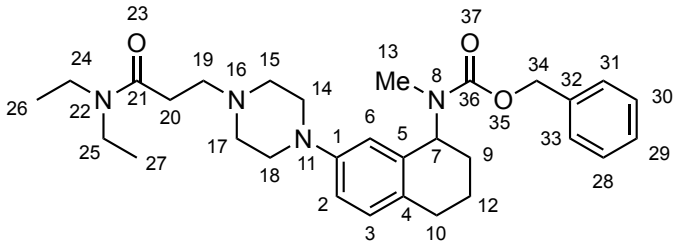

NMR Assignments (**2.41**). ^{1}H NMR (499 MHz, $CDCl_3$) δ 7.45 – 7.28 (comp, 5H, 28, 29, 30, 31, 33), 6.99 (d, *J* = 8.4 Hz, 1H, 3), 6.79 – 6.74 (m, 1H, 2), 6.64 – 6.59 (m, 1H, 6), 5.49 – 5.32 (m, 1H, 7), 5.30 – 5.11 (comp, 2H, 34), 3.42 – 3.30 (comp, 4H, 24, 25), 3.14 – 3.04 (comp, 4H, 14, 18), 2.84 – 2.77 (comp, 2H, 19), 2.74 – 2.61 (comp, 9H, 10, 13, 15, 17), 2.59 – 2.53 (comp, 2H, 20), 2.07 – 1.92 (comp, 2H, 9, 12), 1.80 – 1.71 (comp, 2H, 9, 12), 1.19 (td, *J* = 7.2, 2.0 Hz, 3H, 26, 27), 1.12 (t, *J* = 7.1 Hz, 3H). ^{13}C NMR (126 MHz, $CDCl_3$) δ 170.6 (21), 157.2 (36), 156.9 (36), 149.9 (1), 149.8 (1), 137.1 (5), 137.0 (5), 135.8 (32), 135.7 (32), 130.2 (4), 129.8 (3), 129.8 (3), 129.7 (4), 128.5 (28, 30), 127.9 (29), 127.7 (31, 33), 127.7 (31, 33), 115.6 (2), 115.4 (2), 114.6 (6), 114.2 (6), 67.1 (34), 67.1 (34), 55.6 (7), 55.3 (7), 54.4 (19), 53.3 (15, 17), 53.3 (15, 17), 49.5 (14, 18), 49.4 (14, 18), 42.0 (24, 25), 40.1 (24, 25), 30.8 (20), 30.2 (13), 29.7 (13), 28.7 (10), 28.6 (10), 28.1 (9), 27.6 (9), 22.2 (12), 22.0 (12), 14.4 (26, 27), 13.1 (26, 27).

Representative Procedure H: *N*-alkylation with ethyl acrylate.

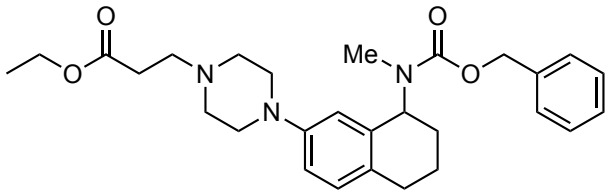

Ethyl 3-(4-(8-(((benzyloxy)carbonyl)(methyl)amino)-5,6,7,8-tetrahydronaphthalen-2-yl)piperazin-1-yl)propanoate (**2.42**) (MDW-2-120). Ethyl acrylate (0.22 g, 0.24 mL, 2.2 mmol) was added to a solution of **2.16** (83 mg, 0.22 mmol)

in EtOH (1.1 mL). The reaction was heated at 40 °C for 18 h. The reaction was cooled to room temperature and the concentrated under reduced pressure. The crude residue was purified via flash chromatography (SiO_2) eluting with hexanes/EtOAc/Et_3N (64:35:1) affording 90 mg (86%) of **2.42** as a colorless oil. ^{1}H NMR (400 MHz, $CDCl_3$) rotamers δ 7.45 – 7.27 (comp, 5H), 6.98 (d, *J* = 8.4 Hz, 1H), 6.81 – 6.72 (m, 1H), 6.61 (dd, *J* = 10.8, 2.6 Hz, 1H), 5.51 – 5.31 (m, 1H), 5.32 – 5.10 (comp, 2H), 4.16 (q, *J* = 7.2 Hz, 2H), 3.15 – 2.99 (comp, 4H), 2.75 (t, *J* = 7.4 Hz, 2H), 2.72 – 2.49 (comp, 11H), 2.07 – 1.92 (comp, 2H), 1.85 – 1.68 (comp, 2H), 1.30 – 1.24 (comp, 3H). ^{13}C NMR (126 MHz, $CDCl_3$) δ 172.6, 157.4, 157.1, 150.0, 137.3, 137.2, 136.0, 135.9, 130.3, 130.0, 129.9, 129.8, 128.6, 128.1, 127.9, 127.9, 115.8, 115.5, 114.7, 114.4, 67.2, 67.2, 60.6, 55.7, 55.5, 53.7, 53.0, 49.7, 49.5, 32.5, 30.3, 29.8, 29.8, 28.9, 28.8, 28.2, 27.8, 22.4, 22.2, 14.4. HRMS (ESI) *m/z* calcd for $C_{28}H_{37}N_3O_4$ $(M+H)^+$, 480.2857; found 480.2860

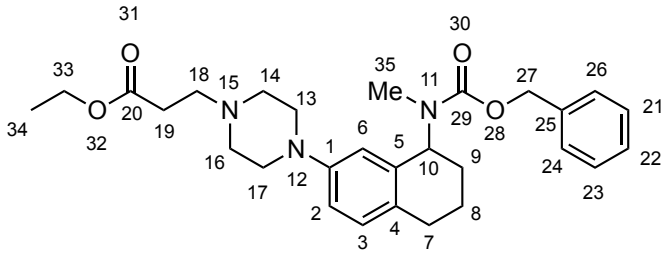

NMR Assignments (**2.42**). ^{1}H NMR (400 MHz, $CDCl_3$) rotamers δ 7.45 – 7.27 (comp, 5H, 21, 22, 23, 24, 26), 6.98 (d, *J* = 8.4 Hz, 1H, 3), 6.81 – 6.72 (m, 1H, 2), 6.61 (dd, *J* = 10.8, 2.6 Hz, 1H, 6), 5.51 – 5.31 (m, 1H, 10), 5.32 – 5.10 (comp, 2H, 27), 4.16 (q, *J* = 7.2 Hz, 2H, 33), 3.15 – 2.99 (comp, 4H, 13, 17), 2.75 (t, *J* = 7.4 Hz, 2H, 18), 2.72 – 2.49 (comp, 11H, 7, 14, 16, 19, 35), 2.07 – 1.92 (comp, 2H, 8, 9), 1.85 – 1.68 (comp, 2H, 8, 9), 1.30 – 1.24 (comp, 3H, 34). ^{13}C NMR (126 MHz, $CDCl_3$) δ 172.6 (20), 157.4 and 157.1 (29), 150.0 (1), 137.3 and 137.2 (5), 136.0 and 135.9 (25), 130.3 and 130.0 (4), 129.9 and 129.8 (3), 128.6 (21, 23), 128.1 (22), 127.9 and 127.9 (24, 26), 115.8 and 115.5

(2), 114.7 and 114.4 (6), 67.2 and 67.2 (27), 60.6 (33), 55.7 and 55.5 (10), 53.7, 53.0 (14, 16), 49.7 and 49.5 (13, 17), 32.5 (19), 30.3 (18), 29.8 and 29.8 (35), 28.9 and 28.8 (7), 28.2 and 27.8 (9), 22.4 and 22.2 (8), 14.4 (34).

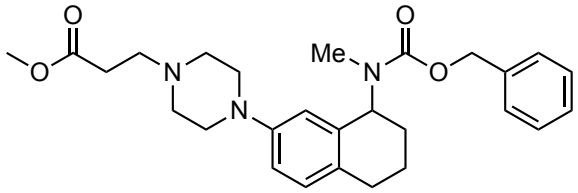

Methyl 3-(4-(8-(((benzyloxy)carbonyl)(methyl)amino)-5,6,7,8-tetrahydronaphthalen-2-yl)piperazin-1-yl)propanoate (**2.43**) (MDW-1-166). Methyl acrylate (0.16 g, 0.17 mL, 1.6 mmol) was added to a solution of **2.16** (60 mg, 0.16 mmol) in MeOH (0.8 mL). The reaction was heated at 40 °C for 18 h. The reaction was cooled to room temperature and the concentrated under reduced pressure. The crude residue was purified via flash chromatography (SiO_2) eluting with hexanes/EtOAc/Et_3N (59:40:1) affording 56 mg (75%) of **2.43** as a colorless oil. ^{1}H NMR (499 MHz, $CDCl_3$) rotamers δ 7.45 – 7.28 (comp, 5H), 6.98 (dd, *J* = 8.4, 1.5 Hz, 1H), 6.80 – 6.73 (m, 1H), 6.61 (dd, *J* = 13.7, 2.6 Hz, 1H), 5.50 – 5.32 (m, 1H), 5.31 – 5.12 (comp, 2H), 3.70 (d, *J* = 1.5 Hz, 3H), 3.13 – 3.01 (comp, 4H), 2.76 (t, *J* = 7.4 Hz, 2H), 2.72 – 2.53 (m, 11H), 2.08 – 1.92 (comp, 2H), 1.84 – 1.68 (comp, 2H). ^{13}C NMR (126 MHz, $CDCl_3$) rotamers δ 173.0, 157.3, 157.0, 150.0, 150.0, 137.2, 137.1, 135.9, 135.8, 130.2, 130.0, 129.9, 129.8, 128.6, 128.0, 127.9, 127.9, 115.7, 115.5, 114.7, 114.3, 67.2, 67.2, 55.7, 55.4, 53.6, 53.0, 53.0, 51.8, 49.6, 49.5, 32.2, 30.3, 29.8, 28.8, 28.7, 28.2, 27.7, 22.3, 22.1. HRMS (ESI) *m/z* calcd for $C_{27}H_{35}N_3O_4$ $(M+Na)^+$, 488.2520; found 488.2541.

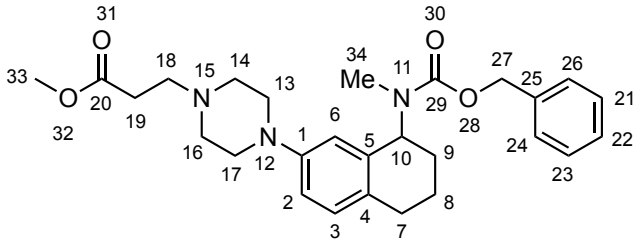

NMR Assignments (**2.43**). ^{1}H NMR (499 MHz, $CDCl_3$) δ 7.45 – 7.28 (comp, 5H, 21, 22, 23, 24, 26), 6.98 (dd, *J* = 8.4, 1.5 Hz, 1H, 3), 6.80 – 6.73 (m, 1H, 2), 6.61 (dd, *J* = 13.7, 2.6 Hz, 1H, 6), 5.50 – 5.32 (m, 1H, 10), 5.31 – 5.12 (comp, 2H, 27), 3.70 (d, *J* = 1.5 Hz, 3H, 33), 3.13 – 3.01 (comp, 4H, 13, 17), 2.76 (t, *J* = 7.4 Hz, 2H, 18), 2.72 – 2.53 (comp, 11H, 7, 14, 16, 19, 34), 2.08 – 1.92 (m, 2H, 8, 9), 1.84 – 1.68 (m, 2H, 8, 9). ^{13}C NMR (126 MHz, $CDCl_3$) rotamers δ 173.0 (20), 157.3 and 157.0 (29), 150.0 and 150.0 (1), 137.2 and 137.1 (5), 135.9 and 135.8 (25), 130.2 and 130.0 (4), 129.9 and 129.8 (3), 128.6 (21, 23), 128.0 (22), 127.9 and 127.9 (24, 26), 115.7 and 115.5 (2), 114.7 and 114.3 (6), 67.2 and 67.2 (27), 55.7 and 55.4 (10), 53.6 (18), 53.0 and 53.0 (14, 16), 51.8 (33), 49.6 and 49.5 (13, 17), 32.2 (19), 30.3 and 29.8 (34), 28.8 and 28.7 (7), 28.2 and 27.7 (9), 22.3 and 22.1 (8).

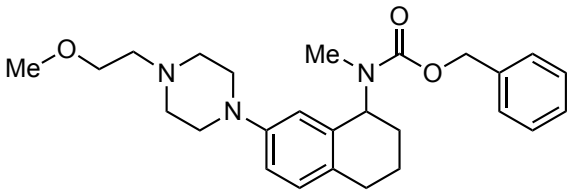

Benzyl (7-(4-(2-methoxyethyl)piperazin-1-yl)-1,2,3,4-tetrahydronaphthalen-1-yl)(methyl)carbamate (**2.44**) (MDW-1-219). Prepared from **2.14** (70 mg 0.19 mmol) and piperazine according to representative procedure B. The crude residue was purified via flash chromatography (SiO_2) eluting with hexanes/EtOAc/Et_3N (59:40:1) to afford 40 mg (49%) of **2.44** as a pale yellow oil. ^{1}H NMR (499 MHz, $CDCl_3$) δ 7.45 – 7.27 (comp, 5H), 6.98 (d, *J* = 8.4 Hz, 1H), 6.79 – 6.74 (m, 1H), 6.65 – 6.58 (m, 1H), 5.50 – 5.31 (m,

1H), 5.31 – 5.11 (comp, 2H), 3.56 (t, J = 5.5 Hz, 2H), 3.38 (s, 3H), 3.17 – 3.06 (comp, 4H), 2.76 – 2.59 (comp, 11H), 2.07 – 1.91 (comp, 2H), 1.83 – 1.68 (comp, 2H). ^{13}C NMR (126 MHz, $CDCl_3$) δ 157.3, 157.0, 150.1, 150.0, 137.3, 137.1, 135.9, 135.8, 130.2, 130.0, 129.9, 129.7, 128.6, 128.0, 127.9, 115.7, 115.4, 114.7, 114.4, 70.3, 70.2, 67.2, 67.2, 59.1, 58.1, 55.7, 55.5, 53.7, 53.7, 49.5, 49.4, 30.3, 29.8, 28.8, 28.8, 28.2, 27.7, 22.3, 22.2. HRMS (ESI) *m/z* calcd for $C_{26}H_{35}N_3O_3$ $(M+H)^+$, 438.2751; found 438.2767.

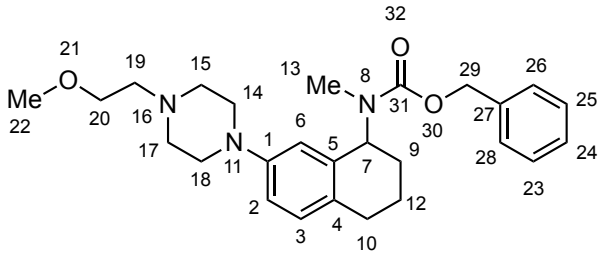

NMR Assignments (**2.44**). ^{1}H NMR (499 MHz, $CDCl_3$) δ 7.45 – 7.27 (comp, 5H, 23, 24, 25, 26, 28), 6.98 (d, J = 8.4 Hz, 1H, 3), 6.79 – 6.74 (m, 1H, 2), 6.65 – 6.58 (m, 1H, 6), 5.50 – 5.31 (m, 1H, 7), 5.31 – 5.11 (comp, 2H, 29), 3.56 (t, J = 5.5 Hz, 2H, 20), 3.38 (s, 3H, 22), 3.17 – 3.06 (comp, 4H, 14, 18), 2.76 – 2.59 (comp, 11H, 10, 13, 15, 17, 19), 2.07 – 1.91 (comp, 2H, 9, 12), 1.83 – 1.68 (comp, 2H, 9, 12). ^{13}C NMR (126 MHz, $CDCl_3$) δ 157.3 (31), 157.0 (31), 150.1 (1), 150.0 (1), 137.3 (5), 137.1 (5), 135.9 (27), 135.8 (27), 130.2 (4), 130.0 (3), 129.9 (3), 129.7 (4), 128.6 (23, 25), 128.0 (24), 127.9 (26, 28), 115.7 (2), 115.4 (2), 114.7 (6), 114.4 (6), 70.3 (20), 70.2 (20), 67.2 (29), 67.2 (29), 59.1 (22), 58.1 (19), 55.7 (7), 55.5 (7), 53.7 (15, 17), 53.7 (15, 17), 49.5 (14, 18), 49.4 (14, 18), 30.3 (13), 29.8 (13), 28.8 (10), 28.8 (10), 28.2 (9), 27.7 (9), 22.3 (12), 22.2 (12).

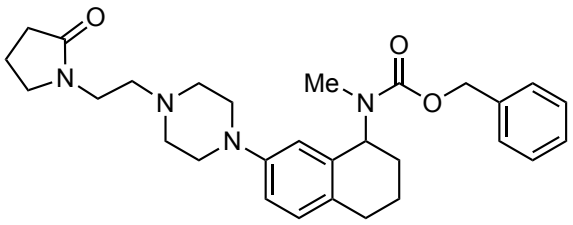

Benzyl methyl(7-(4-(2-(2-oxopyrrolidin-1-yl)ethyl)piperazin-1-yl)-1,2,3,4-tetrahydronaphthalen-1-yl)carbamate (**2.50**) (MDW-2-149). A solution of **2.16** (40 mg, 0.11 mmol), K_2CO_3 (29 mg, 0.21 mmol), and known 1-(2-Chloroethyl)-2-pyrrolidinone (20 mg, 0.14 mmol) in MeCN/THF (2:1, 1.1 mL) was heated at 45 °C for 15 h and then heated at 65 °C for 48 h.[304] The reaction was diluted with saturated aqueous $NaHCO_3$ (10 mL) and extracted with CH_2Cl_2 (3 x 10 mL). The combined organic extracts were washed with brine (1 x 10 mL), dried (Na_2SO_4), and concentrated under reduced pressure. The crude residue was purified via flash chromatography (SiO_2) eluting with EtOAc/MeOH/Et_3N (97:2:1 to 94:5:1) to afford 13 mg (25%) of **2.50** as a pale yellow oil. ^{1}H NMR (499 MHz, $CDCl_3$) rotamers δ 7.44 – 7.29 (comp, 5H), 6.98 (d, *J* = 8.4 Hz, 1H), 6.78 – 6.72 (m, 1H), 6.64 – 6.56 (m, 1H), 5.49 – 5.31 (m, 1H), 5.31 – 5.13 (comp, 2H), 3.52 – 3.42 (comp, 4H), 3.12 – 3.00 (comp, 4H), 2.74 – 2.54 (comp, 11H), 2.38 (t, *J* = 8.1 Hz, 2H), 2.05 – 1.92 (comp, 4H), 1.83 – 1.68 (comp, 2H). ^{13}C NMR (126 MHz, $CDCl_3$) rotamers δ 175.2, 157.3, 157.0, 150.0, 149.9, 137.2, 137.1, 135.9, 135.8, 130.3, 130.0, 129.9, 129.9, 128.6, 128.6, 128.0, 128.0, 127.9, 115.7, 115.6, 114.7, 114.3, 67.2, 67.2, 55.7, 55.6, 55.5, 53.2, 49.6, 49.6, 47.9, 47.8, 39.8, 39.8, 31.1, 30.4, 29.8, 28.8, 28.8, 28.2, 27.7, 22.3, 22.2, 18.2. HRMS (ESI) *m/z* calcd for $C_{29}H_{38}N_4O_3$ $(M+H)^+$, 491.3017; found 491.3025.

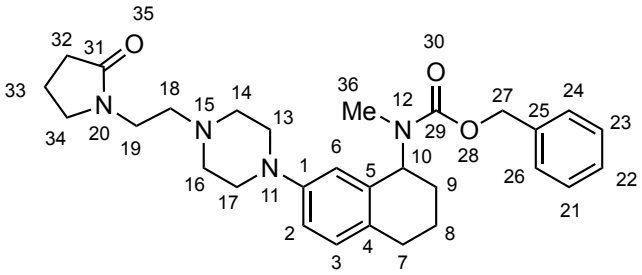

NMR Assignments (**2.50**). ^{1}H NMR (499 MHz, $CDCl_3$) rotamers δ 7.44 – 7.29 (comp, 5H, 21, 22, 23, 24, 26), 6.98 (d, *J* = 8.4 Hz, 1H, 3), 6.78 – 6.72 (m, 1H, 2), 6.64 – 6.56 (m, 1H, 6), 5.49 – 5.31 (m, 1H, 10), 5.31 – 5.13 (comp, 2H, 27), 3.52 – 3.42 (comp, 4H, 19, 34''), 3.12 – 3.00 (comp, 4H, 14, 16), 2.74 – 2.54 (comp, 11H, 7, 13, 17, 18, 36), 2.38 (t, *J* = 8.1 Hz, 2H, 32), 2.05 – 1.92 (comp, 4H, 8, 9, 33), 1.83 – 1.68 (comp, 2H, 8, 9). ^{13}C NMR (126 MHz, $CDCl_3$) δ 175.2 (31), 157.3 and 157.0 (29), 150.0 and 149.9 (1), 137.2 and 137.1 (5), 135.9 and 135.8 (25), 130.3 and 130.0 (4), 129.9 and 129.9 (3), 128.6 and 128.6 (21, 23), 128.0 and 128.0 (22), 127.9 (24, 26), 115.7 and 115.6 (2), 114.7 and 114.3 (6), 67.2 and 67.2 (27), 55.7 (18), 55.6 and 55.5 (10), 53.2 (14, 16), 49.6 and 49.6 (13, 17), 47.9 and 47.8 (34), 39.8 and 39.8 (19), 31.1 (32), 30.4 and 29.8 (36), 28.8 and 28.8 (7), 28.2 and 27.7 (9), 22.3 and 22.2 (8), 18.2 (33).

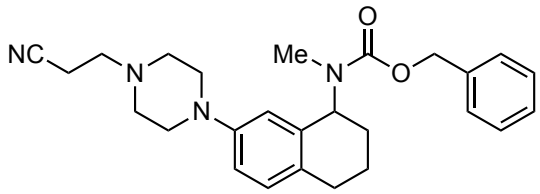

Benzyl (7-(4-(2-cyanoethyl)piperazin-1-yl)-1,2,3,4-tetrahydronaphthalen-1-yl)(methyl)carbamate (**2.52**) (MDW-2-213). Acrylonitrile (61 mg, 75 μL, 1.1 mmol) was added to a solution of **2.16** (0.289 g, 0.762 mmol) in MeOH (3.8 mL) at 0 °C. The reaction was stirred at 0 °C for 1 h and the cooling bath was removed. The reaction was stirred for 22h at room temperature and then concentrated under reduced pressure. The

crude residue was purified via flash chromatography (SiO_2) eluting with hexanes/EtOAc (1:1 to 3:7) to afford 0.230 g (70%) of **2.52** as a pale yellow oil. 1H NMR (500 MHz, $CDCl_3$) δ 7.48 – 7.28 (comp, 5H), 6.99 (d, *J* = 8.3 Hz, 1H), 6.81 – 6.73 (m, 1H), 6.66 – 6.58 (m, 1H), 5.52 – 5.33 (m, 1H,), 5.32 – 5.12 (comp, 2H), 3.18 – 3.03 (comp, 4H), 2.83 – 2.59 (comp, 11H), 2.58 – 2.52 (comp, 2H), 2.11 – 1.92 (comp, 2H), 1.85 – 1.68 (comp, 2H). ^{13}C NMR (126 MHz, $CDCl_3$) rotamers δ 157.2, 156.9, 149.8, 149.7, 137.1, 137.0, 135.9, 135.8, 130.3, 129.9, 129.9, 129.9, 128.5, 127.9, 127.8, 127.8, 118.7, 118.7, 115.8, 115.5, 114.7, 114.4, 67.1, 67.1, 55.6, 55.4, 53.4, 53.4, 52.7, 49.5, 49.4, 30.2, 29.7, 28.7, 28.7, 28.1, 27.6, 22.2, 22.1, 16.0. HRMS (ESI) *m/z* calcd for $C_{26}H_{32}N_4O_2$ $(M+Na)^+$, 455.2417; found 455.2434.

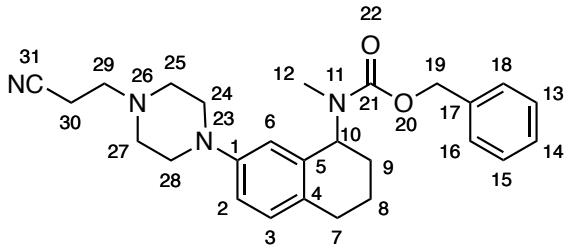

NMR Assignments (**2.52**). 1H NMR (500 MHz, $CDCl_3$) rotamers δ 7.48 – 7.28 (comp, 5H, 13, 14, 15, 16), 6.99 (d, *J* = 8.3 Hz, 1H, 3), 6.81 – 6.73 (m, 1H, 2), 6.66 – 6.58 (m, 1H, 6), 5.52 – 5.33 (m, 1H, 10), 5.32 – 5.12 (comp, 2H, 19), 3.18 – 3.03 (comp, 4H, 24, 28), 2.83 – 2.59 (comp, 11H, 7, 12, 25, 27, 29), 2.58 – 2.52 (comp, 2H, 30), 2.11 – 1.92 (comp, 2H, 8, 9), 1.85 – 1.68 (comp, 2H, 8', 9'). ^{13}C NMR (126 MHz, $CDCl_3$) rotamers δ 157.2 and 156.9 (21), 149.8 and 149.7 (1), 137.1 and 137.0 (5), 135.9 and 135.8 (17), 130.3 and 129.9 (3), 129.9 and 129.9 (4), 128.5 (13, 15), 127.9 (16, 18), 127.8 (14), 127.8 (16, 18), 118.7 and 118.7 (31), 115.8 and 115.5 (2), 114.7 and 114.4 (6), 67.1 and 67.1 (19), 55.6 and 55.4 (10), 53.4 and 53.4 (29), 52.7 (25, 27), 49.5 and 49.4 (24, 28), 30.2 and 29.7 (12), 28.7 and 28.7 (7), 28.1 and 27.6 (9), 22.2 and 22.1 (8), 16.0 (30).

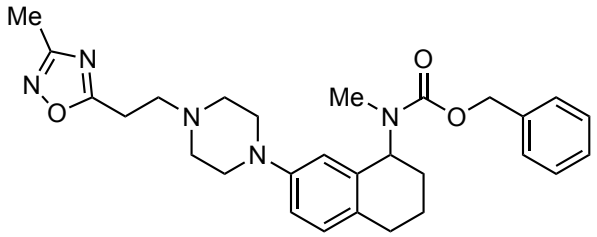

Benzyl methyl(7-(4-(2-(3-methyl-1,2,4-oxadiazol-5-yl)ethyl)piperazin-1-yl)-1,2,3,4-tetrahydronaphthalen-1-yl)carbamate (**2.56**) (MDW-2-255). A stirred solution of **2.42** (24 mg, 0.051 mmol), K_2CO_3 (14 mg, 0.10 mmol), and acetamide oxime (7.5 mg, 0.10 mmol) in PhMe (0.5 mL) was heated at 110 °C in sealed vial for 44 h. The reaction was diluted with 1 N NaOH (5 mL) and extracted with CH_2Cl_2 (3 x 10 mL). The combined organic extracts were washed with brine (1 x 10 mL), dried (Na_2SO_4), and concentrated under reduced pressure. The crude residue was purified via flash chromatography (SiO_2) eluting with hexanes/EtOAc/Et_3N (59:40:1) to afford 18 mg (71%) of **2.56** as a colorless oil. ^{1}H NMR (400 MHz, $CDCl_3$) rotamers δ 7.46 – 7.26 (comp, 5 H), 7.02 – 6.96 (m, 1 H), 6.79 – 6.72 (m, 1 H), 6.63 – 6.57 (m, 1 H), 5.51 – 5.11 (comp, 3 H), 3.14 – 3.00 (comp, 6 H), 2.95 – 2.87 (comp, 2 H), 2.75 – 2.58 (comp, 9 H), 2.39 (s, 3 H), 2.07 – 1.91 (comp, 2 H), 1.81 – 1.67 (comp, 2 H). ^{13}C NMR (126 MHz, $CDCl_3$) rotamers δ 178.2, 167.2, 157.3, 157.0, 149.9, 149.9, 137.2, 137.1, 135.9, 135.8, 130.4, 130.0, 129.9, 128.6, 128.6, 128.0, 127.9, 127.9, 115.8, 115.5, 114.7, 114.4, 67.2, 67.2, 55.7, 55.5, 54.8, 52.9, 49.6, 49.5, 30.3, 29.8, 28.8, 28.7, 28.2, 27.7, 24.8, 22.3, 22.2, 11.7. HRMS (ESI) *m/z* calcd for $C_{28}H_{35}N_5O_3$ $(M+H)^+$, 490.2813; found 490.2819.

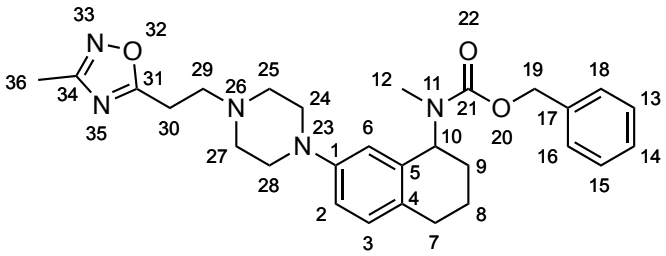

NMR Assignments (**2.56**). ^{1}H NMR (400 MHz, $CDCl_3$) rotamers δ 7.46 – 7.26 (comp, 5 H, 13, 14, 15, 16, 18), 7.02 – 6.96 (m, 1 H, 3), 6.79 – 6.72 (m, 1 H, 2), 6.63 – 6.57 (m, 1 H, 6), 5.51 – 5.11 (comp, 3 H, 10, 19), 3.14 – 3.00 (comp, 6 H, 25, 27, 30), 2.95 – 2.87 (comp, 2 H, 29), 2.75 – 2.58 (comp, 9 H, 7, 12, 24, 28), 2.39 (s, 3 H, 36), 2.07 – 1.91 (comp, 2 H, 8, 9), 1.81 – 1.67 (comp, 2 H, 8, 9). ^{13}C NMR (126 MHz, $CDCl_3$) rotamers δ 178.2 (31), 167.2 (34), 157.3 and 157.0 (21), 149.9 and 149.9 (1), 137.2 and 137.1 (5), 135.9 and 135.8 (17), 130.4 (4), 130.0 and 129.9 (3), 128.6 and 128.6 (13, 15), 128.0 (14), 127.9 and 127.9 (16, 18), 115.8 and 115.5 (2), 114.7 and 114.4 (6), 67.2 and 67.2 (19), 55.7 and 55.5 (10), 54.8 (29), 52.9 (24, 28), 49.6 and 49.5 (25, 27), 30.3 and 29.8 (12), 28.8 and 28.7 (7), 28.2 and 27.7 (9), 24.8 (30), 22.3 and 22.2 (8), 11.7 (36).

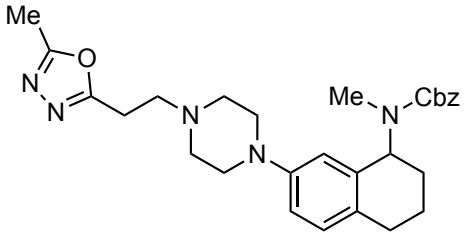

Benzyl methyl(7-(4-(2-(5-methyl-1,3,4-oxadiazol-2-yl)ethyl)piperazin-1-yl)-1,2,3,4-tetrahydronaphthalen-1-yl)carbamate (**2.58**) (MDW-2-251). A mixture of *c.a.* 80% $N_2H_4 \cdot H_2O$ in water (70 μL) was added to a solution of **2.42** (58 mg, 0.12 mmol) in EtOH (1.2 mL), and the reaction was heated under reflux for 21 h. The reaction mixture was concentrated under reduced pressure and dissolved in CH_2Cl_2 (5 mL), whereupon it was washed with 1 N NaOH (5 mL). The organic layer was separated, and the aqueous

layer was extracted with CH_2Cl_2 (2 x 5 mL). The combined organic extracts were dried (Na_2SO_4), and concentrated under reduced pressure. The crude residue was dissolved in triethyl orthoacetate (1.0 mL) and CH_3CO_2H (2 drops) was added. The reaction was heated at 125 °C under microwave irradiation for 1 h. The reaction was cooled to room temperature and concentrated under reduced pressure. The crude crude residue was dissolved in CH_2Cl_2 (5 mL) and washed with 1 N NaOH (5 mL). The organic layer was separated, and the aqueous layer was extracted with CH_2Cl_2 (2 x 5 mL). The combined organic extracts were dried (Na_2SO_4) and concentrated under reduced pressure. The crude residue was purified via flash chromatography (SiO_2) eluting with hexanes/EtOAc/Et_3N (29:70:1 to 0:99:1) to afford 37 mg (63%) of **2.58** as a colorless oil. ^{1}H NMR (400 MHz, $CDCl_3$) rotamers δ 7.46 – 7.27 (comp, 5 H), 7.02 – 6.95 (m, 1 H), 6.79 – 6.72 (m, 1 H), 6.64 – 6.57 (m, 1 H), 5.50 – 5.11 (comp, 3 H), 3.15 – 3.00 (comp, 6 H), 2.91 – 2.83 (comp, 2 H), 2.72 – 2.59 (comp, 9 H), 2.53 – 2.49 (comp, 3 H), 2.08 – 1.90 (comp, 2 H), 1.84 – 1.67 (comp, 2 H). ^{13}C NMR (126 MHz, $CDCl_3$) rotamers δ 165.7, 163.9, 157.3, 157.0, 149.9, 149.9, 137.2, 137.1, 135.9, 135.8, 130.4, 130.0, 129.9, 129.9, 128.6, 128.6, 128.0, 127.9, 127.9, 115.8, 115.5, 114.7, 114.4, 67.2, 67.2, 55.7, 55.4, 54.7, 52.9, 49.6, 49.5, 30.3, 29.8, 28.8, 28.7, 28.2, 27.7, 23.6, 22.3, 22.1, 11.1. HRMS (ESI) *m/z* calcd for $C_{28}H_{35}N_5O_3$ $(M+H)^+$, 490.2813; found 490.2817.

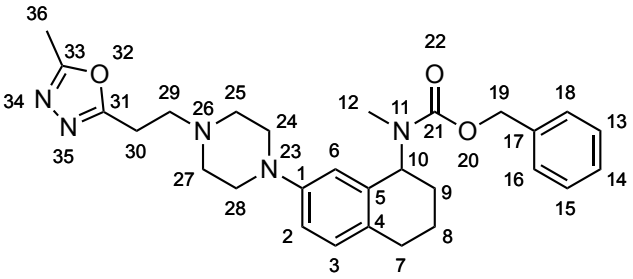

NMR Assignments (**2.58**). ^{1}H NMR (400 MHz, $CDCl_3$) rotamers δ 7.46 – 7.27 (comp, 5 H, 13, 14, 15, 16, 18), 7.02 – 6.95 (m, 1 H, 3), 6.79 – 6.72 (m, 1 H, 2), 6.64 – 6.57 (m, 1 H, 6), 5.50 – 5.11 (comp, 3 H, 10, 19), 3.15 – 3.00 (comp, 6 H, 25, 27, 30), 2.91 – 2.83 (comp, 2 H, 29), 2.72 – 2.59 (comp, 9 H, 7, 12, 24, 28), 2.53 – 2.49 (comp, 3 H, 36), 2.08 – 1.90 (comp, 2 H, 8, 9), 1.84 – 1.67 (comp, 2 H, 8, 9). ^{13}C NMR (126 MHz, $CDCl_3$) rotamers δ 165.7 (33), 163.9 (31), 157.3 and 157.0 (21), 149.9 and 149.9 (1), 137.2 and 137.1 (5), 135.9 and 135.8 (17), 130.4 (4), 130.0 and 129.9 (3), 129.9 (4), 128.6 and 128.6 (13, 15), 128.0 (14), 127.9 and 127.9 (16, 18), 115.8 and 115.5 (2), 114.7 and 114.4 (6), 67.2 and 67.2 (19), 55.7 and 55.4 (10), 54.7 (29), 52.9 (24, 28), 49.6 and 49.5 (25, 27), 30.3 and 29.8 (12), 28.8 and 28.7 (7), 28.2 and 27.7 (9), 23.6 (30), 22.3 and 22.1 (8), 11.1 (36).

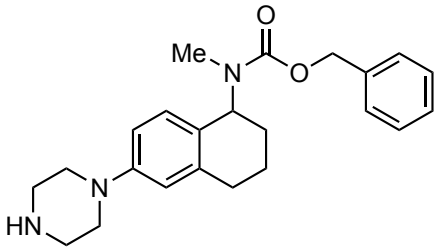

Benzyl methyl(6-(piperazin-1-yl)-1,2,3,4-tetrahydronaphthalen-1-yl)carbamate (**2.61**) (MDW-1-165). Prepared from **2.15** (0.300 g, 0.910 mmol) and piperazine according to representative procedure B. The crude residue was purified via flash chromatography (SiO_2) eluting with DCM/MeOH/Et_3N (97:2:1) to afford 0.114 g (35%) of **2.61** as a pale yellow oil. ^{1}H NMR (400 MHz, $CDCl_3$) rotamers δ 7.44 – 7.23 (comp, 5H), 7.00 – 6.92 (m, 1H), 6.77 – 6.69 (m, 1H), 6.63 – 6.57 (m, 1H), 5.46 – 5.27 (m, 1H), 5.25 – 5.13 (comp, 2H), 3.15 – 3.05 (comp, 4H), 3.04 – 2.96 (comp, 4H), 2.72 – 2.59 (comp, 6H), 2.04 – 1.88 (comp, 2H), 1.82 – 1.63 (comp, 2H). ^{13}C NMR (101 MHz,

$CDCl_3$) rotamers δ 157.1, 156.9, 150.5, 150.4, 139.2, 139.0, 137.1, 137.0, 128.4, 128.2, 128.0, 127.8, 127.8, 127.7, 127.6, 126.5, 126.4, 115.8, 114.6, 67.0, 54.8, 54.6, 50.1, 46.0, 30.0, 30.0, 29.9, 29.4, 28.3, 27.8, 22.1, 22.0. HRMS (ESI) *m/z* calcd for $C_{23}H_{29}N_3O_2$ $(M+H)^+$, 380.2333; found 380.2346.

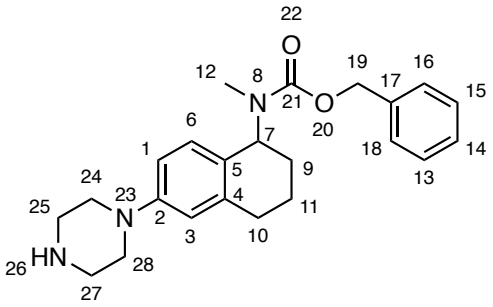

NMR Assignments (**2.61**). ^{1}H NMR (400 MHz, $CDCl_3$) rotamers δ 7.44 – 7.23 (comp, 5H, 13, 14, 15, 16, 18), 7.00 – 6.92 (m, 1H, 6), 6.77 – 6.69 (m, 1H, 1), 6.63 – 6.57 (m, 1H, 3), 5.46 – 5.27 (m, 1H, 7), 5.25 – 5.13 (comp, 2H, 19), 3.15 – 3.05 (comp, 4H, 24, 28), 3.04 – 2.96 (comp, 4H, 25, 27), 2.72 – 2.59 (comp, 6H, 10, 12, 26), 2.04 – 1.88 (comp, 2H, 9, 11), 1.82 – 1.63 (comp, 2H, 9, 11). ^{13}C NMR (101 MHz, $CDCl_3$) δ 157.1 (21), 156.9 (21), 150.5 (2), 150.4 (2), 139.2 (4), 139.0 (4), 137.1 (17), 137.0 (17), 128.4 (13, 15), 128.2 (6), 128.0 (6), 127.8 (14), 127.8 (14), 127.7 (16, 18), 127.6 (16, 18), 126.5 (5), 126.4 (5), 115.8 (3), 114.6 (1), 67.0, 54.8 (7), 54.6 (7), 50.1 (24, 28), 46.0 (25, 27), 30.0 (12), 30.0 (12), 29.9 (10), 29.4 (10), 28.3 (9), 27.8 (9), 22.1 (11), 22.0 (11).

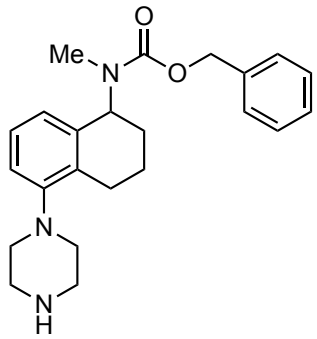

Benzyl methyl(5-(piperazin-1-yl)-1,2,3,4-tetrahydronaphthalen-1-yl)carbamate (**2.60**) (MDW-1-212). Prepared from **2.27** (0.129 g, 0.339 mmol) and piperazine according to representative procedure B. The crude residue was purified via flash chromatography (SiO_2) eluting with DCM/MeOH/Et_3N (97:2:1) to afford 0.0735 g (57%) of **2.60** as a pale yellow oil. ^1H NMR (400 MHz, $CDCl_3$) rotamers δ 7.45 – 7.27 (comp, 5H), 7.13 (t, *J* = 7.8 Hz, 1H), 6.95 – 6.84 (comp, 2H), 5.56 – 5.32 (m, 1H), 5.28 – 5.14 (comp, 2H), 3.07 – 2.92 (comp, 6H), 2.81 – 2.72 (comp, 2H), 2.72 – 2.59 (comp, 5H), 2.55 – 2.42 (m, 1H), 2.10 – 1.93 (comp, 2H), 1.86 – 1.61 (comp, 2H). ^{13}C NMR (126 MHz, $CDCl_3$) rotamers: δ 157.1, 156.8, 151.6, 151.6, 137.0, 136.9, 136.5, 136.4, 134.0, 133.8, 128.5, 128.4, 127.9, 127.8, 127.7, 127.7, 126.4, 126.4, 122.6, 122.5, 117.8, 117.7, 67.1, 55.7, 55.5, 53.1, 46.5, 30.2, 29.6, 27.9, 27.4, 25.3, 25.2, 22.1, 22.0. HRMS (ESI) *m/z* calcd for $C_{23}H_{29}N_3O_2$ $(M+H)^+$, 380.2333; found 380.2348.

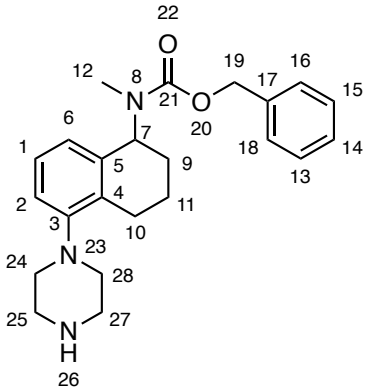

NMR Assignments (**2.60**). ^1H NMR (400 MHz, $CDCl_3$) rotamers δ 7.45 – 7.27 (comp, 5H, 13, 14, 15, 16, 18), 7.13 (t, *J* = 7.8 Hz, 1H, 1), 6.95 – 6.84 (comp, 2H, 2, 6), 5.56 – 5.32 (m, 1H, 7), 5.28 – 5.14 (comp, 2H, 19), 3.07 – 2.92 (comp, 6H, 24, 25, 27, 28), 2.81 – 2.72 (comp, 2H, 25, 27), 2.72 – 2.59 (comp, 5H, 10, 12, 26), 2.55 – 2.42 (m, 1H, 10), 2.10 – 1.93 (comp, 2H, 9, 11), 1.86 – 1.61 (comp, 2H, 9, 11). ^{13}C NMR (101

MHz, $CDCl_3$) δ 157.1 (21), 156.8 (21), 151.6 (3), 151.6 (3), 137.0 (5), 136.9 (5), 136.5 (17), 136.4 (17), 134.0 (1), 133.8 (1), 128.5 (13, 15), 128.4 (13, 15), 127.9 (14), 127.8 (14), 127.7 (16, 18), 127.7 (16, 18), 126.4 (4), 126.4 (4), 122.6 (6), 122.5 (6), 117.8 (2), 117.7 (2), 67.1 (19), 55.7 (7), 55.5 (7), 53.1 (24, 28), 46.5 (25, 27), 30.2 (12), 29.6 (12), 27.9 (9), 27.4 (9), 25.3 (10), 25.2 (10), 22.1 (11), 22.0.

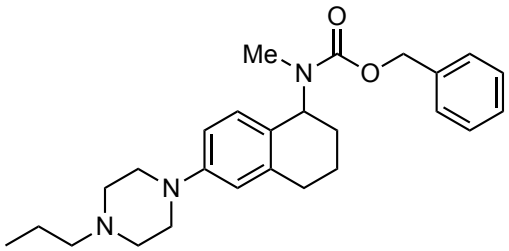

Benzyl methyl(6-(4-propylpiperazin-1-yl)-1,2,3,4-tetrahydronaphthalen-1-yl)carbamate (**2.64**) (MDW-1-204). Prepared from **2.61** (30 mg, 0.079 mmol) and propionaldehyde according to representative procedure E. The crude residue was purified via flash chromatography (SiO_2) eluting with hexanes/EtOAc/Et_3N (76:23:1) to afford 24 mg (71%) of **2.64** as a pale yellow oil. ^{1}H NMR (400 MHz, $CDCl_3$) rotamers δ 7.45 – 7.28 (comp, 5H), 7.01 – 6.95 (m, 1H), 6.75 (d, J = 8.6 Hz, 1H), 6.64 – 6.60 (m, 1H), 5.49 – 5.28 (m, 1H), 5.27 – 5.11 (comp, 2H), 3.25 – 3.14 (comp, 4H), 2.82 – 2.67 (comp, 2H), 2.67 – 2.56 (comp, 7H), 2.40 – 2.32 (comp, 2H), 2.07 – 1.90 (comp, 2H), 1.84 – 1.65 (comp, 2H), 1.56 (h, J = 7.9, 7.4 Hz, 2H), 0.93 (t, J = 7.4 Hz, 3H).^{13}C NMR (101 MHz, $CDCl_3$) rotamers δ 157.3, 157.0, 150.2, 150.1, 139.4, 139.1, 137.2, 137.2, 128.6, 128.6, 128.3, 128.2, 128.0, 128.0, 127.9, 127.8, 126.5, 126.4, 115.8, 114.6, 67.2, 67.2, 60.8, 54.9, 54.8, 53.4, 49.1, 30.2, 30.1, 29.8, 29.6, 28.4, 27.9, 22.3, 22.1, 20.1, 12.1. HRMS (ESI) *m/z* calcd for $C_{26}H_{35}N_3O_2$ $(M+H)^+$, 422.2802; found 422.2819.

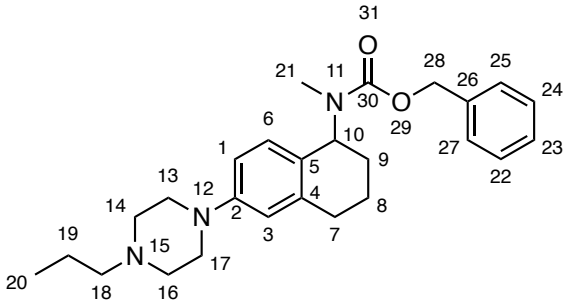

NMR Assignments (**2.64**). ^{1}H NMR (400 MHz, $CDCl_3$) rotamers δ 7.45 – 7.28 (comp, 5H, 22, 23, 24, 25, 27), 7.01 – 6.95 (m, 1H, 6), 6.75 (d, J = 8.6 Hz, 1H, 1), 6.64 – 6.60 (m, 1H, 3), 5.49 – 5.28 (m, 1H, 10), 5.27 – 5.11 (comp, 2H, 28), 3.25 – 3.14 (comp, 4H, 13, 17), 2.82 – 2.67 (comp, 2H, 7), 2.67 – 2.56 (comp, 7H, 14, 16, 21), 2.40 – 2.32 (comp, 2H, 18), 2.07 – 1.90 (comp, 2H, 8, 9), 1.84 – 1.65 (comp, 2H, 8, 9), 1.56 (h, J = 7.9, 7.4 Hz, 2H, 19), 0.93 (t, J = 7.4 Hz, 3H, 20). ^{13}C NMR (101 MHz, $CDCl_3$) rotamers δ 157.3 (30), 157.0 (30), 150.2 (2), 150.1 (2), 139.4 (4), 139.1 (4), 137.2 (26), 137.2 (26), 128.6 (22, 24), 128.6 (22, 24), 128.3 (6), 128.2 (6), 128.0 (23), 128.0 (23), 127.9 (25, 27), 127.8 (25, 27), 126.5 (5), 126.4 (5), 115.8 (3), 114.6 (1), 67.2, 67.2 (28), 60.8 (18), 54.9 (10), 54.8 (10), 53.4 (14, 16), 49.1 (13, 17), 30.2 (7), 30.1 (7), 29.8 (21), 29.6, 28.4 (18), 27.9 (18), 22.3 (9), 22.1 (9), 20.1 (19), 12.1 (20).

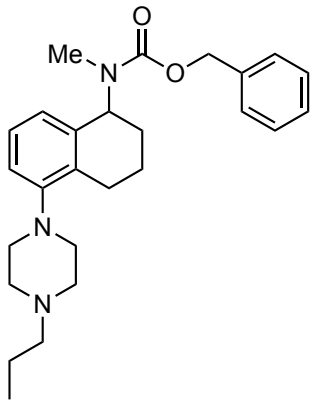

Benzyl methyl(5-(4-propylpiperazin-1-yl)-1,2,3,4-tetrahydronaphthalen-1-yl)carbamate (**2.63**) (MDW-1-215). Prepared from **2.60** (30 mg, 0.079 mmol) and

propionaldehyde according to representative procedure E. The crude residue was purified via flash chromatography (SiO_2) eluting with hexanes/EtOAc/Et_3N (82:17:1) to afford 23 mg (68%) of **2.63** as a pale yellow oil. ^{1}H NMR (499 MHz, $CDCl_3$) rotamers δ 7.43 – 7.28 (comp, 5H), 7.13 (t, *J* = 7.8 Hz, 1H), 6.96 – 6.92 (m, 1H), 6.90 – 6.85 (m, 1H), 5.56 – 5.35 (m, 1H), 5.26 – 5.11 (comp, 2H), 3.07 – 2.93 (comp, 3H), 2.87 – 2.78 (comp, 2H), 2.70 – 2.43 (comp, 8H2.41 – 2.35 (comp, 2H), 2.10 – 1.94 (comp, 2H), 1.85 – 1.64 (comp, 2H), 1.61 – 1.51 (comp, 2H), 0.94 (t, *J* = 7.4 Hz, 3H). ^{13}C NMR (126 MHz, $CDCl_3$) δ 157.3, 156.9, 151.5, 151.4, 137.2, 137.1, 136.6, 136.5, 134.1, 133.9, 128.6, 128.6, 128.0, 128.0, 127.9, 127.8, 126.6, 126.5, 122.7, 122.5, 117.8, 117.8, 67.3, 61.0, 55.9, 55.6, 53.9, 52.0, 30.4, 29.7, 28.1, 27.6, 25.4, 25.4, 22.3, 22.2, 20.2, 12.2. HRMS (ESI) *m/z* calcd for $C_{26}H_{35}N_3O_2$ $(M+H)^+$, 422.2802; found 422.2804.

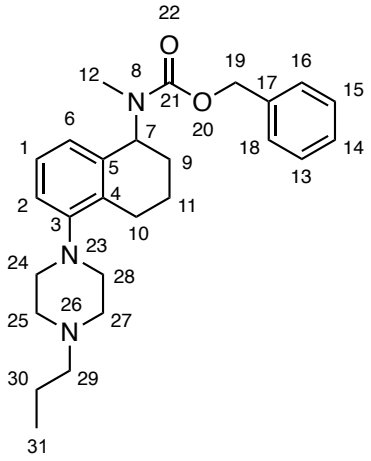

NMR Assignments (**2.63**).^{1}H NMR (499 MHz, $CDCl_3$) rotamers δ 7.43 – 7.28 (comp, 5H, 13, 14, 15, 16, 18), 7.13 (t, *J* = 7.8 Hz, 1H, 1), 6.96 – 6.92 (m, 1H, 6), 6.90 – 6.85 (m, 1H, 2), 5.56 – 5.35 (m, 1H, 7), 5.26 – 5.11 (comp, 2H, 19), 3.07 – 2.93 (comp, 3H, 10, 24, 28), 2.87 – 2.78 (comp, 2H, 24, 28), 2.70 – 2.43 (comp, 8H, 10, 12, 25, 27), 2.41 – 2.35 (comp, 2H, 29), 2.10 – 1.94 (comp, 2H, 9, 11), 1.85 – 1.64 (comp, 2H, 9, 11),

1.61 – 1.51 (comp, 2H, 30), 0.94 (t, J = 7.4 Hz, 3H, 31). ^{13}C NMR (126 MHz, $CDCl_3$) δ 157.3 (21), 156.9 (21), 151.5 (3), 151.4 (3), 137.2 (5), 137.1, 136.6 (17), 136.5 (17), 134.1 (4), 133.9 (4), 128.6 (13, 15), 128.6 (13, 15), 128.0 (14), 128.0 (14), 127.9 (16, 18), 127.8 (16, 18), 126.6 (1), 126.5 (1), 122.7 (6), 122.5 (6), 117.8 (2), 117.8 (2), 67.3 (19), 61.0 (29), 55.9 (7), 55.6 (7), 53.9 (25, 27), 52.0, 30.4 (12), 29.7 (12), 28.1 (9), 27.6 (9), 25.4 (10), 25.4 (10), 22.3 (11), 22.2 (11), 20.2 (30), 12.2 (31).

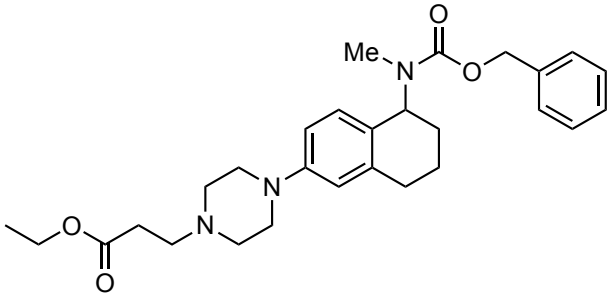

Ethyl 3-(4-(5-(((benzyloxy)carbonyl)(methyl)amino)-5,6,7,8-tetrahydronaphthalen-2-yl)piperazin-1-yl)propanoate (**2.66**) (MDW-1-207). Prepared from **2.61** (30 mg, 0.079 mmol) and ethyl acrylate according to representative procedure H. The crude residue was purified via flash chromatography (SiO_2) eluting with hexanes/EtOAc/Et_3N (69:30:1) to afford 32 mg (84%) of **2.66** as a pale yellow oil.^{1}H NMR (499 MHz, $CDCl_3$) rotamers δ 7.44 – 7.26 (comp, 5H), 7.00 – 6.94 (m, 1H), 6.76 – 6.72 (m, 1H), 6.63 – 6.59 (m, 1H), 5.47 – 5.29 (m, 1H), 5.27 – 5.15 (comp, 2H), 4.15 (q, J = 7.1 Hz, 2H), 3.21 – 3.11 (comp, 4H), 2.79 – 2.70 (comp, 3H), 2.72 – 2.66 (m, 1H), 2.66 – 2.58 (comp, 7H), 2.53 (t, J = 7.8, 6.9 Hz, 2H), 2.06 – 1.91 (comp, 2H), 1.83 – 1.66 (comp, 2H), 1.26 (t, J = 7.1 Hz, 3H). ^{13}C NMR (126 MHz, $CDCl_3$) rotamers δ 172.6, 157.3, 157.0, 150.1, 150.0, 139.4, 139.1, 137.2, 137.1, 128.6, 128.6, 128.3, 128.1, 128.0, 128.0, 127.9, 127.8, 126.6, 126.5, 115.9, 114.6, 67.2, 67.2, 60.6, 54.9, 54.8, 53.7, 53.1,

49.1, 32.5, 30.2, 30.1, 29.8, 29.5, 28.4, 27.9, 22.2, 22.1, 14.4. HRMS (ESI) *m/z* calcd for $C_{28}H_{37}N_3O_4$ $(M+H)^+$, 480.2857; found 480.2876

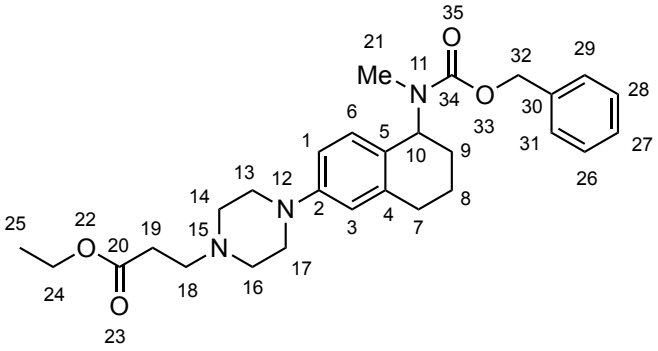

NMR Assignments (**2.66**).^{1}H NMR (499 MHz, CDCl) rotamers δ 7.44 – 7.26 (comp, 5H, 26, 27, 28, 29, 31), 7.00 – 6.94 (m, 1H, 6), 6.76 – 6.72 (m, 1H, 1), 6.63 – 6.59 (m, 1H, 3), 5.47 – 5.29 (m, 1H, 10), 5.27 – 5.15 (comp, 2H, 32), 4.15 (q, *J* = 7.1 Hz, 2H, 24), 3.21 – 3.11 (comp, 4H, 13, 17), 2.79 – 2.70 (comp, 3H, 7, 18), 2.72 – 2.66 (m, 1H, 7), 2.66 – 2.58 (comp, 7H, 14, 16, 21), 2.53 (t, *J* = 7.8, 6.9 Hz, 2H, 19), 2.06 – 1.91 (comp, 2H, 8, 9), 1.83 – 1.66 (comp, 2H, 8, 9), 1.26 (t, *J* = 7.1 Hz, 3H, 25). ^{13}C NMR (126 MHz, CDC_3) rotamers δ 172.6 (20), 157.3 (34), 157.0 (34), 150.1 (2), 150.0 (2), 139.4 (4), 139.1 (4), 137.2 (30), 137.1 (30), 128.6 (26, 28), 128.6 (26, 28), 128.3 (6), 128.1 (6), 128.0 (27), 128.0 (27), 127.9 (29, 31), 127.8 (29, 31), 126.6 (5), 126.5 (5), 115.9 (3), 114.6 (1), 67.2 (32), 67.2 (32), 60.6 (24), 54.9 (10), 54.8 (10), 53.7 (18), 53.1 (14, 16), 49.1 (13, 17), 32.5 (19), 30.2 (7), 30.1 (7), 29.8 (21), 29.5 (21), 28.4 (9), 27.9 (9), 22.2 (8), 22.1 (8), 14.4 (25).

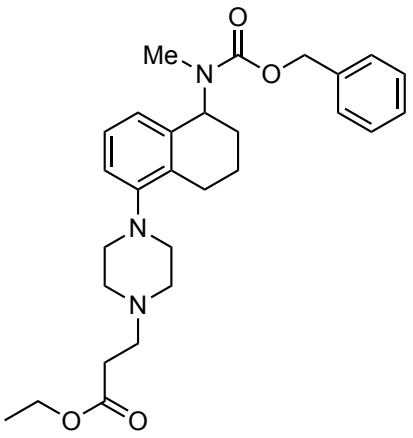

Ethyl 3-(4-(5-(((benzyloxy)carbonyl)(methyl)amino)-5,6,7,8-tetrahydronaphthalen-1-yl)piperazin-1-yl)propanoate (**2.65**) (MDW-1-214). Prepared from **2.60** (30 mg, 0.079 mmol) and ethyl acrylate according to representative procedure H. The crude residue was purified via flash chromatography (SiO_2) eluting with hexanes/EtOAc/Et_3N (79:20:1) to afford 22 mg (59%) of **2.65** as a pale yellow oil. ^1H NMR (499 MHz, $CDCl_3$) rotamers δ 7.43 – 7.27 (comp, 5H), 7.13 (t, *J* = 7.8 Hz, 1H), 6.94 – 6.90 (m, 1H), 6.90 – 6.85 (m, 1H), 5.55 – 5.35 (m, 1H), 5.26 – 5.11 (comp, 2H), 4.16 (q, *J* = 7.2 Hz, 2H), 3.04 – 2.92 (comp, 3H), 2.85 – 2.75 (comp, 4H), 2.71 – 2.41 (comp, 10H), 2.10 – 1.93 (comp, 2H), 1.85 – 1.62 (comp, 2H), 1.27 (t, *J* = 7.1 Hz, 3H). ^{13}C NMR (126 MHz, $CDCl_3$) rotamers δ 172.6, 157.3, 156.9, 151.3, 151.3, 137.1, 137.1, 136.6, 136.5, 134.1, 133.9, 128.6, 128.6, 128.0, 128.0, 127.9, 127.8, 126.6, 126.5, 122.8, 122.6, 117.8, 117.7, 67.3, 60.6, 55.8, 55.6, 53.8, 53.6, 51.9, 32.5, 30.4, 29.7, 28.1, 27.6, 25.4, 25.3, 22.3, 22.1, 14.4. HRMS (ESI) *m/z* calcd for $C_{28}H_{37}N_3O_4$ $(M+H)^+$, 480.2857; found 480.2875.

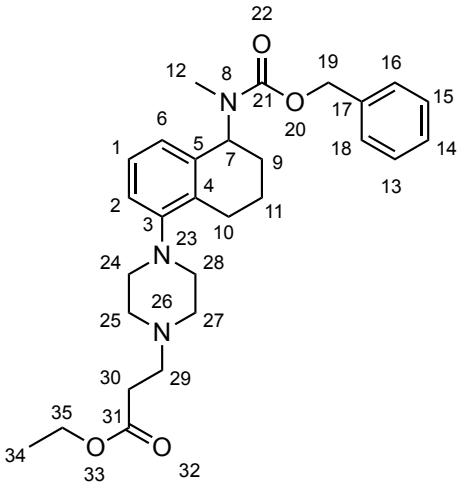

NMR Assignments (**2.65**).^{1}H NMR (499 MHz, $CDCl_3$) rotamers δ 7.43 – 7.27 (comp, 5H, 13, 14, 15, 16, 18), 7.13 (t, *J* = 7.8 Hz, 1H, 1), 6.94 – 6.90 (m, 1H, 6), 6.90 – 6.85 (m, 1H, 2), 5.55 – 5.35 (m, 1H, 7), 5.26 – 5.11 (comp, 2H, 19), 4.16 (q, *J* = 7.2 Hz, 2H, 35), 3.04 – 2.92 (comp, 3H, 10, 24', 28'), 2.85 – 2.75 (comp, 4H, 24'', 28'', 29), 2.71 – 2.41 (comp, 10H, 10, 12, 25, 27, 30), 2.10 – 1.93 (comp, 2H, 9', 11'), 1.85 – 1.62 (comp, 2H, 9'', 11''), 1.27 (t, *J* = 7.1 Hz, 3H, 34). ^{13}C NMR (126 MHz, $CDCl_3$) δ 172.6 (31), 157.3 (21), 156.9 (21), 151.3 (3), 151.3 (3), 137.1 (5), 137.1 (5), 136.6 (17), 136.5 (17), 134.1 (1), 133.9 (1), 128.6 (13, 15), 128.6 (13, 15), 128.0 (14), 128.0 (14), 127.9 (16, 18), 127.8 (16, 18), 126.6 (4), 126.5 (4), 122.8 (6), 122.6 (6), 117.8 (2), 117.7 (2), 67.3 (19), 60.6 (35), 55.8 (7), 55.6 (7), 53.8 (29), 53.6 (24, 28), 51.9 (25, 27), 32.5 (30), 30.4 (12), 29.7 (12), 28.1 (9), 27.6 (9), 25.4 (10), 25.3 (10), 22.3 (11), 22.1 (11), 14.4 (34).

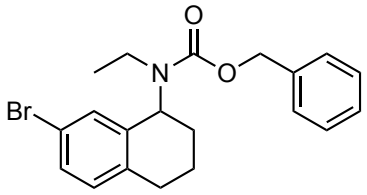

Benzyl (7-bromo-1,2,3,4-tetrahydronaphthalen-1-yl)(ethyl)carbamate (**2.71**) (MDW-1-182). A solution containing 7-bromotetralone (0.500 g, 2.22 mmol), $EtNH_3Cl$

(1.81 g, 22.2 mmol), $NaBH_3CN$ (0.279 g, 4.44 mmol), and Et_3N (2.25 g, 3.1 mL, 22.2 mmol) was stirred at room temperature for 48 h. The reaction was diluted with Et_2O (20 mL) and extracted with 1 N HCl (3 x 30 mL). The combined aqueous extracts were made basic with 6 N NaOH and extracted with CH_2Cl_2 (3 x 100 mL). The combined organic extracts were dried (Na_2SO_4), and concentrated under reduced pressure to afford 0.361 g of a crude residue that was used directly. The crude residue was dissolved in CH_2Cl_2 (14 mL) and cooled to 0 °C, whereupon *i*-Pr_2Net (0.36 g, 0.49 mL, 2.8 mmol) and CbzCl (0.29 g, 0.24 mL, 1.7 mmol) were added sequentially. The reaction was stirred for 1 h and the cooling bath was removed, and the solution was stirred for 14 h at room temperature. The reaction was diluted with CH_2Cl_2 (20 mL) and washed with 1 N HCl (2 x 25 mL), 1 N NaOH (2 x 25 mL), and brine (1 x 25 mL). The organic layer was dried (Na_2SO_4) and concentrated under reduced pressure. The crude residue was purified via flash chromatography (SiO_2) eluting with hexanes/EtOAc (25:4) to afford 0.432 g (50%) of **2.71** as a pale yellow oil. ^1H NMR (400 MHz, $CDCl_3$) rotamers: δ 7.52 – 7.15 (comp, 7 H), 7.01 – 6.87 (m, 1H), 5.50 – 5.01 (comp, 3 H), 3.45 – 3.19 (m, 1 H), 3.08 – 2.57 (comp, 3 H), 2.17 – 1.92 (comp, 2 H), 1.90 – 1.64 (comp, 2 H), 1.28 – 1.07 (m, 3 H). HRMS (ESI) *m/z* calcd for $C_{20}H_{22}BrNO_2$ $(M+Na)^+$, 410.0726; found 410.0736.

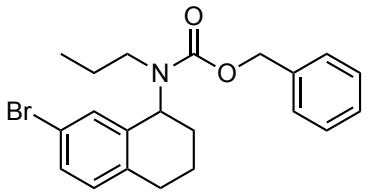

Benzyl (7-bromo-1,2,3,4-tetrahydronaphthalen-1-yl)(propyl)carbamate (**2.72**) (MDW-1-182). A solution containing bromotetralone (0.500 g, 2.22 mmol), propylamine (0.40 g, 0.55 mL 6.7 mmol), $Na(OAc)BH_3$ (0.942 g, 4.44 mmol), and acetic acid (0.24 g, 0.23 mL, 4.0 mmol) was stirred at room temperature for 48 h. The reaction was diluted

with Et_2O (20 mL) and extracted with 1 N HCl (3 x 30 mL). The combined aqueous extracts were made basic with 6 N NaOH and extracted with CH_2Cl_2 (3 x 100 mL). The combined organic extracts were dried (Na_2SO_4), and concentrated under reduced pressure to afford 0.277 g of a crude residue that was used directly. The crude residue was dissolved in CH_2Cl_2 (10 mL) and cooled to 0 °C, whereupon *i*-Pr_2Net (0.27 g, 0.36 mL, 2.8 mmol) and CbzCl (0.22 g, 0.18 mL, 1.7 mmol) were added sequentially. The reaction was stirred for 1 h and the cooling bath was removed, and the solution was stirred for 14 h at room temperature. The reaction was diluted with CH_2Cl_2 (20 mL) and washed with 1 N HCl (2 x 25 mL), 1 N NaOH (2 x 25 mL), and brine (1 x 25 mL). The organic layer was dried (Na_2SO_4) and concentrated under reduced pressure. The crude residue was purified via flash chromatography (SiO_2) eluting with hexanes/EtOAc (25:4) to afford 0.398 g (45%) of **2.72** as a pale yellow oil. ^{1}H NMR (400 MHz, $CDCl_3$) rotamers δ 7.46 – 7.14 (comp, 7H), 6.98 – 6.89 (m, 1H), 5.41 – 4.96 (comp, 3H), 3.33 – 3.14 (m, 1H), 2.99 – 2.60 (comp, 3H), 2.14 – 1.93 (comp, 2H), 1.92 – 1.65 (comp, 3H), 1.64 – 1.47 (m, 1H), 0.94 – 0.75 (comp, 3H). ^{13}C NMR (101 MHz, $CDCl_3$) δ 156.8, 156.0, 139.1, 138.6, 137.0, 136.8, 136.6, 136.5, 130.7, 130.7, 129.7, 129.6, 129.4, 129.2, 128.4, 128.3, 127.8, 127.6, 127.5, 119.6, 67.0, 67.0, 56.5, 56.0, 48.5, 46.7, 28.9, 28.5, 23.5, 22.5, 22.1, 22.0, 11.4. HRMS (ESI) *m/z* calcd for $C_{21}H_{24}BrNO_2$ $(M+Na)^+$, 424.0883; found 424.0891.

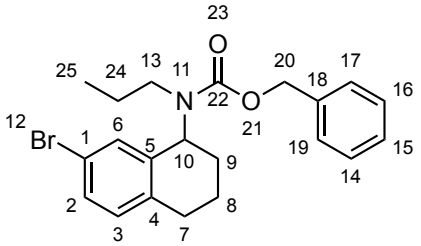

NMR Assignments (**2.72**). ^{1}H NMR (400 MHz, $CDCl_3$) rotamers δ 7.46 – 7.14 (comp, 7H, 2, 6, 14, 15, 16, 17, 19), 6.98 – 6.89 (m, 1H, 3), 5.41 – 4.96 (comp, 3H, 10,

20), 3.33 – 3.14 (m, 1H, 7), 2.99 – 2.60 (comp, 3H, 7, 13), 2.14 – 1.93 (comp, 2H, 8, 9), 1.92 – 1.65 (comp, 3H, 8, 9, 24), 1.64 – 1.47 (m, 1H, 24), 0.94 – 0.75 (comp, 3H, 25). ^{13}C NMR (101 MHz, $CDCl_3$) rotamers δ 156.8 (22), 156.0 (22), 139.1 (5), 138.6 (5), 137.0 (18), 136.8 (18), 136.6 (4), 136.5 (4), 130.7, 130.7 (6), 129.7 (3), 129.6 (3), 129.4 (1), 129.2 (1), 128.4 (14, 16), 128.3 (14, 16), 127.8 (15), 127.6 (17, 19), 127.5 (17, 19), 119.6 (2), 67.0 (20), 67.0 (20), 56.5 (10), 56.0 (10), 48.5 (13), 46.7 (13), 28.9 (7), 28.5 (9), 23.5 (24), 22.5 (24), 22.1 (8), 22.0 (8), 11.4 (25).

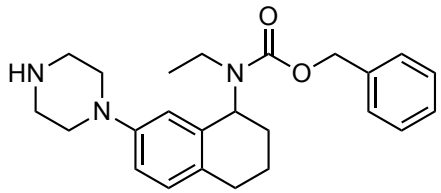

Benzyl ethyl(7-(piperazin-1-yl)-1,2,3,4-tetrahydronaphthalen-1-yl)carbamate (**2.73**) (MDW-1-185). Prepared from **2.71** (0.432 g 1.11 mmol) and piperazine according to representative procedure B. The crude residue was purified via flash chromatography (SiO_2) eluting with DCM/MeOH/Et_3N (97:2:1) to afford 0.320 g (73%) of **2.73** as an orange oil. ^{1}H NMR (400 MHz, $CDCl_3$) rotamers δ 7.41 – 7.17 (comp, 5H), 6.93 (d, J = 8.4 Hz, 1H), 6.70 (dd, J = 8.4, 2.6 Hz, 1H), 6.60 – 6.55 (m, 1H), 5.46 – 4.97 (comp, 4H), 3.35 – 3.06 (comp, 2H), 2.98 – 2.86 (comp, 8H), 2.71 – 2.56 (comp, 2H), 2.07 – 1.94 (comp, 2H), 1.85 – 1.59 (comp, 2H), 1.12 (dt, J = 24.7, 7.0 Hz, 3H). ^{13}C NMR (101 MHz, $CDCl_3$) rotamers δ 156.9, 156.0, 150.0, 149.9, 136.9, 136.8, 136.5, 136.1, 129.5, 129.4, 129.1, 128.2, 128.1, 127.6, 127.5, 115.4, 115.2, 114.2, 113.8, 66.6, 66.5, 56.4, 56.0, 50.4, 50.3, 45.9, 40.3, 38.8, 29.2, 28.8, 28.5, 28.4, 22.3, 22.1, 15.6, 14.5. HRMS (ESI) *m/z* calcd for $C_{24}H_{31}N_3O_2$ $(M+H)^+$, 394.2489; found 394.2507.

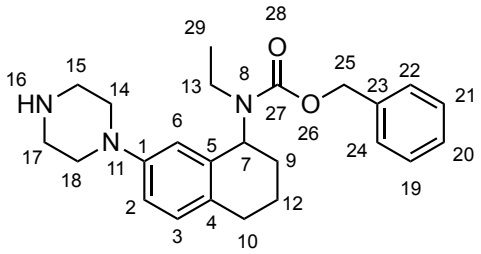

NMR Assignments (**2.73**). ^{1}H NMR (400 MHz, $CDCl_3$) rotamers δ 7.41 – 7.17 (comp, 5H, 19, 20, 21, 22, 24), 6.93 (d, *J* = 8.4 Hz, 1H, 3), 6.70 (dd, *J* = 8.4, 2.6 Hz, 1H, 6), 6.60 – 6.55 (m, 1H, 2), 5.46 – 4.97 (comp, 4H, 7, 16, 25), 3.35 – 3.06 (m, 2H, 13), 2.98 – 2.86 (comp, 8H, 14, 15, 17, 18), 2.71 – 2.56 (comp, 2H, 10), 2.07 – 1.94 (comp, 2H, 9, 12), 1.85 – 1.59 (comp, 2H, 9, 12), 1.12 (dt, *J* = 24.7, 7.0 Hz, 3H, 29). ^{13}C NMR (101 MHz, $CDCl_3$) rotamers δ 156.9 (27), 156.0 (27), 150.0 (1), 149.9 (1), 136.9 (5), 136.8 (5), 136.5 (23), 136.1 (23), 129.5 (4), 129.4 (3), 129.1 (4), 128.2 (19), 128.1 (21), 127.6 (20), 127.5 (22, 24), 115.4 (2), 115.2 (2), 114.2 (6), 113.8 (6), 66.6 (25), 66.5 (25), 56.4, 56.0 (7), 50.4 (14, 18), 50.3 (14, 18), 45.9 (15, 17), 40.3 (13), 38.8 (13), 29.2 (10), 28.8 (10), 28.5 (9), 28.4 (9), 22.3 (12), 22.1 (12), 15.6 (29), 14.5 (29).

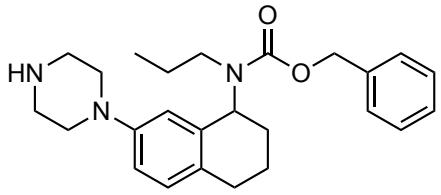

Benzyl (7-(piperazin-1-yl)-1,2,3,4-tetrahydronaphthalen-1-yl)(propyl)carbamate (**2.74**) (MDW-1-186). Prepared from **2.72** (0.398 g 1.02 mmol) and piperazine according to representative procedure B. The crude residue was purified via flash chromatography (SiO_2) eluting with DCM/MeOH/Et_3N (97:2:1) to afford 0.284 g (70%) of **2.74** as an orange oil. ^{1}H NMR (400 MHz, $CDCl_3$) rotamers δ 7.43 – 7.18 (comp, 5H), 6.95 (d, *J* = 8.4 Hz, 1H), 6.73 (dd, *J* = 8.4, 2.6 Hz, 1H), 6.60 – 6.54 (m, 1H), 5.42 – 4.99 (comp, 3H), 3.26 – 3.04 (m, 1H), 3.02 – 2.87 (comp, 8H), 2.83 – 2.59 (comp,

3H), 2.10 – 1.97 (comp, 2H), 1.97 – 1.88 (m, 1H), 1.84 – 1.60 (comp, 3H), 1.59 – 1.44 (m, 1H), 0.77 (dt, J = 30.3, 7.4 Hz, 3H). ^{13}C NMR (101 MHz, $CDCl_3$) rotamers δ 157.0, 156.3, 150.1, 150.0, 137.0, 136.8, 136.3, 129.6, 129.5, 129.1, 128.2, 128.1, 127.6, 127.5, 127.5, 115.5, 115.2, 114.1, 113.6, 66.6, 66.6, 56.7, 56.1, 50.5, 50.4, 46.3, 45.9, 29.3, 28.9, 28.5, 28.5, 23.5, 22.4, 22.2, 11.4. HRMS (ESI) *m/z* calcd for $C_{25}H_{33}N_3O_2$ $(M+H)^+$, 408.2646; found 408.2661.

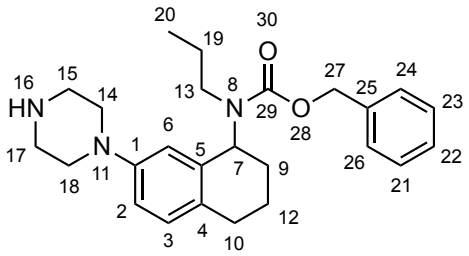

NMR Assignments (**2.74**). ^{1}H NMR (400 MHz, $CDCl_3$) rotamers δ 7.43 – 7.18 (comp, 5H, 21, 22, 23, 24, 26), 6.95 (d, J = 8.4 Hz, 1H, 3), 6.73 (dd, J = 8.4, 2.6 Hz, 1H, 2), 6.60 – 6.54 (m, 1H, 6), 5.42 – 4.99 (comp, 3H, 7, 27), 3.26 – 3.04 (m, 1H, 10), 3.02 – 2.87 (comp, 8H, 14, 15, 17, 18), 2.83 – 2.59 (comp, 3H, 10, 13), 2.10 – 1.97 (comp, 2H, 9, 12), 1.97 – 1.88 (m, 1H, 19), 1.84 – 1.60 (comp, 3H, 9, 12, 19), 1.59 – 1.44 (m, 1H, 16), 0.77 (dt, J = 30.3, 7.4 Hz, 3H, 20). ^{13}C NMR (101 MHz, $cdcl_3$) δ 157.0 (29), 156.3 (29), 150.1 (1), 150.0 (1), 137.0 (5), 136.8 (5, 25), 136.3 (25), 129.6 (4), 129.5 (3), 129.1 (4), 128.2 (21), 128.1 (21, 23), 127.6 (24, 26), 127.5 (24, 26), 127.5 (22), 115.5 (2), 115.2 (2), 114.1 (6), 113.6 (6), 66.6 (27), 66.6 (27), 56.7 (7), 56.1 (7), 50.5 (14, 18), 50.4 (14, 18), 46.3 (13), 45.9 (15, 17), 29.3 (10), 28.9 (10), 28.5 (9), 28.5 (9), 23.5 (12), 22.4 (19), 22.2 (12), 11.4.

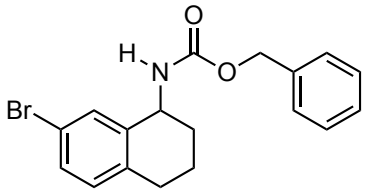

Benzyl (7-bromo-1,2,3,4-tetrahydronaphthalen-1-yl)carbamate (2.75) (MDW-1-193). NH_4OAc (1.71 g, 22.2 mmol), and $NaBH_3CN$ (691 mg, 11.1 mmol) were added to a solution of 7-bromotetralone (0.500 g, 2.22 mmol), in MeOH (11 mL) and the reaction was heated at 60 °C for 24 h. The reaction was concentrated under reduced pressure, and the crude residue was dissolved in Et_2O (30 mL) and extracted with 1 N HCl (3 x 30 mL). The combined aqueous extracts were made basic with 6 N NaOH and extracted with CH_2Cl_2 (3 x 50 mL). The combined organic extracts were dried (Na_2SO_4) and concentrated under reduced pressure. The crude residue was dissolved in CH_2Cl_2 (22 mL) and cooled to 0 °C. *i*-Pr_2Net (0.55 g, 0.75 mL, 4.3 mmol) and CbzCl (0.44 g, 0.37 mL, 2.6 mmol) were added sequentially to the cooled solution. The reaction was stirred for 1 h and the cooling bath was removed, and the solution was stirred for 14 h at room temperature. The reaction was diluted with CH_2Cl_2 (20 mL) and washed with 1 N HCl (2 x 25 mL), 1 N NaOH (2 x 25 mL), and brine (1 x 25 mL). The organic layer was dried (Na_2SO_4) and concentrated under reduced pressure. The crude residue was purified via flash chromatography (SiO_2) eluting with hexanes/EtOAc (9:1) to afford 0.502 g (59%) of **2.75** as a colorless oil. ^1H NMR (400 MHz, $CDCl_3$) δ 7.48 (dd, J = 2.1 Hz, 1H), 7.41 – 7.28 (comp, 5H), 7.25 (dd, J = 8.4, 2.1 Hz, 1H), 6.92 (d, J = 8.2 Hz, 1H), 5.40 (d, J = 9.0 Hz, 1H), 5.11 (s, 2H), 4.89 – 4.79 (m, 1H), 2.76 – 2.60 (comp, 2H), 2.07 – 1.95 (m, 1H), 1.89 – 1.68 (comp, 3H). ^{13}C NMR (101 MHz, $CDCl_3$) δ 155.9, 139.0, 136.4, 136.1, 131.1, 130.6, 130.1, 128.4, 128.0, 127.9, 119.5, 66.7, 49.0, 30.1, 28.6, 19.8. HRMS (ESI) *m/z* calcd for $C_{18}H_{18}BrNO_2$ $(M+Na)^+$, 382.0413; found 382.0417

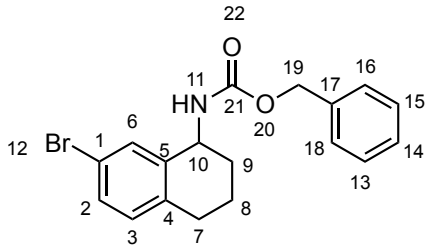

NMR Assignments (**2.75**). ^{1}H NMR (400 MHz, $CDCl_3$) δ 7.48 (dd, *J* = 2.1 Hz, 1H, 6), 7.41 – 7.28 (comp, 5H, 13, 14, 15, 16, 18), 7.25 (dd, *J* = 8.4, 2.1 Hz, 1H, 2), 6.92 (d, *J* = 8.2 Hz, 1H, 3), 5.40 (d, *J* = 9.0 Hz, 1H, 11), 5.11 (s, 2H, 19), 4.89 – 4.79 (m, 1H, 10), 2.76 – 2.60 (comp, 2H, 7), 2.07 – 1.95 (m, 1H, 9), 1.89 – 1.68 (comp, 3H, 8, 9). ^{13}C NMR (101 MHz, $CDCl_3$) δ 155.9 (21), 139.0 (5), 136.4 (4), 136.1 (17), 131.1 (6), 130.6 (2), 130.1 (1), 128.4 (13, 15), 128.0 (14), 127.9 (16, 18), 119.5 (3), 66.7 (19), 49.0 (10), 30.1 (7), 28.6 (9), 19.8 (8).

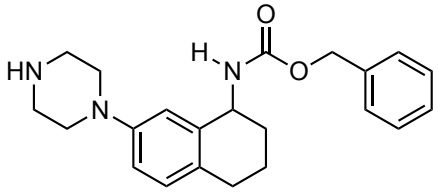

Benzyl (7-(piperazin-1-yl)-1,2,3,4-tetrahydronaphthalen-1-yl)carbamate (**2.76**) (MDW-1-197). Prepared from **2.75** (0.200 g 0.555 mmol) and piperazine according to representative procedure B. The crude residue was purified via flash chromatography (SiO_2) eluting with DCM/MeOH/Et_3N (97:2:1) to afford 89 mg (43%) of **2.76** as a colorless oil. 1H NMR (400 MHz, $CDCl_3$) δ 7.42 – 7.28 (comp, 5H), 6.96 (d, *J* = 8.4 Hz, 1H), 6.84 (d, *J* = 2.6 Hz, 1H), 6.76 (dd, *J* = 8.4, 2.6 Hz, 1H), 5.33 (d, *J* = 8.7 Hz, 1H), 5.13 (dd, *J* = 12.3, 8.9 Hz, 2H), 4.89 – 4.81 (m, 1H), 3.07 – 2.93 (comp, 8H), 2.71 – 2.64 (comp, 2H), 2.61 – 2.49 (m, 1H), 2.04 – 1.94 (m, 1H), 1.87 – 1.73 (comp, 3H). ^{13}C NMR (101 MHz, $CDCl_3$) δ 156.0, 150.3, 137.2, 136.7, 129.7, 128.8, 128.5, 128.1, 128.1, 116.1, 116.0, 66.6, 50.5, 49.6, 46.0, 30.5, 28.4, 19.9.

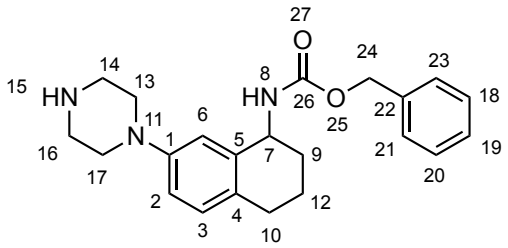

NMR Assignments (**2.75**). ^{1}H NMR (400 MHz, $CDCl_3$) δ 7.42 – 7.28 (comp, 5H, 18, 19, 20, 21, 23), 6.96 (d, *J* = 8.4 Hz, 1H, 3), 6.84 (d, *J* = 2.6 Hz, 1H, 6), 6.76 (dd, *J* = 8.4, 2.6 Hz, 1H, 2), 5.33 (d, *J* = 8.7 Hz, 1H, 8), 5.13 (dd, *J* = 12.3, 8.9 Hz, 2H), 4.89 – 4.81 (m, 1H, 7), 3.07 – 2.93 (comp, 8H, 13, 14, 16, 17), 2.71 – 2.64 (comp, 2H, 10), 2.61 – 2.49 (m, 1H, 15), 2.04 – 1.94 (m, 1H, 9), 1.87 – 1.73 (m, 3H, 9, 12). ^{13}C NMR (101 MHz, $CDCl_3$) δ 156.0 (26), 150.3 (1), 137.2 (5), 136.7 (22), 129.7 (3), 128.8 (4), 128.5 (18, 20), 128.1 (19), 128.1 (21, 23), 116.1 (2), 116.0 (6), 66.6 (24), 50.5 (13, 17), 49.6 (7), 46.0 (14, 16), 30.5 (10), 28.4 (9), 19.9 (12).

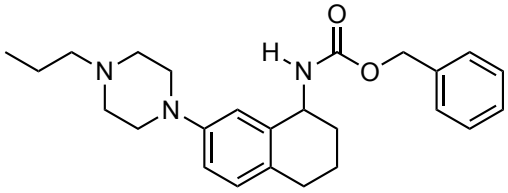

Benzyl (7-(4-propylpiperazin-1-yl)-1,2,3,4-tetrahydronaphthalen-1-yl)carbamate (**2.77**) (MDW-1-202). Prepared from **2.76** (30 mg, 0.082 mmol) and propionaldehyde according to representative procedure E. The crude residue was purified via flash chromatography (SiO_2) eluting with hexanes/EtOAc/Et_3N (74:25:1) to afford 28 mg (84%) of **2.77** as a colorless oil. ^{1}H NMR (499 MHz, $CDCl_3$) δ 7.43 – 7.29 (comp, 5H), 6.98 (d, *J* = 8.4 Hz, 1H), 6.88 (d, *J* = 2.6 Hz, 1H), 6.79 (dd, *J* = 8.4, 2.7 Hz, 1H), 5.20 – 5.10 (comp, 2H), 5.02 (d, *J* = 8.7 Hz, 1H), 4.91 – 4.83 (m, 1H), 3.19 – 3.07 (comp, 4H), 2.75 – 2.62 (comp, 2H), 2.59 (t, *J* = 5.1 Hz, 4H), 2.40 – 2.33 (comp, 2H), 2.10 – 1.97 (comp, 2H), 1.82 – 1.74 (comp, 2H), 1.61 – 1.51 (comp, 2H), 0.93 (t, *J* = 7.4 Hz,

3H). ^{13}C NMR (126 MHz, $CDCl_3$) δ 156.0, 150.0, 137.2, 136.8, 129.9, 128.8, 128.6, 128.2, 116.1, 116.0, 66.8, 60.8, 53.3, 30.6, 28.5, 20.1, 20.0, 12.1. HRMS (ESI) *m/z* calcd for $C_{25}H_{33}N_3O_2$ $(M+H)^+$, 408.2646; found 408.2662.

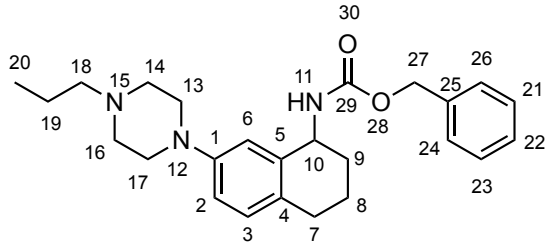

NMR Assignments (**2.77**). ^{1}H NMR (499 MHz, $CDCl_3$) δ 7.43 – 7.29 (comp, 5H, 21, 22, 23, 24, 26), 6.98 (d, *J* = 8.4 Hz, 1H, 3), 6.88 (d, *J* = 2.6 Hz, 1H, 6), 6.79 (dd, *J* = 8.4, 2.7 Hz, 1H, 2), 5.20 – 5.10 (comp, 2H, 27), 5.02 (d, *J* = 8.7 Hz, 1H, 11), 4.91 – 4.83 (m, 1H, 10), 3.19 – 3.07 (comp, 4H, 13, 17), 2.75 – 2.62 (comp, 2H, 7), 2.59 (t, *J* = 5.1 Hz, 4H, 14, 16), 2.40 – 2.33 (comp, 2H, 18), 2.10 – 1.97 (comp, 2H, 8, 9), 1.82 – 1.74 (comp, 2H, 8, 9), 1.61 – 1.51 (m, 2H, 19), 0.93 (t, *J* = 7.4 Hz, 3H, 20). ^{13}C NMR (126 MHz, $CDCl_3$) δ 156.0 (29), 150.0 (1), 137.2 (5), 136.8 (25), 129.9 (3), 128.8 (4), 128.6 (21, 23), 128.2 (22, 24, 26), 116.1 (2), 116.0 (6), 66.8 (27), 60.8 (18), 53.3 (14, 16), 30.6 (9), 28.5 (7), 20.1 (19), 20.0 (8), 12.1 (20).

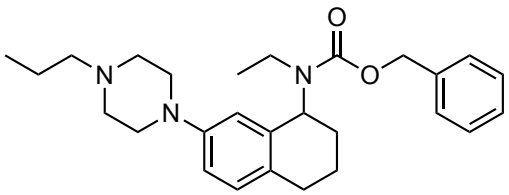

Benzyl ethyl(7-(4-propylpiperazin-1-yl)-1,2,3,4-tetrahydronaphthalen-1-yl)carbamate (**2.78**) (MDW-1-195). Prepared from **2.73** (29 mg, 0.072 mmol) and propionaldehyde according to representative procedure E. The crude residue was purified via flash chromatography (SiO_2) eluting with hexanes/EtOAc/Et_3N (76:23:1) to afford 24

mg (77%) of **2.78** as a pale yellow oil. ^{1}H NMR (499 MHz, $CDCl_3$) rotamers δ 7.45 – 7.22 (comp, 5H), 6.98 (d, *J* = 8.4 Hz, 1H), 6.77 (dd, *J* = 8.4, 2.5 Hz, 1H), 6.65 – 6.59 (m, 1H), 5.47 – 5.04 (comp, 3H), 3.35 – 3.15 (m, 1H), 3.11 – 3.01 (comp, 4H), 2.98 – 2.79 (m, 1H), 2.77 – 2.62 (comp, 2H), 2.60 – 2.52 (comp, 4H), 2.39 – 2.32 (comp, 2H), 2.11 – 2.01 (m, 1H), 2.00 – 1.91 (m, 1H), 1.88 – 1.66 (comp, 2H), 1.55 (h, *J* = 7.4 Hz, 2H), 1.15 (dt, *J* = 32.6, 7.0 Hz, 3H), 0.94 (t, *J* = 7.4 Hz, 3H). ^{13}C NMR (126 MHz, $CDCl_3$) rotamers δ 157.4, 156.5, 150.0, 149.9, 137.3, 137.1, 136.5, 130.0, 129.8, 129.5, 128.6, 128.5, 127.9, 115.8, 115.5, 114.7, 114.2, 67.1, 66.9, 60.8, 56.9, 56.4, 53.4, 49.6, 49.5, 39.2, 29.6, 29.2, 28.9, 28.8, 22.7, 22.4, 20.2, 15.9, 14.9, 12.1. HRMS (ESI) *m/z* calcd for $C_{27}H_{37}N_3O_2$ $(M+H)^+$, 436.2959; found 436.2976.

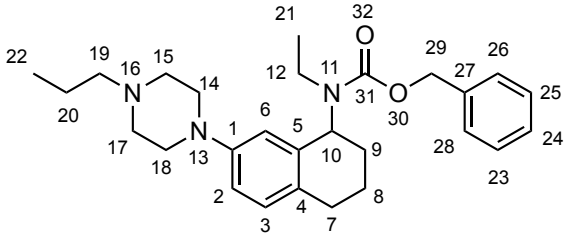

NMR Assignments (**2.78**). ^{1}H NMR (499 MHz, $CDCl_3$) rotamers δ 7.45 – 7.22 (comp, 5H, 23, 24, 25, 26, 28), 6.98 (d, *J* = 8.4 Hz, 1H, 2), 6.77 (dd, *J* = 8.4, 2.5 Hz, 1H, 3), 6.65 – 6.59 (m, 1H, 6), 5.47 – 5.04 (comp, 3H, 10, 29), 3.35 – 3.15 (m, 1H, 7), 3.11 – 3.01 (comp, 4H, 14, 18), 2.98 – 2.79 (m, 1H, 7), 2.77 – 2.62 (comp, 2H, 12), 2.60 – 2.52 (comp, 4H, 15, 17), 2.39 – 2.32 (comp, 2H, 19), 2.11 – 2.01 (m, 1H, 9), 2.00 – 1.91 (m, 1H, 9), 1.88 – 1.66 (comp, 2H, 8), 1.55 (h, *J* = 7.4 Hz, 2H, 20), 1.15 (dt, *J* = 32.6, 7.0 Hz, 3H, 21), 0.94 (t, *J* = 7.4 Hz, 3H, 22). ^{13}C NMR (126 MHz, $CDCl_3$) rotamers δ 157.4 (31), 156.5 (31), 150.0 (1), 149.9 (1), 137.3 (5), 137.1 (5), 136.5 (27), 130.0 (3), 129.8 (3, 4), 129.5 (4), 128.6 (23), 128.5 (25), 127.9 (26, 28), 115.8 (2), 115.5 (2), 114.7 (6), 114.2 (6), 67.1 (29), 66.9 (29), 60.8 (19), 56.9, 56.4 (10), 53.4 (15, 17), 49.6 (14, 18), 49.5 (14,

18), 39.2 (7), 29.6 (9), 29.2 (9), 28.9 (12), 28.8 (12), 22.7 (8), 22.4 (8), 20.2 (20), 15.9 (21), 14.9 (21), 12.1 (22).

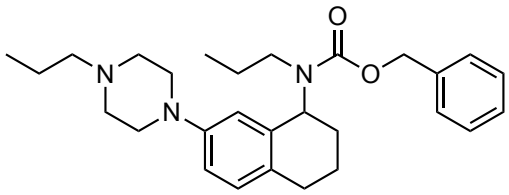

Benzyl propyl(7-(4-propylpiperazin-1-yl)-1,2,3,4-tetrahydronaphthalen-1-yl)carbamate (**2.79**) (MDW-1-196). Prepared from **2.74** (29 mg, 0.071 mmol) and propionaldehyde according to representative procedure E. The crude residue was purified via flash chromatography (SiO_2) eluting with hexanes/EtOAc/Et_3N (76:23:1) to afford 23 mg (72%) of **2.79** as a pale yellow oil. ^{1}H NMR (400 MHz, $CDCl_3$) rotamers δ 7.47 – 7.17 (comp, 5H), 6.98 (d, J = 8.5 Hz, 1H), 6.77 (dd, J = 8.4, 2.5 Hz, 1H), 6.60 (d, J = 2.6 Hz, 1H), 5.44 – 5.01 (comp, 3H), 3.27 – 2.99 (comp, 5H), 2.86 – 2.61 (comp, 3H), 2.60 – 2.51 (comp, 4H), 2.35 (app t, J = 7.8 Hz, 2H), 2.11 – 2.00 (m, 1H), 2.00 – 1.91 (m, 1H), 1.91 – 1.62 (comp, 3H), 1.61 – 1.45 (comp, 3H), 0.94 (t, J = 7.4 Hz, 3H), 0.78 (dt, J = 31.6, 7.4 Hz, 3H). ^{13}C NMR (101 MHz, $CDCl_3$) δ 157.4, 156.7, 150.0, 149.9, 137.4, 137.2, 137.1, 136.6, 129.9, 129.8, 129.4, 128.6, 128.5, 127.9, 127.9, 127.8, 115.8, 115.4, 114.4, 114.0, 67.0, 67.0, 60.8, 57.0, 56.5, 53.4, 49.6, 49.6, 46.7, 29.6, 29.3, 28.9, 28.8, 23.8, 22.8, 22.5, 20.2, 12.1, 11.7, 11.7. HRMS (ESI) *m/z* calcd for $C_{28}H_{39}N_3O_2$ $(M+H)^+$, 450.3115; found 450.3134.

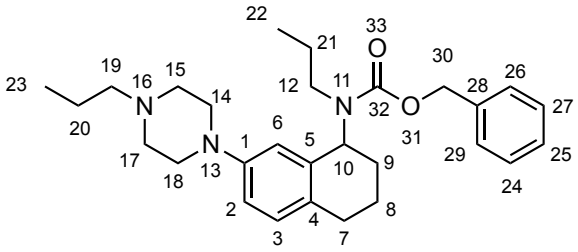

NMR Assignments (**2.79**). ^{1}H NMR (400 MHz, $CDCl_3$) rotamers δ 7.47 – 7.17 (comp, 5H, 24, 25, 26, 27, 29), 6.98 (d, *J* = 8.5 Hz, 1H, 3), 6.77 (dd, *J* = 8.4, 2.5 Hz, 1H, 2), 6.60 (d, *J* = 2.6 Hz, 1H, 6), 5.44 – 5.01 (comp, 3H, 10, 30), 3.27 – 2.99 (comp, 5H, 7, 14, 18), 2.86 – 2.61 (comp, 3H, 7, 12), 2.60 – 2.51 (comp, 4H, 15, 17), 2.35 (app t, *J* = 7.8 Hz, 2H, 19), 2.11 – 2.00 (m, 1H, 9), 2.00 – 1.91 (m, 1H, 9), 1.91 – 1.62 (comp, 3H, 8, 21), 1.61 – 1.45 (comp, 3H, 8, 20), 0.94 (t, *J* = 7.4 Hz, 3H, 23), 0.78 (dt, *J* = 31.6, 7.4 Hz, 3H). ^{13}C NMR (101 MHz, $CDCl_3$) δ 157.4 (32), 156.7 (32), 150.0 (1), 149.9 (1), 137.4 (5), 137.2, 137.1 (28), 136.6 (28), 129.9 (4), 129.8 (3), 129.4 (4), 128.6 (24, 26), 128.5 (24, 26), 127.9 (27, 29), 127.9 (25), 127.8 (27, 29), 115.8 (2), 115.4 (2), 114.4 (6), 114.0 (6), 67.0 (30), 67.0 (30), 60.8 (19), 57.0 (10), 56.5 (10), 53.4 (15, 17), 49.6 (14, 18), 49.6 (14, 18), 46.7 (7), 29.6 (9), 29.3 (9), 28.9, 28.8 (12), 23.8 (21), 22.8, 22.5 (8), 20.2 (20), 12.1 (23), 11.7 (22), 11.7 (22).

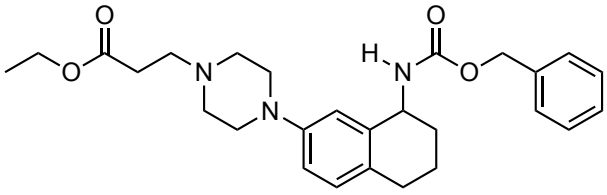

Ethyl 3-(4-(8-(((benzyloxy)carbonyl)amino)-5,6,7,8-tetrahydronaphthalen-2-yl)piperazin-1-yl)propanoate (**2.80**) (MDW-1-206). Prepared from **2.76** (30 mg, 0.082 mmol) and ethyl acylate according to representative procedure H. The crude residue was purified via flash chromatography (SiO_2) eluting with hexanes/EtOAc/Et_3N (69:30:1) to afford 23 mg (80%) of **2.80** as a pale yellow oil. ^{1}H NMR (400 MHz, $CDCl_3$) δ 7.43 –

7.29 (comp, 5H), 6.98 (d, *J* = 8.4 Hz, 1H), 6.86 (d, *J* = 2.6 Hz, 1H), 6.78 (dd, *J* = 8.4, 2.6 Hz, 1H), 5.21 – 5.09 (comp, 2H), 5.02 (d, *J* = 8.7 Hz, 1H), 4.90 – 4.83 (m, 1H), 4.16 (q, *J* = 7.1 Hz, 2H), 3.17 – 3.05 (comp, 4H), 2.75 (app t, *J* = 7.6, 7.1 Hz, 2H), 2.74 – 2.61 (comp, 2H), 2.60 (t, *J* = 5.0 Hz, 4H), 2.54 (app t, *J* = 7.6, 7.2 Hz, 2H), 2.07 – 1.96 (m, 1H), 1.88 – 1.74 (comp, 3H), 1.27 (t, *J* = 7.1 Hz, 3H). ^{13}C NMR (101 MHz, $CDCl_3$) δ 172.6, 156.0, 149.9, 137.3, 136.8, 129.9, 128.9, 128.6, 128.2, 116.1, 66.8, 60.6, 53.7, 53.0, 49.7, 49.5, 32.5, 30.6, 28.5, 20.0, 14.4. HRMS (ESI) *m/z* calcd for $C_{27}H_{35}N_3O_4$ $(M+H)^+$, 466.2700; found 466.2721.

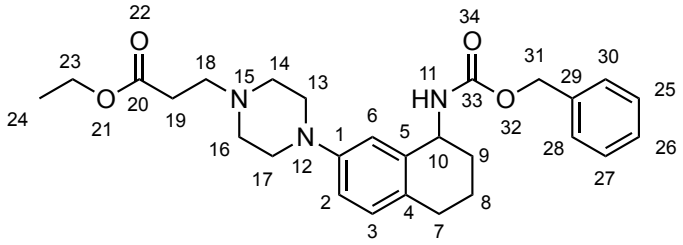

NMR Assignments (**2.80**). ^{1}H NMR (400 MHz, $CDCl_3$) δ 7.43 – 7.29 (comp, 5H, 25, 26, 27, 28, 30), 6.98 (d, *J* = 8.4 Hz, 1H, 3), 6.86 (d, *J* = 2.6 Hz, 1H, 6), 6.78 (dd, *J* = 8.4, 2.6 Hz, 1H, 2), 5.21 – 5.09 (comp, 2H, 31), 5.02 (d, *J* = 8.7 Hz, 1H, 11), 4.90 – 4.83 (m, 1H, 10), 4.16 (q, *J* = 7.1 Hz, 2H, 23), 3.17 – 3.05 (comp, 4H, 13, 17), 2.75 (app t, *J* = 7.6, 7.1 Hz, 2H, 18), 2.74 – 2.61 (comp, 2H, 7), 2.60 (t, *J* = 5.0 Hz, 4H, 14, 16), 2.54 (app t, *J* = 7.6, 7.2 Hz, 2H, 19), 2.07 – 1.96 (m, 1H, 9), 1.88 – 1.74 (comp, 3H, 8, 9), 1.27 (t, *J* = 7.1 Hz, 3H, 24). ^{13}C NMR (101 MHz, $CDCl_3$) δ 172.6 (20), 156.0 (33), 149.9 (1), 137.3 (5), 136.8 (29), 129.9 (3), 128.9 (4), 128.6 (25, 27), 128.2 (28, 30), 116.1 (2, 6), 66.8 (31), 60.6 (23), 53.7 (18), 53.0 (14, 16), 49.7 (10), 49.5 (13, 17), 32.5 (19), 30.6 (9), 28.5 (7), 20.0 (8), 14.4 (24).

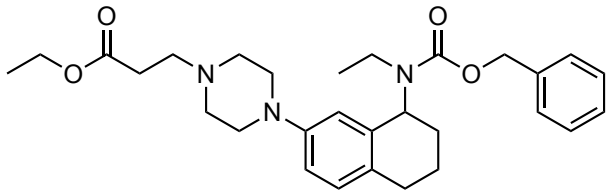

Ethyl 3-(4-(8-(((benzyloxy)carbonyl)(ethyl)amino)-5,6,7,8-tetrahydronaphthalen-2-yl)piperazin-1-yl)propanoate (**2.81**) (MDW-1-190). Prepared from **2.73** (30 mg, 0.076 mmol) and ethyl acylate according to representative procedure H. The crude residue was purified via flash chromatography (SiO_2) eluting with hexanes/EtOAc/Et_3N (69:30:1) to afford 35 mg (92%) of **2.81** as a pale yellow oil. 1H NMR (499 MHz, $CDCl_3$) rotamers δ 7.45 – 7.23 (comp, 5H), 6.97 (d, *J* = 8.3 Hz, 1H), 6.75 (dd, *J* = 8.5, 2.5 Hz, 1H), 6.63 – 6.58 (m, 1H), 5.45 – 5.04 (comp, 3H), 4.16 (q, *J* = 7.1 Hz, 2H), 3.36 – 3.15 (m, 1H), 3.09 – 3.00 (comp, 4H), 2.96 – 2.79 (m, 1H), 2.75 (t, *J* = 7.4 Hz, 2H), 2.72 – 2.62 (comp, 2H), 2.61 – 2.56 (comp, 4H), 2.53 (t, *J* = 7.4 Hz, 2H), 2.11 – 1.91 (comp, 2H), 1.87 – 1.67 (comp, 2H), 1.27 (t, *J* = 7.1 Hz, 3H), 1.15 (dt, *J* = 31.7, 7.0 Hz, 3H). ^{13}C NMR (126 MHz, $CDCl_3$) δ 172.6, 157.3, 156.4, 149.9, 149.7, 137.3, 137.1, 137.0, 136.5, 130.1, 129.8, 129.6, 128.6, 128.5, 128.0, 127.9, 115.8, 115.5, 114.7, 114.2, 67.1, 66.9, 60.6, 56.8, 56.4, 53.7, 53.0, 49.6, 49.5, 39.2, 32.5, 29.8, 29.6, 29.2, 28.9, 28.8, 22.7, 22.4, 15.9, 14.9, 14.4. HRMS (ESI) *m/z* calcd for $C_{29}H_{39}N_3O_4$ $(M+H)^+$, 494.3013; found 494.3034.

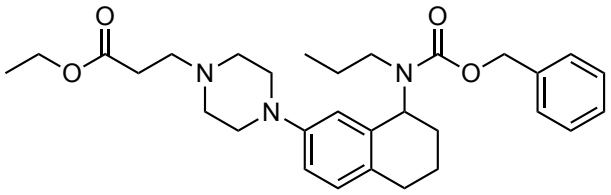

Ethyl 3-(4-(8-(((benzyloxy)carbonyl)(propyl)amino)-5,6,7,8-tetrahydronaphthalen-2-yl)piperazin-1-yl)propanoate (**2.82**) (MDW-1-191). Prepared

from **2.74** (30 mg, 0.074 mmol) and ethyl acylate according to representative procedure H. The crude residue was purified via flash chromatography (SiO_2) eluting with hexanes/EtOAc/Et_3N (69:30:1) to afford 32 mg (86%) of **2.82** as a pale yellow oil. ^1H NMR (499 MHz, $CDCl_3$) rotamers δ 7.43 – 7.19 (comp, 5H), 7.00 – 6.94 (m, 1H), 6.75 (dd, *J* = 8.4, 2.5 Hz, 1H), 6.61 – 6.56 (m, 1H), 5.42 – 5.02 (comp, 3H), 4.16 (q, *J* = 7.1 Hz, 2H), 3.25 – 2.98 (comp, 5H), 2.79 – 2.62 (comp, 5H), 2.62 – 2.51 (comp, 6H), 2.09 – 2.00 (m, 1H), 1.99 – 1.91 (m, 1H), 1.89 – 1.61 (comp, 3H), 1.59 – 1.45 (m, 1H), 1.27 (t, *J* = 7.1 Hz, 3H), 0.78 (dt, *J* = 38.9, 7.4 Hz, 3H). ^{13}C NMR (126 MHz, $CDCl_3$) rotamers δ 172.6, 157.4, 156.6, 149.9, 149.7, 137.3, 137.2, 137.1, 136.7, 130.0, 129.8, 129.5, 128.6, 128.5, 128.0, 127.9, 127.9, 127.8, 115.8, 115.5, 114.4, 114.0, 67.0, 67.0, 60.6, 57.0, 56.4, 53.7, 53.0, 49.6, 49.5, 46.7, 45.9, 32.5, 29.6, 29.2, 28.9, 28.8, 23.8, 22.8, 22.7, 22.5, 14.4, 11.7, 11.6. HRMS (ESI) *m/z* calcd for $C_{30}H_{41}N_3O_4$ $(M+H)^+$, 508.3170; found 508.3191.

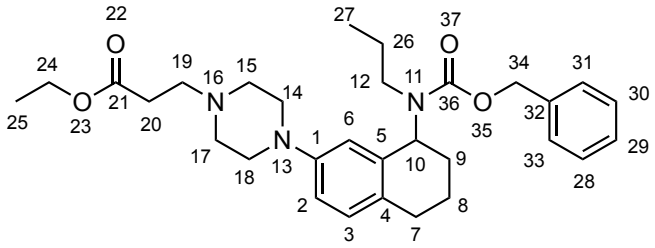

NMR Assignments (**2.82**). ^1H NMR (499 MHz, $CDCl_3$) rotamers δ 7.43 – 7.19 (comp, 5H, 28, 29, 30, 31, 33), 7.00 – 6.94 (m, 1H, 3), 6.75 (dd, *J* = 8.4, 2.5 Hz, 1H, 2), 6.61 – 6.56 (m, 1H, 6), 5.42 – 5.02 (comp, 3H, 10, 34), 4.16 (q, *J* = 7.1 Hz, 2H, 24), 3.25 – 2.98 (comp, 5H, 12, 14, 18), 2.79 – 2.62 (comp, 5H, 7, 12, 19), 2.62 – 2.51 (comp, 6H, 15, 17, 20), 2.09 – 2.00 (m, 1H, 9), 1.99 – 1.91 (m, 1H, 8), 1.89 – 1.61 (comp, 3H, 8, 9, 26), 1.59 – 1.45 (m, 1H, 26), 1.27 (t, *J* = 7.1 Hz, 3H, 25), 0.78 (dt, *J* = 38.9, 7.4 Hz, 3H, 27). ^{13}C NMR (126 MHz, $CDCl_3$) δ 172.6 (21), 157.4, 156.6 (36), 149.9, 149.7 (1), 137.3, 137.2 (5), 137.1, 136.7 (32), 130.0, 129.8 (3), 129.5 (4), 128.6, 128.5 (28, 30),

128.0, 127.9 (31, 33), 127.9, 127.8 (29), 115.8, 115.5 (2), 114.4, 114.0 (6), 67.0, 67.0 (34), 60.6 (24), 57.0, 56.4 (10), 53.7 (19), 53.0 (15, 17), 49.6, 49.5 (14, 18), 46.7, 45.9 (12), 32.5 (20), 29.6, 29.2 (9), 28.9, 28.8 (7), 23.8, 22.8 (26), 22.7, 22.5 (8), 14.4 (25), 11.7, 11.6 (27).

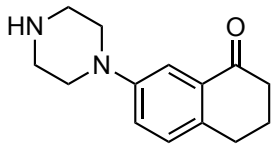

7-(Piperazin-1-yl)-3,4-dihydronaphthalen-1(2*H*)-one (**2.83**) (MDW-2-220). A resealable tube was charged with 7-bromotetralone (1.500 g, 6.664 mmol), piperazine (5.740 g, 66.63 mmol), Cs_2CO_3 (3.257 g, 9.99 mmol). The tube was evacuated and backfilled with N_2 three times, whereupon degassed *t*-BuOH (33 mL) and the suspension was stirred at 45 °C for 15 min. A freshly prepared *t*-BuOH solution (2.0 mL) containing Pd_2dba_3 (122 mg, 0.133 mmol) and RuPhos (124 mg, 0.266 mmol) that had been stirred at 60 °C for 30 min was added. The tube was sealed, and the reaction was stirred at 100 °C for 3 h. After cooling to room temperature, the mixture was filtered through Celite, the filter cake was washed with CH_2Cl_2 (200 mL), and the filtrate was concentrated. The residue was dissolved in Et_2O (75 mL) and extracted with 1 N HCl (4 x 30 mL). The combined acidic aqueous extracts were made basic and extracted with CH_2Cl_2 (3 x 100 mL), after which the combined organic extracts were dried (MgSO) and concentrated under reduced pressure. The crude material was purified via flash chromatography (SiO_2) eluting with CH_2Cl_2/MeOH/Et_3N (97:2:1) affording 1.3574 g (88%) of **2.83** as a red oil. 1H NMR (400 MHz, $CDCl_3$) δ 7.46 (d, *J* = 2.8 Hz, 1H), 7.07 (d, *J* = 8.4 Hz, 1H), 7.01 (dd, *J* = 8.4, 2.8 Hz, 1H), 3.15 – 3.05 (comp, 4H), 3.00 – 2.91 (comp, 4H), 2.78 (t, *J* = 6.1 Hz, 2H, 9), 2.70 (brs, 1H), 2.53 (t, *J* = 6.3 Hz, 3H), 2.01 (p, *J* = 6.3 Hz, 2H). ^{13}C NMR

(101 MHz, $CDCl_3$) δ 198.5, 150.3, 135.8, 132.8, 129.4, 122.0, 112.8, 50.0, 45.8, 39.1, 28.7, 23.4. HRMS (ESI) *m/z* calcd for $C_{14}H_{18}N_2O$ $(M+H)^+$, 231.1492; found 231.1497

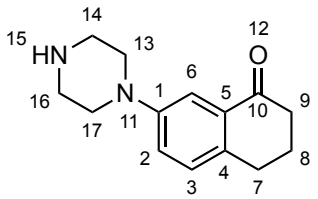

NMR Assignments (**2.83**). 1H NMR (400 MHz, $CDCl_3$) δ 7.46 (d, *J* = 2.8 Hz, 1H, 6), 7.07 (d, *J* = 8.4 Hz, 1H, 3), 7.01 (dd, *J* = 8.4, 2.8 Hz, 1H, 2), 3.15 – 3.05 (comp, 4H, 13, 17), 3.00 – 2.91 (comp, 4H, 14, 16), 2.78 (t, *J* = 6.1 Hz, 2H, 9), 2.70 (brs, 1H, 18), 2.53 (t, *J* = 6.3 Hz, 3H, 7), 2.01 (p, *J* = 6.3 Hz, 2H, 8). ^{13}C NMR (101 MHz, $CDCl_3$) δ 198.5 (10), 150.3 (1), 135.8 (5), 132.8 (4), 129.4 (3), 122.0 (2), 112.8 (6), 77.5, 77.2, 76.8, 50.0 (13, 17), 45.8 (14, 16), 39.1 (9), 28.7 (7), 23.4 (8).

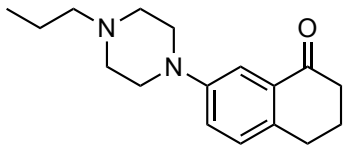

7-(4-Propylpiperazin-1-yl)-3,4-dihydronaphthalen-1(2*H*)-one (**2.84**) (MDW-2-57). A solution of propionaldehyde (1.006 g, 11.29 mmol) in DCE (25 mL) was added dropwise to a solution of amine **2.83** (2.363 g, 10.3 mmol) and $Na(OAc)_3BH$ (4.349 g, 20.5 mmol) in DCE (103 mL), and the reaction was stirred at room temperature for 3 h. The reaction mixture was then washed with saturated aq. $NaHCO_3$ (2 x 50 mL), dried (Na_2SO_4), and concentrated under reduced pressure. The crude material was purified via flash chromatography (SiO_2) eluting with hexanes/EtOAc/Et_3N (74:25:1) affording 2.165 g (77%) of **2.84** as a yellow oil. ^1H NMR (400 MHz, $CDCl_3$) δ 7.54 (d, *J* = 2.7 Hz, 1 H), 7.14 (d, *J* = 8.4 Hz, 1 H), 7.08 (dd, *J* = 8.5, 2.7 Hz, 1 H), 3.24 – 3.19 (comp, 4 H), 2.86 (t,

J = 6.1 Hz, 2 H), 2.64 – 2.55 (comp, 6 H), 2.38 – 2.31 (m, 2 H), 2.09 (m, 2 H), 1.60 – 1.48 (m, 2 H), 0.92 (t, *J* = 7.4 Hz, 3 H). 13C NMR (101 MHz, $CDCl_3$) δ 198.9, 150.1, 135.8, 133.0, 129.6, 122.0, 113.0, 60.8, 53.2, 49.1, 39.3, 28.9, 23.6, 20.1, 12.1. HRMS (ESI) *m/z* calcd for $C_{17}H_{24}N_2O$ $(M+H)^+$, 273.1961; found 273.1965

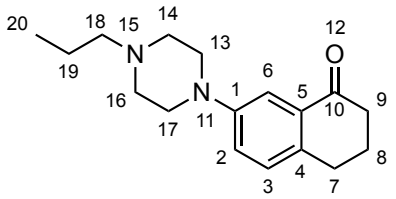

NMR Assignments (**2.84**). ^{1}H NMR (400 MHz, $CDCl_3$) δ 7.54 (d, *J* = 2.7 Hz, 1H, 6), 7.14 (d, *J* = 8.4 Hz, 1H, 3), 7.08 (dd, *J* = 8.5, 2.7 Hz, 1H, 2), 3.24 – 3.19 (comp, 4H, 13, 17), 2.86 (t, *J* = 6.1 Hz, 2H, 9), 2.64 – 2.55 (comp, 7H, 7, 14, 16), 2.38 – 2.31 (comp, 2H, 18), 2.09 (p, *J* = 6.4 Hz, 3H, 19), 1.60 – 1.48 (comp, 2H, 8), 0.92 (t, *J* = 7.4 Hz, 3H, 20). ^{13}C NMR (101 MHz, $CDCl_3$) δ 198.9 (10), 150.1 (1), 135.8 (5), 133.0 (4), 129.6 (3), 122.0 (2), 113.0 (6), 60.8 (18), 53.2 (13, 17), 49.1 (14, 16), 39.3 (9), 28.9 (7), 23.6 (8), 20.1 (19), 12.1 (20).

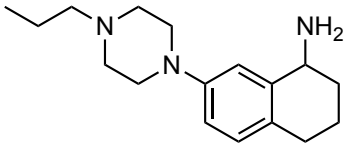

7-(4-Propylpiperazin-1-yl)-1,2,3,4-tetrahydronaphthalen-1-amine (**2.86**) (MDW-2-100). Prepared from **2.84** (0.213 g, 0.782 mmol) mmol) and NH_4OAc according to representative procedure D. The crude residue was purified via flash chromatography (SiO_2) eluting with CH_2Cl_2/MeOH/Et_3N (94:5:1) affording 0.115 g (54%) of **2.86** as a red oil. ^{1}H NMR (400 MHz, $CDCl_3$) δ 7.03 (d, *J* = 2.6 Hz, 1 H), 6.94 (d, *J* = 8.4 Hz, 1 H), 6.74 (dd, *J* = 8.4, 2.6 Hz, 1 H), 4.05 – 3.90 (comp, 3 H), 3.20 – 3.12

(comp, 4 H), 2.75 – 2.50 (comp, 6 H), 2.34 – 2.27 (m, 2 H), 2.04 – 1.82 (comp, 2 H), 1.77 – 1.65 (comp, 2 H), 1.58 – 1.45 (comp, 2 H), 0.90 (t, J = 7.4 Hz, 3 H). ^{13}C NMR (101 MHz, $CDCl_3$) δ 149.8, 139.1, 129.7, 128.0, 115.6, 115.4, 60.7, 53.3, 49.8, 49.4, 32.4, 28.5, 20.0, 19.6, 12.0. HRMS (ESI) *m/z* calcd for $C_{17}H_{27}N_3$ $(M+H)^+$, 274.2278; found 274.2277.

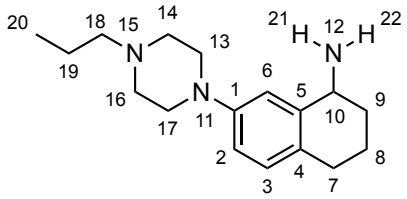

NMR Assignments (**2.86**).^{1}H NMR (400 MHz, $CDCl_3$) δ 7.03 (d, J = 2.6 Hz, 1 H, 6), 6.94 (d, J = 8.4 Hz, 1 H, 3), 6.74 (dd, J = 8.4, 2.6 Hz, 1 H, 2), 4.05 – 3.90 (comp, 3 H, 10, 21, 22), 3.20 – 3.12 (comp, 4 H, 13, 17), 2.75 – 2.50 (comp, 6 H, 7, 14, 16), 2.34 – 2.27 (comp, 2 H, 18), 2.04 – 1.82 (comp, 2 H, 9), 1.77 – 1.65 (comp, 2 H, 8), 1.58 – 1.45 (comp, 2H, 19), 0.90 (t, J = 7.4 Hz, 3 H, 20).^{13}C NMR (101 MHz, $CDCl_3$) δ 149.8 (1), 139.1 (5), 129.7 (4), 128.0 (3), 115.6 (6), 115.4 (2), 60.7 (18), 53.3 (13, 17), 49.8 (10), 49.4 (14, 16), 32.4 (9), 28.5 (7), 20.0 (19), 19.6 (8), 12.0 (20).

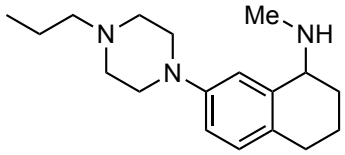

***N*-Methyl-7-(4-propylpiperazin-1-yl)-1,2,3,4-tetrahydronaphthalen-1-amine** (**2.87**) (MDW-2-74). Prepared from **2.84** (0.102 g, 0.375 mmol) mmol) and $MeNH_3Cl$ according to representative procedure D. The crude residue was purified via flash chromatography (SiO_2) eluting with CH_2Cl_2/MeOH/Et_3N (98:1:1) affording 76 mg (78%)

of **2.87** as a pale yellow oil. ^{1}H NMR (400 MHz, $CDCl_3$) δ 6.97 (d, *J* = 8.4 Hz, 1H), 6.92 (d, *J* = 2.6 Hz, 1H), 6.77 (dd, *J* = 8.4, 2.7 Hz, 1H), 3.61 (t, *J* = 4.9 Hz, 1H), 3.20 – 3.14 (comp, 4H), 2.77 – 2.62 (comp, 2H,), 2.62 – 2.57 (comp, 4H), 2.49 (s, 3H), 2.38 – 2.32 (comp, 2H), 1.96 – 1.80 (comp, 3H), 1.75 – 1.65 (m, 1H), 1.60 – 1.49 (comp, 2H), 1.37 (brs, 1H), 0.92 (t, *J* = 7.4 Hz, 3H). ^{13}C NMR (101 MHz, $CDCl_3$) δ 149.7, 139.6, 129.7, 128.8, 116.4, 115.4, 60.8, 57.6, 53.4, 49.8, 34.1, 28.6, 27.9, 20.1, 19.2, 12.1. HRMS (ESI) *m/z* calcd for $C_{18}H_{29}N_3$ $(M+H)^+$, 288.2434; found 288.2438.

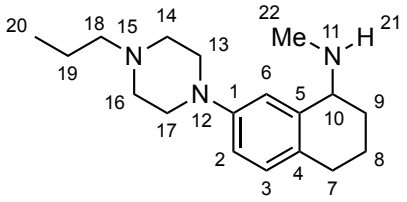

NMR Assignments (**2.87**). ^{1}H NMR (400 MHz, $CDCl_3$) δ 6.97 (d, *J* = 8.4 Hz, 1H, 3), 6.92 (d, *J* = 2.6 Hz, 1H, 6), 6.77 (dd, *J* = 8.4, 2.7 Hz, 1H, 2), 3.61 (t, *J* = 4.9 Hz, 1H, 10), 3.20 – 3.14 (comp, 4H, 13, 17), 2.77 – 2.62 (comp, 2H, 7), 2.62 – 2.57 (comp, 4H, 14, 16), 2.49 (s, 3H, 22), 2.38 – 2.32 (comp, 2H, 18), 1.96 – 1.80 (comp, 3H, 8, 9), 1.75 – 1.65 (m, 1H, 8), 1.60 – 1.49 (comp, 2H, 19), 1.37 (brs, 1H, 21), 0.92 (t, *J* = 7.4 Hz, 3H, 20). ^{13}C NMR (101 MHz, $CDCl_3$) δ 149.7 (1), 139.6 (5), 129.7 (3), 128.8 (4), 116.4 (6), 115.4 (2), 60.8 (18), 57.6 (10), 53.4 (14, 16), 49.8 (13, 17), 34.1 (22), 28.6 (7), 27.9 (9), 20.1 (19), 19.2 (8), 12.1 (20).

Representative Procedure I: Reduction amination using Ti(O*i*-Pr)$_4$ and an alkyl amine.

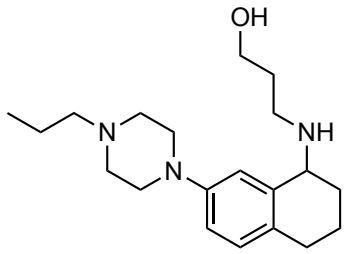

3-((7-(4-Propylpiperazin-1-yl)-1,2,3,4-tetrahydronaphthalen-1-yl)amino)propan-1-ol (**2.88**) (MDW-2-140). TiO(*i*-Pr)$_4$ (0.73 g, 0.76 mL, 2.6 mmol) was added to a solution of **2.84** (70 mg, 0.256 mmol) and 3-amino-1-propanol (0.028 g, 0.029 mL, 0.38 mmol) in EtOH (1.7 mL), and the reaction was stirred at 45 °C for 17 h. The reaction was cooled to 0 °C and $NaBH_4$ (19 mg, 50 mmol) was added in a single portion. The reaction was stirred for 30 min and the cooling bath was removed. The solution was stirred for 4 h at room temperature and poured into 2 M aq. NH_4OH (2 mL). Celite was added to the mixture and it was filtered, washing the filter cake with CH_2Cl_2 (50 mL). The filtrate was concentrated under reduced pressure to remove volatile organics and the mixture obtained was diluted with saturated aqueous $NaHCO_3$ (10 mL), whereupon the aqueous layer was extracted with CH_2Cl_2 (3 x 10 mL). The combined organic extracts were dried (Na_2SO_4) and concentrated. The crude residue was purified via flash chromatography (SiO_2) eluting with CH_2Cl_2/MeOH/Et_3N (97:2:1) affording 77 mg (91%) of **2.88** as a yellow oil.^{1}H NMR (499 MHz, $CDCl_3$) δ 6.95 (d, *J* = 8.4 Hz, 1H), 6.91 (d, *J* = 2.6 Hz, 1H), 6.77 (dd, *J* = 8.4, 2.6 Hz, 1H), 4.37 (brs, 2H), 3.83 – 3.75 (comp, 3H), 3.20 – 3.10 (comp, 4H), 3.04 – 2.90 (comp, 2H), 2.72 – 2.54 (comp, 6H), 2.37 – 2.28 (comp, 2H), 1.93 – 1.80 (comp, 3H), 1.76 – 1.65 (comp, 3H), 1.57 – 1.47 (comp, 2H), 0.90 (t, *J* = 7.4 Hz, 3H). ^{13}C NMR (126 MHz, $CDCl_3$) δ 149.7, 137.9, 129.8,

128.8, 116.3, 115.8, 64.1, 60.8, 56.0, 53.3, 49.5, 47.0, 30.9, 28.4, 27.6, 20.1, 19.1, 12.1. HRMS (ESI) *m/z* calcd for $C_{20}H_{33}N_3O$ $(M+H)^+$, 332.2696; found 332.27110.

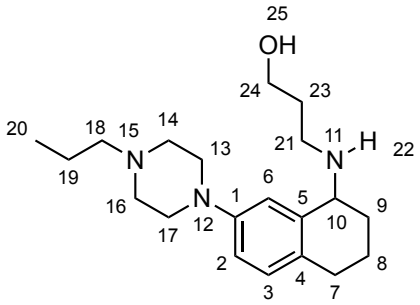

NMR Assignments (**2.88**). ^{1}H NMR (499 MHz, $CDCl_3$) δ 6.95 (d, *J* = 8.4 Hz, 1H, 3), 6.91 (d, *J* = 2.6 Hz, 1H, 6), 6.77 (dd, *J* = 8.4, 2.6 Hz, 1H, 2), 4.37 (brs, 2H, 22, 25), 3.83 – 3.75 (comp, 3H, 10, 24), 3.20 – 3.10 (comp, 4H, 13, 17), 3.04 – 2.90 (comp, 2H, 7), 2.72 – 2.54 (comp, 6H, 14, 16, 21), 2.37 – 2.28 (comp, 2H, 18), 1.93 – 1.80 (comp, 3H, 8, 9), 1.76 – 1.65 (comp, 3H, 8, 23), 1.57 – 1.47 (comp, 2H, 19), 0.90 (t, *J* = 7.4 Hz, 3H, 20). ^{13}C NMR (126 MHz, $CDCl_3$) δ 149.7 (1), 137.9 (5), 129.8 (3), 128.8 (4), 116.3 (6), 115.8 (2), 64.1 (24), 60.8 (18), 56.0 (10), 53.3 (14, 16), 49.5 (13, 17), 47.0 (7), 30.9 (23), 28.4 (21), 27.6 (9), 20.1 (19), 19.1 (8), 12.1 (20).

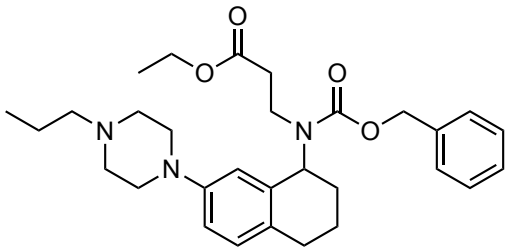

Ethyl 3-((7-(4-propylpiperazin-1-yl)-1,2,3,4-tetrahydronaphthalen-1-yl)amino)propanoate (**2.89**) (MDW-2-123). Ethyl acrylate (35 mg, 38 μL, 0.35 mmol) was added to a solution of **2.86** (79 mg, 0.29 mmol) in EtOH (1.4 mL) and the reaction was stirred at room temperature for 48 h. The reaction was concentrated under reduced

pressure. The crude residue was filtered through a SiO_2 plug rinsing with hexanes/EtOAc/Et_3N (49:49:1), and the filtrate was concentrated under reduced pressure to afford a crude residue (42 mg) that was use directly. The crude residue was dissolved in CH_2Cl_2 (1.1 mL) and cooled to 0 ° C. *i*-Pr_2NEt (29 mg, 39 μL 0.22 mmol) and CbzCl (45 mg, 38 μL, 0.27 mmol) we added sequentially. The reaction was stirred overnight allowing to slowly warm to room temperature. The reaction was diluted with CH_2Cl_2 (5 mL) and washed sequentially with 1 N HCl (2 x5 mL), 1 N NaOH (2 x 5 mL), and saturated aqueous $NaHCO_3$ (1x 5 mL). The organic layer was dried (Na_2SO_4) and concentrated under reduced pressure. The crude residue was purified via flash chromatography (SiO_2) eluting with hexanes/EtOAc/Et_3N (74:25:1) to afford 31 mg (21%) of **2.89** as a colorless oil. ^1H NMR (499 MHz, $CDCl_3$) rotamers δ 7.43 – 7.24 (comp, 5H), 6.97 (dd, *J* = 8.7, 2.4 Hz, 1H), 6.76 (dd, *J* = 8.5, 2.5 Hz, 1H), 6.56 (brs, 1H), 5.47 – 5.05 (comp, 3H), 4.11 – 3.99 (comp, 2H), 3.54 – 3.40 (m, 1H), 3.24 – 3.00 (comp, 5H), 2.81 – 2.45 (comp, 8H), 2.38 – 2.31 (comp, 2H), 2.08 – 1.91 (comp, 2H), 1.81 – 1.67 (comp, 2H), 1.60 – 1.51 (comp, 2H), 1.23 – 1.16 (comp, 3H), 0.93 (t, *J* = 7.4 Hz, 3H). ^{13}C NMR (126 MHz, $CDCl_3$) rotamers δ 171.9, 171.7, 157.1, 156.6, 150.1, 150.0, 137.0, 136.9, 136.0, 130.0, 129.6, 128.7, 128.6, 128.1, 128.0, 128.0, 116.0, 115.7, 114.3, 113.9, 67.3, 67.2, 60.8, 60.6, 60.6, 56.5, 53.4, 49.6, 49.5, 40.2, 35.4, 34.3, 29.5, 29.1, 28.8, 28.7, 22.6, 22.4, 20.2, 14.3, 12.1. HRMS (ESI) *m/z* calcd for $C_{30}H_{41}N_3O_4$ $(M+H)^+$, 508.3170; found 508.3181.

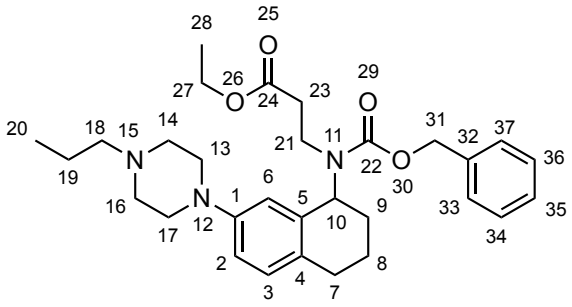

NMR Assignments (**2.89**).[1]H NMR (499 MHz,$CDCl_3$) rotamers δ 7.43 – 7.24 (comp, 5H, 33, 34, 35, 36, 37), 6.97 (dd, *J* = 8.7, 2.4 Hz, 1H, 3), 6.76 (dd, *J* = 8.5, 2.5 Hz, 1H, 2), 6.56 (brs, 1H, 6), 5.47 – 5.05 (comp, 3H, 10, 31), 4.11 – 3.99 (comp, 2H, 27), 3.54 – 3.40 (m, 1H, 23), 3.24 – 3.00 (comp, 5H, 13, 17, 23), 2.81 – 2.45 (comp, 8H, 7, 14, 16, 21), 2.38 – 2.31 (comp, 2H, 18), 2.08 – 1.91 (comp, 2H, 8, 9), 1.81 – 1.67 (comp, 2H, 8, 9), 1.60 – 1.51 (comp, 2H, 19), 1.23 – 1.16 (comp, 3H, 28), 0.93 (t, *J* = 7.4 Hz, 3H, 20). [13]C NMR (126 MHz, $CDCl_3$) rotamers δ 171.9 and 171.7 (24), 157.1 and 156.6 (22), 150.1 and 150.0 (1), 137.0 and 136.9 (5), 136.0 (32), 130.0 (3), 129.6 (4), 128.7 and 128.6 (34, 36), 128.1 and 128.0 (35), 128.0 (33, 37), 116.0 and 115.7 (2), 114.3 and 113.9 (6), 67.3 and 67.2 (31), 60.8 (18), 60.6 and 60.6 (27), 56.5 (10), 53.4 (14, 16), 49.6 and 49.5 (13, 17), 40.2 (23), 35.4 and 34.3 (21), 29.5 and 29.1 (9), 28.8 and 28.7 (7), 22.6 and 22.4 (8), 20.2 (19), 14.3 (28), 12.1 (20).

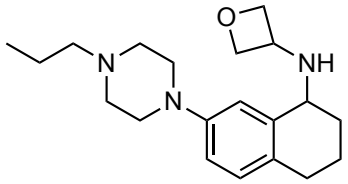

***N*-(7-(4-Propylpiperazin-1-yl)-1,2,3,4-tetrahydronaphthalen-1-yl)oxetan-3-amine** (**S.1**) (MDW-2-193). $TiO(i\text{-}Pr)_4$ (0.64 g, 0.67 mL, 2.3 mmol) was added to a solution of **2.86** (57 mg, 24 mmol) and 3-oxetanone (0.0192 g, 0.017 mL, 0.27 mmol) in EtOH (1.1 mL), and the reaction was stirred for 17 h at room temperature. $NaCNBH_3$

(0.026 g, 0.41 mmol) was added to the solution and the reaction was stirred for 6 h. The reaction was poured into 2 M aq. NH_4OH (10 mL). Celite was added to the mixture and it was filtered. The filter cake was washed with CH_2Cl_2 (100 mL). The filtrate was concentrated under reduced pressure to remove volatile organics and the mixture obtained was diluted with saturated aqueous $NaHCO_3$ (10 mL), whereupon the aqueous layer was extracted with CH_2Cl_2 (3 x 15 mL). The combined organic extracts were dried (Na_2SO_4) and concentrated under reduced pressure. The crude residue was purified via flash chromatography (SiO_2) eluting with CH_2Cl_2/MeOH/Et_3N (99:0:1 to 94:5:1) affording 26 mg (37 %) of **S.1** as an orange oil. ^{1}H NMR (499 MHz, $CDCl_3$) δ 6.97 (d, *J* = 8.4 Hz, 1H), 6.93 (d, *J* = 2.6 Hz, 1H), 6.78 (dd, *J* = 8.4, 2.6 Hz, 1H), 4.84 (q, *J* = 6.4 Hz, 2H), 4.44 (q, *J* = 6.0 Hz, 2H), 4.14 (p, *J* = 6.8 Hz, 1H), 3.69 (t, *J* = 5.3 Hz, 1H), 3.23 – 3.13 (comp, 4H), 2.77 – 2.58 (comp, 6H), 2.43 – 2.34 (comp, 2H), 2.03 – 1.50 (comp, 7H), 0.93 (t, *J* = 7.4 Hz, 3H). ^{13}C NMR (126 MHz, $CDCl_3$) δ 149.7, 139.1, 129.8, 128.9, 116.3, 115.8, 81.4, 81.0, 60.7, 55.2, 53.3, 52.2, 49.6, 30.1, 28.5, 20.0, 19.5, 12.1. HRMS (ESI) *m/z* calcd for $C_{20}H_{31}N_3O$ $(M+H)^+$, 330.2540 found 330.2544.

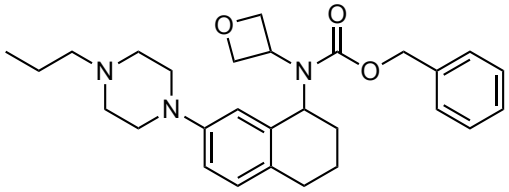

Benzyl oxetan-3-yl(7-(4-propylpiperazin-1-yl)-1,2,3,4-tetrahydronaphthalen-1-yl)carbamate (**2.91**) (MDW-2-197). Prepared from **S.1** (14 mg, 0.042 mmol) and CbzCl according to representative procedure A. The crude residue was purified via flash chromatography (SiO_2) eluting with hexanes/EtOAc/Et_3N (59:40:1) affording 7 mg (35 %) of **2.91** as a colorless oil. ^{1}H NMR (499 MHz, $CDCl_3$) rotamers δ 7.51 – 7.21 (comp, 5 H), 6.91 (d, *J* = 8.4 Hz, 1 H), 6.70 (dd, *J* = 8.4, 2.6 Hz, 1 H), 6.42 (brs, 1 H), 5.43 –

4.25 (comp, 8 H), 3.08 – 2.90 (comp, 4 H), 2.67 – 2.47 (comp, 6 H), 2.34 – 2.26 (comp, 2 H), 2.04 – 1.94 (m, 1 H), 1.90 – 1.82 (m, 1 H), 1.71 – 1.62 (comp, 2 H), 1.53 – 1.46 (comp, 2 H), 0.86 (t, J = 7.4 Hz, 3 H). HRMS (ESI) *m/z* calcd for $C_{28}H_{37}N_3O_3$ $(M+H)^+$, 464.2908 found 464.2909

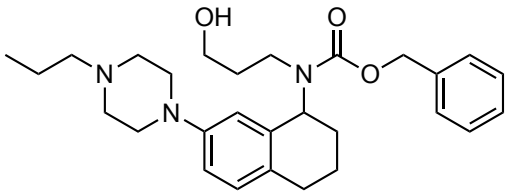

Benzyl (3-hydroxypropyl)(7-(4-propylpiperazin-1-yl)-1,2,3,4-tetrahydronaphthalen-1-yl)carbamate (**2.92**) (MDW-2-143). A solution of **2.88** (77 mg, 0.23 mmol) and *i*-Pr_2NEt (60 mg, 81 μL 0.47 mmol) in CH_2Cl_2 (6 mL) was cooled to 0 ° C. CbzCl (43 mg, 36 μL, 0.25 mmol) was added dropwise to the cooled solution and the reaction was stirred for 1 h at 0 °C. The cooling bath was removed and the solution was stirred at room temperature for 16 h. The reaction was quenched with sequential addition of MeOH (3 mL) and 1 N NaOH (3 mL), and the reaction was stirred for 1 h at room temperature. The reaction was concentrated under reduced pressure to remove volatile organics and the mixture obtained was diluted with saturated aqueous 1 N NaOH (10 mL), whereupon the aqueous layer was extracted with CH_2Cl_2 (3 x 15 mL). The combined organic extracts were dried (Na_2SO_4) and concentrated under reduced pressure. The crude residue was purified via flash chromatography (SiO_2) eluting with EtOAc/hexanes/MeOH/Et_3N (50:44:5:1) affording 20 mg (19%) of **2.92** as a colorless oil. ^1H NMR (499 MHz, $CDCl_3$) rotamers δ 7.46 – 7.15 (comp, 5H), 6.98 (d, J = 8.3 Hz, 1H), 6.75 (dd, J = 8.4, 2.5 Hz, 1H), 6.63 – 6.52 (m, 1H), 5.43 – 5.03 (comp, 3H), 3.66 – 3.41 (comp, 3H), 3.27 – 3.06 (comp, 5H), 2.99 – 2.60 (comp, 7H), 2.59 – 2.46 (comp, 2H), 2.08 – 1.60 (comp, 8H), 0.95 (t, J = 7.3 Hz, 3H). ^{13}C NMR (126 MHz, $CDCl_3$)

rotamers δ 157.9, 157.3, 149.5, 137.0, 136.8, 136.6, 130.8, 130.1, 128.7, 128.6, 128.1, 128.0, 116.2, 115.8, 114.8, 114.3, 67.5, 67.3, 60.6, 60.3, 59.4, 57.4, 56.6, 53.6, 52.9, 48.8, 42.4, 41.8, 33.6, 32.9, 29.5, 29.0, 28.8, 28.7, 22.6, 22.4, 19.3, 19.1, 11.9. HRMS (ESI) *m/z* calcd for $C_{28}H_{39}N_3O_3$ $(M+Na)^+$, 488.2884; found 488.2895.

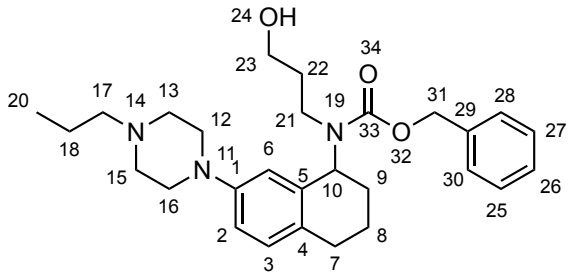

NMR Assignments (**2.92**). ^{1}H NMR (499 MHz, $CDCl_3$) rotamers δ 7.46 – 7.15 (comp, 5H, 25, 26, 27, 28, 30), 6.98 (d, *J* = 8.3 Hz, 1H, 3), 6.75 (dd, *J* = 8.4, 2.5 Hz, 1H, 2), 6.63 – 6.52 (m, 1H, 6), 5.43 – 5.03 (comp 3H, 10, 31), 3.66 – 3.41 (m, 3H, 23, 24), 3.27 – 3.06 (comp, 5H, 12, 16, 21"), 2.99 – 2.60 (comp, 7H, 7, 13, 15, 21'), 2.59 – 2.46 (comp, 2H, 17), 2.08 – 1.60 (comp, 8H, 8, 9, 18, 22), 0.95 (t, *J* = 7.3 Hz, 3H, 20). ^{13}C NMR (126 MHz, $CDCl_3$) δ 157.9 and 157.3 (33), 149.5 (1), 137.0 and 136.8 (5), 136.6 (29), 130.8 (4), 130.1 (3), 128.7 (26), 128.6 (25, 27), 128.1 and 128.0 (28, 30), 116.2 and 115.8 (2), 114.8 and 114.3 (6), 67.5 and 67.3 (31), 60.6 and 60.3 (17), 59.4 (23), 57.4 and 56.6 (10), 53.6 and 52.9 (13, 15), 48.8 (12, 16), 42.4 and 41.8 (21), 33.6 and 32.9 (22), 29.5 and 29.0 (9), 28.8 and 28.7 (7), 22.6 and 22.4 (8), 19.3 and 19.1 (18), 11.9 (20).

Representative Procedure J: Reaction of an amine with an acyl chloride.

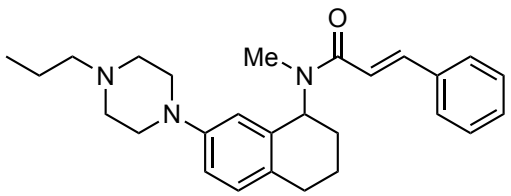

***N*-Methyl-*N*-(7-(4-propylpiperazin-1-yl)-1,2,3,4-tetrahydronaphthalen-1-yl)cinnamamide** (**2.93**) (MDW-2-190). A solution of **2.87** (14 mg, 0.050 mmol) and *i*-Pr_2NEt (13 mg, 17 μL 0.10 mmol) in CH_2Cl_2 (0.5 mL) was cooled to 0 ° C. Cinnamoyl chloride (10 mg, 0.60 mmol) was added to the cooled solution and the solution was stirred for 24 h allowing the reaction to slowly warm to room temperature. The reaction was diluted with 1 N NaOH (10 mL) and the aqueous layer was extracted with CH_2Cl_2 (3 x 10 mL). The combined organic extracts were washed with brine (1 x 20 mL), dried (Na_2SO_4), and concentrated under reduced pressure. The crude residue was purified via flash chromatography (SiO_2) eluting with hexanes/EtOAc/Et_3N (59:40:1) to afford 14 mg (66%) of **2.93** as a colorless oil. ^1H NMR (400 MHz, $CDCl_3$) rotamers δ 7.85 – 7.72 (m, 1H), 7.63 – 7.48 (comp, 2H), 7.45 – 7.32 (comp, 3H), 7.09 – 6.93 (comp, 2H), 6.86 – 6.76 (m, 1H), 6.71 – 6.61 (m, 1H), 6.07 – 5.18 (m, 1H), 3.23 – 3.07 (comp, 4H), 2.89 – 2.77 (comp, 3H), 2.77 – 2.69 (comp, 2H), 2.65 – 2.55 (comp, 4H), 2.41 – 2.31 (comp, 2H), 2.13 – 1.91 (comp, 3H), 1.88 – 1.76 (m, 1H), 1.62 – 1.48 (comp, 2H), 0.97 – 0.88 (comp, 3H).^{13}C NMR (126 MHz, CDCl3) rotamers δ 167.9, 167.3, 150.3, 150.2, 143.1, 142.8, 135.8, 135.5, 135.5, 135.5, 130.5, 130.2, 130.0, 129.8, 129.7, 129.4, 129.0, 128.9, 128.0, 127.9, 117.9, 115.7, 115.6, 114.9, 114.0, 60.7, 60.5, 57.8, 53.5, 53.3, 53.2, 49.6, 49.4, 31.5, 30.1, 29.2, 28.9, 28.6, 27.6, 22.5, 22.2, 20.0, 12.1. HRMS (ESI) *m/z* calcd for $C_{27}H_{35}N_3O_3$ $(M+H)^+$, 418.2853; found 418.2856.

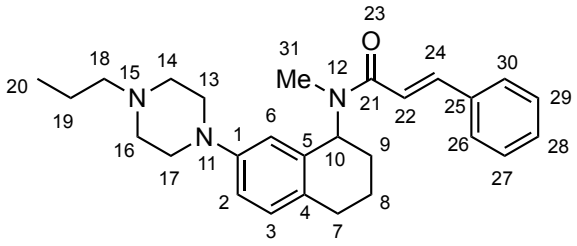

NMR Assignments (**2.93**). ^{1}H NMR (400 MHz, $CDCl_3$) rotamers δ 7.85 – 7.72 (m, 1H, 24), 7.63 – 7.48 (comp, 2H, 26, 30), 7.45 – 7.32 (comp, 3H, 27, 28, 29), 7.09 – 6.93 (comp, 2H, 3, 22), 6.86 – 6.76 (m, 1H, 2), 6.71 – 6.61 (m, 1H, 6), 6.07 – 5.18 (m, 1H, 10), 3.23 – 3.07 (comp, 4H, 13, 17), 2.89 – 2.77 (comp, 3H, 31), 2.77 – 2.69 (comp, 2H, 7), 2.65 – 2.55 (comp, 4H, 14, 16), 2.41 – 2.31 (comp, 2H, 18), 2.13 – 1.91 (comp, 3H, 8, 9), 1.88 – 1.76 (m, 1H, 8'), 1.62 – 1.48 (comp, 2H, 19), 0.97 – 0.88 (m, 3H, 20). ^{13}C NMR (126 MHz, $CDCl_3$) rotamers δ 167.9 and 167.3 (21), 150.3 and 150.2 (1), 143.1 and 142.8 (24), 135.8 and 135.5 (25), 135.5 and 135.5 (5), 130.5 and 130.2 (4), 130.0 and 129.8 (3), 129.7 and 129.4 (28), 129.0 and 128.9 (26, 30), 128.0 and 127.9 (27, 29) and 117.9 (22), 115.7 and 115.6 (2), 114.9 and 114.0 (6), 60.7 and 60.5 (18), 57.8 and 53.5 (10), 53.3 and 53.2 (14, 16), 49.6 and 49.4 (13, 17), 31.5 and 30.1 (31), 29.2 and 28.9 (7), 28.6 and 27.6 (9), 22.5 and 22.2 (8), 20.0 (19), 12.1 (20).

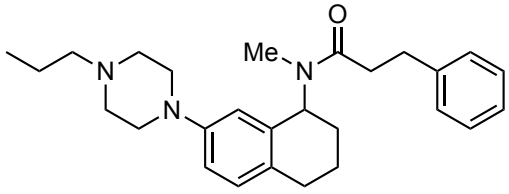

***N*-Methyl-3-phenyl-*N*-(7-(4-propylpiperazin-1-yl)-1,2,3,4-tetrahydronaphthalen-1-yl)propenamide** (**2.94**) (MDW-1-238). Prepared from **2.87** (14 mg, 0.052mmol) and 3-phenylpropionyl chloride according to representative procedure J. The crude residue was purified via flash chromatography (SiO_2) eluting with hexanes/EtOAc/Et_3N (59:40:1) affording 13 mg (61 %) of **2.94** as a colorless oil. ^{1}H NMR (499 MHz, $CDCl_3$) rotamers δ 7.33 – 7.17 (comp, 5H), 7.00 (t, J = 8.2 Hz, 1H), 6.81 – 6.75 (m, 1H), 6.53 (dd, J = 9.3, 2.5 Hz, 1H), 5.94 – 4.89 (m, 1H), 3.15 – 3.00 (comp, 6H), 2.89 – 2.52 (comp, 11H), 2.36 (td, J = 7.9, 2.7 Hz, 2H), 2.02 – 1.66 (comp, 4H), 1.61 – 1.48 (comp, 2H), 0.93 (td, J = 7.4, 2.1 Hz, 3H). ^{13}C NMR (126 MHz, $CDCl_3$)

rotamers δ 173.0, 172.8, 150.3, 150.1, 141.7, 141.5, 135.8, 135.4, 130.4, 130.2, 129.9, 129.4, 128.7, 128.6, 128.6, 128.6, 126.3, 126.2, 115.6, 115.6, 114.7, 113.7, 60.8, 60.8, 57.4, 53.4, 53.3, 53.0, 49.7, 49.5, 36.0, 35.4, 31.9, 31.5, 31.2, 30.5, 29.8, 29.5, 28.9, 28.7, 28.6, 27.6, 22.5, 22.2, 20.2, 12.1. HRMS (ESI) *m/z* calcd for $C_{27}H_{37}N_3O$ $(M+H)^+$, 420.3009; found 420.3009.

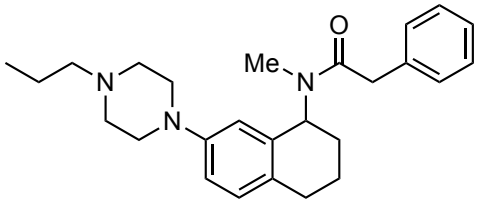

***N*-Methyl-2-phenyl-*N*-(7-(4-propylpiperazin-1-yl)-1,2,3,4-tetrahydronaphthalen-1-yl)acetamide** (**2.95**) (MDW-2-189). Prepared from **2.87** (17 mg, 0.059mmol) and phenylacetyl chloride according to representative procedure J. The crude residue was purified via flash chromatography (SiO_2) eluting with hexanes/EtOAc/Et_3N (59:40:1) affording 11 mg (46%) of **2.95** as a colorless oil. ^1H NMR (499 MHz, $CDCl_3$) rotamers δ 7.43 – 7.21 (comp, 5H), 6.96 (t, *J* = 9.1 Hz, 1H), 6.78 – 6.69 (m, 1H), 6.35 (d, *J* = 2.7 Hz, 1H), 5.95 – 5.01 (m, 1H), 3.93 – 3.78 (comp, 2H), 3.04 – 2.88 (comp, 4H), 2.70 – 2.60 (comp, 5H), 2.59 – 2.50 (comp, 4H), 2.41 – 2.32 (comp, 2H), 2.05 – 1.87 (comp, 2H), 1.78 – 1.49 (comp, 4H), 0.97 – 0.90 (comp, 3H). ^{13}C NMR (126 MHz, $CDCl_3$) roatmers δ 171.9, 171.8, 150.1, 149.9, 135.8, 135.6, 135.3, 135.1, 130.1, 130.0, 129.9, 128.9, 128.9, 128.9, 128.8, 127.0, 126.9, 115.5, 115.3, 114.0, 113.8, 60.8, 57.8, 53.3, 53.2, 53.0, 49.3, 49.3, 42.0, 41.8, 31.5, 29.8, 29.6, 28.8, 28.6, 28.5, 27.4, 22.3, 22.2, 20.1, 20.1, 12.1, 12.1. HRMS (ESI) *m/z* calcd for $C_{26}H_{35}N_3O$ $(M+H)^+$, 406.2853; found 406.2853.

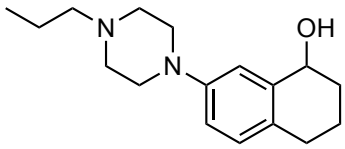

7-(4-Propylpiperazin-1-yl)-1,2,3,4-tetrahydronaphthalen-1-ol (**2.96**) (MDW-2-65). $NaBH_4$ was added to a solution of **2.84** (150 mg, 0.551 mmol) in MeOH (2.7 mL) and the reaction was stirred for 2 h at room temperature. The reaction was quenched with 1 N NaOH (5 mL) and volatile organics were removed under reduced pressure, whereupon the aqueous mixture was extracted with CH_2Cl_2 (3 x 10 mL). The combined organic extracts were washed with brined (1 x 10 mL) dried (Na_2SO_4) and concentrated under reduced pressure to afford 151 mg (100%) of **2.96** as a colorless oil. ^{1}H NMR (400 MHz, $CDCl_3$) δ 6.98 (d, *J* = 2.6 Hz, 1H), 6.94 (d, *J* = 8.4 Hz, 1H), 6.75 (dd, *J* = 8.4, 2.7 Hz, 1H), 4.68 – 4.63 (m, 1H), 3.14 – 3.07 (comp, 4H), 2.93 (brs, 1H), 2.72 – 2.50 (comp, 6H), 2.35 – 2.27 (comp, 2H), 2.00 – 1.64 (comp, 4H), 1.58 – 1.47 (comp, 2H), 0.90 (t, *J* = 7.4 Hz, 3H). ^{13}C NMR (101 MHz, $CDCl_3$) δ 149.7, 139.6, 129.4, 128.3, 116.1, 115.8, 68.3, 60.7, 53.2, 49.4, 32.6, 28.4, 19.9, 19.3, 12.0. HRMS (ESI) *m/z* calcd for $C_{17}H_{26}N_2O$ $(M+H)^+$, 275.2118; found 275.2125.

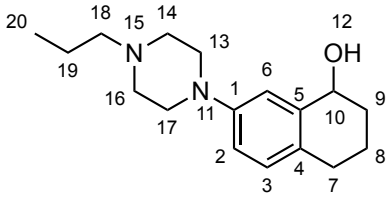

NMR Assignments (**2.96**). ^{1}H NMR (400 MHz, $CDCl_3$) δ 6.98 (d, *J* = 2.6 Hz, 1H, 6), 6.94 (d, *J* = 8.4 Hz, 1H, 3), 6.75 (dd, *J* = 8.4, 2.7 Hz, 1H, 2), 4.68 – 4.63 (m, 1H, 10), 3.14 – 3.07 (comp, 4H, 13, 17), 2.93 (brs, 1H, 12), 2.72 – 2.50 (comp, 6H, 7, 14, 16), 2.35 – 2.27 (comp, 2H, 18), 2.00 – 1.64 (comp, 4H, 8, 9), 1.58 – 1.47 (comp, 2H, 19), 0.90 (t, *J* = 7.4 Hz, 3H, 20). ^{13}C NMR (101 MHz, $CDCl_3$) δ 149.7 (1), 139.6 (5), 129.4

(3), 128.3 (4), 116.1 (2), 115.8 (6), 68.3 (10), 60.7 (18), 53.2 (14, 16), 49.4 (13, 17), 32.6 (7), 28.4 (9), 19.9 (8), 19.3 (19), 12.0 (20).

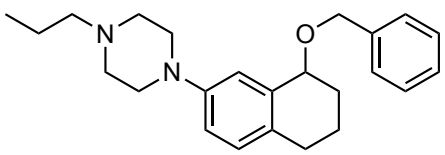

1-(8-(Benzyloxy)-5,6,7,8-tetrahydronaphthalen-2-yl)-4-propylpiperazine (**2.99**) (MDW-1-245). NaH (6 mg of a 60% suspension in mineral oil, 0.1 mmol) was added to a solution of **2.96** (20 mg, 0.073 mmol) in DMF (0.4 mL) and the reaction was stirred at room temperature for 30 min. The reaction was cooled to 0 °C and a solution of benzyl bromide (12 mg, 8.6 μL, 0.073 mmol) in DMF (0.1 mL) was added. The reaction was stirred for 30 min at 0 °C and the cooling bath was removed. The reaction was stirred for 1 h at room temperature and NH_4Cl (10 mL) was added, whereupon the mixture was extracted with CH_2Cl_2 (3 x 10 mL). The combined organic extracts were dried (Na_2SO_4) and concentrated under reduced pressure. The crude residue was purified via flash chromatography (SiO_2) eluting with hexanes/EtOAc/Et_3N (89:10:1) affording 15 mg (58%) of **2.99** as a pale yellow oil. ^{1}H NMR (600 MHz, $CDCl_3$) δ 7.43 – 7.39 (m, 1H), 7.35 (t, *J* = 7.6 Hz, 2H), 7.30 – 7.26 (m, 1H), 6.99 (d, *J* = 8.3 Hz, 1H), 6.86 (d, *J* = 2.7 Hz, 1H), 6.81 (dd, *J* = 8.4, 2.7 Hz, 1H), 4.70 (d, *J* = 12.0 Hz, 1H), 4.59 (d, *J* = 12.0 Hz, 1H), 4.51 – 4.47 (m, 1H), 3.21 – 3.15 (comp, 4H), 2.79 – 2.60 (comp, 6H), 2.41 (t, *J* = 7.9 Hz, 2H), 2.07 – 1.98 (comp, 2H), 1.96 – 1.89 (m, 1H), 1.76 – 1.69 (m, 1H), 1.64 – 1.55 (comp, 2H), 0.94 (t, *J* = 7.4 Hz, 3H). ^{13}C NMR (151 MHz, $CDCl_3$) δ 149.5, 139.3, 137.4, 129.6, 129.4, 128.5, 128.0, 127.6, 116.8, 116.7, 75.1, 70.3, 60.7, 53.3, 49.6, 28.4, 28.2, 19.9, 19.4, 12.1. HRMS (ESI) *m/z* calcd for $C_{24}H_{32}N_2O$ $(M+H)^+$, 365.2587 found 365.2594.

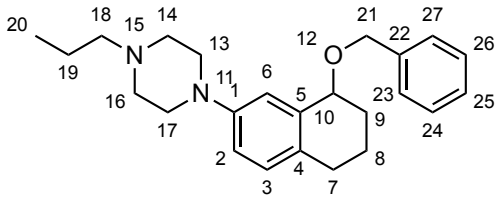

NMR Assignments (**2.99**). ^{1}H NMR (600 MHz, $CDCl_3$) δ 7.43 – 7.39 (m, 1H, 23, 27), 7.35 (t, *J* = 7.6 Hz, 2H, 24, 26), 7.30 – 7.26 (m, 1H, 25), 6.99 (d, *J* = 8.3 Hz, 1H, 3), 6.86 (d, *J* = 2.7 Hz, 1H, 6), 6.81 (dd, *J* = 8.4, 2.7 Hz, 1H, 2), 4.70 (d, *J* = 12.0 Hz, 1H, 21''), 4.59 (d, *J* = 12.0 Hz, 1H, 21'), 4.51 – 4.47 (m, 1H, 10), 3.21 – 3.15 (comp, 4H, 13, 17), 2.79 – 2.60 (comp, 6H, 7, 14, 16), 2.41 (t, *J* = 7.9 Hz, 2H, 18), 2.07 – 1.98 (comp, 2H, 8'', 9''), 1.96 – 1.89 (m, 1H, 9'), 1.76 – 1.69 (m, 1H, 8'), 1.64 – 1.55 (comp, 2H, 19), 0.94 (t, *J* = 7.4 Hz, 3H, 20). ^{13}C NMR (151 MHz, $CDCl_3$) δ 149.5 (1), 139.3 (22), 137.4 (5), 129.6 (3), 129.4 (4), 128.5 (24, 26), 128.0 (23, 27), 127.6 (25), 116.8 (6), 116.7 (2), 75.1 (10), 70.3 (21), 60.7 (18), 53.3 (14, 16), 49.6 (13, 17), 28.4 (7), 28.2 (9), 19.9 (19), 19.4 (8), 12.1 (20).

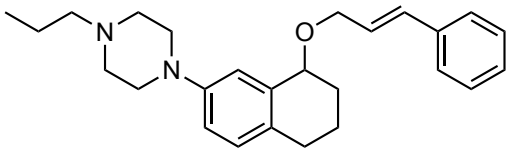

1-(8-(Cinnamyloxy)-5,6,7,8-tetrahydronaphthalen-2-yl)-4-propylpiperazine (**2.100**) (MDW-2-98). A solution of **2.96** (50 mg, 0.18 mmol) in DMF (0.4 mL) was added to a solution of NaH (10 mg of a 60% suspension in mineral oil, 0.25 mmol) in DMF (0.3 mL) and the reaction was stirred for 30 min at room temperature. The reaction was cooled to 0 °C and a solution of cinnamyl bromide (43 mg, 0.22 mmol) in DMF (0.45 mL) was added. The reaction was stirred for 30 min at 0 °C and the cooling bath was removed. The reaction was stirred for 22 h at room temperature and NH_4Cl (10 mL)

was added, whereupon the mixture was extracted with CH_2Cl_2 (3 x 10 mL). The combined organic extracts were dried (Na_2SO_4) and concentrated under reduced pressure. The crude residue was purified via flash chromatography (SiO_2) eluting with hexanes/EtOAc/Et_3N (89:10:1) affording 22 mg (31%) of **2.100** as a pale yellow oil. ^{1}H NMR (400 MHz, $CDCl_3$) δ 7.42 – 7.37 (comp, 2H), 7.35 – 7.29 (comp, 2H), 7.26 – 7.21 (m, 1H), 7.00 (d, *J* = 8.4 Hz, 1H), 6.98 (d, *J* = 2.7 Hz, 1H), 6.82 (dd, *J* = 8.4, 2.7 Hz, 1H), 6.66 (d, *J* = 16.0 Hz, 1H), 6.37 (dt, *J* = 15.9, 5.9 Hz, 1H), 4.50 (t, *J* = 4.9 Hz, 1H), 4.38 – 4.20 (comp, 2H), 3.22 – 3.15 (comp, 4H), 2.82 – 2.57 (comp, 6H), 2.41 – 2.33 (comp, 2H), 2.07 – 1.88 (comp, 3H), 1.78 – 1.67 (m, 1H), 1.63 – 1.50 (comp, 2H), 0.93 (t, *J* = 7.4 Hz, 3H). ^{13}C NMR (101 MHz, $CDCl_3$) δ 149.7, 137.4, 137.1, 131.9, 129.6, 129.3, 128.7, 127.7, 127.2, 126.6, 116.7, 116.6, 75.5, 69.1, 60.8, 53.4, 49.7, 28.5, 28.4, 20.1, 19.4, 12.1. HRMS (ESI) *m/z* calcd for $C_{26}H_{34}N_2O$ $(M+H)^+$, 391.2744 found 391.2754.

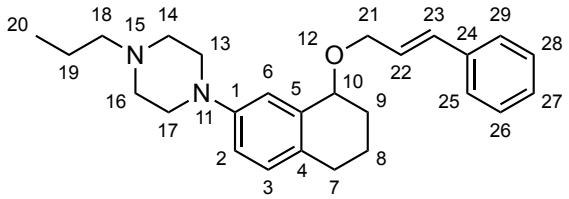

NMR Assignments (**2.100**). ^{1}H NMR (400 MHz, $CDCl_3$) δ 7.42 – 7.37 (comp, 2H, 25, 29), 7.35 – 7.29 (comp, 2H, 26, 28), 7.26 – 7.21 (m, 1H, 27), 7.00 (d, *J* = 8.4 Hz, 1H, 3), 6.98 (d, *J* = 2.7 Hz, 1H, 6), 6.82 (dd, *J* = 8.4, 2.7 Hz, 1H, 2), 6.66 (d, *J* = 16.0 Hz, 1H, 23), 6.37 (dt, *J* = 15.9, 5.9 Hz, 1H, 22), 4.50 (t, *J* = 4.9 Hz, 1H, 10), 4.38 – 4.20 (comp, 2H, 21), 3.22 – 3.15 (comp, 4H, 13, 17), 2.82 – 2.57 (comp, 6H, 7, 14, 16), 2.41 – 2.33 (comp, 2H, 18), 2.07 – 1.88 (comp, 3H, 8", 9), 1.78 – 1.67 (m, 1H, 8'), 1.63 – 1.50 (comp, 2H, 19), 0.93 (t, *J* = 7.4 Hz, 3H, 20). ^{13}C NMR (101 MHz, $CDCl_3$) δ 149.7 (1), 137.4 (5), 137.1 (24), 131.9 (23), 129.6 (3), 129.3 (4), 128.7 (26, 28), 127.7 (27), 127.2

(22), 126.6 (25, 29), 116.7 (6), 116.6 (2), 75.5 (10), 69.1 (21), 60.8 (18), 53.4 (14, 16), 49.7 (13, 17), 28.5 (9), 28.4 (7), 20.1 (19), 19.4 (8), 12.1 (20).

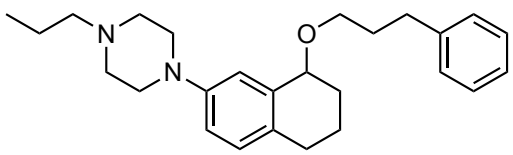

1-(8-(3-Phenylpropoxy)-5,6,7,8-tetrahydronaphthalen-2-yl)-4-propylpiperazine (**2.101**) (MDW-2-126). A solution of ethanol (1 mL) containing **2.100** (18 mg, 0.045 mmol) and 10% Pd/C (5 mg) was sparged with H_2 gas for 5 min and then stirred under an atmosphere of H_2 (1 atm) for 2 h.The reaction was filtered through a pad of Celite and the filter cake was washed with CH_2Cl_2 (20 mL). The filtrate was concentrated under reduced pressure and the crude residue was purified via flash chromatography (SiO_2) eluting with hexanes/Et_2O/Et_3N (59:30:1) to afford 9 mg (50%) of **2.101** as a colorless oil. ^{1}H NMR (499 MHz, $CDCl_3$) δ 7.30 – 7.25 (comp, 2H), 7.22 – 7.16 (comp, 3H), 6.99 (d, *J* = 8.5 Hz, 1H), 6.97 (d, *J* = 2.6 Hz, 1H), 6.83 (dd, *J* = 8.4, 2.7 Hz, 1H), 4.36 (t, *J* = 5.2 Hz, 1H), 3.69 – 3.62 (m, 1H), 3.54 – 3.48 (m, 1H), 3.21 – 3.13 (comp, 4H), 2.79 – 2.71 (comp, 3H), 2.67 – 2.56 (comp, 5H), 2.39 – 2.32 (comp, 2H), 2.03 – 1.88 (comp, 5H), 1.73 – 1.66 (m, 1H), 1.60 – 1.50 (comp, 2H), 0.93 (t, *J* = 7.4 Hz, 3H). ^{13}C NMR (126 MHz, $CDCl_3$) δ 149.8, 142.3, 137.7, 129.6, 129.1, 128.6, 128.4, 125.9, 116.6, 116.6, 76.1, 67.7, 60.9, 53.5, 49.9, 32.7, 32.0, 28.5, 28.3, 20.2, 19.5, 12.1. HRMS (ESI) *m/z* calcd for $C_{26}H_{36}N_2O$ $(M+H)^+$, 393.2900 found 393.2903.

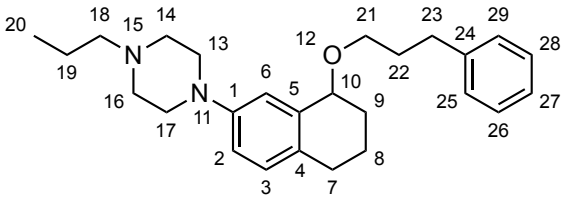

NMR Assignments (**2.101**). ^{1}H NMR (499 MHz, $CDCl_3$) δ 7.30 – 7.25 (comp, 2H, 25, 29), 7.22 – 7.16 (comp, 3H, 26, 27, 28), 6.99 (d, *J* = 8.5 Hz, 1H, 3), 6.97 (d, *J* = 2.6 Hz, 1H, 6), 6.83 (dd, *J* = 8.4, 2.7 Hz, 1H, 2), 4.36 (t, *J* = 5.2 Hz, 1H, 10), 3.69 – 3.62 (m, 1H, 21''), 3.54 – 3.48 (m, 1H, 21'), 3.21 – 3.13 (comp, 4H, 13, 17), 2.79 – 2.71 (comp, 3H, 7'', 23), 2.67 – 2.56 (comp, 5H, 7', 14, 16), 2.39 – 2.32 (comp, 2H, 18), 2.03 – 1.88 (comp, 5H, 8'', 9, 22), 1.73 – 1.66 (m, 1H, 8'), 1.60 – 1.50 (comp, 2H, 19), 0.93 (t, *J* = 7.4 Hz, 3H, 20). ^{13}C NMR (126 MHz, $CDCl_3$) δ 149.8 (1), 142.3 (24), 137.7 (5), 129.6 (3), 129.1 (4), 128.6 (26, 28), 128.4 (25, 29), 125.9 (27), 116.6 (6), 116.6 (2), 76.1 (10), 67.7 (21), 60.9 (18), 53.5 (14, 16), 49.9 (13, 17), 32.7 (23), 32.0 (22), 28.5 (9), 28.3 (7), 20.2 (8), 19.5 (19), 12.1 (20).

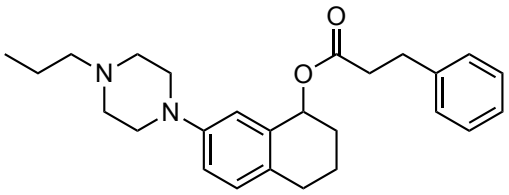

7-(4-Propylpiperazin-1-yl)-1,2,3,4-tetrahydronaphthalen-1-yl 3-phenylpropanoate (**2.103**) (MDW-1-290). A solution of **2.96** (30 mg, 0.11 mmol) and *i*-Pr_2NEt (14 mg, 19 μL 0.11 mmol) in CH_2Cl_2 (1.1 mL) was cooled to 0 ° C. Hydrocinnamoyl chloride (18 mg, 16 μL, 0.11 mmol) was added to the cooled solution and the solution was stirred for 22 h allowing the reaction to slowly warm to room temperature. The reaction was diluted with saturated aqueous $NaHCO_3$ (5 mL) and extracted with CH_2Cl_2 (3 x 10 mL). The combined organic extracts were washed with

brine (1 x 20 mL), dried (Na_2SO_4), and concentrated under reduced pressure. The crude residue was purified via flash chromatography (SiO_2) eluting with hexanes/EtOAc/Et_3N (79:40:1) to afford 14 mg (32%) of **2.103** as a colorless oil. ^{1}H NMR (500 MHz, $CDCl_3$) δ 7.29 – 7.25 (comp, 2H), 7.22 – 7.17 (comp, 3H), 7.02 (d, *J* = 8.4 Hz, 1H), 6.85 (dd, *J* = 8.4, 2.7 Hz, 1H), 6.78 (d, *J* = 2.6 Hz, 1H), 5.95 (t, *J* = 4.2 Hz, 1H), 3.20 – 3.14 (comp, 4H), 2.97 (t, *J* = 7.7 Hz, 2H), 2.80 – 2.73 (m, 1H), 2.70 – 2.60 (comp, 7H), 2.45 – 2.38 (comp, 2H), 1.94 – 1.83 (comp, 3H), 1.79 – 1.71 (m, 1H), 1.64 – 1.54 (comp, 2H), 0.94 (t, *J* = 7.3 Hz, 3H). ^{13}C NMR (126 MHz, $CDCl_3$) δ 172.8, 149.7, 140.6, 135.0, 129.8, 129.5, 128.6, 128.4, 126.3, 117.0, 117.0, 70.5, 60.7, 53.2, 49.3, 36.4, 31.2, 29.3, 28.3, 19.9, 19.0, 12.0. HRMS (ESI) *m/z* calcd for $C_{26}H_{34}N_2O_2$ $(M+H)^+$, 407.2693; found 407.2697

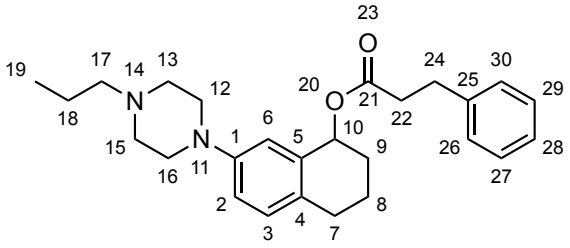

NMR Assignments (**2.103**). ^{1}H NMR (500 MHz, $CDCl_3$) δ 7.29 – 7.25 (comp, 2H, 26, 30), 7.22 – 7.17 (comp, 3H, 27, 28, 29), 7.02 (d, *J* = 8.4 Hz, 1H, 3), 6.85 (dd, *J* = 8.4, 2.7 Hz, 1H, 2), 6.78 (d, *J* = 2.6 Hz, 1H, 6), 5.95 (t, *J* = 4.2 Hz, 1H, 10), 3.20 – 3.14 (comp, 4H, 12, 16), 2.97 (t, *J* = 7.7 Hz, 2H, 24), 2.80 – 2.73 (m, 1H, 7'), 2.70 – 2.60 (comp, 7H, 7'', 13, 15, 22), 2.45 – 2.38 (comp, 2H, 17), 1.94 – 1.83 (comp, 3H, 8', 9), 1.79 – 1.71 (m, 1H, 8''), 1.64 – 1.54 (comp, 2H, 18''), 0.94 (t, *J* = 7.3 Hz, 3H, 19). ^{13}C NMR (126 MHz, $CDCl_3$) δ 172.8 (21), 149.7 (1), 140.6 (5), 135.0 (25), 129.8 (3), 129.5 (4), 128.6 (26, 30), 128.4 (27, 29), 126.3 (28), 117.0 (6), 117.0 (2), 70.5 (10), 60.7 (17),

53.2 (13, 15), 49.3 (12, 16), 36.4 (22), 31.2 (24), 29.3 (9), 28.3 (7), 19.9 (18), 19.0 (8), 12.0 (19).

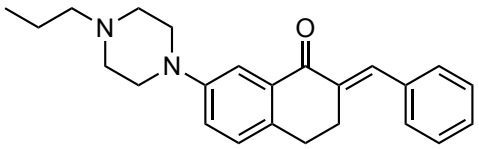

(*E*)-2-Benzylidene-7-(4-propylpiperazin-1-yl)-3,4-dihydronaphthalen-1(2*H*)-one (**2.105**) (MDW-1-292). A solution of **2.84** (46 mg, 0.17 mmol) in EtOH (0.2 mL) was added dropwise to a 5% KOH in EtOH solution containing benzaldehyde (22 mg, 21 μL, 0.21 mmol). The reaction was stirred for 23 h at room temperature and diluted with saturated aqueous NH_4Cl (10 mL), whereupon the solution was extracted with CH_2Cl_2 (3 x 10 mL). The combined organic extracts were washed with brine (1 x 20 mL), dried (Na_2SO_4), and concentrated under reduced pressure. The crude residue was purified via flash chromatography (SiO_2) eluting with hexanes/EtOAc/Et_3N (79:40:1) to afford 36 mg (59%) of **2.105** as a yellow solid: MP 106-110 °C. ^{1}H NMR (499 MHz, $CDCl_3$) δ 7.85 (brs, *J* = 1.9 Hz, 1H), 7.66 (d, *J* = 2.6 Hz, 1H), 7.46 – 7.38 (comp, 4H), 7.36 – 7.32 (m, 1H), 7.15 (d, *J* = 8.3 Hz, 1H), 7.11 (dd, *J* = 8.4, 2.7 Hz, 1H), 3.30 – 3.25 (comp, 4H), 3.09 (td, *J* = 6.9, 1.6 Hz, 2H), 2.88 – 2.84 (comp, 2H), 2.67 – 2.62 (comp, 4H), 2.41 – 2.36 (comp, 2H), 1.62 – 1.53 (comp, 2H), 0.94 (t, *J* = 7.4 Hz, 3H). ^{13}C NMR (126 MHz, $CDCl_3$) δ 188.3, 150.4, 136.5, 136.1, 135.9, 134.7, 133.9, 130.0, 129.1, 128.5, 128.5, 121.8, 114.2, 60.7, 53.2, 49.1, 28.1, 27.5, 20.1, 12.1. HRMS (ESI) *m/z* calcd for $C_{24}H_{28}N_2O$ $(M+H)^+$, 361.2274; found 361.2276

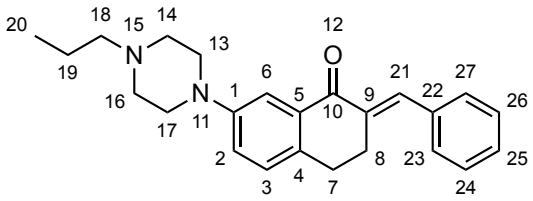

NMR Assignments (**2.105**). ^{1}H NMR (499 MHz, $CDCl_3$) δ 7.85 (brs, J = 1.9 Hz, 1H, 21), 7.66 (d, J = 2.6 Hz, 1H, 6), 7.46 – 7.38 (comp, 4H, 23, 24, 26, 27), 7.36 – 7.32 (m, 1H, 25), 7.15 (d, J = 8.3 Hz, 1H, 3), 7.11 (dd, J = 8.4, 2.7 Hz, 1H, 2), 3.30 – 3.25 (comp, 4H, 13, 17), 3.09 (td, J = 6.9, 1.6 Hz, 2H, 8), 2.88 – 2.84 (comp, 2H, 7), 2.67 – 2.62 (comp, 4H, 14, 16), 2.41 – 2.36 (comp, 2H, 18), 1.62 – 1.53 (comp, 2H, 19), 0.94 (t, J = 7.4 Hz, 3H, 20). ^{13}C NMR (126 MHz, $CDCl_3$) δ 188.3 (10), 150.4 (1), 136.5 (21), 136.1 (9), 135.9 (22), 134.7 (5), 133.9 (4), 130.0 (23, 27), 129.1 (3), 128.5 (25), 128.5 (24, 26), 121.8 (2), 114.2 (6), 60.7 (18), 53.2 (14, 16), 49.1 (13, 17), 28.1 (7), 27.5 (8), 20.1 (19), 12.1 (20).

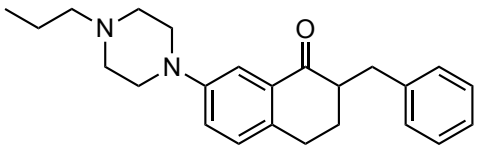

2-Benzyl-7-(4-propylpiperazin-1-yl)-3,4-dihydronaphthalen-1(2*H*)-one (**2.106**) (MDW-1-151). A solution of ethanol (1.1 mL) containing **2.105** (19 mg, 0.054 mmol) and 10% Pd/C (9 mg) was sparged with H_2 gas for 5 min and then stirred under an atmosphere of H_2 (1 atm) for 3 h. The reaction was filtered through a pad of Celite and the filter cake was washed with CH_2Cl_2 (20 mL). The filtrate was concentrated under reduced pressure and the crude residue was purified via flash chromatography (SiO_2) eluting with hexanes/Et_2O/Et_3N (59:30:1) to afford 6 mg (32%) of **2.106** as a pale yellow oil. ^{1}H NMR (499 MHz, $CDCl_3$) δ 7.58 (d, J = 2.4 Hz, 1H), 7.33 – 7.27 (comp, 2H), 7.25 – 7.19 (comp, 3H), 7.14 – 7.07 (comp, 2H), 3.47 (dd, J = 13.6, 4.0 Hz, 1H), 3.28 – 3.20

(m, 4H), 2.92 – 2.77 (comp, 2H), 2.75 – 2.68 (m, 1H), 2.67 – 2.58 (comp, 5H), 2.41 – 2.34 (comp, 2H), 2.11 – 2.03 (m, 1H), 1.80 – 1.71 (m, 1H), 1.61 – 1.51 (comp, 2H), 0.93 (t, J = 7.4 Hz, 3H). ^{13}C NMR (126 MHz, $CDCl_3$) δ 199.9, 150.2, 140.3, 135.4, 133.0, 129.6, 129.4, 128.5, 126.2, 122.0, 113.5, 60.8, 53.3, 49.6, 49.2, 35.9, 28.0, 27.8, 20.1, 12.1. HRMS (ESI) *m/z* calcd for $C_{24}H_{30}N_2O$ $(M+H)^+$, 363.2431 found 363.2435.

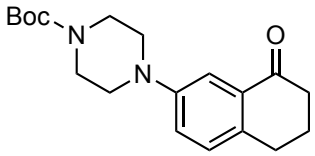

***tert*-Butyl 4-(8-oxo-5,6,7,8-tetrahydronaphthalen-2-yl)piperazine-1-carboxylate** (**2.107**) (DRM-1-43). Boc_2O (3.77 g, 3.97 mL, 17.3 mmol) was added to a solution of **2.83** (2.66 g, 11.5 mmol) and Et_3N (1.75 g, 2.41 mL, 17.3 mmol) in CH_2Cl_2 (60 mL) and the reaction was stirred for 20 h at room temperature. The reaction was diluted with 1 N NaOH (40 mL) and extracted with CH_2Cl_2 (3 x 40 mL). The combined organic extracts were washed with brine (1 x 30 mL), dried (Na_2SO_4), and concentrated under reduced pressure. The crude residue was purified via flash chromatography (SiO_2) eluting with hexanes/EtOAc/Et_3N (74:25:1) to afford 2.85 g (75%) of **2.107** as a yellow solid: mp 114–117 °C. ^{1}H NMR (499 MHz, $CDCl_3$) δ 7.54 (d, J = 2.7 Hz, 1 H), 7.16 (d, J = 8.4 Hz, 1 H), 7.09 (dd, J = 8.4, 2.7 Hz, 1 H), 3.57 (app t, J = 5.1 Hz, 4 H), 3.13 (app t, J = 5.1 Hz, 4 H), 2.87 (t, J = 6.0 Hz, 2 H), 2.62 (t, J = 6.5 Hz, 3 H), 2.13 – 2.06 (m, 2 H), 1.47 (s, 9 H). ^{13}C NMR (126 MHz, $CDCl_3$) δ 198.7, 154.8, 150.1, 136.6, 133.1, 129.8, 122.8, 113.7, 80.1, 49.5, 43.9, 43.3, 39.3, 29.0, 28.5, 23.6. HRMS (ESI) *m/z* calcd for $C_{19}H_{26}N_2O_3$ $(M+H)^+$, 331.2016 found 331.2017.

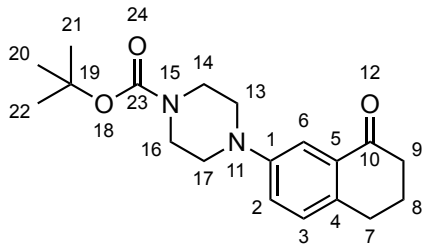

NMR Assignments (**2.107**). ^{1}H NMR (499 MHz, $CDCl_3$) δ 7.54 (d, *J* = 2.7 Hz, 1 H, 6), 7.16 (d, *J* = 8.4 Hz, 1 H, 3), 7.09 (dd, *J* = 8.4, 2.7 Hz, 1 H, 2), 3.57 (t, *J* = 5.1 Hz, 4 H, 14, 16), 3.13 (t, *J* = 5.1 Hz, 4 H, 13, 17), 2.87 (t, *J* = 6.0 Hz, 2 H, 9), 2.62 (t, *J* = 6.5 Hz, 3 H, 7), 2.13 – 2.06 (m, 2 H, 8), 1.47 (s, 9 H, 20, 21, 22). ^{13}C NMR (126 MHz, $CDCl_3$) δ 198.7 (10), 154.8 (23), 150.1 (1), 136.6 (5), 133.1 (4), 129.8 (3), 122.8 (2), 113.7 (6), 80.1 (19), 49.5 (13, 17), 43.9 and 43.3 (14, 16), 39.3 (7), 29.0 (9), 28.5 (20, 21, 22), 23.6 (8).

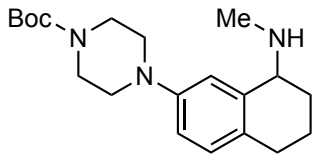

***tert*-Butyl 4-(8-(methylamino)-5,6,7,8-tetrahydronaphthalen-2-yl)piperazine-1-carboxylate** (**2.108**) (MDW-2-178). Prepared from **2.107** (0.300 g, 0.908 mmol) mmol) and $MeNH_3Cl$ according to representative procedure D. The crude residue was purified via flash chromatography (SiO_2) eluting with CH_2Cl_2/MeOH/Et_3N (99:0:1 to 98:1:1) affording 0.266 g (85%) of **2.108** as a brown oil. ^{1}H NMR (499 MHz, $CDCl_3$) δ 6.98 (d, *J* = 8.4 Hz, 1 H), 6.95 (d, *J* = 2.5 Hz, 1 H), 6.76 (dd, *J* = 8.4, 2.5 Hz, 1H), 3.65 – 3.61 (m, 1 H), 3.56 (app t, *J* = 5.2 Hz, 4H), 3.12 – 3.04 (comp, 4 H), 2.76 – 2.59 (comp, 2 H), 2.48 (s, 3 H), 1.96 – 1.81 (comp, 3 H), 1.73 – 1.66 (m, 1 H), 1.47 (s, 9 H). ^{13}C NMR (126 MHz, $CDCl_3$) δ 154.8, 149.6, 139.4, 129.8, 129.6, 117.1, 116.2, 57.5, 50.1, 44.1,

43.4, 33.9, 28.6, 28.5, 27.7, 19.2. HRMS (ESI) *m/z* calcd for $C_{20}H_{31}N_3O_2$ $(M+H)^+$, 315.2067 found 315.2070.

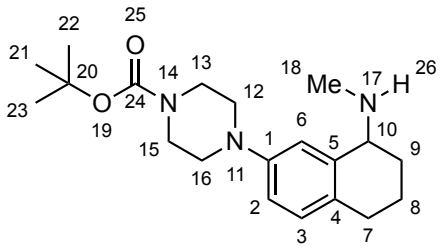

NMR Assignments (**2.108**). ^{1}H NMR (499 MHz, $CDCl_3$) δ 6.98 (d, *J* = 8.4 Hz, 1 H, 3), 6.95 (d, *J* = 2.5 Hz, 1 H, 6), 6.76 (dd, *J* = 8.4, 2.5 Hz, 1 H, 2), 3.65 – 3.61 (m, 1 H, 10), 3.56 (t, *J* = 5.2 Hz, 4 H, 13, 15), 3.12 – 3.04 (comp, 4 H, 12, 16), 2.76 – 2.59 (comp, 2 H, 7), 2.48 (s, 3 H, 18), 1.96 – 1.81 (comp, 4 H, 8, 9, 26), 1.73 – 1.66 (m, 1 H, 8), 1.47 (s, 9 H, 21, 22, 23). ^{13}C NMR (126 MHz, $CDCl_3$) δ 154.8 (24), 149.6 (1), 139.4 (5), 129.8 (3), 129.6 (4), 117.1 (6), 116.2 (2), 57.5 (10), 50.1 (12, 16), 44.1 and 43.4 (13, 15), 33.9 (18), 28.6 (7), 28.5 (21, 22, 23), 27.7 (9), 19.2 (8).

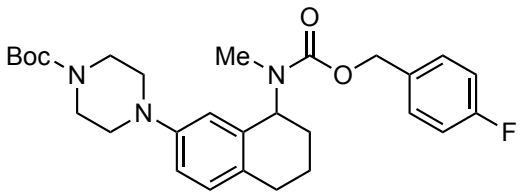

***tert*-Butyl 4-(8-((((4-fluorobenzyl)oxy)carbonyl)(methyl)amino)-5,6,7,8-tetrahydronaphthalen-2-yl)piperazine-1-carboxylate** (**2.110**) (DRM-1-47). A 20% solution of phosgene in PhME (0.8 mL) was added dropwise to a solution of 4-fluorobenzyl alcohol (0.18 g, 0.16 mL, 1.4 mmol) and *i*-Pr_2Net (0.29 g, 0.39 mL, 2.2 mmol) in THF/PhMe (1:1, 1.5 mL) at 0 °C. The reaction was stirred at 0 °C for 20 min, whereupon a solution of **2.108** (0.258 g, 0.747 mmol) in toluene (1.2 mL) was added dropwise to the cooled mixture. The reaction was stirred for 4 h, allowing to slowly warm

to room temperature. The solution was diluted with 1 N NaOH (10 mL) and extracted with CH_2Cl_2 (3 x 10 mL). The combined organic extracts were dried (Na_2SO_4) and concentrated under reduced pressure. The crude residue was purified via flash chromatography (SiO_2) eluting with EtOAc/hexanes (3:7) affording 0.269 g (73%) of **2.110** as a pale-yellow oil**.** ^{1}H NMR (499 MHz, $CDCl_3$) δ 7.43 – 7.30 (comp, 2 H), 7.10 – 6.95 (comp, 3 H), 6.79 – 6.73 (m, 1 H), 6.63 – 6.51 (m, 1 H), 5.48 – 5.26 (m, 1 H), 5.27 – 5.06 (comp, 2 H), 3.56 – 3.51 (comp, 4 H), 3.07 – 2.89 (comp, 4 H), 2.74 – 2.59 (comp, 5 H), 2.05 – 1.91 (comp, 2 H), 1.82 – 1.66 (comp, 2 H), 1.48 (s, 9 H). ^{13}C NMR (126 MHz, $CDCl_3$) δ 163.7, 161.8, 157.3, 157.0, 154.9, 154.9, 150.2, 150.1, 136.1, 136.0, 133.2, 133.1, 133.1, 133.1, 131.0, 130.5, 130.3, 130.2, 130.2, 130.1, 130.1, 116.5, 116.3, 115.7, 115.6, 115.3, 114.9, 80.1, 66.7, 66.7, 55.9, 55.6, 50.1, 44.2, 43.4, 30.5, 29.9, 29.0, 28.9, 28.7, 28.3, 27.8, 22.5, 22.3. HRMS (ESI) *m/z* calcd for $C_{28}H_{36}FN_3O_4$ $(M+H)^+$, 498.2763; found 498.2784.

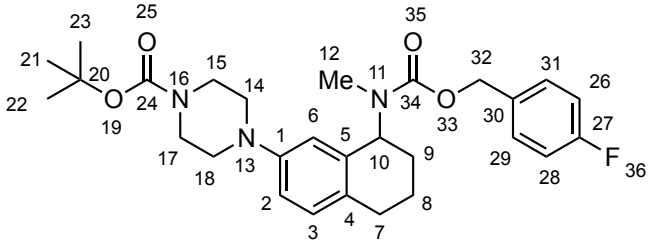

NMR Assignments (**2.110**). ^{1}H NMR (499 MHz, $CDCl_3$) δ 7.43 – 7.30 (comp, 2 H, 26, 28), 7.10 – 6.95 (comp, 3 H, 3, 29, 31), 6.79 – 6.73 (m, 1 H, 2), 6.63 – 6.51 (m, 1 H, 6), 5.48 – 5.26 (m, 1 H, 10), 5.27 – 5.06 (comp, 2 H, 32), 3.56 – 3.51 (comp, 4 H, 15, 17), 3.07 – 2.89 (comp, 4 H, 14, 18), 2.74 – 2.59 (comp, 5 H, 7, 12), 2.05 – 1.91 (comp, 2 H, 8, 9), 1.82 – 1.66 (comp, 2 H, 8, 9), 1.48 (s, 9 H, 21, 22, 23). ^{13}C NMR (126 MHz, $CDCl_3$) δ 163.7 and 161.8 (27), 157.3 and 157.0 (34), 154.9 and 154.9 (24), 150.2 and 150.1 (1), 136.1 and 136.0 (5), 133.2, 133.1, 133.1, and 133.1 (30), 131.0 and 130.5 (4),

130.3 (3), 130.2 (26, 28), 130.2 (3), 130.1 and 130.1 (26, 28), 116.5 and 116.3 (2), 115.7 and 115.6 (29, 31), 115.3 and 114.9 (6), 80.1 (20), 66.7 and 66.7 (32), 55.9 and 55.6 (10), 50.1 (14, 18), 44.2 and 43.4 (15, 17), 30.5 and 29.9 (12), 29.0 and 28.9 (7), 28.7 (21, 22, 23), 28.3 and 27.8 (9), 22.5 and 22.3 (8).

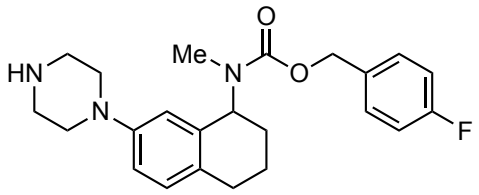

4-Fluorobenzyl methyl(7-(piperazin-1-yl)-1,2,3,4-tetrahydronaphthalen-1-yl)carbamate (**2.111**) (DRM-1-49). TFA (0.33 mL, 4.3 mmol) was added to a solution of **2.110** (0.107 g, 0.215 mmol) in CH_2Cl_2 (2.2 mL) cooled to 0 °C. The reaction was stirred for 17 h, allowing to slowly warm to room. The reaction was was diluted with 1 N NaOH (10 mL) and extracted with CH_2Cl_2 (3 x 10 mL). The combined organic extracts were dried (Na_2SO_4) and concentrated under reduced pressure. The crude residue was purified via flash chromatography (SiO_2) eluting with CH_2Cl_2/MeOH/Et_3N (99:0:1 to 97:2:1) affording 53 mg (61%) of **2.111** as a colorless oil**.** ^{1}H NMR (499 MHz, $CDCl_3$) rotamers δ 7.43 – 7.31 (comp, 2 H), 7.12 – 6.95 (comp, 3 H), 6.79 – 6.73 (m, 1 H), 6.64 – 6.53 (m, 1 H), 5.50 – 5.26 (m, 1 H), 5.26 – 5.06 (comp, 2 H), 3.06 – 2.92 (comp, 7 H), 2.74 – 2.59 (comp, 5 H) 2.04 – 1.65 (comp, 5 H). ^{13}C NMR (126 MHz, $CDCl_3$) rotamers δ 163.5, 161.6, 157.2, 156.9, 150.6, 150.5, 135.8, 135.7, 133.1, 133.0, 133.0, 132.9, 130.2, 130.0, 130.0, 129.9, 129.9, 129.9, 129.7, 115.8, 115.5, 115.4, 114.7, 114.3, 66.5, 66.5, 55.7, 55.5, 50.9, 50.8, 46.2, 46.2, 30.4, 29.8, 28.8, 28.7, 28.2, 27.7, 22.3, 22.1. HRMS (ESI) *m/z* calcd for $C_{29}H_{36}FN_3O_3$ $(M+H)^+$, 398.2238; found 398.2248.

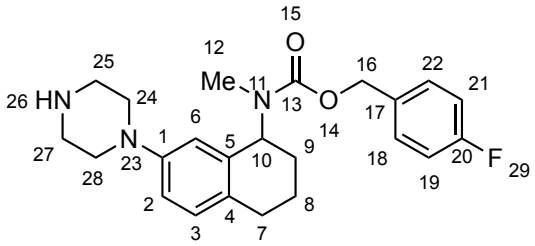

NMR Assignments (**2.111**). ^{1}H NMR (499 MHz, $CDCl_3$) rotamers δ 7.43 – 7.31 (comp, 2 H, 13, 15), 7.12 – 6.95 (comp, 3 H, 3, 16, 18), 6.79 – 6.73 (m, 1 H, 2), 6.64 – 6.53 (m, 1 H, 6), 5.50 – 5.26 (m, 1 H, 10), 5.26 – 5.06 (comp, 2 H, 19), 3.06 – 2.92 (comp, 7 H, 25, 26, 28, 29), 2.74 – 2.59 (comp, 5 H, 7, 12) 2.04 – 1.65 (comp, 5 H, 8, 9, 30). ^{13}C NMR (126 MHz, $CDCl_3$) rotamers δ 163.5 and 161.6 (14), 157.2 and 156.9 (21), 150.6 and 150.5 (1), 135.8 and 135.7 (5), 133.1, 133.0, 133.0, and 132.9 (17), 130.2 and 130.0 (3), 130.0, 129.9, 129.9, 129.9 (4, 13, 15), 129.7 (4), 115.8 (2), 115.5 and 115.4 (2, 16, 18), 114.7 and 114.3 (6), 66.5 and 66.5 (19), 55.7 and 55.5 (10), 50.9 and 50.8 (26, 28), 46.2 and 46.2 (25, 29), 30.4 and 29.8 (12), 28.8 and 28.7 (7), 28.2 and 27.7 (9), 22.3 and 22.1 (8).

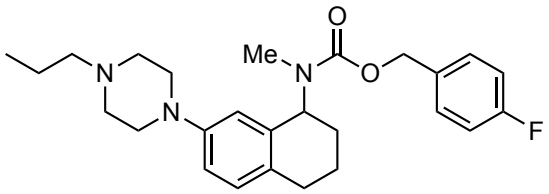

4-Fluorobenzyl methyl(7-(4-propylpiperazin-1-yl)-1,2,3,4-tetrahydronaphthalen-1-yl)carbamate (**2.112**) (DRM-1-54). Prepared from **2.111** (20 mg, 0.051 mmol) and propionaldehyde according to representative procedure E. The crude residue was purified via flash chromatography (SiO_2) eluting with hexanes/EtOAc/Et_3N (74:25:1) to afford 18 mg (81%) of **2.112** as a colorless oil. ^{1}H NMR (600 MHz, $CDCl_3$) rotamers δ 7.40 (dd, J = 8.5, 5.6 Hz, 1H), 7.33 (dd, J = 8.4, 5.5 Hz, 1H), 7.09 – 6.96 (comp, 3H), 6.80 – 6.74 (m, 1H), 6.61 – 6.55 (m, 1H), 5.48 – 5.27

(m, 1H), 5.26 – 5.07 (comp, 2H), 3.13 – 3.02 (comp, 4H), 2.74 – 2.60 (comp, 5H), 2.59 – 2.54 (comp, 4H), 2.39 – 2.33 (comp, 2H), 2.06 – 1.91 (comp, 2H), 1.83 – 1.67 (comp, 2H), 1.60 – 1.51 (comp, 2H), 0.93 (t, J = 7.4 Hz, 3H). ^{13}C NMR (151 MHz, $CDCl_3$) rotamers δ 163.4, 161.8, 157.2, 156.9, 150.2, 150.1, 135.9, 135.7, 133.1, 133.1, 133.0, 133.0, 130.2, 130.1, 130.0, 130.0, 130.0, 129.9, 129.9, 129.7, 115.8, 115.6, 115.5, 115.4, 114.7, 114.2, 66.5, 66.5, 60.8, 60.8, 55.8, 55.5, 53.4, 53.3, 49.7, 49.6, 30.4, 29.8, 28.8, 28.7, 28.2, 27.8, 22.4, 22.2, 20.2, 12.1. HRMS (ESI) *m/z* calcd for $C_{26}H_{34}FN_3O_2$ $(M+H)^+$, 440.2708; found 440.2723.

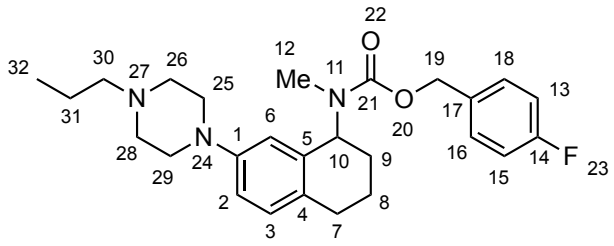

NMR Assignments (**2.112**). ^{1}H NMR (600 MHz, $CDCl_3$) rotamers δ 7.40 (dd, J = 8.5, 5.6 Hz, 1H), 7.33 (dd, J = 8.4, 5.5 Hz, 1H, 13, 15), 7.09 – 6.96 (comp, 3H, 3, 16, 18), 6.80 – 6.74 (m, 1H, 2), 6.61 – 6.55 (m, 1H, 6), 5.48 – 5.27 (m, 1H, 10), 5.26 – 5.07 (comp, 2H, 19), 3.13 – 3.02 (comp, 4H, 26, 28), 2.74 – 2.60 (comp, 5H, 7, 12), 2.59 – 2.54 (comp, 4H, 25, 29), 2.39 – 2.33 (comp, 2H, 30'), 2.06 – 1.91 (comp, 2H, 8", 9"), 1.83 – 1.67 (comp, 2H, 8', 9'), 1.60 – 1.51 (comp, 2H, 31"), 0.93 (t, J = 7.4 Hz, 3H, 32). ^{13}C NMR (151 MHz, $CDCl_3$) rotamers δ 163.4, 161.8, 157.2, and 156.9 (21), 150.2 and 150.1 (1), 135.9 and 135.7 (5), 133.1, 133.1, 133.0, and 133.0 (17), 130.2 and 130.1 (3), 130.0, 130.0, 130.0, and 129.9 (13, 15), 129.9 and 129.7 (4), 115.8, 115.6, 115.5, and 115.4 (16, 18), 114.7 and 114.2 (6), 66.5 and 66.5 (19), 60.8 and 60.8 (30), 55.8 and 55.5 (10), 53.4

and 53.3 (25, 29), 49.7 and 49.6 (26, 28), 30.4 and 29.8 (12), 28.8 and 28.7 (7), 28.2 and 27.8 (9), 22.4 and 22.2 (8), 20.2 (31), 12.1.

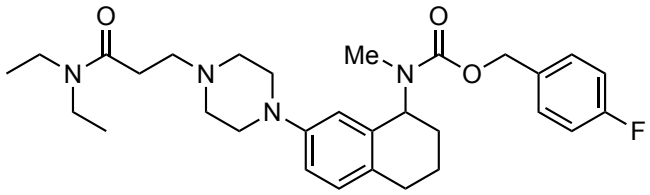

4-Fluorobenzyl (7-(4-(3-(diethylamino)-3-oxopropyl)piperazin-1-yl)-1,2,3,4-tetrahydronaphthalen-1-yl)(methyl)carbamate (**2.114**) (DRM-1-53). Prepared from **2.111** (17 mg, 0.051 mmol) and 3-bromo-N,N-diethylpropanamide, according to representative procedure G.[315] The crude residue was purified via flash chromatography (SiO_2) eluting with hexanes/EtOAc/Et_3N (74:25:1) affording 21 mg (94%) of **2.114** as a colorless oil. ^{1}H NMR (600 MHz,$CDCl_3$) rotamers δ 7.40 (dd, *J* = 8.5, 5.5 Hz, 1H), 7.33 (dd, *J* = 8.5, 5.5 Hz, 1H), 7.10 – 6.96 (comp, 3H), 6.79 – 6.73 (m, 1H), 6.59 – 6.52 (m, 1H), 5.47 – 5.26 (m, 1H), 5.26 – 5.06 (comp, 2H), 3.38 (q, *J* = 7.1 Hz, 2H), 3.33 (q, *J* = 7.0 Hz, 2H), 3.10 – 3.00 (comp, 4H), 2.83 – 2.77 (comp, 2H), 2.74 – 2.59 (comp, 9H), 2.58 – 2.53 (comp, 2H), 2.04 – 1.90 (comp, 2H), 1.82 – 1.66 (comp, 2H), 1.19 (td, *J* = 7.2, 1.9 Hz, 3H), 1.12 (t, *J* = 7.1 Hz, 3H). ^{13}C NMR (151 MHz, $CDCl_3$) rotamers δ 170.8, 163.4, 161.8, 157.2, 156.9, 150.0, 150.0, 135.9, 135.7, 133.1, 133.1, 133.0, 133.0, 130.3, 130.1, 130.1, 130.0, 130.0, 130.0, 129.9, 129.8, 115.8, 115.6, 115.5, 115.4, 114.6, 114.2, 66.5, 66.5, 55.8, 55.5, 54.5, 54.5, 53.4, 53.4, 49.7, 49.5, 42.1, 42.1, 40.3, 31.0, 30.9, 30.4, 29.8, 28.8, 28.7, 28.2, 27.7, 22.4, 22.2, 14.5, 13. HRMS (ESI) *m/z* calcd for $C_{30}H_{41}FN_4O_3$ $(M+H)^+$, 525.3235; found 525.3253.

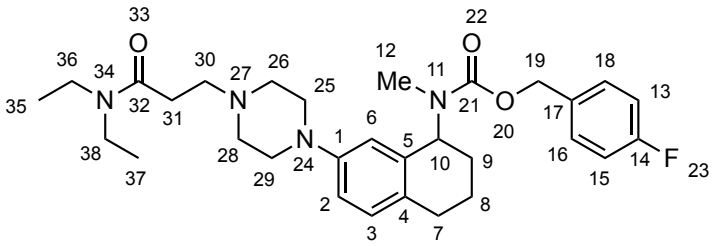

NMR Assignments (**2.114**). ^{1}H NMR (600 MHz, $CDCl_3$) rotamers δ 7.40 (dd, *J* = 8.5, 5.5 Hz, 1H), 7.33 (dd, *J* = 8.5, 5.5 Hz, 1H, 13, 15), 7.10 – 6.96 (comp, 3H, 3, 16, 18), 6.79 – 6.73 (m, 1H, 2), 6.59 – 6.52 (m, 1H, 6), 5.47 – 5.26 (m, 1H, 10), 5.26 – 5.06 (comp, 2H, 19), 3.38 (q, *J* = 7.1 Hz, 2H, 36), 3.33 (q, *J* = 7.0 Hz, 2H, 38), 3.10 – 3.00 (comp, 4H, 26, 28), 2.83 – 2.77 (comp, 2H, 31), 2.74 – 2.59 (comp, 9H, 7, 12, 25, 29), 2.58 – 2.53 (comp, 2H, 30), 2.04 – 1.90 (comp, 2H, 8', 9'), 1.82 – 1.66 (comp, 2H, 8'', 9''), 1.19 (td, *J* = 7.2, 1.9 Hz, 3H, 35, 37), 1.12 (t, *J* = 7.1 Hz, 3H). ^{13}C NMR (151 MHz, $CDCl_3$) rotamers δ 170.8 (32), 163.4 and 161.8 (14), 157.2 and 156.9 (21), 150.0 and 150.0 (1), 135.9 and 135.7 (5), 133.1, 133.1, 133.0, and 133.0 (17), 130.3 and 130.1 (3), 130.1, 130.0, 130.0, and 130.0 (13, 15), 129.9 and 129.8 (4), 115.8, 115.6, 115.5, and 115.4 (16, 18), 114.6, 114.2, 66.5, and 66.5 (19), 55.8 and 55.5 (10), 54.5 and 54.5 (31), 53.4 and 53.4 (25, 29), 49.7 and 49.5 (26, 28), 42.1, 42.1, and 40.3 (36, 38), 31.0 and 30.9 (30), 30.4 and 29.8 (12), 28.8 and 28.7 (7), 28.2 and 27.7 (9), 22.4 and 22.2 (8), 14.5 and 13.2 (35, 37).

Representative Procedure K: Coupling the amine with a cinnamic acid derivative.

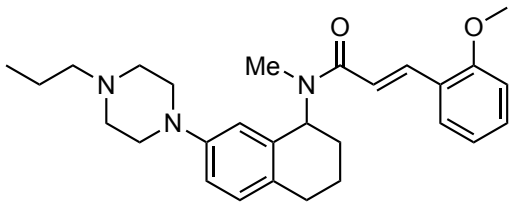

(*E*)-3-(2-Methoxyphenyl)-*N*-methyl-*N*-(7-(4-propylpiperazin-1-yl)-1,2,3,4-tetrahydronaphthalen-1-yl)acrylamide (**2.116**) (DRM-1-64). A solution of **2.87** (64 mg, 0.22 mmol), 2-methoxycinnamic acid (69 mg, 0.39 mmol), EDCI·HCl (74 mg, 0.39 mmol), and *i*-Pr_2Net (130 mg, 18 μL, 1.0 mmol) in THF (2.6 mL) was stirred for 17 h at room temperature. The reaction was diluted with 1 N NaOH (15 mL) and extracted with Et_2O (2 x 15 mL), whereupon the combined organic extracts were extracted with 1 N HCl (3 x 15 mL). The combined acidic aqueous extracts were made basic with 6 N NaOH and extracted with CH_2Cl_2 (3 x 20 mL). The combined organic extracts were dried (Na_2SO_4) and concentrated under reduced pressure. The crude residue was purified via flash chromatography (SiO_2) eluting with hexanes/EtOAc/Et_3N (54:45:1) affording 66 mg (70%) of **2.116** as a colorless oil**.** ^{1}H NMR (400 MHz,$CDCl_3$) rotamers δ 8.04 (dd, *J* = 17.8, 15.5 Hz, 1H), 7.57 – 7.44 (m, 1H), 7.36 – 7.27 (m, 1H), 7.12 – 6.87 (comp, 4H), 6.79 (td, *J* = 8.5, 2.6 Hz, 1H), 6.68 (dd, *J* = 20.4, 2.6 Hz, 1H), 6.11 – 5.17 (m, 1H), 3.94 – 3.83 (comp, 3H), 3.22 – 3.05 (comp, 4H), 2.89 – 2.64 (comp, 5H), 2.63 – 2.52 (comp, 4H), 2.41 – 2.31 (comp, 2H), 2.13 – 1.69 (comp, 4H), 1.54 (h, *J* = 7.3 Hz, 2H), 0.91 (td, *J* = 7.4, 2.1 Hz, 3H). ^{13}C NMR (126 MHz, $CDCl_3$) rotamers δ 168.6, 167.9, 158.4, 158.2, 150.3, 150.1, 138.6, 138.1, 136.0, 135.7, 130.8, 130.7, 130.5, 130.2, 129.9, 129.5, 129.3, 128.9, 124.6, 124.6, 120.8, 120.7, 118.9, 118.9, 115.6, 115.5, 115.0, 114.2, 111.3, 111.2, 60.8, 57.7, 55.6, 53.4, 53.3, 53.3, 49.7, 49.5, 31.4, 29.2, 29.0, 28.7, 27.6, 22.5, 22.2, 20.1, 12.1. HRMS (ESI) *m/z* calcd for $C_{28}H_{37}N_3O_2$ $(M+H)^+$, 448.2959; found 448.2958.

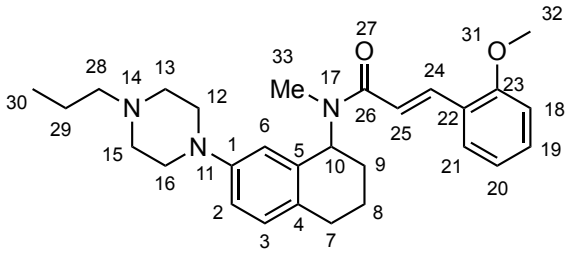

NMR Assignments (**2.116**). ^{1}H NMR (400 MHz, $CDCl_3$) rotamers δ 8.04 (dd, *J* = 17.8, 15.5 Hz, 1H, 24), 7.57 – 7.44 (m, 1H, 19), 7.36 – 7.27 (m, 1H, 21), 7.12 – 6.87 (comp, 4H, 3, 18, 20, 25), 6.79 (td, *J* = 8.5, 2.6 Hz, 1H, 2), 6.68 (dd, *J* = 20.4, 2.6 Hz, 1H, 6), 6.11 – 5.17 (m, 1H, 10), 3.94 – 3.83 (comp, 3H, 32), 3.22 – 3.05 (comp, 4H, 12, 16), 2.89 – 2.64 (comp, 5H, 7, 33), 2.63 – 2.52 (comp, 4H, 13, 15), 2.41 – 2.31 (comp, 2H, 28), 2.13 – 1.69 (comp, 4H, 8, 9), 1.54 (h, *J* = 7.3 Hz, 2H, 29), 0.91 (td, *J* = 7.4, 2.1 Hz, 3H, 30). ^{13}C NMR (126 MHz, $CDCl_3$) rotamers δ 168.6 and 167.9 (26), 158.4 and 158.2 (23), 150.3 and 150.1 (1), 138.6 and 138.1 (24), 136.0 and 135.7 (5), 130.8 and 130.7 (21), 130.5 (4), 130.2 and 129.9 (3), 129.5 (4), 129.3 and 128.9 (19), 124.6 and 124.6 (22), 120.8 and 120.7 (20), 118.9 and 118.9 (25), 115.6 and 115.5 (2), 115.0 and 114.2 (6), 111.3 and 111.2 (18), 60.8 (28), 57.7 (10), 55.6 (32), 53.4 (10), 53.3 and 53.3 (13, 15), 49.7 and 49.5 (12, 16), 31.4 (33), 29.2 and 29.0 (7), 28.7 and 27.6 (9), 22.5 and 22.2 (8), 20.1 (29), 12.1 (30).

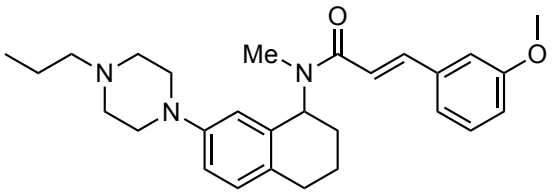

(*E*)-3-(3-Methoxyphenyl)-*N*-methyl-*N*-(7-(4-propylpiperazin-1-yl)-1,2,3,4-tetrahydronaphthalen-1-yl)acrylamide (**2.117**) (DRM-1-63). Prepared from **2.87** (64 mg, 0.22 mmol) and 3-methoxycinnamic acid according to representative procedure K. The crude residue was purified via flash chromatography (SiO_2) eluting with hexanes/EtOAc/Et_3N (54:45:1) to afford 65 mg (94%) of **2.117** as a colorless oil. ^{1}H NMR (500 MHz, $CDCl_3$) δ 7.73 – 7.60 (m, 1H), 7.26 – 7.16 (m, 1H), 7.12 – 6.78 (comp, 5H), 6.76 – 6.68 (m, 1H), 6.62 – 6.53 (m, 1H), 5.98 – 5.09 (m, 1H), 3.79 – 3.70 (comp,

3H), 3.13 – 3.01 (comp, 4H), 2.80 – 2.60 (comp, 5H), 2.58 – 2.50 (comp, 4H), 2.33 – 2.26 (comp, 2H), 2.03 – 1.58 (comp, 4H), 1.53 – 1.43 (comp, 2H), 0.84 (t, J = 7.3 Hz, 3H). ^{13}C NMR (126 MHz, $CDCl_3$) δ 167.7, 167.1, 159.9, 159.8, 150.1, 149.9, 142.9, 142.6, 136.8, 136.8, 135.7, 135.4, 130.5, 130.2, 129.9, 129.9, 129.8, 129.5, 120.5, 120.4, 118.1, 115.6, 115.6, 115.2, 115.2, 114.8, 114.0, 113.2, 113.0, 60.6, 60.6, 57.7, 55.4, 53.4, 53.1, 49.4, 49.3, 31.4, 29.1, 28.8, 28.5, 27.4, 22.4, 22.1, 19.9, 19.8, 12.0. HRMS (ESI) *m/z* calcd for $C_{28}H_{37}N_3O_2$ $(M+H)^+$, 448.2959; found 448.2960.

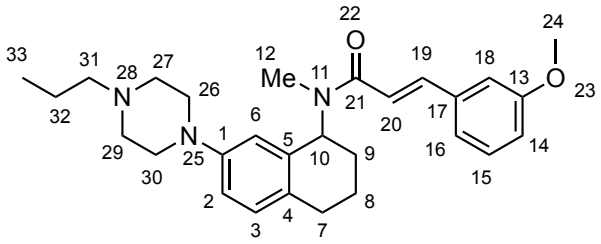

NMR Assignments (**2.117**). ^{1}H NMR (500 MHz, $CDCl_3$) rotamers δ 7.73 – 7.60 (m, 1H, 19), 7.26 – 7.16 (m, 1H, 15), 7.12 – 6.78 (comp, 5H, 3, 14, 16, 18, 20), 6.76 – 6.68 (m, 1H, 2), 6.62 – 6.53 (m, 1H, 6), 5.98 – 5.09 (m, 1H, 10), 3.79 – 3.70 (comp, 3H, 24), 3.13 – 3.01 (comp, 4H, 27, 29), 2.80 – 2.60 (comp, 5H, 7, 12), 2.58 – 2.50 (comp, 4H, 26, 30), 2.33 – 2.26 (comp, 2H, 31), 2.03 – 1.58 (comp, 4H, 8, 9), 1.53 – 1.43 (comp, 2H, 32), 0.84 (t, J = 7.3 Hz, 3H, 33). ^{13}C NMR (126 MHz, $CDCl_3$) δ 167.7 and 167.1 (21), 159.9 and 159.8 (13), 150.1 and 149.9 (1), 142.9 and 142.6 (19), 136.8 and 136.8 (17), 135.7 and 135.4 (5), 130.5 and 130.2 (3), 129.9 and 129.9 (15), 129.8 and 129.5 (4), 120.5 and 120.4 (16), 118.1 (20), 115.6 and 115.6 (14), 115.2 and 115.2 (2), 114.8 and 114.0 (6), 113.2 and 113.0 (18), 60.6 and 60.6 (31), 57.7 (10), 55.4 (24), 53.4 (10), 53.1 (26, 30), 49.4 and 49.3 (27, 29), 31.4 (12), 29.1 and 28.8 (7), 28.5 and 27.4 (9), 22.4 and 22.1 (8), 19.9 and 19.8 (32), 12.0 (33).

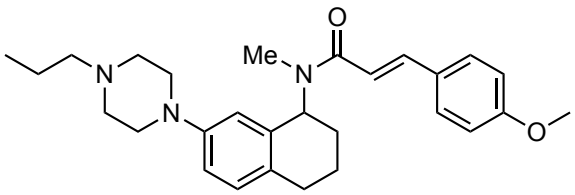

(*E*)-3-(4-methoxyphenyl)-*N*-methyl-*N*-(7-(4-propylpiperazin-1-yl)-1,2,3,4-tetrahydronaphthalen-1-yl)acrylamide (**2.118**) (DRM-1-55). Prepared from **2.87** (85 mg, 0.30 mmol) and 4-methoxycinnamic acid according to representative procedure K. The crude residue was purified via flash chromatography (SiO_2) eluting with hexanes/EtOAc/Et_3N (59:40:1) affording 91 mg (69%) of **2.118** as a colorless oil. ^1H NMR (400 MHz, $CDCl_3$) rotamers δ 7.74 (dd, *J* = 16.8, 15.3 Hz, 1H), 7.49 (dd, *J* = 27.6, 8.7 Hz, 2H), 7.03 (dd, *J* = 12.0, 8.4 Hz, 1H), 6.94 – 6.76 (comp, 4H), 6.66 (dd, *J* = 19.6, 2.3 Hz, 1H), 6.06 – 5.18 (m, 1H), 3.88 – 3.79 (comp, 3H), 3.18 – 3.03 (comp, 4H), 2.86 – 2.68 (comp, 5H), 2.62 – 2.52 (comp, 4H), 2.38 – 2.29 (comp, 2H), 2.11 – 1.69 (comp, 4H), 1.59 – 1.47 (comp, 2H), 0.91 (td, *J* = 7.4, 1.9 Hz, 3H). ^{13}C NMR (126 MHz, $CDCl_3$) δ 168.2, 167.6, 161.0, 160.9, 150.3, 150.2, 142.8, 142.5, 135.9, 135.7, 130.4, 130.2, 129.9, 129.6, 129.5, 128.3, 128.3, 115.6, 115.5, 115.5, 115.4, 114.9, 114.4, 114.3, 114.1, 60.8, 57.7, 55.5, 53.4, 53.3, 53.3, 49.7, 49.5, 31.5, 29.2, 29.0, 28.7, 27.6, 22.6, 22.2, 20.1, 12.1. HRMS (ESI) *m/z* calcd for $C_{28}H_{37}N_3O_2$ $(M+H)^+$, 448.2959; found 448.2960.

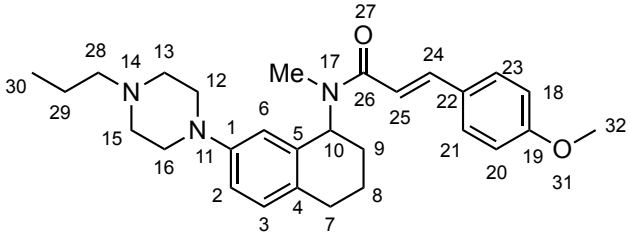

NMR Assignments (**2.118**). ^1H NMR (400 MHz, $CDCl_3$) rotamers δ 7.74 (dd, *J* = 16.8, 15.3 Hz, 1H, 24), 7.49 (dd, *J* = 27.6, 8.7 Hz, 2H, 21, 23), 7.03 (dd, *J* = 12.0, 8.4 Hz, 1H, 3), 6.94 – 6.76 (comp, 4H, 2, 18, 20, 25), 6.66 (dd, *J* = 19.6, 2.3 Hz, 1H, 6), 6.06 –

5.18 (m, 1H, 10), 3.88 – 3.79 (comp, 3H, 32), 3.18 – 3.03 (comp, 4H, 12, 16), 2.86 – 2.68 (comp, 5H, 7, 33), 2.62 – 2.52 (comp, 4H, 13, 15), 2.38 – 2.29 (comp, 2H, 28), 2.11 – 1.69 (comp, 4H, 8, 9), 1.59 – 1.47 (comp, 2H, 29), 0.91 (td, J = 7.4, 1.9 Hz, 3H, 30). ^{13}C NMR (126 MHz, $CDCl_3$) rotamers δ 168.2 and 167.6 (26), 161.0 and 160.9 (19), 150.3 and 150.2 (1), 142.8 and 142.5 (24), 135.9 and 135.7 (5), 130.4 (4), 130.2 and 129.9 (3), 129.6 and 129.5 (21, 23), 128.3 and 128.3 (22), 115.6 and 115.5 (2), 115.5 and 115.4 (25), 114.9 (6), 114.4 and 114.3 (18, 20), 114.1 (6), 60.8 (28), 57.7 (10), 55.5 (32), 53.4 (10), 53.3 and 53.3 (13, 15), 49.7 and 49.5 (12, 16), 31.5 (33), 29.2 and 29.0 (7), 28.7 and 27.6 (9), 22.6 and 22.2 (8), 20.1 (29), 12.1 (30).

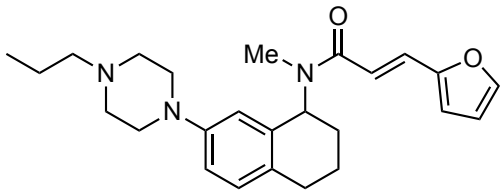

(*E*)-3-(Furan-2-yl)-*N*-methyl-*N*-(7-(4-propylpiperazin-1-yl)-1,2,3,4-tetrahydronaphthalen-1-yl)acrylamide (**2.120**) (DRM-1-72). Prepared from **2.87** (81 mg, 0.28 mmol) and furan-2-acrylic acid according to representative procedure K. The crude residue was purified via flash chromatography (SiO_2) eluting with hexanes/EtOAc/Et_3N (59:40:1) affording 87 mg (76%) of **2.120** as a pale yellow oil. ^{1}H NMR (500 MHz, $CDCl_3$) rotamers δ 7.54 (app dd, J = 15.1, 7.5 Hz, 1H), 7.46 – 7.38 (m, 1H), 7.00 (app dd, J = 13.1, 8.4 Hz, 1H), 6.87 (app dd, J = 28.6, 15.1 Hz, 1H), 6.81 – 6.74 (m, 1H), 6.61 (app dd, J = 20.6, 2.5 Hz, 1H), 6.55 (app dd, J = 17.6, 3.4 Hz, 1H), 6.47 – 6.40 (m, 1H), 6.03 – 5.19 (m, 1H), 3.19 – 3.06 (comp, 4H), 2.86 – 2.66 (comp, 5H), 2.63 – 2.54 (comp, 4H), 2.39 – 2.31 (comp, 2H), 2.10 – 1.63 (comp, 4H), 1.58 – 1.49 (comp, 2H), 0.89 (app td, J = 7.4, 1.2 Hz, 3H). ^{13}C NMR (126 MHz, $CDCl_3$) rotamers δ 167.5, 167.1, 151.8, 151.7, 150.1, 149.9, 144.0, 143.9, 135.7, 135.4, 130.4,

130.1, 129.9, 129.7, 129.7, 129.5, 115.6, 115.5, 115.4, 115.1, 114.7, 114.1, 114.0, 113.7, 112.3, 112.2, 60.6, 57.5, 53.4, 53.1, 49.4, 49.3, 31.3, 29.9, 29.1, 28.8, 28.5, 27.4, 22.4, 22.1, 19.9, 19.9, 12.0. HRMS (ESI) *m/z* calcd for $C_{25}H_{33}N_3O_2$ $(M+H)^+$, 408.2646; found 408.2649.

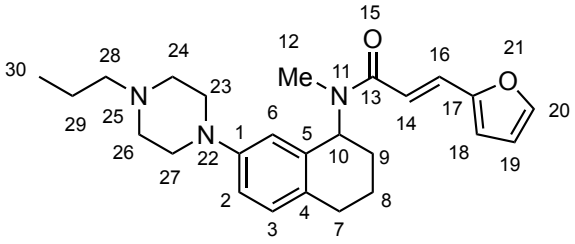

NMR Assignments (**2.87**). ^{1}H NMR (500 MHz, $CDCl_3$) rotamers δ 7.54 (app dd, *J* = 15.1, 7.5 Hz, 1H, 16), 7.46 – 7.38 (m, 1H, 20), 7.00 (app dd, *J* = 13.1, 8.4 Hz, 1H, 3), 6.87 (app dd, *J* = 28.6, 15.1 Hz, 1H, 14), 6.81 – 6.74 (m, 1H, 2), 6.61 (app dd, *J* = 20.6, 2.5 Hz, 1H, 6), 6.55 (app dd, *J* = 17.6, 3.4 Hz, 1H, 18), 6.47 – 6.40 (m, 1H, 19), 6.03 – 5.19 (m, 1H, 10), 3.19 – 3.06 (comp, 4H, 23, 27), 2.86 – 2.66 (comp, 5H, 7, 12), 2.63 – 2.54 (comp, 4H, 24, 26), 2.39 – 2.31 (comp, 2H, 28), 2.10 – 1.63 (comp, 4H, 8, 9), 1.58 – 1.49 (comp, 2H, 29), 0.89 (app td, *J* = 7.4, 1.2 Hz, 3H, 30). ^{13}C NMR (126 MHz, $CDCl_3$) rotamers δ 167.5 and 167.1 (13), 151.8 and 151.7 (17), 150.1 and 149.9 (1), 144.0 and 143.9 (20), 135.7 and 135.4 (5), 130.4 and 130.1 (3), 129.9 and 129.7 (16), 129.7 and 129.5 (4), 115.6 and 115.5 (2), 115.4 and 115.1 (14), 114.7 and 114.1 (6), 114.0 and 113.7 (18), 112.3 and 112.2 (19), 60.6 (28), 57.5 and 53.4 (10), 53.1 (23, 27), 49.4 and 49.3 (24, 26), 31.3 and 29.9 (12), 29.1 and 28.8 (7), 28.5 and 27.4 (9), 22.4 and 22.1 (8), 19.9 and 19.9 (29), 12.0 (30).

(R/*S*)-7-bromo-*N*-methyl-1,2,3,4-tetrahydronaphthalen-1-amine (**(S)-2.121/(R)-2.122**) (MDW-2-105 and 2-106). According to a slightly modified protocol, a solution of (±)-**2.28** (1.276 g, 5.312 mmol) and *N*-acetyl-*L*-phenylalanine (1.101 g, 5.312 mmol) in EtOH (25 mL) was heated to a boil. Additional EtOH was added to the boiling solution until the solids were completely dissolved, whereupon the solution was allowed to slowly cool to room temperature. The crystalline solid that formed was isolated by filtration and washed sequentially with cold EtOH (20 mL) and Et_2O (20 mL), and the *R*–enriched filtrate was reserved. The collected solids (1.041 g) were dissolved in EtOH (20 mL) and subjected to the same recrystallization protocol, and the *R*–enriched filtrate was reserved. The isolated white crystalline solid, $[a]_D^{33}$ = +71.00 (c = 1, MeOH), was partitioned between CH_2Cl_2 (30 mL) and 15% NaOH (20 mL). The organic layer was separated and the aqueous layer was extracted with CH_2Cl_2 (3 x 30 mL). The combined organic extracts were dried (Na_2SO_4) and concentrated under reduced pressure to afford a 0.411 g (32%) of (***S***)–2.121 as a colorless oil. The ^{1}H NMR spectrum was consistent with (±)-**2.28** A portion was converted to the HCl salt for analysis, $[a]_D^{28}$ = + 63.00 (c = 1, MeOH).

The combined *R*–enriched filtrates were concentrated under reduced pressure and the crude residue was partitioned between CH_2Cl_2 (30 mL) and 15% NaOH (20 mL). The organic layer was separated and the aqueous layer was extracted with extracted with CH_2Cl_2 (3 x 30 mL). The combined organic extracts were dried (Na_2SO_4) and concentrated under reduced pressure to afford the *R*–enriched residue (0.693 g, 2.89 mmol) as a red oil. A solution of the *R*–enriched residue and *N*-acetyl-*D*-phenylalanine

(0.598 g, 2.89 mmol) in EtOH (14 mL) was heated to a boil. Additional EtOH was added to the boiling solution until the solids were completely dissolved, whereupon the solution was allowed to slowly cool to room temperature. The crystalline solid that formed was isolated by filtration and washed sequentially with cold EtOH (20 mL) and Et_2O (20 mL). The collected solids (0.879 g) were dissolved in EtOH (10 mL) and subjected to the same recrystallization protocol. The isolated white crystalline solid, $[a]_D^{33} = -61.00$ (c = 1, MeOH), was partitioned between CH_2Cl_2 (30 mL) and 15% NaOH (20 mL). The organic layer was separated and the aqueous layer was extracted with CH_2Cl_2 (3 x 30 mL). The combined organic extracts were dried (Na_2SO_4) and concentrated under reduced pressure to afford a 0.317 g (25%) of (***R***)–2.122 as a colorless oil. The ^{1}H NMR spectrum was consistent with (±)-**2.28** A portion was converted to the HCl salt for analysis, $[a]_D^{24} = -63.00$ (c = 1, MeOH). Lit (***R***)-**2.122** $[a]_D^{22} = -55.2$ (c = 1, MeOH).

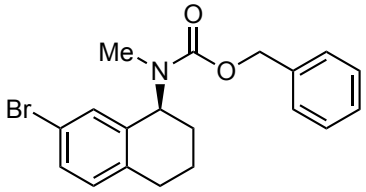

Benzyl (*S*)-(7-bromo-1,2,3,4-tetrahydronaphthalen-1-yl)(methyl)carbamate ((***S***)–**2.123**) (MDW-2-107). Prepared from (***S***)**–2.121** (0.69 g, 1.54 mmol) and CbzCl according to representative procedure A. The crude residue was purified via flash chromatography (SiO_2) eluting with hexanes/EtOAc (10:1) to afford 0.571 g (98%) of (***S***)**–2.123** as a colorless oil ($[a]_D^{24} = -31.00$ (c = 1, MeOH). ^{1}H NMR (400 MHz, $CDCl_3$) (rotamers) δ 7.50 – 7.19 (comp, 7 H), 6.97 – 6.90 (m, 1 H), 5.55 – 5.16 (comp, 3 H), 2.77 – 2.61 (comp, 5 H), 2.09 – 1.92 (comp, 2 H), 1.85 – 1.67 (comp, 2 H). ^{13}C NMR (101 MHz, $CCCl_3$) (rotamers) δ 156.8, 156.3, 137.6, 137.5, 137.2, 136.9, 136.6, 136.6, 130.7, 129.8, 129.7, 129.5, 129.5, 128.3, 128.3, 127.8, 127.7, 127.6, 127.5, 127.5, 119.7, 119.7,

67.1, 55.0, 54.7, 30.1, 29.4, 28.8, 28.7, 27.4, 26.9, 21.6, 21.6. HRMS (ESI) *m/z* calcd for $C_{19}H_{20}BrNO_2$ $(M+Na)^+$, 396.0570; found 396.0574.

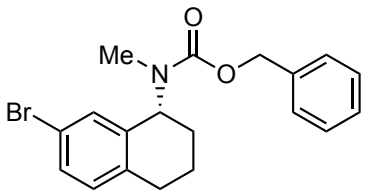

Benzyl (*R*)-(7-bromo-1,2,3,4-tetrahydronaphthalen-1-yl)(methyl)carbamate ((***R***)–**2.124**) (MDW-2-108). Prepared from (***R***)–**2.122** (0.269 g, 1.12 mmol) and CbzCl according to representative procedure A. The crude residue was purified via flash chromatography (SiO_2) eluting with hexanes/EtOAc (10:1) to afford 0.413 g (98%) of (***R***)–**2.124** as a colorless oil ($[a]_D^{24}$ = + 26.33 (c = 1, MeOH). ^{1}H NMR (400 MHz, $CDCl_3$) rotamers δ 7.45 – 7.21 (comp, 7 H), 6.98 – 6.91 (m, 1 H), 5.55 – 5.17 (comp, 3 H), 2.75 – 2.62 (comp, 5 H), 2.10 – 1.92 (comp, 2 H), 1.86 – 1.64 (comp, 2 H). ^{13}C NMR (101 MHz, $CDCl_3$) rotamers δ 156.9, 156.5, 137.7, 137.6, 137.2, 137.0, 136.7, 136.6, 130.8, 129.9, 129.8, 129.6, 129.5, 128.4, 127.9, 127.6, 119.8, 119.8, 67.2, 55.1, 54.8, 30.2, 29.5, 28.9, 28.8, 27.5, 26.9, 21.7, 21.6. HRMS (ESI) *m/z* calcd for $C_{19}H_{20}BrNO_2$ $(M+Na)^+$, 396.0570; found 396.0577.

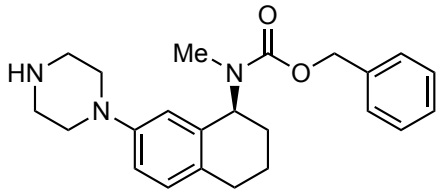

Benzyl (*S*)-methyl(7-(piperazin-1-yl)-1,2,3,4-tetrahydronaphthalen-1-yl)carbamate ((***S***)–**2.125**) (MDW-2-112). Prepared from (***S***)–**2.123** (0.529 g, 1.40 mmol) and piperazine according to representative procedure C. The crude residue was purified

via flash chromatography (SiO_2) eluting with CH_2Cl_2/MeOH/Et_3N (99:0:1 to 97:2:1) to afford 0.362 g (68%) of (***S***)–**2.125** as an orange oil. ^1H NMR (400 MHz, $CDCl_3$) rotamers δ 7.43 – 7.22 (comp, 5 H), 7.00 – 6.93 (m, 1 H), 6.77 – 6.71 (m, 1 H), 6.64 – 6.56 (m, 1 H), 5.49 – 5.08 (comp, 3 H), 3.05 – 2.87 (comp, 8 H), 2.72 – 2.59 (comp, 5 H), 2.06 – 1.87 (comp, 3 H), 1.82 – 1.63 (comp, 2 H). ^{13}C NMR (101 MHz, $CDCl_3$) rotamers δ 156.9, 156.6, 150.3, 150.2, 137.0, 136.8, 135.5, 135.4, 129.8, 129.6, 129.6, 129.4, 128.3, 127.7, 127.6, 127.5, 115.4, 115.2, 114.3, 114.0, 66.8, 66.8, 55.3, 55.1, 50.5, 50.4, 46.0, 45.9, 30.0, 29.4, 28.5, 28.4, 27.9, 27.4, 22.0, 21.9. HRMS (ESI) *m/z* calcd for $C_{23}H_{29}N_3O_2$ $(M+H)^+$, 380.2333; found 380.2341.

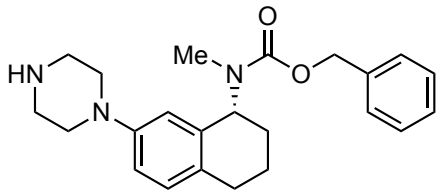

Benzyl (*R*)-methyl(7-(piperazin-1-yl)-1,2,3,4-tetrahydronaphthalen-1-yl)carbamate ((***R***)–**2.126**) (MDW-2-113). Prepared from (***R***)–**2.124** (0.394 g, 1.04 mmol) and piperazine according to representative procedure C. The crude residue was purified via flash chromatography (SiO_2) eluting with CH_2Cl_2/MeOH/Et_3N (99:0:1 to 97:2:1) to afford 0.235 g (60%) of (***R***)–**2.126** as an orange oil. ^1H NMR (500 MHz, $CDCl_3$) rotamers δ 7.45 – 7.25 (comp, 5H), 7.02 – 6.96 (m, 1H), 6.80 – 6.73 (m, 1H), 6.67 – 6.58 (m, 1H), 5.53 – 5.11 (comp, 3H), 3.10 – 2.95 (comp, 8H), 2.75 – 2.63 (comp, 5H), 2.09 – 1.91 (comp, 3H), 1.84 – 1.67 (comp, 2H). ^{13}C NMR (126 MHz, $CDCl_3$) rotamers δ 157.0, 156.7, 150.3, 150.3, 137.0, 136.9, 135.6, 135.5, 129.9, 129.7, 129.6, 129.5, 128.3, 127.7, 127.7, 127.6, 127.6, 115.5, 115.3, 114.4, 114.1, 66.9, 66.9, 55.4, 55.2, 50.6, 50.5, 46.0, 30.1, 29.5, 28.6, 28.5, 28.0, 27.5, 22.1, 22.0. HRMS (ESI) *m/z* calcd for $C_{23}H_{29}N_3O_2$ $(M+H)^+$, 380.2333; found 380.2338.

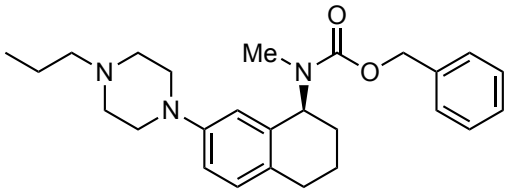

Benzyl (*S*)-methyl(7-(4-propylpiperazin-1-yl)-1,2,3,4-tetrahydronaphthalen-1-yl)carbamate ((***S***)–**2.127**) (MDW-2-118). Prepared from (***S***)–**2.125** (32 mg, 0.084 mmol) and propionaldehyde according to representative procedure E. The crude residue was purified via flash chromatography (SiO_2) eluting with hexanes/EtOAc/Et_3N (79:20:1) to afford 33 mg (91%) of (***S***)–**2.127** (>99% *ee* by analytical HPLC). as a colorless oil. ^1H NMR (500 MHz, $CDCl_3$) rotamers δ 7.44 – 7.26 (comp, 5H), 6.99 (d, *J* = 8.3 Hz, 1H), 6.81 – 6.73 (m, 1H), 6.62 (dd, *J* = 11.8, 2.6 Hz, 1H), 5.50 – 5.32 (m, 1H), 5.32 – 5.11 (comp, 2H), 3.16 – 3.03 (comp, 4H), 2.75 – 2.61 (comp, 5H), 2.61 – 2.53 (comp, 4H), 2.39 – 2.32 (comp, 2H), 2.07 – 1.91 (comp, 2H), 1.84 – 1.68 (comp, 2H), 1.61 – 1.51 (comp, 2H), 0.94 (t, *J* = 7.4 Hz, 3H). ^{13}C NMR (126 MHz, $CDCl_3$) δ 157.3, 157.1, 150.1, 150.1, 137.3, 137.2, 135.9, 135.8, 130.1, 130.0, 129.9, 129.7, 128.6, 128.0, 127.9, 127.9, 115.7, 115.4, 114.7, 114.3, 67.2, 67.2, 60.8, 55.7, 55.5, 53.4, 53.3, 49.7, 49.5, 30.3, 29.8, 29.8, 28.8, 28.8, 28.2, 27.8, 22.3, 22.2, 20.2, 12.1. HRMS (ESI) *m/z* calcd for $C_{26}H_{35}N_3O_2$ $(M+H)^+$, 422.2802; found 422.2819.

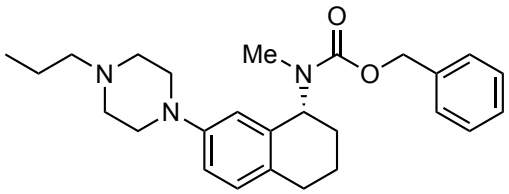

Benzyl (*R*)-methyl(7-(4-propylpiperazin-1-yl)-1,2,3,4-tetrahydronaphthalen-1-yl)carbamate ((***R***)–**2.128**) (MDW-2-119). Prepared from (***R***)–**2.126** (32 mg, 0.084

mmol) and propionaldehyde according to representative procedure E. The crude residue was purified via flash chromatography (SiO_2) eluting with hexanes/EtOAc/Et_3N (79:20:1) to afford 36 mg (100%) of (***R***)–**2.128** (>99% *ee* by analytical HPLC) as a colorless oil. ^1H and ^{13}C NMR are consistent with (±)–**2.31**. ^1H NMR (499 MHz, $CDCl_3$) δ 7.45 – 7.27 (comp, 5H), 6.99 (d, *J* = 8.3 Hz, 1H), 6.81 – 6.74 (m, 1H), 6.62 (dd, *J* = 11.9, 2.6 Hz, 1H), 5.51 – 5.32 (m, 1H), 5.32 – 5.10 (comp, 2H), 3.15 – 3.03 (comp, 4H), 2.75 – 2.62 (comp, 5H), 2.61 – 2.52 (comp, 4H), 2.06 – 1.92 (comp, 2H), 1.83 – 1.68 (comp, 2H), 1.56 (h, *J* = 7.4 Hz, 2H), 0.94 (t, *J* = 7.4 Hz, 3H). ^{13}C NMR (126 MHz, $CDCl_3$) δ 157.3, 157.1, 150.1, 150.1, 137.3, 137.1, 135.9, 135.8, 130.1, 130.0, 129.9, 129.7, 128.6, 128.0, 127.9, 127.9, 115.7, 115.4, 114.7, 114.3, 67.2, 67.2, 60.8, 55.7, 55.5, 53.3, 53.3, 49.7, 49.5, 32.1, 30.3, 29.8, 29.5, 28.8, 28.7, 28.2, 27.7, 22.8, 22.3, 22.2, 20.2, 14.3, 12.1. HRMS (ESI) *m/z* calcd for $C_{26}H_{35}N_3O_2$ $(M+H)^+$, 422.2802; found 422.2297.

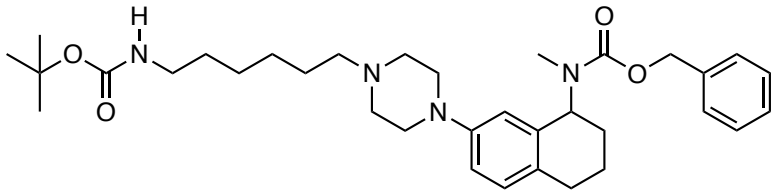

Benzyl (7-(4-(6-((*tert*-butoxycarbonyl)amino)hexyl)piperazin-1-yl)-1,2,3,4-tetrahydronaphthalen-1-yl)(methyl)carbamate (**2.138**) (MDW-1-276). Prepared from **2.16** (60 mg, 0.16 mmol) and the known aldehyde **2.132** according to representative procedure E.[335] The crude residue was purified via flash chromatography (SiO_2) eluting with hexanes/EtOAc/Et_3N (54:45:1) to afford 60 mg (65%) of **2.138** as a colorless oil. ^1H NMR (499 MHz, $CDCl_3$) rotamers δ 7.43 – 7.27 (comp, 5H), 6.98 (d, *J* = 8.4 Hz, 1H), 6.79 – 6.74 (m, 1H), 6.62 (dd, *J* = 12.4, 2.5 Hz, 1H), 5.50 – 5.31 (m, 1H), 5.30 – 5.10 (comp, 2H), 4.56 (brs, 1H), 3.15 – 3.03 (comp, 6H), 2.74 – 2.61 (comp, 5H), 2.60 – 2.52 (comp, 4H), 2.40 – 2.33 (comp, 2H), 2.05 – 1.91 (comp, 2H), 1.83 – 1.66 (comp, 2H),

1.58 – 1.29 (m, 17H). ^{13}C NMR (126 MHz, $CDCl_3$) rotamers δ 157.3, 157.0, 156.1, 150.1, 150.0, 137.2, 137.1, 135.8, 135.7, 130.1, 129.9, 129.9, 129.6, 128.6, 128.0, 127.8, 127.8, 115.7, 115.4, 114.6, 114.3, 79.1, 67.2, 67.1, 58.7, 55.7, 55.4, 53.3, 49.6, 49.5, 40.6, 30.3, 30.1, 29.8, 28.8, 28.7, 28.5, 28.2, 27.7, 27.3, 26.9, 26.8, 22.3, 22.1. HRMS (ESI) *m/z* calcd for $C_{34}H_{50}N_4O_4$ $(M+H)^+$, 579.3905; found 579.3911.

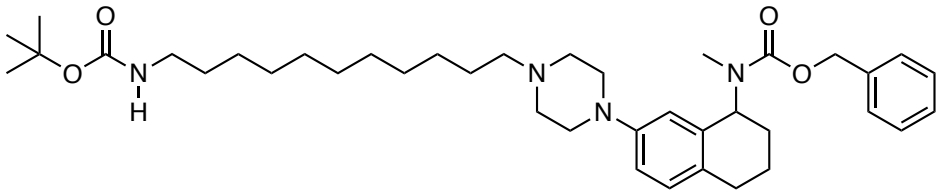

Benzyl (7-(4-(11-((*tert*-butoxycarbonyl)amino)undecyl)piperazin-1-yl)-1,2,3,4-tetrahydronaphthalen-1-yl)(methyl)carbamate (**2.139**) (MDW-1-278). Prepared from **2.16** (60 mg, 0.16 mmol) and the known aldehyde **2.137** according to representative procedure E.[338] The crude residue was purified via flash chromatography (SiO_2) eluting with hexanes/EtOAc/Et_3N (74:25:1) to afford 62 mg (60%) of **2.139** as a colorless oil. ^{1}H NMR (499 MHz, $CDCl_3$) rotamers δ 7.44 – 7.27 (comp, 5H), 6.98 (d, *J* = 8.8 Hz, 1H), 6.79 – 6.74 (m, 1H), 6.62 (dd, *J* = 12.0, 2.5 Hz, 1H), 5.50 – 5.31 (m, 1H), 5.31 – 5.11 (comp, 2H), 4.54 (brs, 1H), 3.16 – 3.01 (comp, 6H), 2.74 – 2.61 (comp, 5H), 2.60 – 2.52 (comp, 4H), 2.41 – 2.33 (comp, 2H), 2.06 – 1.91 (comp, 2H), 1.83 – 1.67 (comp, 2H), 1.57 – 1.40 (comp, 13H), 1.33 – 1.24 (comp, 14H). ^{13}C NMR (126 MHz, $CDCl_3$) rotamers δ 157.3, 157.0, 156.1, 150.1, 150.0, 137.2, 137.1, 135.9, 135.8, 130.1, 129.9, 129.9, 129.6, 128.6, 128.0, 127.9, 127.8, 115.7, 115.4, 114.6, 114.3, 79.1, 67.2, 67.1, 58.9, 55.7, 55.4, 53.4, 49.6, 49.5, 40.7, 30.3, 30.2, 29.8, 29.7, 29.7, 29.6, 29.6, 29.4, 28.8, 28.7, 28.5, 28.2, 27.7, 27.0, 26.9, 22.3, 22.1. HRMS (ESI) *m/z* calcd for $C_{39}H_{60}N_4O_4$ $(M+H)^+$, 649.4687; found 649.4691.

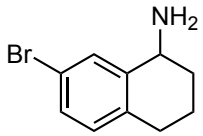

7-bromo-1,2,3,4-tetrahydronaphthalen-1-amine (**2.140**) (MDW-1-274). NH_4OAc (1.71 g, 22.2 mmol), and $NaBH_3CN$ (691 mg, 11.1 mmol) were added to a solution of 7-bromotetralone (0.500 g, 2.22 mmol), in MeOH (11 mL) and the reaction was heated at 60 °C for 24 h. The reaction was concentrated under reduced pressure, and the crude residue was dissolved in Et_2O (30 mL) and extracted with 1 N HCl (3 x 30 mL). The combined aqueous extracts were made basic with 6 N NaOH and extracted with CH_2Cl_2 (3 x 50 mL). The combined organic extracts were dried (Na_2SO_4) and concentrated under reduced pressure to afford 0.486 g (97%) of **2.140** as a colorless oil. ^{1}H NMR (400 MHz, $CDCl_3$) δ 7.56 (d, *J* = 2.3 Hz, 1H), 7.24 (app dd, *J* = 8.2, 2.1 Hz, 1H), 6.94 (d, *J* = 8.2 Hz, 1H), 3.93 (d, *J* = 5.9 Hz, 2H), 2.80 – 2.61 (comp, 2H), 2.06 – 1.97 (m, 1H), 1.97 – 1.86 (m, 1H), 1.81 – 1.70 (m, 1H), 1.69 – 1.60 (m, 1H), 1.53 (brs, 2H). ^{13}C NMR (126 MHz, $CDCl_3$) δ 143.6, 135.8, 131.0, 130.8, 129.7, 119.6, 49.5, 33.6, 29.2, 19.6. HRMS (ESI) *m/z* calcd for $C_{10}H_{12}BrN$ $(M+H)^+$, 226.0226; found 226..0222.

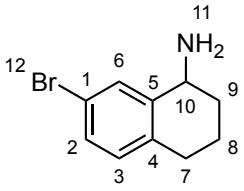

NMR Assignments (**2.140**). ^{1}H NMR (400 MHz, $CDCl_3$) δ 7.56 (d, *J* = 2.3 Hz, 1H, 6), 7.24 (app dd, *J* = 8.2, 2.1 Hz, 1H, 2), 6.94 (d, *J* = 8.2 Hz, 1H, 3), 3.93 (d, *J* = 5.9 Hz, 2H, 10), 2.80 – 2.61 (comp, 2H, 7), 2.06 – 1.97 (m, 1H, 9'), 1.97 – 1.86 (m, 1H, 8'), 1.81 – 1.70 (m, 1H, 8''), 1.69 – 1.60 (m, 1H, 9''), 1.53 (s, 2H, 11). ^{13}C NMR (126 MHz,

$CDCl_3$) δ 143.6 (5), 135.8 (4), 131.0 (6), 130.8 (3), 129.7 (2), 119.6 (1), 49.5 (10), 33.6 (9), 29.2 (7), 19.6 (8).

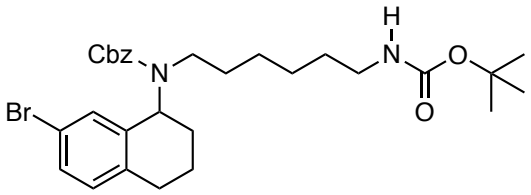

Benzyl (7-bromo-1,2,3,4-tetrahydronaphthalen-1-yl)(6-((*tert*-butoxycarbonyl)amino)hexyl)carbamate (**2.141**) (MDW-1-282). A solution of **2.140** (85 mg, 0.37 mmol) and **2.132** (90 mg, 0.45 mmol) in MeOH (1.9 mL) was stirred with 3 Å MS (200 mg) for 4 h at room temperature, whereupon $NaBH_4$ (14 mg, 3.7 mmol) was added to the solution and the reaction was stirred overnight. The reaction was concentrated under reduced pressure and the crude residue was partitioned between CH_2Cl_2 (10 mL) and saturated aqueous $NaHCO_3$ (10 mL). The organic layer was separated and the aqueous layer was extracted with CH_2Cl_2 (2 x 10 mL). The combined organic extracts were dried (Na_2SO_4) and concentrated under reduced pressure. The crude residue was filtered through a SiO_2 plug washing with hexanes/EtOAc/Et_3N (82:17:1) to afford 102 mg of an oil that was used directly. The crude residue was dissolved in CH_2Cl_2 (1 mL) and cooled to 0 °C. *i*-Pr_2Net (62 mg, 83 μL, 0.48 mmol) and CbzCl (49 mg, 41 μL, 0.29 mmol) were added sequentially to the cooled solution. The reaction was stirred for 20 min and the cooling bath was removed, and the solution was stirred for 3 h at room temperature. The reaction was diluted with CH_2Cl_2 (5 mL) and washed with 1 N HCl (2 x 5 mL), 1 N NaOH (1 x 5 mL), and saturated aqueous $NaHCO_3$ (1 x 10 mL). The organic layer was dried (Na_2SO_4) and concentrated under reduced pressure to afford 141 mg of **2.141** as a colorless oil. ^1H NMR (499 MHz, $CDCl_3$) rotamers δ 7.51 – 7.08 (comp, 7H), 6.98 – 6.88 (comp, 1H), 5.37 – 4.95 (comp, 3H), 4.63 – 4.42 (comp, 1H), 3.31 –

2.56 (comp, 6H), 2.09 – 1.07 (comp, 21H). ^{13}C NMR (126 MHz, $CDCl_3$) rotamers δ 157.0, 156.2, 156.0, 139.1, 138.6, 137.2, 136.9, 136.6, 130.9, 130.9, 129.9, 129.8, 129.7, 129.4, 128.8, 128.6, 128.6, 128.5, 128.4, 128.1, 127.9, 127.8, 119.8, 119.7, 79.0, 67.3, 67.2, 56.6, 56.1, 53.5, 45.0, 40.5, 30.2, 29.9, 29.3, 29.1, 28.6, 28.5, 28.5, 26.8, 26.5, 26.3, 22.2, 22.1. HRMS (ESI) *m/z* calcd for $C_{29}H_{39}BrN_2O_4$ $(M+Na)^+$, 581.1985; found 581.1988.

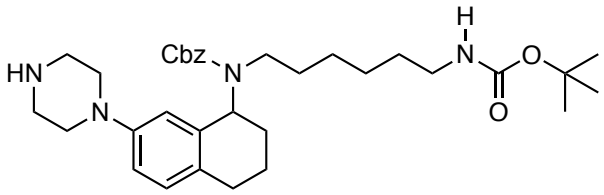

Benzyl (6-((*tert*-butoxycarbonyl)amino)hexyl)(7-(piperazin-1-yl)-1,2,3,4-tetrahydronaphthalen-1-yl)carbamate (2.142) (MDW-1-284). Prepared from **2.141** (141 mg 0.252 mmol) and piperazine according to representative procedure C. The crude residue was purified via flash chromatography (SiO_2) eluting with CH_2Cl_2/MeOH/Et_3N (99:0:1 to 97:2:1) to afford 65 mg (46%) of **2.142** as a pale yellow oil. ^{1}H NMR (499 MHz, $CDCl_3$) rotamers δ 7.42 – 7.19 (comp, 5H), 7.00 – 6.93 (m, 1H), 6.78 – 6.71 (m, 1H), 6.61 – 6.53 (m, 1H), 5.43 – 5.01 (comp, 3H), 4.69 – 4.54 (comp, 1H), 3.22 – 2.90 (comp, 9H), 2.89 – 2.38 (comp, 5H), 2.08 – 1.03 (comp, 22H). ^{13}C NMR (126 MHz, $CDCl_3$) rotamers δ 157.2, 156.5, 155.9, 150.2, 150.1, 137.1, 136.9, 136.4, 130.0, 129.7, 129.5, 128.5, 128.4, 127.9, 127.9, 127.8, 127.8, 115.8, 115.5, 114.5, 114.0, 78.9, 67.0, 66.8, 56.3, 52.9, 50.6, 50.5, 46.1, 46.0, 40.4, 30.2, 29.5, 29.2, 29.1, 28.7, 28.6, 28.4, 26.7, 22.5, 22.3, 10.8, 8.1. HRMS (ESI) *m/z* calcd for $C_{33}H_{48}N_4O_4$ $(M+Na)^+$, 587.3568; found 587.3573.

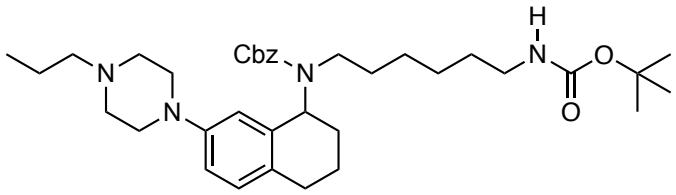

Benzyl (6-((*tert*-butoxycarbonyl)amino)hexyl)(7-(4-propylpiperazin-1-yl)-1,2,3,4-tetrahydronaphthalen-1-yl)carbamate (**2.143**) (MDW-1-286). Prepared from 2.142 (25 mg, 0.044 mmol) and propionaldehyde according to representative procedure E. The crude residue was purified via flash chromatography (SiO_2) eluting with hexanes/EtOAc/Et_3N (69:30:1) to afford 17 mg (63%) of **2/143** as a colorless oil. ^1H NMR (499 MHz, $CDCl_3$) rotamers δ 7.43 – 7.20 (comp, 5H), 6.98 (dd, *J* = 8.4, 2.2 Hz, 1H), 6.77 (dd, *J* = 8.4, 2.5 Hz, 1H), 6.62 – 6.56 (m, 1H), 5.43 – 5.02 (comp, 3H), 4.62 – 4.47 (m, 1H), 3.24 – 2.95 (comp, 7H), 2.86 – 2.50 (comp, 7H), 2.37 (d, *J* = 8.9 Hz, 2H), 2.07 – 1.91 (comp, 2H), 1.83 – 1.66 (comp, 3H), 1.64 – 1.49 (comp, 3H), 1.49 – 1.37 (comp, 11H), 1.35 – 1.25 (comp, 2H), 1.19 – 1.07 (comp, 2H), 0.94 (t, *J* = 7.4 Hz, 3H). HRMS (ESI) *m/z* calcd for $C_{36}H_{54}N_4O_4$ $(M+H)^+$, 607.4218; found 607.4213.

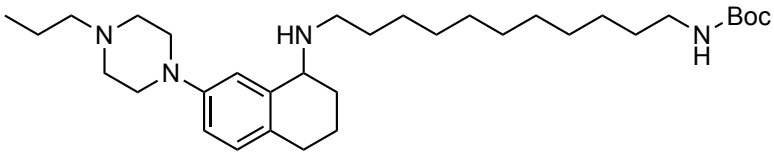

***tert*-Butyl (11-((7-(4-propylpiperazin-1-yl)-1,2,3,4-tetrahydronaphthalen-1-yl)amino)undecyl)carbamate** (**2.146**) (MDW-2-95). Prepared from **2.84** (50.8 mg, 0.186 mmol) and mono-Boc-1,11-diaminoundecane according to representative procedure I.[340] The crude residue was purified via flash chromatography (SiO_2) eluting with hexanes/EtOAc/Et_3N (84:15:1) to afford 87.6 mg (87%) of **2.146** as a colorless oil. ^1H NMR (499 MHz, $CDCl_3$) δ 6.96 (d, *J* = 8.4 Hz, 1 H), 6.93 (d, *J* = 2.6 Hz, 1 H), 6.76 (dd, *J* = 8.4, 2.6 Hz, 1 H), 4.56 (br s, 1 H), 3.69 (t, *J* = 5.0 Hz, 1 H), 3.20 – 3.13 (m, 4 H), 3.08

(comp, J = 6.8 Hz, 2 H), 2.75 – 2.62 (comp, 4 H), 2.61 – 2.57 (comp, 4 H), 2.37 – 2.32 (comp, 2 H), 1.97 – 1.87 (m, 1 H), 1.86 – 1.79 (comp, 2 H), 1.72 – 1.64 (m, 1 H), 1.60 – 1.40 (comp, 15 H), 1.38 – 1.22 (m, 15 H), 0.92 (t, J = 7.4 Hz, 3 H). ^{13}C NMR (126 MHz, $CDCl_3$) δ 156.1, 149.7, 140.1, 129.7, 129.0, 116.4, 115.5, 79.1, 60.9, 56.0, 53.4, 49.9, 47.4, 40.7, 30.7, 30.2, 29.7, 29.7, 29.7, 29.6, 29.4, 28.7, 28.6, 28.5, 27.6, 26.9, 20.2, 19.4, 12.1. HRMS (ESI) *m/z* calcd for $C_{33}H_{58}N_4O_2$ $(M+H)^+$, 543.4633; found 543.4651

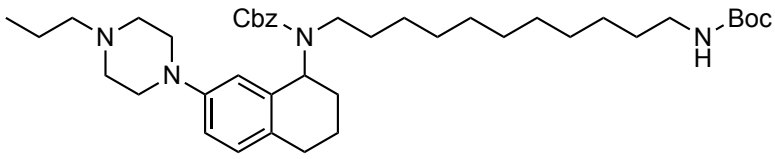

Benzyl (11-((*tert*-butoxycarbonyl)amino)undecyl)(7-(4-propylpiperazin-1-yl)-1,2,3,4-tetrahydronaphthalen-1-yl)carbamate (**2.147**) (MDW-2-97). Prepared from **2.146** (80.4 mg, 0.148 mmol) and CbzCl according to representative procedure A. The crude residue was purified via flash chromatography (SiO_2) eluting with hexanes/EtOAc/Et_3N (74:25:1) to afford 80.6 mg (80%) of **2.147** as a pale yellow oil. ^{1}H NMR (499 MHz, $CDCl_3$) δ 7.43 – 7.19 (comp, 5 H), 6.99 – 6.95 (m, 1 H), 6.76 (dd, J = 8.4, 2.5 Hz, 1 H), 6.60 (d, J = 2.5 Hz, 1 H), 5.42 – 4.98 (m, 3 H), 4.51 (br s, 1 H), 3.29 – 3.01 (comp, 7 H), 2.88 – 2.50 (comp, 7 H), 2.41 – 2.31 (comp, 2 H), 2.10 – 1.38 (comp, 19 H), 1.32 – 1.07 (comp, 14 H) 0.93 (t, J = 7.4 3 H). ^{13}C NMR (126 MHz, $CDCl_3$) δ 157.3, 156.6, 156.1, 150.0, 149.9, 137.3, 137.2, 137.1, 136.7, 130.0, 129.8, 129.5, 128.6, 128.5, 128.0, 127.9, 127.9, 115.7, 115.4, 114.5, 114.0, 79.1, 67.1, 67.0, 60.8, 56.5, 53.3, 49.6, 49.5, 45.0, 40.8, 30.6, 30.5, 30.2, 29.6, 29.6, 29.5, 29.4, 29.3, 29.3, 28.9, 28.8, 28.6, 27.3, 26.9, 22.7, 22.5, 20.2, 12.1. HRMS (ESI) *m/z* calcd for $C_{41}H_{64}N_4O_4$ $(M+H)^+$, 677.5000; found 677.4994

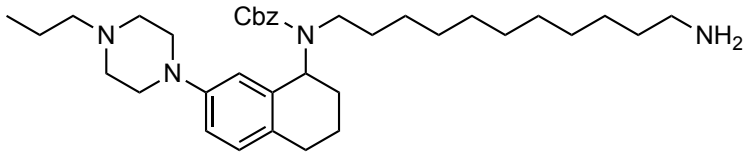

Benzyl (11-aminoundecyl)(7-(4-propylpiperazin-1-yl)-1,2,3,4-tetrahydronaphthalen-1-yl)carbamate (**2.149**) (MDW-2-32). **2.147** (37.3 mg, 0.0551 mmol) was dissolved in a solution of dioxane (0.4 mL) containing HCl (4 M) cooled to 0 °C. The solution was stirred at 0 °C for 3 h and then diluted with CH_2Cl_2 (20 mL). The solution was washed with 1 N NaOH (1 x 20 mL), saturated aqueous $NaHCO_3$ (1 x 20 mL), dried (Na_2SO_4), and concentrated under reduced pressure to afford 30.6 mg of **2.149** (96%) as a pale yellow oil. ^{1}H NMR (499 MHz, $CDCl_3$) δ 7.44 – 7.18 (comp, 5 H), 7.01 – 6.94 (m, 1 H), 6.76 (dd, *J* = 8.4, 2.5 Hz, 1 H), 6.63 – 6.56 (m, 1 H), 5.44 – 5.01 (comp, 3 H), 3.29 – 2.99 (comp, 5 H), 2.86 – 2.60 (comp, 5 H), 2.58 – 2.50 (comp, 4 H), 2.38 – 2.31 (comp, 2 H), 2.07 – 1.41 (comp, 12 H), 1.32 – 1.08 (comp, 14 H), 0.93 (t, *J* = 7.4 Hz, 3 H). ^{13}C NMR (126 MHz, $CDCl_3$) δ 157.2, 156.5, 149.8, 149.7, 137.2, 136.9, 136.5, 129.8, 129.7, 129.3, 128.4, 128.4, 127.8, 127.8, 127.7, 115.6, 115.2, 114.3, 113.8, 66.9, 66.8, 60.7, 56.3, 53.2, 53.2, 49.5, 44.8, 42.1, 33.5, 30.4, 29.6, 29.5, 29.5, 29.4, 29.2, 29.1, 28.7, 28.6, 27.2, 26.9, 22.6, 22.4, 20.1, 12.0. HRMS (ESI) *m/z* calcd for $C_{36}H_{56}N_4O_2$ $(M+H)^+$, 577.4476; found 577.4484

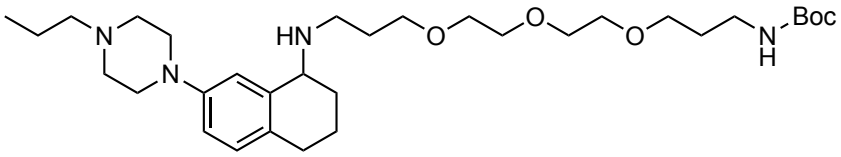

***tert*-Butyl (3-(2-(2-(3-((7-(4-propylpiperazin-1-yl)-1,2,3,4-tetrahydronaphthalen-1-yl)amino)propoxy)ethoxy)ethoxy)propyl)carbamate** (**2.151**) ((MDW-2-85). Prepared from **2.84** (103 mg, 0.377 mmol) and *N*-Boc-4,7,10-trioxa-1,13-

tridecanediamine according to representative procedure I.[341] The crude residue was purified via flash chromatography (SiO_2) eluting with hexanes/acetone/Et_3N (44:35:1) to afford 118 mg (54%) of **2.151** as an orange oil containing some impurities that could not be separated. The residue was used in the subsequent reaction without additional purification. ^{1}H NMR (400 MHz, $CDCl_3$) δ 6.97 – 6.90 (comp, 2H), 6.73 (dd, *J* = 8.3, 2.7 Hz, 1H), 5.20 – 5.10 (m, 1H), 3.66 (t, *J* = 5.0 Hz, 1H), 3.64 – 3.45 (comp, 13H), 3.22 – 3.09 (comp, 6H), 2.83 – 2.46 (comp, 8H), 2.35 – 2.28 (comp, 2H), 1.96 – 1.59 (comp, 9H), 1.52 (h, *J* = 7.4 Hz, 2H), 1.40 (s, 10H), 0.89 (t, *J* = 7.4 Hz, 3H). HRMS (ESI) *m/z* calcd for $C_{32}H_{56}N_4O_5$ $(M+H)^+$, 577.4323; found 577.4340.

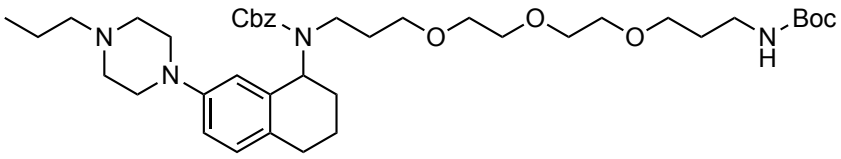

Benzyl (2,2-dimethyl-4-oxo-3,9,12,15-tetraoxa-5-azaoctadecan-18-yl)(7-(4-propylpiperazin-1-yl)-1,2,3,4-tetrahydronaphthalen-1-yl)carbamate (**2.152**) (MDW-2-93). Prepared from **2.151** (0.118 g, 0.204 mmol) and CbzCl according to representative procedure A. The crude residue was purified via flash chromatography (SiO_2) eluting with hexanes/acetone/Et_3N (76:23:1) to afford 118 mg (81%) of **2.152** as a colorless oil. ^{1}H NMR (499 MHz, $CDCl_3$) rotamers δ 7.40 – 7.11 (comp, 5H), 6.89 (d, *J* = 8.4 Hz, 1H), 6.68 (dd, *J* = 8.4, 2.5 Hz, 1H), 6.54 – 6.46 (m, 1H), 5.39 – 4.88 (comp, 4H), 3.55 – 3.08 (comp, 15H), 3.04 – 2.93 (comp, 4H), 2.91 – 2.74 (m, 1H), 2.66 – 2.44 (comp, 6H), 2.32 – 2.21 (comp, 2H), 2.01 – 1.62 (comp, 8H), 1.48 (h, *J* = 7.5 Hz, 2H), 1.36 (s, 9H), 0.86 (t, *J* = 7.3 Hz, 3H). ^{13}C NMR (126 MHz, $CDCl_3$) rotamers δ 157.2, 156.6, 156.0, 149.9, 149.8, 137.1, 136.9, 136.4, 129.9, 129.8, 129.4, 128.5, 128.4, 127.9, 127.9, 127.8, 115.7, 115.3, 114.3, 113.8, 78.9, 70.6, 70.2, 70.1, 70.0, 69.6, 69.2, 69.1, 67.0, 66.9, 60.7, 56.9,

56.4, 53.2, 49.5, 49.4, 42.0, 38.6, 30.5, 29.6, 29.5, 29.4, 29.0, 28.7, 28.6, 28.5, 22.6, 22.4, 20.0, 12.0. HRMS (ESI) *m/z* calcd for $C_{40}H_{62}N_4O_7$ $(M+H)^+$, 711.4691; found 711.4698.

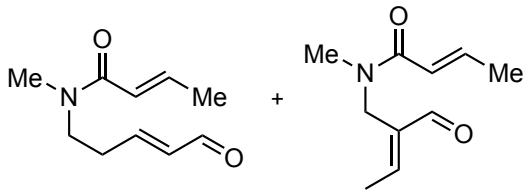

4.4 **4.30**

(*E*)-*N*-Methyl-*N*-((*E*)-5-oxopent-3-en-1-yl)but-2-enamide (**4.4**) (MDW-4-126). Freshly distilled crotonyl chloride (0.998 g, 9.55 mmol) was added dropwise to a solution of 1,3,5-trimethylhexahydro-1,3,5-triazine (0.410 g, 3.17 mmol) in MeCN (16 mL) at 0 °C. The reaction was stirred for 30 min at 0 °C and then transferred to an oil bath preheated to 80 °C and stirred for 2 h. After cooling to 0 °C, TMSOTf (0.06 mL, 0.3 mmol) and 1-(trimethylsiloxy)-1,3-butadiene (1.813 g, 12.74 mmol) were sequentially added dropwise, and the reaction was stirred at 0 °C for 16 h. The reaction was quenched with saturated aqueous $NaHCO_3$ (2 mL), and the MeCN was removed under reduced pressure. The resulting mixture was diluted with saturated aqueous $NaHCO_3$ (20 mL) and extracted with CH_2Cl_2 (3 x 30 mL). The combined organic extracts were dried (Na_2SO_4) and concentrated under reduced pressure, and the crude residue was purified via flash chromatography (SiO_2) eluting with hexanes/*i*-PrOH (90:10 to 40:60) to give 1.073 g (62%) of **4.4** as a pale yellow oil and 168 mg (10%) of **4.30** as a colorless oil.

Compound 4.4 IR (neat): ν_{max}/cm^{-1} 2938, 1684, 1660, 1606, 1484, 1447, 1401, 1143, 1097, 966, 827. ^1H NMR (400 MHz, $CDCl_3$) rotamers δ 9.53 – 9.43 (comp, 1H), 6.98 – 6.67 (comp, 2H), 6.26 – 6.05 (comp, 2H), 3.65 – 3.47 (comp, 2H), 3.08 – 2.94 (comp, 3H), 2.66 – 2.52 (comp, 2H), 1.86 (dd, J = 6.9, 1.7 Hz, 3H). ^{13}C NMR (126 MHz, $CDCl_3$) rotamers δ 193.9, 193.3, 166.8, 166.7, 154.9, 152.8, 142.4, 142.3, 134.8, 134.4,

121.6, 121.2, 48.3, 46.5, 35.7, 34.1, 32.2, 31.1, 18.3, 15.4.HRMS (ESI) *m/z* calcd for $C_{10}H_{15}NO_2$ $(M+H)^+$, 182.1176; found 182.1178.

Compound 4.30. IR (neat): ν_{max}/cm^{-1} 2936, 1681, 1659, 1612, 1447, 1400, 1284, 1260, 1128, 1097, 965, 947, 825. ^1H NMR (400 MHz, $CDCl_3$) δ 9.44 (s, 1H), 6.97 – 6.77 (comp, 2H), 6.23 (d, *J* = 15.0 Hz, 1H), 4.34 – 4.20 (comp, 2H), 3.03 (s, 3H), 2.14 (d, *J* = 7.0 Hz, 3H), 1.87 (d, *J* = 6.5 Hz, 3H). ^{13}C NMR (126 MHz, $CDCl_3$) δ 194.9, 166.7, 155.6, 142.0, 140.2, 121.8, 40.5, 36.2, 18.4, 15.6. HRMS (ESI) *m/z* calcd for $C_{10}H_{15}NO_2$ $(M+Na)^+$, 204.0995; found 204.1002.

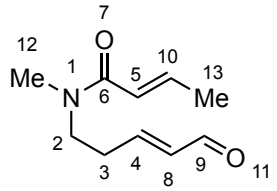

NMR Assignments (**4.4**). ^1H NMR (400 MHz, $CDCl_3$) rotamers δ 9.53 – 9.43 (m, 1H, 9), 6.98 – 6.67 (comp, 2H, 4, 10), 6.26 – 6.05 (comp, 2H, 5, 8), 3.65 – 3.47 (comp, 2H, 2), 3.08 – 2.94 (comp, 3H, 12), 2.66 – 2.52 (comp, 2H, 3), 1.86 (dd, *J* = 6.9, 1.7 Hz, 3H, 13). ^{13}C NMR (126 MHz, $CDCl_3$) δ 193.9 and 193.3 (9), 166.8 and 166.7 (6), 154.9 and 152.8 (4), 142.4 and 142.3 (10), 134.8 and 134.4 (8), 121.6 and 121.2 (5), 48.3 and 46.5 (2), 35.7 and 34.1 (12), 32.2 and 31.1 (3), 18.3 and 15.4 (13).

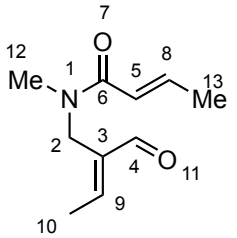

NMR Assignments (**4.30**). ^1H NMR (400 MHz, $CDCl_3$) δ 9.44 (s, 1H, 4), 6.97 – 6.77 (comp, 2H, 8, 9), 6.23 (d, *J* = 15.0 Hz, 1H, 5), 4.34 – 4.20 (comp, 2H, 2), 3.03 (s,

3H, 12), 2.14 (d, *J* = 7.0 Hz, 3H, 10), 1.87 (d, *J* = 6.5 Hz, 3H, 13). ^{13}C NMR (126 MHz, $CDCl_3$) δ 194.9 (4), 166.7 (6), 155.6 (9), 142.0 (8), 140.2 (3), 121.8 (5), 40.5 (2), 36.2 (12), 18.4 (13), 15.6 (10).

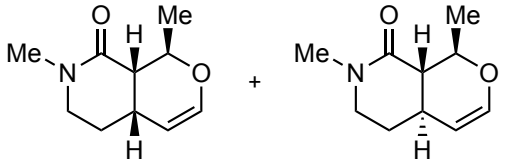

4.31 **4.32**

(±)-((1*R*,4a*R*,8a*S*)-1,7-Dimethyl-1,4a,5,6,7,8a-hexahydro-8*H*-pyrano[3,4-*c*]pyridin-8-one (**4.31**) (MDW-4-127). A solution of **4.4** (1.039 g, 5.733 mmol) in mesitylene (385 mL) was degassed via sparging the solution with N_2 for 1 h. The reaction flask was transferred to an oil bath preheated to 190 °C and heated under reflux for 30 h. Upon cooling, the solvent was removed under reduced pressure, and the crude material was purified via flash chromatography (SiO_2), eluting with hexanes/EtOAc (70:30 to 40:60) to afford 0.677 g (65%) of **4.31** as a colorless oil and 0.125 g of **4.32** (12%) as a waxy white solid.

Compound 4.31. IR (neat): ν_{max}/cm^{-1} 2930, 2869, 1633, 1500, 1443, 1331, 1237, 1097, 1049, 743. ^{1}H NMR (400 MHz, $CDCl_3$) δ 6.38 (dd, *J* = 6.2, 2.1 Hz, 1H), 4.81 (qd, *J* = 6.6, 3.7 Hz, 1H), 4.53 (dd, *J* = 6.3, 2.4 Hz, 1H), 3.36 (ddd, *J* = 12.0, 10.1, 4.5 Hz, 1H), 3.13 (dt, *J* = 12.2, 4.9 Hz, 1H), 2.93 (s, 3H), 2.75 – 2.67 (m, 1H), 2.41 – 2.35 (m, 1H), 2.02 – 1.92 (m, 1H), 1.83 – 1.73 (m, 1H), 1.33 (d, *J* = 6.7 Hz, 3H). ^{13}C NMR (126 MHz, $CDCl_3$) δ 169.0, 144.6, 100.6, 70.3, 46.8, 44.6, 35.3, 27.2, 26.1, 18.4. HRMS (ESI) *m/z* calcd for $C_{10}H_{15}NO_2$ $(M+H)^+$, 182.1176; found 182.1180.

Compound 4.32. IR (neat): ν_{max}/cm^{-1} 2975, 2933, 1630, 1501, 1439, 1327, 1226, 1073, 1042, 738. ^{1}H NMR (400 MHz, $CDCl_3$) δ 6.35 (dd, *J* = 6.0, 2.4 Hz, 1H), 4.58 (dd,

J = 6.1, 1.7 Hz, 1H), 4.10 (dq, *J* = 9.9, 6.1 Hz, 1H), 3.40 (ddd, *J* = 12.4, 7.6, 2.7 Hz, 1H), 3.30 (ddd, *J* = 12.4, 10.1, 7.0 Hz, 1H), 2.90 (d, *J* = 0.7 Hz, 3H), 2.45 – 2.36 (m, 1H), 2.05 – 1.95 (comp, 2H), 1.67 (d, *J* = 6.1 Hz, 3H), 1.64 – 1.54 (m, 1H). ^{13}C NMR (126 MHz, $CDCl_3$) δ 170.1, 143.7, 102.8, 73.1, 48.6, 48.2, 34.5, 32.0, 29.5, 21.8. HRMS (ESI) *m/z* calcd for $C_{10}H_{15}NO_2$ $(M+H)^+$, 182.1176; found 182.1179.

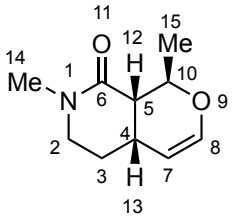

NMR Assignments (**4.31**). ^{1}H NMR (400 MHz, $CDCl_3$) δ 6.38 (dd, *J* = 6.2, 2.1 Hz, 1H, 8), 4.81 (qd, *J* = 6.6, 3.7 Hz, 1H, 10), 4.53 (dd, *J* = 6.3, 2.4 Hz, 1H, 7), 3.36 (ddd, *J* = 12.0, 10.1, 4.5 Hz, 1H, 2''), 3.13 (dt, *J* = 12.2, 4.9 Hz, 1H, 2'), 2.93 (s, 3H, 14), 2.75 – 2.67 (m, 1H, 13), 2.41 – 2.35 (m, 1H, 12), 2.02 – 1.92 (m, 1H, 3'), 1.83 – 1.73 (m, 1H, 3''), 1.33 (d, *J* = 6.7 Hz, 3H, 15). ^{13}C NMR (126 MHz, $CDCl_3$) δ 169.0 (6), 144.6 (8), 100.6 (7), 70.3 (10), 46.8 (2), 44.6 (5), 35.3 (14), 27.2 (3), 26.1 (4), 18.4 (15).

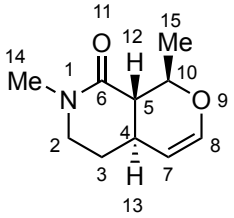

NMR Assignments (**4.32**). ^{1}H NMR (400 MHz, $CDCl_3$) δ 6.35 (dd, *J* = 6.0, 2.4 Hz, 1H, 8), 4.58 (dd, *J* = 6.1, 1.7 Hz, 1H, 7), 4.10 (dq, *J* = 9.9, 6.1 Hz, 1H, 10), 3.40 (ddd, *J* = 12.4, 7.6, 2.7 Hz, 1H, 2''), 3.30 (ddd, *J* = 12.4, 10.1, 7.0 Hz, 1H, 2'), 2.90 (d, *J* = 0.7 Hz, 3H, 14), 2.45 – 2.36 (m, 1H, 13), 2.05 – 1.95 (comp, 2H, 3'', 12), 1.67 (d, *J* = 6.1 Hz, 3H, 15), 1.64 – 1.54 (m, 1H, 3'). ^{13}C NMR (126 MHz, $CDCl_3$) δ 170.1 (6), 143.7 (8), 102.8 (7), 73.1 (10), 48.6 (2), 48.2 (5), 34.5 (14), 32.0 (4), 29.5 (3), 21.8 (15).

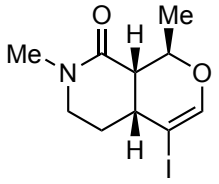

(±)-((1*R*,4a*R*,8a*S*)-4-Iodo-1,7-dimethyl-1,4a,5,6,7,8a-hexahydro-8*H*-pyrano[3,4-*c*]pyridin-8-one (**4.46**) (MDW-4-129). A foil-wrapped flask containing *cis*-oxahydroisoquinolone **4.31** (0.677 g, 3.74 mmol) was evacuated and backfilled with N_2 five times, whereupon MeCN (31 mL) was added. Under a positive flow of N_2, $AgNO_3$ (63 mg, 0.37 mmol) and recrystallized NIS (1.008 g, 4.480 mmol) were added sequentially. The flask was transferred to an oil bath preheated to 80 °C and stirred in the dark for 2.5 h. After cooling the mixture to room temperature, it was filtered through a pad of Celite into a foil-wrapped flask, and the filter cake was washed with MeCN (50 mL). The filtrate was concentrated under reduced pressure, whereupon the resulting residue was dissolved in CH_2Cl_2 (30 mL) and washed with saturated aqueous $Na_2S_2O_3$ (1 x 30 mL). The organic layer was separated, and the aqueous layer was washed with CH_2Cl_2 (2 x 20 mL). The combined organic layers were washed with H_2O (3 x 30 mL), brine, (1 x 40 mL), dried (Na_2SO_4), and concentrated under reduced pressure. The crude residue was purified via flash chromatography (SiO_2) eluting with hexanes/EtOAc (80:20 to 40:60) to give 0.954 g (83%) of **4.46** as a yellow oil. IR (neat): ν_{max}/cm^{-1} 2931, 1636, 1500, 1442, 1197, 1161, 1136, 1018, 983. ^1H NMR (400 MHz, $CDCl_3$) δ 6.72 (d, J = 1.8 Hz, 1H), 4.83 (qd, J = 6.7, 4.3 Hz, 1H), 3.33 (dt, J = 12.4, 6.9 Hz, 1H), 3.14 (dt, J = 12.4, 5.1 Hz, 1H), 2.94 (s, 3H), 2.78 – 2.71 (m, 1H), 2.57 (dd, J = 6.2, 4.3 Hz, 1H), 2.09 – 2.02 (m, 2H), 1.36 (d, J = 6.6 Hz, 3H).^{13}C NMR (126 MHz, $CDCl_3$) δ 167.8, 148.9, 72.4, 70.9, 46.5, 46.4, 35.4, 34.8, 27.5, 18.4. HRMS (ESI) *m/z* calcd for $C_{10}H_{14}INO_2$ $(M+H)^+$, 308.0142; found 308.0150.

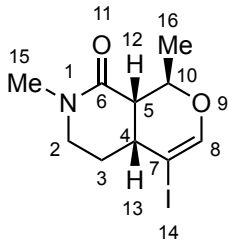

NMR Assignments (4.46). ^{1}H NMR (400 MHz, $CDCl_3$) δ 6.72 (d, *J* = 1.8 Hz, 1H, 8), 4.83 (qd, *J* = 6.7, 4.3 Hz, 1H, 10), 3.33 (dt, *J* = 12.4, 6.9 Hz, 1H, 2''), 3.14 (dt, *J* = 12.4, 5.1 Hz, 1H, 2'), 2.94 (s, 3H, 15), 2.78 – 2.71 (m, 1H, 13), 2.57 (dd, *J* = 6.2, 4.3 Hz, 1H, 12), 2.09 – 2.02 (comp, 2H, 3), 1.36 (d, *J* = 6.6 Hz, 3H, 16). ^{13}C NMR (126 MHz, $CDCl_3$) δ 167.8 (6), 148.9 (8), 72.4 (7), 70.9 (10), 46.5 (2), 46.4 (5), 35.4 (15), 34.8 (13), 27.5 (3), 18.4 (16).

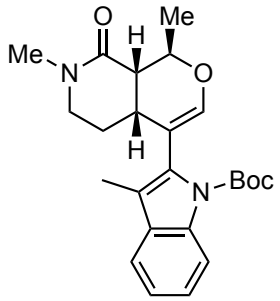

(±)-*tert*-Butyl 2-((1*R*,4a*R*,8a*S*)-1,7-dimethyl-8-oxo-4a,5,6,7,8,8a-hexahydro-1*H*-pyrano[3,4-*c*]pyridin-4-yl)-3-methyl-1*H*-indole-1-carboxylate (4.55) (MDW-4-131). *tert*-BuLi (8.0 mL of a 1.8 M solution in pentane) was added dropwise over 10 min to a solution of *N*-Boc-3-methylindole[487] (2.908 g, 13.38 mmol) in THF (67 mL) at -78 °C. After stirring for 1 h at –78 °C, $B(OMe)_3$ (3.4 g, 3.7 mL, 33 mmol) was added rapidly, and the reaction was stirred for 1 h at –78 °C. The reaction was transferred to a cooling bath at 0 °C, and stirring was continued for 30 min, whereupon saturated aqueous NH_4Cl (10 mL) was added. The flask was removed from the cooling bath and stirred for

30 min. The mixture was diluted with saturated aqueous NH_4Cl (20 mL) and extracted with Et_2O (3 x 30 mL). The combined organic extracts were dried ($MgSO_4$) and concentrated under reduced pressure to afford crude boronic acid **17** that was used immediately. The flask containing the crude **17** was evacuated and backfilled with N_2 five times, whereupon PhMe (19 mL) was added, and N_2 was bubbled through the solution for 10 min. The solution was transferred via cannula to a N_2 flushed flask containing vinyl iodide **4.46** (1.017 g, 3.311 mmol), SPhos Pd G2 (0.239 g, 0.332 mmol), and K_3PO_4 (2.811 g, 13.24 mmol), rinsing with PhMe (3 x 12 mL). Degassed H_2O (11 mL) was added to the mixture, and the flask was immediately transferred to an oil bath preheated to 60 °C and stirred in the dark for 2 h. The reaction was cooled to room temperature, and the mixture was diluted with saturated aqueous NH_4Cl (1 x 50 mL) and extracted with Et_2O (3 x 50 mL). The combined organic extracts were dried ($MgSO_4$), concentrated under reduced pressure, and the crude residue was purified via flash chromatography (SiO_2) eluting with hexanes/EtOAc (70:30 to 50:50) to afford 1.071 g (79%) of **4.55** as a pale yellow solid: mp 67-72 °C. IR (neat): ν_{max}/cm^{-1} 2933, 1727, 1640,1455, 1318, 1144, 1073, 866, 747. ^1H NMR (400 MHz, $CDCl_3$) δ 8.01 (dd, *J* = 7.3, 1.0 Hz, 1H), 7.50 – 7.45 (comp, 1H), 7.32 – 7.21 (m, 2H), 6.49 (d, *J* = 1.3 Hz, 1H), 4.64 (p, *J* = 6.5 Hz, 1H), 3.14 – 2.99 (m, 3H), 2.93 (s, 3H), 2.68 (t, *J* = 6.2 Hz, 1H), 2.22 (s, 3H), 1.85 – 1.67 (m, 2H), 1.66 (s, 9H), 1.53 (d, *J* = 6.5 Hz, 3H). ^{13}C NMR (126 MHz, $CDCl_3$) δ 168.8, 150.2, 144.8, 135.9, 133.2, 130.6, 124.3, 122.6, 118.8, 117.2, 115.7, 107.3, 83.6, 70.4, 48.2, 45.5, 35.2, 31.7, 28.5, 25.9, 19.6, 9.9. HRMS (ESI) *m/z* calcd for $C_{24}H_{30}N_2O_4$ $(M+H)^+$, 411.2278; found 411.2281.

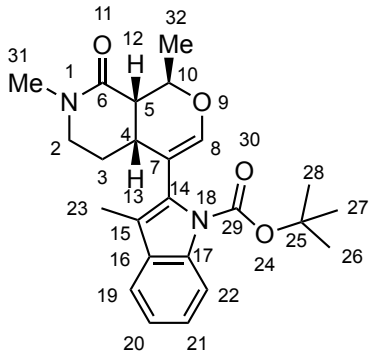

NMR Assignments 4.55). ^{1}H NMR (400 MHz, $CDCl_3$) δ 8.01 (dd, *J* = 7.3, 1.0 Hz, 1H, 19), 7.50 – 7.45 (m, 1H, 22), 7.32 – 7.21 (comp, 2H, 20, 21), 6.49 (d, *J* = 1.3 Hz, 1H, 8), 4.64 (p, *J* = 6.5 Hz, 1H, 10), 3.14 – 2.99 (comp, 3H, 2, 13), 2.93 (s, 3H, 24), 2.68 (t, *J* = 6.2 Hz, 1H, 12), 2.22 (s, 3H, 23), 1.85 – 1.67 (comp, 2H, 3), 1.66 (s, 9H, 28, 29, 30), 1.53 (d, *J* = 6.5 Hz, 3H, 25). ^{13}C NMR (126 MHz, $CDCl_3$) δ 168.8 (6), 150.2 (29), 144.8 (8), 135.9 (17), 133.2 (16), 130.6 (14), 124.3 (21), 122.6 (20), 118.8 (22), 117.2 (15), 115.7 (19), 107.3 (7), 83.6 (25), 70.4 (10), 48.2 (2), 45.5 (5), 35.2 (31), 31.7 (13), 28.5 (26, 27, 28), 25.9 (3), 19.6 (32), 9.9 (23).

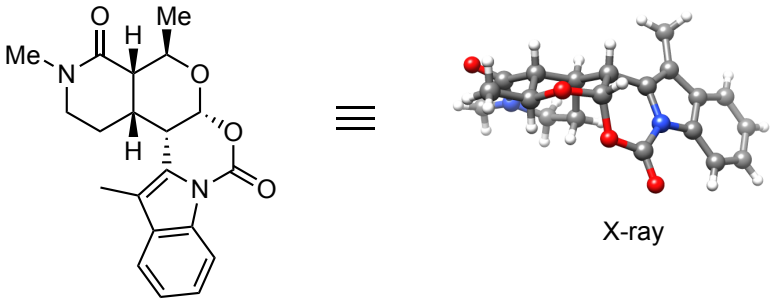

(±)-(4a*S*,5*R*,6a*R*,14b*S*,14c*S*)-3,5,14-Trimethyl-1,2,3,4a,5,6a,14b,14c-octahydro-4*H*,8*H*-pyrido[4'',3'':4',5']pyrano[3',2':5,6][1,3]oxazino[3,4-*a*]indole-4,8-dione (**4.61**) (MDW-4-145). A solution of HCl (4 M in dioxane, 0.75 mL) was added dropwise to a solution of indolyl oxahydroisoquinolone **4.55** (0.155 g, 0.378 mmol) in dioxane (6.8 mL) at room temperature, and the flask was sealed. The reaction was stirred

for 31 h, whereupon it was poured into saturated aqueous $NaHCO_3$ (10 mL) and extracted with CH_2Cl_2 (3 x 15 mL). The combined organic extracts were dried (Na_2SO_4), concentrated under reduced pressure, and the crude residue was purified via flash chromatography (SiO_2) eluting with EtOAc/CH_2Cl_2 (10:90 to 30:70) affording 0.103 g (77%) of **4.61** as a white solid: mp 107-111 °C. IR (neat): ν_{max}/cm^{-1} 2925, 1724, 1627,1461, 1378, 1336, 1317, 1183, 1131, 1089, 998, 951, 907, 755. ^1H NMR (400 MHz, $CDCl_3$) δ 8.31 – 8.26 (comp, 1H), 7.53 – 7.49 (comp, 1H), 7.41 – 7.31 (m, 2H), 5.84 (d, *J* = 3.6 Hz, 1H), 4.43 (dq, *J* = 10.5, 6.1 Hz, 1H), 3.58 (dd, *J* = 6.2, 3.6 Hz, 1H), 3.18 (ddd, *J* = 12.3, 6.2, 1.5 Hz, 1H), 3.07 (td, *J* = 12.1, 5.0 Hz, 1H), 2.88 (s, 3H), 2.73 – 2.67 (m, 1H), 2.53 – 2.44 (comp, 1H), 2.31 – 2.17 (m, 4H), 1.48 (d, *J* = 6.2 Hz, 3H), 1.32 – 1.26 (comp, 1H). ^{13}C NMR (126 MHz, $CDCl_3$) δ 167.4, 147.1, 134.8, 131.1, 128.2, 125.3, 124.2, 118.8, 115.7, 114.5, 98.3, 65.5, 49.6, 47.7, 35.0, 34.7, 34.5, 21.4, 19.9, 8.5. HRMS (ESI) *m/z* calcd for $C_{20}H_{22}N_2O_4$ $(M+Na)^+$, 377.1472; found 377.1474.

An analytical sample of **4.61** was recrystallized from THF and water via slow evaporation to afford colorless thin needles. Crystallographic data for **19** has been deposited with the Cambridge Crystallographic Data Center, Deposition number 1947103

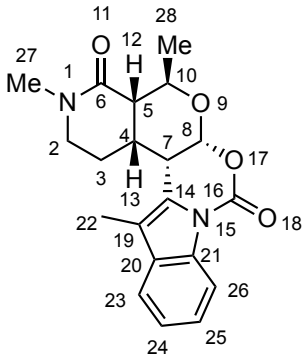

NMR Assignments (**4.61**). ^1H NMR (400 MHz, $CDCl_3$) δ 8.31 – 8.26 (m, 1H, 23), 7.53 – 7.49 (m, 1H, 26), 7.41 – 7.31 (comp, 2H, 24, 25), 5.84 (d, *J* = 3.6 Hz, 1H, 8),

4.43 (dq, *J* = 10.5, 6.1 Hz, 1H, 10), 3.58 (dd, *J* = 6.2, 3.6 Hz, 1H, 7), 3.18 (ddd, *J* = 12.3, 6.2, 1.5 Hz, 1H, 2''), 3.07 (td, *J* = 12.1, 5.0 Hz, 1H, 2'), 2.88 (s, 3H, 27), 2.73 – 2.67 (m, 1H, 12), 2.53 – 2.44 (m, 1H, 13), 2.31 – 2.17 (comp, 4H, 3', 22), 1.48 (d, *J* = 6.2 Hz, 3H, 28), 1.32 – 1.26 (m, 1H, 3''). ^{13}C NMR (126 MHz, $CDCl_3$) δ 167.4 (6), 147.1 (16), 134.8 (21), 131.1 (14), 128.2 (20), 125.3 (25), 124.2 (24), 118.8 (26), 115.7 (23), 114.5 (19), 98.3 (8), 65.5 (10), 49.6 (2), 47.7 (5), 35.0 (27), 34.7 (13), 34.5 (7), 21.4 (3), 19.9 (28), 8.5 (22).

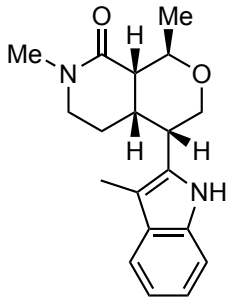

(±)-(1*R*,4*S*,4a*S*,8a*S*)-1,7-Dimethyl-4-(3-methyl-1*H*-indol-2-yl)octahydro-8*H*-pyrano[3,4-*c*]pyridin-8-one (**4.63**) (MDW-4-147). Triethylsilane (0.33 g, 0.46 mL, 2.9 mmol) was added to a solution of acetal **4.61** (0.102 g, 0.288 mmol) in CH_2Cl_2 (4.8 mL) at –40 °C. $EtAlCl_2$ (1.1 mL of a 1.8 M solution in PhMe) was added dropwise over 5 min, and the reaction was stirred at –40 °C for 30 min. The reaction was transferred to a cooling bath at 0 °C and stirred for 3 h. The solution was poured into saturated aqueous $NaHCO_3$ (10 mL), whereupon saturated aqueous Rochelle salt (10 mL) was added. The mixture was stirred for 2 h and then extracted with CH_2Cl_2 (3 x 20 mL). The combined organic extracts were dried (Na_2SO_4) and concentrated under reduced pressure, and the crude residue was purified via flash chromatography (SiO_2) eluting with EtOAc/CH_2Cl_2 (30:60 to 60:40) to furnish 87 mg (97%) of **4.63** as a white solid: mp 107-112 °C. IR (neat): ν_{max}/cm^{-1} 3292, 2930, 1619, 1501, 1462, 1337, 1243, 1101, 1049, 907. ^{1}H NMR

(400 MHz, $CDCl_3$) δ 7.91 (s, 1H), 7.51 (d, *J* = 1.3 Hz, 1H), 7.29 (d, *J* = 1.0 Hz, 1H), 7.18 – 7.07 (comp, 2H), 4.13 – 4.00 (comp, 3H), 3.51 (dt, *J* = 10.0, 4.9 Hz, 1H), 3.19 – 3.02 (comp, 2H), 2.79 (s, 3H), 2.60 – 2.46 (comp, 2H), 2.31 – 2.16 (comp, 4H), 1.62 – 1.53 (m, 1H), 1.44 (d, *J* = 6.2 Hz, 3H). ^{13}C NMR (126 MHz, $CDCl_3$) δ 169.1, 135.4, 132.7, 129.0, 121.8, 119.5, 118.4, 110.6, 108.5, 70.6, 64.8, 49.2, 49.0, 37.1, 36.0, 35.0, 20.3, 20.2, 8.9. HRMS (ESI) *m/z* calcd for $C_{19}H_{24}N_2O_2$ $(M+Na)^+$, 335.1730; found 335.1730.

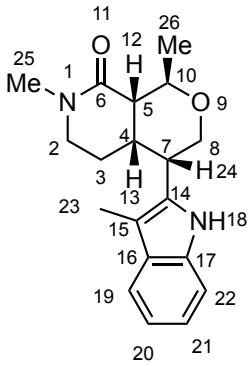

NMR Assignments (**4.63**).^1H NMR (400 MHz, $CDCl_3$) δ 7.91 (s, 1H, 18), 7.51 (d, *J* = 1.3 Hz, 1H, 19), 7.29 (d, *J* = 1.0 Hz, 1H, 22), 7.18 – 7.07 (comp, 2H, 20, 21), 4.13 – 4.00 (comp, 3H, 8, 10), 3.51 (dt, *J* = 10.0, 4.9 Hz, 1H, 24), 3.19 – 3.02 (comp, 2H, 2), 2.79 (s, 3H, 25), 2.60 – 2.46 (comp, 2H, 12, 13), 2.31 – 2.16 (comp, 4H, 3', 23), 1.62 – 1.53 (m, 1H, 3''), 1.44 (d, *J* = 6.2 Hz, 3H, 26). ^{13}C NMR (126 MHz, $CDCl_3$) δ 169.1 (6), 135.4 (14), 132.7 (17), 129.0 (16), 121.8 (21), 119.5 (20), 118.4 (19), 110.6 (22), 108.5 (15), 70.6 (8), 64.8 (10), 49.2 (5), 49.0 (2), 37.1 (7), 36.0 (4), 35.0 (25), 20.3 (3), 20.2 (26), 8.9 (23).

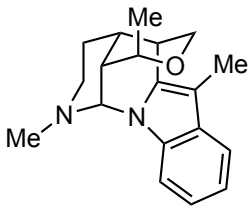

(±)-Alstoscholarisine E (**3.5**) (MDW-4-147). A flask containing tetrahydropyran **4.63** (79 mg, 0.25 mmol) and $IrCl(CO)(PPh_3)_2$ (3.9 mg, 0.0050 mmol) was evacuated and backfilled with N_2 three times, followed by addition of CH_2Cl_2 (5 mL). 1,1,3,3–Tetramethyldisiloxane (99 mg, 0.13 mL, 0.74 mmol) was added and the resulting solution was stirred at room temperature for 2.5 h. The reaction was concentrated under reduced pressure, and the crude residue was purified via flash chromatography (SiO_2) eluting with EtOAc/hexane/Et_3N (20:79:1 to 40:59:1) to provide 58 mg (77%) of **3.5** as a pale yellow solid: mp 119-122 °C (from MeOH) (lit[488] 138–140 °C). IR (neat): ν_{max}/cm^{-1} 2918, 1682, 1456, 1329, 1314, 1132, 1043, 736. 1H NMR (600 MHz, CD_3OD) δ 7.50 (d, *J* = 8.2 Hz, 1H), 7.42 (d, *J* = 7.9 Hz, 1H), 7.04 (td, *J* = 8.2, 1.2 Hz, 1H), 6.98 (td, *J* = 7.9, 1.0 Hz, 1H), 5.39 (d, *J* = 2.5 Hz, 1H), 4.06 (q, *J* = 6.8 Hz, 1H), 3.96 (dd, *J* = 10.4, 1.8 Hz, 1H), 3.40 (dd, *J* = 10.4, 2.6 Hz, 1H), 3.13 (brs, 1H), 2.56 – 2.52 (m, 1H), 2.36 (dd, *J* = 11.7, 5.9 Hz, 1H), 2.29 (s, 3H), 2.23 (s, 3H), 2.19 (brs, 1H), 2.10 – 2.03 (m, 1H), 1.90 (dd, *J* = 12.5, 4.1 Hz, 1H), 1.87 – 1.82 (m, 1H), 1.35 (d, *J* = 6.7 Hz, 3H). ^{13}C NMR (126 MHz, CD_3OD) δ 138.8, 137.0, 130.3, 121.3, 119.8, 118.6, 111.6, 105.1, 73.4, 72.5, 68.9, 47.1, 45.5, 43.5, 36.1, 31.0, 28.6, 18.4, 8.0. HRMS (ESI) *m/z* calcd for $C_{19}H_{24}N_2O$ $(M+H)^+$, 297.1961; found 297.1970.

Table S1. Comparison of ^{1}H-NMR for natural,[488] and synthetic alstoscholarisine E (3.5) in CD_3OD.

	^{1}H NMR (δ in ppm, multiplicity , *J* in Hz)	
Atom	Synthetic (600 MHz)	Natural (600 MHz)
H–18	1.35 (d, J = 6.7 Hz, 3H)	1.32 (d, J = 6.8 Hz, 3H)
H–14'	1.87-1.82 (m, 1H)	1.81 (m, 1H)
H–3'	1.90 (dd, J = 12.5, 4.1 Hz, 1H)	1.85 (td, J = 11.3, 4.0 Hz, 1H)
H–14"	2.10-2.03 (m, 1H)	2.03 (m, 1 H)
H–20	2.19 (brs, 1H)	2.16 (brs, 1H)
H–6	2.23 (s, 3H)	2.21 (s, 3H)
NCH_3	2.29 (s, 3H)	2.26 (s, 3H)
H–3"	2.36 (dd, J = 11.7, 5.9 Hz, 1H)	2.33 (dd, J = 11.3, 6.8 Hz, 1H)
H–15	2.56-2.52 (m, 1H)	2.50 (m, 1H)
H–16	3.13 (brs, 1H)	3.09 (brs, 1H)
H–17'	3.40 (dd, J = 10.4, 2.6 Hz, 1H)	3.37 (dd, J = 10.2, 2.6 Hz, 1H)
H–17"	3.96 (dd, J = 10.4, 1.8 Hz, 1H)	3.92 (dd, J = 10.2, 1.9 Hz, 1H)
H–19	4.06 (q, J = 6.8 Hz, 1H)	4.04 (q, J = 6.8 Hz, 1H)
H–21	5.39 (d, J = 2.5 Hz, 1H)	5.37 (d, J = 2.3 Hz, 1H)
H–10	6.98 (td, J = 7.9, 1.0 Hz, 1H)	6.99 (t, J = 8.0 Hz, 1H)
H–11	7.04 (td, J = 8.2, 1.2 Hz, 1H)	7.04 (t, J = 8.0 Hz, 1H)
H–9	7.42 (d, J = 7.9 Hz, 1H)	7.41 (d, J = 8.0 Hz, 1H)
H–12	7.50 (d, J = 8.2 Hz, 1H)	7.49d, J = 8.0 Hz, 1H)

Table S2. Comparison of ^{13}C-NMR for natural,[488] and synthetic alstoscholarisine E (**3.5**) in CD_3OD.

	^{1}H NMR (δ in ppm, multiplicity , *J* in Hz)	
Atom	Synthetic (600 MHz)	Natural (600 MHz)
C–6	8.0	8.0

C–18	18.4	18.3
C–15	28.6	28.5
C–14	31.0	31.0
C–16	36.1	36.0
C–20	43.5	43.4
NCH_3	45.5	45.5
C–3	47.1	47.1
C–17	68.9	68.8
C–21	72.5	72.4
C–19	73.4	73.3
C–7	105.1	105.0
C–12	111.6	111.6
C–9	118.6	118.6
C–10	119.8	119.8
C–11	121.3	121.3
C–8	130.3	130.2
C–2	137.0	137.0
C–13	138.8	138.7

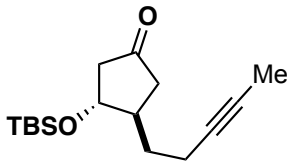

(±)-(3*R*,4*R*)-3-((*tert*-Butyldimethylsilyl)oxy)-4-(pent-3-yn-1-yl)cyclopentan-1-one (**5.20**) (MDW-3-114). *tert*-BuLi (1.3 mL of a 1.5 M solution in pentane) was added dropwise over 2 min to a solution of known iodoalkyne **5.17** (0.183 g, 0.943 mmol) in

Et_2O (1.9 mL) at -78 °C and the reaction was stirred for 2 h.[460] A solution of CuI•0.75DMS (89 mg, 0.38 mmol) and DMS (0.06 mL, 51 mg, 0.82 mmol) in THF (0.5 mL) was added dropwise and the reaction was stirred at – 78 °C for 5 min, whereupon the reaction was transferred to a cooling bath at -40 °C and the mixture was stirred for 20 min. The reaction was cooled to -78 °C and HMPA (0.08 mL, 80 mg, 0.4 mmol) was added followed by dropwise addition of a solution of known 4-silyloxy-cyclopentenone (**5.15**) (50 mg, 0.24 mmol) and TMSCl (50 mg, 0.5 mmol) in THF (1.2 mL) over 20 min.[450] The reaction was stirred for 30 min at -78 °C and was quenched with sequential addition of a solution of saturated aqueous NH_4Cl and aqueous NH_4OH (9:1, 10 mL) and Et_2O (10 mL). After warming to room temperature, the organic layer was separated and washed with saturated aqueous NH_4Cl (1 x 10 mL). The organic layer was separated and the combined aqueous extracts were extracted with Et_2O (2 x 10 mL). The combined organic extracts were dried ($MgSO_4$) and concentrated under reduced pressure. The crude residue was dissolved in THF (1.0 mL) and H_2O (0.1 mL) and glacial AcOH (0.1 mL) were added sequentially. The reaction was stirred for 8 h and was diluted with saturated aqueous $NaHCO_3$ (10 mL), whereupon the solution was extracted with Et_2O (3 x 10 mL). The combined organic extracts were dried ($MgSO_4$) and concentrated under reduced pressure. The crude residue was purified via flash chromatography (SiO_2) eluting with hexanes/Et_2O (93:7 to 80:20) to afford 41 mg (61%) of **5.20** as a pale yellow oil. ^{1}H NMR (400 MHz, $CDCl_3$) δ 4.09 (q, *J* = 6.0 Hz, 1H), 2.60 (ddd, *J* = 18.5, 8.1, 1.7 Hz, 1H), 2.53 – 2.45 (m, 1H), 2.32 – 2.12 (comp, 4H), 1.90 – 1.79 (comp, 2H), 1.77 (t, *J* = 2.5 Hz, 3H), 1.42 – 1.31 (m, 1H), 0.89 (s, 9H), 0.08 (d, *J* = 11.9 Hz, 6H). ^{1}H NMR (400 MHz, $CDCl_3$) δ 4.09 (q, *J* = 6.0 Hz, 1H), 2.60 (ddd, *J* = 18.5, 8.1, 1.7 Hz, 1H), 2.53 – 2.45 (m, 1H), 2.32 – 2.12 (m, 4H), 1.90 – 1.79 (m, 2H), 1.77 (t, *J* = 2.5 Hz, 3H), 1.42 – 1.31 (m, 1H), 0.89 (s, 9H), 0.08 (d, *J* = 11.9 Hz, 6H). ^{13}C NMR (126 MHz, $CDCl_3$) δ

216.1, 78.4, 76.4, 74.6, 47.5, 44.7, 42.7, 32.3, 25.9, 18.1, 17.5, 3.6, -4.5, -4.7. HRMS (ESI) *m/z* calcd for $C_{16}H_{29}O_2Si$ $(M+H)^+$, 281.1937; found 281.1934.

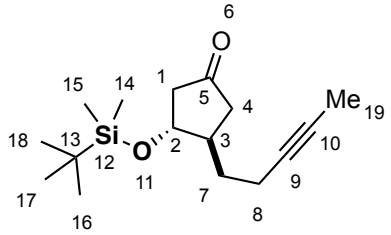

NMR Assignments (**5.20**).^{1}H NMR (400 MHz, $CDCl_3$) δ 4.09 (q, *J* = 6.0 Hz, 1H, 2), 2.60 (ddd, *J* = 18.5, 8.1, 1.7 Hz, 1H, 1), 2.53 – 2.45 (m, 1H, 4''), 2.32 – 2.12 (comp, 4H, 3, 4', 8''), 1.90 – 1.79 (comp, 2H, 1, 7'), 1.77 (t, *J* = 2.5 Hz, 3H, 19), 1.42 – 1.31 (m, 1H, 7''), 0.89 (s, 9H, 16, 17, 18), 0.08 (d, *J* = 11.9 Hz, 6H, 14, 15). ^{13}C NMR (126 MHz, $CDCl_3$) δ 216.1 (5), 78.4 (9), 76.4 (10), 74.6 (2), 47.5 (4), 44.7 (3), 42.7 (1), 32.3 (7), 25.9 (16, 17, 18), 18.1 (13), 17.5 (8), 3.6 (19), -4.5 (14), -4.7 (15).

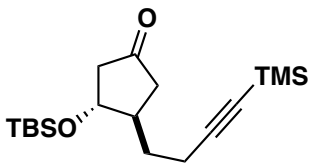

(±)-(3*R*,4*R*)-3-((*tert*-Butyldimethylsilyl)oxy)-4-(4-(trimethylsilyl)but-3-yn-1-yl)cyclopentan-1-one (**5.26**) (MDW-3-217). *tert*-BuLi (8.0 mL of a 1.9 M solution in pentane) was added dropwise via syringe pump over 4 min to a solution of known iodoalkyne **5.23** (2.060 g, 8.169 mmol) in Et_2O (16 mL) at -78 °C and the reaction was stirred for 1 h. *n*-BuLi (2.0 mL of a 2.6 M solution in hexanes) was added to a solution of thiophene (0.39 mL, 0.41 g, 4.9 mmol) in Et_2O (6.0 mL) at 0 °C and the reaction was stirred for 10 min, whereupon the cooling bath was removed and the reaction was stirred at room temperature for 30 min. The freshly prepared 2-thienyllithium solution was cooled to -78 °C and transferred dropwise via cannula to a suspension of CuI•0.75DMS

(1.161 mg, 4.898 mmol) in Et_2O (6.0 mL) at -78 °C and the reaction was stirred for 10 min. The solution of freshly prepared lithiated alkyne **5.24** was allowed to settle at -78 °C and the supernatant was transferred dropwise via cannula to the suspension of CuI•0.75DMS and the mixture was stirred at -78 °C for 10 min, whereupon the reaction was transferred to a cooling bath at -40 °C and the reaction was stirred for 20 min. The reaction was cooled to -78 °C and HMPA (1.3 mL, 1.3 g, 7.3 mmol) was added followed by dropwise addition of a solution of known 4-silyloxy-cyclopentenone (**5.15**) (0.803 g, 3.78 mmol) and TMSCl (1.4 mL, 1.2 g, 11 mmol) in Et_2O (19 mL) over 1 h via syringe pump.[450] The reaction was stirred at -78 °C for 20 min and was quenched with glacial AcOH/H_2O (1:1, 6 mL). The cooling bath was removed and the reaction was stirred for 10 min. The mixture was diluted with saturated aqueous $NaHCO_3$ (50 mL) and the organic layer was separated. The aqueous solution was extracted with Et_2O (3 x 50 mL) and the combined organic extracts were dried ($MgSO_4$) and concentrated under reduced pressure. The crude residue was dissolved in THF (50 mL) and a solution of glacial AcOH/H_2O (1:1, 12 mL) was added. The reaction was stirred at room temperature for 6 h and diluted with saturated aqueous $NaHCO_3$ (100 mL) and Et_2O (100 mL). The organic layer was separated and extracted with saturated aqueous $NaHCO_3$ (3 x 100 mL). The combined aqueous extracts were extracted with Et_2O (2 x 200 mL) and the combined organic extracts were dried ($MgSO_4$) and concentrated under reduced pressure. The crude residue was purified via flash chromatography (SiO_2) eluting with hexanes/Et_2O (95:5 to 88:12) to afford 0.927 g (72%) of **5.26** as a colorless oil. ^{1}H NMR (400 MHz, $CDCl_3$) δ 4.11 (q, J = 5.8 Hz, 1H), 2.61 (ddd, J = 18.4, 8.1, 1.7 Hz, 1H), 2.49 (dd, J = 18.0, 6.0 Hz, 1H), 2.39 – 2.23 (comp, 3H), 2.23 – 2.14 (m, 1H), 1.92 – 1.80 (comp, 2H), 1.47 – 1.36 (m, 1H), 0.89 (s, 9H), 0.15 (s, 9H), 0.08 (d, J = 11.9 Hz, 6H). ^{13}C NMR (126 MHz,

$CDCl_3$) δ 216.1, 106.5, 85.5, 74.6, 47.4, 44.7, 42.6, 32.0, 25.9, 18.6, 18.1, 0.2, -4.4, -4.6. HRMS (ESI) *m/z* calcd for $C_{18}H_{35}O_2Si_2$ $(M+H)^+$, 339.2176; found 339.2179.

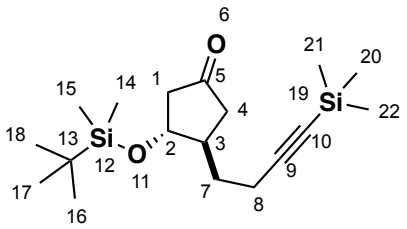

NMR Assignments (**5.26**).^{1}H NMR (400 MHz, $CDCl_2$) δ 4.11 (q, *J* = 5.8 Hz, 1H, 2), 2.61 (ddd, *J* = 18.4, 8.1, 1.7 Hz, 1H, 1''), 2.49 (dd, *J* = 18.0, 6.0 Hz, 1H, 4''), 2.39 – 2.23 (comp, 3H, 3, 8), 2.23 – 2.14 (m, 1H, 4'), 1.92 – 1.80 (comp, 2H, 1', 7''), 1.47 – 1.36 (m, 1H, 7'), 0.89 (s, 9H, 16, 17, 18), 0.15 (s, 9H, 20, 21, 22), 0.08 (d, *J* = 11.9 Hz, 6H, 14, 15). ^{13}C NMR (126 MHz, $CDCl_3$) δ 216.1, 106.5, 85.5, 74.6, 47.4, 44.7, 42.6, 32.0, 25.9, 18.6, 18.1, 0.2, -4.4, -4.6.

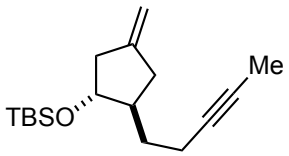

(±)-*tert*-Butyldimethyl(((1*R*,2*R*)-4-methylene-2-(pent-3-yn-1-yl)cyclopentyl)oxy)silane (**5.27**) (MDW-3-217). Petasis reagent (0.87 mL of a 12.3% solution in PhMe) was added to **5.20** (50 mg, 0.18 mmol) in a foil wrapped flask and the reaction was transferred to an oil bath preheated to 65 °C. The reaction was stirred for 8 h and diluted with pentane (5 mL). The mixture was filtered through celite and the filter cake was washed with pentane (30 mL). The combined filtrate and washings were concentrated and the crude residue was purified via flash chromatography (SiO_2) eluting with hexanes/Et_2O (99:1) to afford 23 mg (46%) of **5.27** as a colorless oil. ^{1}H NMR (500 MHz, $CDCl_3$) δ 4.77 (s, 2H), 3.72 (q, *J* = 7.1 Hz, 1H), 2.59 – 2.46 (comp, 2H), 2.25 –

2.02 (comp, 3H), 1.91 – 1.77 (comp, 2H), 1.73 (s, 3H), 1.29 – 1.16 (comp, 2H), 0.84 (s, 9H), 0.01 (d, J = 7.2 Hz, 6H). ^{13}C NMR (126 MHz, $CDCl_3$) δ 148.2, 106.8, 79.3, 78.0, 75.6, 47.0, 42.2, 36.0, 32.7, 26.0, 18.2, 17.6, 3.6, -4.3, -4.6. HRMS (ESI) *m/z* calcd for $C_{17}H_{31}OSi$ $(M+H)^+$, 279.2144; found 279.2146.

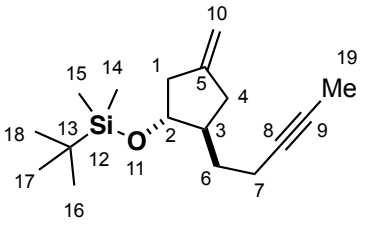

NMR Assignments (**5.27**). ^{1}H NMR (500 MHz, $CDCl_3$) δ 4.77 (s, 2H, 10), 3.72 (q, J = 7.1 Hz, 1H, 2), 2.59 – 2.46 (comp, 2H, 1", 4"), 2.25 – 2.02 (comp, 3H, 1', 7), 1.91 – 1.77 (comp, 2H, 3, 4'), 1.73 (s, 3H, 19), 1.29 – 1.16 (comp, 2H, 6), 0.84 (s, 9H, 16, 17, 18), 0.01 (d, J = 7.2 Hz, 6H, 14, 15). ^{13}C NMR (126 MHz, $CDCl_3$) δ 148.2 (5), 106.8 (10), 79.3 (8), 78.0 (2), 75.6 (9), 47.0 (3), 42.2 (1), 36.0 (4), 32.7 (6), 26.0 (16, 17, 18), 18.2 (13), 17.6 (7), 3.6 (19), -4.3 (14, 15), -4.6.

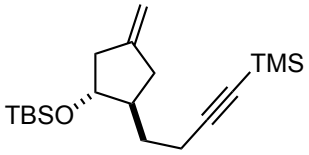

(±)-*tert*-Butyldimethyl(((1*R*,2*R*)-4-methylene-2-(4-(trimethylsilyl)but-3-yn-1-yl)cyclopentyl)oxy)silane (**5.28**) (MDW-3-221). Petasis reagent (11.7 mL of a 12% solution in PhMe) was added to a solution of **5.26** (0.898 g, 2.65 mmol) in PhMe (1.5 mL) in a foil wrapped flask and the reaction was transferred to an oil bath preheated to 65 °C. The reaction was stirred for 7 h and diluted with pentane (5 mL). The mixture was concentrated and filtered through a SiO_2 plug rinsing with hexanes/Et_2O (7:3, 100 mL). The filtrate was concentrated and the crude residue was purified via flash

chromatography (SiO_2) eluting with hexanes/Et_2O (99:1 to 85:15) to afford 0.473 g (53%) of **5.28** as a colorless oil. ^{1}H NMR (400 MHz, $CDCl_3$) δ 4.83 (brs, 2H), 3.77 (q, *J* = 6.9 Hz, 1H), 2.69 – 2.52 (comp, 2H), 2.33 – 2.14 (comp, 3H), 1.98 – 1.73 (comp, 3H), 1.39 – 1.27 (m, 1H), 0.89 (s, 9H), 0.14 (s, 9H), 0.05 (d, *J* = 5.3 Hz, 6H). ^{13}C NMR (126 MHz, $CDCl_3$) δ 148.2, 107.7, 106.9, 84.6, 78.0, 47.1, 42.1, 36.1, 32.2, 26.0, 18.8, 18.2, 0.3, -4.3, -4.6. HRMS (ESI) *m/z* calcd for $C_{19}H_{37}OSi_2$ $(M+H)^+$, 337.2383; found 337.2386.

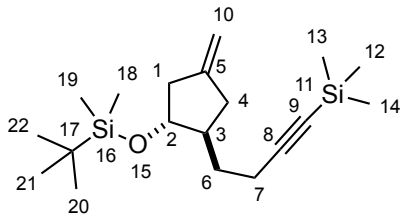

NMR Assignments (**5.28**). ^{1}H NMR (400 MHz, $CDCl_3$) δ 4.83 (brs, 2H, 10), 3.77 (q, *J* = 6.9 Hz, 1H, 2), 2.69 – 2.52 (comp, 2H, 1", 4"), 2.33 – 2.14 (comp, 3H, 1', 7), 1.98 – 1.73 (comp, 3H, 3, 4', 6'), 1.39 – 1.27 (m, 1H, 6"), 0.89 (s, 9H, 20, 21, 22), 0.14 (s, 9H, 12, 13, 14), 0.05 (d, *J* = 5.3 Hz, 6H, 18, 19). ^{13}C NMR (126 MHz, $CDCl_3$) δ 148.2 (5), 107.7 (9), 106.9 (10), 84.6 (8), 78.0 (2), 47.1 (3), 42.1 (1), 36.1 (4), 32.2 (6), 26.0 (6, 20, 21, 22), 18.8 (7), 18.2 (17), 0.3 (12, 13, 14), -4.3 (18), -4.6 (19).

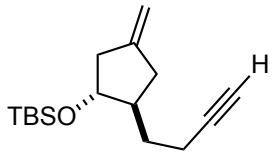

(±)-(((1*R*,2*R*)-2-(but-3-yn-1-yl)-4-methylenecyclopentyl)oxy)(*tert*-butyl)dimethylsilane (**5.29**) (MDW-3-214). A solution of **5.29** (0.147 g, 0.437 mmol) and K_2CO_3 (0.121 g, 0.875 mmol) in MeOH (4.4 mL) was stirred for 15 h at room temperature. The reaction was concentrated under reduced pressure and the crude residue

was dissolved in Et_2O (10 mL). The solution was washed with saturated aqueous $NaHCO_3$ (1 x 10 mL). The organic layer was separated and the aqueous solution was extracted with Et_2O (2 x 10 mL). The combined organic extracts were dried ($MgSO_4$) and concentrated under reduced pressure. The crude residue was purified via flash chromatography (SiO_2) eluting with hexanes/Et_2O (99:1) to afford 0.108 g (94%) of **5.29** as a colorless oil. ^1H NMR (400 MHz, $CDCl_3$) δ 4.83 (brs, 2H), 3.76 (q, *J* = 7.2 Hz, 1H), 2.65 – 2.53 (comp, 2H), 2.31 – 2.13 (comp, 3H), 1.99 – 1.78 (comp, 4H), 1.40 – 1.28 (m, 1H), 0.89 (s, 9H), 0.06 (d, *J* = 5.2 Hz, 6H). ^{13}C NMR (126 MHz, $CDCl_3$) δ 147.9, 107.0, 84.7, 78.0, 68.4, 46.9, 42.2, 35.9, 32.1, 26.0, 18.2, 17.4, -4.3, -4.6. HRMS (ESI) *m/z* calcd for $C_{16}H_{29}OSi$ $(M+H)^+$, 265.1988; found 265.1996.

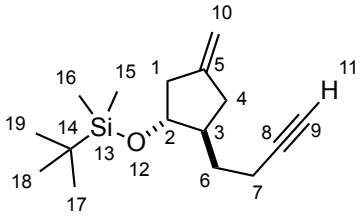

NMR Assignments (**5.29**). ^1H NMR (400 MHz,$CDCl_3$) δ 4.83 (brs, 2H, 10), 3.76 (q, *J* = 7.2 Hz, 1H, 2), 2.65 – 2.53 (comp, 2H, 1", 4"), 2.31 – 2.13 (comp, 3H, 1', 7), 1.99 – 1.78 (comp, 4H, 3, 4', 6", 11), 1.40 – 1.28 (m, 1H, 6'), 0.89 (s, 9H, 17, 18, 19), 0.06 (d, *J* = 5.2 Hz, 6H, 15, 16). ^{13}C NMR (126 MHz, $CDCl_3$) δ 147.9 (5), 107.0 (10), 84.7 (8), 78.0 (2), 68.4 (9), 46.9 (3), 42.2 (1), 35.9 (4), 32.1 (6), 26.0 (17, 18, 19), 18.2 (14), 17.4 (7), -4.3 (15), -4.6 (16).

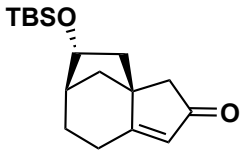

(±)-(3a*S*,5*R*,6*R*)-5-((*tert*-butyldimethylsilyl)oxy)-5,6,7,8-tetrahydro-3*H*-3a,6-methanoazulen-2(4*H*)-one (**5.42**) (MDW-3-214). A solution of **5.27** (0.159 g, 0.601 mmol) and dicobalt octacarbonyl (0.216 g, 0.632 mmol) in pentane (6 mL) was stirred for 2 h at room temperature and concentrated under reduced pressure. The crude residue was filtered through a SiO_2 plug washing with hexanes/Et_2O (99:1, 50 mL) and the filtrate was concentrated to afford 0.303 g (91% mass recovery) of **5.43** as a dark red oil that was used directly. A portion of the crude residue (28 mg, 0.051 mmol) was dissolved in PhMe (1.0 mL) and heated under microwave irradiation at 130 °C for 2.5 h. The solution was filtered through a SiO_2 plug washing with hexanes (20 mL) and discarding the flow through. The SiO_2 plug was then washed with hexanes/EtOAc (50 mL) and the collected filtrate was concentrated under reduced pressure. The crude residue was purified via flash chromatography (SiO_2) eluting with hexanes/EtOAc (95:5 to 85:15) to afford 3.0 mg (20%) of **5.42** as a pale yellow oil. ^{1}H NMR (500 MHz, $CDCl_3$) δ 5.58 (s, 1H), 4.11 (dd, *J* = 7.0, 2.9 Hz, 1H), 2.62 (dd, *J* = 16.0, 6.5 Hz, 1H), 2.41 – 2.31 (comp, 2H), 2.26 – 2.15 (comp, 2H), 2.12 (q, *J* = 3.2, 2.5 Hz, 1H), 2.07 (ddd, *J* = 13.9, 6.8, 2.0 Hz, 1H), 1.78 (ddd, *J* = 14.2, 7.3, 4.2 Hz, 1H), 1.68 (dd, *J* = 13.8, 2.9 Hz, 1H), 1.55 – 1.52 (m, 1H), 1.28 (d, *J* = 11.1 Hz, 1H), 0.83 (s, 9H), 0.01 (s, 3H), -0.00 (s, 3H). ^{13}C NMR (126 MHz, $CDCl_3$) δ 207.5, 185.6, 123.2, 50.6, 46.0, 44.0, 43.4, 40.4, 27.7, 24.8, 24.0, 17.1, -0.0, -5.7. HRMS (ESI) *m/z* calcd for $C_{17}H_{29}O_2Si$ $(M+H)^+$, 293.1937; found 293.1936.

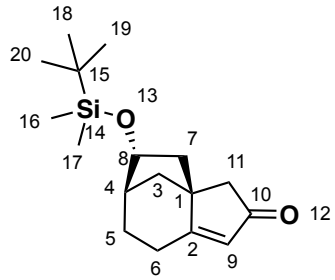

NMR Assignments (**5.42**). ^{1}H NMR (500 MHz, $CDCl_3$) δ 5.58 (s, 1H, 9), 4.11 (dd, *J* = 7.0, 2.9 Hz, 1H, 8), 2.62 (dd, *J* = 16.0, 6.5 Hz, 1H, 6'), 2.41 – 2.31 (comp, 2H, 7), 2.26 – 2.15 (comp, 2H, 3", 6"), 2.12 (q, *J* = 3.2, 2.5 Hz, 1H, 4), 2.07 (ddd, *J* = 13.9, 6.8, 2.0 Hz, 1H, 11"), 1.78 (ddd, *J* = 14.2, 7.3, 4.2 Hz, 1H, 5"), 1.68 (dd, *J* = 13.8, 2.9 Hz, 1H, 11'), 1.55 – 1.52 (m, 1H, 5'), 1.28 (d, *J* = 11.1 Hz, 1H, 3'), 0.83 (s, 9H, 18, 19, 20), 0.01 (s, 3H, 16), -0.00 (s, 3H, 17). ^{13}C NMR (126 MHz, $CDCl_3$) δ 207.5 (10), 185.6 (2), 123.2 (9), 50.6 (1), 46.0 (11), 44.0, 43.4 (7), 40.4 (3), 27.7 (5), 24.8 (18, 19, 20), 24.0 (6), 17.1 (15), -0.0 (16), -5.7 (17).

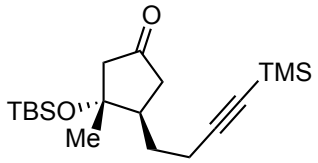

5.47
major diastereomer

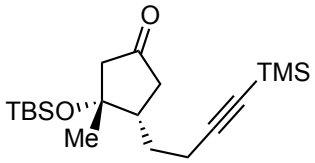

S.2
minor diastereomer

(3*R*,4*R*)-3-((*tert*-Butyldimethylsilyl)oxy)-3-methyl-4-(4-(trimethylsilyl)but-3-yn-1-yl)cyclopentan-1-one (**5.47**) (MDW-4-206). *tert*-BuLi (10.2 mL of a 2.4 M solution in pentane) was added dropwise via syringe pump over 4 min to a solution of known iodoalkyne **5.23** (2.942 g, 11.67 mmol) in degassed Et_2O (23 mL) at -78 °C and the reaction was stirred for 1 h. *n*-BuLi (2.2 mL of a 3.4 M solution in hexanes) was added to a solution of thiophene (0.55 mL, 0.58 g, 6.9 mmol) in degassed Et_2O (6.0 mL) at 0 °C and the reaction was stirred for 15 min, whereupon the cooling bath was removed and the reaction was stirred at room temperature for 30 min. The freshly prepared 2-thienyllithium solution was cooled to -78 °C and transferred dropwise via cannula over 10 min to a suspension of CuI•0.75DMS (1.629 g, 6.872 mmol) in degassed Et_2O (8.6 mL) at -78 °C and the reaction was stirred for 10 min. The solution of freshly prepared lithiated alkyne **5.24** was allowed to settle at -78 °C and the supernatant was transferred

dropwise via cannula to the suspension of CuI•0.75DMS and the mixture was stirred at -78 °C for 10 min, whereupon the reaction was transferred to a cooling bath at -40 °C and the reaction was stirred for 20 min. The reaction was cooled to -78 °C and HMPA (1.8 mL, 1.9 g, 10 mmol) was added, followed by dropwise addition of a solution of known 4-silyloxy-cyclopentenone (**5.11**) (1.196 g, 5.283 mmol) and TMSCl (2.0 mL, 1.7 g, 16 mmol) in degassed Et_2O (23 mL) over 1.5 h via syringe pump.[450] The reaction was stirred at -78 °C for 20 min and was diluted with THF (20 mL) followed by slow addition of glacial AcOH/H_2O (1:1, 13 mL). The cooling bath was removed and the reaction was stirred for 12 h. The solution was diluted with Et_2O (50 mL) and extracted with saturated aqueous NH_4Cl/NH_4OH (9:1, 3 x 50 mL). The combined aqueous extracts were extracted with Et_2O (2 x 100 mL) and the combined organic extracts were dried ($MgSO_4$) and concentrated under reduced pressure. The crude residue was filtered through a SiO_2 plug washing with hexanes/Et_2O (95:5, 200 mL) to afford 1.202 g of a residue containing the silyl enol ether intermediate **5.46**. The SiO_2 plug was washed with hexanes/Et_2O (90:10, 200 mL) to afford 0.7420 g of a residue containing **5.47** (mixture of diastereomers). The residue containing the silyl enol ether intermediate **5.46** (1.202 g) was dissolved in THF (28 mL), whereupon glacial AcOH/H_2O (1:1, 4.7 mL) was added and the reaction was stirred for 22 h. The reaction was diluted with saturated aqueous $NaHCO_3$ (50 mL) and extracted with Et_2O (3 x 50 mL). The combined organic extracts were dried ($MgSO_4$) and concentrated under reduced pressure. The crude residue was combined with the residue containing **5.47** (0.7420 g) that was previously collected and was purified via flash chromatography (SiO_2) eluting with hexanes/Et_2O (95:5 to 90:10) to afford 1.191 g (64%) of **5.47** as a pale yellow oil and 56 mg (3%) of **S.2** as a pale yellow oil.

Compound **5.47**. ^{1}H NMR (400 MHz, $CDCl_3$) δ 2.58 (dd, J = 18.8, 8.4 Hz, 1H), 2.46 – 2.29 (comp, 4H), 2.28 – 2.18 (m, 1H), 1.95 – 1.83 (comp, 2H), 1.44 – 1.31 (m,

1H), 1.24 (s, 3H), 0.86 (s, 9H), 0.14 (s, 9H), 0.09 (d, J = 6.8 Hz, 6H). ^{13}C NMR (126 MHz, $CDCl_3$) δ 215.6, 106.6, 85.3, 79.1, 54.9, 47.7, 42.7, 28.9, 25.8, 23.3, 18.9, 18.0, 0.2, -2.2, -2.4. HRMS (CI) *m/z* calcd for $C_{19}H_{37}O_2Si$ $(M+H)^+$, 353.2332; found 353.2321.

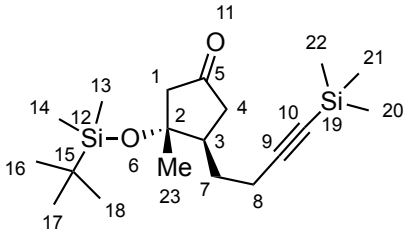

NMR Assignments (**5.47**). ^{1}H NMR (400 MHz, $CDCl_3$) δ 2.58 (dd, J = 18.8, 8.4 Hz, 1H, 4''), 2.46 – 2.29 (comp, 4H, 1, 3, 8''), 2.28 – 2.18 (m, 1H, 8'), 1.95 – 1.83 (comp, 2H, 4', 7'), 1.44 – 1.31 (m, 1H, 7''), 1.24 (s, 3H, 23), 0.86 (s, 9H, 16, 17, 18), 0.14 (s, 9H, 20, 21, 22), 0.09 (d, J = 6.8 Hz, 6H, 13, 14). ^{13}C NMR (126 MHz, $CDCl_3$) δ 215.6 (5), 106.6 (10), 85.3 (9), 79.1 (2), 54.9 (1), 47.7 (3), 42.7 (4), 28.9 (7), 25.8 (16, 17, 18), 23.3 (23), 18.9 (8), 18.0 (15), 0.2 (20, 21, 22), -2.2 (13), -2.4 (14).

NOE Correlations (**5.47**).

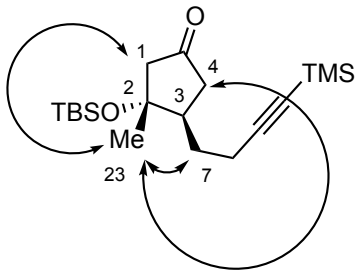

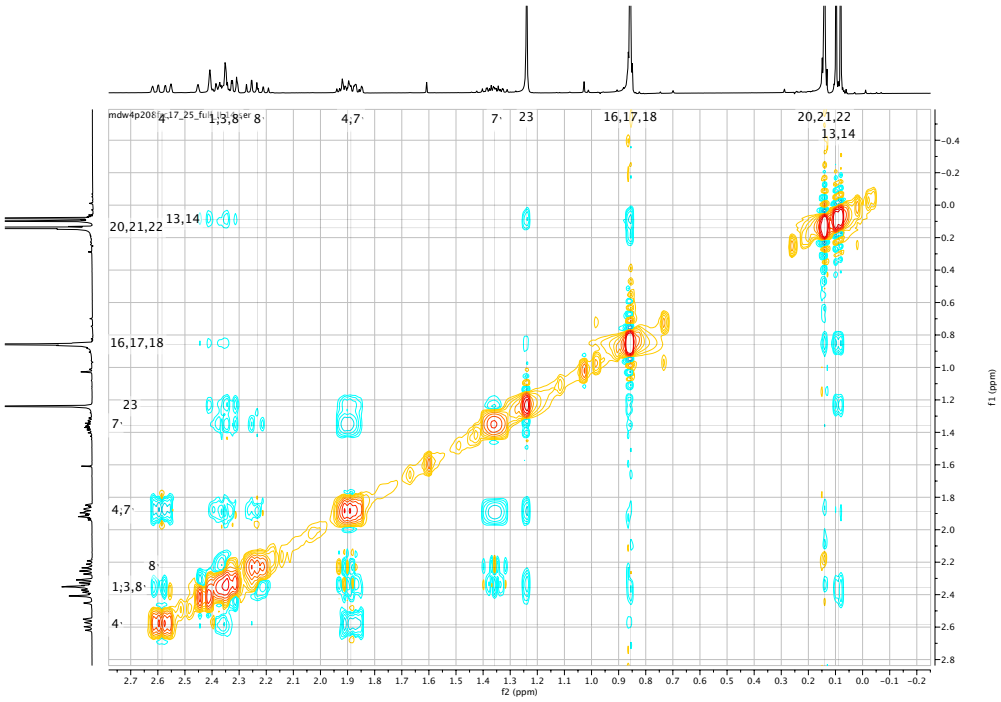

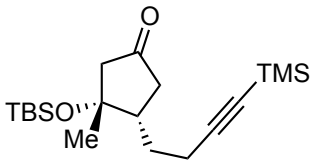

S.??

(3*R*,4*S*)-3-((*tert*-butyldimethylsilyl)oxy)-3-methyl-4-(4-(trimethylsilyl)but-3-yn-1-yl)cyclopentan-1-one (**S.2**). ^{1}H NMR (400 MHz, $CDCl_3$) δ 2.47 – 2.40 (m, 2H), 2.39 – 2.30 (m, 1H), 2.27 (d, *J* = 17.6 Hz, 1H), 2.23 – 2.13 (m, 1H), 2.12 – 2.03 (m, 2H), 1.97 – 1.82 (m, 1H), 1.66 – 1.55 (m, 1H), 1.45 (s, 3H), 0.83 (s, 9H), 0.14 (s, 9H), 0.08 (d, *J* = 11.8 Hz, 6H). ^{13}C NMR (126 MHz, $CDCl_3$) δ 216.6, 107.0, 85.3, 79.7, 55.2, 47.9, 42.5, 27.7, 25.9, 25.2, 18.9, 18.3, 0.3, -2.2, -2.5. HRMS (ESI) *m/z* calcd for $C_{19}H_{36}O_2Si_2$ $(M+Na)^+$, 375.2146; found 375.2151.

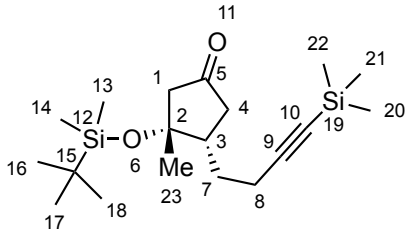

NMR Assignments (**S.2**). ^{1}H NMR (400 MHz, $CDCl_3$) δ 2.47 – 2.40 (comp, 2H, 1', 4'), 2.39 – 2.30 (m, 1H, 8''), 2.27 (d, *J* = 17.6 Hz, 1H, 1''), 2.23 – 2.13 (m, 1H, 8'), 2.12 – 2.03 (comp, 2H, 3, 4''), 1.97 – 1.82 (m, 1H, 7'), 1.66 – 1.55 (m, 1H, 7''), 1.45 (s, 3H, 23), 0.83 (s, 9H, 16, 17, 18), 0.14 (s, 9H, 20, 21, 22), 0.08 (d, *J* = 11.8 Hz, 6H, 13, 14).^{13}C NMR (126 MHz, $CDCl_3$) δ 216.6 (5), 107.0 (10), 85.3 (9), 79.7 (2), 55.2 (1), 47.9 (3), 42.5 (4), 27.7 (7), 25.9 (16, 17, 18), 25.2 (23), 18.9 (8), 18.3 (15), 0.3 (20, 21, 22), -2.2 (13), -2.5 (14).

NOE Correlations (**S.2**).

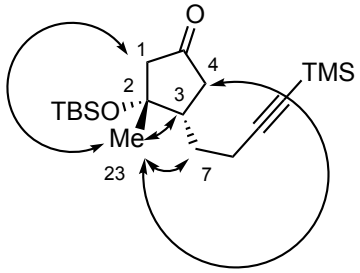

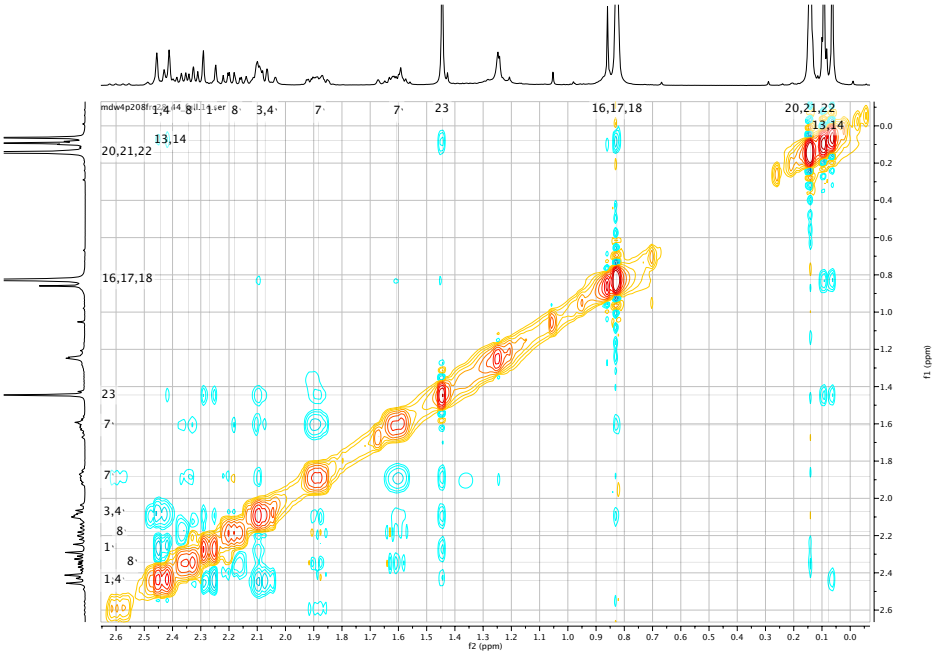

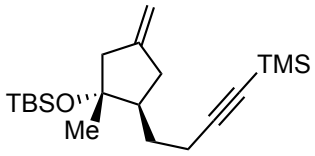

***tert*-Butyldimethyl(((1*R*,2*R*)-1-methyl-4-methylene-2-(4-(trimethylsilyl)but-3-yn-1-yl)cyclopentyl)oxy)silane** (**5.48**) (MDW-4-196). Petasis reagent (1.2 mL of a 16% solution in PhMe) was added to **5.47** (0.111 g, 0.315 mmol) in a foil wrapped flask and the reaction was transferred to an oil bath preheated to 65 °C and stirred for 8 h. The reaction was filtered through a SiO_2 plug rinsing with hexanes/Et_2O (7:3, 100 mL). The filtrate was concentrated and the crude residue was purified via flash chromatography (SiO_2) eluting with hexanes/Et_2O (99:1 to 85:15) to afford 71 mg (64%) of **5.48** as a colorless oil. ^{1}H NMR (400 MHz, Chloroform-*d*) δ 4.86 – 4.82 (m, 1H), 4.81 – 4.75 (m, 1H), 2.60 (dd, *J* = 16.8, 8.5 Hz, 1H), 2.49 (dd, *J* = 15.6, 2.9 Hz, 1H), 2.37 – 2.17 (comp,

3H), 2.10 – 1.99 (m, 1H), 1.88 – 1.71 (comp, 2H), 1.37 – 1.27 (m, 1H), 1.08 (d, J = 0.9 Hz, 3H), 0.86 (s, 9H), 0.15 (s, 9H), 0.08 (s, 6H). ^{13}C NMR (126 MHz, $CDCl_3$) δ 147.9, 107.5, 106.6, 84.1, 80.8, 49.5, 49.4, 35.3, 28.7, 25.6, 22.2, 18.7, 17.8, -0.0, -2.4, -2.6. HRMS (CI) *m/z* calcd for $C_{20}H_{38}OSi_2$ $(M+H)^+$, 350.2461; found 350.2452.

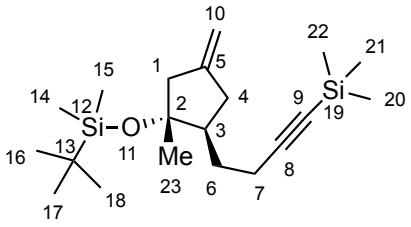

NMR Assignments (**5.48**). ^{1}H NMR (400 MHz, $CDCl_3$) δ 4.86 – 4.82 (m, 1H, 10''), 4.81 – 4.75 (m, 1H, 10'), 2.60 (dd, J = 16.8, 8.5 Hz, 1H, 4'), 2.49 (dd, J = 15.6, 2.9 Hz, 1H, 1''), 2.37 – 2.17 (comp, 3H, 1', 7), 2.10 – 1.99 (m, 1H, 3), 1.88 – 1.71 (comp, 2H, 4'', 6''), 1.37 – 1.27 (m, 1H, 6'), 1.08 (d, J = 0.9 Hz, 3H, 23), 0.86 (s, 9H, 16, 17, 18), 0.15 (s, 9H, 20, 21, 22), 0.08 (s, 6H, 14, 15). ^{13}C NMR (126 MHz, $CDCl_3$) δ 147.9 (5), 107.5 (9), 106.6 (10), 84.1 (8), 80.8 (2), 49.5 (3), 49.4 (1), 35.3 (4), 28.7 (6), 25.6 (16, 17, 18), 22.2 (23), 18.7 (7), 17.8 (13), -0.0 (20, 21, 22), -2.4 (14), -2.6 (15).

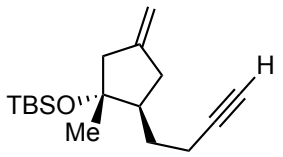

(((1*R*,2*R*)-2-(But-3-yn-1-yl)-1-methyl-4-methylenecyclopentyl)oxy)(*tert*-butyl)dimethylsilane (**5.49**) (MDW-4-198). A solution of **5.48** (0.125 g, 0.256 mmol) and K_2CO_3 (99 mg, 0.72 mmol) in MeOH (3.6 mL) was stirred for 16 h at room temperature. The reaction was concentrated under reduced pressure and the crude residue was dissolved in Et_2O (10 mL). The solution was washed with saturated aqueous $NaHCO_3$ (1 x 10 mL). The organic layer was separated and the aqueous solution was

extracted with Et_2O (2 x 10 mL). The combined organic extracts were dried ($MgSO_4$) and concentrated under reduced pressure. The crude residue was purified via flash chromatography (SiO_2) eluting with hexanes/Et_2O (99:1) to afford 92 mg (92%) of **5.49** as a colorless oil. ^{1}H NMR (400 MHz, $CDCl_3$) δ 4.87 – 4.82 (m, 1H), 4.81 – 4.76 (m, 1H), 2.59 (dd, *J* = 16.7, 8.4 Hz, 1H), 2.50 (dd, *J* = 15.2, 2.8 Hz, 1H), 2.35 (dq, *J* = 15.4, 1.5 Hz, 1H), 2.31 – 2.14 (comp, 2H), 2.10 – 2.00 (m, 1H), 1.94 (t, *J* = 2.6 Hz, 1H), 1.89 – 1.73 (comp, 2H), 1.40 – 1.31 (m, 1H), 1.09 (d, *J* = 1.0 Hz, 3H), 0.86 (s, 9H), 0.07 (d, *J* = 0.9 Hz, 6H). ^{13}C NMR (126 MHz, $CDCl_3$) δ 148.0, 107.1, 85.0, 81.0, 68.3, 49.8, 49.7, 35.6, 28.9, 25.9, 22.4, 18.1, 17.7, -2.1, -2.3. HRMS (CI) *m/z* calcd for $C_{17}H_{30}OSi$ $(M+H)^+$, 278.2066; found 278.2064.

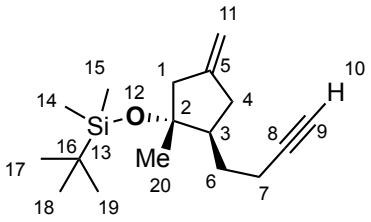

NMR Assignments (**5.49**). ^{1}H NMR (400 MHz, $CDCl_3$) δ 4.87 – 4.82 (m, 1H, 11''), 4.81 – 4.76 (m, 1H, 11'), 2.59 (dd, *J* = 16.7, 8.4 Hz, 1H, 4''), 2.50 (dd, *J* = 15.2, 2.8 Hz, 1H, 1''), 2.35 (dq, *J* = 15.4, 1.5 Hz, 1H, 1'), 2.31 – 2.14 (comp, 2H, 7), 2.10 – 2.00 (m, 1H, 3), 1.94 (t, *J* = 2.6 Hz, 1H, 10), 1.89 – 1.73 (comp, 2H, 4', 6''), 1.40 – 1.31 (m, 1H, 6'), 1.09 (d, *J* = 1.0 Hz, 3H, 20), 0.86 (s, 9H, 17, 18, 19), 0.07 (d, *J* = 0.9 Hz, 6H, 14, 15). ^{13}C NMR (126 MHz, $CDCl_3$) δ 148.0 (5), 107.1 (11), 85.0 (8), 81.0 (2), 68.3 (9), 49.8 (3), 49.7 (1), 35.6 (4), 28.9 (6), 25.9, 22.4 (20), 18.1 (16), 17.7 (7), -2.1 (14), -2.3 (15).

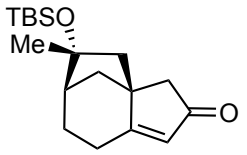

(3a*S*,5*R*,6*R*)-5-((*tert*-Butyldimethylsilyl)oxy)-5-methyl-5,6,7,8-tetrahydro-3*H*-3a,6-methanoazulen-2(4*H*)-one (**5.51**) (MDW-4-199). A solution of **5.49** (8.4 mg, 0.030 mmol) and dicobalt octacarbonyl (13 mg, 0.038 mmol) in PhMe (0.6 mL) was stirred for 2 h at room temperature and concentrated under reduced pressure. The crude residue was filtered through a SiO_2 plug washing with pentane (30 mL) and the filtrate was concentrated to afford 13 mg (76% mass recovery) of **5.50** as a dark red oil that was used directly. The crude residue (13 mg, 0.022 mmol) was dissolved in PhMe (0.6 mL) and heated under microwave irradiation at 130 °C for 4 h. The solution was concentrated and the crude residue was purified via preparative TLC eluting with hexanes/EtOAC (85:15) to afford 0.97 mg (11% from **5.49**) of **5.51** as a pale yellow oil. ^{1}H NMR (600 MHz, $CDCl_3$) δ 5.64 (d, *J* = 2.0 Hz, 1H), 2.69 (dd, *J* = 16.6, 7.2 Hz, 1H), 2.53 (ddd, *J* = 11.1, 4.8, 2.2 Hz, 1H), 2.45 – 2.35 (m, 3H), 2.10 (d, *J* = 3.9 Hz, 1H), 2.04 (dd, *J* = 14.2, 1.6 Hz, 1H), 1.92 – 1.85 (m, 1H), 1.81 (dd, *J* = 14.2, 1.9 Hz, 1H), 1.66 – 1.62 (m, 1H), 1.45 (s, 3H), 1.37 (dd, *J* = 11.1, 1.7 Hz, 1H), 0.87 (s, 9H), 0.10 (d, *J* = 11.5 Hz, 6H). ^{13}C NMR (151 MHz, $CDCl_3$) δ 208.7, 187.7, 123.7, 83.2, 52.5, 51.2, 48.9, 46.0, 43.5, 26.6, 25.9, 24.9, 24.6, 18.1, -2.1. HRMS (CI) *m/z* calcd for $C_{18}H_{31}O_2Si$ $(M+H)^+$, 307.2093; found 307.2090.

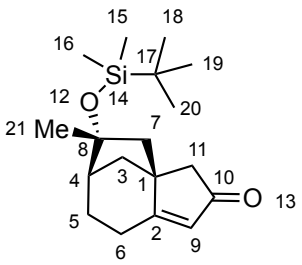

NMR Assignments (**5.51**). ^{1}H NMR (600 MHz, $CDCl_3$) δ 5.64 (d, *J* = 2.0 Hz, 1H, 9), 2.69 (dd, *J* = 16.6, 7.2 Hz, 1H, 6''), 2.53 (ddd, *J* = 11.1, 4.8, 2.2 Hz, 1H, 3''), 2.45 – 2.35 (comp, 3H, 6', 7), 2.10 (d, *J* = 3.9 Hz, 1H, 4), 2.04 (dd, *J* = 14.2, 1.6 Hz, 1H, 11'), 1.92 – 1.85 (m, 1H, 5''), 1.81 (dd, *J* = 14.2, 1.9 Hz, 1H, 11''), 1.66 – 1.62 (m, 1H, 5'), 1.45 (s, 3H, 21), 1.37 (dd, *J* = 11.1, 1.7 Hz, 1H, 3'), 0.87 (s, 9H, 18, 19, 20), 0.10 (d, *J* = 11.5 Hz, 6H, 15, 16). ^{13}C NMR (151 MHz, $CDCl_3$) δ 208.7 (10), 187.7 (2), 123.7 (9), 83.2 (8), 52.5 (11), 51.2 (1), 48.9 (4), 46.0 (7), 43.5 (3), 26.6 (5), 25.9 (18, 19, 20), 24.9 (21), 24.6 (6), 18.1 (17), -2.1 (15, 16).

6.3 HPLC TRACES FOR ENANTIOENRICHED (*S*)-2.127 AND (*R*)-*2.128*.

Chiralcel OD: 5% *i*-PrOH/hexanes, 0.7 mL/min, obs:250 nm.

Racemic (±)-**2.26**:

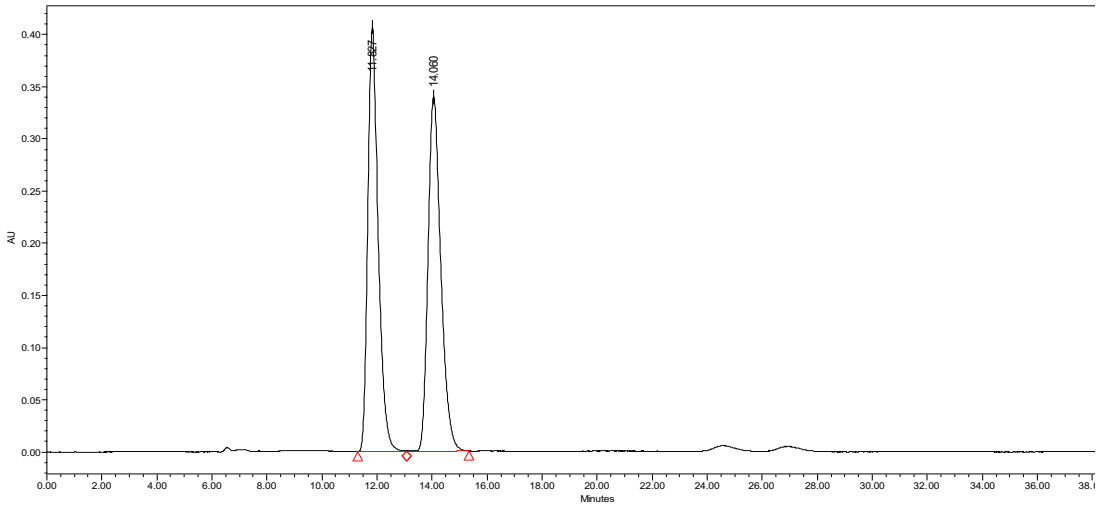

	Retention time (min)	Area (μV*sec)	% area	Height (μV)	Int Type
1	11.827	10907640	50.07	407227	bb
2	14.060	10675181	49.93	340180	bb

Enantioenriched (*S*)-**2.127**:

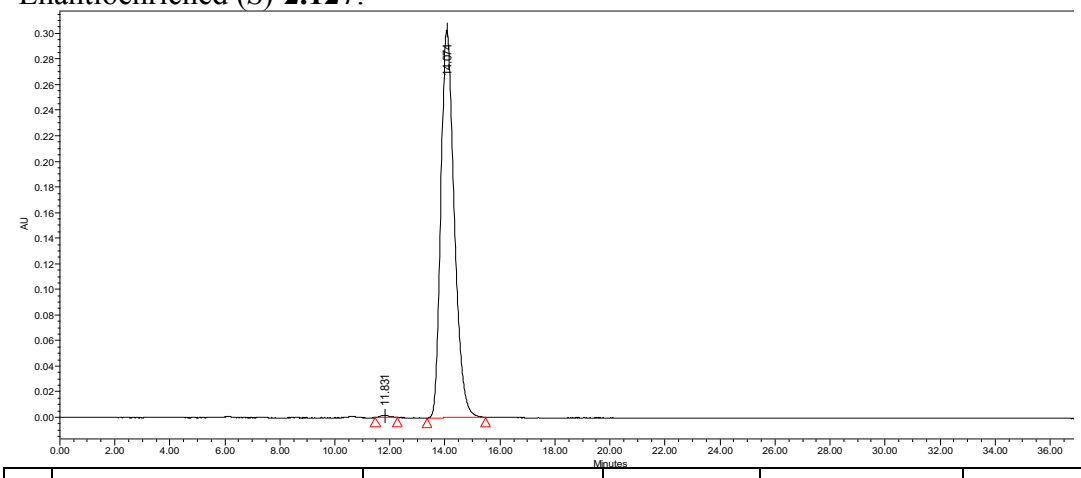

	Retention time (min)	Area (μV*sec)	% area	Height (μV)	Int Type
1	11.831	43484	0.42	1685	bb
2	14.074	10355600	99.58	302813	bb

Enantioenriched (*R*)-2.118:

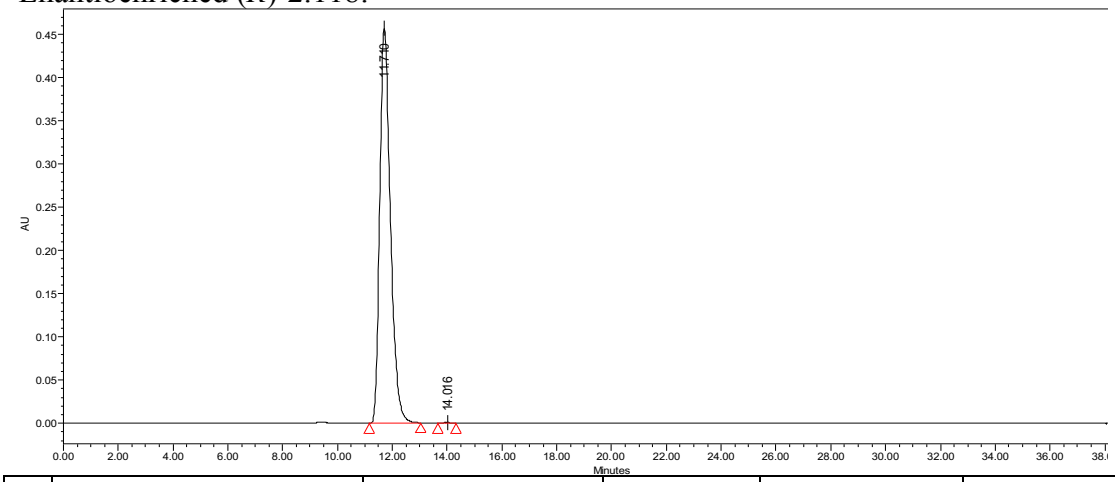

	Retention time (min)	Area (μV*sec)	% area	Height (μV)	Int Type
1	11.710	12350948	99.9	456831	bb
2	14.016	11908	0.1	562	bb

6.4 JVW-1601 Binding Profile at Non-Sigma Receptor Sites

Table S.1. JVW-1601 binding profile at non-sigma receptor sites.

Target	K_i (nM)	Target	K_i (nM)
$5HT_{1A}$	156	Beta3	>10,000
$5HT_{1B}$	362	BZP Rat Brain	>10,000
$5HT_{1D}$	135	Calcium Channel	>10,000
$5HT_{1e}$	>10,000	D_1	690
$5HT_{2A}$	315	D_2	>10,000
$5HT_{2B}$	100	D_3	438
$5HT_{2C}$	762	D_4	6,660
$5HT_3$	>10,000	D_5	3,964
$5HT_{5a}$	NA	DOR	>10,000
$5HT_6$	778	GabaA	>10,000
$5HT_7$	459	H_1	20
A2B2	NA	H_3	1,351
A2B4	NA	hERG	NA
A3B2	NA	KOR	>10,000
A3B4	NA	M_1	>10,000
A4B2	NA	M_2	>10,000
A4B2**	NA	M_3	>10,000
A4B4	NA	M_4	>10,000
A7	NA	M_5	6,621
A7**	NA	MOR	>10,000
$Alpha_{1a}$	2,356	NET	>10,000
$Alpha_{1b}$	>10,000	NMDA	NA
$Alpha_{1d}$	2,595	PBR	8,325
$Alpha_{2a}$	1,031	SERT	>10,000
$Alpha_{2b}$	3,326	Sig1	200
$Alpha_{2c}$	> 10,000	V1A	NA
AMPA	NA	V1B	NA
Beta1	>10,000	V2	NA
Beta2	>10,000		

Appendix A: Crystallographic Data

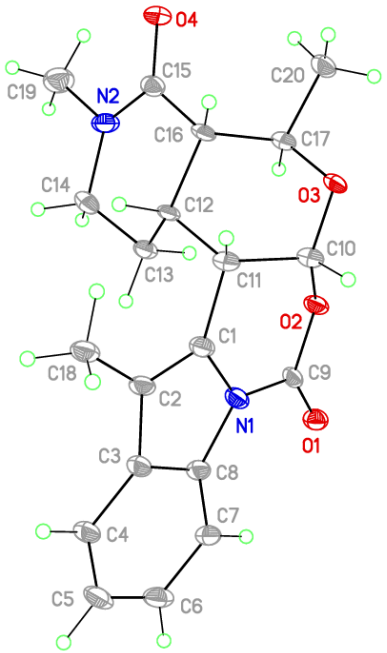

Figure A.1. Crystal structure of **4.61** Showing the atom labeling scheme. Displacement ellipsoids are scaled to the 50% probability level

X-ray Experimental for $C_{20}H_{22}N_2O_4$: Crystals grew as clusters of colorless needles by slow evaporation from THF and water. The data crystal was cut from a cluster of crystals and had approximate dimensions; 0.18 x 0.048 x 0.038 mm. The data were collected on an Agilent Technologies SuperNova Dual Source diffractometer using a μ-focus Cu Kα radiation source (λ = 1.5418Å) with collimating mirror monochromators. A total of 669 frames of data were collected using ω-scans with a scan range of 1° and a counting time of 15.9 seconds per frame for frames collected with a detector offset of - 42.4° and 58.47 seconds per frame with frames collected with a

detector offset of 110.8°. The data were collected at 100 K using an Oxford Cryostream low temperature device. Details of crystal data, data collection and structure refinement are listed in Table 1. Data collection, unit cell refinement and data reduction were performed using Rigaku Oxford Diffraction's CrysAlisPro V 1.171.40.53.[489] The structure was solved by direct methods using SHELXT[490] and refined by full-matrix least-squares on F2 with anisotropic displacement parameters for the non-H atoms using SHELXL-2016/6.[490] Structure analysis was aided by use of the programs PLATON[491], OLEX2[492] and WinGX.6[493] The hydrogen atoms on the carbon atoms were calculated in ideal positions with isotropic displacement parameters set to 1.2xUeq of the attached atom (1.5xUeq for methyl hydrogen atoms).

The function, Σw(|Fo|2 - |Fc|2)2, was minimized, where w = 1/[(σ (Fo))2 + (0.0759*P)2 + (0.5009*P)] and P = (|Fo|2 + 2|Fc|2)/3. Rw(F2) refined to 0.115, with R(F) equal to 0.0439 and a goodness of fit, S, = 1.05. Definitions used for calculating R(F), Rw(F2) and the goodness of fit, S, are given below.[494] The data were checked for secondary extinction effects but no correction was necessary. Neutral atom scattering factors and values used to calculate the linear absorption coefficient are from the International Tables for X-ray Crystallography (1992).[495] All figures were generated using SHELXTL/PC.[496] Tables of positional and thermal parameters, bond lengths and angles, torsion angles and figures are found elsewhere.

Table A.1. Crystal data and structure refinement for **4.61.**

Empirical formula	C20 H22 N2 O4	
Formula weight	354.39	
Temperature	100(2) K	
Wavelength	1.54184 Å	
Crystal system	monoclinic	
Space group	C c	
Unit cell dimensions	a = 13.4799(5) Å	α= 90°.
	b = 10.2973(3) Å	β= 111.392(4)°.
	c = 13.3063(4) Å	γ = 90°.
Volume	1719.76(11) $Å^3$	
Z	4	
Density (calculated)	1.369 Mg/m^3	
Absorption coefficient	0.785 mm^{-1}	
F(000)	752	
Crystal size	0.180 x 0.048 x 0.038 mm^3	
Theta range for data collection	5.557 to 70.060°.	
Index ranges	-15<=h<=16, -12<=k<=9, -16<=l<=16	
Reflections collected	3270	
Independent reflections	2242 [R(int) = 0.0268]	
Completeness to theta = 67.684°	98.6 %	
Absorption correction	Gaussian and multi-scan	
Max. and min. transmission	1.00 and 0.806	
Refinement method	Full-matrix least-squares on F^2	
Data / restraints / parameters	2242 / 2 / 238	
Goodness-of-fit on F^2	1.053	
Final R indices [I>2sigma(I)]	R1 = 0.0439, wR2 = 0.1132	
R indices (all data)	R1 = 0.0453, wR2 = 0.1154	
Absolute structure parameter	0.0(3)	
Extinction coefficient	n/a	
Largest diff. peak and hole	0.255 and -0.373 e.$Å^-$	

References

(1) Martin, S. F. Natural Products and Their Mimics as Targets of Opportunity for Discovery. *J. Org. Chem.* **2017**, *82*, 10757-10794.

(2) Martin, S. F.; Benage, B.; Hunter, J. E. A concise strategy for the syntheses of indole alkaloids of the heteroyohimboid and corynantheioid families. Total syntheses of (.+-.)-tetrahydroalstonine, (.+-.)-cathenamine and (.+-.)-geissoschizine. *J. Am. Chem. Soc.* **1988**, *110*, 5925-5927.

(3) Sahn, J. J.; Granger, B. A.; Martin, S. F. Evolution of a strategy for preparing bioactive small molecules by sequential multicomponent assembly processes, cyclizations, and diversification. *Org. Biomol. Chem.* **2014**, *12*, 7659-7672.

(4) Sahn, J. J.; Hodges, T. R.; Chan, J. Z.; Martin, S. F. Norbenzomorphan Framework as a Novel Scaffold for Generating Sigma 2 Receptor/PGRMC1 Subtype-Selective Ligands. *ChemMedChem* **2016**, *11*, 556-561.

(5) Schmidt, H. R.; Kruse, A. C. The Molecular Function of σ Receptors: Past, Present, and Future. *Trends Pharmacol. Sci.* **2019**, *40*, 636-654.

(6) Schmidt, H. R.; Zheng, S.; Gurpinar, E.; Koehl, A.; Manglik, A.; Kruse, A. C. Crystal structure of the human σ1 receptor. *Nature* **2016**, *532*, 527-530.

(7) Zeng, C.; Mach, R. H.: The Evolution of the Sigma-2 (σ2) Receptor from Obscure Binding Site to Bona Fide Therapeutic Target. In *Sigma Receptors: Their Role in Disease and as Therapeutic Targets*; Smith, S. B., Su, T.-P., Eds.; Springer International Publishing: Cham, 2017; pp 49-61.

(8) Linkens, K.; Schmidt, H. R.; Sahn, J. J.; Kruse, A. C.; Martin, S. F. Investigating isoindoline, tetrahydroisoquinoline, and tetrahydrobenzazepine scaffolds for their sigma receptor binding properties. *Eur. J. Med. Chem.* **2018**, *151*, 557-567.

(9) Sahn, J. J.; Hodges, T. R.; Chan, J. Z.; Martin, S. F. Norbenzomorphan Scaffold: Chemical Tool for Modulating Sigma Receptor-Subtype Selectivity. *ACS Med. Chem. Lett.* **2017**, *8*, 455-460.

(10) Maurice, T.; Su, T.-P. The pharmacology of sigma-1 receptors. *Pharmacology & Therapeutics* **2009**, *124*, 195-206.

(11) Sahn, J. J.; Mejia, G. L.; Ray, P. R.; Martin, S. F.; Price, T. J. Sigma 2 Receptor/Tmem97 Agonists Produce Long Lasting Antineuropathic Pain Effects in Mice. *ACS Chem. Neurosci.* **2017**, *8*, 1801-1811.

(12) Yi, B.; Sahn, J. J.; Ardestani, P. M.; Evans, A. K.; Scott, L. L.; Chan, J. Z.; Iyer, S.; Crisp, A.; Zuniga, G.; Pierce, J. T.; Martin, S. F.; Shamloo, M. Small molecule modulator of sigma 2 receptor is neuroprotective and reduces cognitive deficits

and neuroinflammation in experimental models of Alzheimer's disease. *J. Neurochem*. **2017**, *140*, 561-575.

(13) Scott, L. L.; Sahn, J. J.; Ferragud, A.; Yen, R. C.; Satarasinghe, P. N.; Wood, M. D.; Hodges, T. R.; Shi, T.; Prakash, B. A.; Friese, K. M.; Shen, A.; Sabino, V.; Pierce, J. T.; Martin, S. F. Small molecule modulators of σ2R/Tmem97 reduce alcohol withdrawal-induced behaviors. *Neuropsychopharmacology* **2018**, *43*, 1867-1875.

(14) Vázquez-Rosa, E.; Watson, M. R.; Sahn, J. J.; Hodges, T. R.; Schroeder, R. E.; Cintrón-Pérez, C. J.; Shin, M.-K.; Yin, T. C.; Emery, J. L.; Martin, S. F.; Liebl, D. J.; Pieper, A. A. Neuroprotective Efficacy of a Sigma 2 Receptor/TMEM97 Modulator (DKR-1677) after Traumatic Brain Injury. *ACS Chem. Neurosci*.**2019**, *10*, 1595-1602.

(15) Martin, S. F.; Hunter, J. E.; Benage, B.; Geraci, L. S.; Mortimore, M. Unified strategy for synthesis of indole and 2-oxindole alkaloids. *J. Am. Chem. Soc*. **1991**, *113*, 6161-6171.

(16) Martin, S. F.; Grzejszczak, S.; Rueeger, H.; Williamson, S. A. Total synthesis of (.+-.)-reserpine. *J. Am. Chem. Soc*. **1985**, *107*, 4072-4074.

(17) Martin, S. F.; Rueger, H.; Williamson, S. A.; Grzejszczak, S. General strategies for the synthesis of indole alkaloids. Total synthesis of (.+-.)-reserpine and (.+-.)-.alpha.-yohimbine. *J. Am. Chem. Soc*. **1987**, *109*, 6124-6134.

(18) Martin, S. F.; Williamson, S. A.; Gist, R. P.; Smith, K. M. Aspects of the intramolecular Diels-Alder reactions of some 1,3,9-trienic amides, amines, and esters. An approach to the pentacyclic skeleton of the yohimboid alkaloids. *J. Org. Chem*. **1983**, *48*, 5170-5180.

(19) Martin, S. F.; Desai, S. R.; Philips, G. W.; Miller, A. C. General methods for alkaloid synthesis via intramolecular [4 + 2] cycloaddition reactions of enamides. A new approach to the synthesis of Aspidosperma alkaloids. *J. Am. Chem. Soc*. **1980**, *102*, 3294-3296.

(20) Martin, S. F.; Benage, B. Applications of intramolecular diels-alder reactions of heterodienes. Facile syntheses of the heteroyohimbine alkaloids tetrahydroalstonine and akuammigine. *Tetrahedron Lett*. **1984**, *25*, 4863-4866.

(21) Martin, S. F. Evolution of the Vinylogous Mannich Reaction as a Key Construction for Alkaloid Synthesis. *Acc. Chem. Res*. **2002**, *35*, 895-904.

(22) Martin, S. F.; Clark, C. W.; Corbett, J. W. Applications of Vinylogous Mannich Reactions. Asymmetric Synthesis of the Heteroyohimboid Alkaloids (-)-Ajmalicine, (+)-19-epi-Ajmalicine, and (-)-Tetrahydroalstonine. *J. Org. Chem*. **1995**, *60*, 3236-3242.

(23) Martin, S. F.; Barr, K. J.; Smith, D. W.; Bur, S. K. Applications of Vinylogous Mannich Reactions. Concise Enantiospecific Total Syntheses of (+)-Croomine. *J. Am. Chem. Soc.* **1999**, *121*, 6990-6997.

(24) Martin, S. F.; Bur, S. K. Vinylogous Mannich reactions. Stereoselective formal synthesis of pumiliotoxin 251D. *Tetrahedron* **1999**, *55*, 8905-8914.

(25) Liras, S.; Lynch, C. L.; Fryer, A. M.; Vu, B. T.; Martin, S. F. Applications of Vinylogous Mannich Reactions. Total Syntheses of the Ergot Alkaloids Rugulovasines A and B and Setoclavine. *J. Am. Chem. Soc.* **2001**, *123*, 5918-5924.

(26) Reichelt, A.; Bur, S. K.; Martin, S. F. Applications of vinylogous Mannich reactions. Total synthesis of the angiotensin converting enzyme inhibitor (–)-A58365A. *Tetrahedron* **2002**, *58*, 6323-6328.

(27) Corey, E. J.; Cheng, X.-m.: *The logic of chemical synthesis*; John Wiley: New York, 1989.

(28) Schreiber, S. L. Target-Oriented and Diversity-Oriented Organic Synthesis in Drug Discovery. *Science* **2000**, *287*, 1964-1969.

(29) Burke, M. D.; Schreiber, S. L. A Planning Strategy for Diversity-Oriented Synthesis. *Angew. Chem. Int. Ed.* **2004**, *43*, 46-58.

(30) Galloway, W. R. J. D.; Isidro-Llobet, A.; Spring, D. R. Diversity-oriented synthesis as a tool for the discovery of novel biologically active small molecules. *Nature Commun.* **2010**, *1*, 1-13.

(31) Biggs-Houck, J. E.; Younai, A.; Shaw, J. T. Recent advances in multicomponent reactions for diversity-oriented synthesis. *Curr. Opin. Chem. Biol.* **2010**, *14*, 371-382.

(32) Gracias, V.; Darczak, D.; Gasiecki, A. F.; Djuric, S. W. Synthesis of fused triazolo-imidazole derivatives by sequential van Leusen/alkyne–azide cycloaddition reactions. *Tetrahedron Lett.* **2005**, *46*, 9053-9056.

(33) Kumagai, N.; Muncipinto, G.; Schreiber, S. L. Short Synthesis of Skeletally and Stereochemically Diverse Small Molecules by Coupling Petasis Condensation Reactions to Cyclization Reactions. *Angew. Chem. Int. Ed.* **2006**, *45*, 3635-3638.

(34) Ribelin, T. P.; Judd, A. S.; Akritopoulou-Zanze, I.; Henry, R. F.; Cross, J. L.; Whittern, D. N.; Djuric, S. W. Concise Construction of Novel Bridged Bicyclic Lactams by Sequenced Ugi/RCM/Heck Reactions. *Org. Lett.* **2007**, *9*, 5119-5122.

(35) Banfi, L.; Basso, A.; Giardini, L.; Riva, R.; Rocca, V.; Guanti, G. Tandem Ugi MCR/Mitsunobu Cyclization as a Short, Protecting-Group-Free Route to Benzoxazinones with Four Diversity Points. *Eur. J. Org. Chem.* **2011**, *2011*, 100-109.

(36) Nielsen, T. E.; Schreiber, S. L. Towards the Optimal Screening Collection: A Synthesis Strategy. *Angew. Chem. Int. Ed.* **2008**, *47*, 48-56.

(37) Pellissier, H. Stereocontrolled Domino Reactions. *Chem. Rev.* **2013**, *113*, 442-524.

(38) Nicolaou, K. C.; Edmonds, D. J.; Bulger, P. G. Cascade Reactions in Total Synthesis. *Angew. Chem. Int. Ed.* **2006**, *45*, 7134-7186.

(39) Austin, C. P. Molecular Biology: NIH Molecular Libraries Initiative. *Science* **2004**, *306*, 1138-1139.

(40) Zerhouni, E. Medicine: The NIH Roadmap. *Science* **2003**, *302*, 63-72.

(41) Sunderhaus, J. D.; Dockendorff, C.; Martin, S. F. Applications of Multicomponent Reactions for the Synthesis of Diverse Heterocyclic Scaffolds. *Org. Lett.* **2007**, *9*, 4223-4226.

(42) Sunderhaus, J. D.; Dockendorff, C.; Martin, S. F. Synthesis of diverse heterocyclic scaffolds via tandem additions to imine derivatives and ring-forming reactions. *Tetrahedron* **2009**, *65*, 6454-6469.

(43) Sahn, J. J.; Martin, S. F. Facile syntheses of substituted, conformationally-constrained benzoxazocines and benzazocines via sequential multicomponent assembly and cyclization. *Tetrahedron Lett.* **2011**, *52*, 6855-6858.

(44) Donald, J. R.; Martin, S. F. Synthesis and Diversification of 1,2,3-Triazole-Fused 1,4-Benzodiazepine Scaffolds. *Org. Lett.* **2011**, *13*, 852-855.

(45) Donald, J. R.; Wood, R. R.; Martin, S. F. Application of a Sequential Multicomponent Assembly Process/Huisgen Cycloaddition Strategy to the Preparation of Libraries of 1,2,3-Triazole-Fused 1,4-Benzodiazepines. *ACS Combi. Sci.* **2012**, *14*, 135-143.

(46) Granger, B. A.; Kaneda, K.; Martin, S. F. Multicomponent Assembly Strategies for the Synthesis of Diverse Tetrahydroisoquinoline Scaffolds. *Org. Lett.* **2011**, *13*, 4542-4545.

(47) Granger, B. A.; Kaneda, K.; Martin, S. F. Libraries of 2,3,4,6,7,11b-Hexahydro-1H-pyrido[2,1-a]isoquinolin-2-amine Derivatives via a Multicomponent Assembly Process/1,3-Dipolar Cycloaddition Strategy. *ACS Combi. Sci.* **2012**, *14*, 75-79.

(48) Sahn, J. J.; Su, J. Y.; Martin, S. F. Facile and Unified Approach to Skeletally Diverse, Privileged Scaffolds. *Org. Lett.* **2011**, *13*, 2590-2593.

(49) Hardy, S.; Martin, S. F. Multicomponent, Mannich-type assembly process for generating novel, biologically-active 2-arylpiperidines and derivatives. *Tetrahedron* **2014**, *70*, 7142-7157.

(50) Sahn, J. J.; Martin, S. F. Expedient Synthesis of Norbenzomorphan Library via Multicomponent Assembly Process Coupled with Ring-Closing Reactions. *ACS Comb. Sci.* **2012**, *14*, 496-502.

(51) Kanematsu, K.; Takeda, M.; Jacobson, A. E.; May, E. L. Synthesis of 6,7-benzomorphan and related nonquaternary carbon structures with marked analgetic activity. *J. Med. Chem.* **1969**, *12*, 405-408.

(52) Jacobson, A. E.; Mokotoff, M. Azabicyclo chemistry. I. Synthesis of 1,5-methano-7-methoxy-2,3,4,5-tetrahydro-1H-2-benzazepines. B-norbenzomorphans. *J. Med. Chem.***1970**, *13*, 7-9.

(53) Chen, Y. L.; Liston, D.; Nielsen, J.; Chapin, D.; Dunaiskis, A.; Hedberg, K.; Ives, J.; Johnson, J., Jr.; Jones, S. Syntheses and Anticholinesterase Activity of Tetrahydrobenzazepine Carbamates. *J. Med. Chem.* **1994**, *37*, 1996-2000.

(54) [Ki determinations, receptor binding profiles, agonist and/or antagonist functional data, HERG data, MDR1 data, etc. as appropriate] was generously provided by the National Institute of Mental Health's Psychoactive Drug Screening Program, Contract # HHSN-271-2018-00023-C (NIMH PDSP). The NIMH PDSP is Directed by Bryan L. Roth at the University of North Carolina at Chapel Hill and Project Officer Jamie Driscoll at NIMH, Bethesda MD, USA. For experimental details please refer to the PDSP web site https://pdsp.unc.edu/ims/investigator/web/.

(55) Martin, W. R.; Eades, C. G.; Thompson, J. A.; Huppler, R. E.; Gilbert, P. E. The effects of morphine- and nalorphine- like drugs in the nondependent and morphine-dependent chronic spinal dog. *J. Pharmacol. Exp. Ther.* **1976**, *197*, 517.

(56) Su, T. P. Evidence for sigma opioid receptor: binding of [3H]SKF-10047 to etorphine-inaccessible sites in guinea-pig brain. *J. Pharmacol. Exp. Ther.***1982**, *223*, 284-290.

(57) Tam, S. W. Naloxone-inaccessible sigma receptor in rat central nervous system. *Proc. Natl. Acad. Sci. U.S.A.* **1983**, *80*, 6703-6707.

(58) Pert, C. B.; Snyder, S. H. Opiate Receptor: Demonstration in Nervous Tissue. *Science* **1973**, *179*, 1011-1014.

(59) Pasternak, G. W.: Opioid Receptors: The Early Years. In *The Opiate Receptors*; Pasternak, G. W., Ed.; Humana Press: Totowa, NJ, 2011; pp 59-91.

(60) Kosterlitz, H. W.; Paterson, S. J.; Robson, L. E. Characterization of the k-subtype of the opiate receptor in the guinea-pig brain. *Br. J. Pharmacol.* **1981**, *73*, 939-949.

(61) Mendelsohn, L. G.; Kalra, V.; Johnson, B. G.; Kerchner, G. A. Sigma opioid receptor: characterization and co-identity with the phencyclidine receptor. *J. Pharmacol. Exp. Ther.* **1985**, *233*, 597-602.

(62) Quirion, R.; Hammer, R. P.; Herkenham, M.; Pert, C. B. Phencyclidine (angel dust)/sigma "opiate" receptor: visualization by tritium-sensitive film. *Proc. Natl. Acad. Sci. U.S.A.***1981**, *78*, 5881-5885.

(63) Holtzman, S. G. Phencyclidine-like discriminative effects of opioids in the rat. *J. Pharmacol. Exp. Ther.* **1980**, *214*, 614-619.

(64) Shannon, H. E. Evaluation of phencyclidine analogs on the basis of their discriminative stimulus properties in the rat. *J. Pharmacol. Exp. Ther.* **1981**, *216*, 543-551.

(65) Brady, K.; Balster, R.; May, E. Stereoisomers of N-allylnormetazocine: phencyclidine-like behavioral effects in squirrel monkeys and rats. *Science* **1982**, *215*, 178-180.

(66) Zukin, S. R.; Brady, K. T.; Slifer, B. L.; Balster, R. L. Behavioral and biochemical stereoselectivity of sigma opiate/PCP receptors. *Brain Res.* **1984**, *294*, 174-177.

(67) Magaros, W. F.; Chu, D. C. M.; Greenamyre, J. T.; Penney, J. B.; Young, A. B. High correlation between the localization of [3H]TCP binding and NMDA receptors. *Eur. J. Pharmacol.* **1986**, *123*, 173-174.

(68) Wong, E. H. F.; Knight, A. R.; Woodruff, G. N. [3H]MK-801 Labels a Site on the N-Methyl-D-Aspartate Receptor Channel Complex in Rat Brain Membranes. *J. Neurochem.* **1988**, *50*, 274-281.

(69) Majewska, M. D.; Parameswaran, S.; Vu, T.; London, E. D. Divergent ontogeny of sigma and phencyclidine binding sites in the rat brain. *Dev. Brain Res.* **1989**, *47*, 13-18.

(70) Quirion, R.; Chicheportiche, R.; Contreras, P. C.; Johnson, K. M.; Lodge, D.; William Tam, S.; Woods, J. H.; Zukin, S. R. Classification and nomenclature of phencyclidine and sigma receptor sites. *Trends Neurosci.* **1987**, *10*, 444-446.

(71) Largent, B. L.; Gundlach, A. L.; Snyder, S. H. Psychotomimetic opiate receptors labeled and visualized with (+)-[3H]3-(3-hydroxyphenyl)-N-(1-propyl)piperidine. *Proc. Natl. Acad. Sci. U.S.A.* **1984**, *81*, 4983-4987.

(72) Weber, E.; Sonders, M.; Quarum, M.; McLean, S.; Pou, S.; Keana, J. F. 1,3-Di(2-[5-3H]tolyl)guanidine: a selective ligand that labels sigma-type receptors for psychotomimetic opiates and antipsychotic drugs. *Proc. Natl. Acad. Sci. U.S.A.* **1986**, *83*, 8784-8788.

(73) Glasel, J. A.; Venn, R. F. The sensitivity of opiate receptors and ligands to short wavelength ultraviolet light. *Life Sci.* **1981**, *29*, 221-228.

(74) Bowen, W. D.; Hellewell, S. B.; McGarry, K. A. Evidence for a multi-site model of the rat brain σ receptor. *Eur. J. Pharmacol.***1989**, *163*, 309-318.

(75) Hellewell, S. B.; Bowen, W. D. A sigma-like binding site in rat pheochromocytoma (PC12) cells: decreased affinity for (+)-benzomorphans and lower molecular weight suggest a different sigma receptor form from that of guinea pig brain. *Brain Res*. **1990**, *527*, 244-253.

(76) Quirion, R.; Bowen, W. D.; Itzhak, Y.; Junien, J. L.; Musacchio, J.; Rothman, R. B.; Tsung-Ping, S.; Tam, S. W.; Taylor, D. P. A proposal for the classification of sigma binding sites. *Trends Pharmacol. Sci*. **1992**, *13*, 85-86.

(77) Mach, R. H.; Zeng, C.; Hawkins, W. G. The σ2 Receptor: A Novel Protein for the Imaging and Treatment of Cancer. *J. Med. Chem*. **2013**, *56*, 7137-7160.

(78) Hanner, M.; Moebius, F. F.; Flandorfer, A.; Knaus, H. G.; Striessnig, J.; Kempner, E.; Glossmann, H. Purification, molecular cloning, and expression of the mammalian sigma1-binding site. *Proc. Natl. Acad. Sci. U.S.A*. **1996**, *93*, 8072-8077.

(79) Kekuda, R.; Prasad, P. D.; Fei, Y.-J.; Leibach, F. H.; Ganapathy, V. Cloning and Functional Expression of the Human Type 1 Sigma Receptor (hSigmaR1). *Biochem. Biophys. Res. Commun*. **1996**, *229*, 553-558.

(80) Seth, P.; Leibach, F. H.; Ganapathy, V. Cloning and Structural Analysis of the cDNA and the Gene Encoding the Murine Type 1 Sigma Receptor. *Biochem. Biophys. Res. Commun*. **1997**, *241*, 535-540.

(81) Seth, P.; Fei, Y.-J.; Li, H. W.; Huang, W.; Leibach, F. H.; Ganapathy, V. Cloning and Functional Characterization of a σ Receptor from Rat Brain. *J. Neurochem*. **2002**, *70*, 922-931.

(82) Nguyen, L.; Lucke-Wold, B. P.; Mookerjee, S. A.; Cavendish, J. Z.; Robson, M. J.; Scandinaro, A. L.; Matsumoto, R. R. Role of sigma-1 receptors in neurodegenerative diseases. *J. Pharmacol. Sci*. **2015**, *127*, 17-29.

(83) Guitart, X.; Codony, X.; Monroy, X. Sigma receptors: biology and therapeutic potential. *Psychopharmacology* **2004**, *174*.

(84) Mei, J.; Pasternak, G. W. Molecular cloning and pharmacological characterization of the rat sigma1 receptor. *Biochem. Pharmacol*. **2001**, *62*, 349-355.

(85) Aydar, E.; Palmer, C. P.; Klyachko, V. A.; Jackson, M. B. The Sigma Receptor as a Ligand-Regulated Auxiliary Potassium Channel Subunit. *Neuron* **2002**, *34*, 399-410.

(86) *Sigma Receptors Chemistry, Cell Biology and Clinical Implications / edited by Tsung-Ping Su, Rae R. Matsumoto, Wayne D. Bowen*; Springer US: Boston, MA, 2007.

(87) Laurini, E.; Col, V. D.; Mamolo, M. G.; Zampieri, D.; Posocco, P.; Fermeglia, M.; Vio, L.; Pricl, S. Homology Model and Docking-Based Virtual Screening for Ligands of the σ1 Receptor. *ACS Med. Chem. Lett*. **2011**, *2*, 834-839.

(88) Alonso, G.; Phan, V. L.; Guillemain, I.; Saunier, M.; Legrand, A.; Anoal, M.; Maurice, T. Immunocytochemical localization of the sigma1 receptor in the adult rat central nervous system. *Neuroscience* **2000**, *97*, 155-170.

(89) Zamanillo, D.; Andreu, F.; Ovalle, S.; Pérez, M. P.; Romero, G.; Farré, A. J.; Guitart, X. Up-regulation of sigma1 receptor mRNA in rat brain by a putative atypical antipsychotic and sigma receptor ligand. *Neuroscience Lett*. **2000**, *282*, 169-172.

(90) Shamsul Ola, M.; Moore, P.; El-Sherbeny, A.; Roon, P.; Agarwal, N.; Sarthy, V. P.; Casellas, P.; Ganapathy, V.; Smith, S. B. Expression pattern of sigma receptor 1 mRNA and protein in mammalian retina. *Mol. Brain Res*. **2001**, *95*, 86-95.

(91) Hayashi, T.; Su, T.-P. Sigma-1 Receptor Chaperones at the ER- Mitochondrion Interface Regulate Ca2+ Signaling and Cell Survival. *Cell* **2007**, *131*, 596-610.

(92) Vance, J. E. MAM (mitochondria-associated membranes) in mammalian cells: Lipids and beyond. *Biochim. Biophys. Acta* **2014**, *1841*, 595-609.

(93) Weng, T.-Y.; Tsai, S.-Y. A.; Su, T.-P. Roles of sigma-1 receptors on mitochondrial functions relevant to neurodegenerative diseases. *J. Biomed. Sci.* **2017**, *24,* 74.

(94) Su, T.-P.; Su, T.-C.; Nakamura, Y.; Tsai, S.-Y. The Sigma-1 Receptor as a Pluripotent Modulator in Living Systems. *Trends Pharmacol. Sci*. **2016**, *37*, 262-278.

(95) Mori, T.; Hayashi, T.; Hayashi, E.; Su, T.-P. Sigma-1 Receptor Chaperone at the ER-Mitochondrion Interface Mediates the Mitochondrion-ER-Nucleus Signaling for Cellular Survival. *PLoS ONE* **2013**, *8*, e76941.

(96) Chu, U. B.; Ruoho, A. E. Biochemical Pharmacology of the Sigma-1 Receptor. *Mol. Pharmacol*. **2016**, *89*, 142-153.

(97) Tsai, S.-Y. A.; Chuang, J.-Y.; Tsai, M.-S.; Wang, X.-F.; Xi, Z.-X.; Hung, J.-J.; Chang, W.-C.; Bonci, A.; Su, T.-P. Sigma-1 receptor mediates cocaine-induced transcriptional regulation by recruiting chromatin-remodeling factors at the nuclear envelope. *Proc. Natl. Acad. Sci. U.S.A*. **2015**, *112*, E6562-E6570.

(98) Ganapathy, M. E.; Prasad, P. D.; Huang, W.; Seth, P.; Leibach, F. H.; Ganapathy, V. Molecular and Ligand-Binding Characterization of the Sigma-Receptor in the Jurkat Human T Lymphocyte Cell Line. *J. Pharmacol. Exp. Ther*. **1999**, *289*, 251-260.

(99) Su, T.; London, E.; Jaffe, J. Steroid binding at sigma receptors suggests a link between endocrine, nervous, and immune systems. *Science* **1988**, *240*, 219-221.

(100) Waterhouse, R. N.; Chang, R. C.; Atuehene, N.; Collier, T. L. In vitro and in vivo binding of neuroactive steroids to the sigma-1 receptor as measured with the positron emission tomography radioligand [18F]FPS. *Synapse* **2007**, *61*, 540-546.

(101) Fontanilla, D.; Johannessen, M.; Hajipour, A. R.; Cozzi, N. V.; Jackson, M. B.; Ruoho, A. E. The Hallucinogen N,N-Dimethyltryptamine (DMT) Is an Endogenous Sigma-1 Receptor Regulator. *Science* **2009**, *323*, 934-937.

(102) Frecska, E.; Szabo, A.; Winkelman, M. J.; Luna, L. E.; McKenna, D. J. A possibly sigma-1 receptor mediated role of dimethyltryptamine in tissue protection, regeneration, and immunity. *J. Neural Transm.* **2013**, *120*, 1295-1303.

(103) Nichols, D. E. N,N-dimethyltryptamine and the pineal gland: Separating fact from myth. *J. Psychopharmacol.* **2018**, *32*, 30-36.

(104) Ramachandran, S.; Chu, U. B.; Mavlyutov, T. A.; Pal, A.; Pyne, S.; Ruoho, A. E. The sigma1 receptor interacts with N-alkyl amines and endogenous sphingolipids. *Eur. J. Pharmacol.* **2009**, *609*, 19-26.

(105) *Sigma Proteins: Evolution of the Concept of Sigma Receptors edited by Felix J. Kim, Gavril W. Pasternak*; 1st ed. 2017. ed.; Springer International Publishing: Cham, 2017.

(106) McCracken, K. A.; Bowen, W. D.; De Costa, B. R.; Matsumoto, R. R. Two novel σ receptor ligands, BD1047 and LR172, attenuate cocaine-induced toxicity and locomotor activity. *Eur. J. Pharmacol.* **1999**, *370*, 225-232.

(107) Matsumoto, R. R.; McCracken, K. A.; Pouw, B.; Miller, J.; Bowen, W. D.; Williams, W.; De Costa, B. R. N-alkyl substituted analogs of the σ receptor ligand BD1008 and traditional σ receptor ligands affect cocaine-induced convulsions and lethality in mice. *Eur. J. Pharmacol.* **2001**, *411*, 261-273.

(108) Maurice, T.; Goguadze, N.: Sigma-1 (σ1) Receptor in Memory and Neurodegenerative Diseases. In *Sigma Proteins: Evolution of the Concept of Sigma Receptors*; Kim, F. J., Pasternak, G. W., Eds.; Springer International Publishing: Cham, 2017; pp 81-108.

(109) Jin, J.-L.; Fang, M.; Zhao, Y.-X.; Liu, X.-Y. Roles of sigma-1 receptors in Alzheimer's disease. *Int. J. Clin. Exp. Med.* **2015**, *8*, 4808-4820.

(110) Mori, T.; Hayashi, T.; Su, T.-P. Compromising σ-1 Receptors at the Endoplasmic Reticulum Render Cytotoxicity to Physiologically Relevant Concentrations of Dopamine in a Nuclear Factor-κB/Bcl-2-Dependent Mechanism: Potential Relevance to Parkinson's Disease. *J. Pharmacol. Exp. Ther.* **2012**, *341*, 663-671.

(111) Hong, J.; Sha, S.; Zhou, L.; Wang, C.; Yin, J.; Chen, L. Sigma-1 receptor deficiency reduces MPTP-induced parkinsonism and death of dopaminergic neurons. *Cell Death Dis.* **2015**, *6*, e1832-e1832.

(112) Hyrskyluoto, A.; Pulli, I.; Törnqvist, K.; Huu Ho, T.; Korhonen, L.; Lindholm, D. Sigma-1 receptor agonist PRE084 is protective against mutant huntingtin-induced cell degeneration: involvement of calpastatin and the NF-κB pathway. *Cell Death Dis.* **2013**, *4*, e646-e646.

(113) Fukunaga, K.; Shinoda, Y.; Tagashira, H. The role of SIGMAR1 gene mutation and mitochondrial dysfunction in amyotrophic lateral sclerosis. *J. Pharmacol. Sci.* **2015**, *127*, 36-41.

(114) Mavlyutov, T. A.; Guo, L.-W.; Epstein, M. L.; Ruoho, A. E. Role of the Sigma-1 receptor in Amyotrophic Lateral Sclerosis (ALS). *J. Pharmacol. Sci.* **2015**, *127*, 10-16.

(115) Dong, H.; Ma, Y.; Ren, Z.; Xu, B.; Zhang, Y.; Chen, J.; Yang, B. Sigma-1 Receptor Modulates Neuroinflammation After Traumatic Brain Injury. *Cell. Mol. Neurobiol.* **2016**, *36*, 639-645.

(116) Zhang, X.; Wu, F.; Jiao, Y.; Tang, T.; Yang, L.; Lu, C.; Zhang, Y.; Zhang, Y.; Bai, Y.; Chao, J.; Teng, G.; Yao, H. An Increase of Sigma-1 Receptor in the Penumbra Neuron after Acute Ischemic Stroke. *J. Stroke Cerebrovasc. Dis.* **2017**, *26*, 1981-1987.

(117) Ruscher, K.; Shamloo, M.; Rickhag, M.; Ladunga, I.; Soriano, L.; Gisselsson, L.; Toresson, H.; Ruslim-Litrus, L.; Oksenberg, D.; Urfer, R.; Johansson, B. B.; Nikolich, K.; Wieloch, T. The sigma-1 receptor enhances brain plasticity and functional recovery after experimental stroke. *Brain* **2011**, *134*, 732-746.

(118) Zamanillo, D.; Romero, L.; Merlos, M.; Vela, J. M. Sigma 1 receptor: A new therapeutic target for pain. *Eur. J. Pharmacol.***2013**, *716*, 78-93.

(119) Bruna, J.; Velasco, R. Sigma-1 receptor: a new player in neuroprotection against chemotherapy-induced peripheral neuropathy. *Neural Regen. Res.* **2018**, *13*, 775.

(120) Bruna, J.; Videla, S.; Argyriou, A. A.; Velasco, R.; Villoria, J.; Santos, C.; Nadal, C.; Cavaletti, G.; Alberti, P.; Briani, C.; Kalofonos, H. P.; Cortinovis, D.; Sust, M.; Vaqué, A.; Klein, T.; Plata-Salamán, C. Efficacy of a Novel Sigma-1 Receptor Antagonist for Oxaliplatin-Induced Neuropathy: A Randomized, Double-Blind, Placebo-Controlled Phase IIa Clinical Trial. *Neurotherapeutics* **2018**, *15*, 178-189.

(121) Urfer, R.; Moebius, H. J.; Skoloudik, D.; Santamarina, E.; Sato, W.; Mita, S.; Muir, K. W. Phase II Trial of the Sigma-1 Receptor Agonist Cutamesine (SA4503) for Recovery Enhancement After Acute Ischemic Stroke. *Stroke* **2014**, *45*, 3304-3310.

(122) Anavex Life Sciences Corp. ANAVEX2-73 Study in Parkinson's Disease Dementia (report no. NCT03774459). https://clinicaltrials.gov/ct2/show/NCT03774459 (accessed May 9, 2020 2020).

(123) Anavex Life Sciences Corp. ANAVEX2-73 for Treatment of Early Alzheimer's Disease (report no. NCT03790709). https://clinicaltrials.gov/ct2/show/study/NCT03790709 (accessed May 9, 2020 2020).

(124) Anavex Life Sciences Corp. An Extension Study of ANAVEX2-73 in Patients With Mild to Moderate Alzheimer's Disease (record no. NCT02756858). https://clinicaltrials.gov/ct2/show/NCT02756858 (accessed May 9, 2020 2020).

(125) Kim, F. J.; Maher, C. M.: Sigma1 Pharmacology in the Context of Cancer. In *Sigma Proteins: Evolution of the Concept of Sigma Receptors*; Kim, F. J., Pasternak, G. W., Eds.; Springer International Publishing: Cham, 2017; pp 237-308.

(126) Van Waarde, A.; Rybczynska, A. A.; Ramakrishnan, N. K.; Ishiwata, K.; Elsinga, P. H.; Dierckx, R. A. J. O. Potential applications for sigma receptor ligands in cancer diagnosis and therapy. *Biochim. Biophys. Acta - Biomembranes* **2015**, *1848*, 2703-2714.

(127) Spruce, B. A.; Campbell, L. A.; McTavish, N.; Cooper, M. A.; Appleyard, M. V. L.; O'Neill, M.; Howie, J.; Samson, J.; Watt, S.; Murray, K.; McLean, D.; Leslie, N. R.; Safrany, S. T.; Ferguson, M. J.; Peters, J. A.; Prescott, A. R.; Box, G.; Hayes, A.; Nutley, B.; Raynaud, F.; Downes, C. P.; Lambert, J. J.; Thompson, A. M.; Eccles, S. Small Molecule Antagonists of the σ-1 Receptor Cause Selective Release of the Death Program in Tumor and Self-Reliant Cells and Inhibit Tumor Growthin Vitroandin Vivo. *Cancer Res.* **2004**, *64*, 4875-4886.

(128) Colabufo, N.; Berardi, F.; Contino, M.; Niso, M.; Abate, C.; Perrone, R.; Tortorella, V. Antiproliferative and cytotoxic effects of some σ2 agonists and σ1 antagonists in tumour cell lines. *Naunyn-Schmiedeberg's Arch. Pharmacol.* **2004**, *370*.

(129) Aydar, E.; Onganer, P.; Perrett, R.; Djamgoz, M. B.; Palmer, C. P. The expression and functional characterization of sigma (σ) 1 receptors in breast cancer cell lines. *Cancer Lett.* **2006**, *242*, 245-257.

(130) Ogawa, K.; Kanbara, H.; Kiyono, Y.; Kitamura, Y.; Kiwada, T.; Kozaka, T.; Kitamura, M.; Mori, T.; Shiba, K.; Odani, A. Development and evaluation of a radiobromine-labeled sigma ligand for tumor imaging. *Nucl. Med. Biol.* **2013**, *40*, 445-450.

(131) Xie, F.; Bergmann, R.; Kniess, T.; Deuther-Conrad, W.; Mamat, C.; Neuber, C.; Liu, B.; Steinbach, J.; Brust, P.; Pietzsch, J.; Jia, H. 18 F-Labeled 1,4-Dioxa-8-azaspiro[4.5]decane Derivative: Synthesis and Biological Evaluation of a σ 1 Receptor Radioligand with Low Lipophilicity as Potent Tumor Imaging Agent. *J. Med. Chem.* **2015**, *58*, 5395-5407.

(132) Narita, N.; Hashimoto, K.; Tomitaka, S.-I.; Minabe, Y. Interactions of selective serotonin reuptake inhibitors with subtypes of σ receptors in rat brain. *Eur. J. Pharmacol.***1996**, *307*, 117-119.

(133) Ossa, F.; Schnell, J. R.; Ortega-Roldan, J. L.: A Review of the Human Sigma-1 Receptor Structure. In *Sigma Receptors: Their Role in Disease and as*

Therapeutic Targets; Smith, S. B., Su, T.-P., Eds.; Springer International Publishing: Cham, 2017; pp 15-29.

(134) Manallack, D. T.; Beart, P. M. Quantitative conformational analyses predict distinct receptor sites for PCP-like and σ drugs. *Eur. J. Pharmacol.* **1987**, *144*, 231-235.

(135) Manallack, D. T.; Wong, M. G.; Costa, M.; Andrews, P. R.; Beart, P. M. Receptor site topographies for phencyclidine-like and sigma drugs: predictions from quantitative conformational, electrostatic potential, and radioreceptor analyses. *Mol. Pharmacol.* **1988**, *34*, 863-879.

(136) Largent, B. L.; Wikström, H.; Gundlach, A. L.; Snyder, S. H. Structural determinants of sigma receptor affinity. *Mol. Pharmacol.* **1987**, *32*, 772-784.

(137) Glennon, R. A.; Yousif, M. Y.; Ismaiel, A. M.; El-Ashmawy, M. B.; Herndon, J. L.; Fischer, J. B.; Server, A. C.; Howie, K. J. B. Novel 1-phenylpiperazine and 4-phenylpiperidine derivatives as high-affinity .sigma. ligands. *J. Med. Chem.* **1991**, *34*, 3360-3365.

(138) Gilligan, P. J.; Cain, G. A.; Christos, T. E.; Cook, L.; Drummond, S.; Johnson, A. L.; Kergaye, A. A.; McElroy, J. F.; Rohrbach, K. W. Novel piperidine .sigma. receptor ligands as potential antipsychotic drugs. *J. Med. Chem.* **1992**, *35*, 4344-4361.

(139) Glennon, R. A.; Smith, J. D.; Ismaiel, A. M.; El-Ashmawy, M.; Battaglia, G.; Fischer, J. B. Identification and exploitation of the .sigma.-opiate pharmacophore. *J. Med. Chem.* **1991**, *34*, 1094-1098.

(140) Glennon, R. A.; Ablordeppey, S. Y.; Ismaiel, A. M.; El-Ashmawy, M. B.; Fischer, J. B.; Howie, K. B. Structural Features Important for .sigma.1 Receptor Binding. *J. Med. Chem.* **1994**, *37*, 1214-1219.

(141) Ablordeppey, S. Y.; Glennon, R. A.: Pharmacophore Models for σ1 Receptor Binding. In *Sigma Receptors: Chemistry, Cell Biology and Clinical Implications*; Su, T.-P., Matsumoto, R. R., Bowen, W. D., Eds.; Springer US: Boston, MA, 2007; pp 71-98.

(142) Zampieri, D.; Mamolo, M. G.; Laurini, E.; Florio, C.; Zanette, C.; Fermeglia, M.; Posocco, P.; Paneni, M. S.; Pricl, S.; Vio, L. Synthesis, Biological Evaluation, and Three-Dimensional in Silico Pharmacophore Model for σ1Receptor Ligands Based on a Series of Substituted Benzo[d]oxazol-2(3H)-one Derivatives. *J. Med. Chem.* **2009**, *52*, 5380-5393.

(143) Adapted with permission from Zampieri, D. M., M. G.; Laurini, E.; Florio, C.; Zanette, C.; Fermeglia, M.; Posocco, P.; Paneni, M. S.; Pricl, S.; Vio, L. Synthesis, Biological Evaluation, and Three-Dimensional in Silico Pharmacophore Model for σ1Receptor Ligands Based on a Series of Substituted

Benzo[d]oxazol-2(3H)-one Derivatives. *J. Med. Chem.* **2009**, *52*, 5380-5393. Copyright (2009) American Chemical Society

(144) Seth, P.; Ganapathy, M. E.; Conway, S. J.; Bridges, C. D.; Smith, S. B.; Casellas, P.; Ganapathy, V. Expression pattern of the type 1 sigma receptor in the brain and identity of critical anionic amino acid residues in the ligand-binding domain of the receptor. *Biochim Biophys. Acta.* **2001**, *1540*, 59-67.

(145) Adapted with permission from Laurini, E. C., V. D.; Mamolo, M. G.; Zampieri, D.; Posocco, P.; Fermeglia, M.; Vio, L.; Pricl, S. Homology Model and Docking-Based Virtual Screening for Ligands of the σ1 Receptor. *ACS Med. Chem. Lett.* **2011**, *2*, 834-839. Copyright (2011) American Chemical Society.

(146) Laurini, E.; Marson, D.; Dal Col, V.; Fermeglia, M.; Mamolo, M. G.; Zampieri, D.; Vio, L.; Pricl, S. Another Brick in the Wall. Validation of the σ 1 Receptor 3D Model by Computer-Assisted Design, Synthesis, and Activity of New σ 1 Ligands. *Mol. Pharmaceutics* **2012**, *9*, 3107-3126.

(147) Meyer, C.; Schepmann, D.; Yanagisawa, S.; Yamaguchi, J.; Dal Col, V.; Laurini, E.; Itami, K.; Pricl, S.; Wünsch, B. Pd-Catalyzed Direct C–H Bond Functionalization of Spirocyclic σ1Ligands: Generation of a Pharmacophore Model and Analysis of the Reverse Binding Mode by Docking into a 3D Homology Model of the σ1 Receptor. *J. Med. Chem.* **2012**, *55*, 8047-8065.

(148) Rossi, D.; Marra, A.; Picconi, P.; Serra, M.; Catenacci, L.; Sorrenti, M.; Laurini, E.; Fermeglia, M.; Pricl, S.; Brambilla, S.; Almirante, N.; Peviani, M.; Curti, D.; Collina, S. Identification of RC-33 as a potent and selective σ1 receptor agonist potentiating NGF-induced neurite outgrowth in PC12 cells. Part 2: g-Scale synthesis, physicochemical characterization and in vitro metabolic stability. *Bioorg. Med. Chem.* **2013**, *21*, 2577-2586.

(149) Zampieri, D.; Laurini, E.; Vio, L.; Golob, S.; Fermeglia, M.; Pricl, S.; Mamolo, M. G. Synthesis and receptor binding studies of some new arylcarboxamide derivatives as sigma-1 ligands. *Bioorg. Med. Chem. Lett.* **2014**, *24*, 1021-1025.

(150) Laurini, E.; Harel, D.; Marson, D.; Schepmann, D.; Schmidt, T. J.; Pricl, S.; Wünsch, B. Identification, pharmacological evaluation and binding mode analysis of novel chromene and chromane based σ1 receptor ligands. *Eur. J. Med. Chem.* **2014**, *83*, 526-533.

(151) Zampieri, D.; Laurini, E.; Vio, L.; Fermeglia, M.; Pricl, S.; Wünsch, B.; Schepmann, D.; Mamolo, M. G. Improving selectivity preserving affinity: New piperidine-4-carboxamide derivatives as effective sigma-1-ligands. *Eur. J. Med. Chem.* **2015**, *90*, 797-808.

(152) Brune, S.; Schepmann, D.; Klempnauer, K. H.; Marson, D.; Dal Col, V.; Laurini, E.; Fermeglia, M.; Wünsch, B.; Pricl, S. The Sigma Enigma: In Vitro/in Silico

Site-Directed Mutagenesis Studies Unveil σ1 Receptor Ligand Binding. *Biochemistry* **2014**, *53*, 2993-3003.

(153) Ortega-Roldan, J. L.; Ossa, F.; Amin, N. T.; Schnell, J. R. Solution NMR studies reveal the location of the second transmembrane domain of the human sigma-1 receptor. *FEBS Lett*. **2015**, *589*, 659-665.

(154) Schmidt, H. R.; Betz, R. M.; Dror, R. O.; Kruse, A. C. Structural basis for σ1 receptor ligand recognition. *Nat. Struct. Mol. Biol*. **2018**, *25*, 981-987.

(155) Alon, A.; Schmidt, H.; Zheng, S.; Kruse, A. C.: Structural Perspectives on Sigma-1 Receptor Function. In *Sigma Receptors: Their Role in Disease and as Therapeutic Targets*; Smith, S. B., Su, T.-P., Eds.; Springer International Publishing: Cham, 2017; pp 5-13.

(156) Yamamoto, H.; Miura, R.; Yamamoto, T.; Shinohara, K.; Watanabe, M.; Okuyama, S.; Nakazato, A.; Nukada, T. Amino acid residues in the transmembrane domain of the type 1 sigma receptor critical for ligand binding. *FEBS Lett*. **1999**, *445*, 19-22.

(157) Gromek, K. A.; Suchy, F. P.; Meddaugh, H. R.; Wrobel, R. L.; Lapointe, L. M.; Chu, U. B.; Primm, J. G.; Ruoho, A. E.; Senes, A.; Fox, B. G. The Oligomeric States of the Purified Sigma-1 Receptor Are Stabilized by Ligands. *J. Biol. Chem*. **2014**, *289*, 20333-20344.

(158) Mishra, A. K.; Mavlyutov, T.; Singh, D. R.; Biener, G.; Yang, J.; Julie; Ruoho, A.; Raicu, V. The sigma-1 receptors are present in monomeric and oligomeric forms in living cells in the presence and absence of ligands. *Biochem. J*. **2015**, *466*, 263-271.

(159) Kruse, A.: Structural Insights into Sigma1 Function. In *Sigma Proteins: Evolution of the Concept of Sigma Receptors*; Kim, F. J., Pasternak, G. W., Eds.; Springer International Publishing: Cham, 2017; pp 13-25.

(160) Alon, A.; Schmidt, H. R.; Wood, M. D.; Sahn, J. J.; Martin, S. F.; Kruse, A. C. Identification of the gene that codes for the σ2 receptor. *Proc. Natl. Acad. Sci. U.S.A*. **2017**, *114*, 7160-7165.

(161) Zeng, C.; McDonald, E. S.; Mach, R. H.: Molecular Probes for Imaging the Sigma-2 Receptor: In Vitro and In Vivo Imaging Studies. In *Sigma Proteins: Evolution of the Concept of Sigma Receptors*; Kim, F. J., Pasternak, G. W., Eds.; Springer International Publishing: Cham, 2017; pp 309-330.

(162) Georgiadis, M.-O.; Karoutzou, O.; Foscolos, A.-S.; Papanastasiou, I. Sigma Receptor (σR) Ligands with Antiproliferative and Anticancer Activity. *Molecules* **2017**, *22*, 1408.

(163) Mondal, S.; Hegarty, E.; Sahn, J. J.; Scott, L. L.; Gökçe, S. K.; Martin, C.; Ghorashian, N.; Satarasinghe, P. N.; Iyer, S.; Sae-Lee, W.; Hodges, T. R.; Pierce,

J. T.; Martin, S. F.; Ben-Yakar, A. High-Content Microfluidic Screening Platform Used To Identify σ2R/Tmem97 Binding Ligands that Reduce Age-Dependent Neurodegeneration in C. elegans SC_APP Model. *ACS Chem. Neurosci.* **2018**, *9*, 1014-1026.

(164) Izzo, N. J.; Staniszewski, A.; To, L.; Fa, M.; Teich, A. F.; Saeed, F.; Wostein, H.; Walko, T.; Vaswani, A.; Wardius, M.; Syed, Z.; Ravenscroft, J.; Mozzoni, K.; Silky, C.; Rehak, C.; Yurko, R.; Finn, P.; Look, G.; Rishton, G.; Safferstein, H.; Miller, M.; Johanson, C.; Stopa, E.; Windisch, M.; Hutter-Paier, B.; Shamloo, M.; Arancio, O.; Levine, H.; Catalano, S. M. Alzheimer's Therapeutics Targeting Amyloid Beta 1–42 Oligomers I: Abeta 42 Oligomer Binding to Specific Neuronal Receptors Is Displaced by Drug Candidates That Improve Cognitive Deficits. *PLoS ONE* **2014**, *9*, e111898.

(165) Izzo, N. J.; Xu, J.; Zeng, C.; Kirk, M. J.; Mozzoni, K.; Silky, C.; Rehak, C.; Yurko, R.; Look, G.; Rishton, G.; Safferstein, H.; Cruchaga, C.; Goate, A.; Cahill, M. A.; Arancio, O.; Mach, R. H.; Craven, R.; Head, E.; Levine, H.; Spires-Jones, T. L.; Catalano, S. M. Alzheimer's Therapeutics Targeting Amyloid Beta 1–42 Oligomers II: Sigma-2/PGRMC1 Receptors Mediate Abeta 42 Oligomer Binding and Synaptotoxicity. *PLoS ONE* **2014**, *9*, e111899.

(166) Grundman, M.; Morgan, R.; Lickliter, J. D.; Schneider, L. S.; Dekosky, S.; Izzo, N. J.; Guttendorf, R.; Higgin, M.; Pribyl, J.; Mozzoni, K.; Safferstein, H.; Catalano, S. M. A phase 1 clinical trial of the sigma-2 receptor complex allosteric antagonist CT1812, a novel therapeutic candidate for Alzheimer's disease. *Alzheimers Dement. (NY)* **2019**, *5*, 20-26.

(167) Davidson, M.; Saoud, J.; Staner, C.; Noel, N.; Luthringer, E.; Werner, S.; Reilly, J.; Schaffhauser, J.-Y.; Rabinowitz, J.; Weiser, M.; Luthringer, R. Efficacy and Safety of MIN-101: A 12-Week Randomized, Double-Blind, Placebo-Controlled Trial of a New Drug in Development for the Treatment of Negative Symptoms in Schizophrenia. *Am. J. Psychiatry* **2017**, *174*, 1195-1202.

(168) Terada, K.; Migita, K.; Matsushima, Y.; Kamei, C. Sigma-2 receptor as a potential therapeutic target for treating central nervous system disorders. *Neural Regen. Res.* **2019**, *14*, 1893.

(169) Gordon, D. E.; Jang, G. M.; Bouhaddou, M.; Xu, J.; Obernier, K.; White, K. M.; O'Meara, M. J.; Rezelj, V. V.; Guo, J. Z.; Swaney, D. L.; Tummino, T. A.; Huettenhain, R.; Kaake, R. M.; Richards, A. L.; Tutuncuoglu, B.; Foussard, H.; Batra, J.; Haas, K.; Modak, M.; Kim, M.; Haas, P.; Polacco, B. J.; Braberg, H.; Fabius, J. M.; Eckhardt, M.; Soucheray, M.; Bennett, M. J.; Cakir, M.; McGregor, M. J.; Li, Q.; Meyer, B.; Roesch, F.; Vallet, T.; Mac Kain, A.; Miorin, L.; Moreno, E.; Naing, Z. Z. C.; Zhou, Y.; Peng, S.; Shi, Y.; Zhang, Z.; Shen, W.; Kirby, I. T.; Melnyk, J. E.; Chorba, J. S.; Lou, K.; Dai, S. A.; Barrio-Hernandez, I.; Memon, D.; Hernandez-Armenta, C.; Lyu, J.; Mathy, C. J. P.; Perica, T.; Pilla,

K. B.; Ganesan, S. J.; Saltzberg, D. J.; Rakesh, R.; Liu, X.; Rosenthal, S. B.; Calviello, L.; Venkataramanan, S.; Liboy-Lugo, J.; Lin, Y.; Huang, X.-P.; Liu, Y.; Wankowicz, S. A.; Bohn, M.; Safari, M.; Ugur, F. S.; Koh, C.; Savar, N. S.; Tran, Q. D.; Shengjuler, D.; Fletcher, S. J.; O'Neal, M. C.; Cai, Y.; Chang, J. C. J.; Broadhurst, D. J.; Klippsten, S.; Sharp, P. P.; Wenzell, N. A.; Kuzuoglu, D.; Wang, H.-Y.; Trenker, R.; Young, J. M.; Cavero, D. A.; Hiatt, J.; Roth, T. L.; Rathore, U.; Subramanian, A.; Noack, J.; Hubert, M.; Stroud, R. M.; Frankel, A. D.; Rosenberg, O. S.; Verba, K. A.; Agard, D. A.; Ott, M.; Emerman, M.; Jura, N. A SARS-CoV-2 protein interaction map reveals targets for drug repurposing. *Nature* **2020**, *582*, 459-468.

(170) Bouchard, P.; Quirion, R. [3H]1,3-di(2-tolyl)guanidine and [3H](+)pentazocine binding sites in the rat brain: Autoradiographic visualization of the putative sigma 1 and sigma 2 receptor subtypes. *Neuroscience* **1997**, *76*, 467-477.

(171) Hellewell, S. B.; Bruce, A.; Feinstein, G.; Orringer, J.; Williams, W.; Bowen, W. D. Rat liver and kidney contain high densities of σ1 and σ2 receptors: characterization by ligand binding and photoaffinity labeling. *Eur. J. Pharmacol. Mol. Pharmacol.* **1994**, *268*, 9-18.

(172) Vilner, B. J.; John, C. S.; Bowen, W. D. Sigma-1 and Sigma-2 Receptors Are Expressed in a Wide Variety of Human and Rodent Tumor Cell Lines. *Cancer Res.* **1995**, *55*, 408-413.

(173) Zeng, C.; Vangveravong, S.; Xu, J.; Chang, K. C.; Hotchkiss, R. S.; Wheeler, K. T.; Shen, D.; Zhuang, Z.-P.; Kung, H. F.; Mach, R. H. Subcellular Localization of Sigma-2 Receptors in Breast Cancer Cells Using Two-Photon and Confocal Microscopy. *Cancer Res.* **2007**, *67*, 6708-6716.

(174) Gebreselassie, D.; Bowen, W. D. Sigma-2 receptors are specifically localized to lipid rafts in rat liver membranes. *Eur. J. Pharmacol.* **2004**, *493*, 19-28.

(175) Nicholson, H. E.; Alsharif, W. F.; Comeau, A. B.; Mesangeau, C.; Intagliata, S.; Mottinelli, M.; McCurdy, C. R.; Bowen, W. D. Divergent Cytotoxic and Metabolically Stimulative Functions of Sigma-2 Receptors: Structure-Activity Relationships of 6-Acetyl-3-(4-(4-(4-fluorophenyl)piperazin-1-yl)butyl)benzo[d]oxazol-2(3H)-one (SN79) Derivatives. *J. Pharmacol. Exp. Ther.* **2019**, *368*, 272-281.

(176) Matsumoto, R. R.; Bowen, W. D.; Tom, M. A.; Vo, V. N.; Truong, D. D.; De Costa, B. R. Characterization of two novel σ receptor ligands: antidystonic effects in rats suggest σ receptor antagonism. *Eur. J. Pharmacol.* **1995**, *280*, 301-310.

(177) Mach, R. H.; Smith, C. R.; Al-Nabulsi, I.; Whirrett, B. R.; Childers, S. R.; Wheeler, K. T. σ2 Receptors as Potential Biomarkers of Proliferation in Breast Cancer. *Cancer Res.* **1997**, *57*, 156-161.

(178) Hedley, D. W.; Clark, G. M.; Cornelisse, C. J.; Killander, D.; Kute, T.; Merkel, D. Consensus review of the clinical utility of dna cytometry in carcinoma of the breast. *Cytometry* **1993**, *14*, 482-485.

(179) Masunaga, S.-I.; Ono, K. Significance of the Response of Quiescent Cell Populations within Solid Tumors in Cancer Therapy. *J. Rad. Res.* **2002**, *43*, 11-11.

(180) Wheeler, K. T.; Wang, L. M.; Wallen, C. A.; Childers, S. R.; Cline, J. M.; Keng, P. C.; Mach, R. H. Sigma-2 receptors as a biomarker of proliferation in solid tumours. *Br. J. Cancer* **2000**, *82*, 1223-1232.

(181) Mach, R. H.; Huang, Y.; Freeman, R. A.; Wu, L.; Vangveravong, S.; Luedtke, R. R. Conformationally-flexible benzamide analogues as dopamine D3 and σ2 receptor ligands. *Bioorg. Med. Chem. Lett.* **2004**, *14*, 195-202.

(182) Tu, Z.; Dence, C. S.; Ponde, D. E.; Jones, L.; Wheeler, K. T.; Welch, M. J.; Mach, R. H. Carbon-11 labeled σ2 receptor ligands for imaging breast cancer. *Nucl. Med. Biol.* **2005**, *32*, 423-430.

(183) Tu, Z.; Xu, J.; Jones, L. A.; Li, S.; Dumstorff, C.; Vangveravong, S.; Chen, D. L.; Wheeler, K. T.; Welch, M. J.; Mach, R. H. Fluorine-18-Labeled Benzamide Analogues for Imaging the σ2 Receptor Status of Solid Tumors with Positron Emission Tomography. *J. Med. Chem.* **2007**, *50*, 3194-3204.

(184) Dehdashti, F.; Laforest, R.; Gao, F.; Shoghi, K. I.; Aft, R. L.; Nussenbaum, B.; Kreisel, F. H.; Bartlett, N. L.; Cashen, A.; Wagner-Johnson, N.; Mach, R. H. Assessment of Cellular Proliferation in Tumors by PET Using 18F-ISO-1. *J. Nucl. Med.* **2013**, *54*, 350-357.

(185) Shoghi, K. I.; Xu, J.; Su, Y.; He, J.; Rowland, D.; Yan, Y.; Garbow, J. R.; Tu, Z.; Jones, L. A.; Higashikubo, R.; Wheeler, K. T.; Lubet, R. A.; Mach, R. H.; You, M. Quantitative Receptor-Based Imaging of Tumor Proliferation with the Sigma-2 Ligand [18F]ISO-1. *PLoS ONE* **2013**, *8*, e74188.

(186) Berridge, M. J.; Bootman, M. D.; Lipp, P. Calcium - a life and death signal. *Nature* **1998**, *395*, 645-648.

(187) Vilner, B. J.; Bowen, W. D. Modulation of Cellular Calcium by Sigma-2 Receptors: Release from Intracellular Stores in Human SK-N-SH Neuroblastoma Cells. *J. Pharmacol. Exp. Ther.* **2000**, *292*, 900-911.

(188) Zeng, C.; Rothfuss, J.; Zhang, J.; Chu, W.; Vangveravong, S.; Tu, Z.; Pan, F.; Chang, K. C.; Hotchkiss, R.; Mach, R. H. Sigma-2 ligands induce tumour cell death by multiple signalling pathways. *Br. J. Cancer* **2012**, *106*, 693-701.

(189) Cassano, G.; Gasparre, G.; Contino, M.; Niso, M.; Berardi, F.; Perrone, R.; Colabufo, N. A. The sigma-2 receptor agonist PB28 inhibits calcium release from

the endoplasmic reticulum of SK-N-SH neuroblastoma cells. *Cell Calcium* **2006**, *40*, 23-28.

(190) Cassano, G.; Gasparre, G.; Niso, M.; Contino, M.; Scalera, V.; Colabufo, N. A. F281, synthetic agonist of the sigma-2 receptor, induces Ca2+ efflux from the endoplasmic reticulum and mitochondria in SK-N-SH cells. *Cell Calcium* **2009**, *45*, 340-345.

(191) Ferorelli, S.; Abate, C.; Colabufo, N. A.; Niso, M.; Inglese, C.; Berardi, F.; Perrone, R. Design and Evaluation of Naphthol- and Carbazole-Containing Fluorescent σ Ligands as Potential Probes for Receptor Binding Studies. *J. Med. Chem.* **2007**, *50*, 4648-4655.

(192) Kaushal, N.; Robson, M. J.; Vinnakota, H.; Narayanan, S.; Avery, B. A.; McCurdy, C. R.; Matsumoto, R. R. Synthesis and Pharmacological Evaluation of 6-Acetyl-3-(4-(4-(4-fluorophenyl)piperazin-1-yl)butyl)benzo[d]oxazol-2(3H)-one (SN79), a Cocaine Antagonist, in Rodents. *AAPS J.* **2011**, *13*, 336-346.

(193) Nicholson, H.; Mesangeau, C.; McCurdy, C. R.; Bowen, W. D. Sigma-2 Receptors Play a Role in Cellular Metabolism: Stimulation of Glycolytic Hallmarks by CM764 in Human SK-N-SH Neuroblastoma. *J. Pharmacol. Exp. Ther.* **2016**, *356*, 434-445.

(194) Vilner, B.; De Costa, B.; Bowen, W. Cytotoxic effects of sigma ligands: sigma receptor-mediated alterations in cellular morphology and viability. *J. Neurosci.* **1995**, *15*, 117-134.

(195) Bowen, W. D.: σ2 Receptors: Regulation of Cell Growth and Implications for Cancer Diagnosis and Therapeutics. In *Sigma Receptors: Chemistry, Cell Biology and Clinical Implications*; Su, T.-P., Matsumoto, R. R., Bowen, W. D., Eds.; Springer US: Boston, MA, 2007; pp 215-235.

(196) Crawford, K. W.; Bowen, W. D. Sigma-2 Receptor Agonists Activate a Novel Apoptotic Pathway and Potentiate Antineoplastic Drugs in Breast Tumor Cell Lines. *Cancer Res.* **2002**, *62*, 313-322.

(197) Perregaard, J.; Moltzen, E. K.; Meier, E.; Sanchez, C. .sigma. Ligands with Subnanomolar Affinity and Preference for the .sigma.2 Binding Site. 1. 3-(.omega.-Aminoalkyl)-1H-indoles. *J. Med. Chem.* **1995**, *38*, 1998-2008.

(198) Ostenfeld, M. S.; Fehrenbacher, N.; Høyer-Hansen, M.; Thomsen, C.; Farkas, T.; Jäättelä, M. Effective Tumor Cell Death by σ-2 Receptor Ligand Siramesine Involves Lysosomal Leakage and Oxidative Stress. *Cancer Res.* **2005**, *65*, 8975-8983.

(199) Ostenfeld, M. S.; Høyer-Hansen, M.; Bastholm, L.; Fehrenbacher, N.; Olsen, O. D.; Groth-Pedersen, L.; Puustinen, P.; Kirkegaard-Sørensen, T.; Nylandsted, J.; Farkas, T.; Jäättelä, M. Anti-cancer agent siramesine is a lysosomotropic

detergent that induces cytoprotective autophagosome accumulation. *Autophagy* **2008**, *4*, 487-499.

(200) Hafner Česen, M.; Repnik, U.; Turk, V.; Turk, B. Siramesine triggers cell death through destabilisation of mitochondria, but not lysosomes. *Cell Death Dis*. **2013**, *4*, e818-e818.

(201) Zeng, C.; Rothfuss, J. M.; Zhang, J.; Vangveravong, S.; Chu, W.; Li, S.; Tu, Z.; Xu, J.; Mach, R. H. Functional assays to define agonists and antagonists of the sigma-2 receptor. *Anal. Biochem*. **2014**, *448*, 68-74.

(202) Zeng, C.; Weng, C.-C.; Schneider, M. E.; Puentes, L.; Riad, A.; Xu, K.; Makvandi, M.; Jin, L.; Hawkins, W. G.; Mach, R. H. TMEM97 and PGRMC1 do not mediate sigma-2 ligand-induced cell death. *Cell Death Discov*. **2019**, *5*.

(203) Huang, Y.-S.; Lu, H.-L.; Zhang, L.-J.; Wu, Z. Sigma-2 Receptor Ligands and Their Perspectives in Cancer Diagnosis and Therapy. *Med. Res. Rev*. **2014**, *34*, 532-566.

(204) Nicholson, H.; Comeau, A.; Mesangeau, C.; McCurdy, C. R.; Bowen, W. D. Characterization of CM572, a Selective Irreversible Partial Agonist of the Sigma-2 Receptor with Antitumor Activity. *J. Pharmacol. Exp. Ther*. **2015**, *354*, 203-212.

(205) Ghelardini, C.; Galeotti, N.; Bartolini, A. Pharmacological identification of SM-21, the novel σ2 antagonist. *Pharmacol. Biochem. Behav*. **2000**, *67*, 659-662.

(206) Lever, J. R.; Miller, D. K.; Green, C. L.; Fergason-Cantrell, E. A.; Watkinson, L. D.; Carmack, T. L.; Fan, K.-H.; Lever, S. Z. A selective sigma-2 receptor ligand antagonizes cocaine-induced hyperlocomotion in mice. *Synapse* **2014**, *68*, 73-84.

(207) Colabufo, N. A.; Berardi, F.; Contino, M.; Perrone, R.; Tortorella, V. A new method for evaluating σ2 ligand activity in the isolated guinea-pig bladder. *Naunyn-Schmiedeberg's Arch. Pharmacol*. **2003**, *368*, 106-112.

(208) Lin, G.; Xuechu, Z. Sigma-2 Receptor Ligands: Neurobiological Effects. *Curr. Med. Chem*. **2015**, *22*, 989-1003.

(209) Clinical Trial of CT1812 in Mild to Moderate Alzheimer's Disease. (report no. NCT02907567) https://clinicaltrials.gov/ct2/show/NCT02907567 (accessed June 5, 2020.

(210) Keefe, R. S. E.; Harvey, P. D.; Khan, A.; Saoud, J. B.; Staner, C.; Davidson, M.; Luthringer, R. Cognitive effects of MIN-101 in patients with schizophrenia and negative symptoms : Results from a randomized controlled trial. *J. Clin. Psych*. **2018**, *79*, 17m11753.

(211) Study to Evaluate Efficacy and Safety of Roluperidone (MIN-101) in Adult Patients With Negative Symptoms of Schizophrenia (report no. NCT03397134). https://clinicaltrials.gov/ct2/show/NCT03397134 (accessed June 5, 2020.

(212) Kim, F. J.; Pasternak, G. W. Cloning the sigma2 receptor: Wandering 40 years to find an identity. *Proc. Natl. Acad. Sci. U.S.A.* **2017**, *114*, 6888-6890.

(213) Rix, U.; Superti-Furga, G. Target profiling of small molecules by chemical proteomics. *Nat. Chem. Biol.* **2009**, *5*, 616-624.

(214) Tamura, T.; Terada, T.; Tanaka, A. A Quantitative Analysis and Chemical Approach for the Reduction of Nonspecific Binding Proteins on Affinity Resins. *Bioconjug. Chem.* **2003**, *14*, 1222-1230.

(215) Hashimoto, M.; Yang, J.; Holman, G. D. Cell-Surface Recognition of Biotinylated Membrane Proteins Requires Very Long Spacer Arms: An Example from Glucose-Transporter Probes. *ChemBioChem* **2001**, *2*, 52-59.

(216) Tamura, S.; Inomata, S.; Ebine, M.; Genji, T.; Iwakura, I.; Mukai, M.; Shoji, M.; Sugai, T.; Ueda, M. Triazoyl–phenyl linker system enhancing the aqueous solubility of a molecular probe and its efficiency in affinity labeling of a target protein for jasmonate glucoside. *Bioorg. Med. Chem. Lett.* **2013**, *23*, 188-193.

(217) Colabufo, N. A.; Berardi, F.; Abate, C.; Contino, M.; Niso, M.; Perrone, R. Is the σ2Receptor a Histone Binding Protein? *J. Med. Chem.* **2006**, *49*, 4153-4158.

(218) Berardi, F.; Ferorelli, S.; Abate, C.; Colabufo, N. A.; Contino, M.; Perrone, R.; Tortorella, V. 4-(Tetralin-1-yl)- and 4-(Naphthalen-1-yl)alkyl Derivatives of 1-Cyclohexylpiperazine as σ Receptor Ligands with Agonist σ2Activity. *J. Med. Chem.* **2004**, *47*, 2308-2317.

(219) Colabufo, N. A.; Abate, C.; Contino, M.; Inglese, C.; Ferorelli, S.; Berardi, F.; Perrone, R. Tritium radiolabelling of PB28, a potent sigma-2 receptor ligand: pharmacokinetic and pharmacodynamic characterization. *Bioorg. Med. Chem. Lett.* **2008**, *18*, 2183-2187.

(220) Abate, C.; Niso, M.; Berardi, F. Sigma-2 receptor: past, present and perspectives on multiple therapeutic exploitations. *Future Med. Chem.* **2018**, *10*, 1997-2018.

(221) Xu, J.; Zeng, C.; Chu, W.; Pan, F.; Rothfuss, J. M.; Zhang, F.; Tu, Z.; Zhou, D.; Zeng, D.; Vangveravong, S.; Johnston, F.; Spitzer, D.; Chang, K. C.; Hotchkiss, R. S.; Hawkins, W. G.; Wheeler, K. T.; Mach, R. H. Identification of the PGRMC1 protein complex as the putative sigma-2 receptor binding site. *Nature Commun.* **2011**, *2*, 380.

(222) Meyer, C.; Schmid, R.; Scriba, P. C.; Wehling, M. Purification and Partial Sequencing of High-Affinity Progesterone-Binding Site(s) from Porcine Liver Membranes. *Eur. J. Biochem.* **1996**, *239*, 726-731.

(223) Ryu, C. S.; Klein, K.; Zanger, U. M. Membrane Associated Progesterone Receptors: Promiscuous Proteins with Pleiotropic Functions – Focus on Interactions with Cytochromes P450. *Front. Pharmacol.* **2017**, *8*.

(224) Cahill, M. A.; Jazayeri, J. A.; Catalano, S. M.; Toyokuni, S.; Kovacevic, Z.; Richardson, D. R. The emerging role of progesterone receptor membrane component 1 (PGRMC1) in cancer biology. *Biochim. Biophys. Acta* **2016**, *1866*, 339-349.

(225) Mifsud, W.; Bateman, A. Membrane-bound progesterone receptors contain a cytochrome b5-like ligand-binding domain. *Genome Biol.* **2002**, *3*, research0068.0061.

(226) Kabe, Y.; Nakane, T.; Koike, I.; Yamamoto, T.; Sugiura, Y.; Harada, E.; Sugase, K.; Shimamura, T.; Ohmura, M.; Muraoka, K.; Yamamoto, A.; Uchida, T.; Iwata, S.; Yamaguchi, Y.; Krayukhina, E.; Noda, M.; Handa, H.; Ishimori, K.; Uchiyama, S.; Kobayashi, T.; Suematsu, M. Haem-dependent dimerization of PGRMC1/Sigma-2 receptor facilitates cancer proliferation and chemoresistance. *Nature Commun.* **2016**, *7*, 11030.

(227) Kabe, Y.; Handa, H.; Suematsu, M. Function and structural regulation of the carbon monoxide (CO)-responsive membrane protein PGRMC1. *J. Clin. Biochem. Nut.* **2018**, *63*, 12-17.

(228) Hughes, A. L.; Powell, D. W.; Bard, M.; Eckstein, J.; Barbuch, R.; Link, A. J.; Espenshade, P. J. Dap1/PGRMC1 Binds and Regulates Cytochrome P450 Enzymes. *Cell Metab.* **2007**, *5*, 143-149.

(229) Klein, M.; Canoll, P. D.; Musacchio, J. SKF 525-A and cytochrome P-450 ligands inhibit with high affinity the binding of [3H]dextromethorpan and σ ligands to guinea pig brain. *Life Sci.* **1991**, *48*, 543-550.

(230) Ross, S. B. Heterogeneous Binding of Sigma Radioligands in the Rat Brain and Liver: Possible Relationship to Subforms of Cytochrome P-450. *Pharmacol. Toxicol.* **1991**, *68*, 293-301.

(231) Ghosh, K.; Thompson, A. M.; Goldbeck, R. A.; Shi, X.; Whitman, S.; Oh, E.; Zhiwu, Z.; Vulpe, C.; Holman, T. R. Spectroscopic and Biochemical Characterization of Heme Binding to Yeast Dap1p and Mouse PGRMC1p. *Biochemistry* **2005**, *44*, 16729-16736.

(232) Min, L.; Strushkevich, N. V.; Harnastai, I. N.; Iwamoto, H.; Gilep, A. A.; Takemori, H.; Usanov, S. A.; Nonaka, Y.; Hori, H.; Vinson, G. P.; Okamoto, M. Molecular identification of adrenal inner zone antigen as a heme-binding protein. *FEBS J.* **2005**, *272*, 5832-5843.

(233) Cahill, M. A. Progesterone receptor membrane component 1: An integrative review. *J. Steroid Biochem. Mol. Biol.* **2007**, *105*, 16-36.

(234) Peluso, J. J.; Romak, J.; Liu, X. Progesterone Receptor Membrane Component-1 (PGRMC1) Is the Mediator of Progesterone's Antiapoptotic Action in Spontaneously Immortalized Granulosa Cells As Revealed by PGRMC1 Small

Interfering Ribonucleic Acid Treatment and Functional Analysis of PGRMC1 M. *Endocrinology* **2008**, *149*, 534-543.

(235) Johannessen, M.; Fontanilla, D.; Mavlyutov, T.; Ruoho, A. E.; Jackson, M. B. Antagonist action of progesterone at σ-receptors in the modulation of voltage-gated sodium channels. *Am. J. Physiol. Cell Physiol.* **2011**, *300*, C328-C337.

(236) Meyer, C.; Schmieding, K.; Falkenstein, E.; Wehling, M. Are high-affinity progesterone binding site(s) from porcine liver microsomes members of the σ receptor family? *Eur. J. Pharmacol.* **1998**, *347*, 293-299.

(237) Clark, N. C.; Friel, A. M.; Pru, C. A.; Zhang, L.; Shioda, T.; Rueda, B. R.; Peluso, J. J.; Pru, J. K. Progesterone receptor membrane component 1 promotes survival of human breast cancer cells and the growth of xenograft tumors. *Cancer Biol.* **2016**, 1-10.

(238) Mir, S. U.; Schwarze, S. R.; Jin, L.; Zhang, J.; Friend, W.; Miriyala, S.; St Clair, D.; Craven, R. J. Progesterone receptor membrane component 1/Sigma-2 receptor associates with MAP1LC3B and promotes autophagy. *Autophagy* **2013**, *9*, 1566-1578.

(239) Mir, S. U. R.; Ahmed, I. S. A.; Arnold, S.; Craven, R. J. Elevated progesterone receptor membrane component 1/sigma-2 receptor levels in lung tumors and plasma from lung cancer patients. *Int. J. Cancer* **2012**, *131*, E1-E9.

(240) Bali, N.; Arimoto, J. M.; Morgan, T. E.; Finch, C. E. Progesterone Antagonism of Neurite Outgrowth Depends on Microglial Activation via Pgrmc1/S2R. *Endocrinology* **2013**, *154*, 2468-2480.

(241) Chu, U. B.; Mavlyutov, T. A.; Chu, M.-L.; Yang, H.; Schulman, A.; Mesangeau, C.; McCurdy, C. R.; Guo, L.-W.; Ruoho, A. E. The Sigma-2 Receptor and Progesterone Receptor Membrane Component 1 are Different Binding Sites Derived From Independent Genes. *EBioMedicine* **2015**, *2*, 1806-1813.

(242) Abate, C.; Niso, M.; Infantino, V.; Menga, A.; Berardi, F. Elements in support of the 'non-identity' of the PGRMC1 protein with the σ2 receptor. *Eur. J. Pharmacol.* **2015**, *758*, 16-23.

(243) Fontanilla, D.; Hajipour, A. R.; Pal, A.; Chu, U. B.; Arbabian, M.; Ruoho, A. E. Probing the Steroid Binding Domain-like I (SBDLI) of the Sigma-1 Receptor Binding Site Using N-Substituted Photoaffinity Labels. *Biochemistry* **2008**, *47*, 7205-7217.

(244) Bertha, C. M.; Vilner, B. J.; Mattson, M. V.; Bowen, W. D.; Becketts, K.; Xu, H.; Rothman, R. B.; Flippen-Anderson, J. L.; Rice, K. C. (E)-8-Benzylidene Derivatives of 2-Methyl-5-(3-hydroxyphenyl)morphans: Highly Selective Ligands for the .sigma.2 Receptor Subtype. *J. Med. Chem.* **1995**, *38*, 4776-4785.

(245) Nastasi, G.; Miceli, C.; Pittalà, V.; Modica, M. N.; Prezzavento, O.; Romeo, G.; Rescifina, A.; Marrazzo, A.; Amata, E. S2RSLDB: a comprehensive manually curated, internet-accessible database of the sigma-2 receptor selective ligands. *J. Cheminform.* **2017**, *9,* 3.

(246) Cratteri, P.; Romanelli, M. N.; Cruciani, G.; Bonaccini, C.; Melani, F. GRIND-derived pharmacophore model for a series of α-tropanyl derivative ligands of the sigma-2 receptor. *J. Comput. Aided Mol. Des.* **2004**, *18*, 361-374.

(247) Laurini, E.; Zampieri, D.; Mamolo, M. G.; Vio, L.; Zanette, C.; Florio, C.; Posocco, P.; Fermeglia, M.; Pricl, S. A 3D-pharmacophore model for σ2 receptors based on a series of substituted benzo[d]oxazol-2(3H)-one derivatives. *Bioorg. Med. Chem. Lett.* **2010**, *20*, 2954-2957.

(248) Bertha, C. M.; Mattson, M. V.; Flippen-Anderson, J. L.; Rothman, R. B.; Xu, H.; Cha, X.-Y.; Becketts, K.; Rice, K. C. A Marked Change of Receptor Affinity of the 2-Methyl-5-(3-hydroxyphenyl)morphans upon Attachment of an (E)-8-Benzylidene Moiety: Synthesis and Evaluation of a New Class of .sigma. Receptor Ligands. *J. Med. Chem.* **1994**, *37*, 3163-3170.

(249) Bowen, W. D.; Bertha, C. M.; Vilner, B. J.; Rice, K. C. CB-64D and CB-184: ligands with high σ2 receptor affinity and subtype selectivity. *Eur. J. Pharmacol.* **1995**, *278*, 257-260.

(250) Bonhaus, D. W.; Loury, D. N.; Jakeman, L. B.; To, Z.; DeSouza, A.; Eglen, R. M.; Wong, E. H. [3H]BIMU-1, a 5-hydroxytryptamine3 receptor ligand in NG-108 cells, selectively labels sigma-2 binding sites in guinea pig hippocampus. *J. Pharmacol. Exp. Ther.* **1993**, *267*, 961-970.

(251) Gualtieri, F.; Conti, G.; Dei, S.; Giovannoni, M. P.; Nannucci, F.; Romanelli, M. N.; Scapecchi, S.; Teodori, E.; Fanfani, L.; Ghelardini, C.; Giotti, A.; Bartolini, A. Presynaptic Cholinergic Modulators as Potent Cognition Enhancers and Analgesic Drugs. 1. Tropic and 2-Phenylpropionic Acid Esters. *J. Med. Chem.* **1994**, *37*, 1704-1711.

(252) Gualtieri, F.; Bottalico, C.; Calandrella, A.; Dei, S.; Giovannoni, M. P.; Mealli, S.; Romanelli, M. N.; Scapecchi, S.; Teodori, E. Presynaptic Cholinergic Modulators as Potent Cognition Enhancers and Analgesic Drugs. 2. 2-Phenoxy-, 2-(Phenylthio)-, and 2-(Phenylamino)alkanoic Acid Esters. *J. Med. Chem.* **1994**, *37*, 1712-1719.

(253) Mach, R. H.; Wu, L.; West, T.; Whirrett, B. R.; Childers, S. R. The analgesic tropane analogue (±)-SM 21 has a high affinity for σ2 receptors. *Life Sci.* **1999**, *64*, PL131-PL137.

(254) Prezzavento, O.; Gualtieri, F.; Marrazzo, A.; Romanelli, M. N.; Ronsisvalle, G.; Teodori, E. Sigma Receptor Binding Profile of a Series of Analgesic Tropane Derivatives. *Arch. Pharm.* **2002**, *335*, 39-43.

(255) Mach R. H., Y. B., Wu L,, Kuhner R., Whirrett B., West T. Synthesis and sigma receptor binding affinities of 8-azabicyclo[3.2.1]octan-3a-yl and 9-azabicyclo[3.3.1]nonan-3a-yl phenyl carbamates. *Med. Chem. Res.* **2001**, *10*, 339-355.

(256) Mach R. H., V. S., Huang Y. S., Yang B., Blair J. B., Wu L. . Synthesis of N-substituted 9-azabicyclo[3.3.1]nonan-3α-yl phenylcarbamate analogs as sigma-2 receptor ligands. *Med. Chem. Res.* **2003**, *11*, 380-398.

(257) Vangveravong, S.; Xu, J.; Zeng, C.; Mach, R. H. Synthesis of N-substituted 9-azabicyclo[3.3.1]nonan-3α-yl carbamate analogs as σ2 receptor ligands. *Bioorg. Med. Chem.* **2006**, *14*, 6988-6997.

(258) Mach, R. H.; Huang, Y.; Freeman, R. A.; Wu, L.; Blair, S.; Luedtke, R. R. Synthesis of 2-(5-Bromo-2,3-dimethoxyphenyl)-5-(aminomethyl)-1H-pyrrole analogues and their binding affinities for dopamine D2, D3, and D4 receptors. *Bioorg. Med. Chem.* **2003**, *11*, 225-233.

(259) Huang, Y.; Luedtke, R. R.; Freeman, R. A.; Wu, L.; Mach, R. H. Synthesis and Structure−Activity Relationships of Naphthamides as Dopamine D3 Receptor Ligands. *J. Med. Chem.* **2001**, *44*, 1815-1826.

(260) Xu, R.; Lever, J. R.; Lever, S. Z. Synthesis and in vitro evaluation of tetrahydroisoquinolinyl benzamides as ligands for σ receptors. *Bioorg. Med. Chem. Lett.* **2007**, *17*, 2594-2597.

(261) Abate, C.; Ferorelli, S.; Contino, M.; Marottoli, R.; Colabufo, N. A.; Perrone, R.; Berardi, F. Arylamides hybrids of two high-affinity σ2 receptor ligands as tools for the development of PET radiotracers. *Eur. J. Med. Chem.* **2011**, *46*, 4733-4741.

(262) Berardi, F.; Abate, C.; Ferorelli, S.; Uricchio, V.; Colabufo, N. A.; Niso, M.; Perrone, R. Exploring the Importance of Piperazine N-Atoms for σ2Receptor Affinity and Activity in a Series of Analogs of 1-Cyclohexyl-4-[3-(5-methoxy-1,2,3,4-tetrahydronaphthalen-1-yl)propyl]piperazine (PB28). *J. Med. Chem.* **2009**, *52*, 7817-7828.

(263) Hodges, T. R. Development of Norbenzomorphan Derived Sigma 2 Receptor Ligands and the Synthesis of (±) Gliocladin C and Related Epipolythiodiketopiperazine Alkaloids. The Univeristy of Texas at Austin Dissertation, 2016.

(264) Morgenthaler, M.; Schweizer, E.; Hoffmann-Röder, A.; Benini, F.; Martin, R. E.; Jaeschke, G.; Wagner, B.; Fischer, H.; Bendels, S.; Zimmerli, D.; Schneider, J.; Diederich, F.; Kansy, M.; Müller, K. Predicting and Tuning Physicochemical Properties in Lead Optimization: Amine Basicities. *ChemMedChem* **2007**, *2*, 1100-1115.

(265) O'Brien, R. J.; Wong, P. C. Amyloid Precursor Protein Processing and Alzheimer's Disease. *Annual. Rev. Neurosci,* **2011**, *34*, 185-204.

(266) Hulme, S. E.; Whitesides, G. M. Chemistry and the Worm: Caenorhabditis elegans as a Platform for Integrating Chemical and Biological Research. *Angew. Chem. Int. Ed.* **2011**, *50*, 4774-4807.

(267) Runko, E. Caenorhabditis elegans VEM-1, a Novel Membrane Protein, Regulates the Guidance of Ventral Nerve Cord-Associated Axons. *J. Neurosci.* **2004**, *24*, 9015-9026.

(268) Colloca, L.; Ludman, T.; Bouhassira, D.; Baron, R.; Dickenson, A. H.; Yarnitsky, D.; Freeman, R.; Truini, A.; Attal, N.; Finnerup, N. B.; Eccleston, C.; Kalso, E.; Bennett, D. L.; Dworkin, R. H.; Raja, S. N. Neuropathic pain. *Nat. Rev. Dis. Primers* **2017**, *3*, 17002.

(269) Finnerup, N. B.; Attal, N.; Haroutounian, S.; McNicol, E.; Baron, R.; Dworkin, R. H.; Gilron, I.; Haanpää, M.; Hansson, P.; Jensen, T. S.; Kamerman, P. R.; Lund, K.; Moore, A.; Raja, S. N.; Rice, A. S. C.; Rowbotham, M.; Sena, E.; Siddall, P.; Smith, B. H.; Wallace, M. Pharmacotherapy for neuropathic pain in adults: a systematic review and meta-analysis. *Lancet Neurol.* **2015**, *14*, 162-173.

(270) Gris, G.; Portillo-Salido, E.; Aubel, B.; Darbaky, Y.; Deseure, K.; Vela, J. M.; Merlos, M.; Zamanillo, D. The selective sigma-1 receptor antagonist E-52862 attenuates neuropathic pain of different aetiology in rats. *Sci. Rep.* **2016**, *6*, 24591.

(271) Decosterd, I.; Woolf, C. J. Spared nerve injury: an animal model of persistent peripheral neuropathic pain. *Pain* **2000**, *87*, 149-158.

(272) Werner, C.; Engelhard, K. Pathophysiology of traumatic brain injury. *Br. J. Anaesth.* **2007**, *99*, 4-9.

(273) Corrigan, J. D.; Selassie, A. W.; Orman, J. A. The Epidemiology of Traumatic Brain Injury. *J. Head Trauma Rehabil.* **2010**, *25*, 72-80.

(274) Roozenbeek, B.; Lingsma, H. F.; Maas, A. I. New considerations in the design of clinical trials for traumatic brain injury. *Clin. Investig.* **2012**, *2*, 153-162.

(275) Yin, T. C.; Voorhees, J. R.; Genova, R. M.; Davis, K. C.; Madison, A. M.; Britt, J. K.; Cintrón-Pérez, C. J.; McDaniel, L.; Harper, M. M.; Pieper, A. A. Acute Axonal Degeneration Drives Development of Cognitive, Motor, and Visual Deficits after Blast-Mediated Traumatic Brain Injury in Mice. *eneuro* **2016**, *3*, ENEURO.0220-0216.

(276) Osier, N.; Dixon, C. Mini Review of Controlled Cortical Impact: A Well-Suited Device for Concussion Research. *Brain Sci.* **2017**, *7*, 88.

(277) Anton, R. F.; O'Malley, S. S.; Ciraulo, D. A.; Cisler, R. A.; Couper, D.; Donovan, D. M.; Gastfriend, D. R.; Hosking, J. D.; Johnson, B. A.; Locastro, J. S.; Longabaugh, R.; Mason, B. J.; Mattson, M. E.; Miller, W. R.; Pettinati, H. M.;

Randall, C. L.; Swift, R.; Weiss, R. D.; Williams, L. D.; Zweben, A.; Combine Study Research Group, F. T. Combined Pharmacotherapies and Behavioral Interventions for Alcohol Dependence. *JAMA* **2006**, *295*, 2003.

(278) Mann, K.; Lehert, P.; Morgan, M. Y. The Efficacy of Acamprosate in the Maintenance of Abstinence in Alcohol-Dependent Individuals: Results of a Meta-Analysis. *Alcohol Clin. Exp. Res.* **2004**, *28*, 51-63.

(279) Koob, G. F.; Roberts, A. J.; Schulteis, G.; Parsons, L. H.; Heyser, C. J.; Hyytia, P.; Merlo-Pich, E.; Weiss, F. Neurocircuitry Targets in Ethanol Reward and Dependence. *Alcohol Clin. Exp. Res.* **1998**, *22*, 3-9.

(280) Winward, J. L.; Bekman, N. M.; Hanson, K. L.; Lejuez, C. W.; Brown, S. A. Changes in Emotional Reactivity and Distress Tolerance Among Heavy Drinking Adolescents During Sustained Abstinence. *Alcohol Clin. Exp. Res.* **2014**, *38*, 1761-1769.

(281) Garcés-Ramírez, L.; Green, J. L.; Hiranita, T.; Kopajtic, T. A.; Mereu, M.; Thomas, A. M.; Mesangeau, C.; Narayanan, S.; McCurdy, C. R.; Katz, J. L.; Tanda, G. Sigma Receptor Agonists: Receptor Binding and Effects on Mesolimbic Dopamine Neurotransmission Assessed by Microdialysis. *Biol. Psychiatry* **2011**, *69*, 208-217.

(282) Klawonn, A. M.; Nilsson, A.; Radberg, C. F.; Lindstrom, S. H.; Ericson, M.; Granseth, B.; Engblom, D.; Fritz, M. The Sigma-2 Receptor Selective Agonist Siramesine (Lu 28-179) Decreases Cocaine-Reinforced Pavlovian Learning and Alters Glutamatergic and Dopaminergic Input to the Striatum. *Front. Pharmacol.* **2017**, *8*.

(283) Mitchell, P.; Mould, R.; Dillon, J.; Glautier, S.; Andrianakis, I.; James, C.; Pugh, A.; Holden-Dye, L.; O'Connor, V. A Differential Role for Neuropeptides in Acute and Chronic Adaptive Responses to Alcohol: Behavioural and Genetic Analysis in Caenorhabditis elegans. *PLoS ONE* **2010**, *5*, e10422.

(284) Scott, L. L.; Davis, S. J.; Yen, R. C.; Ordemann, G. J.; Nordquist, S. K.; Bannai, D.; Pierce, J. T. Behavioral Deficits Following Withdrawal from Chronic Ethanol Are Influenced by SLO Channel Function inCaenorhabditis elegans. *Genetics* **2017**, *206*, 1445-1458.

(285) Grotewiel, M.; Bettinger, J. C. DrosophilaandCaenorhabditis elegansas Discovery Platforms for Genes Involved in Human Alcohol Use Disorder. *Alcohol Clin. Exp. Res.* **2015**, *39*, 1292-1311.

(286) Sabino, V.; Cottone, P.; Zhao, Y.; Iyer, M. R.; Steardo, L.; Steardo, L.; Rice, K. C.; Conti, B.; Koob, G. F.; Zorrilla, E. P. The σ-Receptor Antagonist BD-1063 Decreases Ethanol Intake and Reinforcement in Animal Models of Excessive Drinking. *Neuropsychopharmacology* **2009**, *34*, 1482-1493.

(287) Walters, W. P.; Green, J.; Weiss, J. R.; Murcko, M. A. What Do Medicinal Chemists Actually Make? A 50-Year Retrospective. *J. Med. Chem.* **2011**, *54*, 6405-6416.

(288) Wang, S.; Dong, G.; Sheng, C. Structural simplification: an efficient strategy in lead optimization. *Acta Pharma. Sin. B* **2019**, *9*, 880-901.

(289) Zhao, H. Scaffold selection and scaffold hopping in lead generation: a medicinal chemistry perspective. *Drug Discov. Today* **2007**, *12*, 149-155.

(290) Jarrige, L.; Carboni, A.; Dagousset, G.; Levitre, G.; Magnier, E.; Masson, G. Photoredox-Catalyzed Three-Component Tandem Process: An Assembly of Complex Trifluoromethylated Phthalans and Isoindolines. *Org. Lett.* **2016**, *18*, 2906-2909.

(291) Molander, G. A.; Rivero, M. R. Suzuki Cross-Coupling Reactions of Potassium Alkenyltrifluoroborates. *Org. Lett.* **2002**, *4*, 107-109.

(292) Lee, J.; Kim, H. Y.; Oh, K. Tandem Reaction Approaches to Isoquinolones from 2-Vinylbenzaldehydes and Anilines via Imine Formation–6π-Electrocyclization–Aerobic Oxidation Sequence. *Org. Lett.* **2020**, *22*, 474-478.

(293) Yung-Chi, C.; Prusoff, W. H. Relationship between the inhibition constant (KI) and the concentration of inhibitor which causes 50 per cent inhibition (I50) of an enzymatic reaction. *Biochem. Pharmacol.* **1973**, *22*, 3099-3108.

(294) Cornelius, L. A. M.; Combs, D. W. A Convenient Synthesis of Mono- and Polyhalogenated Benzocyclanones. *Synthetic Commun.* **1994**, *24*, 2777-2788.

(295) Neidigh, K. A.; Avery, M. A.; Williamson, J. S.; Bhattacharyya, S. Facile preparation of N-methyl secondary amines by titanium(IV) isopropoxide-mediated reductive amination of carbonyl compounds. *J. Chem. Soc. Perkin Trans. 1* **1998**, 2527-2532.

(296) Surry, D. S.; Buchwald, S. L. Dialkylbiaryl phosphines in Pd-catalyzed amination: a user's guide. *Chem. Sci.* **2011**, *2*, 27-50.

(297) Harris, M. C.; Huang, X.; Buchwald, S. L. Improved Functional Group Compatibility in the Palladium-Catalyzed Synthesis of Aryl Amines. *Org. Lett.* **2002**, *4*, 2885-2888.

(298) Meanwell, N. A. Improving Drug Design: An Update on Recent Applications of Efficiency Metrics, Strategies for Replacing Problematic Elements, and Compounds in Nontraditional Drug Space. *Chem. Res. Toxicol.* **2016**, *29*, 564-616.

(299) Hann, M. M. Molecular obesity, potency and other addictions in drug discovery. *MedChemComm* **2011**, *2*, 349.

(300) Hann, M. M.; Keserü, G. M. Finding the sweet spot: the role of nature and nurture in medicinal chemistry. *Nat. Rev. Drug Discov.* **2012**, *11*, 355-365.

(301) Lipinski, C. A.; Lombardo, F.; Dominy, B. W.; Feeney, P. J. Experimental and computational approaches to estimate solubility and permeability in drug discovery and development settings. *Adv. Drug Deliv. Rev.* **1997**, *23*, 3-25.

(302) Gleeson, M. P. Generation of a Set of Simple, Interpretable ADMET Rules of Thumb. *J. Med. Chem.* **2008**, *51*, 817-834.

(303) Waring, M. J.; Johnstone, C. A quantitative assessment of hERG liability as a function of lipophilicity. *Bioorg. Med. Chem. Lett.* **2007**, *17*, 1759-1764.

(304) Puetzer, B.; Katz, L.; Horwitz, L. Preparatory Method for N-Vinyl-2-pyrrolidone. *J. Am. Chem. Soc.* **1952**, *74*, 4959-4960.

(305) Meanwell, N. A. Synopsis of Some Recent Tactical Application of Bioisosteres in Drug Design. *J. Med. Chem.* **2011**, *54*, 2529-2591.

(306) Yang, X.; Liu, G.; Li, H.; Zhang, Y.; Song, D.; Li, C.; Wang, R.; Liu, B.; Liang, W.; Jing, Y.; Zhao, G. Novel Oxadiazole Analogues Derived from Ethacrynic Acid: Design, Synthesis, and Structure−Activity Relationships in Inhibiting the Activity of GlutathioneS-Transferase P1-1 and Cancer Cell Proliferation. *J. Med. Chem.* **2010**, *53*, 1015-1022.

(307) Chiou, S.; Shine, H. J. A simplified procedure for preparing 3,5-disubstituted-1,2,4-oxadiazoles by reaction of amidoximes with Acyl chlorides in pyridine solution. *J. Heterocycl. Chem.* **1989**, *26*, 125-128.

(308) Borg, S.; Estenne-Bouhtou, G.; Luthman, K.; Csoeregh, I.; Hesselink, W.; Hacksell, U. Synthesis of 1,2,4-Oxadiazole-, 1,3,4-Oxadiazole-, and 1,2,4-Triazole-Derived Dipeptidomimetics. *J. Org. Chem.* **1995**, *60*, 3112-3120.

(309) Gangloff, A. R.; Litvak, J.; Shelton, E. J.; Sperandio, D.; Wang, V. R.; Rice, K. D. Synthesis of 3,5-disubstituted-1,2,4-oxadiazoles using tetrabutylammonium fluoride as a mild and efficient catalyst. *Tetrahedron Lett.* **2001**, *42*, 1441-1443.

(310) Fortuna, C. G.; Bonaccorso, C.; Bulbarelli, A.; Caltabiano, G.; Rizzi, L.; Goracci, L.; Musumarra, G.; Pace, A.; Palumbo Piccionello, A.; Guarcello, A.; Pierro, P.; Cocuzza, C. E. A.; Musumeci, R. New linezolid-like 1,2,4-oxadiazoles active against Gram-positive multiresistant pathogens. *Eur. J. Med. Chem.* **2013**, *65*, 533-545.

(311) Amarasinghe, K. K. D.; Maier, M. B.; Srivastava, A.; Gray, J. L. One-pot synthesis of 1,2,4-oxadiazoles from carboxylic acid esters and amidoximes using potassium carbonate. *Tetrahedron Lett.* **2006**, *47*, 3629-3631.

(312) Iyer, V. B.; Gurupadayya, B.; Koganti, V. S.; Inturi, B.; Chandan, R. S. Design, synthesis and biological evaluation of 1,3,4-oxadiazoles as promising anti-inflammatory agents. *Med. Chem. Res.* **2017**, *26*, 190-204.

(313) Hagishita, S.; Kuriyama, K. Confirmation of the Sector Rule of the Benzenoid Chromophore. *Bull. Chem. Soc. Jpn.* **1982**, *55*, 3216-3224.

(314) Morin, F. G.; Horton, W. J.; Grant, D. M.; Dalling, D. K.; Pugmire, R. J. Carbon-13 magnetic resonance of hydroaromatics. II. Conformation of Tetralin and tetrahydroanthracene and their methyl derivatives. *J. Am. Chem. Soc.* **1983**, *105*, 3992-3998.

(315) Gearien, J. E.; Liska, K. J. Synthetic Oxytocics. Derivatives of N-2-Naphthylglycine and N-2-Naphthyl-β-alanine 1,2. *J. Am. Chem. Soc.* **1954**, *76*, 3554-3555.

(316) Fogassy, E.; Nogradi, M.; Kozma, D.; Egri, G.; Palovics, E.; Kiss, V. Optical resolution methods. *Org. Biomol. Chem.* **2006**, *4*, 3011-3030.

(317) Welch, W. M.; Williams, M. T. Synthesis of 7-H-3-(1s,4s)-4-(3,4-Dichlorophenyl)-1,2,3,4-Tetrahydro-N-Methyl-L-Naphthalenamine Hydrochloride (7-H-3-Sertraline). *J. Labelled Compd. Rad.* **1993**, *33*, 119-125.

(318) 2020 Alzheimer's disease facts and figures. *Alzheimer's Dement.* **2020**, *16*, 391-460.

(319) Hardy, J. The Amyloid Hypothesis of Alzheimer's Disease: Progress and Problems on the Road to Therapeutics. *Science* **2002**, *297*, 353-356.

(320) Takahashi, R. H.; Capetillo-Zarate, E.; Lin, M. T.; Milner, T. A.; Gouras, G. K. Co-occurrence of Alzheimer's disease β-amyloid and tau pathologies at synapses. *Neurobiol. Aging* **2010**, *31*, 1145-1152.

(321) Zhang, Z.-G.; Li, Y.; Ng, C. T.; Song, Y.-Q. Inflammation in Alzheimer's Disease and Molecular Genetics: Recent Update. *Arch. Immunol. Ther. Exp.* **2015**, *63*, 333-344.

(322) Sly, L. M.; Krzesicki, R. F.; Brashler, J. R.; Buhl, A. E.; McKinley, D. D.; Carter, D. B.; Chin, J. E. Endogenous brain cytokine mRNA and inflammatory responses to lipopolysaccharide are elevated in the Tg2576 transgenic mouse model of Alzheimer's disease. *Brain Res. Bull.* **2001**, *56*, 581-588.

(323) Shaftel, S. S.; Griffin, W. S. T.; O'Banion, M. K. The role of interleukin-1 in neuroinflammation and Alzheimer disease: an evolving perspective. *J. Neuroinflamm.* **2008**, *5*.

(324) Oakley, H.; Cole, S. L.; Logan, S.; Maus, E.; Shao, P.; Craft, J.; Guillozet-Bongaarts, A.; Ohno, M.; Disterhoft, J.; Van Eldik, L.; Berry, R.; Vassar, R. Intraneuronal beta-Amyloid Aggregates, Neurodegeneration, and Neuron Loss in Transgenic Mice with Five Familial Alzheimer's Disease Mutations: Potential Factors in Amyloid Plaque Formation. *J. Neurosci.* **2006**, *26*, 10129-10140.

(325) Karran, E.; Mercken, M.; Strooper, B. D. The amyloid cascade hypothesis for Alzheimer's disease: an appraisal for the development of therapeutics. *Nat. Rev. Drug Discov.* **2011**, *10*, 698-712.

(326) Ricciarelli, R.; Fedele, E. The Amyloid Cascade Hypothesis in Alzheimer's Disease: It's Time to Change Our Mind. *Curr. Neuropharmacol.* **2017**, *15*.

(327) Ferreira, S. T.; Lourenco, M. V.; Oliveira, M. M.; De Felice, F. G. Soluble amyloid-β oligomers as synaptotoxins leading to cognitive impairment in Alzheimer's disease. *Front. Cell. Neurosci.* **2015**, *9*.

(328) Walsh, D. M.; Selkoe, D. J. A beta Oligomers–a decade of discovery. *J. Neurochem.* **2007**, *101*, 1172-1184.

(329) Feng, B.; Mills, J. B.; Davidson, R. E.; Mireles, R. J.; Janiszewski, J. S.; Troutman, M. D.; de Morais, S. M. In vitro P-glycoprotein assays to predict the in vivo interactions of P-glycoprotein with drugs in the central nervous system. *Drug Metab. Dispos.* **2008**, *36*, 268-275.

(330) Wager, T. T.; Chandrasekaran, R. Y.; Hou, X. J.; Troutman, M. D.; Verhoest, P. R.; Villalobos, A.; Will, Y. Defining Desirable Central Nervous System Drug Space through the Alignment of Molecular Properties, in Vitro ADME, and Safety Attributes. *ACS Chem. Neurosci.* **2010**, *1*, 420-434.

(331) BlumDegen, D.; Muller, T.; Kuhn, W.; Gerlach, M.; Przuntek, H.; Riederer, P. Interleukin-1 beta and interleukin-6 are elevated in the cerebrospinal fluid of Alzheimer's and de novo Parkinson's disease patients. *Neuroscience Lett.* **1995**, *202*, 17-20.

(332) Memar Ardestani, P.; K. Evans, A.; Bitna Yi; Tiffany Nguyen; Laurence Coutellier; Mehrdad Shamloo. Modulation of neuroinflammation and pathology in the 5XFAD mouse model of Alzheimer's disease using a biased and selective beta-1 adrenergic receptor partial agonist. *Neuropharmacology* **2017**, *116*, 371-386.

(333) Pekny, M.; Pekna, M. Reactive gliosis in the pathogenesis of CNS diseases. *Biochim. Biophys. Acta* **2016**, *1862*, 483-491.

(334) Burda, J. E.; Sofroniew, M. V. Reactive Gliosis and the Multicellular Response to CNS Damage and Disease. *Neuron* **2014**, *81*, 229-248.

(335) Xiao, X.; Antony, S.; Kohlhagen, G.; Pommier, Y.; Cushman, M. Design, synthesis, and biological evaluation of cytotoxic 11-aminoalkenylindenoisoquinoline and 11-diaminoalkenylindenoisoquinoline topoisomerase I inhibitors. *Bioorg. Med. Chem.* **2004**, *12*, 5147-5160.

(336) Osada, S.; Sano, S.; Ueyama, M.; Chuman, Y.; Kodama, H.; Sakaguchi, K. Fluoroalkene modification of mercaptoacetamide-based histone deacetylase inhibitors. *Bioorg. Med. Chem.* **2010**, *18*, 605-611.

(337) Kane, B. E.; Grant, M. K. O.; El-Fakahany, E. E.; Ferguson, D. M. Synthesis and evaluation of xanomeline analogs - Probing the wash-resistant phenomenon at the M-1 muscarinic acetylcholine receptor. *Bioorg. Med. Chem.* **2008**, *16*, 1376-1392.

(338) Amatore, M.; Beeson, T. D.; Brown, S. P.; Macmillan, D. W. C. Enantioselective Linchpin Catalysis by SOMO Catalysis: An Approach to the Asymmetric α-Chlorination of Aldehydes and Terminal Epoxide Formation. *Angew. Chem. Int. Ed.* **2009**, *48*, 5121-5124.

(339) Kong, F.; Morais, G. R.; Falconer, R. A.; Sutton, C. W. An optimized method for the synthesis of amino-functionalized phosphatidylcholine. *Tetrahedron Lett.* **2012**, *53*, 546-549.

(340) Morrell, A.; Placzek, M. S.; Steffen, J. D.; Antony, S.; Agama, K.; Pommier, Y.; Cushman, M. Investigation of the Lactam Side Chain Length Necessary for Optimal Indenoisoquinoline Topoisomerase I Inhibition and Cytotoxicity in Human Cancer Cell Cultures. *J. Med. Chem.* **2007**, *50*, 2040-2048.

(341) Braun, M.; Hartnagel, U.; Ravanelli, E.; Schade, B.; Böttcher, C.; Vostrowsky, O.; Hirsch, A. Amphiphilic [5:1]- and [3:3]-Hexakisadducts of C60. *Eur. J. Org. Chem.* **2004**, 1983-2001.

(342) Kakumani, P. K.; Malhotra, P.; Mukherjee, S. K.; Bhatnagar, R. K. A draft genome assembly of the army worm, Spodoptera frugiperda. *Genomics* **2014**, *104*, 134-143.

(343) Micah; Kenneth; Armand; Bruno; Ichu, T.-A.; Olucha, J.; Steven; Kundu, S.; Piscitelli, F.; Rosen, H.; Benjamin. A Global Map of Lipid-Binding Proteins and Their Ligandability in Cells. *Cell* **2015**, *161*, 1668-1680.

(344) Murphy, M.; Pykett, M. J.; Harnish, P.; Zang, K. D.; George, D. L. Identification and Characterization of Genes Differentially Expressed in Meningiomas. *Cell Growth Differ.* **1993**, *4*, 715-722.

(345) Xu, X.-Y.; Zhang, L.-J.; Yu, Y.-Q.; Zhang, X.-T.; Huang, W.-J.; Nie, X.-C.; Song, G.-Q. Down-Regulated MAC30 Expression Inhibits Proliferation and Mobility of Human Gastric Cancer Cells. *Cell Physol. Biochem.* **2014**, *33*, 1359-1368.

(346) Kayed, H.; Kleeff, J.; Ding, J.; Hammer, J.; Giese, T.; Zentgraf, H.; Buchler, M. W.; Friess, H. Expression analysis of MAC30 in human pancreatic cancer and tumors of the gastrointestinal tract. *Histol. Histopathol.* **2004**, *19*, 1021-1031.

(347) Xiao, M.; Li, H.; Yang, S.; Huang, Y.; Jia, S.; Wang, H.; Wang, J.; Li, Z. Expression of MAC30 protein is related to survival and clinicopathological variables in breast cancer. *J. Surg. Oncol.* **2013**, *107*, 456-462.

(348) Moparthi, S.; Arbman, G.; Wallin, Å.; Kayed, H.; Kleeff, J.; Zentgraf, H.; Sun, X.-F. Expression of MAC30 protein is related to survival and biological variables in primary and metastatic colorectal cancers. *Int. J. Oncol.* **2007**.

(349) Zhao, Z.-R.; Zhang, L.-J.; He, X.-Q.; Zhang, Z.-Y.; Zhang, F.; Li, F.; Pei, Y.-B.; Hu, Y.-M.; Wang, M.-W.; Sun, X.-F. Significance of mRNA and Protein Expression of MAC30 in Progression of Colorectal Cancer. *Chemotherapy* **2011**, *57*, 394-401.

(350) Han, K.-Y.; Gu, X.; Wang, H.-R.; Liu, D.; Lv, F.-Z.; Li, J.-N. Overexpression of MAC30 is associated with poor clinical outcome in human non-small-cell lung cancer. *Tumor Biol.* **2013**, *34*, 821-825.

(351) Bartz, F.; Kern, L.; Erz, D.; Zhu, M.; Gilbert, D.; Meinhof, T.; Wirkner, U.; Erfle, H.; Muckenthaler, M.; Pepperkok, R.; Runz, H. Identification of Cholesterol-Regulating Genes by Targeted RNAi Screening. *Cell Metab.* **2009**, *10*, 63-75.

(352) Ebrahimi-Fakhari, D.; Wahlster, L.; Bartz, F.; Werenbeck-Ueding, J.; Praggastis, M.; Zhang, J.; Joggerst-Thomalla, B.; Theiss, S.; Grimm, D.; Ory, D. S.; Runz, H. Reduction of TMEM97 increases NPC1 protein levels and restores cholesterol trafficking in Niemann-pick type C1 disease cells. *Human Mol. Genet.* **2016**, *25*, 3588-3599.

(353) Moebius, F. F.; Striessnig, J.; Glossmann, H. The mysteries of sigma receptors: new family members reveal a role in cholesterol synthesis. *Trends Pharmacol. Sci.* **1997**, *18*, 67-70.

(354) Hayashi, T.; Su, T.-P.: Cholesterol at the Endoplasmic Reticulum: Roles of the Sigma-1 Receptor Chaperone and Implications thereof in Human Diseases. In *Cholesterol Binding and Cholesterol Transport Proteins: Structure and Function in Health and Disease*; Harris, J. R., Ed.; Springer Netherlands: Dordrecht, 2010; pp 381-398.

(355) Hopf, T. A.; Scharfe, C. P. I.; Rodrigues, J. P. G. L. M.; Green, A. G.; Kohlbacher, O.; Sander, C.; Bonvin, A. M. J. J.; Marks, D. S. Sequence co-evolution gives 3D contacts and structures of protein complexes. *Elife* **2014**, *3*.

(356) Riad, A.; Zeng, C.; Weng, C.-C.; Winters, H.; Xu, K.; Makvandi, M.; Metz, T.; Carlin, S.; Mach, R. H. Sigma-2 Receptor/TMEM97 and PGRMC-1 Increase the Rate of Internalization of LDL by LDL Receptor through the Formation of a Ternary Complex. *Sci. Rep.* **2018**, *8*.

(357) Riad, A.; Lengyel-Zhand, Z.; Zeng, C.; Weng, C.-C.; Lee, V. M. Y.; Trojanowski, J. Q.; Mach, R. H. The Sigma-2 Receptor/TMEM97, PGRMC1, and LDL Receptor Complex Are Responsible for the Cellular Uptake of Aβ42 and Its Protein Aggregates. *Mol. Neurobiol.* **2020**.

(358) Gan, L.; Cookson, M. R.; Petrucelli, L.; La Spada, A. R. Converging pathways in neurodegeneration, from genetics to mechanisms. *Nat. Neurosci.* **2018**, *21*, 1300-1309.

(359) Duncan, T.; Valenzuela, M. Alzheimer's disease, dementia, and stem cell therapy. *Stem Cell Res. Ther.* **2017**, *8,* 111.

(360) Johnson, T. C.; Siegel, D. Directing Stem Cell Fate: The Synthetic Natural Product Connection. *Chem. Rev.* **2017**, *117*, 12052-12086.

(361) Wilson, R. M.; Danishefsky, S. J. Applications of Total Synthesis to Problems in Neurodegeneration: Fascinating Chemistry along the Way. *Acc. Chem. Res.* **2006**, *39*, 539-549.

(362) Yang, X.-W.; Yang, C.-P.; Jiang, L.-P.; Qin, X.-J.; Liu, Y.-P.; Shen, Q.-S.; Chen, Y.-B.; Luo, X.-D. Indole Alkaloids with New Skeleton Activating Neural Stem Cells. *Org. Lett.* **2014**, *16*, 5808-5811.

(363) Bihelovic, F.; Ferjancic, Z. Total Synthesis of (±)-Alstoscholarisine A. *Angew. Chem. Int. Ed.* **2016**, *55*, 2569-2572.

(364) Liang, X.; Jiang, S.-Z.; Wei, K.; Yang, Y.-R. Enantioselective Total Synthesis of (–)-Alstoscholarisine A. *J. Am. Chem. Soc.* **2016**, *138*, 2560-2562.

(365) Mason, J. D.; Weinreb, S. M. Total Syntheses of the Monoterpenoid Indole Alkaloids (±)-Alstoscholarisine B and C. *Angew. Chem. Int. Ed.* **2017**, *56*, 16674-16676.

(366) Mason, J. D.; Weinreb, S. M. Synthesis of Alstoscholarisines A–E, Monoterpene Indole Alkaloids with Modulating Effects on Neural Stem Cells. *J. Org. Chem.* **2018**, *83*, 5877-5896.

(367) Hu, L.; Li, Q.; Yao, L.; Xu, B.; Wang, X.; Liao, X. Enantioselective and Divergent Syntheses of Alstoscholarisines A, E and Their Enantiomers. *Org. Lett.* **2018**, *20*, 6202-6205.

(368) Reyes-Gutiérrez, P. E.; Torres-Ochoa, R. O.; Martínez, R.; Miranda, L. D. Synthesis of azepino[4,5-b]indolones via an intermolecular radical oxidative substitution of N-Boc tryptamine. *Org. Biomol. Chem.* **2009**, *7*, 1388.

(369) Blechert, S.; Knier, R.; Schroers, H.; Wirth, T. Domino Reactions - New Concepts in the Synthesis of Indole Alkaloids and Other Polycyclic Indole Derivatives. *Synthesis* **1995**, *1995*, 592-604.

(370) Helmboldt, H.; Aho, J. E.; Pihko, P. M. Synthetic Studies Toward Pectenotoxin 2. Part II. Synthesis of the CDE and CDEF Ring Systems. *Org. Lett.* **2008**, *10*, 4183-4185.

(371) Schafroth, M. A.; Sarlah, D.; Krautwald, S.; Carreira, E. M. Iridium-Catalyzed Enantioselective Polyene Cyclization. *J. Am. Chem. Soc.* **2012**, *134*, 20276-20278.

(372) Tlais, S. F.; Danheiser, R. L. N-Tosyl-3-Azacyclohexyne. Synthesis and Chemistry of a Strained Cyclic Ynamide. *J. Am. Chem. Soc.* **2014**, *136*, 15489-15492.

(373) Hanessian, S.; Giroux, S.; Larsson, A. Efficient Allyl to Propenyl Isomerization in Functionally Diverse Compounds with a Thermally Modified Grubbs Second-Generation Catalyst. *Org. Lett.* **2006**, *8*, 5481-5484.

(374) Villar, I. S. D.; Gradillas, A.; Domínguez, G.; Pérez-Castells, J. Nitrogen ylide-mediated cyclopropanation of lactams and lactones. *Tetrahedron Lett.* **2010**, *51*, 3095-3098.

(375) Dou, X.; Huang, Y.; Hayashi, T. Asymmetric Conjugate Alkynylation of Cyclic α,β-Unsaturated Carbonyl Compounds with a Chiral Diene Rhodium Catalyst. *Angew. Chem. Int. Ed.* **2016**, *55*, 1133-1137.

(376) Trost, B. M.; Rhee, Y. H. A Rh(I)-Catalyzed Cycloisomerization of Homo- and Bis-homopropargylic Alcohols. *J. Am. Chem. Soc.* **2003**, *125*, 7482-7483.

(377) Dharuman, S.; Vankar, Y. D. N-Halosuccinimide/AgNO3-Efficient Reagent Systems for One-Step Synthesis of 2-Haloglycals from Glycals: Application in the Synthesis of 2C-Branched Sugars via Heck Coupling Reactions. *Org. Lett.* **2014**, *16*, 1172-1175.

(378) Cox, P. A.; Leach, A. G.; Campbell, A. D.; Lloyd-Jones, G. C. Protodeboronation of Heteroaromatic, Vinyl, and Cyclopropyl Boronic Acids: pH–Rate Profiles, Autocatalysis, and Disproportionation. *J. Am. Chem. Soc.* **2016**, *138*, 9145-9157.

(379) Kinzel, T.; Zhang, Y.; Buchwald, S. L. A New Palladium Precatalyst Allows for the Fast Suzuki–Miyaura Coupling Reactions of Unstable Polyfluorophenyl and 2-Heteroaryl Boronic Acids. *J. Am. Chem. Soc.* **2010**, *132*, 14073-14075.

(380) Düfert, M. A.; Billingsley, K. L.; Buchwald, S. L. Suzuki-Miyaura Cross-Coupling of Unprotected, Nitrogen-Rich Heterocycles: Substrate Scope and Mechanistic Investigation. *J. Am. Chem. Soc.* **2013**, *135*, 12877-12885.

(381) Medley, J. W.; Movassaghi, M. A Concise and Versatile Double-Cyclization Strategy for the Highly Stereoselective Synthesis and Arylative Dimerization of Aspidosperma Alkaloids. *Angew. Chem. Int. Ed.* **2012**, *51*, 4572-4576.

(382) Klosowski, D. W. Applications of Enantioselective Halolactonization Reactions, Synthesis of Photocaged Compounds for Identifying Neurons Based on Function, and Progress Towards the Total Synthesis of Alstoscholarisine E. The University of Texas at Austin Dissertation, 2018.

(383) Wood, M. D.; Klosowski, D. W.; Martin, S. F. Stereoselective Total Synthesis of (±)-Alstoscholarisine E. *Org. Lett.* **2020**, *22*, 786-790.

(384) Martin, S. F.; Li, W. Applications of intramolecular Diels-Alder reactions to alkaloid synthesis. A formal total synthesis of (.+-.)-dendrobine. *J. Org. Chem.* **1991**, *56*, 642-650.

(385) Ito, M.; Clark, C. W.; Mortimore, M.; Goh, J. B.; Martin, S. F. Biogenetically Inspired Approach to the Strychnos Alkaloids. Concise Syntheses of (±)-Akuammicine and (±)-Strychnine. *J. Am. Chem. Soc.* **2001**, *123*, 8003-8010.

(386) Fu, T.-H.; McElroy, W. T.; Shamszad, M.; Heidebrecht, R. W.; Gulledge, B.; Martin, S. F. Studies toward welwitindolinones: formal syntheses of N-methylwelwitindolinone C isothiocyanate and related natural products. *Tetrahedron* **2013**, *69*, 5588-5603.

(387) Granger, B. A.; Jewett, I. T.; Butler, J. D.; Hua, B.; Knezevic, C. E.; Parkinson, E. I.; Hergenrother, P. J.; Martin, S. F. Synthesis of (±)-Actinophyllic Acid and Analogs: Applications of Cascade Reactions and Diverted Total Synthesis. *J. Am. Chem. Soc.* **2013**, *135*, 12984-12986.

(388) Bian, Z.; Marvin, C. C.; Martin, S. F. Enantioselective Total Synthesis of (−)-Citrinadin A and Revision of Its Stereochemical Structure. *J. Am. Chem. Soc.* **2013**, *135*, 10886-10889.

(389) Martin, S. F.; Benage, B.; Williamson, S. A.; Brown, S. P. Applications of the intramolecular Diels-Alder reactions of heterodienes to the syntheses of indole alkaloids. *Tetrahedron* **1986**, *42*, 2903-2910.

(390) Martin, S. F.; Clark, C. W.; Ito, M.; Mortimore, M. A Biomimetic Approach to the Strychnos Alkaloids. A Novel, Concise Synthesis of (±)-Akuammicine and a Route to (±)-Strychnine. *J. Am. Chem. Soc.* **1996**, *118*, 9804-9805.

(391) Deiters, A.; Chen, K.; Eary, C. T.; Martin, S. F. Biomimetic Entry to the Sarpagan Family of Indole Alkaloids: Total Synthesis of (+)-Geissoschizine and (+)-N-Methylvellosimine. *J. Am. Chem. Soc.* **2003**, *125*, 4541-4550.

(392) Martin, S. F.; Chen, K. X.; Eary, C. T. An Enantioselective Total Synthesis of (+)-Geissoschizine†. *Org. Lett.* **1999**, *1*, 79-82.

(393) Martin, S. F.; Humphrey, J. M.; Ali, A.; Hillier, M. C. Enantioselective Total Syntheses of Ircinal A and Related Manzamine Alkaloids. *J. Am. Chem. Soc.* **1999**, *121*, 866-867.

(394) Humphrey, J. M.; Liao, Y.; Ali, A.; Rein, T.; Wong, Y.-L.; Chen, H.-J.; Courtney, A. K.; Martin, S. F. Enantioselective Total Syntheses of Manzamine A and Related Alkaloids. *J. Am. Chem. Soc.* **2002**, *124*, 8584-8592.

(395) Desimoni, G.; Tacconi, G. Heterodiene syntheses with .alpha.,.beta.-unsaturated carbonyl compounds. *Chem. Rev.* **1975**, *75*, 651-692.

(396) Tantillo, D. J.; Houk, K. N.; Jung, M. E. Origins of Stereoselectivity in Intramolecular Diels–Alder Cycloadditions of Dienes and Dienophiles Linked by Ester and Amide Tethers. *J. Org. Chem.* **2001**, *66*, 1938-1940.

(397) Gronowitz, S.; Lidert, Z. A Convenient Synthesis of N-Substituted N-Chloromethyl Carboxamides. *Synthesis* **1979**, *1979*, 810-810.

(398) Amoroso, R.; Cardillo, G.; Tomasini, C.; Tortoreto, P. A new route to the synthesis of amino acids through the mercury cyclization of chiral amidals. *J. Org. Chem.* **1992**, *57*, 1082-1087.

(399) Majumdar, S.; Sloan, K. B. Synthesis, hydrolyses and dermal delivery of N-alkyl-N-alkyloxycarbonylaminomethyl (NANAOCAM) derivatives of phenol, imide and thiol containing drugs. *Bioorg. Med. Chem. Lett.* **2006**, *16*, 3590-3594.

(400) Siver, K. G.; Sloan, K. B. Alkylation of 6-Mercaptopurine (6-MP) with N-Alkyl-N-alkoxycarbonyl)aminomethyl Chlorides: S6-(N-Alkyl-N-alkoxycarbonyl)aminomethyl-6-MP Prodrug Structure Effect on the Dermal Delivery of 6-MP. *J. Pharm. Sci.* **1990**, *79*, 66-73.

(401) Ikeda, K.; Terao, Y.; Sekiya, M. New syntheses of alpha;-N-alkylacetamidomethylated carbonyl compounds. *Chem. Pharm. Bull.* **1981**, *29*, 1156-1159.

(402) Trost, B. M.; Chupak, L. S.; Lübbers, T. Short preparation of (S)-(E)-1-(O-methylmandeloxy)butadiene. *J. Org. Chem.* **1997**, *62*, 736-736.

(403) Desimoni, G.; Faita, G.; Quadrelli, P. Forty Years after "Heterodiene Syntheses with α,β-Unsaturated Carbonyl Compounds": Enantioselective Syntheses of 3,4-Dihydropyran Derivatives. *Chem. Rev.* **2018**, *118*, 2080-2248.

(404) Gademann, K.; Chavez, D. E.; Jacobsen, E. N. Highly enantioselective inverse-electron-demand hetero-Diels-Alder reactions of alpha,beta-unsaturated aldehydes. *Angew. Chem. Int. Ed.* **2002**, *41*, 3059-3061.

(405) Graven, A.; Johannsen, M.; Jørgensen, K. A. A highly chemo- and enantio-selective hetero-Diels–Alder reaction catalysed by chiral aluminium complexes. *Chem. Commun.* **1996**, 2373-2374.

(406) Wang, B.; Feng, X.; Huang, Y.; Liu, H.; Cui, X.; Jiang, Y. A Highly Enantioselective Hetero-Diels–Alder Reaction of Aldehydes with Danishefsky's Diene Catalyzed by Chiral Titanium(IV) 5,5‘,6,6‘,7,7‘,8,8‘-Octahydro-1,1‘-bi-2-naphthol Complexes. *J. Org. Chem.* **2002**, *67*, 2175-2182.

(407) Laupichle, L.; Sowa, C. E.; Thiem, J. Synthesis and structural studies of asparagine-modified 2-deoxy-α-N-glycopeptides associated with the renin-Angiotensin system. *Bioorg. Med. Chem.* **1994**, *2*, 1281-1294.

(408) Bruno, N. C.; Tudge, M. T.; Buchwald, S. L. Design and preparation of new palladium precatalysts for C–C and C–N cross-coupling reactions. *Chem. Sci.* **2013**, *4*, 916-920.

(409) De Koning, C. B.; Michael, J. P.; Pathak, R.; Van Otterlo, W. A. L. The synthesis of indolo- and pyrrolo[2,1- a]isoquinolines. *Tetrahedron Lett.* **2004**, *45*, 1117-1119.

(410) Ito, S.; Taguchi, T.; Yamada, T.; Ubukata, T.; Yamaguchi, Y.; Asami, M. Indolylbenzothiadiazoles with varying substituents on the indole ring: a systematic study on the self-recovering mechanochromic luminescence. *RSC Adv.* **2017**, *7*, 16953-16962.

(411) W. Gribble, G. Sodium borohydride in carboxylic acid media: a phenomenal reduction system. *Chem. Soc. Rev.* **1998**, *27*, 395.

(412) Schwartz, B. D.; Denton, J. R.; Lian, Y.; Davies, H. M. L.; Williams, C. M. Asymmetric [4 + 3] Cycloadditions between Vinylcarbenoids and Dienes: Application to the Total Synthesis of the Natural Product (–)-5-epi-Vibsanin E. *J. Am. Chem. Soc.* **2009**, *131*, 8329-8332.

(413) Larson, G. L.; Fry, J. L.: Ionic and Organometallic-Catalyzed Organosilane Reductions. In *Organic Reactions*; Denmark, S. E., Ed.; Wiley and Sons, 2008; Vol. 71.

(414) Anderson, E.; Campbell, C.: Reduction of O,O-, N,O-, and S,O-Acetals to Ethers. Elsevier Ltd., 2014; Vol. 8; pp 339-367.

(415) Li, W.; Mead, K. T.; Smith, L. T. Studies towards diarylheptanoid synthesis. Part 1: Synthesis and ring cleavage reactions of hexahydro-2H,5H-pyrano[2,3-b]pyran-2-ones. *Tetrahedron Lett.* **2003**, *44*, 6351-6353.

(416) Gaertzen, O.; Misske, A. M.; Wolbers, P.; Hoffmann, H. M. R. Synthesis of Enantiopure C-Glycosides and Pseudo C-Glycosides. Lewis Acid Mediated Cleavage of [3.3.1] Oxabicyclic Lactones. *Synlett* **1999**, *1999*, 1041-1044.

(417) Yin, J.; Linker, T. Stereoselective diversity-oriented syntheses of functionalized saccharides from bicyclic carbohydrate 1,2-lactones. *Tetrahedron* **2011**, *67*, 2447-2461.

(418) Volkov, A.; Tinnis, F.; Slagbrand, T.; Trillo, P.; Adolfsson, H. Chemoselective reduction of carboxamides. *Chem. Soc. Rev.* **2016**, *45*, 6685-6697.

(419) Mizutani, M.; Inagaki, F.; Nakanishi, T.; Yanagihara, C.; Tamai, I.; Mukai, C. Total Syntheses of (–)- and (+)-Goniomitine. *Org. Lett.* **2011**, *13*, 1796-1799.

(420) Spletstoser, J. T.; White, J. M.; Tunoori, A. R.; Georg, G. I. Mild and selective hydrozirconation of amides to aldehydes using Cp2Zr(H)Cl: Scope and mechanistic insight. *J. Am. Chem. Soc.* **2007**, *129*, 3408-3419.

(421) Addis, D.; Das, S.; Junge, K.; Beller, M. Selective Reduction of Carboxylic Acid Derivatives by Catalytic Hydrosilylation. *Angew. Chem. Int. Ed.* **2011**, *50*, 6004-6011.

(422) Bower, S.; Kreutzer, K. A.; Buchwald, S. L. A Mild General Procedure for the One-Pot Conversion of Amides to Aldehydes. *Angew. Chem. Int. Ed.* **1996**, *35*, 1515-1516.

(423) Laval, S.; Dayoub, W.; Favre-Reguillon, A.; Demonchaux, P.; Mignani, G.; Lemaire, M. A mild titanium-based system for the reduction of amides to aldehydes. *Tetrahedron Lett.* **2010**, *51*, 2092-2094.

(424) Motoyama, Y.; Aoki, M.; Takaoka, N.; Aoto, R.; Nagashima, H. Highly efficient synthesis of aldenamines from carboxamides by iridium-catalyzed silane-reduction/dehydration under mild conditions. *Chem. Commun.* **2009**, 1574.

(425) Gabriel, P.; Gregory, A. W.; Dixon, D. J. Iridium-Catalyzed Aza-Spirocyclization of Indole-Tethered Amides: An Interrupted Pictet–Spengler Reaction. *Org. Lett.* **2019**, *21*, 6658-6662.

(426) Nakajima, M.; Sato, T.; Chida, N. Iridium-Catalyzed Chemoselective Reductive Nucleophilic Addition to N -Methoxyamides. *Org. Lett.* **2015**, *17*, 1696-1699.

(427) Yoritate, M.; Takahashi, Y.; Tajima, H.; Ogihara, C.; Yokoyama, T.; Soda, Y.; Oishi, T.; Sato, T.; Chida, N. Unified Total Synthesis of Stemoamide-Type Alkaloids by Chemoselective Assembly of Five-Membered Building Blocks. *J. Am. Chem. Soc.* **2017**, *139*, 18386-18391.

(428) Gammack Yamagata, A. D.; Dixon, D. J. Enantioselective Construction of the ABCDE Pentacyclic Core of the Strychnos Alkaloids. *Org. Lett.* **2017**, *19*, 1894-1897.

(429) Huang, P.-Q.; Ou, W.; Han, F. Chemoselective reductive alkynylation of tertiary amides by Ir and Cu(i) bis-metal sequential catalysis. *Chem. Commun.* **2016**, *52*, 11967-11970.

(430) Hu, X.-N.; Shen, T.-L.; Cai, D.-C.; Zheng, J.-F.; Huang, P.-Q. The iridium-catalysed reductive coupling reaction of tertiary lactams/amides with isocyanoacetates. *Org. Chem. Front.* **2018**, *5*, 2051-2056.

(431) Gregory, A. W.; Chambers, A.; Hawkins, A.; Jakubec, P.; Dixon, D. J. Iridium-Catalyzed Reductive Nitro-Mannich Cyclization. *Chem. Eur. J.* **2015**, *21*, 111-114.

(432) Tan, P. W.; Seayad, J.; Dixon, D. J. Expeditious and Divergent Total Syntheses of Aspidosperma Alkaloids Exploiting Iridium(I)-Catalyzed Generation of Reactive Enamine Intermediates. *Angew. Chem. Int. Ed.* **2016**, *55*, 13436-13440.

(433) Fuentes De Arriba, Á. L.; Lenci, E.; Sonawane, M.; Formery, O.; Dixon, D. J. Iridium-Catalyzed Reductive Strecker Reaction for Late-Stage Amide and Lactam Cyanation. *Angew. Chem. Int. Ed.* **2017**, *56*, 3655-3659.

(434) Xie, L.-G.; Dixon, D. J. Tertiary amine synthesis via reductive coupling of amides with Grignard reagents. *Chem. Sci.* **2017**, *8*, 7492-7497.

(435) Xie, L.-G.; Dixon, D. J. Iridium-catalyzed reductive Ugi-type reactions of tertiary amides. *Nature Commun.* **2018**, *9*.

(436) Wang, L.-Q.; Chen, S.-N.; Qin, G.-W.; Cheng, K.-F. Grayanane Diterpenoids from Pieris formosa. *J. Nat. Prod.* **1998**, *61*, 1473-1475.

(437) Niu, C.-S.; Li, Y.; Liu, Y.-B.; Ma, S.-G.; Liu, F.; Li, L.; Xu, S.; Wang, X.-J.; Wang, R.-B.; Qu, J.; Yu, S.-S. Pierisketolide A and Pierisketones B and C, Three Diterpenes with an Unusual Carbon Skeleton from the Roots of Pieris formosa. *Org. Lett.* **2017**, *19*, 906-909.

(438) Li, C.-H.; Yan, X.-T.; Zhang, A.-L.; Gao, J.-M. Structural Diversity and Biological Activity of the Genus Pieris Terpenoids. *J. Agric. Food Chem.* **2017**, *65*, 9934-9949.

(439) Riehl, P. S.; DePorre, Y. C.; Armaly, A. M.; Groso, E. J.; Schindler, C. S. New avenues for the synthesis of ent-kaurene diterpenoids. *Tetrahedron* **2015**, *71*, 6629-6650.

(440) Niu, C.-S.; Li, Y.; Liu, Y.-B.; Ma, S.-G.; Li, L.; Qu, J.; Yu, S.-S. Analgesic diterpenoids from the twigs of Pieris formosa. *Tetrahedron* **2016**, *72*, 44-49.

(441) Liu, Y.; Zhang, Y. Intramolecular and intermolecular ketone–ester reductive coupling reactions promoted by samarium(II) iodide. *Tetrahedron Lett.* **2001**, *42*, 5745-5748.

(442) Szostak, M.; Fazakerley, N. J.; Parmar, D.; Procter, D. J. Cross-Coupling Reactions Using Samarium(II) Iodide. *Chem. Rev.* **2014**, *114*, 5959-6039.

(443) Schiavo, L.; Lebedel, L.; Massé, P.; Choppin, S.; Hanquet, G. Access to Wieland–Miescher Diketone-Derived Building Blocks by Stereoselective Construction of the C-9 Quaternary Carbon Center Using the Mukaiyama Aldol Reaction. *J. Org. Chem.* **2018**, *83*, 6247-6258.

(444) Li, C.; Tu, S.; Wen, S.; Li, S.; Chang, J.; Shao, F.; Lei, X. Total Synthesis of the G2/M DNA Damage Checkpoint Inhibitor Psilostachyin C. *J. Org. Chem.* **2011**, *76*, 3566-3570.

(445) Kerr, W. J.; McLaughlin, M.; Morrison, A. J.; Pauson, P. L. Formal Total Synthesis of (±)-α- and β-Cedrene by Preparation of Cedrone. Construction of the Tricyclic Carbon Skeleton by the Use of a Highly Efficient Intramolecular Khand Annulation. *Org. Lett.* **2001**, *3*, 2945-2948.

(446) Crawford, J. J.; Kerr, W. J.; McLaughlin, M.; Morrison, A. J.; Pauson, P. L.; Thurston, G. J. Use of a highly effective intramolecular Pauson–Khand cyclisation for the formal total synthesis of (±)-α- and β-cedrene by preparation of cedrone. *Tetrahedron* **2006**, *62*, 11360-11370.

(447) Kerr, W. J.; McLaughlin, M.; Paterson, L. C.; Pearson, C. M. Total synthesis 2-epi-α-cedren-3-one via a cobalt-catalysed Pauson-Khand reaction. *Tetrahedron* **2018**, *74*, 5062-5068.

(448) Chirkin, E.; Michel, S.; Porée, F.-H. Viability of a [2 + 2 + 1] Hetero-Pauson–Khand Cycloaddition Strategy toward Securinega Alkaloids: Synthesis of the BCD-Ring Core of Securinine and Related Alkaloids. *J. Org. Chem.* **2015**, *80*, 6525-6528.

(449) Brill, Z. G.; Grover, H. K.; Maimone, T. J. Enantioselective synthesis of an ophiobolin sesterterpene via a programmed radical cascade. *Science* **2016**, *352*, 1078-1082.

(450) Reiser, O.; Ulbrich, K.; Kreitmeier, P. Microwave- or Microreactor-Assisted Conversion of Furfuryl Alcohols into 4-Hydroxy-2-cyclopentenones. *Synlett* **2010**, *2010*, 2037-2040.

(451) Kluge, A. F.; Untch, K. G.; Fried, J. H. Prostaglandins. X. Synthesis of prostaglandin models and prostaglandins by conjugage addition of a functionalized organocopper reagent. *J. Am. Chem. Soc.* **1972**, *94*, 7827-7832.

(452) Alvarez, F. S.; Wren, D.; Prince, A. Prostaglandins. IX. Synthesis of (+-)-prostaglandin E1, (+-)-11-deoxyprostaglandins E1,F1.alpha., and F1.beta., and (+-)-9-oxo-13-cis-prostenoic acid by conjugate addition of vinylcopper reagents. *J. Am. Chem. Soc.* **1972**, *94*, 7823-7827.

(453) Suzuki, M.; Yanagisawa, A.; Noyori, R. Prostaglandin synthesis. 16. The three-component coupling synthesis of prostaglandins. *J. Am. Chem. Soc.* **1988**, *110*, 4718-4726.

(454) Robertson, J.; Hatley, R. J. D.; Watkin, D. J. Preparation of the tricyclic ketopyrrole core of roseophilin by radical macrocyclisation and Paal–Knorr condensation. *J. Chem. Soc. Perkin Trans. 1* **2000**, 3389-3396.

(455) Gu, J.; Dirr, M. J.; Wang, Y.; Soper, D. L.; De, B.; Wos, J. A.; Johnson, C. R. An Efficient Synthesis of 3-Hetero-13,14-dihydro Prostaglandin F1αAnalogues. *Org. Lett.* **2001**, *3*, 791-794.

(456) Borrelly, S.; Paquette, L. A. Studies Directed to the Synthesis of the Unusual Cardiotoxic Agent Kalmanol. Enantioselective Construction of the Advanced Tetracyclic 7-Oxy-5,6-dideoxy Congener. *J. Am. Chem. Soc.* **1996**, *118*, 727-740.

(457) Corey, E. J.; Boaz, N. W. The reactions of combined organocuprate-chlorotrimethylsilane reagents with conjugated carbonyl compounds. *Tetrahedron* **1985**, *26*, 6019-6022.

(458) Bertz, S. H.; Miao, G.; Rossiter, B. E.; Snyder, J. P. New Copper Chemistry. 25. Effect of TMSCl on the Conjugate Addition of Organocuprates to .alpha.-Enones: A New Mechanism. *J. Am. Chem. Soc.* **1995**, *117*, 11023-11024.

(459) Taylor, R. J. K. Organocopper Conjugate Addition-Enolate Trapping Reactions. *Synthesis* **1985**, *1985*, 364-392.

(460) Hickmann, V.; Kondoh, A.; Gabor, B.; Alcarazo, M.; FüRstner, A. Catalysis-Based and Protecting-Group-Free Total Syntheses of the Marine Oxylipins Hybridalactone and the Ecklonialactones A, B, and C. *J. Am. Chem. Soc.* **2011**, *133*, 13471-13480.

(461) Bailey, W. F.; Punzalan, E. R. Convenient general method for the preparation of primary alkyllithiums by lithium-iodine exchange. *J. Org. Chem.* **1990**, *55*, 5404-5406.

(462) Pangborn, A. B.; Giardello, M. A.; Grubbs, R. H.; Rosen, R. K.; Timmers, F. J. Safe and Convenient Procedure for Solvent Purification. *Organometallics* **1996**, *15*, 1518-1520.

(463) Huang, H.; Greenberg, M. M. Synthesis and Analysis of Oligonucleotides Containing Abasic Site Analogues. *J. Org. Chem.* **2008**, *73*, 2695-2703.

(464) Bisacchi, G. S.; Chao, S. T.; Bachard, C.; Daris, J. P.; Innaimo, S.; Jacobs, G. A.; Kocy, O.; Lapointe, P.; Martel, A.; Merchant, Z.; Slusarchyk, W. A.; Sundeen, J. E.; Young, M. G.; Colonno, R.; Zahler, R. BMS-200475, a novel carbocyclic 2′-deoxyguanosine analog with potent and selective anti-hepatitis B virus activity in vitro. *Bioorg. Med. Chem. Lett.* **1997**, *7*, 127-132.

(465) Petasis, N. A.; Bzowej, E. I. Titanium-mediated carbonyl olefinations. 1. Methylenations of carbonyl compounds with dimethyltitanocene. *J. Am. Chem. Soc.* **1990**, *112*, 6392-6394.

(466) Hartley, R. C.; McKiernan, G. J. Titanium reagents for the alkylidenation of carboxylic acid and carbonic acid derivatives. *J. Chem. Soc. Perkin Trans. 1* **2002**, 2763-2793.

(467) Khand, I. U.; Knox, G. R.; Pauson, P. L.; Watts, W. E.; Foreman, M. I. Organocobalt complexes. Part II. Reaction of acetylenehexacarbonyldicobalt complexes, (R1C2R2)Co2(CO)6, with norbornene and its derivatives. *J. Chem. Soc. Perkin Trans. 1* **1973**, 977-981.

(468) Magnus, P.; Principe, L. M. Origins of 1,2- and 1,3-stereoselectivity in dicobaltoctacarbonyl alkene-alkyne cyclizations for the synthesis of substituted bicyclo[3.3.0]octenones. *Tetrahedron Lett.* **1985**, *26*, 4851-4854.

(469) Xacobe C. Cambeiro, M. A. P.: The Mechanism of the Pauson-Khand Reaction: Hypothesis, Experimental Facts, and Theoretical Investigations. In *The Pauson-Khand Reaction*; Torres, R. R., Ed., 2012; pp 23-48.

(470) Jeong, N.: 5.24 The Pauson–Khand Reaction. In *Comprehensive Organic Synthesis II (2nd Ed.)*; Knochel, P., Ed.; Elsevier: Amsterdam, 2014; pp 1106-1178.

(471) Schore, N. E.; Croudace, M. C. Preparation of bicyclo[3.3.0]oct-1-en-3-one and bicyclo[4.3.0]non-1(9)-en-8-one via intramolecular cyclization of .alpha.,.omega.-enynes. *J. Org. Chem.* **1981**, *46*, 5436-5438.

(472) Chang, Y.; Shi, L.; Huang, J.; Shi, L.; Zhang, Z.; Hao, H.-D.; Gong, J.; Yang, Z. Stereoselective Total Synthesis of (±)-5-epi-Cyanthiwigin I via an Intramolecular Pauson–Khand Reaction as the Key Step. *Org. Lett.* **2018**, *20*, 2876-2879.

(473) Chuang, K. V.; Xu, C.; Reisman, S. E. A 15-step synthesis of (+)-ryanodol. *Science* **2016**, *353*, 912-915.

(474) You, L.; Liang, X.-T.; Xu, L.-M.; Wang, Y.-F.; Zhang, J.-J.; Su, Q.; Li, Y.-H.; Zhang, B.; Yang, S.-L.; Chen, J.-H.; Yang, Z. Asymmetric Total Synthesis of Propindilactone G. *J. Am. Chem. Soc.* **2015**, *137*, 10120-10123.

(475) Liu, D.-D.; Sun, T.-W.; Wang, K.-Y.; Lu, Y.; Zhang, S.-L.; Li, Y.-H.; Jiang, Y.-L.; Chen, J.-H.; Yang, Z. Asymmetric Total Synthesis of Lancifodilactone G Acetate. *J. Am. Chem. Soc.* **2017**, *139*, 5732-5735.

(476) Miller, K. A.; Martin, S. F. Concise, Enantioselective Total Synthesis of (–)-Alstonerine. *Org. Lett.* **2007**, *9*, 1113-1116.

(477) Chen, J.-P.; He, W.; Yang, Z.-Y.; Yao, Z.-J. Synthesis of Tricyclo[4,3,1,0 1,5]decane Core of Plumisclerin A Using Pauson–Khand Annulation and SmI 2 -Mediated Radical Cyclization. *Org. Lett.* **2015**, *17*, 3379-3381.

(478) Sugihara, T.; Yamada, M.; Yamaguchi, M.; Nishizawa, M. The Intra- and Intermolecular Pauson-Khand Reaction Promoted by Alkyl Methyl Sulfides. *Synlett* **1999**, *1999*, 771-773.

(479) Sugihara, T.; Yamada, M.; Ban, H.; Yamaguchi, M.; Kaneko, C. Rate Enhancement of the Pauson–Khand Reaction by Primary Amines. *Angew. Chem. Int. Ed.* **1997**, *36*, 2801-2804.

(480) Shambayani, S.; Crowe, W. E.; Schreiber, S. L. N-oxide promoted Pauson-Khand cyclizations at room temperature. *Tetrahedron Lett.* **1990**, *31*, 5289-5292.

(481) Iqbal, M.; Vyse, N.; Dauvergne, J.; Evans, P. Microwave promoted Pauson–Khand reactions. *Tetrahedron Lett.* **2002**, *43*, 7859-7862.

(482) Shibata, T.; Toshida, N.; Takagi, K. Rhodium Complex-Catalyzed Pauson–Khand-Type Reaction with Aldehydes as a CO Source. *J. Org. Chem.* **2002**, *67*, 7446-7450.

(483) Cabré, A.; Khaizourane, H.; Garçon, M.; Verdaguer, X.; Riera, A. Total Synthesis of (R)-Sarkomycin Methyl Ester via Regioselective Intermolecular Pauson–Khand Reaction and Iridium-Catalyzed Asymmetric Isomerization. *Org. Lett.* **2018**, *20*, 3953-3957.

(484) Lam, F. L., Lee, H.W., Wang, J. and Kwong, F.Y.: Recent Advancement of Catalytic Pauson-Khand-type Reactions. In *The Pauson-Khand Reaction*; Torres, R. R., Ed., 2012; pp 181-210.

(485) Still, W. C.; Kahn, M.; Mitra, A. Rapid Chromatographic Technique for Preparative Separations with Moderate Resolution. *J. Org. Chem.* **1978**, *43*, 2923-2925.

(486) Cui, Y.; Jiang, H.; Li, Z. T.; Wu, N.; Yang, Z.; Quan, J. M. Unexpected Regioselectivity in the Synthesis of Pyranonaphthoquinone via the Diels-Alder Reaction. *Org. Lett.* **2009**, *11*, 4628-4631.

(487) Kuwano, R.; Kashiwabara, M. Ruthenium-catalyzed asymmetric hydrogenation of N-Boc-indoles. *Org. Lett.* **2006**, *8*, 2653-2655.

(488) Yang, X. W.; Yang, C. P.; Jiang, L. P.; Qin, X. J.; Liu, Y. P.; Shen, Q. S.; Chen, Y. B.; Luo, X. D. Indole Alkaloids with New Skeleton Activating Neural Stem Cells. *Org. Lett.* **2014**, *16*, 5808-5811.

(489) CrysAlisPro. Rigaku Oxford Diffraction (2019). CrysAlicPro Software System, 1.171.40.53.

(490) SHELXT. (2015). G. M. Sheldrick. A program for crystal structure solution. Acta Cryst. A71, 3-8.

(491) Spek, A. L. (2009). PLATON, A Multipurpose Crystallographic Tool. Utrecht University, The Netherlands. Acta Cryst. D65, 148-155.

(492) Dolomanov, O. V.; Bourhis, L. J.; Gildea, R. J.; Howard, J. A. K.; Puschmann, H. OLEX2: a complete structure solution, refinement and analysis program. *J Appl Crystallogr* **2009**, *42*, 339-341.

(493) WinGX 1.64. (1999). An Integrated System of Windows Programs for the Solution, Refinement and Analysis of Single Crystal X-ray Diffraction Data. Farrugia, L. J. J. Appl. Cryst. 32. 837-838.

(494) $Rw(F^2) = w(|Fo|2 - |Fc|2)2/\square w(|Fo|)4\}1/2$ where w is the weight given each reflection.

$R(F) = \Sigma(|F_o| - |F_c|)/\Sigma|F_o|\}$ for reflections with $F_o > 4(\sigma(F_o))$.

$S = [\Sigma w(|F_o|^2 - |F_c|^2)^2/(n - p)]^{1/2}$, where n is the number of reflections and p is the number of refined parameters.

(495) International Tables for X-ray Crystallography (1992). Vol. C, Tables 4.2.6.8 and 6.1.1.4, A. J. C. Wilson, editor, Boston: Kluwer Academic Press.

(496) Sheldrick, G. M. (1994). SHELXTL/PC (Version 5.03). Siemens Analytical X-ray Instruments, Inc., Madison, Wisconsin, USA.